CHEMICAL REVIEWS

Review

pubs.acs.org/CR

The Halogen Bond

Gabriella Cavallo,[†] Pierangelo Metrangolo,[*,†,‡] Roberto Milani,[‡] Tullio Pilati,[†] Arri Priimagi,[§] Giuseppe Resnati,[*,†] and Giancarlo Terraneo[†]

[†]Laboratory of Nanostructured Fluorinated Materials (NFMLab), Department of Chemistry, Materials and Chemical Engineering "Giulio Natta", Politecnico di Milano, Via L. Mancinelli 7, I-20131 Milano, Italy

[‡]VTT-Technical Research Centre of Finland, Biologinkuja 7, 02150 Espoo, Finland

[§]Department of Chemistry and Bioengineering, Tampere University of Technology, Korkeakoulunkatu 8, FI-33101 Tampere, Finland

ABSTRACT: The halogen bond occurs when there is evidence of a net attractive interaction between an electrophilic region associated with a halogen atom in a molecular entity and a nucleophilic region in another, or the same, molecular entity. In this fairly extensive review, after a brief history of the interaction, we will provide the reader with a snapshot of where the research on the halogen bond is now, and, perhaps, where it is going. The specific advantages brought up by a design based on the use of the halogen bond will be demonstrated in quite different fields spanning from material sciences to biomolecular recognition and drug design.

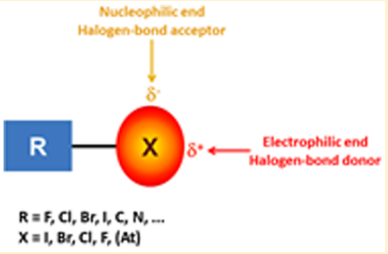

CONTENTS

Special Issue: Frontiers in Macromolecular and Supramolecular Science

Received: August 17, 2015
Published: January 26, 2016

DOI: 10.1021/acs.chemrev.5b00484
Chem. Rev. 2016, 116, 2478−2601

1. INTRODUCTION

Halogen atoms in haloorganics are typically considered as sites of high electron density because of their high electronegativity. Consistent with this well-established understanding, it is commonly accepted that halogen atoms can form attractive interactions by functioning as electron donor sites (i.e., nucleophiles). The ability of halogen atoms to work as hydrogen bond acceptors was recognized as early as the 1920s,[1−4] and halogen atoms of halocarbons can function as electron donor sites also to several other elements, e.g., when coordinating alkali-metal or alkaline-earth-metal cations. However, the electron density in halogen atoms is anisotropically distributed whenever the atom is covalently bound to one or more atoms.[5−7] In compounds wherein the halogen atom is involved in the formation of one covalent bond, by far the most common case, there is a region of higher electron density, where the electrostatic potential is negative in nearly all cases, which forms a belt orthogonal to the covalent bond, and a region of lower electron density (the so-called σ-hole) where the potential is frequently positive, mainly in the heavier halogens, which generates a cap of depleted electron density on the elongation of the covalent bond. This region can form attractive interactions with electron-rich sites, and the general ability of halogen atoms to attractively interact with electron donor sites (nucleophiles) has been fully recognized and comprehensively understood only recently.

In 2009 the International Union of Pure and Applied Chemistry (IUPAC) started a project (project no. 2009-032-1-100) having the aim "to take a comprehensive look at intermolecular interactions involving halogens as electrophilic species and classify them".[8] An IUPAC recommendation[9] defining these interactions as halogen bonds was issued in 2013 when the project was concluded: This definition states that "A halogen bond occurs when there is evidence of a net attractive interaction between an electrophilic region associated with a halogen atom in a molecular entity and a nucleophilic region in another, or the same, molecular entity." A schematic representation of the halogen bond is given in Figure 1.

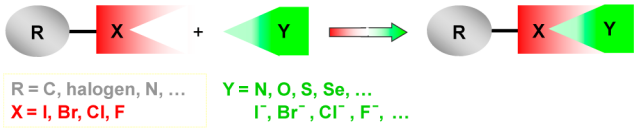

Figure 1. Schematic representation of the halogen bond.

The IUPAC definition categorizes unambiguously an interaction responsible for the formation of adducts prepared as early as 1814 but which had been overlooked for decades. This interaction developed into a routine and predictable tool to direct self-assembly phenomena in all phases only after its effectiveness in crystal engineering was demonstrated in the late 1990s.[10]

This review will focus on supramolecular systems assembled via the halogen bond (XB). The practice and concept of the interaction developed through a rather patchy course, and it seems instructive to open this review with a brief historical perspective of the topic as it may help the reader to identify Ariadne's thread which enabled the present situation to come about. This perspective may also help in anticipating future directions.

1.1. Historical Perspective

The beginning of the XB story can be traced back approximately to two centuries ago, when $I_2\cdots NH_3$, probably the first halogen-bonded complex ever prepared, was serendipitously synthesized by J. J. Colin while working in the laboratory of J. L. Gay-Lussac. In fact, in 1814 Colin reported the formation of a blue-black color upon combination of iodine with amilose[11] and of a liquid with a somewhat metallic luster upon reaction of dry iodine and dry gaseous ammonia.[12] The exact molecular composition of this liquid was established only 50 years later, when F. Guthrie obtained the same material in pure form by adding powdered iodine to aqueous ammonia and first proposed the $I_2\cdots NH_3$ structure for the formed liquid.[13] Notwithstanding this, it required another century before pioneering discoveries on charge-transfer interactions by R. Mulliken[14] and O. Hassel[15] allowed for major advancements in the understanding of the nature of the interaction driving the formation of such a complex. In the two centuries after Colin's report, many theoretical and experimental studies, performed in quite different contexts, provided information relevant to XB identification and outlining. However, these pieces of information remained long fragmented, their contextualization was limited to their respective areas, and a unifying and comprehensive categorization was missing. In this section we will mention the experimental and theoretical findings which gave major contributions for the development of the XB concept and practice. Some of these contributions will be discussed in greater detail and after a different perspective in the following sections of this review.

Soon after Colin's discovery, in 1819 P. Pelletier and J. B. Caventou[16] reported the first experimental evidence revealing the ability of dihalogens to interact attractively with anions. Specifically, they published the synthesis of strychnine triiodide, where the I_3^- anion was formed on interaction of I^- with I_2. The formation of triiodide anions has also been invoked by several other investigators to rationalize the greater solubility of I_2 in different solvents on addition of metal iodides as well as the reaction between metal halides and I_2.[17] In 1870 S. M. Jörgensen proposed that polyiodide alkaloids contain iodide anions as well as I_2 and published the first systematic investigation on the topic.[18]

In 1883 O. Rhoussopoulos[19] reported the synthesis of the quinoline/iodoform adduct, showing that halocarbons behave as dihalogens and form adducts with Lewis bases.

The formation of halogen-bonded complexes involving bromine and chlorine as electron acceptor species was first reported at the end of the 19th century by I. Remsen and J. F. Norris, who described the 1:1 dimers formed by Br_2 and Cl_2 with various amines.[20] On the other hand, the first XB adduct involving F_2 was reported only 80 years later[21−23] when it was possible to isolate the F_3^- anion by using very extreme conditions, and the synthesis of $F_2\cdots NH_3$ and $F_2\cdots OH_2$ adducts appeared only in the 1990s.[24] These early data were already suggesting, and today it is well established,[25−27] that the XB strength scales with the polarizability of the XB donor atom, that is, F < Cl < Br < I. In fact, F is the least prone to be involved in XB, being the less polarizable halogen atom, and can act as an XB donor only when attached to particularly strong electron-withdrawing groups.[28−31] The polarizability of astatine, the heaviest halogen, has been calculated to be higher than that of iodine,[32] and according to the trend described above, it can be foreseen that it may function as an XB donor

DOI: 10.1021/acs.chemrev.5b00484
Chem. Rev. 2016, 116, 2478−2601

too, even better than I. Although computational data support this hypothesis,[33,34] astatine is a radioactive element with short-lived isotopes, little is known about its chemistry,[35] and no halogen-bonded adducts involving At have been reported, so far.

The whole 20th century saw a flourishing of the research activity in the field. Lots of experimental observations and phenomena, where we are now acknowledging the role played by the XB, were reported. Albeit not yet named so, XB was at the core of some important achievements in chemistry, being relevant to the work of R. Mulliken (Nobel Prize in chemistry in 1966)[36,37] on the chemical bond and central to the conformational studies of O. Hassel (Nobel Prize in chemistry in 1969).[15]

Compilations collecting closely related results began to appear in the mid-20th century;[38−48] however, single findings were understood within conceptual frames different from each other, and the common features were not recognized until the end of the 20th century. The most important discoveries reported in the past 70 years are described below.

It has long been known that when I_2 is dissolved in organic solvents, solutions of different colors are formed:[49] Brown or red-brown solutions are obtained with acetone, alcohols, ethers, amines, and benzene, while violet solutions, resembling the color of the I_2 vapors, are obtained with aliphatic hydrocarbons, carbon tetrachloride, and chloroform. In 1948 H. A. Benesi and J. H. Hildebrand rationalized these phenomena when identifying the first cases of intermolecular donor−acceptor interactions in solution.[50,51] Similar complexes involving ethers, thioethers, and carbonyl derivatives were soon after reported by R. S. Mulliken in 1950,[14,52,53] and two years later he rationalized them as a subclass of the electron donor−acceptor molecular complex family.[53] UV−vis spectroscopy indicated that a charge transfer to the halogen occurs in all of these complexes, even in the weaker ones, such as those involving dihalogens and aromatics[54] or perfluorocarbons and amines.[55]

X-ray crystallographic studies reported by O. Hassel in the 1950s were crucial in identifying the structural features of the intermolecular interaction occurring in several complexes formed by dihalogens or halocarbons with electron donor molecules. In particular, in 1954 Hassel described the structure of the $Br_2\cdots O(CH_2CH_2)_2O$ adduct[56] as an infinite chain containing "halogen molecule bridges" linking together dioxane molecules (Figure 2, top). In this adduct the covalent Br−Br distance was found to be slightly longer than in the isolated Br_2 molecule, the Br···O intermolecular distance was shorter than the sum of their respective van der Waals radii, and the Br−Br···O angle was close to 180°.[57] These three features are general and distinctive of the XB. The "halogen molecule bridges" observed in the $Br_2\cdots O(CH_2CH_2)_2O$ adduct were also found in similar systems formed upon reaction of Br_2 and Cl_2 with benzene (Figure 2, bottom). Hassel himself reported in 1958 and 1959, respectively, the crystal structures of the adducts $Br_2\cdots C_6H_6$ and $Cl_2\cdots C_6H_6$, containing endless chains built up of alternating benzene and dihalogen molecules.[58,59] These two structures were particularly interesting since they showed π-systems working as donors of electron density toward dihalogens also in the solid state[60] and suggested that halogen-bonded adducts are on the reaction pathways of halogenation reactions of aromatics and other unsaturated systems. In the successive decades this hypothesis was forcefully confirmed,[61,62] and J. K. Kochi showed that π-donating moieties form solid adducts also with halocarbons.[54]

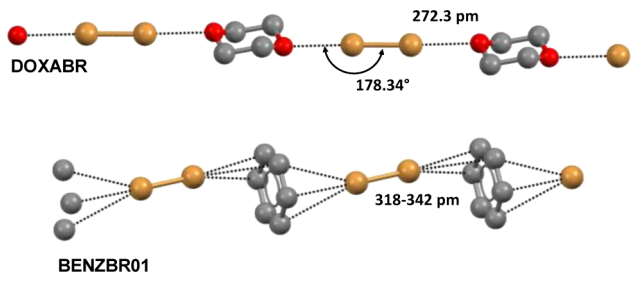

Figure 2. Ball-and-stick representation (Mercury 3.3) of the $Br_2\cdots O(CH_2CH_2)_2O$[56] (top) and $Br_2\cdots C_6H_6$[58] (bottom) adducts. Both adducts contain infinite chains formed by dibromine as the bidentate XB donor and dioxane, or benzene, as the bidentate XB acceptor. Color code: carbon, gray; oxygen, red; bromine, light brown. XBs are dotted black lines. Hydrogen atoms are omitted for clarity. CSD Refcodes are reported. Reprinted with permission from ref 63. Copyright 2015 Springer.

A comprehensive discussion of the crystal structures of halogen-bonded systems known at that time was given by H. A. Bent in the review he published in 1968 on the chemistry of donor−acceptor adducts. In this paper, the most distinctive geometric features of the interactions were clearly highlighted, i.e., the short interatomic distances and high directionality mentioned above.[64] Bent's analysis evidenced that in all complexes the distances between the electron donor atom and the halogen atom were shorter than the sum of their respective van der Waals radii and that the two atoms lay nearly on a straight line (i.e., the corresponding angles were close to 180°). These geometric features were confirmed 20 years later through statistical analysis of the structures in the Cambridge Structural Database (CSD) by R. Parthasarathy and G. R. Desiraju.[65] In 1983 J.-M. Dumas, M. Gomel, and M. Guerin[66] analyzed the intermolecular interactions involving haloorganics in solution through a variety of techniques (e.g., UV−vis, IR, Raman, NMR, nuclear quadrupole resonance (NQR), dielectric polarization, etc.), and they showed that the interaction features in the liquid phase parallel those in the solid phase.

A. Legon and co-workers[24,67] were the first to undertake a systematic analysis of a wide variety of halogen-bonded adducts formed in the gas phase via microwave spectroscopy. Their results on geometries and charge distributions revealed close similarities between "isolated" adducts and adducts in the condensed phase, showing that the lattice and solvent effects, present in the solid and in solution, respectively, have a minor influence on basic XB features.

In the same period some of us proved systematically that both anions[68−75] and lone-pair-possessing heteroatoms[76−87] form with halocarbons adducts showing consistent geometrical features (Figures 3 and 4). We also expanded the range of halocarbons which can work as effective XB donors[10,88] and identified the key role of residues close to covalently bound halogen atoms in determining their strength as electrophilic sites.

Gradually, it became clear that it was possible to design and fine-tune the structural and functional features of self-assembled adducts by choosing conveniently the nature and the structure of the molecules involved in XB formation. However, it took a long time before it was recognized that the electrophilic behavior of halogen atoms is commonplace and can drive the predictable formation of strong and highly directional interactions in the solid, liquid, and gas phases. Halogens are

DOI: 10.1021/acs.chemrev.5b00484
Chem. Rev. 2016, 116, 2478−2601

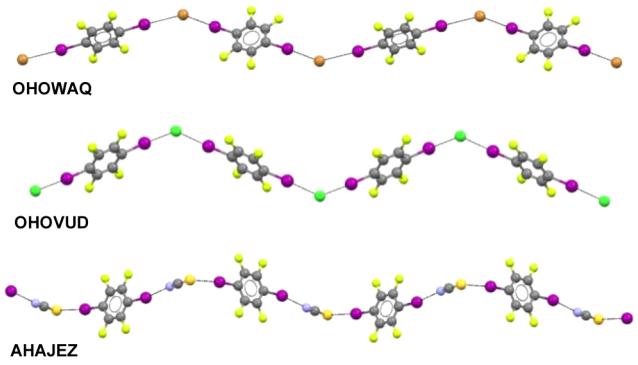

Figure 3. Ball-and-stick representation (Mercury 3.3) of the halogen-bonded infinite chains containing 1,4-diiodotetrafluorobenzene as the bidentate XB donor and *n*-$Bu_4N^+Br^-$ (OHOWAQ),[72] *n*-$Bu_4N^+Cl^-$ (OHOVUD),[72] and *n*-$Bu_4N^+SCN^-$ (AHAJEZ)[73] as XB acceptors. Quite similar infinite chains are obtained when *n*-$Bu_4P^+Br^-$,[73] $Me_4N^+Br^-$,[74] *n*-$Bu_4P^+Cl^-$,[75] and $Me_4N^+Cl^-$ [74] are used. Cations are omitted for clarity. Color code: carbon, gray; nitrogen, blue; bromine, light brown; chlorine, light green, sulfur, dark yellow; fluorine, yellow. XBs are dotted black lines. CSD Refcodes are reported.

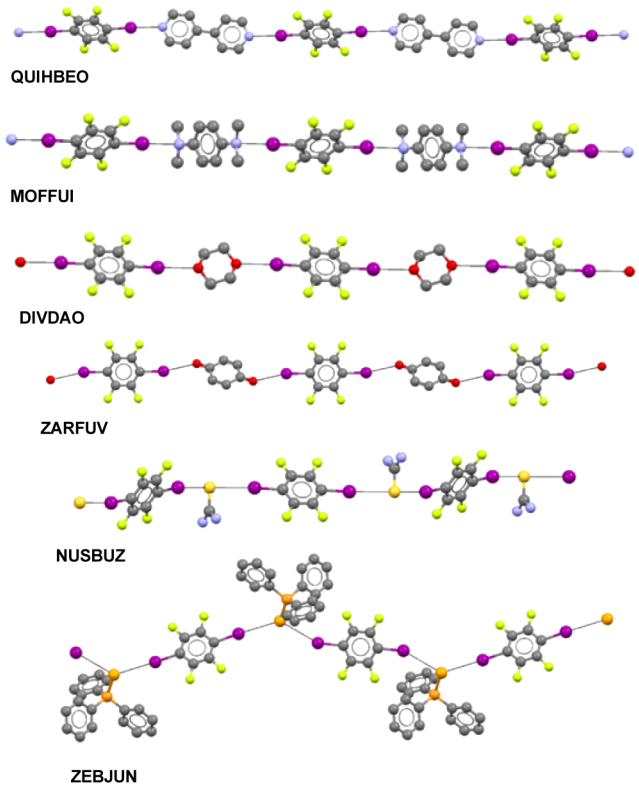

Figure 4. Ball-and-stick representation (Mercury 3.3) of the halogen-bonded infinite chains containing 1,4-diiodotetrafluorobenzene as the bidentate XB donor and neutral Lewis bases as bidentate XB acceptors. The selected Lewis bases are 4,4′-dipyridine (QUIHBEO),[76] *N*,*N*,*N*′,*N*′-tetramethyl-*p*-phenylendiamine (MOFFUI),[85] dioxane (DIVDAO),[77] 1,4-benzoquinone (ZARFUV),[86] thiourea (NUSBUZ),[78] and triphenylphosphine selenide (ZEBJUN).[79] Quite similar infinite chains are obtained when other nitrogen-centered nucleophiles,[80−83,87] oxygen-centered nucleophiles,[84] and sulfur-centered nucleophiles[77] are used. Color code: carbon, gray; nitrogen, blue; oxygen, red; iodine, purple; sulfur, dark yellow; phosphorus, orange; selenium, dark orange; fluorine, yellow. XBs are dotted black lines. Hydrogen atoms are omitted for clarity. CSD Refcodes are reported.

among the most electronegative elements in the periodic table, and their ability to function as electrophilic species appeared quite strange and counterintuitive. A decisive contribution to the stereoelectronic understanding of the XB was given by computational studies on the distribution of the electron density in halogen atoms which began to appear in the early 1990s. The studies by P. Politzer and J. S. Murray were particularly significant as they demonstrated the anisotropic charge distribution on halogen atoms forming one covalent bond[89−91] and paved the way to the definition of the "σ-hole": a region of depleted and often positive electrostatic potential on the surface of halogen atoms.

All these findings and related rationalizations clearly demanded a unification process which was initiated by some of us with the paper entitled "Halogen Bonding: A Paradigm in Supramolecular Chemistry".[10] This paper showed how the electrophilic behavior of halogen atoms is a general phenomenon impacting "all the fields where design and manipulation of aggregation processes play a key role". Soon after we published a review paper in *Accounts of Chemical Research*,[92] highlighting the main and common features of adducts formed when dihalogens, halocarbons, or other halogenated derivatives attractively interact with lone-pair-possessing atoms, π-systems, or anions and afford adducts in the gas, liquid, or solid phase.

This unification process boosted the interest of the scientific community on the topic. Thanks to the strength of the interaction (section 2) and its intrinsic tunability resulting from the possibility to span the four halogen atoms as electron density acceptor sites, in recent years the number of papers on XB has been growing very rapidly, and the interaction has quickly evolved from a scientific curiosity to one of the routinely used tools to direct and control molecular assembly phenomena (Figure 5).[93]

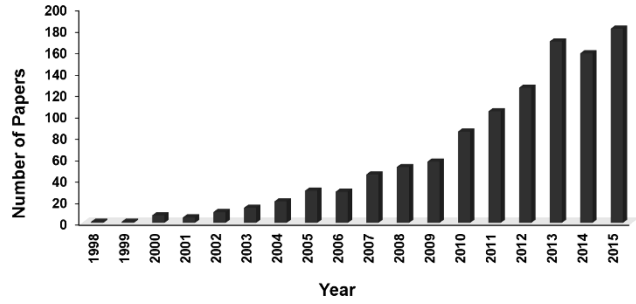

Figure 5. Number of papers per year having "halogen bonding" in the title and/or abstract (source SciFinder, search performed in November 2015).

A symposium devoted to the XB was organized in the frame of the 238th National Meeting of the American Chemical Society (Washington, DC, Aug 16, 2009), and had the seminal role to allow for the emerging consensus on some features of the interaction to be acknowledged. This consensus was further tuned in the kick-off event of the IUPAC project mentioned above (Sigüenza, Spain, Aug 20−21, 2011). At the end point of a 200 year long process, the IUPAC definition of the XB[9] finally registered the agreement reached by the scientific community on self-assembly and recognition processes controlled by electrophilic halogens, a topic that is nowadays well-established, understood, and used.

DOI: 10.1021/acs.chemrev.5b00484
Chem. Rev. 2016, 116, 2478−2601

1.2. Definition of the Halogen Bond

In the two centuries of research on phenomena where halogen atoms function as electrophilic sites, a remarkably wide variety of terms were coined to describe this type of behavior, thus pointing out the struggle to understand the phenomenon. Already in 1968 Bent[64] reported a list of 20 descriptive phrases used during the "first century" of the XB: "Electron clutching", 'saturation of residual affinities', "bumps-in hollow", "pairs-in-pocket", "points-in-holes", "locks-in-keys", "exaltation of valency", "donor−acceptor interactions", "charge-transfer interactions", and "filling of antibonding orbitals" are just some of the proposed names. Some of them are quite imaginative and imply that intermolecular interactions can be described in terms of properties of the starting molecules, i.e., "bumps-in hollow" or "pairs-in-pocket", while others aim at emphasizing different aspects of the intermolecular interaction, i.e., the saturation of bonding potential and the directional character, the creation of formal charges and expanded octets, or the fact that the increased nucleus−electron attraction is the driving force behind the intermolecular interaction. In an attempt to highlight the differences with respect to the hydrogen bond (HB), the term "anti-hydrogen bond" has also been used by W. Klemperer and co-workers[94] while considering the intermolecular interaction in the F−Cl···F−H complex, while G. R. Desiraju and T. Steiner[95] and I. Alkorta et al.[96] had used the term "inverse hydrogen bonding" referring to the intermolecular interaction occurring between hydrides and covalently bonded halogen atoms.

It is difficult to establish exactly when the term *halogen bond* was first proposed for interactions formed by electrophilic halogens and even more difficult to give an exact date for when the concept was developed and accepted. The concept began to emerge in the middle of the 20th century when the XB began to be identified as the cause of a well-defined and relatively homogeneous set of phenomena. In 1961 R. Zingaro and R. Hedges,[97] while describing the complexes formed in solution by halogens and interhalogens with phosphine oxides and sulfides, were probably the first to use the term *halogen bond* to describe interactions were halogens act as electrophilic species, in analogy to the behavior of hydrogen in the HB. In 1976 D. E. Martire et al. used the term to describe adducts formed in the gas phase by haloforms with ethers and amines.[98] However, it was the review of J.-M. Dumas, M. Gomel, and M. Guerin in 1983[66] that first separated results obtained by using several experimental techniques in the gas, liquid, and solid phases from other domains (e.g., other electron donor−acceptor interactions) and organized them under the term *halogen bond*. The name began to be used regularly after the *concept* paper by P. Metrangolo and G. Resnati[92] afforded general heuristic principles to correlate the structure of the XB donor and acceptor sites and the strength of the resulting interaction. An exponential growth of the interest of the scientific community has resulted in the past 15 years or so (Figure 5). The terms halogen bond and halogen bonding are used interchangeably, both terms having XB as an acronym.

In 2006 R. Glaser et al.[99] suggested to use the term halogen bond to designate any interaction involving halogen atoms, regardless of whether they act as electrophiles or nucleophiles. Without a general and univocal criterion for assessing if an interaction is a halogen bond, confusion may arise, as in the case when halogens interact with positive hydrogen atoms through the belt of higher electron density on their electrostatic potential surface. Clearly these interactions are and have to be named hydrogen bonds,[4] and cannot be confused with halogen bonds; otherwise the wrong electronic and geometric information is delivered. The IUPAC project 2009-032-1-100 was started in 2009 with the task to give a unified conceptual frame to interactions involving halogens as electrophilic species and to finally classify them in an unequivocal way.[8] The definition of the halogen bond reported in the previous section was the IUPAC recommendation proposed in 2013 at the end of the project.[9] According to this definition, a typical XB is denoted as

$$R{-}X\cdots Y \quad (1)$$

with the three dots representing the bond. R−X is the XB donor, and X is a halogen atom covalently bound to the R group and having an electrophilic region, or a potentially electrophilic region, on its electrostatic potential surface. It may happen that X is covalently bound to more than one group. In such cases the halogen may also form more than one halogen bond (Figure 6). Y is the XB acceptor (donor of electron density) and can be an anion or a neutral species possessing at least one nucleophilic region, e.g., a lone-pair-possessing atom or π-system. This IUPAC definition has been framed as simply and comprehensively as possible to account for all the cases wherein there is evidence of bond formation involving a nucleophile and a positive region on a halogen atom X from a molecule or molecular fragment R−X.

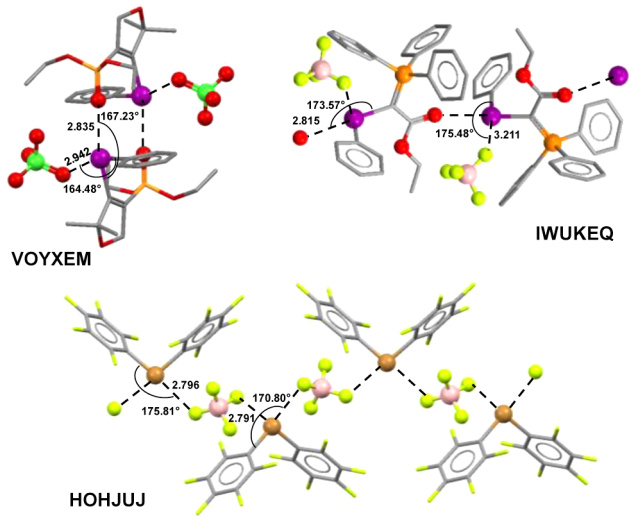

Figure 6. Short and directional XBs existing in halonium salts. Phenyl[2,2-dimethyl-4-(diethylphosphono)-2,5-dihydro-3-furyl]-iodonium perchlorate (VOYXEM[108]): one oxygen of the phosphonate residue and one oxygen of the perchlorate anion work as XB acceptors. [2-Ethoxy-2-oxo-1-(triphenyl-λ^5-phosphanylidene)ethyl]-phenyliodonium tetrafluoroborate (IWUKEQ[109]): the carbonyl oxygen of the carbethoxy residue and a fluorine atom of the fluoroborate anion work as XB acceptors. Bis(pentafluorophenyl)bromonium tetrafluoroborate (HOHJUJ[110]): BF_4^- works as a bidentate XB acceptor as the XB donor ability of Br is increased by strong electron-withdrawing residues. Hydrogen atoms have been omitted, XBs are dashed lines, and the numbers are the C−X···nucleophile angles (deg) and lengths of the halogen bonds (Å). Color code: carbon, gray; oxygen, red; iodine, purple; chlorine, light green; phosphorus, orange; fluorine, yellow; boron, pink. XBs are dotted black lines. Hydrogen atoms are omitted for clarity. CSD Refcodes are reported.

DOI: 10.1021/acs.chemrev.5b00484
Chem. Rev. 2016, 116, 2478−2601

Iodine, bromine, chlorine, and in some circumstances also fluorine can act as XB donors. Occasionally the terms fluorine bond,[100−102] chlorine bond,[103,104] bromine bond,[105] and iodine bond[106,107] have appeared in the literature to designate the specific interactions involving one of the four halogen atoms as an electrophilic site. Clearly, these terms address subsets of the most general set of interactions named halogen bonds. An advantage of the term XB, with respect to the aforementioned subsets, is that it gives the instruments to make a direct and meaningful comparison among the behaviors of the four halogens.

With respect to the different expressions suggested over the years to designate interactions formed by electrophilic halogens, the term halogen bond presents the advantage to declare immediately the most characteristic and general aspect of the interaction, namely, that it involves halogen atoms. A possible further advantage of this term is that it recalls immediately the alliterating term hydrogen bond, and by analogy, halogens are surmised to work as electrophiles as the hydrogen atoms do in the hydrogen bond. The main similarity for the two interactions is the role of the positive site (electron density acceptor, Lewis acid, electrophile) played by the halogen and hydrogen atoms, respectively; the inherent difference is that atoms of the XVII and I groups are involved.

1.3. Pivotal Role of the Halogen Bond in Rationalizing Other Interactions

The mindset developed in relation to XB studies favored the rationalization of the attractive interactions that elements of groups XIV−XVI form with nucleophiles after a general framework. In this section it will be described how the anisotropic distribution of the electron density around covalently bonded atoms is a general phenomenon and the presence of positive σ-holes on the extensions of single covalent bonds is commonplace and frequently results in attractive interactions with incoming nucleophiles.[111−119] It will also be described how this rationalization was the basis for the development of a fairly comprehensive nomenclature of intermolecular interactions, which helped to clarify the intrinsic and extrinsic relationships between names and concepts.

Many elements when involved in the formation of covalent bond(s) show a strong anisotropicity of their electrostatic potential surface. Areas of lower electron density, often positive, coexist with areas of higher electron density, often negative. This anisotropic charge distribution results in an amphoteric behavior, which is a common property for many elements, rather than an exception. For instance, it has been known since the end of the 1960s that chalcogen atoms (mainly S and Se) can form highly directional short contacts with both nucleophiles and electrophiles, the former entering preferentially on the elongations of the covalent bonds[120−123] involving the chalcogen atoms, and the latter lateral to the covalent bonds, above and below the plane that the chalcogen forms with the covalently bonded atoms. A survey of the Protein Data Bank (PDB) revealed that S···O interactions are common in proteins and they can play important roles in their functions, stability, and folding.[124] For instance, F. T. Burling and B. M. Goldstein[125] demonstrated that S···O and Se···O interactions stabilize the final molecular conformations of some thiazole and selenazole nucleosides possessing antitumor activity (Figure 7), and affect their biological activity and their binding to a target enzyme.

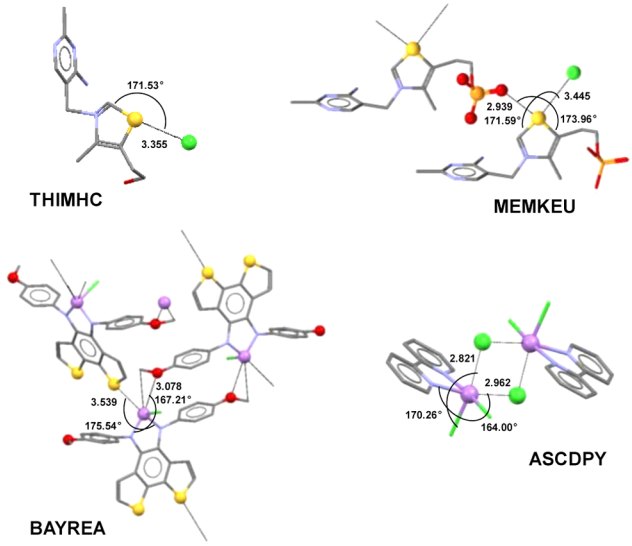

Figure 7. Selected examples of σ-hole interactions. Short and directional chalcogen bonds formed in the solid state by the sulfur atom of two derivatives of thiamin, a vitamin of the B complex, on the elongation of one (THIMHC)[137] or both (MEMKEU)[138] of its covalent bonds. Pnicogen bonds formed by arsenic atoms in 2-chloro-1,3-bis(4-methoxyphenyl)-2,3-dihydro-1*H*-bisthieno[3,2-*e*:2′,3′-*g*]-[1,3,2]benzodiazarsole (BAYREA)[139] and arsenic trichloride dipyridyl (ASCDPY).[140] Hydrogen atoms are omitted for clarity, chalcogen and pnicogen bonds are dotted lines, and the numbers are the angles (deg) and lengths of the chalcogen and pnicogen bonds (Å). Color code: carbon, gray; nitrogen, blue; oxygen, red; chlorine, light green; sulfur, dark yellow; phosphorus, orange; arsenic, violet. CSD Refcodes are reported.

Examples of attractive intermolecular interactions wherein groups XV and XIV atoms get close to nucleophiles are also known. The ability of PF_3 to act as a Lewis acid has been known since 1991,[126] P···P[127] and P···N[128] interactions have been observed through structural analyses, and Si···N and Ge···N attractive interactions have been determined to be responsible for anomalous Si−O−N and Ge−O−N angles in some silane and germane derivatives.[129,130] Pnicogen···π interactions (Figure 7) have been found also in many biological systems where, for instance, they participate in the inhibition of Sb-based drugs used for leishmaniasis treatment.[131]

Recent theoretical investigations aimed at understanding the structural and electronic properties of elements of groups XIV−XVI, when interacting with incoming nucleophiles,[132] proved that the amphoteric behavior known for halogen atoms is not at all an exception, as it is paralleled by an analogous behavior of chalcogens, pnicogens, and tetrels. A theoretical basis was given for the attractive interactions that covalently bonded atoms of groups XVI,[120−125] XV,[133,134] and XIV[6,135,136] can form with nucleophiles, the strength of such interactions even being comparable to that of HBs.[132]

Atoms of groups XIV−XVI can have as many σ-holes as the covalent bonds they form: There can be two σ-holes on chalcogen atoms, three on atoms of group XV, and four on atoms of group XIV,[7,141,142] and if the atom is hypervalent, σ-holes can even be more numerous than in atoms with the typical valency of the group.[6,112] For example, the positive σ-holes on the electrostatic potential surfaces of sulfur, arsenic, and silicon in SCl_2,[143] $As(CN)_3$,[133] and $SiCl_4$[6] are shown as red areas in parts A, B, and C and D, respectively, of Figure 8. In SCl_2, two σ-holes are visible on the sulfur surface and are both

DOI: 10.1021/acs.chemrev.5b00484
Chem. Rev. 2016, 116, 2478−2601

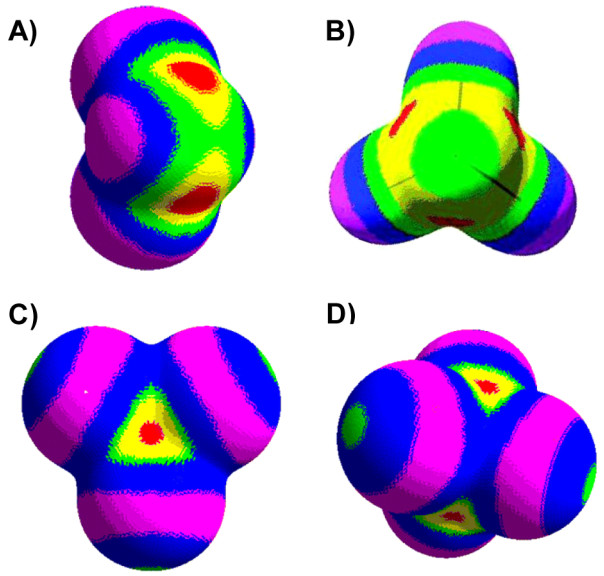

Figure 8. Calculated B3PW91/6-31G** electrostatic potentials of SCl_2[143] (A), $As(CN)_3$[133] (B), and $SiCl_4$[6] (C, D) computed on the 0.001 electron/bohr^3 contour of the electronic density. (A) SCl_2: the sulfur is in the foreground, and the chlorines are at the back. Color ranges (kcal/mol): purple, negative; blue, between 0 and 8; green, between 8 and 15; yellow, between 15 and 20; red, more positive than 20. (B) $As(CN)_3$: the arsenic is in the middle, toward the viewer. Color ranges (kcal/mol): red, greater than 45; yellow, between 30 and 45; green, between 15 and 30; blue, between 0 and 15; purple, less than 0 (negative). (C, D) $SiCl_4$: electron density views of different orientations of the molecule. In the (C) view three chlorine atoms are toward the viewer, and the σ-hole, due to the Cl−Si bond to the fourth chlorine, is in red in the center and on the extension of that Cl−Si bond. In the (D) view two chlorine atoms are toward the viewer. Color ranges (kcal/mol): purple, negative; blue, between 0 and 8; green, between 8 and 11; yellow, between 11 and 18; red, more positive than 18. Panel A adapted with permission from ref 143. Copyright 2008 Springer. Panel B adapted with permission from ref 133. Copyright 2007 John Wiley and Sons. Panels C and D adapted with permission from ref 6. Copyright 2008 Springer.

along the extension of a Cl−S bond, the Cl−S−($V_{S,max}$) angles being 180° ($V_{S,max}$ is the most positive surface electrostatic potential). $V_{S,max}$ on the sulfur surface has been calculated to be 25.1 kcal/mol, while the most negative surface electrostatic potential, $V_{S,min}$, is on the sides of the sulfur ($V_{S,min}$ = −5.9 kcal/mol). In $As(CN)_3$, the entire arsenic surface is positive due to the high electron-withdrawing ability of the CN groups, but the potential is most positive (51.4 kcal/mol) at three areas located approximately on the extensions of the NC−As bonds (in red in Figure 8B). Silicon in $SiCl_4$ has four σ-holes on the extension of each Cl−Si with a $V_{S,max}$ of 20.2 kcal/mol.

Similar to that in halogens, the magnitude of the σ-hole in elements of groups XIV−XVI is affected by the atom polarizability and electronegativity: The more polarizable and less electronegative the element, the more positive the σ-holes. The magnitude of the σ-hole in elements of any such groups thus increases when moving from the lighter to the heavier atoms. Similar to what has already been observed for fluorine, attractive interactions due to the entrance of nucleophiles in the σ-hole are therefore the least common for carbon, nitrogen, and oxygen, since atoms in the first period of the periodic table are the most electronegative and the least polarizable and tend to have relatively weakly positive (typically negative) σ-holes. As in the group XVII elements, the size of the σ-holes in elements of groups XIV−XVI increases, and their potential becomes more positive when electron-withdrawing substituents are present on the molecules; for instance, it has been calculated that when fluorine is the substituent, positive σ-holes typically develop for carbon,[6] nitrogen,[133] and oxygen.[111]

Moreover, in asymmetric molecules where the elements of groups XIV−XVI bear substituents with different electron-attracting abilities, σ-holes with different $V_{S,max}$ values are formed, and their magnitude depends on the nature of the substituents. In Figure 9 the electrostatic potential calculated at

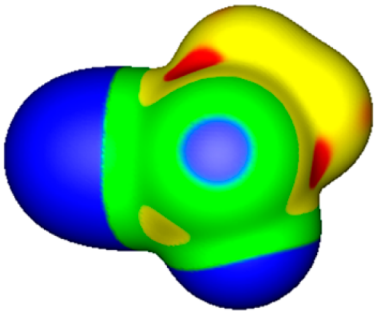

Figure 9. Electrostatic potential calculated at the M06-2X/aug-cc-pVTZ computational level on the 0.001 au molecular surface of $PF(CH_3)(CN)$. Phosphorus is in the middle facing the viewer, the cyano group is to the left, the methyl group is to the top right, and fluorine is to the bottom right. Color ranges: red, greater than 1.26 V; yellow, from 1.26 to 0.65 V; green, from 0.65 to 0 V; blue, less than 0 V (negative). Reprinted with permission from ref 144. Copyright 2015 Springer.

the 0.001 au molecular surface for $PF(CH_3)(CN)$ is reported. The phosphorus surface presents three σ-holes and, consistent with the different electronegativities of the CN, F, and CH_3 substituents, the most positive electrostatic potentials (red areas) are on the extensions of the P−CN (1.52 V) and P−F (1.41 V) bonds, while the σ-hole on the extension of the P−CH_3 bond (yellow area on the bottom left) is less positive (0.95 V).

While the surface electrostatic potential of group XV or group XVI elements can have both positive and negative regions, if the element is bonded to highly electron-withdrawing partners, its surface electrostatic potential may be completely positive (e.g., $As(CN)_3$ in Figure 8). On the other end, if the group XV or group XVII atoms are more electronegative than the bonded partners, then the surface electrostatic potential will be entirely negative and the σ-hole, the area with the lowest electrostatic potential, will be negative, although less negative than its surroundings. This is the case for fluorine in H_3C−F and nitrogen in $(H_3C)_3N$: Their σ-holes are negative, and they are not expected to behave as electrophiles in interactions. The opposite situation typically occurs with tetravalent group XIV atoms, which have entirely positive surfaces in nearly all cases, regardless of the bonding partners.[7] Nevertheless, interactions do not occur in some cases as σ-holes in the elements of this group are less accessible to nucleophiles than in group XVII elements due to the greater steric hindrance.

As outlined above, σ-hole features in elements of groups XIV−XVII present numerous and important similarities, but a few differences have also been observed. For instance, the origin of σ-holes on halogen atoms has been explained by T.

DOI: 10.1021/acs.chemrev.5b00484
Chem. Rev. 2016, 116, 2478−2601

Clark et al.[145] as the results of an electron deficiency arising in the outer lobe of a half-filled p orbital involved in a covalent bond. It was initially believed that the more positive σ-holes originate with a pure p orbital, and the minimal mixing of s character into the p orbital was considered as a fundamental condition to have a strong σ-hole. This interpretation can be easily and successfully extended also to atoms of groups XV and XVI; however, it is not really satisfactory when applied to group XIV atoms, which are essentially sp^3-hybridized and yet in some cases have been calculated to have very high σ-hole $V_{S,max}$ values.[6] Moreover, Clark et al.[112] studied two hypervalent sulfur derivatives, $(H_3C)_2SO$ and $(H_3C)_2SO_2$, and found, respectively, one σ-hole with $V_{S,max}$ = 26.2 kcal/mol and two σ-holes with $V_{S,max}$ = 30.2 kcal/mol on the sulfur surface on the extensions of the O−S bonds. Natural bond orbital (NBO) analysis of these O−S bonds revealed that they are single, with both electrons being provided by the sulfur, and the sulfur orbitals involved in these bonds show a significant s character. The same has been found for the O−P bond in Cl_3PO, where a positive σ-hole is present on the phosphorus surface on the elongation of the O−P bond, although the phosphorus orbital involved in the O−P bond is doubly occupied and shows more than 50% s character.[6] These findings led to an expansion of the σ-hole concept:[6] Although the high p character of bonding orbitals remains a fundamental condition, a sizable s contribution is not precluded, and it is possible for the bonding orbital to be doubly occupied and involved in a coordinate covalent bond.

The understanting of the interactions given by halogen derivatives had a seminal role in the rationalization of the interactions given by elements of groups XIV−XVI after a general and unified mode. Due to the numerous and significant analogies, and the few and minor differences, between the attractive interactions that nucleophiles form with elements of groups XIV−XVI and with elements of group XVII, the mindset developed in relation to the XB paved the way to the development of a systematic and consistent terminology for understanding and naming interactions wherein elements of groups XIV−XVI are the electrophilic sites. Specifically, the names chalcogen bond,[116,146] pnicogen (or pnictogen) bond,[134,147−149] and tetrel bond[135,150−153] have been proposed, and widely accepted, to designate interactions where elements of groups XVI, XV, and XIV function as the electrophile, respectively. The XB thus inspired a general terminology for all interactions wherein it is possible to identify an element, or moiety, working as the electrophile.[154] The resulting classification of interactions links the name of attractive interactions to the group of the element at the electrophilic site. This classification offers the advantage that, paralleling the classification of elements in the periodic table, periodicities in noncovalent interactions can be easily anticipated or identified.

1.4. General Aspects of the Interaction

Directionality, strength tunability, hydrophobicity, and donor atom dimensions are unique features of the XB which allowed the interaction to develop as a routinely used tool in the design and preparation of self-assembled systems. These features will be the focus of this section, and some other general characteristics of the interaction will be discussed.

At a first approximation, atoms in molecules are frequently considered as interpenetrating spheres, but the distribution of the electron density around the nucleus is not spherical, and the XB is a straight consequence of this. The halogen atom anisotropy in molecules has been noted since early times; for instance, solid Cl_2 was reported in 1952 to assume a layered structure[155] which differed from the close-packed structure of other diatomic molecules such as N_2 and H_2. This structure is determined by short contacts between the nonbonded charge concentration of one Cl atom and the charge depletion of another Cl atom (Figure 10).[156]

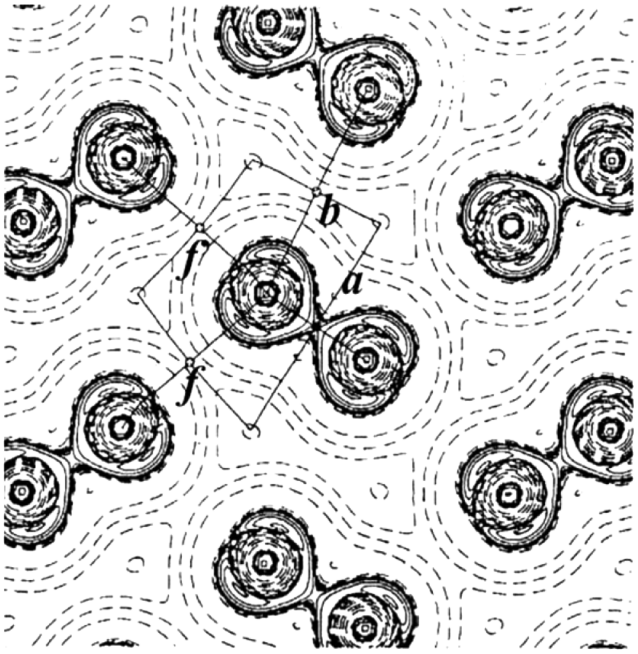

Figure 10. Laplacian distribution for the (100) plane of solid chlorine, solid contours denoting negative values for the gradient of electron density. Reprinted with permission from ref 156. Copyright 1995 International Union of Crystallography.

In 1963 T. Sakurai et al.[157] noted that R−X···X−R contacts (X = halogen atom) occur preferentially according to two different geometries, which, years later, G. R. Desiraju and R. Parthasarathy[158] classified as type I (symmetrical interactions where $\theta_1 = \theta_2$) and type II (bent interactions where $\theta_1 \approx 180°$ and $\theta_2 \approx 90°$) (Figures 11 and 12). This classification is still

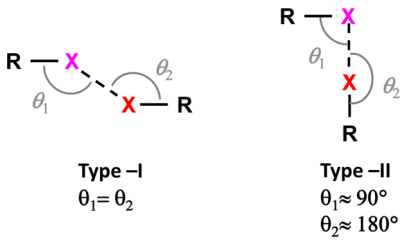

Figure 11. Structural scheme for type I (left) and type II (right) halogen···halogen short contacts. X = halogen atom, and R = C, N, O, halogen atom, etc. Type II contacts are XBs.

used nowadays, and the type I contacts have been further subdivided into *trans* and *cis* systems[159] depending on the relative positions of the R groups covalently bound to X. There is a clear geometric and chemical distinction between type I and type II X···X interactions. Type I interactions are geometry-based contacts that arise from close-packing requirements, are found for all halogens, and are not XBs according to the IUPAC definition. Type II interactions arise from the pairing between the electrophilic area on one halogen atom and the

DOI: 10.1021/acs.chemrev.5b00484
Chem. Rev. 2016, 116, 2478−2601

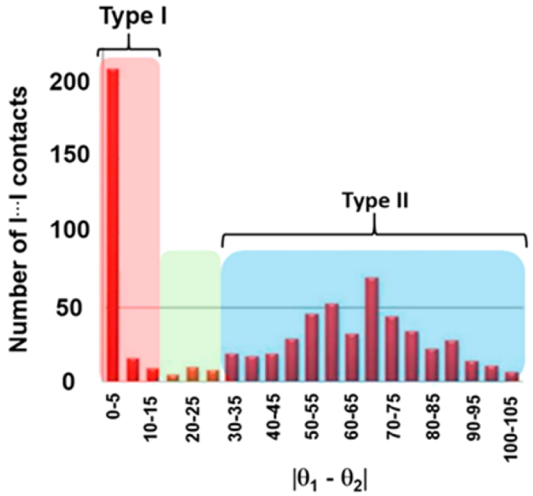

Figure 12. Histogram of I···I contacts and assignment of type I and type II geometries. Adapted from ref 160. Copyright 2014 American Chemical Society.

electrophilic area on the other and are true XBs.[4] Recently, Desiraju and co-workers[160] reanalyzed on a larger data set the occurrence of halogen···halogen (X_1···X_2) contacts in the solid state by a CSD[161] search. It was found that type II contacts are most favored in iodinated derivatives, less in brominated derivatives, and the least in chlorinated derivatives.

Analyses of the type I and type II I···I contacts in the CSD as a function of the interaction distance afforded a further outcome. At distances shorter than the van der Waals contacts, the type I interactions were more frequent at the shortest distances, while XB were more frequent closer to the van der Waals limit. This behavior has been explained as a direct consequence of the electrostatic nature of the XB, which allowed I···I contacts to be formed at longer distances, while type I contacts, being dispersive forces, operated preferentially at shorter distances. The authors also found that unsymmetrical X1···X2 (X1 ≠ X2) short contacts always had the geometry of XBs.

Depending on the interacting partners, XB covers a wide energy range spanning from 10 kJ/mol for weak XBs (e.g., N···Cl contacts)[162] to 150 kJ/mol (e.g., the very strong interaction observed in the I_2···I^- adduct).[163] The remarkable strength of some XBs allows the interaction to often prevail over other weak noncovalent interactions (e.g., $\pi-\pi$ stacking, dipole–dipole interactions, and hydrophobic forces).[164] Alternatively, during the formation of supramolecular systems, XB can cooperate with or surrender to HB, and other interactions when of comparable or lower strength, respectively, and nice examples of hierarchical self-assembly processes have been reported.[80,165,166]

1.4.1. Directionality. The XB is a particularly directional interaction,[167] more directional than the HB. This peculiar feature is a consequence of the localization of the σ-hole exactly on the elongation of the covalent bond(s) the halogen atom is involved in.[145] Both theoretical[26] and experimental[168] studies have shown that, in monovalent halogen atoms, the effective atomic radius along the extended R–X bond axis (R = C, N, halogen atom, etc.) is smaller than in the direction perpendicular to this axis. This smaller radius, also named polar flattering, corresponds to the region of depleted electron density named the σ-hole. The great directionality of the XB is due to the fact that on interaction formation the nucleophile enters the halogen atom σ-hole which is narrowly confined on the elongation of the R–X covalent bond axis, and the R–X···Y angle between the covalent and noncovalent bonds around the halogen is approximately 180°.[26,169] Figure 13 shows the CSD

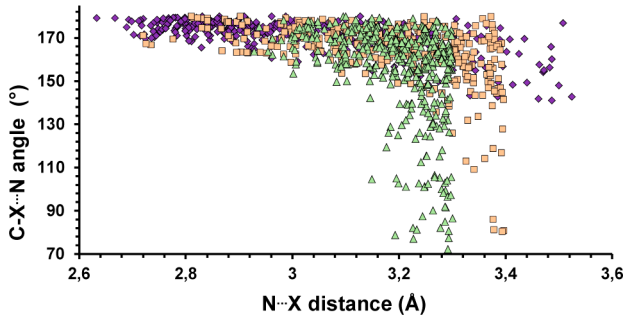

Figure 13. Scatterplot derived from a CSD search reporting the C–X···N angle (deg) versus the X···N distance (Å) for crystal structures containing X···N contacts. Color code: blue rhombuses, I···N contacts; pink squares, Br···N contacts; green triangles, Cl···N contacts. Only error-free and nonpolymeric structures containing single-bonded I, Br, or Cl atoms and showing no disorder with $R < 0.05$ are considered.

(version 5.35) scatterplots of intermolecular C–X···N interaction versus X···N distance (X = I, Br, and Cl). Clearly, short and strong XBs are more directional that the long and weak ones, and by reducing the polarizability of the XB donor, the linearity slightly drops (mean values for the C–X···N angle are 171.4° for I, 164.1° for Br, and 154.6° for Cl). This trend is general and has also been observed when XB acceptor sites other than nitrogen are used.

As far as the interaction directionality from the XB acceptor site is concerned, it is interesting to note that when the interaction involves heteroatoms Y possessing n-pairs, the XB is preferentially along the axis of the donated n-pair on Y. For instance, in halogen-bonded adducts where pyridines are the XB acceptors, the C–X group is almost coplanar with the pyridyl ring, and the two C–N···X angles are close to 120°.[170,171] The same geometrical features are observed for other nitrogen heteroaromatics such as pyrazine or quinoline.[172−174] When carbonyl groups act as XB acceptors, the oxygen may function as both a monodentate[175] and a bidentate[176] site, and the XB donor(s) are pinned in a trigonal planar geometry. Sulfonyl[177,178] and phosphoryl[179] groups behave similarly to carbonyl moieties, and also imines[180] form XBs along the respective n-pair axis. XBs around ethers,[56,181] thioethers,[182,183] and amines[184,185] usually adopt a tetrahedral arrangement with preferential axial directions for the XBs around hexacyclic amines[186] and equatorial directions for hexacyclic thioethers[64] (Figure 14).

When the XB acceptor is an isolated π-system, the axis of the R–X covalent bond (R = halogen,[24,187] carbon;[188,189] X = Cl, Br, I) lies, in the equilibrium geometry, approximately along the symmetry axis of the π-bonding orbital of the XB acceptor (Figure 15). When two conjugated and equivalent π bonds are present on the electron donor system, such as in 1,3-butadiene, R–X lies perpendicular to the plane containing the four carbon atoms of the double bonds and is localized at one π-bonding orbital site with no evidence of tunneling. Adducts involving aromatic π donors (e.g., benzene) exhibit a C_{6v}-symmetric-top-type arrangement, the intersection between the elongation of the R–X covalent bond and the plane of the benzene ring being closer to the carbon atom than to the middle point of the π-

DOI: 10.1021/acs.chemrev.5b00484
Chem. Rev. 2016, 116, 2478−2601

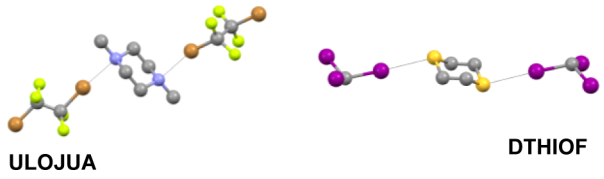

Figure 14. XBs around hexacyclic amines and thioethers feature axial (left) and equatorial (right) directions, respectively. XBs are dotted black lines. Color code: carbon, gray; nitrogen, blue; iodine, purple; bromine, light brown; sulfur, dark yellow. Hydrogen atoms are omitted for clarity. CSD Refcodes are reported. In ULOJUA the disorder on 1,2-dibromotetrafluoroethane is omitted.

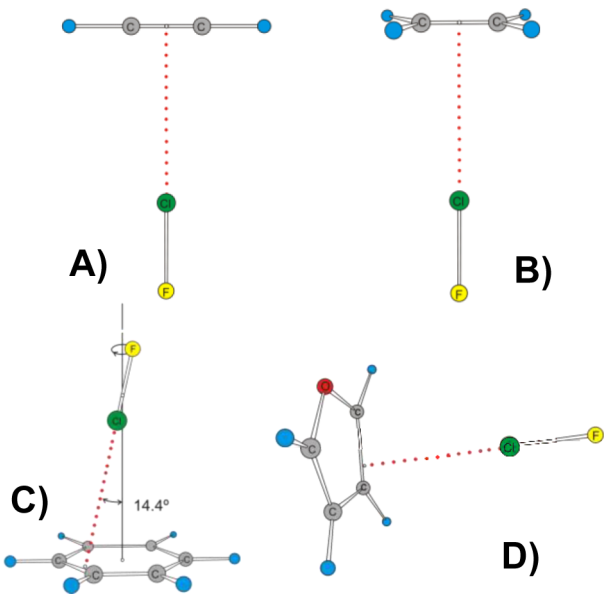

Figure 15. Angular geometries of complexes formed by FCl with simple π-electron donors (A) FCl···ethyne and (B) FCl···ethene and with aromatic π-electron donors (C) FCl···benzene and (D) FCl···furan.

bonding orbital. When both n-pairs and aromatic π-pairs are present in the XB acceptor, n-pairs are preferentially involved in XB formation. Furan and thiophene are exceptions where the π-bonding orbitals prevail over the n-pairs.

1.4.2. Tunability. As already mentioned in section 1.1, the XB donor ability changes in the order I > Br > Cl > F, and this scale can be explained through the positive character of the corresponding σ-holes, which increases with the polarizability, and decreases with the electronegativity, of the halogen atom (Figures 16 and 17).[190,191]

A nice example of this trend can be observed in the 3-X-cyanoacetylene series (X = I, Br, Cl): All three compounds work as self-complementary modules, and the N···X distance is consistent with the scale reported above, being 2.932, 2.978, and 2.984 Å in the iodo, bromo, and chloro derivatives, respectively.[192,193] The same tendency is exemplified by the 4-halobenzonitrile series, the iodo derivative displaying a shorter XB distance than the bromo compound, while the chloro and fluoro analogues do not show XB contacts.[194]

The fluorine atom is the poorest XB donor; however, a positive σ-hole is found when fluorine is bound to another fluorine atom and sometimes when it is linked to O, N, C, or other atoms bearing particularly strong electron-withdrawing substituents.[29,195] $CF_3C(O)OF$, $(CF_3SO_2)_2NF$, and CF_3SO_2-

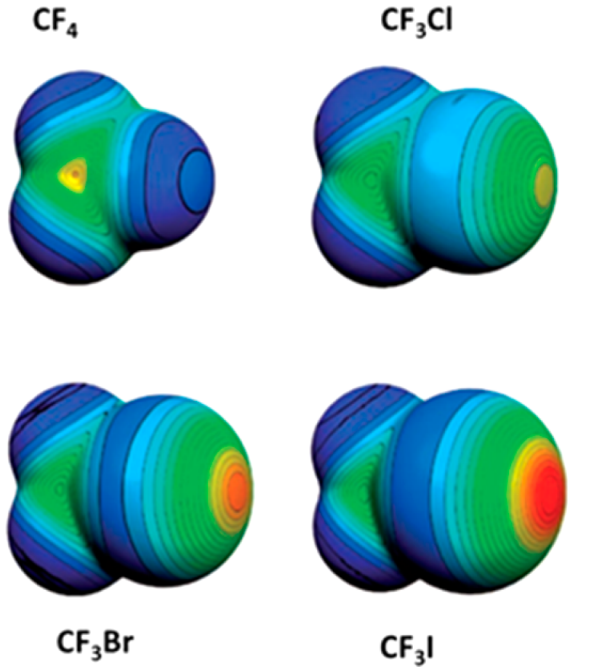

Figure 16. Molecular electrostatic potential at the isodensity surface with 0.001 au for CF_4, CF_3Cl, CF_3Br, and CF_3I. Color ranges: red, greater than 27 kcal/mol; yellow, between 20 and 14 kcal/mol; green, between 12 and 6 kcal/mol; blue, negative. Adapted with permission from ref 145. Copyright 2007 Springer.

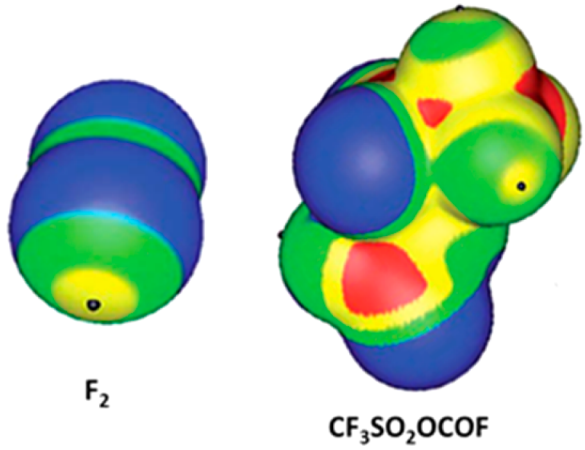

Figure 17. Molecular electrostatic potential at the isodensity surface with 0.001 au of F_2 and CF_3SO_2OCOF (the CF_3 group is on top). Color ranges: red, greater than 20 kcal/mol; yellow, between 20 and 9 kcal/mol; green, between 9 and 0 kcal/mol; blue, negative. The black hemispheres denote the positions of the most positive potentials associated with the fluorine atoms. Reprinted with permission from ref 195. Copyright 2011 Royal Society of Chemistry.

OCOF are prototypical cases where fluorine bears a positive σ-hole (Figure 17).

Importantly, the presence of a region of charge depletion on fluorine atoms was experimentally observed by electron density studies of the homometric crystal of pentafluorophenyl-2,2′-bis-thiazole, among others.[31] Two fluorine atoms are involved in XB contacts. One fluorine interacts with the lone pair of the sulfur atom in the thiazole ring, while the other fluorine atom acts as the XB donor interacting with the negative belt of a closeby fluorine, leading to an F···F XB.

DOI: 10.1021/acs.chemrev.5b00484
Chem. Rev. 2016, 116, 2478−2601

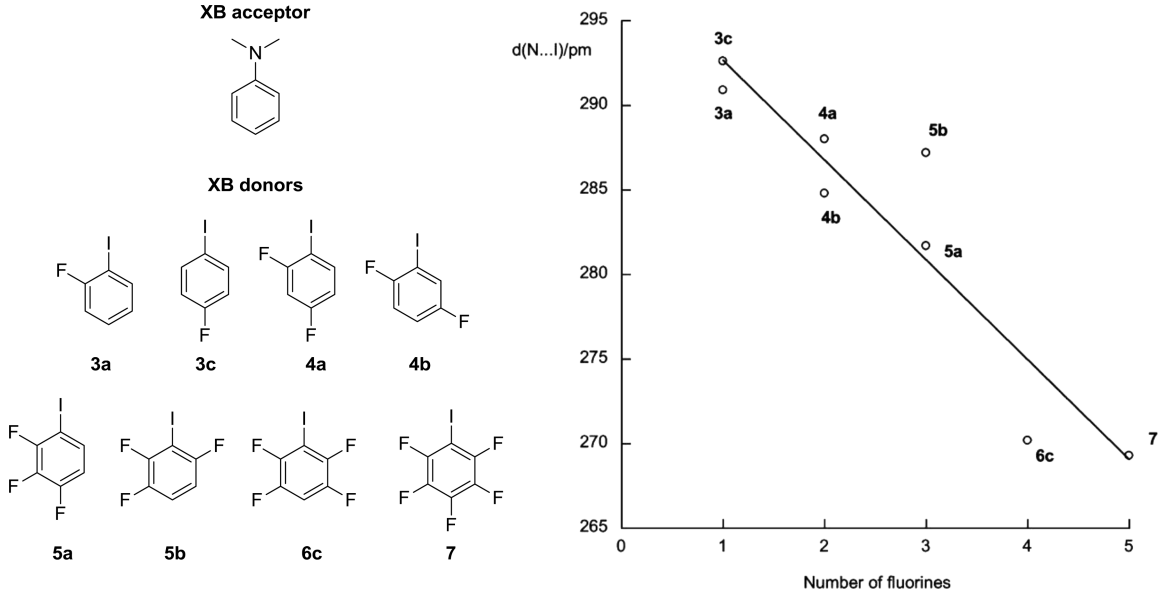

Figure 18. XB donors and XB acceptor and plot of the N···I separation in the corresponding adducts as a function of the number of fluorine atoms on the donor. N···I distances are reported in picometers. Adapted from ref 202. Copyright 2009 American Chemical Society.

The XB donor ability of a given compound can thus be easily tuned by choosing the most convenient halogen atom as the donor site. A quite large range of interaction energies can be spanned by single-atom mutation on the XB donor tecton, namely, by changing an iodine atom into a bromine atom, or a chlorine atom; usually fluorine introduction precludes the XB from working as the driving force of the self-assembly process.

An alternative approach to tune the σ-hole magnitude, i.e., the XB strength, consists in modifying the hybridization of the carbon atom bound to the XB donor site. The greater the s component in an sp-hybridized carbon, the greater its electron-withdrawing ability, and many experimental observations and theoretical studies confirm that, for organic XB donors where no other structural differences are present, the strength order is $C(sp)-X > C(sp^2)-X > C(sp^3)-X$.[25] Haloalkynes, such as diiodoacetylene and (bromoethynyl)- or (iodoethynyl)-benzene, are very good XB donors.[196,197] One example of the sp-hybridization-based trend is observed in the cocrystallization of diiodoacetylene and tetraiodoethylene with 1,4-dioxane. When interacting, these molecules give rise to infinite and halogen-bonded chains where the XB donors and acceptors alternate, the I···O interaction length being shortest in the diiodoacetylene system, 2.668 Å, versus 3.004 Å in the tetraiodoethylene cocrystal.[198,199] The same trend is seen when 1,4-diselenane interacts with diiodoacetylene[182] and iodoform;[200] the I···Se distances are 3.336 and 3.464 Å, respectively.

In general, the strength of the XB can be tuned by any compositional or structural modification affecting the electron-withdrawing ability of the atom(s), or moieties, covalently bound to a given halogen atom. For instance, the presence of strong electron-withdrawing moieties strengthens the σ-hole on the XB donor atom, leading to strong XBs, and the closer the electron-withdrawing moiety is to the halogen atom, the greater the effect. Haloarenes have been routinely used in XB-based crystal engineering and, in general, are good XB donors.[201] The partial or full substitution of hydrogen atoms with fluorine atoms on the aromatic ring is a well-established strategy to increase the size and positive potential of the σ-hole on the halogen atom, but the same occurs when a cyano or a nitro substitutes for the hydrogen. For instance, it has been shown how increasing the number of fluorine substituents onto a iodobenzene ring results in a uniform decrease in the N···I bond distance (Figure 18).[202] A similar effect was described earlier by P. Metrangolo and G. Resnati et al.[203] and by W. T. Pennington et al.,[76] who compared the structures and spectral properties of the three diiodobenzene isomers and corresponding tetrafluoro analogues when interacting with a variety of N acceptors. In all cases, the N···I bond distances were much shorter for the perfluorinated iodoarene.[76] This fluorine ability in tuning the XB strength is corroborated by several computational studies, which show very good correlation between the interaction energies, the positive electrostatic potentials on the halogens, and the fluorination degree.[204] It is also shown that aromatic fluorine substitutions affect the optimal geometries of the halogen-bonded complexes, often as the result of secondary interactions such as weak F···H or F···F type I interactions.[205]

Haloheteroarenes offer a further opportunity to modulate the XB. In some cases, in fact, the heteroarene moiety can be made positively charged, for instance, when a halopyridine is transformed into a halopyridinium derivative via protonation or alkylation. This converts the heterosystem into a strong electron-withdrawing group that enhances the XB donor ability of the halogen atom.[206,207] Similarly, the Lewis acidity of the halogen atom of monohaloalkanes is dramatically boosted by the perfluorination of the hydrocarbon chain[208] or when a positively charged residue is geminal to the halogen (as is the case for various iodomethyl onium salts, e.g., $Ph_3P^+-CH_2-I$), where the presence of the positive charge close to the halogen atom drastically increases its σ-hole and its XB donor ability.

In summary, the XB interaction strength can be tuned (I) by single-atom mutation, (II) by changing the sp hybridization on the carbon atom the XB donor is bound to, and (III) by modifying the electron-withdrawing ability of the moiety the XB donor is bound to.

An aspect related to tunability is the possibility to rank XB donors according to their effectiveness. This opportunity

DOI: 10.1021/acs.chemrev.5b00484
Chem. Rev. 2016, 116, 2478−2601

becomes important in XB-based supramolecular synthesis since the classification of the XB donor strength could help in anticipating the preferred binding patterns in a polydentate module, namely, in the development of general heuristic principles for hierarchical supramolecular syntheses. In principle, it may also allow for a multistep and sequential supramolecular synthesis where a simpler adduct self-assembled via a stronger interaction (e.g., metal coordination) is the building block for a successive self-assembly process driven by a weaker interaction. For instance, C. Aakeröy and some of us[209] recently tried to establish an XB donor ability ranking of various molecules by a combination of infrared spectroscopy data, structural characterizations by X-rays, and computational studies, namely, by calculating the molecular electrostatic potential surfaces. The halogen atom donor site, the sp hybridization on the carbon atom the XB donor is bound to, and the presence of fluorine atoms on the donor molecule were systematically varied to tune the XB strength (Figure 19). The

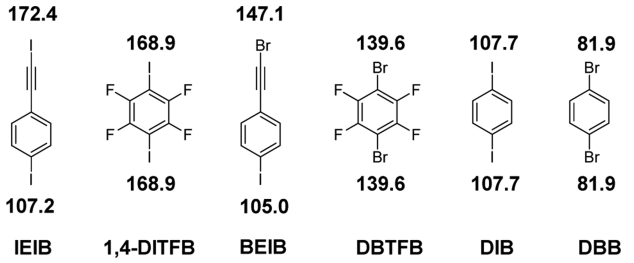

Figure 19. Chemical structures of C(sp)-bonded XB donors (IEIB and BEIB), activated C(sp^2)-bonded donors (1,4-DITFB and DBTFB), and nonactivated C(sp^2)-bonded donors (DIB and DBB) cocrystallized using a solvent-drop grinding methodology. The six XB donor molecules are reported in order of decreasing $V_{S,max}$ values (from left to right) associated with the most positive σ-hole on their halogen atoms. $V_{S,max}$ values are the numbers reported near the corresponding atom and are given in kilojoules per mole. Adapted with permission from ref 209. Copyright 2013 John Wiley and Sons.

preferential self-assembly of 21 XB acceptors with iodoethynyl donors, iodoperfluorocarbon donors, and iodophenyl donors or with analogous bromine derivatives was assessed by cocrystallizing the modules using solvent-drop grinding methodology. 1-(Iodoethynyl)-4-iodobenzene and 1,4-diiodotetrafluorobenzene were the best donors of the series and were found to have similar σ-hole magnitudes. The tendency of other XB donors to form cocrystals paralleled the electrostatic potential on the donor halogen atom.

The presence in the same molecular structure of two different XB donor sites complements the competitive cocrystal formation when an assessment of the relative XB donor abilities of the sites is pursued. For instance, in 1-(iodoethynyl)-4-iodobenzene the iodine bound to the sp-hybridized carbon proved to be a stronger donor than the iodine bound to the sp^2 carbon. The crystal structure of the cocrystal with 4-phenylpyridine (Cambridge Crystallographic Data Centre (CCDC) Refcode BISBIQ) showed the presence of a strong XB between the iodoethynyl moiety and the nitrogen atom. The second halogen atom on the molecule was, instead, involved in a type I I···I contact with an adjacent molecule. An analogous situation was observed in a cocrystal where the same XB donor was interacting with a benzimidazole derivative (BISBEM). In fact, the iodoethynyl iodine formed a short XB with the nitrogen atom, while the iodine on the sp^2 carbon atom was involved in an iodine···π interaction with the benzimidazole ring of another XB acceptor molecule. These two examples, among others presented in the same paper, demonstrated that the best donor–best acceptor pairing, well-known to occur in hydrogen-bonded systems,[210] also applies to halogen-bonded supramolecular systems (Figure 20).

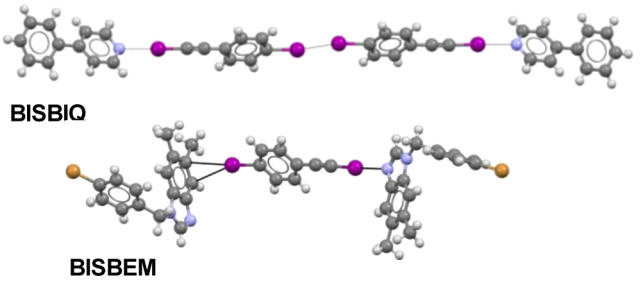

Figure 20. Ball-and-stick representation of the cocrystals of 1-(iodoethynyl)-4-iodobenzene with 4-phenylpyridine (BISBIQ) and (bromophenyl)benzimidazole (BISBEM). XBs, type I iodine···iodine contacts, and iodine···π interactions are represented as dotted black lines. Color code: carbon, gray; nitrogen, blue; iodine, purple; bromine, light brown; hydrogen, white. CSD Refcodes are reported.

Similarly, the relative XB acceptor ability of two different XB acceptor sites could be established when they are simultaneously present in the same molecular structure. On self-assembly of methyl isonicotinate with 1,4-DITFB, both the N and the O atoms of methyl isonicotinate interact with the iodine atoms, giving rise to I···N and I···O interactions. By varying the composition of the reaction mixture, the hierarchy between these interactions allows for the control of the composition and thus the structure of the supramolecular complex.[211]

1.4.3. Hydrophobicity. Halogen atoms are typically regarded as hydrophobic residues. In fact, a typical XB donor site (e.g., an I or Br atom) is remarkably less hydrophilic than a typical HB donor site (e.g., an OH or an NH group). This difference between the two donor sites brings about many consequences and many useful and complementary applications. For instance, absorption of a drug and its delivery to the target tissue tipically requires the compound to cross cell membranes, and halogen atoms are frequently introduced in a lead compound to increase its lipophilicity and its ability to pass through cell membranes. On the other hand, oral administration of a drug often requires the compound to have a fair water solubility, and the presence of $-OH$ and $-NH_2$ substituents may be helpful for this purpose.

XB can be considered as a hydrophobic analogue of HB as XB donor tectons and halogen-bonded adducts are, in nearly all cases, much more lipophilic than the structurally analogous HB donor tectons and corresponding hydrogen-bonded adducts. For instance, 1,2-diiodotetrafluoroethane and iodopentafluorobenzene are insoluble in water, while ethylene glycol is miscible with water in any ratio, and the phenol solubility is greater than 66 g/L. The thermodynamic aspects of the recognition events leading to either halogen-bonded or hydrogen-bonded adducts (e.g., solvation free energy, solvation shell, and solvophobic effects) are quite different, and the use of tailored and different procedures becomes pivotal if the formation of a given supramolecular complex is pursued. In relation to the topic of this review, it may be interesting to mention that both alcohols and iodoperfluoroalkanes effectively

DOI: 10.1021/acs.chemrev.5b00484
Chem. Rev. 2016, 116, 2478–2601

enter the first coordination sphere of anions, but only the second class of compounds work as effective agents for anion transport across lipid bilayers.[212−214] This behavior has been related to the very poor hydrophilicity of iodoperfluoroalkane−anion adducts.

1.4.4. Donor Atom Dimensions. The van der Waals radii[215] of halogen atoms (1.47, 1.75, 1.85, and 1.98 Å for F, Cl, Br, and I, respectively) are bigger than that of hydrogen (1.20 Å), and this causes differences in some properties of interactions involving these atoms. For the reason stated above, XB is, in general, more sensitive to steric hindrance than HB. In the infinite chain formed by 1,4-diiodotetrafluorobenzene with 4,4′- and 2,2′-bipyridine, the C−I···N distances are 2.864 and 3.158 Å, respectively;[84,216] when 2,4′-bipyridine forms heteromeric crystals with the same XB donor, only the 4-pyridyl nitrogen is halogen-bonded, and trimers are formed wherein the C−I···N distance is 2.821 Å. In section 5, Biomolecular Systems, we will see how, in the formation of DNA base pairs wherein XB substitutes for HB, the most stable pairing was given by bromine as the advantage offered by the greater polarizability of iodine was overwhelmed by the disadvantage resulting from its greater size. Similarly, in section 6.2, Optical and Optoelectronic Systems, it will be shown how the size of the halogen atoms may significantly influence the optoelectronic properties of the obtained supramolecular complex by promoting singlet-to-triplet intersystem crossing.

2. NATURE OF THE HALOGEN BOND

Although the successful use of XB in the design of self-assembly processes is mastered to the point that the forefront of the studies on the interaction is moving to its use for the design of advanced functional systems, some basic features of this interaction are still debated, and interest in fundamental issues remain vibrant.

The σ-hole concept, introduced by Politzer,[145] elegantly rationalized the behavior of halogen atoms as electrophiles, and actually it is quite commonly used. However, there are documented examples of halogen-bonded complexes whose characteristics cannot be explained on the exclusive basis of the σ-hole,[217,218] and the profile of the nature of the XB is still at the center of a heated debate between computational chemists.[26,219−227] Charge-transfer, electrostatic, dispersion, and polarization interactions plus a repulsive component resulting from the Pauli exclusion principle have all been invoked to cooperate in determining the strength and directionality of XB. Different theoretical methods have been suggested for the decomposition of the binding energy into the different components and quantify their contributions.[169,224,225,227−229] However, there is not a universal consensus on this approach. P. Politzer and T. Clark have, for instance, rebutted it,[119,144,230] emphasizing that only the total binding energy is a physical observable while the various proposed components have just a conceptual significance, are not uniquely defined, and are not independent from each other. Although all the suggested models are just intellectual constructs and the several bonding components are not totally independent quantities, they may help in rationalizing the bonding patterns for a better understanding of the nature of the XB.

The following sections give an overview of computational studies on the nature of the XB, and readers are directed to the specialized literature for a more comprehensive discussion on the topic.[119,144,225,231−234]

2.1. Modeling and Theoretical Studies

2.1.1. Electrostatic Component. The electrostatic point of view focuses on the distribution of the electron density in the ground state of the starting, and isolated, modules. Areas of depleted electron density on the XB donor are identified, and the XB is interpreted as the outcome of the attraction between these areas as the donor of electron density.

The analysis of crystal structures in the CSD by P. Murray-Rust et al.[65,235,236] revealed the amphoteric character of covalently bonded halogen atoms by proving that they can interact attractively with both nucleophiles and electrophiles, and electrophiles tend to enter orthogonal to the C−X bond, while nucleophiles have a preference for the elongation of the C−X bond, the angles between the covalent and noncovalent bonds at X spanning the 90−120° and 160−180° ranges, respectively. These experimental data were the starting point for extensive computational studies aimed at mapping the electrostatic potential on the surface of covalently bonded halogen atoms. Through these studies P. Politzer et al.[89,90] gave a rationalization for the ability of electronegative halogens to interact attractively with nucleophiles.

It is commonly recognized that the electron density distribution around a free halogen atom in its ground state is, on average, spherically symmetrical,[237] and the electrostatic potential $V(r)$ created around the atom is positive everywhere,[238,239] since the contribution of the nucleus dominates those of the dispersed electrons. $V(r)$ is a real physical property of a system, which turned out to be quite effective in predicting noncovalent interactions. It can be, in fact, determined computationally and experimentally by diffraction techniques.[240,241] Generally, $V(r)$ is computed on the surface of the molecule, since it is primarily this outer potential ($V_S(r)$) that is seen by nearby molecules. As suggested by R. F. W. Bader et al.,[242] $V(r)$ is computed at the 0.001 au (electron/bohr^3) contour of its $\rho(r)$, which encompasses roughly 97% of the molecule's electronic charge. It has been demonstrated that this contour is somewhat beyond atomic van der Waals radii (except for hydrogen).[243]

When halogen atoms are involved in covalent bonds, an electron density redistribution occurs, and the electrostatic potential becomes anisotropic; a similar behavior is shown by any other element.[119,154,156,244−247] An atom's electron density diminishes in its outer region along the extension of the covalent bond and increases in the direction perpendicular to it. The shape of halogen atoms becomes oblate with the shorter radius always along the covalent bond (Figure 21). The term "polar flattening" has been introduced to describe this phenomenon, which was experimentally proven through a detailed analysis of the CSD[245] and studies of electron density via X-ray analyses.[29,195,248]

As a result, a region of positive electrostatic potential along the C−X covalent bond develops on the outermost portion of the halogen surface. This positive region has been denoted by Politzer et al.[145] as a "σ-hole" because it can be seen as a local deficit of electron charge opposite a σ-bond. The σ-hole is surrounded by a belt which has a negative electrostatic potential and is orthogonal to the bond responsible for σ-hole formation.

This model elegantly explains the interaction pattern of covalently bonded halogen atoms, and their directional preferences, i.e., linear interactions with nucleophiles and lateral interactions with electrophiles. The presence of a positive σ-hole accounts for the electrophilic behavior of halogen atoms, while the focused nature of the σ-hole accounts

DOI: 10.1021/acs.chemrev.5b00484
Chem. Rev. 2016, 116, 2478−2601

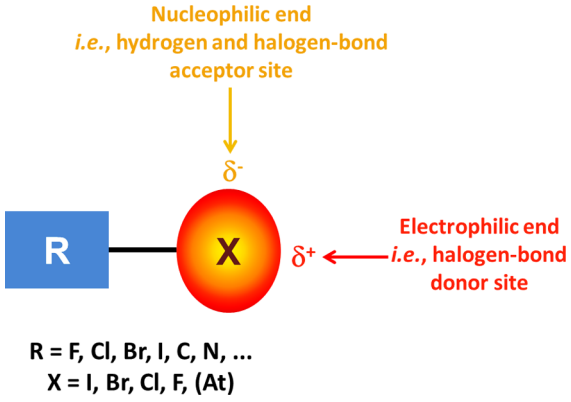

Figure 21. Schematic representation of the anisotropic distribution of the electron density around covalently bound halogen atoms and the pattern of the resulting interactions.

for the high directionality of XB, and the magnitude of the σ-hole can be correlated to the XB strength.

Such an interpretation of XB has also been supported by computational studies carried out by several other groups, among others P. Auffinger et al.,[249] F. F. Awwadi et al.,[246] and P. S. Ho et al. These authors also confirmed that, in short contacts of the R−X···H type, hydrogen atoms tend to enter the halogen orthogonal to the covalent bond,[250] nicely consistent with the amphoteric character of halogens according to which a (positive) hydrogen enters the negative belt of the halogen.

Both the size (the spatial range) and the magnitude (the value of $V_{S,max}$) of the σ-hole can vary significantly from one halogen to the other and, for a given halogen, from one compound to the other (Table 1) as they are affected by the polarizability and electronegativity of the halogen atom and the electron-withdrawing ability of the residue bound to the halogen.[142] As a general trend, the more polarizable the halogen atom and the more electron-attracting the covalently bound residue, the more positive and large the halogen σ-hole.[7,26,142,223]

This is exemplified by the $V_{S,max}$ on iodine in CH_3−I vs $CH_{3-n}F_n$−I (n = 1−3)[204] and NC−I (Table 1), which increases in the order CH_3−I < CF_3−I < NC−I.[136,144] Strong electron-withdrawing substituents can cause the potential $V_S(r)$ of the entire surface of the halogen to be positive, as is the case for fluorine in NC−F.[144] Indeed, also fluorine can form σ-hole bonds, and this has been demonstrated computationally[136,195,251] and, to some extent, also experimentally.[29,100] However, in general, fluorine tends to have negative σ-holes[136,145] (see CH_3−F and CF_3−F in Table 1), although less negative than the surroundings, and routinely it is not involved in attractive σ-hole interactions. In fact, in most cases the fluorine electronegativity, combined with the significant sp hybridization of C in the C−F bond, causes an influx of electronic charge on the outermost portion of the halogen that neutralizes the σ-hole.[252]

In Figure 22 the computed electrostatic potentials on 0.001 au molecular surfaces of different halobenzenes are reported to exemplify how, for a given R in R−X, $V_{S,max}$ becomes more positive when the polarizability of the halogen X increases; namely, $V_{S,max}$ changes in the order F < Cl < Br < I. In Figure 23 the analogous potentials of F_3C−Br and NC−Br are reported to exemplify how, for a given halogen, $V_{S,max}$ becomes more positive when the electron-withdrawing ability of R increases.[253]

Table 1. Most Positive ($V_{S,max}$) and Most Negative ($V_{S,min}$) Electrostatic Potentials (V) on the 0.001 au Surfaces of the Indicated Halogen Atoms[a]

molecule	atom	bond producing a σ-hole	$V_{S,max}$	$V_{S,min}$	ref
		Focus on General Trends			
H_3C−F	F	C−F	−1.07	−1.10	136
H_3C−Cl	Cl	C−Cl	−0.04	−0.68	136
H_3C−Br	Br	C−Br	0.25	−0.65	136
H_3C−I	I	C−I	0.56	−0.56	136
F_3C−F	F	C−F	−0.06	−0.12	136
F_3C−Cl	Cl	C−Cl	0.86	−0.03	136
F_3C−Br	Br	C−Br	1.10	−0.09	136
F_3C−I	I	C−I	1.38	−0.08	136
NC−F	F	C−F	0.56	0.47	144
NC−Cl	Cl	C−Cl	1.56	0.45	144
NC−Br	Br	C−Br	1.85	0.37	144
NC−I	I	C−I	2.11	0.31	144
		Dihalogens			
F−F	F	F−F	0.49	−0.11	144
Cl−Cl	Cl	Cl−Cl	1.11	−0.12	142
Br−Br	Br	Br−Br	1.26	−0.18	142
		Focus on Bromine			
Br—C≡C—Br	Br	C−Br	1.31	−0.09	144
H_3Si−Br	Br	C−Br	0.02	−0.51	136
F_3Si−Br	Br	Si−Br	0.79	0.09	136
H_3Ge−Br	Br	Ge−Br	−0.07	−0.58	136
H_2N−Br	Br	N−Br	0.77	−0.35	142
F_2N−Br	Br	N−Br	1.48	−0.07	142
H_2P−Br	Br	P−Br	0.15	−0.62	142
F_2P−Br	Br	P−Br	0.42	−0.33	142
HO−Br	Br	O−Br	1.42	−0.46	142
FO−Br	Br	O−Br	1.99	−0.02	142
HS−Br	Br	S−Br	0.75	−0.42	142
FS−Br	Br	S−Br	0.98	−0.20	142
F−Br	Br	F−Br	2.31	−0.004	142
Cl−Br	Br	Cl−Br	1.54	−0.10	142

[a]Computational method: M06-2X/6-311G.

It is interesting to note that positive σ-holes appear also in free halogen atoms if considered in the asymmetric valence state configuration $s^2p_x^2p_y^2p_z^1$, the same that they take when forming a covalent bond.[145,223,254] The half-filled p_z orbital is directly involved in the covalent bonding, and positive σ-holes are clearly visible in both the $+z$ and $-z$ directions for this valence state of chlorine, while the equatorial ring of negative potential is due to the doubly occupied p_x and p_y orbitals (Figures 24 and 25). It is worth noting that these σ-holes are not present in a neutral, spherically symmetric halogen atom where electrons are equally distributed on the three p orbitals, each of which contains, on average, 5/3 electrons.[252]

The σ-hole model explains well XBs where a halogen atom in one molecule interacts through its σ-hole with the negative region of a halogen in another, possibly identical, molecule.[143] In this context DFT studies carried out by Y. Lu et al.[255] on trimers $(R-X)_3$ (R = hydrocarbon or fluorocarbon residue; X = Br or I) predicted that it is possible to obtain triangular structures (Figure 26) stabilized by intermolecular interactions involving the σ-hole on a Br or I atom and the negative lateral region of a neighboring Br or I. Analogously, F. F. Wang et al.

DOI: 10.1021/acs.chemrev.5b00484
Chem. Rev. 2016, 116, 2478−2601

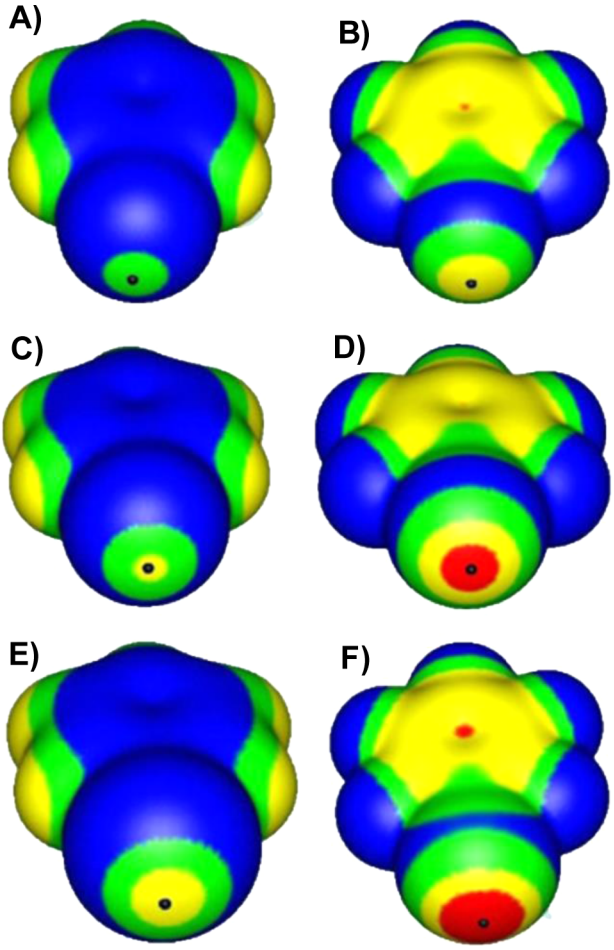

Figure 22. Computed electrostatic potentials on 0.001 au molecular surfaces of (A) chlorobenzene, (B) pentafluorochlorobenzene, (C) bromobenzene, (D) pentafluorobromobenzene, (E) iodobenzene, and (F) pentafluoroiodobenzene. Color range (kcal/mol): red, greater than 20; yellow, between 20 and 10; green, between 10 and 0; blue, negative. Black hemispheres denote the positions of the halogen $V_{S,max}$. Adapted with permission from ref 205. Copyright 2011 Springer.

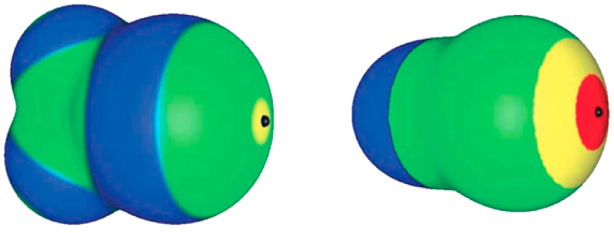

Figure 23. Computed electrostatic potential $V_S(r)$ on the 0.001 au surface of F_3C-Br (top) and NC−Br (bottom). For each molecule bromine is at the right. Color range (kcal/mol): red, more positive than 35; yellow, 20−35; green, 0−20; blue, negative. The position of the bromine $V_{S,max}$ is indicated as a black dot. In F_3C-Br, the σ-hole is an area of positive (yellow and green) $V_S(r)$ on the outer surface of the bromine; the lateral sides of bromine are negative (blue) because of the two pairs of electrons in the $4p_x$ and $4p_y$ orbitals. In NC−Br the presence on bromine of an electron-withdrawing substituent stronger than CF_3 causes such a polarization of the charge in the doubly occupied $4p_x$ and $4p_y$ orbitals of Br that the potential $V_S(r)$ becomes positive over the entire surface of the halogen atom. Adapted with permission from ref 254. Copyright 2010 John Wiley and Sons.

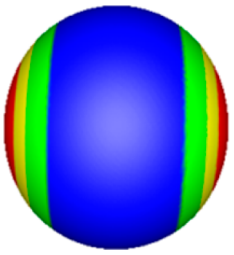

Figure 24. Calculated electrostatic potential on the 0.001 au molecular surface of a chlorine atom in the $s^2p_x^2p_y^2p_z^1$ valence state configuration. Color ranges (V): red, greater than 0.43; yellow, from 0.43 to 0.22; green, from 0.22 to 0; blue, less than 0 (negative). The most positive potentials on the chlorine surface, shown in red at the left and right, have a $V_{S,max}$ of 0.95 V. Computational level: M06-2X/aug-cc-pVTZ. Reprinted with permission from ref 144. Copyright 2015 Springer.

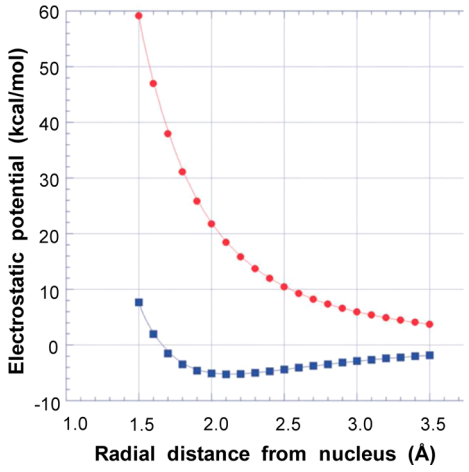

Figure 25. Computed electrostatic potential, B3PW91/6-311G(3d), of the chlorine atom in its valence state, $3s^23p_x^23p_y^23p_z^1$, as a function of the radial distance from the nucleus. The upper and red curve corresponds to the z-axis, the lower and blue curve to the x- and y-axes. In this valence state, $V(r)$ is still positive at all radial distances along the z-axis, corresponding to the half-filled p_z orbital. Along the x- and y-axes, however, $V(r)$ is positive near the nucleus but then becomes negative, reflecting the doubly occupied p_x and p_y orbitals. Reprinted with permission from ref 26. Copyright 2010 Royal Society of Chemistry.

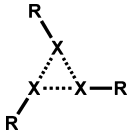

Figure 26. Triangular structure for the $(R-X)_3$ trimer.

predicted through ab initio calculations that the halogen-bonded complex FBr···BrF can be stable in the gas phase thanks to these halogen···halogen interactions.[256]

Several papers document both experimentally and theoretically the good correlation between the interaction energy ΔE of the halogen-bonded adduct and the $V_{S,max}$ of the σ-hole on the halogen. For instance, Politzer et al.[7] calculated the interaction energy at the M06-2X/aug-cc-pVTZ level for several complexes with NH_3 and HCN as XB acceptors, proving that ΔE becomes more negative as $V_{S,max}$ becomes more positive and that the $\Delta E/V_{S,max}$ linear correlation is good. K. Riley et al.[205] quantified the effects of aromatic fluorine substitution on the XB strength in adducts formed by

DOI: 10.1021/acs.chemrev.5b00484
Chem. Rev. 2016, 116, 2478−2601

halobenzene donors with acetone as the acceptor. The interaction energy computed through the MP2 method correlated well with the magnitudes of the σ-holes on the halogens, further confirming the high tunability of the XB. This is also the case for complexes between substituted bromobenzene and bromopyrimidine donors with acetone[257] as shown in Figure 27. Symmetry-adapted perturbation theory interaction energy decomposition on the same adducts revealed that electrostatics plays the key role in these XBs.

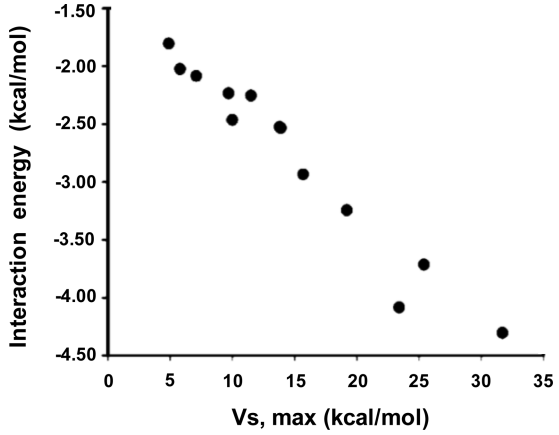

Figure 27. Interaction energy vs bromine $V_{S,max}$ for 13 Ar—Br···O=C$(CH_3)_2$ complexes, where Ar = substituted benzene or pyrimidine (R = 0.976). Reprinted from ref 257 Copyright 2009 American Chemical Society.

The important role of electrostatics in the binding was also revealed by a study of the complexes between a range of halogenated aromatics and HF as the XB acceptor.[258] Calculation of the size and magnitude of the σ-hole on halogen atoms in the donors allowed also for proving that both in-ring and out-of-ring chemical substitutions affect the σ-hole, which systematically increases in size and magnitude going from Cl to I.

2.1.2. Charge-Transfer Component. Several adducts now considered as formed under XB control have long been interpreted as charge-transfer adducts, and this rationalization was strongly motivated by UV−vis observations. Within this frame XB directionality was rationalized as a consequence of donation of electron density to the R−X antibonding orbital (e.g., adducts between diiodine and amines were rationalized as n → σ* interactions). These aspects will be discussed in detail in the rest of this section.

As early as in 1950, R. Mulliken[14,52,53] examined in detail the nature of intermolecular interactions occurring between dihalogens or halogenated compounds and benzene or other organics containing O, S, or N heteroatoms. The appearance of strong and different colors upon dissolution of I_2 in organic solvents was explained by Mulliken in terms of a weak and reversible intermolecular association. In general agreement with considerations advanced by H. A. Benesi and J. H. Hildebrand,[50] Mulliken[14] suggested, except for the "violet" solutions obtained with aliphatic hydrocarbons and other apolar solvents, the existence of specific 1:1 complexes resulting from "an acid−base interaction in the electron donor−acceptor sense" in which iodine functions as the Lewis acid, namely, the electron acceptor. The charge-transfer (CT) theory developed by Mulliken explained well the spectroscopic properties and the dipole moments of these complexes in the ground and excited states.[14] R. Mulliken and W. Person[36] postulated the existence of two types of charge-transfer complexes based on the extent of charge transfer accompanying complex formation: the "outer complexes", characterized by weak interactions and little charge transfer between the components, and the "inner complexes", characterized by stronger interactions and a substantial charge redistribution. Both outer and inner complexes, in Mulliken's notation AX···B and $[BX]^+(sol)A^-(sol)$, respectively, have been invoked in describing halogen-bonded complexes.[259,260] It is worth mentioning that the formation of an inner complex does not imply a complete transfer of one electron from the Lewis base B to the halogen X, but simply means that there is a significant charge transfer.

In 1998, I. Alkorta et al.[261] reported a theoretical study on the charge-transfer complexes formed by dihalogens (F_2, Cl_2, and Br_2) or interhalogens (FBr, FCl, and ClBr) with Lewis bases (HF, H_2O, NH_3, CO, HCN, and C_2H_2) by using hybrid Hartree−Fock density functional theory (HF-DFT) B3LYP and second-order Møllet−Plesset perturbation MP2 methods. As expected, the interaction energy increased with the halogen atom polarizability (F_2 < Cl_2 < Br_2); in the case of interhalogens, the largest interaction energies were associated with the largest dipole moments (FBr > FCl > ClBr); and regarding the Lewis base, NH_3 afforded the strongest complexes. The electron distribution was also analyzed using the atoms in molecules (AIM) methodology. The highest charge transfers, related to the formation of highly dipolar complexes, were observed in NH_3-containing complexes (around 0.16 e^- in the complexes with FCl and FBr), .

Microwave spectroscopy has been applied by A. Legon et al.[262] to study the interaction of dihalogen molecules (R−X; R, X = halogen) with simple Lewis bases (Y) in the gas phase. The changes in the halogen nuclear quadrupole coupling constants upon complex formation allowed for the evaluation of the amount of charge transfer from the Lewis bases Y to the halogen X, as well as the extent of electric charge redistribution in R−X. It was found that, for a number of small Lewis bases, including NH_3 and PH_3, the smaller the energy required to remove the most loosely bound electron (n-type or π-type) from Y, the greater the extent of electron transfer from Y to R−X on formation of the R−X···Y complex. Moreover, the amount of charge transfer increased with the halogen polarizability, and it was usually less than 0.1 e^-, except when Y = NH_3 and PH_3 and R−X = ClBr and ClI (Figure 28). These results suggest that all the studied complexes are Mulliken outer complexes.[24]

UV−vis spectra of complexes containing the same halocarbon but different electron donors[105] revealed a linear correlation between the absorption energy and the oxidation potential of the XB acceptor, and this correlation is, according to Mulliken,[36] the most characteristic feature of charge-transfer complexes. A charge transfer to the σ* orbital of the R−X bond was confirmed through X-ray analysis which showed that the C−I bond of 1,4-DITFB was elongated, relative to that of the pure compound, in a variety of adducts with nitrogen-based XB acceptors.[76] Similarly, a lengthening of the C−Br bond was observed in various bromocarbons involved in XB with bromide[263] and bromometalate[218] anions as electron donors. In all the crystalline structures of the bromocarbon/bromometalate adducts, the short intermolecular C−Br···Br−M XBs (Figure 29) were influential in determining the packing and were always directed toward the bromide ligands where the highest occupied molecular orbitals (HOMOs) of bromometalates are located, while the analysis of the electrostatic

DOI: 10.1021/acs.chemrev.5b00484
Chem. Rev. 2016, 116, 2478−2601

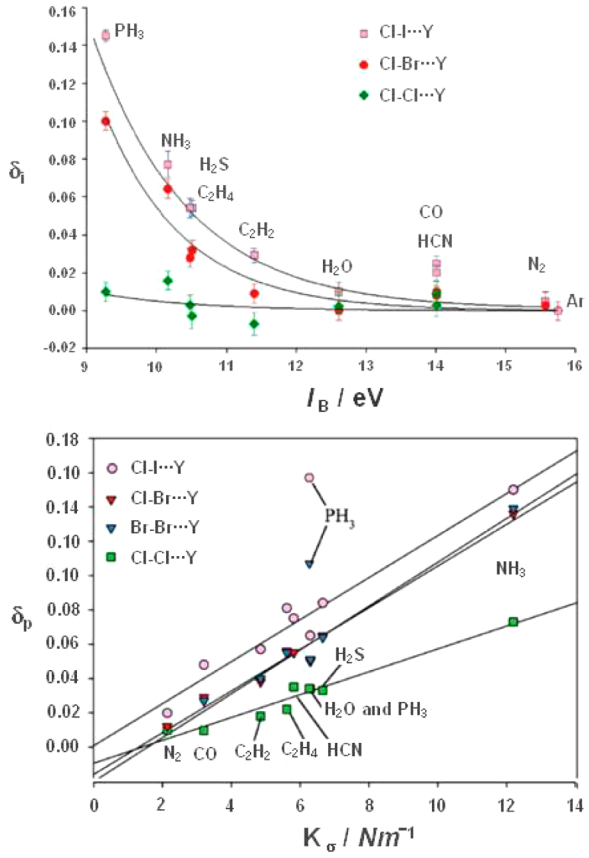

Figure 28. Top: variation of the fraction δ_i of an electronic charge transferred from B to YX on formation of the YX···B complex with the ionization energy I_B of B for the series YX = Cl_2, ClBr, and ClI. Each set of points can be fitted reasonably well by the function $\delta_i = A\exp(-aI_B)$, which is represented as a solid curve on the graph. It is evident that there is a family relationship among the curves. Bottom: variation of the fraction δ_p of an electronic charge transferred from X to Y on formation of the YX···B complex plotted against the intermolecular stretching force constant k_σ for the series YX = Cl_2, Br_2, ClBr, and ClI. The solid line represents the least-squares fit of the points for each YX···B series for a given YX, and δ_p is an approximately linear function of k_σ and hence of the strength of the interaction. Moreover, for a given B δ_p increases with the polarizabilities of the interacting atoms X in YX···B.

potential revealed that HOMO localization did not necessarily coincide with the most negative areas on the surfaces of the bromometalates. A purely electrostatic interaction would be expected to occur preferably between the most positive areas of the bromocarbons and the most negative areas on the surfaces of the bromometalates, but this is true only in the CBr_4···$[CuBr_2]^-$ complex. The experimentally observed directional preference suggests that in all complexes there is a significant HOMO and LUMO overlap (LUMO is the lowest unoccupied molecular orbital) and demonstrates the importance of the covalent component of XB.

A further confirmation that also the charge-transfer component plays a significant role in XB stabilization came from a recent experimental and computational analysis of a series of complexes containing electrophilic bromocarbons (CBr_3F, CBr_3NO_2, CBr_3COCBr_3, CBr_3CONH_2, CBr_3 CN, etc.) as XB donors and bromide anions[264] or pseudohalide anions[265] (N_3^-, NCO^-, and NCS^-) as acceptors. The interaction energies for a wide range of complexes with

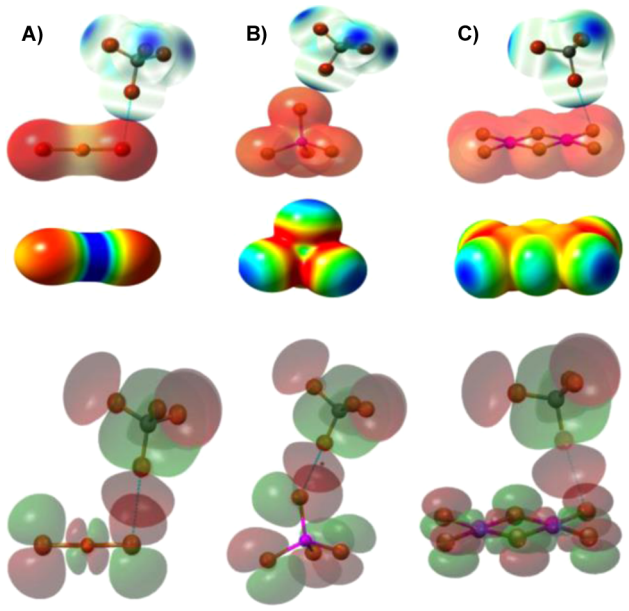

Figure 29. (Top) $V_S(r)$ (calculated at the B3LYP/6-311+G(dp) level on the 0.001 electron/bohr^3 molecular surfaces) of the XB donors and acceptors superimposed onto X-ray structures of their complexes: (A) $CBr_4/[CuBr_2]^-$; (B) $CBr_4/[ZnBr_4]^{2-}$; (C) $CBr_4/[Pt_2Br_6]^{2-}$. Blue and red colors depict positive and negative potentials, respectively. (Middle) The electrostatic potentials of bromometalate anions are negative everywhere, but noticeable variations of their values are also observed and depicted with a color gradient from the most negative (red) to the least negative (blue) values (kcal/mol): (A) $[CuBr_2]^-$, from −100 (red) to −80 (blue); (B) $[ZnBr_4]^{2-}$, from −170 (red) to −150 (blue); (C) $[Pt_2Br_6]^{2-}$, from −155 (red) to −125 (blue). (Bottom) MO shapes (B3LYP/6-311+G(dp) level) of CBr_4 and halometalates, superimposed onto crystal structures of their complexes. HOMOs of bromometalates are mostly located on the bromide ligands. Adapted from ref 218. Copyright 2012 American Chemical Society.

bromide anions showed a good correlation with the combination of electrostatic and orbital components, while the correlation with V_{max} was rather poor. As far as the pseudohalides are concerned, the amount of charge transferred to the electrophile has been calculated through the natural bond orbital analysis.[265] Its value varies from 0.028 e^- for CH_3Br···OCN^- in dichloromethane to 0.316 e^- for CBr_3NO_2···N_3^- in the gas phase. A linear correlation has been found between the amount of charge transferred and the elongation of the C−Br bonds of the bromocarbons: The C−Br bond length increases, and the intermolecular distance between interacting species decreases, as the amount of charge transfer increases. As a result, in the NO_2CBr_3···N_3^- complex, the length of the intermolecular Br···N bond is comparable to that of the adjacent intramolecular C−Br bond, suggesting that one electron is essentially delocalized between the two interacting species in the C−Br···N fragment. This electron delocalization can be explained considering the orbital mixing[266] and the resulting reduction of the barrier for electron transfer[267] between halogenated electrophiles and nucleophiles. This result further supports the hypothesis that halogen-bonded complexes are prereactive intermediates in the reactions of halogenated molecules with nucleophiles,[24,61,268] and suggests that XB may also affect the conducting properties of solid-state materials.

HOMO/LUMO charge transfer and polarization are suggested as the main factors responsible for XB in a set of

DOI: 10.1021/acs.chemrev.5b00484
Chem. Rev. 2016, 116, 2478−2601

$H_3C—X\cdots O{=}CH_2$ and $F_3C—X\cdots O{=}CH_2$ (X = Cl, Br, I) molecular complexes when the nature of the interaction is investigated by using the Kohn–Sham molecular orbital (MO) theory.[224] This supports a remarkable covalent component of XB in these complexes. This understanding is also supported by other studies where the Kohn–Sham MO theory was used coupled with energy decomposition analysis and Voronoi deformation density analysis of the charge distribution to build a physical model of the XB.[219,228] In particular, the structure and bonding mechanism in trihalides $R—X\cdots Y^-$ (R, X, Y = F, Cl, Br, and I) were compared with those in analogous hydrogen-bonded complexes $R—H\cdots Y^-$, and it was found that both XB and HB are characterized by significant charge transfer from the halide Y^- to the antibonding σ^* orbital (LUMO) on the R–X or R–H fragment (Figure 30).

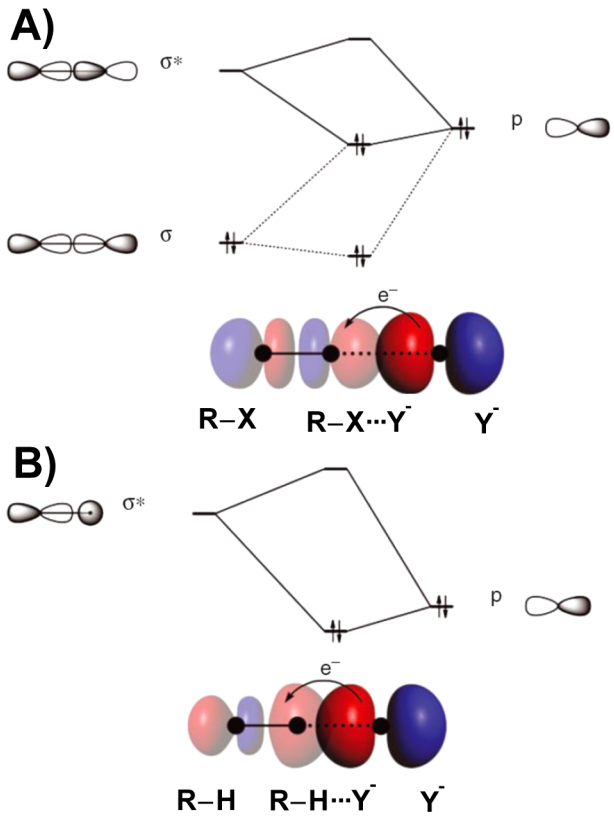

Figure 30. Orbital interaction diagrams for (A) XB and (B) HB arising in $R—X\cdots Y^-$ and $R—H\cdots Y^-$ complexes. Only the σ interactions are shown. Adapted with permission from ref 219. Copyright 2014 John Wiley and Sons.

An ab initio study of the halogen-bonded complexes between pyridine and a series of dihalogen and interhalogen molecules (R–X; R, X = halogen) has been performed[269] with the aim to gain information about the preferred geometry of these systems and to clarify the nature of the intermolecular interactions driving their formation. The natural bond orbital analysis suggests that the $n(Py) \rightarrow \sigma^*(R—X)$ charge transfer plays a key role in the formation of these dimers, while the symmetry-adapted perturbation theory energy decomposition analysis indicates that the XB in R–X···pyridine complexes is predominantly inductive in nature.

Halogen-bonded systems containing one or two XBs were analyzed by using the natural orbitals for chemical valence (NOCV) method combined with the extended-transition-state (ETS) method.[270] The obtained results confirmed the role of the σ-hole that is responsible for the electrostatic stabilization of the interaction; however, in each analyzed system, the XB contained a large degree of covalent component due to a charge transfer from the Lewis base to the empty $\sigma^*(C—X)$ orbital (Figure 31).

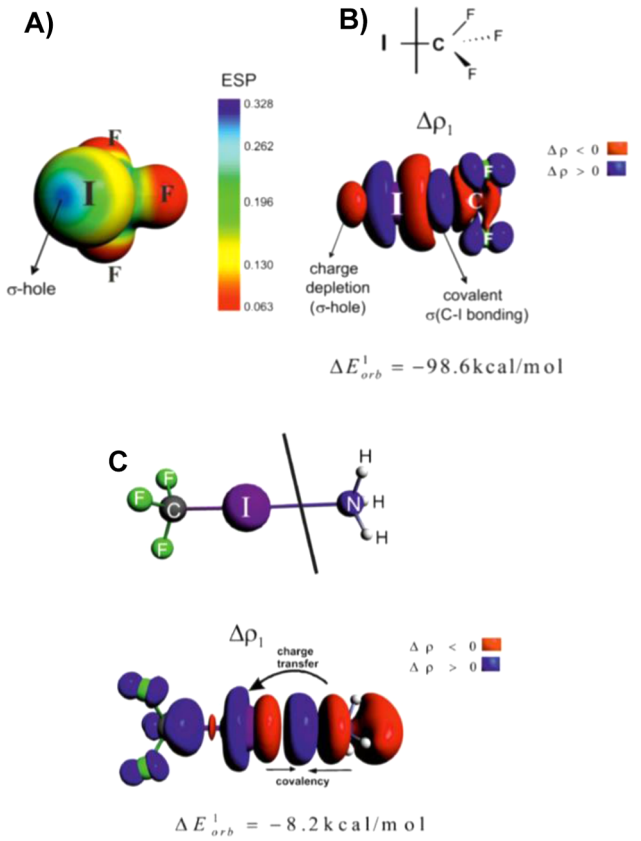

Figure 31. (A) $V_S(r)$ of the CF_3I molecule and represented in blue the σ-hole. (B) Visualization of σ-hole formation using the deformation density contributions originating from NOCV. The contour of the deformation density contribution $\Delta\rho_1$ describes the formation of the C–I bond in the CF_3I molecule starting from an iodine atom and the CF_3 radical (each carrying one unpaired electron with opposite spin polarization). A charge accumulation at iodine is observed due to formation of the C–I bond, which confirms significant charge anisotropy around this atom. An outflow of electron density emerges from the outer area of the iodine atom, which clearly corresponds to the formation of the σ-hole. The corresponding ETS-NOCV-based energy is shown. The numerically smallest contour values are ±0.0006 au. (C) Contour of the deformation density contribution $\Delta\rho_1$ describing the formation of the XB in the $CF_3I\cdots NH_3$ complex.

The observed trend in the XB strength in adducts involving $CY_3—I$ (Y = F, Cl, Br, I) as XB donors and chloride anions or trimethylamine as XB acceptors could not be rationalized on the basis of a purely electrostatic model.[217] Specifically, it was found that the XB strength decreases going from CI_4 to $CF_3—I$, a trend opposite that of the σ-hole on iodine (Figure 32). The same trends were found also with $CY_3—Cl$ and $CY_3—Br$ as XB donors when fluoride, bromide, and iodide anions were the Lewis bases, and it was suggested that these observations were evidence of the importance to consider a charge-transfer contribution from the XB acceptor to the XB donor.

The nature of XB in a series of 55 complexes has been studied by means of ab initio valence bond theory and block

DOI: 10.1021/acs.chemrev.5b00484
Chem. Rev. 2016, 116, 2478–2601

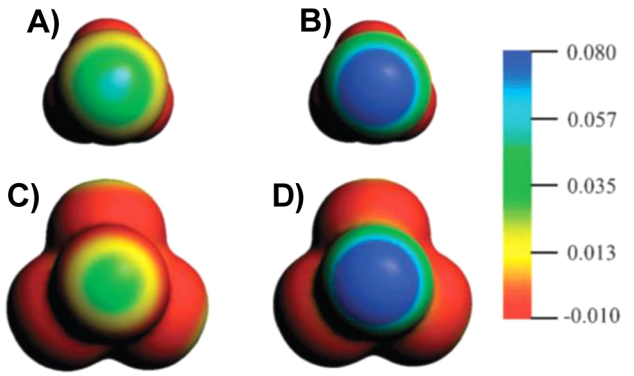

Figure 32. Molecular electrostatic potential at the isodensity surface of CF_3–I (A) and CI_4 (C) at the same contour value of 0.001 electron/bohr^3. The red color shows the most negative potential, while the blue color represents the most positive one. The σ-holes of CF_3–I (B) and CI_4 (D) in the presence of a 1.0 point charge are also depicted. Energies are expressed in atomic units. Reprinted with permission from ref 217. Copyright 2012 Royal Society of Chemistry.

localized wave function theory.[226] The authors found a good linear correlation between charge-transfer energies and total interaction energies and concluded that, in most of the studied complexes, the XB is a charge-transfer interaction.

2.1.3. Dispersion and Polarization Components. The origin of the attractive interaction occurring in halogen-bonded complexes was originally imputed to charge-transfer phenomena, possibly as this was the frame within which some of the earliest studies were performed.[14,36,52,53,64,271,272] These studies frequently employed strong XB donors, and in the resulting adducts the net transfer of electron density from the site entering the halogen atom was indeed nonminor. Then the emphasis moved to electrostatic forces largely because of the close analogy between halogen and hydrogen-bonded complexes.[24,80,273,274] In fact, it is well established that the major contribution to the attraction in hydrogen-bonded systems comes from the electrostatic interaction between a positively charged hydrogen and a negatively charged electron donor, and by analogy, it was proposed, and commonly accepted, that attraction in halogen-bonded systems comes from the electrostatic interaction between a positively charged halogen and a negatively charged electron donor. Recently, P. Hobza et al.[222] established for the iodobenzene···trimethylamine system a stabilization energy of 5.8 kcal/mol, comparable to that of strong H-bonds. Moreover, stabilization energies of 17.1 and 15.3 kcal/mol have been calculated for FI···NH_3 and FBr···NH_3, respectively,[220] while stabilization energies of 8.0 and 15.0 kcal/mol have been reported[275] for the crystals of the complexes of diiodine, I_2, with 1,3-dithiole-2-thione-4-carboxyclic acid and 1,4-diazabicyclo[2.2.2]octane, respectively, and it was considered that these data ask for a further and improved analysis of the origin of these large stabilization energies.

In halogen-bonded systems, the electrostatic attraction is important, but since two atoms with high polarizability (the halogen and the electron donor) are closer than the sum of their van der Waals (vdW) radii, polarization and dispersion contributions cannot be overlooked. Neglecting these components led to the assertion that the electrostatic interpretation of XB is inadequate as in the case of the complexes involving CH_3Cl as the XB donor. In fact, a completely negative surface around the chlorine atom was found in this molecule[252] (see Table 1), and on this basis, it has been assumed that CH_3Cl does not form XB. On the contrary, the existence of the complex CH_3Cl···O=CH_2 was also predicted,[225] and this apparent inconsistency led to thoughts about a failure of the σ-hole theory.[276] However, it should be taken into account[231,277] that, while in an isolated CH_3Cl molecule the chlorine electrostatic potential is negative everywhere, as soon as the molecule begins to interact with O=CH_2, the electron density of each component is polarized by the electric field of the other, resulting in a positive σ-hole on the chlorine (Figure 33)

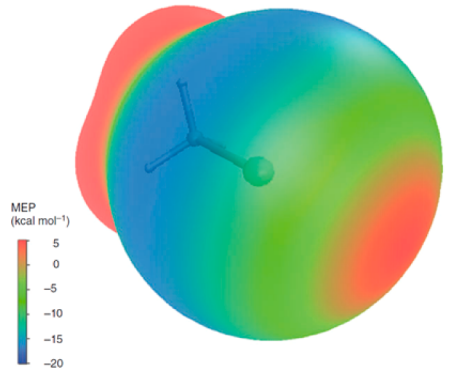

Figure 33. Molecular electrostatic potential (MEP) calculated at the MP2/aug-cc-pVDZ level on the 0.001 au isodensity surface of CH_3Cl in the presence of a charge of −0.2692 at a distance of 3.0 Å from the chlorine atom along the extension of the C–Cl bond. The MEP on the chlorine reflects the polarization caused by the electric field of the negative charge, and a region of positive electrostatic potential (σ-hole) appears on the chlorine surface. Reprinted with permission from ref 231. Copyright 2015 Wiley and Sons.

surface and finally in an attractive interaction.[231,277] In general, recognizing the role of polarization and dispersion is of paramount importance for a correct interpretation of noncovalent interactions.

Decomposition of the total interaction energy into well-defined energy terms is becoming a common approach to analyze noncovalent interactions since it can be helpful in rationalizing the bonding patterns. Several decomposition analyses have been applied, producing different bonding models each describing the XB as a complex mixture of several bonding components. All these bonding models are mathematical constructs, and a universal consensus has not been reached yet.[144,231,277] Different computational methods and decomposition analyses can produce different results, depending on the weight of each energy component on a given XB system. Nevertheless, they are tools that can help in understanding the nature of the XB if great care is taken in their interpretation.

Particularly interesting is the symmetry-adapted perturbation theory (SAPT) and its density functional theory version (DFT-SAPT), which allows for the treatment of extended complexes (up to ∼35 atoms). This method decomposes the total interaction energy into four components, electrostatics (E^{ES}), induction or polarization (E^{I}), dispersion (E^{D}), and exchange repulsion (E^{ER}), and its application allows for the contribution of each component to the total binding energy to be evaluated. The DFT-SAPT method was applied to a series of halogen-bonded complexes, including the X_2···benzene systems (X = F, Cl, and Br), the set of $H_nF_{3-n}CBr$···NH_3 complexes, and some complexes containing formaldehyde as the XB acceptor and chloroform, halothane, enflurane, or isoflurane as the XB donor.[278] The analysis revealed the mixed dispersion–electro-

DOI: 10.1021/acs.chemrev.5b00484
Chem. Rev. 2016, 116, 2478–2601

static nature of XB. The dispersion energy was dominant in 8 out of 10 different halogen-bonded complexes investigated by SAPT, while only in two cases the electrostatic term was slightly larger than the dispersion one. In particular, it was found that dispersion plays an important role in stabilizing type II halogen···halogen contacts where two large and polarizable halogen atoms are in close proximity. The electrostatic component, on the other end, is responsible for the directionality and the tunability of an XB. Figure 34, left,

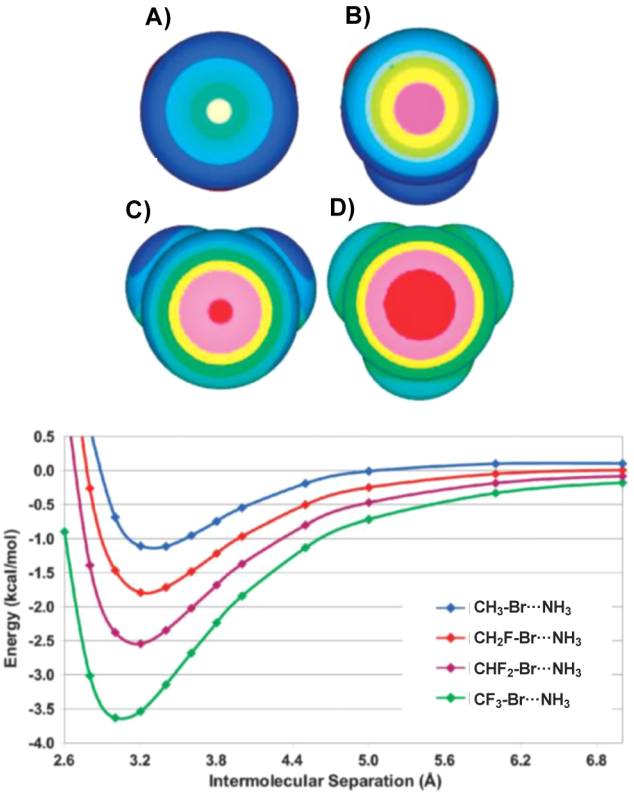

Figure 34. Top: electrostatic potentials of H_3C-Br (A), H_2FC-Br (B), HF_2C-Br (C), and F_3C-Br (D). Color code: lightest blue, <−5 kcal/mol; intermediate blue, between −5 and −2.5 kcal/mol; dark blue, between −2.5 and 0 kcal/mol; green, between 0 and 4 kcal/mol; yellow, between 4 and 8 kcal/mol; pink, between 8 and 16 kcal/mol; red, >16 kcal/mol. Bottom: potential energy curves calculated at the CCSD(T)/aug-cc-pVTZ level for the four complexes $H_nF_{3-n}CBr\cdots NH_3$. Reprinted with permission from ref 278. Copyright 2013 Royal Society of Chemistry.

shows the B3LYP/aug-cc-pVDZ electrostatic potentials calculated on the 0.001 au molecular surface for the $H_nF_{3-n}C-Br$ set of molecules (with n spanning the range from 0 to 3). Here it can be clearly seen that incremental fluorine substitutions result in larger bromine σ-holes and stronger XB interactions with NH_3 as the Lewis base.[204] In fact, the potential energy minima for the $H_nF_{3-n}C-Br\cdots NH_3$ complexes become progressively greater on going from H_3C-Br to F_3C-Br, and the intermolecular separations become shorter (Figure 34, right).

The intermolecular separation can obviously affect the character of the noncovalent interaction in the $H_nF_{3-n}CBr\cdots NH_3$ complexes, i.e., the relative importance of dispersion, electrostatics, and induction. DFT-SAPT energy dissection reveals that for these systems the most important contributions to stabilization come from the electrostatic and dispersion terms, with induction playing a smaller role (Figure 35).

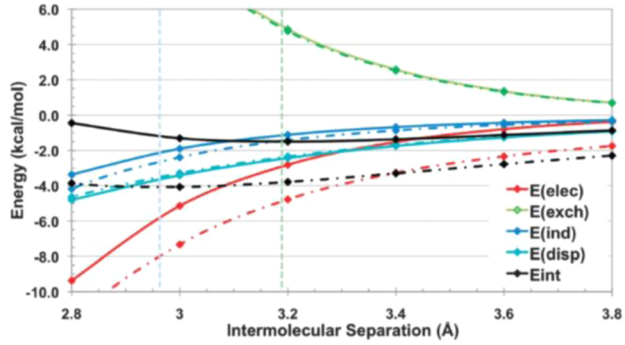

Figure 35. DFT-SAPT components, electrostatics (E(elec)), induction or polarization (E(ind)), dispersion (E(disp)), and exchange (E(exch)), and total binding energies ($E(\text{int})^T$), for the $H_3CBr\cdots NH_3$ (solid lines) and $F_3CBr\cdots NH_3$ complexes (dashed lines) (kcal/mol). Potential energy minima are shown as vertical dashed lines. $H_3CBr\cdots NH_3$ is green, and $F_3CBr\cdots NH_3$ is light blue. Reprinted with permission from ref 278. Copyright 2013 Royal Society of Chemistry.

Halogen-bonded complexes involving FCl as the XB donor were studied using the DFT-SAPT theory with the aim of understanding the factors responsible for the high linearity of this interaction.[279] In particular, the variation of the total binding energy and its components was calculated upon tilting FCl away from its linear orientation (Figure 36). It was found that the linearity is preferred because it minimizes the exchange repulsion, and although the electrostatic component is usually the largest attractive term, in many cases electrostatic energy alone does not predict the structure, and it is necessary to take into account induction and dispersion components.

DFT-SAPT calculations by using the aug-cc-pVDZ and aug-cc-pVTZ basis sets were carried out on 128 halogen-bonded complexes of different sizes and origins to study a set of molecules as large as possible.[233] For each XB donor, the magnitude and size of the σ-hole were calculated as well as the LUMO energy. In perfect agreement with previous results, the magnitude and size of the σ-hole correlate well (correlation coefficient R = 0.86), and both of them increase with the atomic number of the halogen atom and with the presence of fluorine atoms on the remainder of the molecule. Differently, the magnitudes of the σ-hole and LUMO energy anticorrelate with R = −0.76. This confirms that strong electron acceptors (i.e., molecules with the most negative LUMO energies) have more positive σ-holes. An analysis of the stabilization energy allowed for the halogen-bonded complexes to be divided into two groups.

The first group comprises the strongest complexes (stabilization energy larger than 7 kcal/mol) where the most important terms are polarization and induction, consistent with a strong charge-transfer contribution to the binding. The second group comprises weaker halogen-bonded complexes (stabilization energies below 7 kcal/mol), and in this class of complexes, the dispersion component provides the greatest contribution to the total binding energy. In the whole set of 128 halogen-bonded complexes, the polarization (electrostatic) energy is dominant in 62% of the adducts, while the dispersion energy is the dominant attractive term in the remaining 38%. The authors conclude that the concerted action of polarization and dispersion energies is responsible for the characteristic properties of the XB.

The Laplacian of the electron density, $\nabla^2\rho$, provides information about the regions where electronic charge is

DOI: 10.1021/acs.chemrev.5b00484
Chem. Rev. 2016, 116, 2478−2601

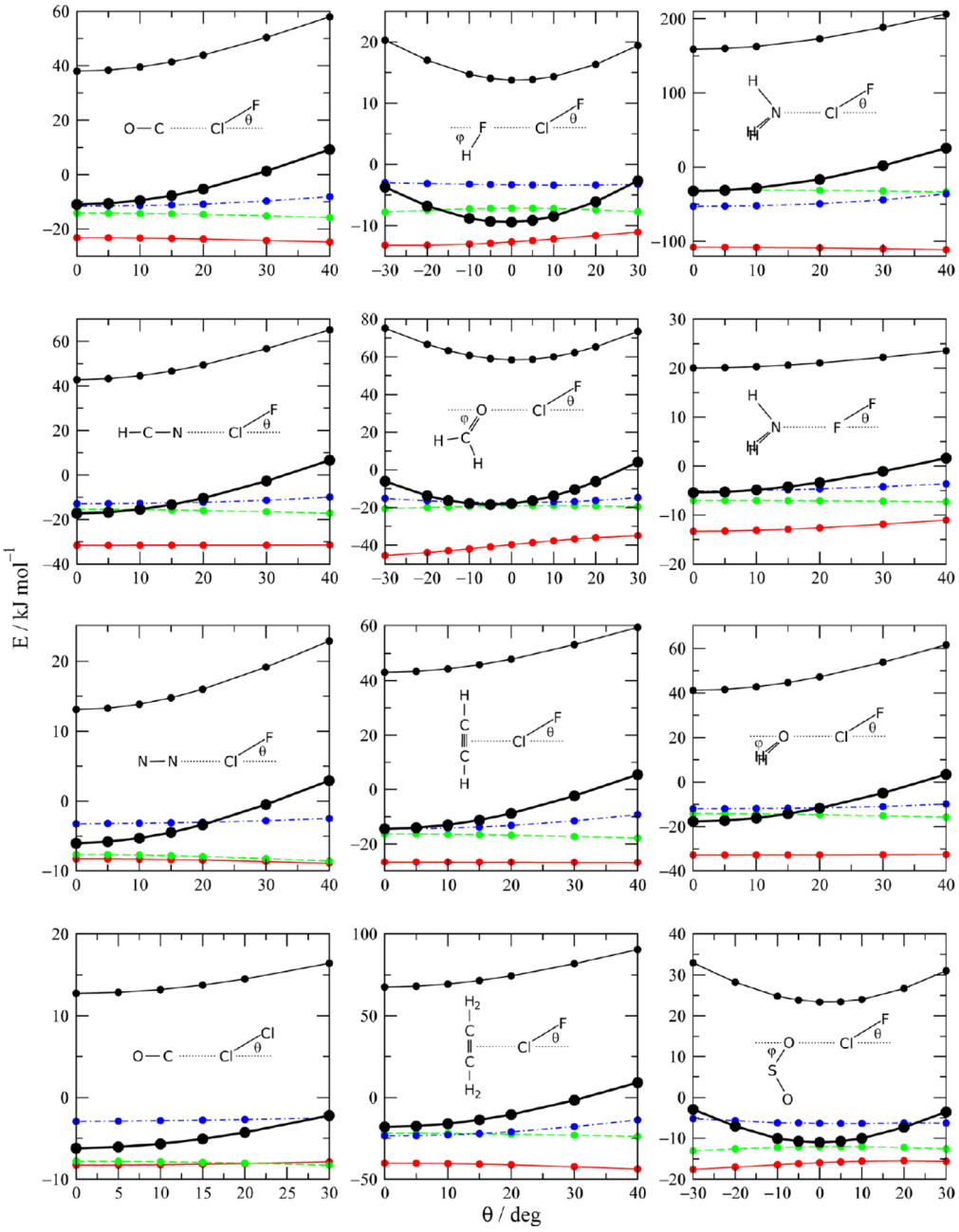

Figure 36. Variation of energy components with the tilt angle θ of FCl···B complexes away from linearity (B is the electron donor). The angle φ was held at 55° for FCl···FH, 69° for FCl···O=CH_2, 0° for FCl···OH_2, and 48° for FCl···O_2S. The components are (black solid) exchange repulsion, (red solid) electrostatics, (green dashed) dispersion, and (blue dashed−dotted) induction. The heavy black line represents the total. Reprinted from ref 279. Copyright 2013 American Chemical Society.

concentrated, discriminating between "lumps" (when $\nabla^2\rho < 0$) or depleted "holes" (when $\nabla^2\rho > 0$), and has also been applied to describe the XB interaction.[280,281] In close analogy with the σ-hole model, this approach considers the XB as an interaction between a "hole" in a halogen atom and a "lump" in a Lewis base.[280] However, unlike the σ-hole model, $\nabla^2\rho$ values depend on both the electrostatic potential $V(r)$ and the kinetic energy $G(r)$, and its sign determines which of these two contributions dominates: When the Laplacian is negative, $V(r)$ dominates, while when the Laplacian is positive, the kinetic energy $G(r)$ is the dominant factor.[281] The advantage of analyzing the $\nabla^2\rho$ function rather than simply the electrostatic potential ($V(r)$), is that $\nabla^2\rho$ allows contributions different from the electrostatics and coming from electron redistribution (polarization and charge transfer) to also be taken into account. From a topological point of view, it is convenient and more intuitive to introduce the function $L(r) = -\nabla^2\rho$, which is positive in a region with higher concentration of electron density and negative in a region with electron density depletion. The Laplacian of electron density has been employed in the description of halogen-bonded complexes formed between ammonia and several halogenated molecules, including CH_3F, CH_3Cl, CH_3Br, and other chloroorganic molecules.[280] In good agreement with the σ-hole model, the distribution of the Laplacian of electron density predicts the absence of "holes" for fluorine in CH_3F and the presence of a hole on bromine in

DOI: 10.1021/acs.chemrev.5b00484
Chem. Rev. 2016, 116, 2478−2601

Table 2. Angular Geometries, Intermolecular I···Y Distances (r_0, Å), and Intermolecular Stretching Force Constants (k_σ, N m^{-1}) As Derived Experimentally from Rotational Spectroscopy in the Gas Phase for a Series of Halogen-Bonded Complexes with ClI and CF_3–I

R–I···Y complex	Point group, r_0 (Å), k_σ (N m^{-1})	
	R = Cl	R = CF_3
	$C_{\infty v}$ 3.180(2) 5.35(2) [333]	C_{3v} 3.438(1) 2.94(2) [342]
	$C_{\infty v}$ 3.011(1) 7.96(3) [334]	C_{3v} 3.428(1) 3.950(2) [343]
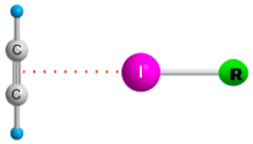	C_{2v} 3.115(2) 12.1(1) [335]	C_s [a] 3.442(2) 4.96(7) [188]
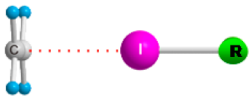	C_{2v} 3.032(2) 14.0(1) [336]	C_s [b] 3.434(2) 4.95(1) [189]
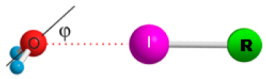	C_s/C_{2v}, φ = 46(2)° 2.828(1) 15.9(2) [337]	C_s [b], φ =34(2)° 3.053(2) 8.8(1) [344]
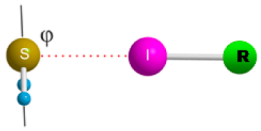	C_s, φ= 91.9(2)° 3.154 16.55(5) [338]	C_s [b], φ= 93.7(2)° 3.559(1) 6.7(1) [344]
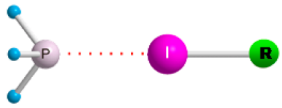	C_{3v} 2.963(1) 20.7(1) [340]	C_{3v} [b] 3.571(3) 6.27(2) [188]
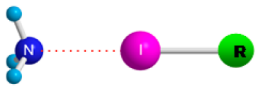	C_{3v} 2.711(2) 30.4(3) [339]	C_{3v} [b] 3.038(1) 11.6(2) [345]

[a] C_s at equilibrium, C_{2v} in the zero-point state. [b] These molecules possess low barriers to internal rotation/other motion. The point group of highest symmetry achieved during the motion is given.

CH_3Br. Therefore, the first halomethane is unable to interact attractively with ammonia, while CH_3Br can, instead, form stable complexes with NH_3.

2.2. Experimental Studies

Long before the "rediscovery" of the XB in the late 1990s, the ability of chlorine and heavier halogens to be involved in attractive interactions with lone-pair-possessing atoms had been revealed by several analytical techniques such as, among others, microwave, infrared, UV–vis, NMR, NQR, and X-ray analysis.[64,88] Later on, as XB started to attract increasing interest, the number of studies aimed at identifying the fingerprints of the interaction rose significantly, and these same techniques are now used more or less routinely to assess the occurrence of XB. Moreover, thanks to technological advancements in available instrumentation, analytical techniques (often complemented by modeling studies) have also allowed advancements in the understanding of the fundamental features of the XB, such as its geometry and thermodynamic parameters.

Giving an account of every single use of these experimental techniques would be a formidable task encompassing nearly the whole XB history. In the next sections we will instead offer selected examples to describe the main advances in XB characterization brought forth through some of the most useful and informative techniques.

2.2.1. Microwave Spectroscopy. Microwave spectroscopy enables measurement under conditions of effective isolation of molecules, avoiding perturbations of the ground-state structure from either solvent or lattice effects. Thus, it is one of the most used techniques to investigate halogen-bonded complexes in the gas phase, although other notable work has been

DOI: 10.1021/acs.chemrev.5b00484
Chem. Rev. 2016, 116, 2478–2601

performed, e.g., by using vibrational spectroscopy. As an example, J. W. Bevan and co-workers have recently shown high-resolution vibration−rotation spectroscopic studies on Cl_2···CO complexes using quantum cascade lasers.[282]

Importantly, the observation of the pure rotational spectra in the microwave region can provide information on several fundamental properties of the studied complexes, and it is particularly suitable for a comparison with the results of ab initio calculations. The analysis of ground-state spectra leads to the determination of a series of ground-state constants. Rotational constants allow for determining the angular and radial geometries of complexes from the changes in their zero-point moments of inertia, centrifugal distortion constants can be used to derive the intermolecular stretching force constant k_σ by modeling the R−X···Y complex as a pair of rigid molecules held together by a weak intermolecular bond, and nuclear quadrupole constants can in certain cases provide insight into the electric charge redistribution of the complexes through the Townes−Dailey model.[283] More detailed information on how these properties can be derived from spectroscopic rotational data has been conveniently collected elsewhere.[24,188]

Two techniques have been most frequently used to study the rotational spectra of halogen-bonded complexes. They are pulsed-jet, Fourier transform microwave spectroscopy (PJ-FTMW) in a Fabry−Perot cavity[284,285] and chirped-pulse, Fourier transform microwave spectroscopy (CP-FTMW).[286,287] In both techniques, a mixture of the two interacting compounds in an inert gas undergoes a supersonic expansion to produce a short gas pulse (about 1 ms) containing the complex to be studied. The mixture then expands into a vacuum chamber in essentially collisionless conditions, which allow for studying the complexes in their vibrational ground state and in their lower energy rotational states. A short pulse of microwave radiation is used to electrically polarize rotational transitions, and when the polarizing radiation has decayed enough to avoid significant background radiation, the amplitude of spontaneous coherent emission as a function of time is recorded. Finally, a Fourier transform of the time-domain signal is performed to yield intensity-versus-frequency spectra.

The series of halogen-bonded complexes R−X···Y involving dihalogens as Lewis acids (R, X = halogen atoms; Y = Lewis base) have been extensively characterized by rotational spectroscopy. Complexes of F_2,[288−292] Cl_2,[293−302] Br_2,[303,304] ClF,[305−325] and BrCl[326−332] were studied by T. Legon's group with a series of systematically varied Lewis bases, and the results of this comprehensive series of investigations have been previously summarized.[24] More recently, this body of work was expanded by the same group to include and compare the gas-phase rotational spectra of new molecular pairs such as ClI···Y[24,67,262,273,333−341] and CF_3I···Y.[188,189,342−345]

Through a systematic variation of R−X and Y and by studying the corresponding changes in the derived properties, it was possible to draw some generalizations about XB,[294,326,346−349] for example, the geometry of complexes and principles to predict the intermolecular stretching force constant k_σ from the nucleophilicity of the Lewis base Y and the electrophilicity of the XB donors.[24,347] The angular geometries for R−X were found to substantially follow a model based on empirical rules which was originally proposed for hydrogen-bonded complexes involving HX molecules[188,350−352] and which is derived from electrostatic considerations. In its form extended to R−X···Y halogen-bonded complexes in the gas phase, this model states that the R−X internuclear axis at equilibrium lies preferably along the axis of a nonbonding electron pair (n-pair) carried by Y or, if there are no n-pairs available, along the local symmetry axis of a π orbital of the Lewis base. When modules possessing both n-pair(s) and π-pair(s) are used, the former prevail over the latter in function as XB acceptors. The only exceptions were found for complexes with furan and thiophene, in which π orbitals dominated over the n-pairs in the tendency to interact with the electrophile.[24,323,324] These rules also apply to the halogen series of CF_3−I···Y complexes, which have geometries very similar to those of their R−X···Y and R−H···Y counterparts. However, it should be noted that the presence of CF_3−I makes the interpretation of spectra more complicated, due to the appearance of vibrational satellites coming from a low-energy barrier related to the rotation of the CF_3 group. The angular geometries for a number of ClI···Y (representative of the interhalogen series) and CF_3−I···Y complexes are summarized as examples in Table 2.

Notably, the differences in angular geometry between the complexes formed with H_2O and H_2S by a dihalogen,[24] an iodoperfluoroalkane,[344] and X−H[352] showed a set of correspondences for all XB donors. In the case of H_2O, the complexes were shown to be essentially planar with a rapid inversion between equivalent pyramidal geometries at oxygen, while for H_2S the configurations at S were observed to be permanently pyramidal. These findings are in agreement with the results of ab initio calculations performed at the CCSD(T)(F12c)/cc-pVDZ-F12 level, which found significantly wider and higher energy barriers for the inversion of configuration at S in H_2S complexes than at O in H_2O complexes[187,188,353,354] (Figure 37).

The radial geometries, i.e., the distances r_0 between XB donor and acceptor atoms, afforded another indication of the existing parallelism between the halogen- and hydrogen-bonded complexes. The experimental distances were found to be below the sum of the van der Waals radii of the corresponding atoms, in agreement with Politzer's electrostatic model of the σ-hole.[26] The R-X···Y distances were always found to be shorter than the corresponding R-H···Y ones, and this difference was attributed, at least in part, to the anisotropy of the X atom radius in R−X molecules, as also supported by ab initio calculations performed on Cl_2 and FCl.[355] This shortening was not observed, instead, for the complexes with F_2, probably due to their weakness. The intermolecular bond distances appeared to always be longer in complexes with CF_3−I when compared to those formed by Cl−I (Table 2).

Rotational spectra can also afford the intermolecular stretching contant k_σ, which can be used as an indication of the strength of the XB. The values derived for k_σ mirrored those obtained for radial geometry, yielding smaller k_σ values for longer interatomic distances. The results for the Cl−I and CF_3−I series are reported in Table 2.

The study of intermolecular stretching constants highlighted one more similarity between HB and XB. For R−X···Y complexes, the constant k_σ was proportional to the nucleophilicity of the Lewis base Y,[24,347] according to the expression $k_\sigma = cN_YE_{RX}$, where c = 0.25 N m^{-1}, N_Y is a numerical nucleophilicity assigned to the Lewis base Y, and E_{RX} is the numerical electrophilicity of the interhalogen RX. An analogous expression holds for hydrogen-bonded complexes, with RH substituting for RX.[356] The plot of k_σ versus N_Y reported in Figure 38A was built from six series of complexes of the dihalogens F_2, FCl, Cl_2, ClBr, Br_2, and ClI with several

DOI: 10.1021/acs.chemrev.5b00484
Chem. Rev. 2016, 116, 2478−2601

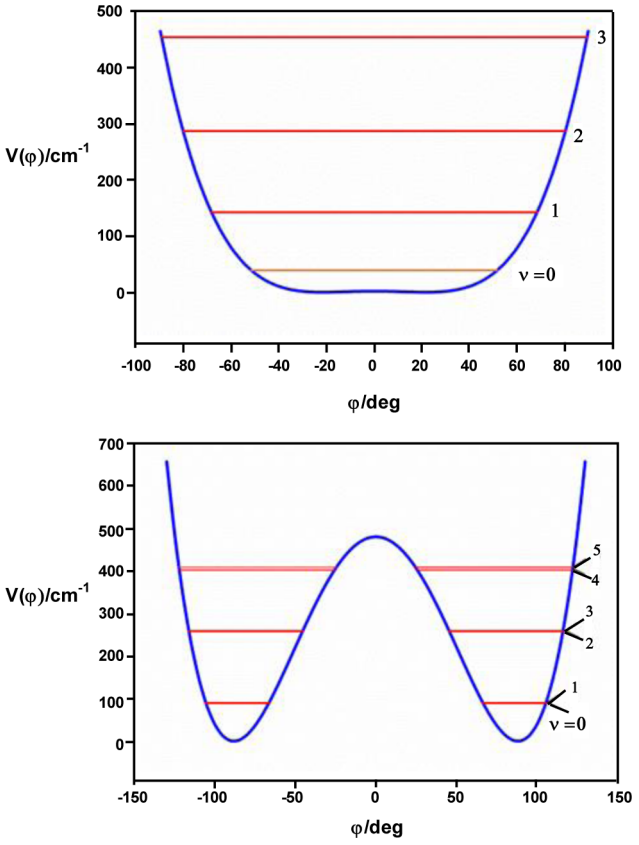

Figure 37. Potential energy $V(\varphi)$ of the molecules ClI···OH_2 (top) and ClI···SH_2 (bottom) as a function of the angle φ made by the extension of the C_2 axis of the H_2O and H_2S molecules with the I···O and I···S internuclear axes (as defined in Table 2). Reprinted with permission from ref 188. Copyright 2015 Springer.

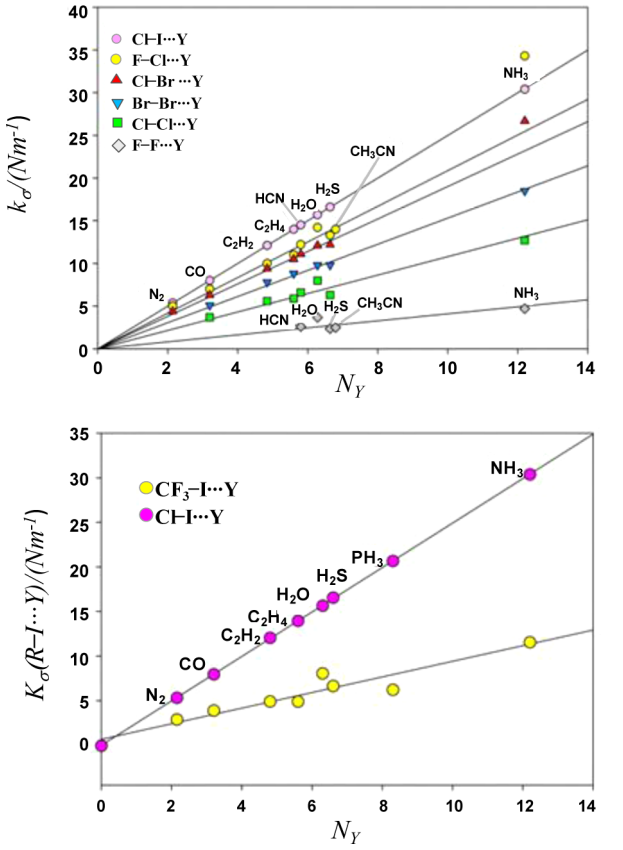

Figure 38. Intermolecular force constant k_σ against the nucleophilicity N_Y of Lewis bases Y for six series of halogen-bonded complexes RX···Y (top) and the two series ClI···Y and CF_3–I···Y (bottom). The slope of each line yields the electrophilicity E_{RX} by means of the expression $k_\sigma = cN_YE_{RX}$, and the value $c = 0.25$ N m^{-1}. Reprinted with permission from ref 188. Copyright 2015 Springer.

Lewis bases Y; in this diagram the N_Y scale was defined by setting $E_{Cl–I} = 10$ and requiring all points of the corresponding plot to lie on a straight line.[188]

The resulting plots for all other dihalogens were substantially linear; some deviations were observed for the Lewis base NH_3, possibly due to significant charge polarization effects occurring in the corresponding complexes. Since the slopes of the lines are proportional to E_{RX}, these plots allowed for drawing a scale of electrophilicity of the dihalogens as $F_2 < Cl_2 < Br_2 < ClBr \approx FCl < ClI$. The same linearity principle was shown to apply to CF_3–I···Y complexes (Figure 38, bottom), albeit with a slope about one-third of that of Cl–I···Y interactions, and somewhat comparable to that of Cl_2···Y interactions.[188] The binding strength scale suggested by these findings is consistent with the σ-hole model, and is supported by the values of the equilibrium dissociation energies D_σ obtained by various groups through theoretical modeling. Ab initio calculations were performed for a series of R–H···Y, R–X···Y,[357] and CF_3–I···Y[188] complexes at the CCSD(T)(F12*)/cc-pVDZ-F12 level, for complexes of C_2H_2 and C_2H_4 with CF_3I at the MP2/cc-aug-pVTZ level,[358] for CF_3–I···NH_3 at the MP2/DZVP level,[204] and for Cl–I···NH_3 at the CCSDT(F12b)/VTZ level.[359]

Finally, the nuclear quadrupole coupling constants derived from rotational spectra allowed for an estimate of the fraction δ_i of charge transferred from the XB acceptor to the donor, which was generally found to be on the order of a few hundredths of an electronic charge; exceptions were observed for stronger complexes,[24] such as those with ammonia and especially with trimethylamine. By plotting δ_i versus the first ionization energies (I_Y) of the corresponding Lewis bases (Figure 39), the charge-transfer fraction appears to increase at lower I_Y values, as well as with the polarity of the XB donor group (ClI > ClBr > Cl_2).[262,273]

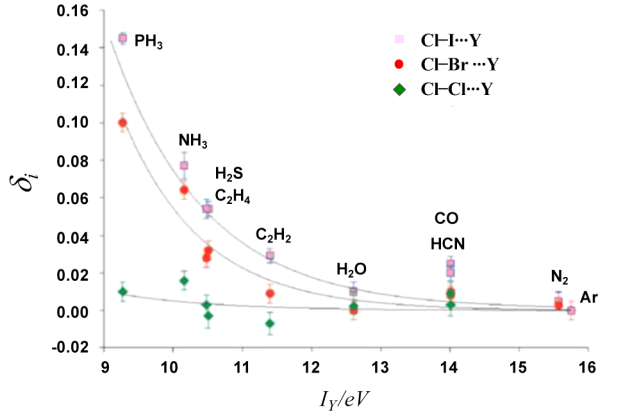

Figure 39. Fraction δ_i of an electronic charge transferred from Y to RX upon complexation, plotted versus the ionization energy I_Y of Y for a series of dihalogen molecules and fitted with negative exponential curves. Adapted with permission from ref 273. Copyright 2010 Royal Society of Chemistry.

DOI: 10.1021/acs.chemrev.5b00484
Chem. Rev. 2016, 116, 2478–2601

A similar kind of plot could not be prepared for complexes formed by CF_3–I, due to the lack of a second quadrupolar nucleus.[188] However, the results exposed above suggest that it is reasonable to suppose that CF_3–I···Y complexes are significantly weaker than those afforded by Cl–I and possibly comparable to those formed with Cl_2 and thus involving negligible charge-transfer components.

Overall, the combination of observed electric charge redistribution and binding energies in almost all the studied R–X···Y complexes has been rationalized as these complexes being Mulliken outer adducts, with a simple electrostatic term acting as a dominating contribution to the interaction energy.[24] The complexes of F_2[292] and FCl[325] with trimethylamine were the most notable exceptions, for which a significant contribution from the form $[(CH_3)_3NX]^+\cdots Y^-$ had to be invoked in a valence-bond description of the complexes.

2.2.2. Infrared and Raman Spectroscopies. The observation of vibrational shifts upon complex formation is a powerful tool to establish the presence of an XB; FTIR spectroscopy, along with X-ray diffraction and NMR spectroscopy, is among the techniques most commonly employed to study the interaction. While slightly less commonly used, the complementarity of Raman spectroscopy allows vibrational modes with low FTIR intensity to be observed, and it is particularly useful at far-IR wavelengths, where C–X modes are found between 100 and 500 cm^{-1}. In this section we will discuss specific studies based on vibrational spectroscopies and allowing for the general features of XB to be established in solid complexes, and to a minor extent liquid complexes. These general features (e.g., the relative effectiveness of different XB donors and acceptors and the effect of the structural features of interacting modules on the XB profile) largely parallel those established for complexes in the gas phase via microwave spectroscopy and discussed in section 2.2.1. It results that fundamental XB characteristics are poorly affected by solvent and lattice effects if these effects are of generic nature, namely, if they do not involve specific XB acceptor, or XB donor, sites. The rationale for the format adopted in this section is that, far from representing a duplication of the section on microwave spectroscopy, it confirms the general validity of some XB features, and the same holds for the format in sections 2.2.3 and 2.2.4.

FTIR is most frequently used to monitor C–H and C–F stretching modes in the 2800–3000 and 1000–1200 cm^{-1} regions, respectively, although far-IR measurements are also feasible and afford useful information. Most commonly, the focus is on C–H modes of Lewis bases involved in XBs, while C–F modes are monitored when haloperfluorocarbons are used as XB donors. One common assumption for R–X···Y–R′ complexes (Y = Lewis base; X = I, Br, or Cl) was first expressed by N. F. Cheetham and A. D. E. Pullin[360] and presumes that since the X···Y bond is weak, it is reasonable to discuss the spectra of the complexes mainly in terms of modified modes of R–X and Y–R′; this assumption is generally supported by the fact that the vibrational spectra of similar complexes display analogous changes.

The interactions between Lewis base atoms (most often nitrogen) and diiodine,[42,45,48,271,361−367] dibromine,[45,361,364,365,368] interhalogens,[45,48,361,363,364,367,369−373] or pseudohalogens such as NC–I[45,361,374] have been extensively studied by infrared and Raman spectroscopies since the 1950s. Some common fundamental features were found from the very early works; this was the case for a small red shift of the R–I stretching (R = halogen or carbon) in the far-IR region, accompanied by a significant intensity increase in the bands of the infrared spectra. These findings were explained with Mulliken's charge-transfer model.[52] According to this interpretation, as the R–I···Y weak bond gains in strength due to n → σ* transfer, the corresponding resonance formula $(R–I)^-\cdots Y^+$ acquires importance.[374] Thus, the R–I force constant decreases, and the effective charge on the R atom increases, thus leading, respectively, to a red-shifted and higher intensity mode observed in FTIR (Figure 40). This red shift was also clearly observed when 1,2-diiodotetrafluoroethane was complexed with diazabicyclooctane.[375]

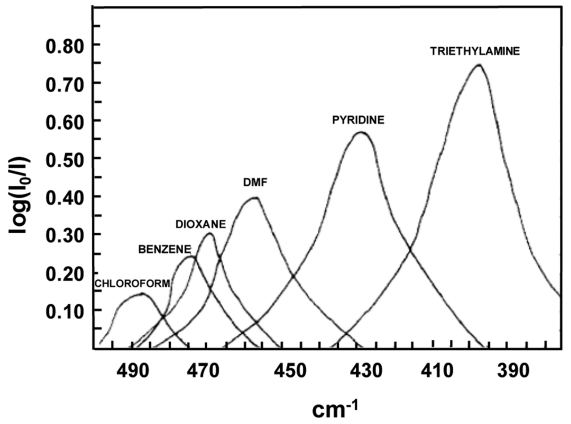

Figure 40. Infrared absorption of the C–I fundamental stretching frequency for NC–I and its complexes with the compound reported above the respective bands. Reprinted from ref 374. Copyright 1959 American Chemical Society.

These early vibrational spectroscopy investigations allowed a wealth of important information on what would later be recognized as XB to be gathered. A. I. Popov and co-workers highlighted noteworthy features such as (i) the similarity between the spectral changes on formation of R–I···Y complexes and corresponding changes in hydrogen-bonded complexes,[374] (ii) the appearance upon complexation of new bands in the infrared spectra of, e.g., pyridine bases due to the breaking of the charge symmetry distribution,[369] and (iii) the formation of stronger complexes for ClI than BrI, when these were used as Lewis acids.[370] In 1963, the solution infrared studies of adducts between nitriles and ClI[363] provided evidence that the interhalogen molecule was situated along the 3-fold symmetry axis of the nitrile group, and that the strength of the interaction was dependent on the inductive effect of substituents close to the nitrogen.

The complexes of pyridine[371] and picolines and lutidines[361,376] with I_2, BrI, and ClI were investigated in the 1960s. Infrared studies gave evidence for complex dissociation in a variety of solvents in the presence of excess base, according to the equilibrium $2(RI\cdot Py) \leftrightarrows Py_2I^+ + IR_2^-$ (R = I, Br, Cl). T. Tassaing and M. Besnard[377,378] later reported an intensity enhancement of the vibrational bands of I_3^- and [bis(pyridine)-iodine]$^+$ upon increased concentration of acetonitrile in CCl_4/acetonitrile solvent mixtures and suggested that the polarity of the solvent plays a role in favoring dissociation.

I. Haque and J. L. Wood determined that the linear geometry observed in the solid state for bis(pyridine) complexes with iodine and bromine is maintained in solution, the solvent polarity being uninfluential.[379] However, more recent infrared

DOI: 10.1021/acs.chemrev.5b00484
Chem. Rev. 2016, 116, 2478−2601

studies performed on dicoordinated complexes of picolines with dihalogens showed a band splitting in the 1030−990 cm^{-1} region, which was interpreted with a steric hindrance-induced breaking of symmetry.[380]

On the basis of vibrational spectroscopy investigations, the structure of trihalide ions in solution was described as slightly asymmetric and easily affected by weak forces.[44,381] This was confirmed also by studies performed on ammonium salt trihalides,[47] which indicated slightly lower symmetry in solution than in the solid state; conversely, the occurrence of both symmetric and asymmetric geometries was demonstrated for Cl_2I^-.[382] Further surveys were aimed at determining possible effects of the solvent nature and polarity on the geometry of the I_3^- ion. Investigations with UV laser-excited Raman spectroscopy afforded evidence for greater asymmetry in alcohols than in water,[46,383] while other studies indicated that the degree of symmetry of the same anion varies with the solvent according to the order acetonitrile > ethyl acetate > ethanol, suggesting that polar protic solvents have a stronger symmetry-destabilizing effect;[384−386] however, an asymmetric bent geometry was also recently suggested in dichloromethane.[387] The results of all these experimental investigations have been supported by several computational studies,[388−393] which claimed that the asymmetry observed in polar protic solvents is a result of HB-induced polarization, and that the energy barrier for the interconversion between symmetric and asymmetric species is higher in water than in ethanol, while flat single-well or very low barrier double-well potentials are expected for polar aprotic solvents.

A series of infrared spectra of the complex between dimethylacetamide and iodine showed the onset of a second C═O stretching band with a 43 cm^{-1} red shift, while the C−N stretching showed a 70 cm^{-1} blue shift.[394] These results were interpreted as an indication of iodine coordination to the oxygen rather than the nitrogen, and several X-ray structures confirm this binding mode. The intensities of the complexed and free carbonyl bands increased and decreased, respectively, with the iodine/dimethylacetamide ratio, and an isosbestic point was observed. This suggested the presence of only two main species, i.e., free amide and a complex (Figure 41). These studies also allowed for a measurement of a binding enthalpy of the complex as high as −5.1 kcal/mol. Interestingly, a comparative study with an iodine−acetone mixture pointed out the importance of the inductive effect of the dimethylamino group in dimethylacetamide, which increases the basicity of the carbonyl oxygen and thus leads to a more stable complex.

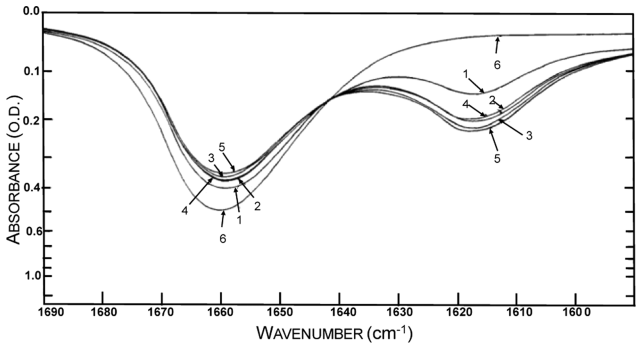

Figure 41. Infrared spectrum of the dimethylacetamide/iodine complex. As the I_2 concentration increases, the intensity of the free amide peak (1662 cm^{-1}) decreases, while the intensity of the complex peak (1619 cm^{-1}) increases. Reprinted from ref 394. Copyright 1960 American Chemical Society.

The ability of iodoacetylenes to act as Lewis acids in complexes was also first observed in the 1960s by vibrational spectroscopy. Early Raman[395] and infrared[396] studies gave evidence for self-association of NCC≡CI in the solid state, occurring by charge transfer between the N and I atoms. The existence of complexes of 1-iodopentyne with carbonyl, sulfuryl, and phosphoryl electron donors in apolar solvents was first shown by means of infrared spectroscopy[397] and later confirmed through ^{13}C NMR[196,398] and X-ray[399] studies. Later on, a systematic study on complexes of substituted 1-iodoacetylenes RC≡C—I with various Lewis bases in apolar solvents[400,401] allowed the strength of the complexes to be obtained from the changes in the infrared spectra of the electron donors. The results showed that the studied 1-iodoacetylenes are weaker Lewis bases than NC−I, and that their acidity increases with the electron-withdrawing power of the R substituent, according to the order *n*-Pr < $SiEt_3$ < Ph < I ≈ CH_2Br < C_6H_4-*p*-NO_2 < COOEt < CN.

The vibrational spectra of CF_3−X (X = I, Br) in mixtures with several Lewis bases were studied in detail by Cheetham and Pullin.[360,402−405] Mixtures were prepared as vapors, CCl_4 solutions (at room temperature), liquids (at lower temperatures), and solid films (at 80 K). These authors observed several important features, in particular for the trimethylamine complexes: (i) the appearance of a low-frequency band at around 100 cm^{-1}, which was attributed to X···N stretching; (ii) a red-shifted C−X band with significantly enhanced intensity around 260 cm^{-1} (X = I) and 330 cm^{-1} (X = Br), with a shift magnitude following the electron-donating ability of the used base; (iii) a blue shift in the symmetric C−F stretching mode ν_1, accompanied by a red shift of the degenerate C−F stretching mode ν_4 in the 1000−1200 cm^{-1} region; (iv) a frequency increase in the C−N−C symmetric bending and C−H stretching of trimethylamine in the 400 and 2800−3000 cm^{-1} regions, respectively; (v) a dependence of the observed shifts on the complex aggregation state, according to the order solid (80 K) > liquid ≈ CCl_4 solution > vapor.

One further step was taken by P. Metrangolo and G. Resnati et al., who began in the late 1990s a systematic investigation by FTIR of halogen-bonded complexes involving iodoperfluoroalkanes[10,28,80,88,190,375,406] and iodoperfluoroarenes.[10,80,84,407] Their observations supported those of Cheetham and Pullin, particularly regarding C−F, C−X, and C−H stretching shifts, and confirmed their validity for longer haloperfluoroalkanes as well as for aromatic systems when used as either XB donors or XB acceptors. Some important additional observations were (i) smaller red shifts in longer haloperfluoroalkanes, consistent with the hypothesis that vibrations of difluoromethylene groups further away from the XB site are significantly less affected,[375] and (ii) lower intensities of C−H stretching bands in FTIR spectra, consistent with a higher positive charge on the H atoms as a consequence of the n → σ^* character of the established XB.[84,375]

Recently, the FTIR spectra of heptafluoro-2-iodopropane and heptafluoro-1-iodopropane complexed with pyridine in a variety of solvents were compared,[408] and proof was obtained for stronger I···N XB with the *iso* compound consistent with the greater electron-withdrawing ability of a trifluoromethyl group with respect to a fluorine atom. Particularly small spectral changes were observed in chloroform, which was attributed to the ability of this solvent to form hydrogen bonds with pyridine

DOI: 10.1021/acs.chemrev.5b00484
Chem. Rev. 2016, 116, 2478−2601

and fluorocarbons. Interestingly, in the same work a combination of FTIR and ^{19}F NMR dilution studies gave evidence of the onset of *self-halogen bonds* for heptafluoro-2-iodopropane in nonpolar solvents. In concentrated cyclohexane solutions, a broad band was observed at around 900 cm^{-1}, attributed to the bending of a C_α–F group geminal to the C–I one and directly engaged in XB. At increasing dilutions, a sharp absorption appeared at 905 cm^{-1}, which was assigned to the same vibration for a free C_α–F (Figure 42). Only free C_α–F was observed in acetone and acetonitrile, which are known to form XBs with iodoperfluoroalkanes.

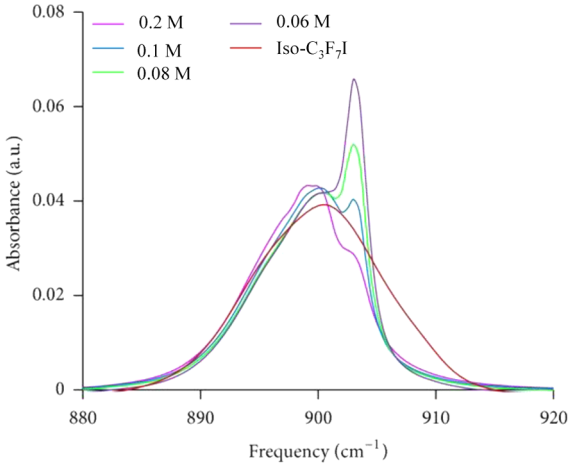

Figure 42. FTIR absorbance of C_α–F bending for heptafluoro-2-iodopropane in cyclohexane at various dilutions. Reprinted with permission from ref 408. Copyright 2013 Hindawi Publishing Corp.

One clear problem related to vibrational spectroscopic investigations of weak interactions in solution is the influence of the environment on the complexes, which results in changes in the observed frequencies. On the other hand, measurements performed on solid matrixes are generally not in thermodynamical equilibrium and thus cannot yield information on the stability of the complexes. These shortcomings can be avoided by performing FTIR and Raman spectroscopy measurements in cryogenic solutions using liquefied rare gases, which also yield spectra with sharper bands and thus facilitate assignments.

Extensive work has been performed on cryogenic solutions of complexes of halotrifluoromethanes with trimethylamine,[409] dimethyl ether,[410] dimethyl sulfide,[411] alkyl halides,[412] and π-systems.[358,413,414] These experimental studies were supported by a variety of quantum chemical calculations to predict the structural, thermodynamic, and spectroscopic properties of the studied species, and by Monte Carlo free energy perturbation methods[415,416] to simulate solvent effects and predict complexation enthalpies. The instrumentation and methodologies involved in these measurements have been recently described in detail elsewhere[417] and will not be reported herein.

The fundamental vibrational modes of halotrifluoromethanes and the recorded shifts in cryogenic solutions in the presence of several Lewis bases are reported in Tables 3 and 4.

One first important result is that these cryogenic FTIR and Raman investigations allowed for the direct observation of XBs involving Cl atoms, although the weakness of these bonds usually required the very low temperatures provided by liquid Ar to provide observable band shifts. Second, while the early results of Pullin and co-workers were confirmed with regard to blue-shifting symmetric (ν_1) and red-shifting antisymmetric (ν_4) CF_3 stretching modes, important new observations were made in the 200–400 cm^{-1} region, where vibrations were assigned to $\nu_3(CF_3X)$ (with significantly increased intensity compared to that of the free compounds, e.g., 900-fold for the complex between CF_3I and trimethylamine) and to ν_6(C–X). In particular, it was possible to point out clear blue shifts of these modes for CF_3Br complexes with both methyl and ethyl fluoride. This is remarkable because these were the first experimental evidence of blue-shifting C–X fundamental vibrations in XBs, which had been only predicted by theoretical studies[418–420] as connected to a shortening of the C–X distance, but had not been experimentally observed before. Perhaps even more remarkably, blue shifts were observed also for complexes with CF_3I, while it had been previously suggested that iodoperfluoroalkanes could be involved only in red-shifting XBs.[418]

The vibrational spectra for complexes of halotrifluoromethanes and dimethyl ether in cryosolutions are reported as examples in Figures 43 and 44. The new bands appearing in the complexes are marked with asterisks in trace a of each panel; particularly remarkable features include the observation of the ν_3 isotopic doublet close to 350 cm^{-1} in the infrared spectrum of the complex with CF_3Br (Figure 43B), and the weak, blue-shifted ν_6 (C–I) mode visible in the Raman spectrum of the complex with CF_3I (Figure 44C) at 268.4 cm^{-1}.

From the analysis of the shifts reported in Tables 3 and 4, it is evident that shift magnitudes follow the well-known XB strength scale, i.e., I > Br > Cl, and that larger shifts are observed for stronger Lewis bases, with trimethylamine dominating the series of studied compounds. One noteworthy feature is that comparable shifts are observed for dimethyl ether and dimethyl sulfide, at variance with the observation that, in HB, when a sulfur atom substitutes for an oxygen, the interaction is weaker.[421] The importance of inductive effects on the XB acceptor, or donor, can be pinpointed by comparing the shifts obtained for several of the studied adducts. For complexes with alkyl halides, it was clearly shown by the shifts and band intensities that ethyl complexes were more stable than methyl ones. Analogous considerations can be made for XBs involving π-systems, as it could be inferred that complex stability followed the order propene > ethene for alkenes, 2-butyne > propyne > ethyne for alkynes, and toluene > benzene for aromatics.

In these cryogenic studies, complex stoichiometries were determined from the band areas of vibrations in the monomers and complexes. For a complex formation equilibrium

$$mA + nB \leftrightarrows A_mB_n$$

by combining Lambert–Beer's law with the expression of the equilibrium constant, it can be shown that

$$S_{A_mB_n} = C(S_A)^m(S_B)^n$$

where S_Z is the monomer band area for species Z and C is a constant related to the equilibrium constant. Therefore, by plotting $S_{A_mB_n}$ versus the product $(S_A)^x(S_B)^y$ in a series of isothermal studies where concentrations are varied systematically, the stoichiometric coefficients can be found by evaluating the linearity observed for different integer values of x and y.

In the series of experiments reported above, 1:1 stoichiometries were generally found. However, for dimethyl sulfide, propene, 2-butyne, and benzene, coordination with two

DOI: 10.1021/acs.chemrev.5b00484
Chem. Rev. 2016, 116, 2478–2601

Table 3. Experimental Frequencies of the Fundamental Vibrational Modes of CF_3−X (X = I, Br, Cl) in Liquid Argon (89 K) and Shifts Recorded upon Complexation with Different Lewis Bases in Various Cryogenic Solutions[a]

		Δν						
	free[b]	Me_3N[c]	Me_2O[b]	Me_2S[d]	MeF[e]	MeCl[e]	EtF[e]	EtCl[e]
				CF_3I				
ν_1	1068.9	+15.1	+11.4	+8.9	+5.5	+3.4	+6.1	+3.1
ν_2	741.3	−10.7	−4.1	−6.5	−1.3	−1.3	−2.0	−1.7
ν_3	286.4[b]	−18.1	−2.3[b]	−12.0	+0.8	−1.0	+0.6	−1.2
ν_4	1177.3	−32.9	−18.8	−19.5	−8.8	−7.1	−10.3	−8.2
ν_5	539.8			−1.3				
ν_6	266.2[b]		+2.2[b]	−0.2	+2.2		+1.7	+1.2
				CF_3Br				
ν_1	1077.1	+5.1	+7.4	+3.8	+4.5		+4.9	+2.8
ν_2	759.9	−8.4	−3.0	−3.8	−1.0	−0.8	−0.9	−1.0
ν_3	350.2/348.5[b]	−14.9/−14.4	−1.1/−1.1[b]	−7.8/−6.0	+1.3/+1.3	−0.1/−0.2	+1.5/+1.4	−0.2/−0.3
ν_4	1199.7	−22.2	−13.8	−11.1	−6.6	−4.3	−7.7	−5.2
ν_5	546.7		−1.3	−1.2	−0.5	−0.2	−0.5	−0.6
ν_6	301.3[b]		+2.6[b]	+1.4			+1.8	
				CF_3Cl				
ν_1	1099.4	+8.1	+7.0					
ν_2	781.0	−4.5	−1.0					
ν_3	476.3/468.4	−3.9/−3.9	+2.0/+2.0					
ν_4	1208.0	−13.8	−10.6					
ν_5	561.2		−0.8					
ν_6	348.1							

[a]All shifts are calculated from the FTIR and Raman spectra of the free and complexed CF_3−X recorded at the same temperatures. Frequencies and shifts are reported in inverse centimeters. [b]Reference 410. Measurements performed in liquid Ar (89 K). For CF_3I and CF_3Br (both free and in complex with DME), ν_3 and ν_6 were obtained in liquid Kr (123 K). [c]Reference 409. Measurements performed in different cryosolutions: for CF_3I in liquid Xe (173 K), for CF_3Br in liquid Kr (123 K), for CF_3Cl in liquid Ar (96K). [d]Reference 411. Measurements performed in liquid Kr (123 K). For mixed solutions of CF_3Cl and dimethyl sulfide, no features suggesting the formation of a complex were detected. This is not surprising when considering that the complexes of the same Lewis acid with dimethyl ether and trimethylamine could be observed only at the lower temperatures provided by the use of liquid Ar. [e]Reference 412. Measurements performed in liquid Kr (123 K).

Table 4. Experimental Frequency Shifts of the Fundamental Vibrational Modes of CF_3−X (X = I, Br, Cl) upon Complexation with π-Systems in Various Cryogenic Solutions[a]

	Δν						
	C═C[b]	C═CC[b]	C≡C[c]	C≡CC[c]	CC≡CC[c]	benzene[d]	toluene[d]
				CF_3I			
ν_1	+4.8	+4.9		+7.1	+8.1	+2.7	+3.1
ν_2	−1.8	−2.4		−1.8	−3.0		−2.1
ν_3	−2.6	−3.6		−2.7	−3.4	−0.8	−1.3
ν_4	−7.9	−10.0	−6.8	−10.0	−12.4	−10.3	−10.8
ν_5	−0.2	+0.7	−1.1	+0.5	−0.8		
ν_6	+0.4	+0.6					
				CF_3Br			
ν_1	+2.0	+2.2		+3.4	+3.9		
ν_2	−1.1	−1.7		−1.4	−2.3	−0.8	−1.4
ν_3	−1.0	−1.7				−0.1	−0.6
ν_4	−4.4	−6.0		−6.8	−8.7	−7.7	−8.3
ν_5	−0.9	−0.5		−0.2	−0.5		
ν_6	+0.5	+0.5					

[a]All shifts are calculated from the FTIR and Raman spectra of the free and complexed CF_3−X recorded at the same temperatures. Frequencies and shifts are reported in inverse centimeters. Alkenes and alkynes are identified by their carbon atoms and multiple bonds. [b]Reference 358. The experimental data refer to a solution in liquid Ar (93 K). No features suggesting the formation of complexes with CF_3Cl were detected, suggesting that the complexes are too weak to be observed. [c]Reference 414. Measurements performed in liquid Kr (120 K). No features suggesting the formation of complexes with CF_3Cl were detected, suggesting that the complexes are too weak to be observed at this temperature. For the solutions containing ethyne, weak spectral features illustrating the occurrence of halogen-bonded complexes were observed only with CF_3I. [d]Reference 413. Measurements performed in liquid Kr (120 K). No features suggesting the formation of complexes with CF_3Cl were detected, suggesting that the complexes are too weak to be observed at this temperature.

CF_3−I molecules could also be observed at lower temperatures and higher XB donor concentrations.

By performing measurements at variable temperature, the complexation enthalpy could also be determined from the van't

DOI: 10.1021/acs.chemrev.5b00484
Chem. Rev. 2016, 116, 2478−2601

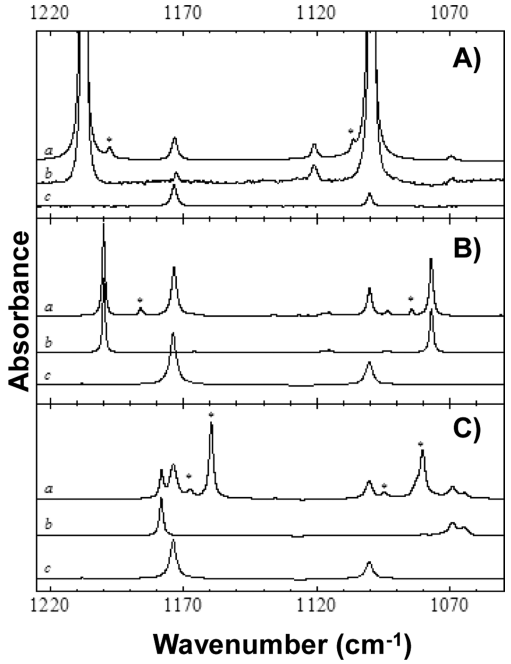

Figure 43. Infrared spectra in the 1225−1050 cm^{-1} region for solutions of mixtures of CF_3Cl (A), CF_3Br (B), and CF_3I (C) with dimethyl ether dissolved in liquid Ar (89 K). Tracs a in each panel represents the spectrum of the mixed solutions, while traces b and c are the spectra of the monomers CF_3X and dimethyl ether, respectively. The new bands assigned to the complex are marked with an asterisk. Reprinted with permission from ref 410. Copyright 2013 John Wiley & Sons, Inc.

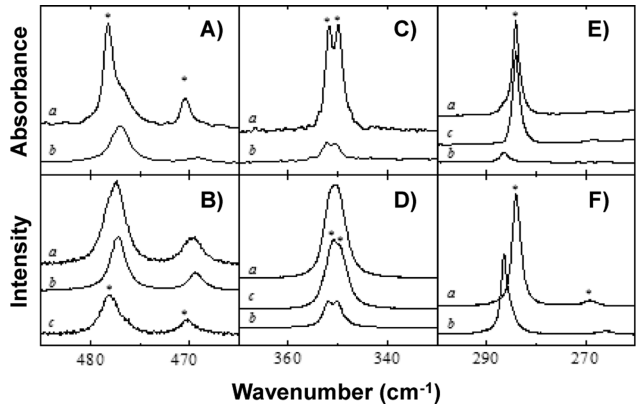

Figure 44. Infrared (A, C, and E) and Raman (B, D, and F) spectra of the $\nu_3(CF_3X)$ region for solutions of mixtures of CF_3Cl (A, B), CF_3Br (C, D), and CF_3I (E, F) with dimethyl ether dissolved in liquid Ar (89 K). Trace a represents the spectrum of the mixed solution, trace b is the spectrum of the monomer CF_3X, and trace c is the spectrum of the complex, obtained by subtracting trace b from trace a. The new bands assigned to the complex are marked with an asterisk. Reprinted with permission from ref 410. Copyright 2013 John Wiley & Sons, Inc.

Hoff plot of the logarithm of the complex:monomer intensity ratio versus the inverse of the temperature, according to the following equation:[417]

$$\ln\left[\frac{I_{A_mB_n}}{I_A^m I_B^n}\right] = -\left[\frac{\Delta H^\circ + (n+m-1)Rb}{R}\right]\frac{1}{T} - (\text{constant}+a)$$

where a and b are temperature-independent constants which define the dependency of the cryosolvent density on the temperature and R is the ideal gas constant.

Finally, in more recent times FTIR and Raman investigations in cryogenic solutions were mostly focused on the evaluation of systems with competing interactions. A series of systematic studies were performed using halothane ($CF_3CBrClH$) as an example of a Lewis acid containing both hydrogen and halogen bond donor sites;[421−425] in all cases, however, only hydrogen-bonded species were found. Conversely, when iododifluoromethane (CHF_2I) was used as a Lewis acid, hydrogen- and halogen-bonded complexes were simultaneously observed with trimethylamine and dimethyl ether, whereas only HBs formed with methyl fluoride.[426] The competition between XB and lone pair···π interactions involving an electron-poor double bond was examined by studying the complexes of C_2F_3−X (X = F, Cl, Br, I) with dimethyl ether.[427] Interestingly, only the halogen-bonded and lone pair···π complexes were observed, respectively, for X = I and X = F, while mixtures of both were found in the other cases.

2.2.3. Nuclear Magnetic and Quadrupolar Resonance Spectroscopies. Nuclear magnetic resonance (NMR) spectroscopy has been used extensively to assess the presence of XBs and to study the XB features usually in solution; it is also one of the methods of choice for investigatiing the nature of XB. NMR parameters such as chemical shifts and coupling constants can yield a wealth of information regarding the occurrence, thermodynamics, and local structure of XBs.

Similar to vibrational spectroscopy investigations, and in many cases presented together with them as a complementary characterization technique, the earliest NMR studies on XB typically regarded dihalogen and pseudohalogen complexes with nitrogen Lewis bases. Solutions of I_2 and dimethylpropionamide in CCl_4 showed spectral changes similar to those observed for dimethylacetamide in aqueous HCl,[428] thus suggesting a similarity between interactions occurring in the two systems. In particular, a broadening of the methyl signals was observed at increased iodine concentration and for dimethylacetamide at low pH values. The thermodynamic parameters and lifetimes of complexes of I_2 with *para*-substituted phenyl methyl sulfides[429] and 2,4,6-trimethylpyridine[430] were calculated from ^1H NMR shifts of the methyl groups at variable temperature. It was demonstrated that I_2··· Lewis base association is influenced by inductive effects and both ionic and nonionic complexes exist with trimethylpyridine (inner and outer complexes after Muilliken's terminology). The ionic form was found to be favored in the more polar environment offered by nitromethane in comparison to CCl_4. Two shifted peaks with increasing intensity at higher I_2 concentration were observed, and these peaks became broader and weaker at higher temperatures. A similar study of complexes of CF_3−I with trimethylpyridine[431] showed that this haloalkane forms complexes weaker than I_2, association ΔH values being −5.0 and −7.8 kcal/mol for CF_3I and I_2, respectively.

A ^1H and ^{13}C NMR study on complexes of I_2 and ClI with a series of pyridyl compounds (Figure 45) evidenced the formation of three species, i.e., a halogen-bonded complex, X−I···Py, an *N*-iodopyridinium salt, Py−$I^+\cdot[X_nI_{n-1}]^-$, and an *N*-iododipyridinium salt, $Py_2I^+\cdot[X_nI_{n-1}]^-$ (X = I, Cl). The relative proportions of these three species were shown to depend on the Lewis basicity of the pyridine derivatives and the acidity of the iodine atom, on the solvent polarity, and on the

DOI: 10.1021/acs.chemrev.5b00484
Chem. Rev. 2016, 116, 2478−2601

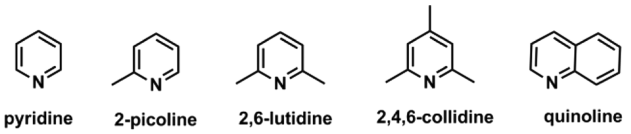

Figure 45. Pyridyl compounds used in the study of Schuster and Roberts.[432]

concentration of the two starting compounds.[432] The ^{13}C shifts of the α-carbons and α-methyl carbons were proposed as useful indicators to identify the nature of the formed species, as they were found to be shielded with respect to the starting base in the monocoordinated iodine(I) complexes, and deshielded in the dicooordinated iodine(I) cations. Conversely, in halogen-bonded complexes shielding was observed for the α-carbons and deshielding for the α-methyl carbons.

Analogous investigations on the ^{1}H NMR spectra of charged dicoordinated iodine(I) and bromine(I) complexes with pyridine, picoline, and lutidine indicated larger deshielding of the pyridine protons in the β and γ positions rather than in the α position, which was attributed to a redistribution of π electron density, the effect being stronger in bromine rather than iodine species.[433]

Further research on dicoordinated halogen(I) systems was carried out by M. Erdelyi's group, who investigated solvent effects on flexible and restrained [bis(pyridine)halogen]$^{+}$ complexes (Figure 46).[434−436] By using Saunder's isotopic

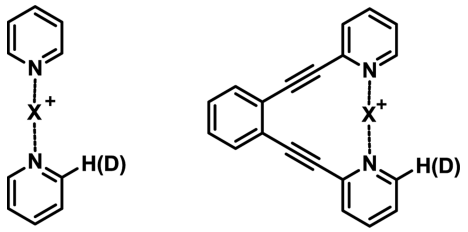

Figure 46. Structure of [bis(pyridine)iodine]$^{+}$ complexes used to study the symmetry of halonium XBs in solution. The bis-(pyridinylethynyl)benzene was exploited to introduce a restraint to the complex geometry.

perturbation technique with ^{13}C NMR and deuterium substitution,[437,438] slightly increased complex stability was observed in higher polarity nonprotic solvents, and it was determined that the charge distribution was unaffected by the solvent polarity, thus suggesting the formation of symmetric three-center−four-electron complexes.

The geometry of dihalogen complexes with nitrogen Lewis bases was also studied by nuclear quadrupole resonance (NQR). This technique allowed for measuring the values of the isomer shift and quadrupole interaction at the ^{129}I nucleus in complexes of BrI and ClI with pyridyl compounds, wherein the presence of a linear X−I···N bond was observed.[439] A dependence of the isomer shift on the base strength could be observed for BrI, but not for ClI.

Recently, ^{1}H NMR titrations and UV−vis spectra showed that the XB between molecular iodine and tetramethylthiourea is rather insensitive to the nature of the solvent environment, as similar association constants were calculated in media as different as alkanes and alcohols.[440] This may suggest that charge transfer plays a significant role in this system, at variance with HBs where thermodynamic stability is determined by electrostatics.

Moving up from dihalogens in the molecular complexity scale, the presence of hydrogen and carbon atoms in XB donors allowed for using ^{1}H and ^{13}C NMR as tools to gain further insight into the nature of XBs and perform a more direct comparison between HBs and XBs in solution. Complexes of trihalomethanes with tetraalkylammonium salts[441] were studied in acetonitrile and CCl_4 solutions. The shifts observed for CHF_3 and $CHCl_3$ suggested decreased proton shielding and were compatible with HB rather than XB; differently, CHI_3 showed increased shielding, which was explained through an involvement of the iodine rather than the hydrogen atom in interaction formation. This hypothesis was supported by FTIR spectra, which gave evidence for polarization of C−I valence electrons by a nearby anion. $CHBr_3$ was reported to be in a somewhat intermediate situation, where both interactions occur. An increased shielding in ^{1}H NMR spectra was also observed for other complexes of CHI_3 with organic ammonium iodides,[442] and a deshielding effect in the ^{13}C NMR spectra of certain complexes was also observed. This was attributed to concurrent C−I bond lengthening and reduction of the I−C−I angles, which decreases the shielding influence of iodine atoms adjacent to the carbon.

A proton NMR[98] study of the interaction of $CHCl_3$ and $CHBr_3$ with a neutral lone-pair donor (hereinafter n-donor) such as dioctyl ether, dioctyl thioether, and dioctylmethylamine allowed the conclusion that the energies of halogen···n-donor interactions in the studied systems were small, with enthalpies following the order $CHBr_3 > CHCl_3$ and N > O > S. It has to be observed here that the XB enthalpy is determined by the balance of several contributions which are sometimes coherent and sometimes contrasting. As a result, the relative strength of the interactions given by a set of XB acceptors may depend on the used XB donor (and conversely the relative strength of the interactions given by a set of XB donors may depend on the used XB acceptor), or in other words, a scale of XB donors may depend on the used acceptor and vice versa. For instance, by using XB donors different from halomethanes, the scale N > S ≥ O was found (see onward) as the difference in the strength of the XBs given by sulfur and oxygen sites is usually not so large to be independent of the used XB donor and the employed sulfur and oxygen moieties.

A large variety of n-donor solvents showed deviations in the linear dependence of the solvent-induced proton shifts of CHX_3[443] and CH_2X_2[444] (X = I, Br) with respect to $CHCl_3$ and CH_2Cl_2. These deviations were attributed to XB occurring in competition with HB. For $CHBr_3$, XB was found to occur only to a small extent in chlorocarbon and amine solutions. Conversely, for CHI_3 XB was always clearly visible, increased with solvent basicity, and became predominant in amine solutions. No indication of XB was found for dibromomethane, while in the case of diiodomethane solutions the predominance of one interaction over the other depended on the solvent: XB was found to prevail in amines, while HB was favored in ethers.

Iodoalkynes are a class of well-known and particularly effective XB donors, and their ^{13}C NMR spectra are a sensitive tool to assess the involvement of these iodine atoms in XB formation. The ^{13}C NMR signals of the iodinated carbon in several iodoalkynes were found to correlate with signals in the corresponding hydrogen-terminated alkynes,[445] but deviations were observed as early as 1983 for iodoalkynes possessing electron donor ending groups such as nitrile and ethoxycarbonyl. In 2000 an initial study of the solvent effect on the ^{13}C spectrum of iodoalkynes showed that the resonance of the C−I

DOI: 10.1021/acs.chemrev.5b00484
Chem. Rev. 2016, 116, 2478−2601

carbon was significantly shifted to higher frequencies in electron donor solvents; e.g., a 12−15 ppm shift was observed in DMSO-d_6 with respect to chloroform.[399] These investigations were subsequently extended by performing a wider study with 1-iodo-1-hexyne and diiodoethyne in a variety of solvents[398] (Figure 47). A combination of calculations

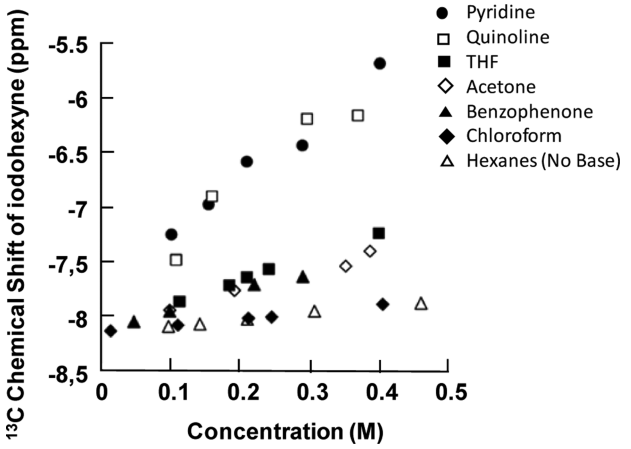

Figure 47. ^{13}C chemical shift of the C−I carbon of 1-iodo-1-hexyne as a function of the concentration of an n-donor compound in hexanes. The concentrations of the iodohexyne and the n-donor were kept approximately equal. Reprinted from ref 398 Copyright 2004 American Chemical Society.

performed with different methods and experimental studies led to the conclusion that this is a result of shielding rather than spin−orbit effects, due to electron donation from the DMSO oxygen to the iodine.[196] It was suggested at first that the alkynyl triple bond would absorb a significant portion of the additional charge and thus bring forth the observed chemical shift changes, but later observations on very similar or even slightly stronger chemical shift changes for the symmetric diiodoacetylene suggested a more complex picture.[398]

Interestingly, DFT and MP2 calculations on ^{13}C NMR shifts of the C−I carbon in complexes of several iodoarenes and iodoacetylene with DMSO suggested that the nonrelativistic complexation shifts and the change in the spin−orbit-induced heavy atom effect of iodine compensate and may cancel each other so that the onset of XB in solution does not necessarily translate into observable ^{13}C NMR shifts.[201]

While ^{1}H and ^{13}C NMR can be highly informative, further data can be obtained by including other nuclei in both NMR and NQR experiments. The use of solvent acceptor numbers (derived by ^{31}P NMR using triethylphosphine oxide as a probe in a series of XB donor solvents) was suggested as a tool to determine the XB strength.[446] DFT calculations were performed to study the effect of HB and XB interactions on NQR[447] and ^{17}O, ^{35}Cl, and ^{1}H NMR[448] parameters by using dichloroacetic acid as a model molecule. On the basis of the quantum theory of atoms in molecules, a partial covalent character was attributed to the O−H···O HBs in dichloroacetic acid, whereas all C−H···O, Cl···O, and Cl···Cl intermolecular contacts were found to be essentially electrostatic in nature.

A combined nuclear Overhauser effect (NOE) NMR/DFT approach based on $^{1}H-^{19}F$ heteronuclear Overhauser effect spectroscopy (HOESY) experiments was employed to discriminate between adducts held together by XB and other noncovalent interactions.[449] The method was tested on complexes of 1-iodoperfluorohexane, iodopentafluorobenzene, and bromopentafluorobenzene with 1,4-diazabicyclo[2.2.2]-octane (DABCO) and trimethylpyridine and allowed for a rough quantification of the occurrence and relative strength of XBs with respect to other interactions.

Whenever fluorine is present in the XB donor, ^{19}F NMR spectroscopy is a particularly powerful and selective tool to study halogen-bonded complexes thanks to the high sensitivity and wide chemical shift range of the nucleus. One early study reported in 1974 that equimolar liquid mixtures of CF_3I, C_2F_5I, and C_3F_7I with trimethylamine showed significant upfield shifts in the ^{19}F NMR resonances of atoms geminal to the iodines.[405] The shifts increased at lower temperatures, thus suggesting a corresponding rise in the concentration of complexed species. When complexation of C_3F_7I was studied with other amines, the magnitude of the ^{19}F NMR shifts changes followed the order NMe_3 > NEt_3 > NPr_3 > NH_3, and this scale was considered the result of a combination of steric effects and ionization potentials.

It was however in the late 1990s that Metrangolo, Resnati, and co-workers reported the first comprehensive series of solution NMR studies[10,28,191] of complexes formed by haloperfluoroalkanes with a variety of Lewis bases, including quinuclidine,[190] diamines,[80,88,375,450] and bipyridines,[406] and of complexes formed by haloperfluoroarenes with pyridyl and pyridyl oxide moieties.[28,80,84,406,407] In the first paper of the series, ^{1}H and ^{13}C NMR spectra of the complex between 1-iodoperfluoropropane and quinuclidine[190] showed chemical shift variations suggesting the onset of a specific interaction. A 7 ppm upfield shift was found in the ^{14}N NMR spectrum for the complex, accompanied by a significant line broadening indicative of an increased quadrupolar relaxation associated with the N···I bond formation. The upfield shifts of $-CF_2-$ resonances in the ^{19}F NMR spectra decreased with increasing distance from the iodine atom and varied significantly with the iodide:amine ratio. A single signal was always observed

Table 5. ^{19}F NMR Chemical Shifts of $-CF_2X$ for 1,2-Dihaloperfluoroethanes in Solvents Having Different n-Donor Abilities

solvent	$I(CF_2)_2I$ $\Delta\delta_{CF_2I}$	$Br(CF_2)_2Br$ $\Delta\delta_{CF_2Br}$	solvent	$I(CF_2)_2I$ $\Delta\delta_{CF_2I}$	$Br(CF_2)_2Br$ $\Delta\delta_{CF_2Br}$
piperidine	11.03	2.35	1,3-propanediol	4.10	0.85
N-methylpiperidine	9.69	2.02	1,3-propanedithiol	3.25	0.53
morpholine	10.39	1.90	pyridine	7.12	1.07
N-methylmorpholine	8.19	1.66	furan	0.91	0.08
thiomorpholine	9.74	1.57	thiophene	1.21	0.21
tetrahydrofuran	3.93	0.90	acetone	3.43	0.85
tetrahydrothiophene	5.18	0.71	DMSO	7.02	1.98
3,6-dioxaoctane	3.16	0.92	HMPA	8.03	2.71
3,6-dithiooctane	5.30	0.72	acetonitrile	2.54	0.40

DOI: 10.1021/acs.chemrev.5b00484
Chem. Rev. 2016, 116, 2478−2601

independent of the iodide:amine ratio, indicating the complex formation−dissociation process was rapid on the NMR time scale.

A systematic study of the ^{19}F NMR chemical shift variation of 1-haloperfluoroalkanes, 2-haloperfluoroalkanes, α,ω-dihaloperfluoroalkanes,[190] and 1,4-dihaloperfluorobenzenes in a series of n-donor solvents (Table 5) revealed a few important trends. On the XB donor side, the observed shift changes, namely, the interaction strengths, followed the halogen polarizability scale (I > Br > Cl, no appreciable interaction with F) and increased with the electron-withdrawing ability of the groups close to the heavy halogen, as demonstrated by the larger shift changes observed for 2-iodoperfluorobutane in comparison to 1-iodoperfluorobutane. On the XB acceptor side, the interaction strength varied with the electron donor heteroatom as N > S ≥ O (see an alternative ranking reported above). The presence of electron-withdrawing groups close to the XB acceptor site and a greater percentage of s character in the donated lone pair resulted in weaker complexes. Increased steric hindrance, at either the donor or the acceptor site, disfavored the formation of tightly bound complexes, XB being more sensitive to steric hindrance than HB. Stronger interactions were observed for secondary over primary and tertiary amines, probably as a result of a balance between inductive and steric effects. All these trends were consistent with n → σ^* electron donation.

The scale of XB donor ability mentioned above (I > Br > Cl) was also suggested by an investigation of the ^{19}F NMR deshielding[451] and its temperature coefficients[452] for the complexes that 1-haloperfluorooctanes give with partners having different *n*-electron-donating ability: Strong association was observed for 1-iodoperfluorooctane with acetone, methyl acetate, acetonitrile, and hexanenitrile, only a moderate association was found on interaction of 1-bromoperfluorooctane with *N*-methylpyrrolidine, and no evidence for association could be observed for 1-chloroperfluorooctane.

^{1}H, ^{19}F, and ^{31}P NMR spectroscopies have been used to study the complexation of 1-iodoperfluorohexane with eight Lewis bases in benzene, CCl_4, and chloroform. The study suggested that XBs have many similarities with HBs and that both interactions can be treated, at least in a first approximation, by using a simple electrostatic solvent competition model.[453] However, complexes involving cyclic amines, such as DABCO and quinuclidine, had significantly higher stability than predicted by the electrostatic model, possibly due to charge-transfer effects.

A purely electrostatic model was also shown to incur significant limitations (when faced with solvent effects and with tectons having a wide set of donor and acceptor abilities) by a systematic ^{19}F NMR titration study of the complex formation between a variety of electron donors and iodoperfluoroalkanes or *para*-substituted iodoperfluoroarenes.[454] The complex association constants were determined, and a linear free energy relationship was found with both empirically derived substituent parameters and calculated molecular electrostatic potentials for several commonly employed XB donors and acceptors (Figure 48). On the other hand, DFT-calculated binding constants yielded moderate correlations with all experimental data, except for the strongly bound couples iodoperfluoroalkane−quinuclidine. This study also highlighted that solvents forming HBs are detrimental to XB formation in solution and that Lewis basic solvents compete with trimethylamine for XBs in a less efficient manner than expected on the basis of a purely electrostatic approach. Once again, it seems

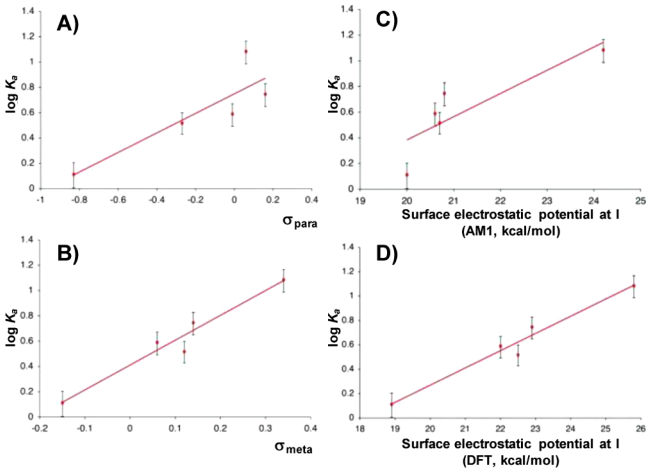

Figure 48. Correlation of the log K_a for the halogen-bonded adducts 4-X-C_6F_4—I···O═PBu_3 with the (A) σ_{para} and (B) σ_{meta} substituent constants of X and with the electrostatic potential at the iodine atom, calculated with the (C) AM1 and (D) DFT (B3LYP/6-31+G**-LANLdp) computational methods. Adapted from ref 454. Copyright 2010 American Chemical Society.

that HBs and XBs possess consistent similarities but also subtle differences.

As described in greater detail in the FTIR/Raman section, evidence for self-halogen bonding of both 1- and 2-iodoheptafluoropropane in cyclohexane was obtained by dilution FTIR and ^{19}F NMR studies. In agreement with most published literature, larger C−I···N association constants were observed in less polar solvents.[408] It should be noted however that remarkable differences can be found even among nonpolar solvents. Considerably stronger C−I···F interaction was found in heptane than in toluene when the complex of iodopentafluorobenzene with *trans*-(tetrafluoropyrid-2-yl)bis(triethylphosphine)fluoronickel(II) was studied.[455] The difference as large as almost 1 order of magnitude between the two K_a values was explained here with a competing π stacking effect in the aromatic solvent, which could weaken the apparent bond strength. Indeed, the π-system of haloperfluoroarenes can also receive electron density from the heteroatoms of solvents such as methanol, dimethyl sulfoxide, acetonitrile, and acetone;[456] this interaction can be even stronger than XBs involving bromo- and chloropentafluorobenzene, and may also have significant effects on the NMR chemical shifts for iodopentafluorobenzene. 1,2-Aryldiyne-linked haloperfluoroarenes and pyridyl moieties were used as a model system to study intramolecular XBs without the influence of entropy effects.[457] The observed ^{19}F NMR chemical shifts were solvent dependent and decreased according to the order cyclohexane > toluene > benzene > dichloromethane > acetone > pyridine. ^{15}N NMR and ^{13}C NMR signals were also investigated in this study, and their nonminor changes afforded useful information.

^{19}F NMR studies on haloperfluoroarenes were also performed as a part of investigations on XB-based anion receptors, and provided valuable information on negatively charged halogen-bonded complexes. Studies on systems employing halide anions as Lewis bases[458] indicated that the affinity of complexes with iodoperfluoroarenes in acetone followed the anion charge density order Cl^- > Br^- > I^-; this scale was also recently confirmed for a different set of anion receptors based on halo-1,2,3-triazoliums.[459] The reverse order was found by P. Beer for analogous interactions in a mixture of

DOI: 10.1021/acs.chemrev.5b00484
Chem. Rev. 2016, 116, 2478−2601

chloroform, methanol, and water, this difference being possibly related to the ability of protic solvents to compete with XB[460] (see the discussion reported above on the difficulty of filing a single and general ranking of XB donors and acceptors).

In comparison to solution NMR spectroscopy, solid-state NMR (SSNMR) offers the advantage to eliminate possible solvent effects on the chemical shifts of halogen-bonded complexes, without requiring long-range crystalline order as is the case for some other solid-state techniques (e.g., X-ray). Unfortunately, crystal packing can also be influential on the spectral characteristics. Another possible drawback consists in the difficulty of studying directly the XB donor sites. SSNMR spectroscopy of chlorine, bromine, and iodine generally yields very broad patterns because of the large quadrupole moments of their NMR-active isotopes.[461] One direct observation of $^{35/37}$Cl SSNMR was performed recently by D. L. Bryce and F. A. Perras for several chlorinated compounds, which however required an ultrahigh magnetic field and state-of-the art pulse sequences.[462]

Nuclear quadrupole resonance (NQR) can be more informative, thanks to the large quadrupolar interactions of heavier halogen atoms involved in covalent bonds. Already in the early 1970s, the ^{127}I NQR frequencies of α,ω-diiodoperfluoroalkanes were reported to change in complexes with secondary and tertiary amines, and the effect was attributed to charge-transfer phenomena.[463] A series of NQR studies of trihalide ions[372] and complexes of dihalogens with various amines, including 3,5-dibromopyridine,[464] 3,5-dichloropyridine,[465] and trimethylamine,[466] afforded conclusions analogous to those discussed above on the role of charge-transfer phenomena in the formation of complexes.

Direct SSNMR investigation of carbon atoms covalently bound to the heavier halogens is also challenging for several reasons, including residual dipolar broadening caused by the presence of iodine.[461] However, Bryce's group reported ^{13}C cross-polarization (CP)/magic angle spinning (MAS) SSNMR spectra from complexes of diiodotetrafluorobenzene with ammonium and phosphonium halides,[74] where weak C−I signals could be studied. By comparing these data with those obtained from single-crystal X-ray diffraction, it could be demonstrated that the related ^{13}C chemical shift increased along with the C−I distance for different complexes, although a clear correlation could not be derived (Figure 49).

Nearly all reported SSNMR investigations, however, focus on signals belonging to the XB acceptors, which are generally much more easily observed. Another work by Bryce's group reported a systematic study on complexes of thiocyanates and selenocyanates with diiodotetrafluorobenzenes, using ^{77}Se as a more attractive alternative to ^{33}S for SSNMR. A clear indication was obtained of increased chemical shift upon XB formation,[467] and these results were also supported by ^{13}C and ^{15}N spectra for both thio- and selenocyanate adducts. Importantly, analysis of the ^{77}Se chemical shift tensor revealed that XB caused molecular perturbations in the plane perpendicular to the axis of the anion, in accordance with the crystal structures.

More recently, the same authors further extended this approach to iodoperfluorobenzene−triphenylphosphine selenide complexes, demonstrating that ^{77}Se chemical shifts increase with the onset of C—I···Se═P XBs and correlate with the P═Se distance and the interaction strength.[468] Importantly, $J(^{77}\text{Se},^{31}\text{P})$ coupling constants increase in magnitude with the weakening of the XB.

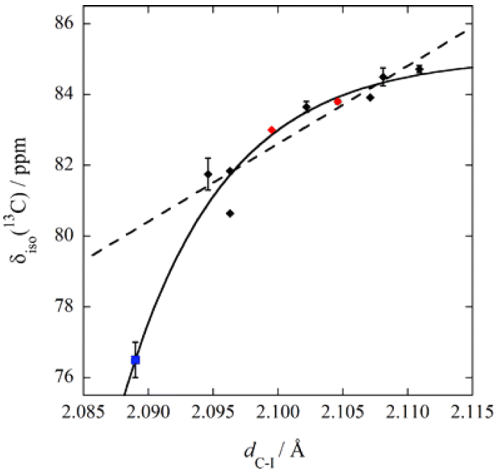

Figure 49. ^{13}C SSNMR chemical shift as a function of the C−I distance for several diiodotetrafluorobenzene complexes with ammonium and phosphonium salts. The solid line represents the best exponential fit, while the dashed line represents a linear fit. Reproduced with permission from ref 74. Copyright 2013 Royal Society of Chemistry.

Bryce and co-workers also investigated haloanilinium halides, recording ^{35}Cl, ^{81}Br, and ^{127}I SSNMR spectra of the halide acceptors.[469] They derived information on space group packing of the compounds from quadrupolar data, and observed that for several compounds of the series the bromine isotropic chemical shift and the chemical shift tensor span increased for shorter halogen−bromide distance. In another recent work, the same authors used multinuclear SSNMR to study complexes of decamethonium diiodides with hydrogenated and perfluorinated *p*-dihalobenzenes, and found a systematic decrease in the ^{14}N quadrupolar coupling constant upon XB formation.[470]

The slight differences observed in the ^{15}N chemical shifts of complexes between 1-(2,3,3-triiodoallyl)imidazole and morpholinium iodide, morpholine, imidazole, and 1-(3-iodopropargyl)imidazole were attributed to XBs with varying strength.[471]

The ^{13}C and ^{15}N SSNMR analysis of halogen-bonded complexes involving nitrogen electron donors has been reported in a fair number of works. One early report is that of J. K. Kochi and co-workers, who studied the interaction between tetrahalomethanes and several amines and found a slightly higher chemical shift when DABCO was halogen bonded to CBr_4.[472]

CP/MAS ^{13}C NMR was also employed to characterize halogen-bonded polymeric systems obtained by interaction of poly(4-vinylpyridine) and α,ω-diiodoperfluoroalkanes.[473] In this case, the signals of the carbon atoms in the *para* position of the pyridyl ring were observed to undergo a clear line broadening.

Evidence for self-halogen bonding was also observed through SSNMR, as reported in studies of benzylbis(4-iodobenzyl)-amine,[474] *C*-aryl-4-halo-1*H*-pyrazoles,[475] and itraconazole in a cocrystal with succinic acid.[476]

Pharmaceutical cocrystals of the antimicrobial 3-iodo-2-propynyl-*N*-butylcarbamate with $CaCl_2$, tetra-*n*-butylammonium iodide, and dipyridyl compounds were investigated by Metrangolo, Resnati, Chierotti, and co-workers through ^{1}H MAS and combined rotation and multiple-pulse spectroscopy (CRAMPS), ^{13}C and ^{15}N CP/MAS, and NQS spectral editing.[477] Larger ^{13}C shifts were observed for complexes

DOI: 10.1021/acs.chemrev.5b00484
Chem. Rev. 2016, 116, 2478−2601

featuring I···N rather than I···X$^-$ interactions, although the shifts could not be directly correlated to the XB strength due to the different crystalline environments experienced by the C≡C—I moiety. A low-frequency shift was observed in ^{15}N spectra when pyridyl derivatives were used as XB acceptors.

Another system comprising an iodoalkynyl XB donor was studied as a part of ultrafast rotors with a potential use as crystalline molecular machines. The authors characterized their systems by ^{1}H wide-line and ^{13}C CP/MAS SSNMR, and used the ^{1}H spin−lattice relaxation and second moment as a function of temperature to investigate the rotation dynamics.

Finally, ^{31}P SSNMR can also be a useful tool to characterize certain halogen-bonded structures.[478,479] The examination of diiodophosphoranes by ^{31}P SSNMR suggested a molecular four-coordinate R_3P−I−I structure for these compounds, rather than a five-coordinate trigonal bipyramidal structure.

2.2.4. X-ray Diffraction Techniques. Single-crystal X-ray analysis affords detailed information on the geometrical features of single molecules and their relative arrangement in the crystal. It is thus no surprise the technique played a key role from the very beginning in the identification of the ability of halogen atoms to attractively interact with electron donor species. O. Hassel reported the infinite chains wherein Br_2 alternates with dioxane[56] or benzene[58,59] as early as 1954 and 1958, respectively. As outlined, among others,[57,64] in his Nobel Lecture,[15] the technique was central in Hassel's studies on adducts which are now understood as halogen-bonded systems, and Hassel's fruitful use of X-ray structural characterization of halogen-bonded adducts went on until the 1970s.[480] Structural studies based on single-crystal X-ray analyses were once again crucial in the "rediscovery" of the XB, which occurred in the late 1990s, specifically when P. Metrangolo and G. Resnati developed XB-based crystal engineering and proved that iodoperfluorocarbons are particularly versatile and effective XB donors.[10,63,69,70,481−483] Also other X-ray techniques (e.g., small-angle X-ray scattering, SAXS)[484] were used to study halogen-bonded systems, and powder X-ray diffraction (PXRD) was by far the most frequently and profitably employed.[83,477,485−489]

The XB donor···XB acceptor separation and the angle between the covalent and noncovalent bonds around the halogen atom are two pieces of structural information afforded by single-crystal X-ray analyses and routinely used to assess the XB presence. Notwithstanding influences from the overall crystal packing, the stronger the XB, the shorter the separation and the more linear the angle.[490,491] The R−X bond dinstance is a more subtle but equally informative indication of XB which is afforded by X-ray analyses. This distance is typically longer in the halogen-bonded adduct than in the pure XB donor,[84] and this lengthening has been associated with the n → σ^* character of the XB. X-ray analyses also afford relevant information on the XB acceptor, and extensive confirmations are available in the CSD that the σ-hole on the electrophilic halogen atom enters preferentially along the axis of the lone pair of an n-donor of electron density and along the local symmetry axis of a π orbital when double or triple bonds or aromatic systems are the electron density donors. In these latter cases it was occasionally possible to distinguish among over-the-ring, over-the-bond,[54,60] and over-the-atom arrangements.[492] These and other information afforded by X-ray analyses allow a ranking of XB donor sites (I > Br > Cl > F) parallel to those suggested by vibrational, IR, Raman, NMR, and NQR spectroscopies and discussed in previous sections. When X-ray techniques are used, also the steric and electronic effects that residues close to the XB donor and acceptor sites have on the energetic and geometric features of the interaction are recognized in close analogy with effects identified through the technicques mentioned above.

For these reasons, in the remaining part of this section, rather than using crystalline structures to exemplify and confirm all these XB features, we will itemize and discuss some crystalline structures with the aim of filing an inventory of the most commonly used XB donor and acceptor moieties.[9,493] X-ray figures in this section are ball-and-stick representations prepared with Mercury 3.5, and XBs have been indicated both with solid lines (as covalent bonds) and with dotted lines in relation to their length. CSD Refcodes are given, and the numbers reported close to these lines are the "normalized contact" (N_c) values, defined as the ratio $D_{xy}/(r_{X_x} + r_{Y_y})$, where D_{xy} is the experimental distance between the XB donor atom X and the XB acceptor atom Y and r_{X_x} and r_{Y_y} are the corresponding vdW radius for the XB donor and vdW radius, or Pauling ionic radius, for the neutral or anionic XB acceptor, respectively. N_c is a useful indicator of the interaction strength, more useful than the XB distance itself, because it allows distances between different interacting sites to be compared.

2.2.4.1. Inventory of XB Donor Moieties. Dihalogens and interhalogens (e.g., I_2,[494] BrI,[495] ClI,[496] Br_2,[497] Cl_2,[498,499] and ClF[498]), as well as pseudohalogens (e.g., NC−I),[500,501] have been extensively involved in adduct formation with lone-pair-possessing (Figure 50) and anionic (Figure 51) XB acceptors. For instance, I_3^- is probably one of the most frequently occurring halogen-bonded motifs in the CSD (355 entries in ConQuest 1.17), and many other polyiodides adopting the

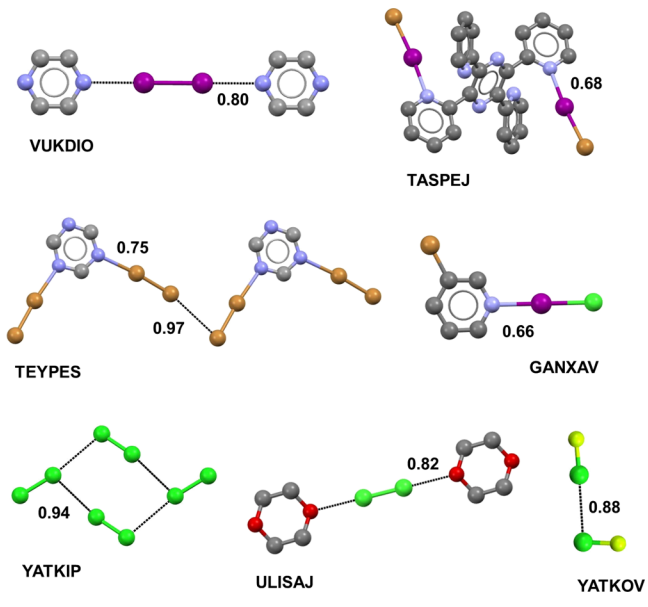

Figure 50. Representation of halogen-bonded crystal structures involving I_2 (VUKDIO), BrI (TASPEJ), Br_2 (TEYPES), ClI (GANXAV), Cl_2 (YATKIP and ULISAJ), and FCl (YATKOV). XBs are represented as solid lines, similar to covalent bonds, when their length is as short as a covalent bond, or as dotted black lines, when their length is close to the sum of the vdW radii of the involved atoms. Hydrogen atoms are omitted for clarity. Color code: carbon, gray; nitrogen, blue; oxygen, red; iodine, purple; bromine, light brown; chlorine, light green, fluorine, yellow. CSD Refcodes are reported.

DOI: 10.1021/acs.chemrev.5b00484
Chem. Rev. 2016, 116, 2478−2601

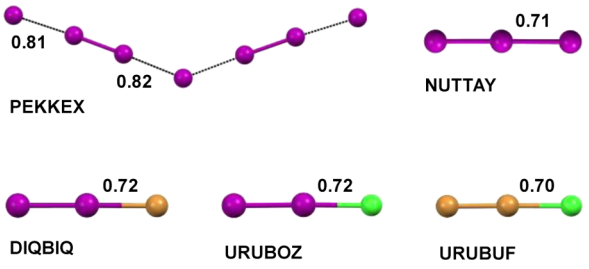

Figure 51. Representation of halogen-bonded crystal structures involving dihalogen molecules as XB donors and anionic XB acceptors. XBs are represented as solid lines, similar to covalent bonds, when their length is as short as a covalent bond, or as dotted black lines, when their length is close to the sum of the vdW and Pauling radii of the involved species. Cations are omitted for clarity. Color code: iodine, purple; bromine, light brown; chlorine, light green. CSD Refcodes are reported.

convenient geometric requirements are commonly recurring XB systems. When interacting with weak XB acceptors, halogens and interhalogens can work as mono- or bidentate XB donors; when interacting with strong acceptors, the nonminor charge transfer to the donor makes the σ-hole on the noninteracting halogen less positive, and the entrance of a second acceptor becomes exceptional.[171,494,502] When interhalogens function as monodentate donors, the heavier halogen, hosting the more positive σ-hole, is preferentially involved in XB formation.

Many structures in the CSD show XBs involving halogen atoms bound to an sp^3-hybridized carbon atom, especially if they are close to strong electron-withdrawing residues or in a polyhalogenated moiety (Figure 52).

Similar to the inclusion in crystals of hydroxylic solvents (e.g., water and alcohols), which is favored by the HBs the solvents form with HB acceptor sites in the crystallized molecule, the inclusion and tight binding of halogenated solvents is favored whenever XB acceptor sites are present in the crystal components. Many solvates wherein $CHCl_3$ and CH_2Cl_2[503−523] or, less frequently, CCl_4 and CCl_2CCl_2[524,525] are halogen-bonded to a variety of anions have been obtained serendipitously. The same holds for solvated systems wherein a lone-pair-possessing XB donor pins the halocarbon. In these systems, the inherent ability of anions and n-donors to function as XB acceptors works synergistically with the need to fill potential voids of the crystal packing, and the formation of supramolecular and halogen-bonded anions or neutral adducts results (Figure 53).

CBr_4[472,526,527] and $CHBr_3$[54,105,267,526] are better XB donors (namely, they give adducts with smaller N_c values) than analogous chlorinated methanes and have been systematically used, among others, by J. K. Kochi for studies both in the solid state and in solution. CHI_3[528] is an even better donor, and adducts with both neutral and anionic Lewis bases are available in the CSD: Interestingly, in the same database no cocrystal can be found wherein CI_4[529] is the donor, possibly due to the high reactivity of the compound with electron donor species. The engineered use of CH_2X_2 and CH_3X (X = Cl, Br, I) as reliable XB donor tectons is virtually undocumented in the solid state, consistent with the fact that with nucleophiles these compounds tend to afford S_N-type products rather than halogen-bonded adducts. The same holds for RCH_2X molecules unless the R residue has a strong electron-withdrawing ability (e.g., CN and CO substituents).[530,531]

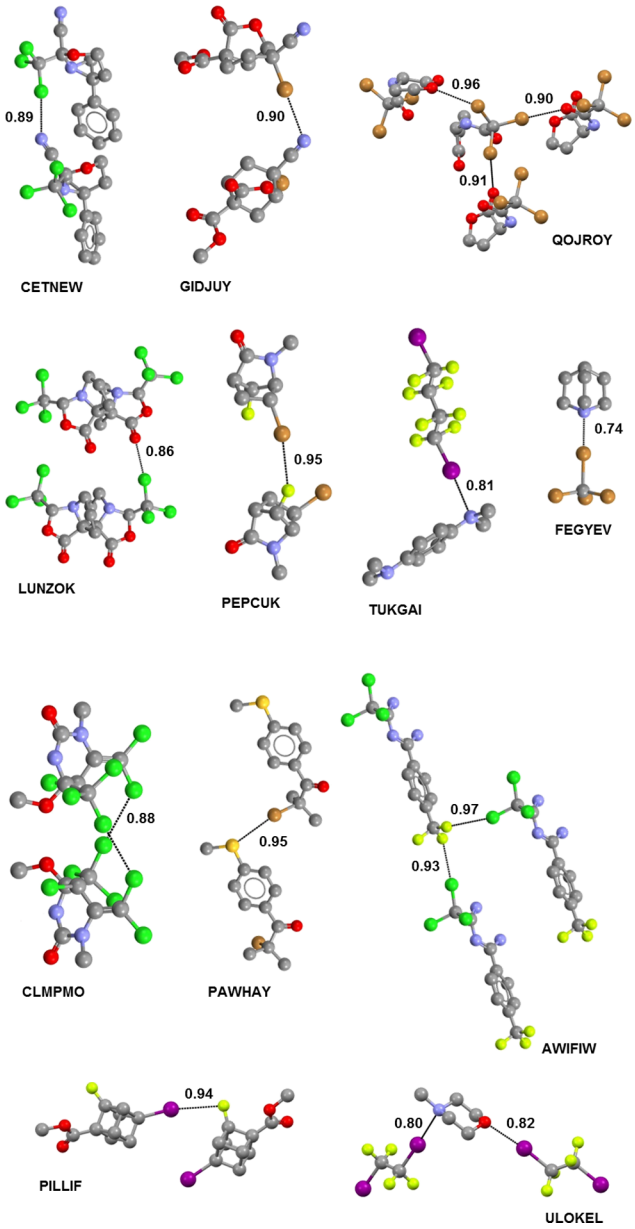

Figure 52. Library of halogen-bonded cocrystals involving haloalkanes as XB donors. Color code: carbon, gray; nitrogen, blue; oxygen, red; iodine, purple; sulfur, dark yellow; chlorine, light green; fluorine, yellow. XBs are dotted black lines. Hydrogen atoms are omitted for clarity. CSD Refcodes are reported: CETNEW, (2*R*,6*S*)-6-phenyl-2-(trichloromethyl)-3-oxa-1-azabicyclo[4.1.0]heptane-2-carbonitrile; GIDJUY, methyl 4-bromo-4-cyano-6-oxabicyclo(3.2.1)octan-7-one-1-carboxylate; QOJROY, *N*-tribromoacetylhomoserine lactone; LUNZOK, 3,3′-bis(trichloromethyl)tetrahydro-5*H*,5′*H*-7a,7a′-bipyrrolo-[1,2-*c*][1,3]oxazole-1,1′-dione; PEPCUK, 6-bromo-7-fluoro-2-methyl-2-azabicyclo[2.2.1]heptan-3-one; TUKGAI, *N*,*N*,*N*′,*N*′-tetramethyl-benzene-1,4-diamine−1,4-diiodoperfluorobutane; FEGYEV, quinuclidine carbon tetrabromide; CLMPMO, 5-chloro-6-(dichloromethylene)-4-methoxy-1-methyl-4-(trichloromethyl)hexahydropyrimidin-2-one; PAWHAY, 2-bromo-2-methyl-1-[4-(methylsulfanyl)phenyl]-propan-1-one; AWIFIW, 4-(trifluoromethyl)-*N*′-(2,2,2-trichloroethanimidoyl)benzene-1-carboximidamide; PILLIF, methyl 2-fluoro-4-iodocubane-1-carboxylate; ULOKEL, *N*-methylmorpholine−1,2-diiodotetrafluoroethane.

Indeed, calculations suggest that the σ-hole in these molecules is weakly positive or even negative and becomes more and

DOI: 10.1021/acs.chemrev.5b00484
Chem. Rev. 2016, 116, 2478−2601

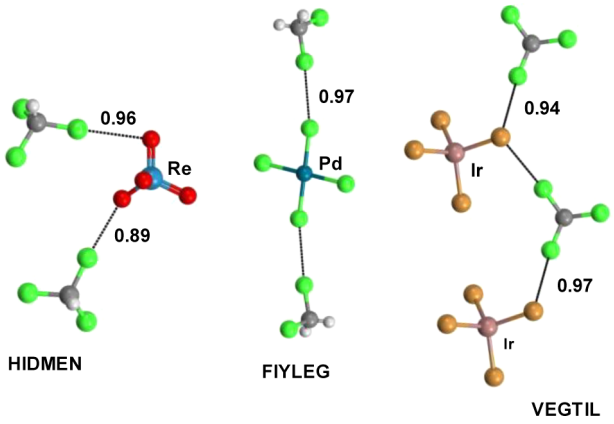

Figure 53. Examples of solvates wherein the chlorinated solvents are pinned by XBs. For the sake of clarity, only the supramolecular anion is reported. Metal atoms are labeled. Color code: carbon, gray; oxygen, red; bromine, light brown; chlorine, light green, hydrogen, white. XBs are dotted black lines. CSD Refcodes are reported: HIDMEN, trichloro(tripyrazolylmethane-*N*,*N*′,*N*″)rhenium(IV) perrhenate chloroform solvate; FIYLEG, [μ_2-1,1′-bis[(1,3-dimethylimidazolidin-2-ylidene)amino]ferrocene]chloropalladium hemi-(tetrachloropalladium) dichloromethane solvate; VEGTIL, [*N*,*N*′-bis(2,6-diisopropylphenyl)triptycenylimidoformamidium]-tetrabromoindium(II) chloroform solvate.

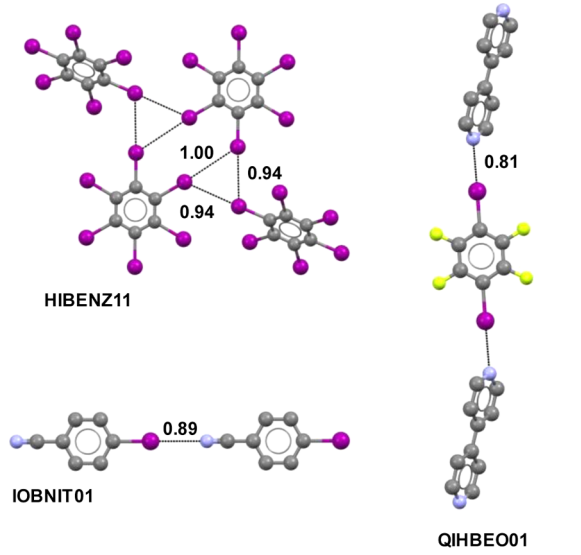

Figure 54. Representation of halogen-bonded crystal structures involving neutral haloarenes and haloperfluoroarenes: HIBENZ11, XB trigonal synthon present in the hexaiodobenzene structure; QIHBEO01, repeating unit in the infinite chain where 4,4′-bipyridine and 1,4-DITFB alternate; IOBNIT01, repeating unit in the 4-iodobenzonitrile infinite chain. Hydrogens are omitted for clarity. Color code: carbon, gray; nitrogen, blue; iodine, purple; fluorine, yellow. XBs are dotted black lines. CSD Refcodes are reported.

more negative, or less positive, if the number of CH_2 units between the electron-withdrawing group R and X increases.

As discussed in previous sections, CF_3I forms fairly strong XBs, and CF_3Br and CF_3Cl give weaker and much weaker adducts, respectively, as confirmed, for instance, through FTIR studies of their complexes with trimethylamine in argon, krypton, and xenon matricxes.[422] However, they have quite low boiling points, and less volatile perfluoroalkanes, namely, C_3 to C_8 analogues, have been preferred over trifluorohalomethanes for obtaining crystalline and halogen-bonded adducts. The CF_3I moiety is present in several hypervalent iodine derivatives (e.g., Togni's reagent, i.e., the electrophilic trifluoromethylating agent 3,3-dimethyl-1-(trifluoromethyl)-1,2-benziodoxole and the carbonyl analogue 1-(trifluoromethyl)-1,2-benziodoxol-3-(1*H*)-one),[532−534] and the bonding pattern around the iodine atom in these compounds can be rationalized as the result of the formation of so strong XBs that they are comparable in length to the other bonds involving iodine.[535]

Monohaloperfluoroalkanes $CF_3(CF_2)_nCF_2X$ (X = I, Br, Cl; *n* = 1,2,4,5,6) have been frequently used in solution studies,[191] but their employment in the obtainment of crystalline systems is occasional.[214,536] Differently, α,ω-diiodoperfluoroalkanes $ICF_2(CF_2)_nCF_2I$ (*n* = 0,2,4,6), and to a lesser extent their brominated analogues,[186,208] have been extensively employed in crystal engineering and gave a major contribution in the "rediscovery" of the XB.[10,28,92]

As for XB donors where the halogen atom is bound to an sp^2 carbon, both haloarenes and haloheteroarenes have been used frequently (Figure 54). Structures reported in the CSD prove that haloarenes having from one up to six XB donor sites[537] have been involved in the formation of adducts so that systems where haloarenes work as mono-,[538] di-,[71] tri-,[539] and polydentate XB donors are all described. For instance, the radical cation of hexaiodobenzene functions as a hexadentate donor forming short and directional XBs with incoming fluorine and oxygen anions.[540] The XB donor ability of the haloarene varies in relation to the number and strength of the electron-donating/withdrawing groups bound to the aromatic moiety and to their relative position respect to the halogen atom. NO_2,[541,542] CN,[194] and halogens[543] are some of the groups more frequently used to enhance the XB donor ability in haloarenes. Unfuctionalized haloarenes have been used occasionally as key tectons in XB-based crystal engineering and, more generally, in supramolecular chemistry, while iodopentafluorobenzene and its derivatives are among the most commonly used XB donor motifs.[10] The availability of general synthetic methodologies[544] to append in high yields a 4-iodotetrafluorophenyl residue onto a hydroxy or amine residue or onto an aromatic ring had an instrumental role in paving the way to such common use. The use of brominated arenes and their (per)fluorinated analogues in crystal engineering is much less common than that of iodoarenes, and when chloroarenes are tested in systematic studies, the obtained structures typically do not show the presence of XBs, while their brominated and iodinated analogues do.

The most commonly used classes of haloheteroarenes are those containing nitrogen atom(s) in the ring. Both neutral and positively charged haloheteroarenes can function as scaffolds for an XB donor site (Figure 55); the cationic form is typically obtained by reacting the neutral form with an alkyl halide or a hydrogen halide, and the released anion works as an XB acceptor for the activated XB donor site.[545] Indeed, for a given halogen and a given heteroaromatic, the cationic form has a much greater XB donor ability than the neutral form thanks to the increased electron-withdrawing ability of the positively charged scaffold. The 5-iodo-1,2,3-triazole moiety[546−549] is a particularly interesting neutral system due to its easy preparation via click chemistry. Its cationic form also has a good XB donor ability and has been recently used in anion recognition processes driven by XB in solution.[550]

Halopyridinium[551−562] and haloimidazolium[563−566] moieties are two other positively charged systems which have been

DOI: 10.1021/acs.chemrev.5b00484
Chem. Rev. 2016, 116, 2478−2601

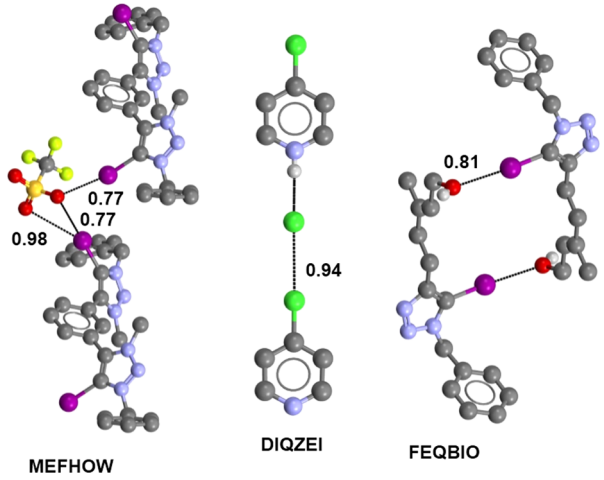

Figure 55. Representation of halogen-bonded crystal structures involving neutral and positively charged haloheteroarenes as XB donors. Hydrogen atoms are omitted for clarity, except for acidic ones in DIQZEI and FEQBIO. Color code: carbon, gray; nitrogen, blue; oxygen, red; iodine, purple; sulfur, dark yellow; chlorine, light green, fluorine, yellow. XBs and HBs are dotted black lines. CSD Refcodes are reported: MEFHOW, trimeric unit present in 5,5′-(1,3-phenylene)bis(3-benzyl-4-iodo-1-methyl-1*H*-1,2,3-triazol-3-ium) bis-(trifluoromethanesulfonate); DIQZEI, repeating unit in the infinite chain formed by 4-chloropyridinium chloride; FEQBIO, dimer formed by 5-(1-benzyl-5-iodo-1*H*-1,2,3-triazol-4-yl)-3-methylpent-2-en-1-ol.

commonly used to study XB via crystallographic techniques, to recognize anions, and to perform chemical catalysis.

The ability of a carbon atom to withdraw electron density from a bound atom increases with the increased s orbital contribution to the atomic orbital used to bind the atom. It is no surprise that halogen atoms bound to an sp carbon atom show particularly positive σ-holes;[209] namely, 1-haloalkynes are particularly strong XB donors and form adducts characterized by quite low N_c values. 1-Iodoalkynes[197,398,399,567−569] have been used much more frequently (Figure 56) than brominated analogues,[209,570,571] and to the best of our knowledge, the

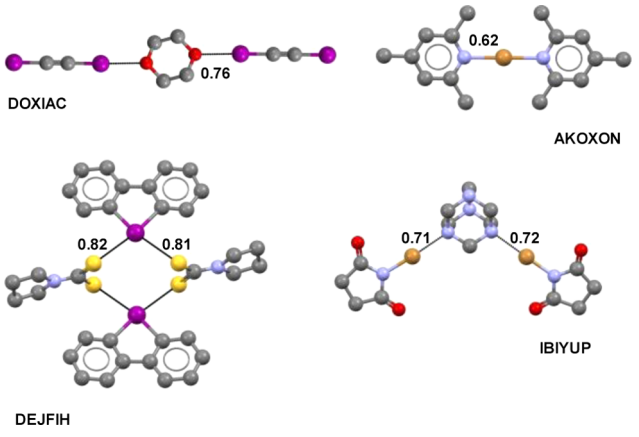

Figure 56. Representation of halogen-bonded crystal structures involving highly polarized halogen atoms. Hydrogen atoms are omitted for clarity. Color code: carbon, gray; nitrogen, blue; oxygen, red; iodine, purple; bromine, light brown; sulfur, dark yellow. XBs are dotted black lines. CSD Refcodes are reported: DOXIAC, 1,4-dioxane and diiodoacetylene; AKOXON, bis(2,4,6-collidine)bromonium perchlorate; DEJFIH, dibenzoiodolyl pyrrolidinedithiocarbamate; IBIYUP, hexamethylenetetramine and *N*-bromosuccinimide.

structures of only two halogen-bonded 1-chloroalkynes are reported.[192,572] The remarkable ability of 1-iodoalkynes to work as XB donors, control the structure of solid architectures, and switch on or tune functional properties has been exploited in the obtainment of supramolecular liquid crystals[573] and organic conductors and magnets.[574−576]

Halonium ions (X^+, X = Cl, Br, I) are the ultimately polarized halogen atoms, and a halonium complex is denoted as $[XY_2]Z$, where X is the XB donor halonium ion (Cl^+, Br^+, or I^+), Y is the XB acceptor, and Z is any anion. Br^+ or I^+ halonium ions have been studied more frequently,[436] and they act as extremely strong XB donors[577] when interacting with several Lewis bases such as nitrogen,[578] sulfur,[579] or selenium[580] atoms. λ^3-Iodanes and -bromanes[581] show bonding patterns which can be rationalized as the formation of halogen-bonded systems, for instance, when an anion and/or a lone-pair-possessing heteroatom enters the σ-hole(s) on the halogen of a diaryliodonium or (aryl)alkynyliodonium salt (Figure 56).[582−594]

In by far the great majority of the described XB donor moieties, the electrophilic halogen is bound to a carbon atom or to another halogen atom, but crystalline structures are also available where the electrophilic halogen is bound to heteroatoms other than halogens, and *N*-haloimides are probably the best known such cases. The electron density on the imide nitrogen is depleted by the two carbonyl residues, and *N*-haloinimides are quite good XB donors and typically form fairly short contacts with XB acceptors (Figure 56).[595−599]

Tetrathiafulvalene (TTF) derivatives are among the most versatile and better known molecules endowed with outstanding redox properties and remarkable electron donor characters. TTFs have been extensively used to prepare organic conductors and magnets. Control of the structure of these materials plays a key role in the functional property optimization, and XB has been used, among other interactions, to fine-tune solid arcitectures and maximize the pursued properties.[576] The first TTF-based complex assembled via XB was reported by T. Imakubo and R. Kato et al.[600] when they described the crystalline structure of 2:1 salts between the cation radical of mono- and diiodinated TFF derivatives (the XB donor) and halide, sulfide, or cianometalate anions (the XB acceptor). The oxidation of the TTF moiety to the cation radical state boosts the σ-hole in the polar region of the iodine and favors the formation of particularly short, and strong, iodine···anion interactions (Figure 57). During the years, several iodine- and bromide-functionalized TTFs[601] and their tetraselena or dithiadiselena analogues have been synthesized, and their single-crystal structures proved they were very efficient XB donors toward different anion systems.[576,602] A few other halogenated radical compounds have been shown to have an XB donor character, among others *p*-iodophenyl nitronyl nitroxide[603] and tribromo-functionalized trioxotriangulene neutral radical (Figure 57).

2.2.4.2. Inventory of XB Acceptor Moieties. When the geometric features of crystalline architectures are determined via X-ray single-crystal analyses, confirmation is obtained that the three most common XB acceptor moieties identified in previous sections, namely, neutral and lone-pair-possessing heteroatoms (n-donors), π-systems (π-donors), and anions, can all work as acceptors in the solid.

Nitrogen functionalities are the most frequently recurring n-donor moieties in molecular crystalline solids. sp^3-hybridized nitrogen atoms in acyclic or cyclic, aliphatic[77] or aromatic[483]

DOI: 10.1021/acs.chemrev.5b00484
Chem. Rev. 2016, 116, 2478−2601

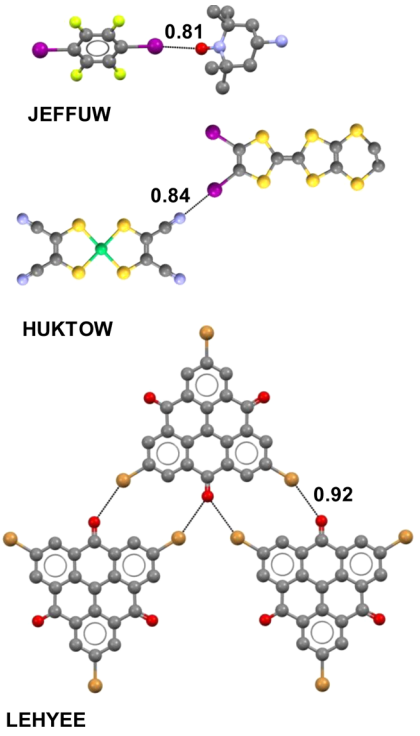

Figure 57. Representation of halogen-bonded crystal structures involving radicals as XB acceptors. Hydrogen atoms are omitted for clarity. Color code: carbon, gray; nitrogen, blue; oxygen, red; iodine, purple; bromine, light brown; sulfur, dark yellow; fluorine, yellow. In HUKTOW, Ni is green. XBs are dotted black lines. CSD Refcodes are reported: JEFFUW, (4-amino-2,2,6,6-tetramethylpiperidin-1-yl)oxy radical, 1,4-DITFB; HUKTOW, bis[3,4-bisiodo-3′,4′-(ethylenedithio)-tetrathiafulvalene) bis(*cis*-1,2-dicyanoethylene-1,2-dithiolato-*S*,*S*′)-nickel; LEHYEE, 2,6,10-tribromo-12-hydroxy-4*H*,8*H*-dibenzo[*cd*,*mn*]-pyrene-4,8-dione.

amines all give small N_c values. Tertiary amines are the XB acceptor in most of the adducts,[197,472,595,604−608] but secondary[77,450,609] and primary[610,611] amines have also been occasionally employed.

Pyridines[612] and pyridine derivatives,[613] pyrimidines,[614] pyrazines,[615] and triazines[616,617] are some of the six-membered nitrogen heterocycles that most frequently afford crystalline and halogen-bonded adducts. sp^2-hybridized nitrogen atoms in five-membered rings (e.g., imidazoles,[618] triazoles,[619] or purines[620]) have been used as XB acceptors less frequently than those in six membered analogues. Also the imine functionality attractively interacts with electrophilic halogens, and the XB is formed along the expected axis of the nitrogen lone pair.[180]

As discussed above, the hybridization state of the halogen-bound carbon influences the XB donor ability of the halogen; similarly, the hybridization state of the nitrogen influences its XB acceptor ability. Also the sp-hybridized nitrogen atom of cyano groups[621,622] works as an XB acceptors, but it tends to be a weaker acceptor than sp^2- and sp^3-hybridized nitrogen atoms. Interestingly, both the π[73] and the sp[622,623] electrons of cyano groups can enter the σ-hole.[573,623−628]

Also the heavier elements of the 15th group of the periodic table, specifically P and As, are shown to function as Lewis bases in halogen-bonded systems where dihalogens are most frequently the XB donor.[629,630] In general, the distribution of the electron density and the bonding pattern in R_3PnX_2 products (R = alkyl, aryl, alkoxy, aryloxy, dialkylamino, etc.; Pn = pnicogen atom; X = Cl, Br, I) can be quite diversified, and three main structural classes can be identified: (i) halogen-bonded adducts (also called charge-transfer or "spoke" adducts in the less recent literature), (ii) ionic halide salts, and (iii) molecular five-coordinate species adopting a trigonal bipyramidal geometry (Figure 58). The pnicogen atom in the first

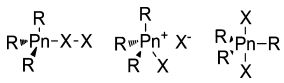

Figure 58. Three main structural types of R_3PnX_2 adducts: the halogen-bonded adduct (left), the phosphonium halide (center), the pentacoordinated addition product (right).

and second classes of compounds has a tetrahedral geometry, and ionic halide salts can be considered products where XBs are so strong that the X−Pn distances are as short as typical "covalent" bonds, and the charge transfer from Pn to X is so remarkable that the heterolytic cleavage of the X−X covalent bonds is enabled and phosphonium halides are formed. The nature of the pnicogen heavily influences the most common structure of the product R_3PnX_2.

sp^3-hybridized neutral oxygen atoms (e.g., those in acyclic[631] and cyclic[77] ethers and alcohols)[632,633] form crystalline adducts with XB donors, but the N_c values are usually larger than those of analogous adducts with sp^3-hybridized neutral nitrogen atoms (e.g., those in amines), consistent with the N > O scale of electron donor abilities identified in previous sections. sp^2-hybridized neutral O atoms (e.g., those in carbonyl,[634] sulfonyl,[635] sulfoxide,[636,637] and phosphonyl[178] groups) can function as XB acceptors (Figure 59). The halogen σ-hole

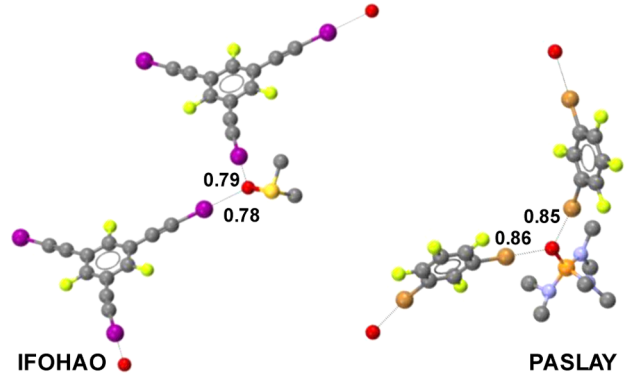

Figure 59. Partial view of the halogen-bonded infinite chains formed by dimethyl sulfoxide with 1,3,5-trifluoro-2,4,6-tris(iodoethynyl)-benzene (IFOHAO) and hexamethylphosphoric triamide with 1,3-dibromotetrafluorobenzene (PASLAY). Hydrogen atoms are omitted for clarity. Color code: carbon, gray; nitrogen, blue; oxygen, red; iodine, purple; bromine, light brown; sulfur, dark yellow; fluorine, yellow. XBs are dotted black lines. CSD Refcodes are reported.

typically enters the oxygen atom along its lone pair axis. Oxygen having more than one lone pair, one or two XBs can be formed; e.g., carbonyl groups may pin one or two halogen atom(s) after a trigonal and planar geometry.[176]

Sulfur atoms can act as XB acceptors, and the R−X···S synthon is quite abundant in the CSD. Halogen-bonded complexes typically involve dihalogens as XB donors and thiols,[148] thioethers,[149] isothiocyanate units,[639] and thione units[640] as acceptors.

DOI: 10.1021/acs.chemrev.5b00484
Chem. Rev. 2016, 116, 2478−2601

Selenium and tellurium analogues of ethers, R_2Ch (Ch = Se, Te; R = alkyl and aryl), are shown to function as electron density donor sites toward an electrophilic halogen, most often a dihalogen. The bonding pattern around the heavy chalcogens recalls that described above for R_3Pn derivatives: Both halogen-bonded systems (also named charge-transfer or "spoke" adducts) and oxidative addition products (having either a see-saw or a T shape) are formed depending on the nature of R, Ch, and the incoming halogen. The heavier the chalcogen, the less favored the formation of the halogen-bonded adducts, but various such systems have been described for both selenium[641] and tellurium.[642]

It is well-known that halogen atoms X in metal halides $M-X_n$ (M = metal; X = Cl, Br, I) can work as HB acceptors,[4,643] consistent with the fact that the low electronegativity of metals boosts the inherent electron donor ability by the halogen. It is thus no surprise that X in $M-X_n$ can funtion as an XB acceptor.[4] In 2005, Brammer et al.[644] demonstrated that the electronic differences between organic (C−X) and inorganic (M−X′) halogen atoms can be exploited in crystal engineering, which enables the C−X···X′−M motif to become a reliable supramolecular synthon. In fact, the metal-bound halogen atom functions as the electron density donor site toward the carbon-bound and electrophilic halogen, and the resulting interaction presents all the electronic and geometric features of a typical XB. Interestingly, for a given XB donor halogen, the N_c value is smaller for the lighter inorganic halogen M−X, thus suggesting that the interaction is stronger.[645]

Also metal hydrides (M−H) are well-established HB acceptors,[646] and recently it has been shown that they can work as XB acceptors too. R. N. Perutz et al.[647] have demonstrated, by solution NMR studies, the formation of halogen-bonded complexes between a serie of bis(η^5-cyclopentadienyl)metal hydrides and iodopentafluorobenzene. The thermodynamic studies showed that the formation of the halogen-bonded complex was energetically favored over the hydrogen-bonded one given by indole.

Electrophilic halogens have formed halogen-bonded crystalline complexes with a variety of π-systems, for instance, double or triple bonds[485,648] (Figure 60) and aromatic (Figure 2) moieties.[649] Adducts in the solid state are similar to those formed in solution, and these latter systems are of particular relevance as they are prereactive states in addition reaction to olefins[62,650] and substitution reactions of aromatics.[651] In principle, any systems possessing π-electrons can work as XB acceptors in the solid state; however, they are involved in the interaction formation only in the absence of other more effective acceptors, e.g., the nitrogen atoms of an amine or a pyridine. This confirms π-systems are less efficient acceptors than most lone-pair-possessing heteroatoms, probably due to the minor localization of the electron density in π-clouds.

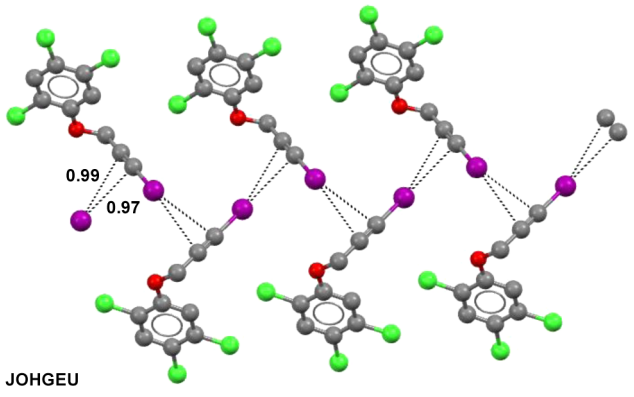

Figure 60. Partial view of the infine chain formed by XBs between iodine atoms and the π-electrons of the triple bonds in one of the polymorphs of haloprogin, the active pharmaceutical ingredient used in antimycotic topical drugs. Hydrogens are omitted for clarity. Color code: carbon, gray; nitrogen, blue; oxygen, red; iodine, purple; chlorine, light green. XBs are dotted black lines. The CSD Refcode is reported.

Several anionic species work as effective XB acceptors, and some anion classes, e.g., halides, halometalates, and cyanometalates, have been extensively used in the anion-driven self-assembly of a wide diversity of XB donors, for instance, iodoperfluorocarbons and 1-iodoalkynes.[69,154,491,652] Under common conditions, HB and XB are competing interactions in driving the formation of the first coordination sphere of anions. As a result, it seems that the greater the hydrophilicity of an anion (identified, for instance, via the Hofmeister series), the less easy its involvement in the formation of anion-templated assembly of halogen-bonded crystals. This inverse relation holds independent of the relative strength of the XBs that the more hydrophilic and less hydrophilic anions form. Iodides, perchlorates, and other poorly hydrophilic anions are particularly reliable and robust tectons and can easily afford halogen-bonded crystals assembled thanks to anion-driven coordination processes. Conversely, the fluoride anion has served as the XB acceptor in cocrystal formation in quite a few cases.[653] The anion recognition occurring in solution has also been used for anion sensing[460,654−658] and transport,[212−214] which seem to be promising fields for XB exploitation, probably as the XB might be tailored to such functions thanks to its hydrophobic character.

Halides form a particularly large number of halogen-bonded crystalline adducts. The topology of these systems is heavily influenced by the cation nature and, even more important, by the number and geometry of the electrophilic halogen(s) present on the XB donor tecton. Due to their spherical shape and their high nucleophilic character, halides can form a variable number of XB contacts.[161] Generally, a moderate bias toward the formation of two or three XBs is observed, but a careful crystal engineering or compelling crystal packing requirements can force halides to adopt other coordination numbers, and a given halide can form up to eight XBs (Figure 61).

Trihalide anions, such as I_3^-, Br_3^-, IBr_2^-, and ICl_2^- are halogen-bonded adducts, as they result from the entrance of a halide anion on a dihalogen or interhalogen, but can also function as XB acceptors, and more complex adducts are formed. Also polyhalometalates can form halogen-bonded supramolecular anions, and linear,[659] tetrahedral,[554] square planar,[660] and bipyramidal[661] geometries have been obtained depending on the anion geometry. However, not all of the halogen atoms bound to a given metal usually work as XB acceptors, and the geometry of the polyhalometalate anion is not univocally translated into the geometry of the supramolecular anion.

Polycyanometalates are by far the most frequently encountered anionic and nitrogen-centered XB acceptors. The high delocalization of the negative charge in these anions results in a lengthening of the distance between the XB donor and acceptor; namely, these anions do not form strong XBs. Nevertheless, directional I···NC interactions have been used

DOI: 10.1021/acs.chemrev.5b00484
Chem. Rev. 2016, 116, 2478−2601

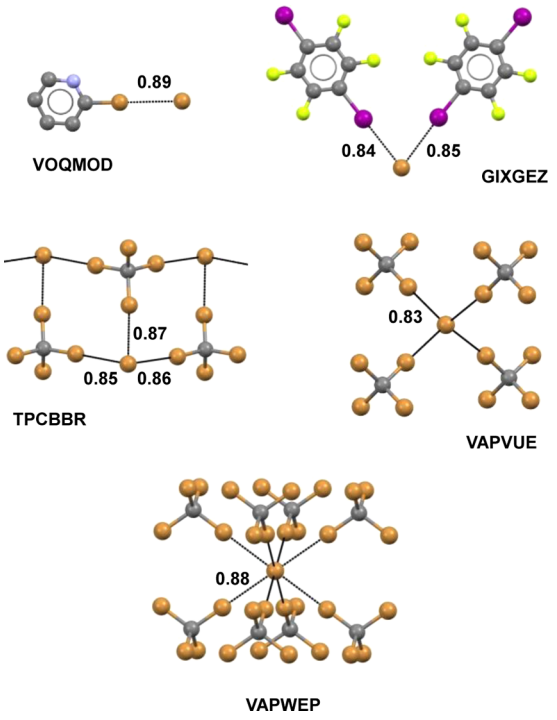

Figure 61. Bromide anions can form from one to eight XBs: VOQMOD, 2-bromopyridinium bromide; GIXGEZ, part of the infinite chain formed by tetramethylammonium bromide and 1,4-DITFB; TPCBBR, part of the ribbon formed by tetraphenylphosphonium bromide and tetrabromomethane; VAPVUE, part of the adamantanoid network formed by tetraethylammonium bromide and tetrabromomethane; VAPWEP, supramolecular anion formed by tetramethylammonium bromide and tetrabromomethane. For the sake of clarity, cations have been omitted, except in the first adduct. Color code: carbon, gray; iodine, purple; bromine, light brown; fluorine, yellow. XBs are dotted black lines. CSD Refcodes are reported.

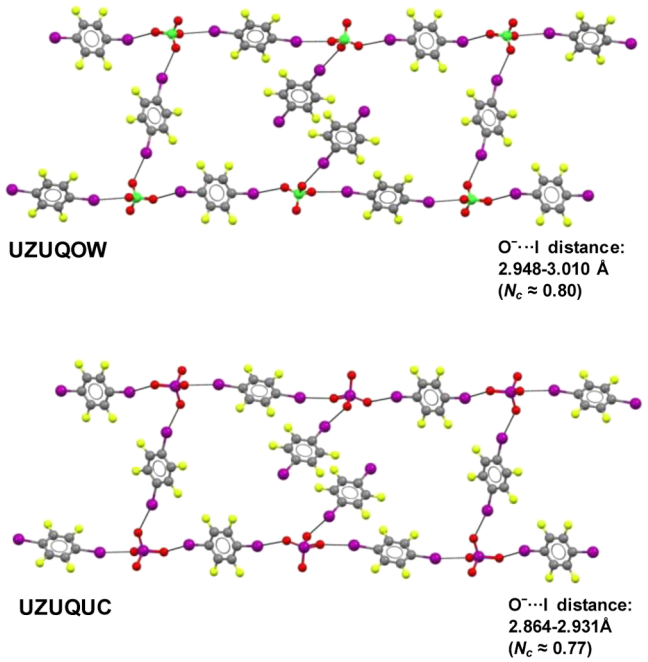

Figure 62. Isomorphous (6,3) networks where perchlorate (UZUQOW) and periodate (UZUQUC) anions are the nodes and 1,4-DITFB is the spacer. Cations were omitted for clarity. Color code: carbon, gray; oxygen, red; iodine, purple; chlorine, light green, fluorine, yellow. XBs are dotted black lines. CSD Refcodes are reported.

effectively for the fine-tuning of crystal and electronic structures in molecular conductors,[194,662−665] an example being bis(diiodo(ethylenedithio)diselenadithiafulvalene) tetracyanoaurate.[666]

Oxyanions, by far the most frequently occurring anions in organic chemistry, have afforded a large variety of adducts under XB control. The obtained systems involve both organic and inorganic oxyanions and span over a wide diversity of electronic and geometric features.[162] The perchlorate anion is the inorganic oxyanion that most frequently affords halogen-bonded adducts, and it gives one, two, three, or four XBs depending on the number of XB donor sites available and on the overall crystal packing requirements (Figure 62). Carboxylate anions are the most represented organic oxyanions in crystalline systems where XB is present. These anions usually act as monodentate XB acceptors.

Several other anions occasionally function as XB acceptors. The ability of the thiocyanate anion to interact with XB donors in the solid state was recently demonstrated.[73,667] It was shown that SCN^- is a weaker XB acceptor than I^-.[68] It is interesting to observe that the thiocyanate anion can work as a bidentate acceptor, with an electrophilic halogen entering the sulfur and another halogen entering the nitrogen,[73] or as a monodentate acceptor, and in these cases sulfur is preferentially involved in XB formation.[105]

Radical molecules can act as XB acceptors, and three main types of radical species have been identified: nitronyl radicals, paramagnetic metallic complexes, and metal complexes with noninnocent ligands. Nitronyl radicals function as very good XB acceptors,[610,668,669] and two paramagnetic metalate systems worth mentioning are the $S = 5/2$ Fe^{III} complex $FeCl_4^-$ and the $S = 3/2$ Cr^{III} complex $[Cr(isoq)_2(NCS)_4]^-$.[670,671] Some dithiolene complexes, such as $[M(mnt)_2]^{\bullet-}$ and $[M(dmit)_2]^{\bullet-}$ (M = Ni, Pd, Pt; mnt = maleonitrileditihionate; dmit = 2-thioxo-1,3-dithiole-4,5-dithiolato), are paramagnetic species ($S = 1/2$) with a spin density strongly delocalized on the two dithiolene moieties, and they can act as XB acceptors, either through the CN group in $[Ni(mnt)_2]^-$ or through the sulfur atoms in $[Pd(dmit)_2]^-$.[672,673]

This brief inventory of XB acceptors is ended with a discussion of studies aimed at filing a ranking of their ability to donate electron density. C. Laurence and J. Graton et al. formulated an I_2 basicity scale ($pK_{B_{I2}} = \log K_a$) by using spectroscopic data for complexes between I_2 and different Lewis bases.[101,674] It was found that molecular entities containing N, P, Se, and S donor sites give rise to stronger XB contacts with I_2 than those having O, F, Cl, Br, and I atoms. This behavior mirrors the evolution of the nucleophilic character in the periodic table, which increases moving down into the group and decreases across the period.

The I_2 basicity scale was used to correlate electron density donor ability and XB strength in a nitrogen-based XB acceptor series. Reduction of the p character of the lone pair of the nitrogen atom results in an elongation of the XB donor−acceptor distance, the distance increasing in the order amine < pyridine < nitrile.

The approach used for the diiodine scale was also adopted by the same authors to rank XB acceptors when the XB donors are

DOI: 10.1021/acs.chemrev.5b00484
Chem. Rev. 2016, 116, 2478−2601

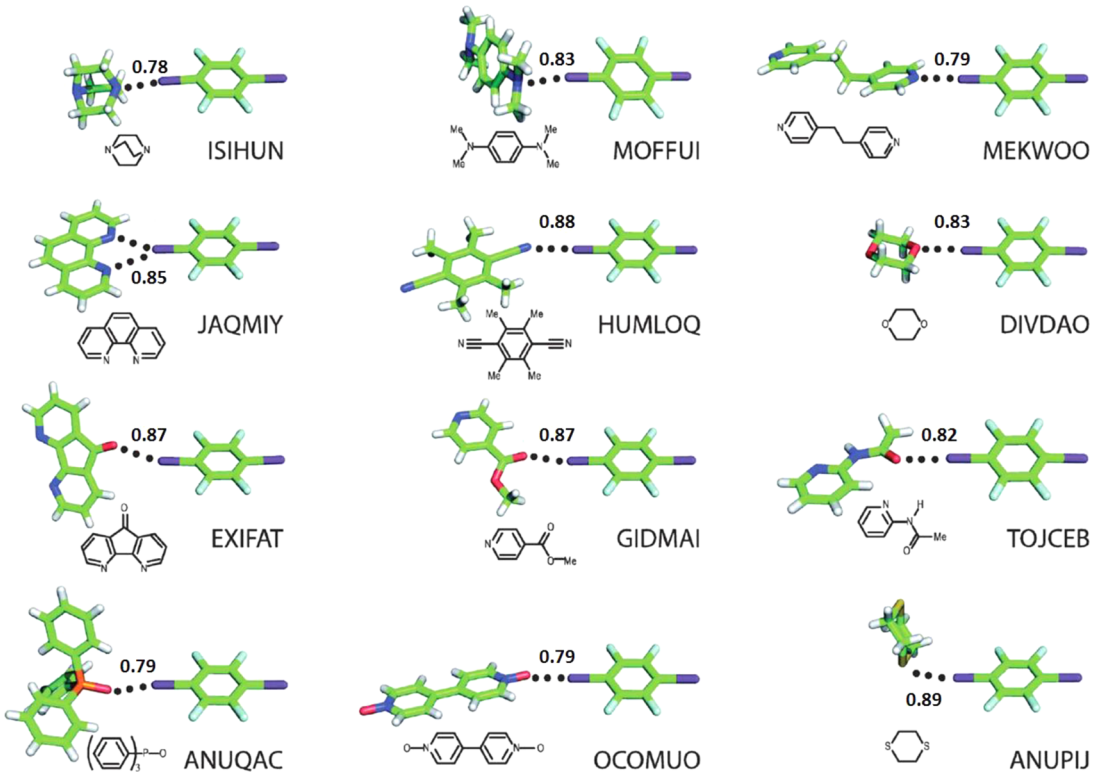

Figure 63. Crystal structures of 1,4-DITFB with various XB acceptors. N_c values and Refcodes are reported. XBs are dotted black lines. Adapted with permission from ref 674. Copyright 2013 Royal Society of Chemistry.

iodoorganic derivatives. In this case, crystal structures reported in the CSD and involving 1,4-diiodotetrafluorobenzene as the XB donor were used (Figure 63). In the nitrogen series, the lengthening of the C−I bond follows the shortening of the interaction, and as expected, aliphatic amines show normalized contacts just slightly shorter than those of pyridines, but significantly shorter than those of nitriles. The nature of the groups close to N_{sp^3} strongly influences the XB contacts. For instance, in anilines the conjugation between the nitrogen lone pair and the aromatic moiety is probably responsible for the longer and less linear I···N interactions compared to those of the corresponding aliphatic amines. Similarly, in the N_{sp^2} series the structure and nature of the XB acceptor impact the XB contact, as exemplified by phenanthroline derivatives, which are weaker XB acceptors than pyridines because in these compounds the XB interaction is three-centered and the second interaction, involving the second nitrogen atom, leads to a lengthening of the donor−acceptor distances.

Laurence and Graton found a quasi-exhaustive diversity of halogen-bonded oxygen bases in the CSD which allowed them to carry out a detailed analysis for the I···O distances. The mean normalized contacts for the I···O distance increase in the following order: NO < PO < R−CO−NR′R″ < SO < RO−CO−NR′R″ < R−O−R′ < R−CO−R′ < R−CO−OR′ < R−SO_2−R′ < NO_2 < Ph−O−R′ < RCO−O−R′. This trend is in good agreement with the ranking established by the diiodine basicity scale.

3. CRYSTAL ENGINEERING

During the second half of the past century, the chemistry behind the development of organic functional materials has progressively shifted its focus from the well-documented methodologies based on covalent synthesis toward approaches based on supramolecular synthesis.[675] A great variety of different self-assembly strategies has been proposed, and their impact in the construction of new supramolecular systems becomes apparent by considering the extensive scientific literature describing the important achievements obtained across the years.[676−679] Molecular organic frameworks (MOFs),[680,681] molecular receptors,[682] responsive systems,[683] organogels,[684,685] supramolecular polymers,[686] and biomimetic materials[687] are only some examples of these outstanding new systems.

When aimed at the design and synthesis of supramolecular materials, a self-assembly approach implies that the components (molecular building blocks, i.e., tectons) are programmed to create an ordered structure tailored to the pursued function. The intermolecular recognition and self-assembly processes, which can occur at any dimensional length scale, are the result of the balanced action of steric and electronic factors related to shape complementarity and size compatibility of the assembled modules and specific anisotropic interactions.

Although self-assembly approaches have generated new systems in all aggregation states of matter,[688,689] the supramolecular synthesis in the solid state has attracted particular attention, leading to a well-defined new area named crystal engineering.[690] Specifically, crystal engineering[691] is the understanding of intermolecular interactions in the context of crystal packing and the way in which such interactions are employed for controlling the assembly of molecular building blocks into designed architectures.

Supramolecular chemists have attempted to assemble molecular modules by using different intermolecular interactions such as HB, $\pi-\pi$ stacking, metal−ligand interactions, electrostatic forces, strong dipole−dipole association, hydrophobic forces, etc. Among all these interactions, HB is by far

DOI: 10.1021/acs.chemrev.5b00484
Chem. Rev. 2016, 116, 2478−2601

the most used one, and many reliable supramolecular synthons[692] have been discovered for the assembly of new supramolecular systems.[693] The persistent bias resulting from the approximation that halogen atoms are neutral entities in dihalogens or fully negative elements in halocarbon moieties has long prevented electrophilic halogens from being considered responsible for the frequent formation of strong attractive interactions, and XB[10] has not been explored to the same extent as HB. Only recently, XB has evolved from a scientific curiosity to a chemical interaction widely used to direct and control assembly phenomena.[93]

This section is focused on the contribution that XB has made to crystal engineering and, more in general, to the wider field of supramolecular synthesis. This discussion will serve as an introduction to successive sections wherein the use of XB to switch on or tune functional properties in supramolecular materials will be presented. Herein, the described results will be organized from the viewpoint of the *dimensionality* of the obtained supramolecular architecture. Specifically, the described structures will be grouped, at least as far as is reasonably possible, into discrete (zero-dimensional, 0D) aggregates and mono-, di-, and tridimensional networks (1D, 2D, and 3D nets, respectively). Discrete and interlocked structures will be discussed, bringing the focus onto the XB itself and the way it generates a molecular recognition event. Then some representative studies will be reported that attempt to combine multiple recognition events and to result in the formation of networks and frameworks, either interpenetrated or porous. In all cases, adducts formed by neutral, lone-pair-possessing donors will be discussed first, and then attention will be on aggregates given by anions. Applications in porous systems and solid-state synthesis will finally be presented at the end of the section.

3.1. Structures

3.1.1. Zero-Dimensional (0D) Systems. The basic approach to form discrete halogen-bonded adducts by design typically involves the self-assembly of a monotopic XB donor with a mono- or polytopic acceptor (or vice versa). If fairly small and strong XB donors and acceptors are used, all the binding sites are paired during the self-assembly process, and trimeric complexes are obtained starting from a bidentate donor and two monodentate acceptors (or vice versa), while multimeric complexes, such as tetrameric or pentameric systems, are obtained by using multidentate donors capped with an equal number of monodentate acceptors (or vice versa). However, if the donor and/or the acceptor modules are quite large molecules, the overall packing requirements, and the tendency to avoid the formation of architectures with large empty volumes, may prevent a saturation of all binding sites, and the obtained aggregates will contain fewer components, or have a lower dimensionality, than the potential maximum attainable. The same happens when the donor and/or the acceptor sites can give rise only to weak XBs and factors other than XB formation drive, or influence, the self-assembly process.

In general, the formation of halogen-bonded 0D systems is more straightforwardly designed or performed and better exemplified when "minimal" donor/acceptor units are used, and several such examples will be presented. This simplification of the structural complexity of the modules maximizes the role of the XB and minimizes the possible interferences of other noncovalent interactions. However, a careful design of the structural complexity of the starting building blocks can also produce quite sophisticated discrete systems as is the case for anion receptors, rotaxanes, and catenanes, which will be exemplified at the end of the section.

Iodopentafluorobenzene (IPFB) is one the most representative compounds of the class of "minimal" XB donors. IPFB gives dimers with 2,6-dimethylpyridine (Figure 64, LEZPOW)

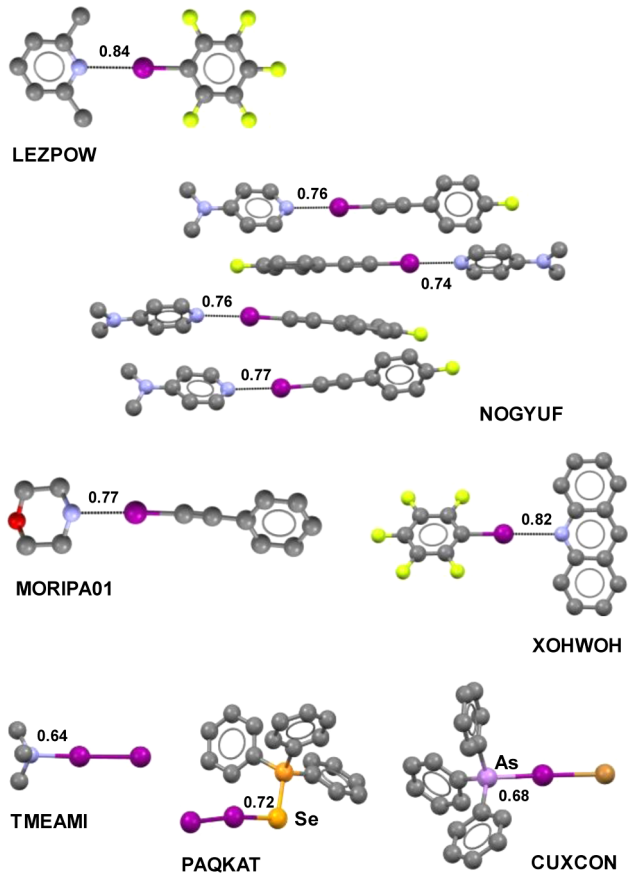

Figure 64. Crystal structures of selected discrete halogen-bonded dimers. Color code: carbon, gray; nitrogen, blue; oxygen, red; iodine, purple; bromine, light brown; fluorine, yellow. XBs are shown as dotted black lines or as colored solid lines. CSD Refcodes are reported: LEZPOW, 2,6-dimethylpyridine−pentafluoroiodobenzene; NOGYUF, *N*,*N*,*N*-Dimethylpyridin-4-amine−1-fluoro-4-(iodoethynyl)benzene; MORIPA01, morpholine−1-iodo-2-phenylacetylene; XOHWOH, acridine−iodopentafluorobenzene; TMEAMI, trimethylamine−diiodine; PAQKAT, triphenylphosphineselenido−diiodine; CUXCON, triphenylarsine−iodine monobromine.

and 2,4,6-trimethylpyridine[538] (LEZPIQ), and in both cases, the activated iodine atom acts as a powerful XB donor and short contacts are formed. Trimethylpyridine gives a shorter contact than dimethylpyridine as the extra methyl group further activates the electron donor ability of the nitrogen and the presence of a tweezer motif due to HBs between the hydrogen atoms on the 2,6-methyl groups and the negative belt on the iodine atom further promotes the reduction of the donor−acceptor distance.

The dimer between IPFB and 4-(*N*,*N*-dimethylamino)-pyridine shows an even shorter N···I distance (2.693 Å, N_c = 0.76),[202] further confirming the role of the substituents on the XB acceptor modules in tuning the strength of the formed XB(s). Not surprisingly, medium or weak XB acceptors (e.g.,

DOI: 10.1021/acs.chemrev.5b00484
Chem. Rev. 2016, 116, 2478−2601

hexamethylenetetramine and 1,3,5-triazine) form even shorter XBs when giving dimers with very strong XB donors (e.g., *N*-iodosuccinimide or other *N*-haloimides).[595,694,695]

(*N*,*N*-Dimethylamino)pyridine is a potentially ditopic XB acceptor, but the dimethylamino moiety was not halogen-bonded to IPFB, and the same happened on crystallization with 4-fluoro-1-(2′-iodoethynyl)benzene where a dimer was obtained (Figure 64, NOGYUF).[696] Similarly, morpholine and *β*-(iodophenyl)acetylene form a dimer (Figure 64, MORIPA01) where the iodine atom selectively interacts with the nitrogen site and not with the oxygen site.[697] This behavior where an XB donor interacts selectively with one XB acceptor is in line with the general heuristic principle that the best XB donor interacts preferentially with the best acceptor.

IPFB and acridine form another discrete halogen-bonded dimer (Figure 64, XOHWOH),[698] and when phenazine is used rather that acridine, a dimer isostructural with XOHWOH is formed; namely, one of the two nitrogen atoms of phenazine is not halogen-bonded. Replacing IPFB with bromopentafluorobenzene (BrPFB), the obtained dimer was isostructural with the IPFB−acridine adduct, demostrating that Br and I can be equivalent in XB-driven self-assembly.

Also molecular iodine has been involved in the formation of discrete systems with neutral XB acceptors. Both iodine atoms in I_2 have large positive *σ*-holes in the isolated molecule, and I_2 can function as a bidentate XB donor, but as discussed above, when one iodine atom is halogen-bonded to a strong acceptor, the charge-transfer component of the interaction may significantly increase the electron density of the other iodine, and its ability to function as an electron density acceptor site is hampered. The dimer between trimethylamine and I_2 is the minimal example of this behavior (Figure 64, TMEAMI).[699] Other discrete adducts can be found in solid-state chemistry where I_2 forms a single XB with sulfur[640] and selenium and arsenic.[700] ClI[701] and BrI[702] give similar 0D systems where in all of the cases the iodine atom functions as an XB donor (Figure 64, PAQKAT and CUXCON).

As mentioned in the XB donor/acceptor inventory in section 2.2.4, the halogen atoms of halogenated heteroarenium cations are effective XB donor sites, while anions can function as effective XB acceptor sites, and X-ray structures frequently show the presence of strong XBs in crystalline haloheteroarenium salts. Anions may potentially accept multiple XB contacts, but the number of XB donor sites on the haloheteroarenium cation becomes the limiting factor for the number of XBs given by the anion in haloheteroarenium salts. In the structures of halogenated organic salts, discrete adducts are more common than infinite nets, probably not due to an inherent preference of anions to work as monodentate XB acceptors but, rather, due to the fact that monohalogenated organic cations are much more numerous than di- or polyhalogenated ones. In monohalopyridinium halides[703−705] and monohaloanilinium halides[706−708] the monodentate cation prevents the anion from functioning as a polydentate unit, and discrete adducts are formed (Figure 65, LEJKUG, WUWMAD, WOQREB, VOQMUJ, CICRAI, HOLLID, and ZONXOP).

Importantly, molecular halogens could interact with anion species, yielding polyhalide entities. In general, polyhalide chains X_{2m+n}^{n-} (X = F, Cl, Br, or I) give rise to a particularly wide variety of structures that are assembled starting from X^-, X_2, and X_3^- building blocks, where X^- and X_3^- may be considered as the XB acceptors (electron donor moieties) and X_2 as the XB donor (electron acceptor). The simplest

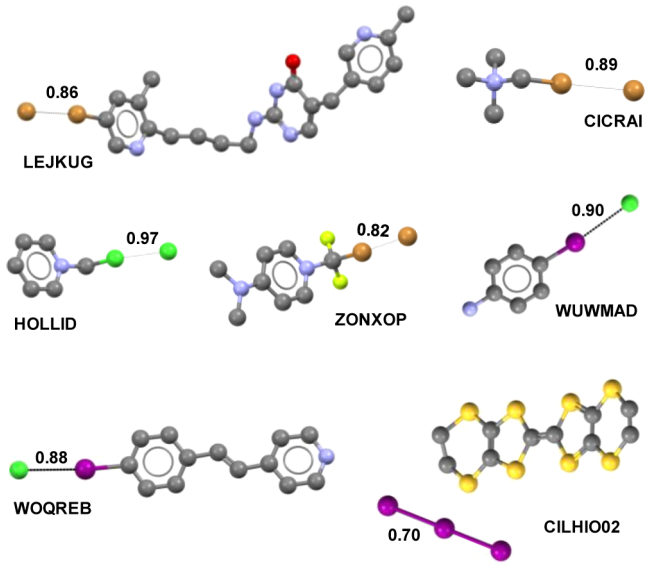

Figure 65. From LEJKUG to WUWMAD: representation of crystal structures of 0D dimeric adducts involving halogen atoms activated by positively charged scaffolds and halide anions. CILHIO22: crystal structure of a TTF derivative containing the triiodide anion. Hydrogen atoms are omitted for clarity. Color code: carbon, gray; nitrogen, blue; iodine, purple; bromine, light brown; chlorine, light green, sulfur, dark yellow; fluorine, yellow. XBs are dotted black lines and colored solid lines. CSD Refcodes are reported: LEJKUG, 2-[[4-(5-bromo-3-methyl-2-pyridyl)butyl]amino]-5-(6-methyl-3-pyridylmethyl)-4-pyrimidone trihydrobromide; CICRAI, (bromomethyl)-trimethylammonium bromide; HOLLID, 1-(chloromethyl)pyridinium chloride; ZONXOP, 1-(bromodifluoromethyl)-4-(dimethylamino)-pyridinium bromide; WUWMAD, 4-iodoanilinium chloride; WOQREB, *trans*-4-[2-(4-iodophenyl)ethenyl]pyridinium chloride; CILHIO02, bis[bis(ethylenedithio)tetrathiafulvalene] triiodide.

polyhalide species and thus the smallest 0D dimeric adduct involving molecular halogens and halide anions is the trihalide X_3^-. Depending on the halogen atoms that form the X_3^- species, these can be homoatomic trihalides X_3^- $[(X_1\cdots X_2-X_3)^-$; $X_1 = X_2 = X_3$ = F, Cl, Br, I) or heteroatomic mixed trihalides X_2Y^- $[(Y_1\cdots X_2-X_3)^-]$; Y_1, $X_2 = X_3$ = Cl, Br, I). The most common trihalide unit is I_3^-, where I_2 is halogen-bonded to I^- (Figure 65, CILHIO22).[17,709]

In the CSD, trimeric discrete systems are quite common, although less common than infinite chains. Some selected examples involving 1,4-DITFB are shown in Figure 66 (TOKFEG, ANUQAC, LICBIK). 1,4-DITFB typically functions as a bidentate tecton, consistent with calculations which show that both the iodine atoms of this module present a remarkably positive *σ*-hole. Trimers are thus formed when two equivalents of a monodentate XB acceptor (such as N,[211] O,[183] and *π*-systems[710]) are available, and similar trimeric complexes are obtained by using other analogous tectons, e.g., 1,3-diiodotetrafluorobenzene,[711] 1,2-diiodotetrafluorobenzene,[618] or 1,4-bis(iodoethynyl)benzene[573] and its brominated analogue. Alternatively, all these tectons afford halogen-bonded systems with higher dimensionality (e.g., infinite chains, honeycomb-like nets, etc.) when interacting with di- or tridentate acceptors, but not when crystal packing requirements or the formation of other intermolecular interactions interfere.[618,634,712]

Discrete and trimeric motifs are also obtained when the code is reverted, namely, when a bidentate XB acceptor self-assembles with two monodentate donor molecules. 4,4′-

DOI: 10.1021/acs.chemrev.5b00484
Chem. Rev. 2016, 116, 2478−2601

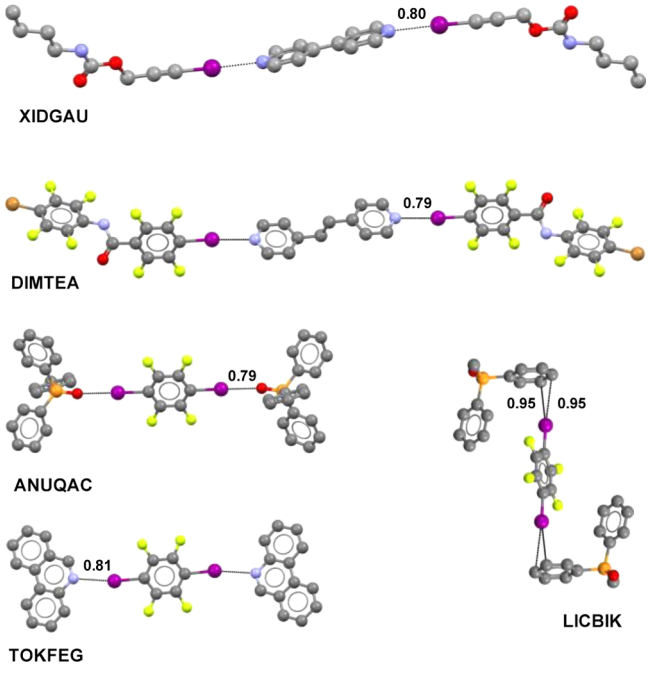

Figure 66. Trimeric discrete complexes formed by 1,4-DITFB with phenanthridine (TOKFEG),[713] triphenylphosphine oxide (ANUQAC),[183] and methyl(diphenyl)phosphine oxide (LICBIK).[710] Trimeric complexes assembled by *N*-(4-bromo-2,3,5,6-tetrafluorophenyl)-2,3,5,6-tetrafluoro-4-iodobenzamide with *t*-BPE (DIMTEA)[714] and by 3-iodoprop-2-yn-1-ylbutyl carbamate with 4,4′-bipyridine (XIDGAU).[477] Color code: carbon, gray; nitrogen, blue; oxygen, red; iodine, purple; bromine, light brown; chlorine, light green; phosphorus, orange; fluorine, yellow. XBs are dotted black lines. CSD Refcodes are reported.

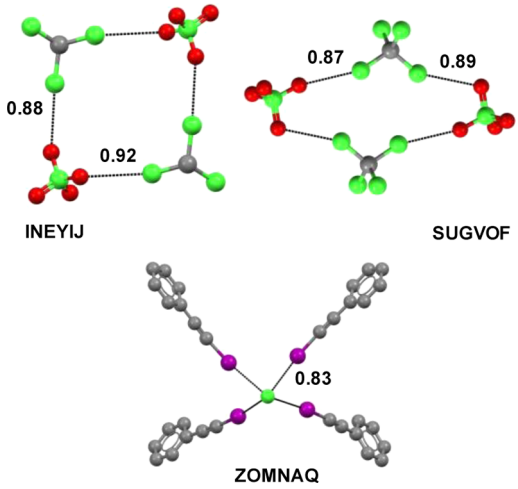

Figure 67. Representation of the cyclic tetrameric superanions formed by $CHCl_3$ and the perchlorate anion of bis[μ_2-8-[(2-pyridylsulfanyl)-methyl]quinoline]disilver(I) diperchlorate (INEYIJ) and CCl_4 and the perchlorate anion of (*cis*-2,6,9,13-tetrathiabicyclo(12.4.0)octadecane)-nickel(II) diperchlorate (SUGVOF). Representation of the pentameric superanion assembled thanks to I$l\cdots Cl^-$ XBs in tetraphenylphosphonium chloride−tetrakis(1-iodo-2-phenylacetylene) (ZOMNAQ). Cations are omitted for clarity. Color code: carbon, gray; oxygen, red; iodine, purple; chlorine, light green. XBs are dotted black lines. CSD Refcodes are reported.

Bipyridine and *t*-BPE are two "minimal" XB acceptors, and examples are reported in Figure 66 (DIMTEA and XIDGAU).[477,485,638]

Anionic XB acceptors can also be involved in trimeric adduct formation. However, the well-known ability of these electron density donors to accept multiple XB donors makes the design and assembly of defined and discrete units quite challenging and rare. Two interesting examples are the inclusion complexes of 1,4-DITFB in decamethonium diiodide where two iodide anions pin the two iodine atoms of the XB donor[470] and the motif between chloride anion and two monoiodoperfluoropropane molecules.[214] The latter example was used as structural confirmation to explain the ability of monoiodoperfluoroalkanes to act as anion transporters through membranes. Several other examples of trimeric complexes involving ionic species are discussed in two review papers on anion coordination under XB control.[69,70]

The achievement of multimeric discrete systems by design is even more demanding if compared with that of dimeric or trimeric adducts. This is also related to limitations or complications experienced during the covalent synthesis of preorganized starting modules. Some examples of discrete systems involving multiple XBs are discussed in the following section on porous systems and cages (3.2.1). Some others[70,523,715,716] are presented in Figure 67 or can be found in the CSD. In general, they have been obtained by chance rather than by design.

Anion receptors could be considered as a functional class of discrete assemblies, and in the final part of this section some of the most relevant examples will be discussed. A common feature of all these systems is that their molecular structure is preorganized to allow for the targeted function to merge, for instance, the recognition of the guest by eliciting a specific binding mode relative to all the other possible interaction modes. This structure-imposed selectivity is also a key feature in the construction of complex topologies such as catenanes and rotaxanes.

The first example of a preorganized anion receptor incorporating XB donor groups was reported by P. Metrangolo and G. Resnati et al. in 2005 (Figure 68).[717] The receptor TIPTEA was obtained by appending three *p*-iodotetrafluorophenyl groups to the tris[2-(ethylene glycol)ethyl]amine moiety. The resulting heteroditopic tripodal receptor bound separated alkali-metal halide ion pairs. Specifically, the alkali metals interacted attractively with the Lewis basic podand portion of the receptor, while their counteranions were recognized through XBs to the iodoperfluoroarene groups at the periphery of the receptor. X-ray studies of TIPTEA with NaI confirmed the binding mode (Figure 68, DAXGIT). The selectivity of the receptor for the halides was evaluated by competitive electrospray ionization mass spectrometry (ESI-MS) experiments and followed the trend $I^- > Br^- > Cl^-$.

In 2010, M. S. Taylor and co-workers developed the tripodal anionic receptor TIBTM, where three 2-iodoperfluorobenzoic acid units are appended onto a 1,3,5-tris(hydroxymethyl)-benzene core (Figure 68).[458] This unit oriented the XB donor sites to allow a high selectivity for anionic guests. One year later, the same group synthesized another anion receptor (DIBU) containing one urea and two 2-iodotetrafluorophenyl groups. The presence of both HB and XB donor groups in the receptor scaffold enhanced the affinity for the halide anion with respect to that of DIBU.[718]

The use of positively charged XB donors as anion receptors allows for Coulombic attraction to make a major contribution

DOI: 10.1021/acs.chemrev.5b00484
Chem. Rev. 2016, 116, 2478−2601

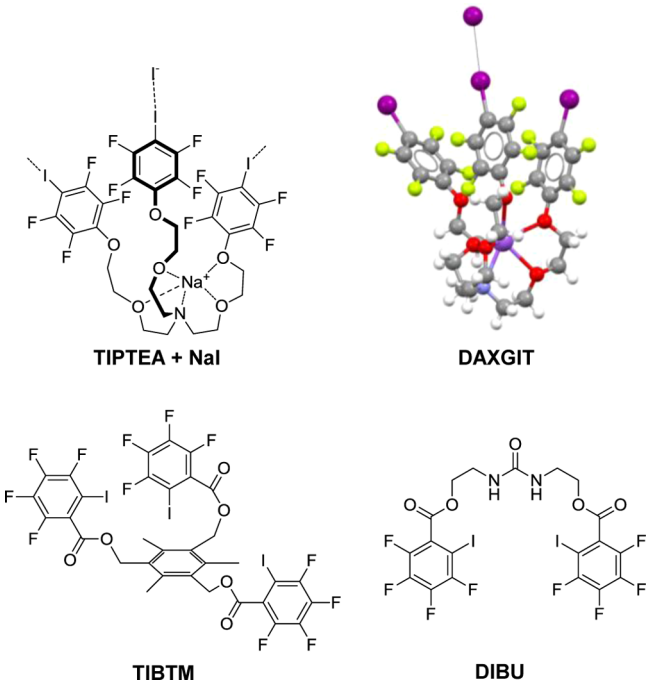

Figure 68. Top: molecular formula of TIPTEA (left) and representation of the single-crystal X-ray structure of the complex of TIPTEA with NaI (right). The I···I$^-$ XB is shown as a black dotted line. Bottom: molecular formulas of TIBTM and of DIBU. Color code: carbon, gray; nitrogen, blue; oxygen, red; iodine, purple; fluorine, yellow; sodium, light purple. XBs are dotted black lines. The CSD Refcodes are reported.

to anion binding. The approach has evolved as a general strategy to strengthen the anion recognition process. In this context some of us proposed a monodentate 2-iodoimidazolium system (AMII) which showed a good affinity, in solution, for halide anions and, importantly, a particularly high affinity for the poorly explored $H_2PO_4^-$ anion (Figure 69). The crystal

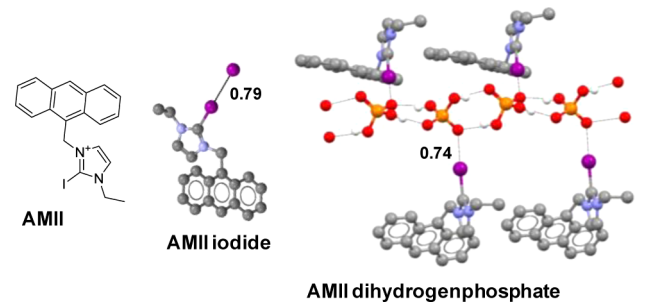

Figure 69. Left: molecular formula of AMII. Middle: single-crystal X-ray structure of the AMII iodide salt. Right: single-crystal X-ray structure of the AMII dihydrogen phosphate salt. Color code: carbon, gray; nitrogen, blue; oxygen, red; iodine, purple; phosphorus, orange; hydrogen, white. XBs and HBs are dotted black lines. CSD Refcodes are reported.

structures of AMII as iodide and dihydrogen phosphate salts revealed short I···I$^-$ and I···O$^-$ contacts, respectively, and confirmed the behavior observed in solution.[563]

Using positively charged modules, P. Beer and co-workers recently reported several interlocked receptors showing complex supramolecular structures such as self-assembled rotaxanes and catenanes. In the first rotaxane reported, ITIPA, an iodotriazolium-based unit, the axle, was assembled with an isophthalamide-based macrocycle, the ring. The rotaxane formation was driven by cooperative HB and XB interactions involving the bromide anion (Figure 70). Structural details of the binding of the bromide ion in the cavity of the rotaxane were afforded by X-ray analysis.[460] Similar rotaxanes showed strong and selective recognition for anions in water, demonstrating the superiority of XB over HB for strong anion binding.[657]

In 2014 the same group reported the first rotaxane host system totally based on XB, DITDIT. In this case both the axle and the macrocycle integrated XB donor units, namely, two iodotriazole and two iodotriazolium motifs, respectively (Figure 70, top).[550] The cooperative and convergent XB interaction with chloride allowed for the formation of the interlocked adduct as confirmed by X-ray analysis.

Similar catenate structures were targeted using either an approach based on HB and XB (CAT1)[719] or an approach based on XB only (CAT2) (Figure 70, bottom).[658] These systems were formed upon interaction with halide anions.

Two other examples where the preorganization of the structure is instrumental in the recognition phenomena are the foldamer reported by J. Lin et al. (HTF)[720] and the anion receptor developed by P. Molina et al. (BITN) (Figure 71).[721] In the first case, the intramolecular HBs imposed a preorganized cavity where the tris(iododifluoroacetate) guest was trapped by XB. In the second system, the bidentate HB and XB triazolium-based receptors showed a very high affinity for the hydrogen pyrophosphate ($HP_2O_7^{3-}$) anion, which was not observed for the receptor based only on HB.

3.1.2. One-Dimensional (1D) Systems. 1D halogen-bonded architectures can be homomeric systems, obtained on self-assembly of self-complementary modules bearing both XB donor and acceptor sites. Alternatively, they can be heteromeric systems, obtained on self-assembly of a ditopic XB donor and a ditopic XB acceptor. Several examples of homomeric halogen-bonded 1D chains formed by iodotetrafluorophenyl derivatives bearing different neutral XB acceptor sites (e.g., sp^3-hybridized,[722] sp^2-hybridized,[723] or sp-hybridized[623] nitrogen atoms, oxygen-centered sites,[724] and π-systems[725]) are shown in Figure 72.

In all cases, the activated iodine atoms act as powerful XB donors, and the acceptors provide the complementary link for 1D chain formation. The C–I···XB acceptor angles are close to linear, consistent with the high directionality of the interaction. Similar adducts are formed using activated chlorine[623] or bromine[725−727] atoms as XB donor sites. Not only iodotetrafluorobenzene derivatives give rise to halogen-bonded infinite chains, but other neutral self-complementary systems are found in the CSD, such as 3-iodo-propiononitrile[193] and 4-iodonitrobenzene,[690] which are two other "minimal" tectons.

Also charged self-complementary systems can assemble into infinite chains, as is the case for halogen-substituted zwitterions where the XB donor and acceptor sites interact to form homomeric crystals (Figure 73).[728−730]

The heteromeric 1D chain is by far the most common motif among halogen-bonded cocrystals obtained by design. Generally, complexes with linear geometry are obtained when the axes of the donor and acceptor sites are parallel and coaxial. This is the case for 1D chains formed by flat XB donor and acceptor modules (Figure 74, IKUHUR).[168,203,731] Differently, stepped infinite chains are obtained when the binding sites are parallel, but not collinear, as is the case when α,ω-

DOI: 10.1021/acs.chemrev.5b00484
Chem. Rev. 2016, 116, 2478−2601

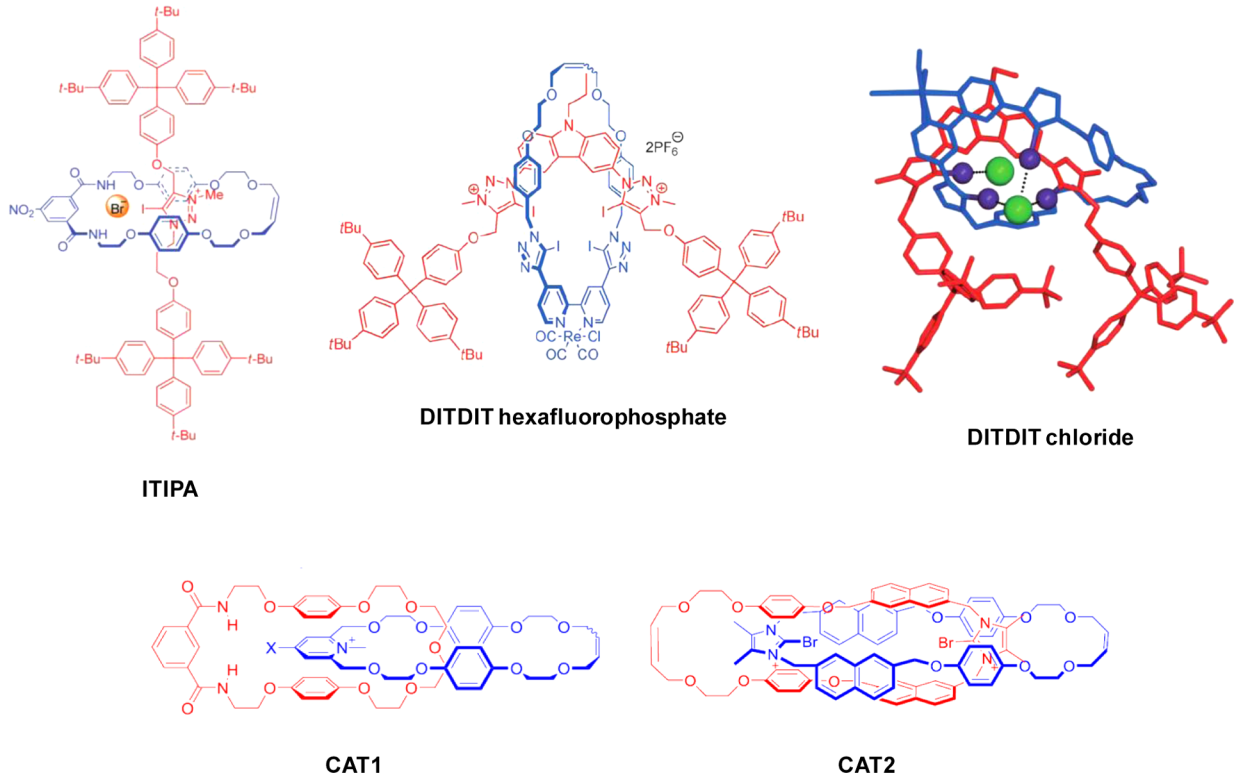

Figure 70. Top: molecular formula of ITIPA, molecular formula of DITDIT hexafluorophosphate salt, and single-crystal X-ray structure of DITDIT chloride salt. Adapted with permission from ref 551. Copyright 2014 John Wiley and Sons. Bottom: molecular formulas of CAT1 (left) and CAT2 (right). Adapted with permission from refs 719 and 659. Copyright 2014 and 2012, respectively, John Wiley and Sons.

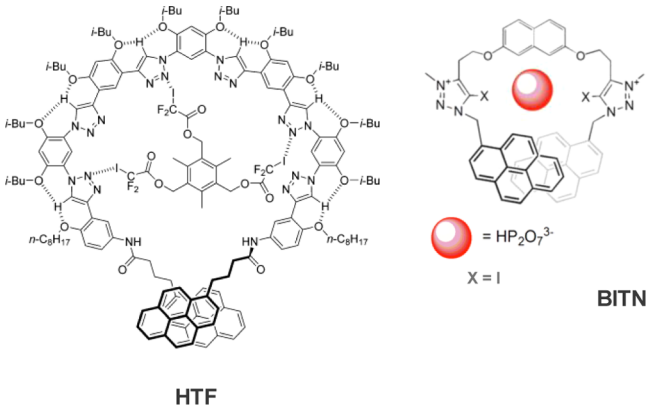

Figure 71. Left: cartoon representing the binding of the tris-(iododifluoroacetate) guest to the folded structure of HTF by multiple I···N XBs, which further fastens the folded state and leads to an increase of the excimer emission of the appended pyrene units. Adapted with permission from ref 720. Copyright 2012 John Wiley and Sons. Right: molecular structure of BITN bound to the $HP_2O_7^{3-}$ anion. Here, too, the recognition event leads to an increase of the excimer emission of the appended pyrene units. Adapted from ref 721. Copyright 2014 American Chemical Society.

dihaloperfluoroalkanes are used as XB donors (Figure 74, QANRUS and LOQBAU).[28,85,406,732−734]

Herringbone supramolecular chains appear when the axes of the donor sites on the XB donor tecton, or of the acceptor sites on the XB acceptor tecton, are not parallel. Thanks to the high directionality of XB, the angle between the axes of the binding sites corresponds to the angle along the resulting 1D chain, or in other words, the XB directionality translates the molecular geometry into the supramolecular geometry. Illustrative examples are the linear chain that 4,4′-bipyridine affords with DITFB[76] and the weavy chains formed by the same acceptor with 1,3- and 1,2-diiodotetrafluorobenzenes or their dibromo analogues[203,735] (Figure 75, IKUJON and IKUJIH).[736] Many other cases have been described where the XB donor,[190,472] the XB acceptor,[399,407,450,544,737] or both tectons[105,738] present an angular geometry translated into the chain geometry. A particularly nice example is the cocrystal between 3,5-bis(pyrid-4′-yl)-1,2,4-oxadiazole and 1,4-diiodoperfluorobutane or its analogue with 1,6-diiodoperfluorohexane (Figure 75, BEWXIM).[167]

Heteromeric 1D chains can also be obtained via self-assembly of a ditopic XB donor with a monotopic XB acceptor bearing a functional site with two lone pairs. Examples reported in the CSD usually involve oxygen[727] and sulfur[78] atoms, which frequently behave as bifurcated sites (Figure 76, FEQVON and NUSBUZ). This ability of oxygen atoms, discovered thanks to in situ cryocrystallization, allowed for the obtainment of 1D polymeric architectures between 1,3-dibromotetrafluoroben-zene,[178] or 1,2-dihalotetrafluoroethane,[179] and dimethyl sulf-oxide (DMSO) or hexamethylphosphoramide (HMPA).

Also XB donor sites can work as bifurcated sites. This behavior is quite rare and requires pairing with the appropriate XB acceptors,[216] as was the case for a set of tectons where two electron density donor sites were locked in place in such a way to favor the formation of a symmetric bifurcated XB with a single electrophilic halogen atom (Figure 76, EXIFEX).[614]

Anionic species, mainly halides, have been frequently used to build up linear architectures by design. Many chains in the CSD are given by chlorides, bromides, and iodides, and only a few involve fluoride anions.[653] Examples can be found both among

DOI: 10.1021/acs.chemrev.5b00484
Chem. Rev. 2016, 116, 2478−2601

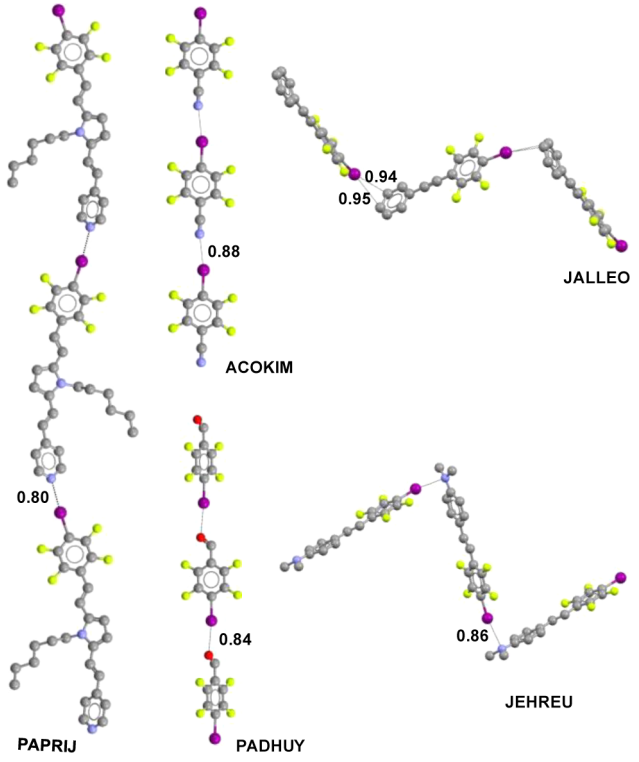

Figure 72. Representation of single-crystal structures of halogen-bonded 1D infinite chains assembled via self-complementary modules. Color code: carbon, gray; nitrogen, blue; oxygen, red; iodine, purple; fluorine, yellow. XBs are dotted black lines. CSD Refcodes are reported: PAPRIJ, 4-[2-[1-hexyl-5-[2-(tetrafluoro-4-iodophenyl)-vinyl]-1*H*-pyrrol-2-yl]vinyl]pyridine; ACOKIM, 4-iodo-2,3,5,6-fluoro-benzonitrile; PADHUY, 4-iodotetrafluorobenzaldehyde; JALLEO, 1-iodo-4-(phenylethynyl)tetrafluorobenzene; JEHREU, *N*,*N*-dimethyl-4-(*E*)-[2-(tetrafluoro-4-iodophenyl)vinyl]aniline.

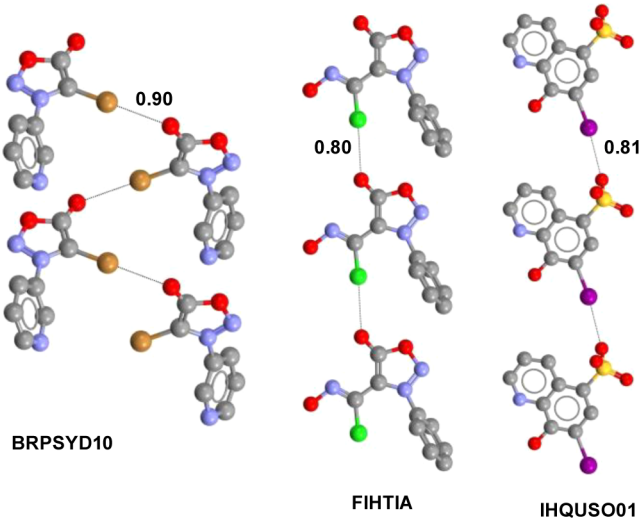

Figure 73. 1D infinite chains of halogen-substituted zwitterions: 4-bromo-3-(3-pyridyl)sydnone (BRPSYD10), (*Z*)-3-phenylsydnone-4-hydroximic acid chloride (FIHTIA), and 7-iodo-8-hydroxyquinolinium 5-sulfonate (IHQUSO01). Color code: carbon, gray; nitrogen, blue; oxygen, red; iodine, purple; bromine, light brown; chlorine, light green; sulfur, dark yellow. XBs are dotted black lines. CSD Refcodes are reported.

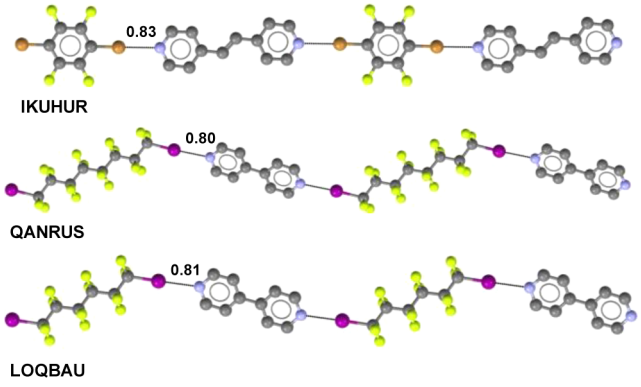

Figure 74. Partial representation of the 1D chain: linear chain formed by *t*-BPE and 1,4-dibromotetrafluorobenzene (IKUHUR), stepped chains formed on self-assembly of 4,4′-dipyridyl and DIPFH (QANRUS) and DIPFO (LOQBAU). Hydrogen atoms are omitted for clarity. Color code: carbon, gray; nitrogen, blue; iodine, purple; bromine, light brown; fluorine, yellow. XBs are dotted black lines. CSD Refcodes are reported.

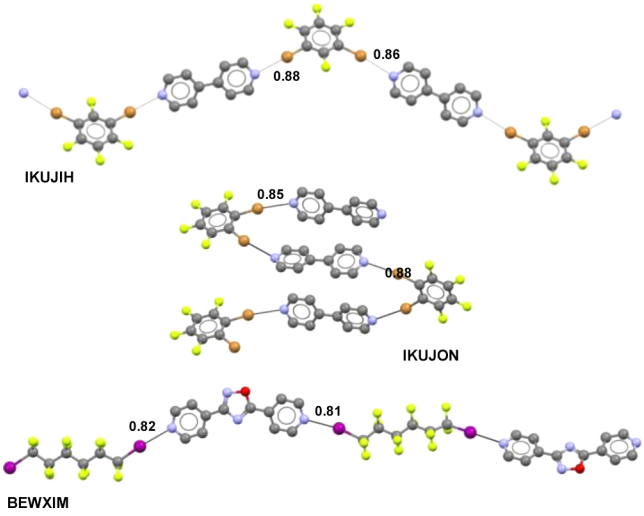

Figure 75. Representation of a part of the infinite chains between 4,4′dipyridyl and 1,3-dibromotetrafluorobenzene (IKUJIH)) and 1,2-dibromotetrafluorobenzene (IKUJON) and between 3,5-bis(pyrid-4′-yl)-1,2,4-oxadiazole and 1,6-diiodoperfluorohexane (BEWXIN). In BEWXIN the angle between the two pyridyl pendants of the XB acceptor (149.1°) is quite similar to the angle between the two formed XBs (141.5°). Hydrogen atoms are omitted for clarity. Color code: carbon, gray; nitrogen, blue; oxygen, red; iodine, purple; bromine, light brown; fluorine, yellow. XBs are dotted black lines. CSD Refcodes are reported.

the heteromeric two-component systems[207,739] and among the heteromeric three-component systems.[263] Linear, zigzag, or helicoidal arrangements are formed as a function of the overall crystal packing requirements (Figure 77, IKUXER, BOCGAB, PAVZIV, and AHULEU).

Finally, unusual 1D architectures have been assembled using anionic species such as a "rings and sticks" chain[740] or a comblike system.[741] A supramolecular ribbonlike arrangement is another peculiar assembly formed, for instance, when halide anions, working as tridentate and XB acceptor nodes, self-assemble with bidentate dihalocarbons, functioning as linear spacers of the nodes (Figure 77, UGULAK, DOXTOA, GIXGOJ, and NUZKIC).

DOI: 10.1021/acs.chemrev.5b00484
Chem. Rev. 2016, 116, 2478−2601

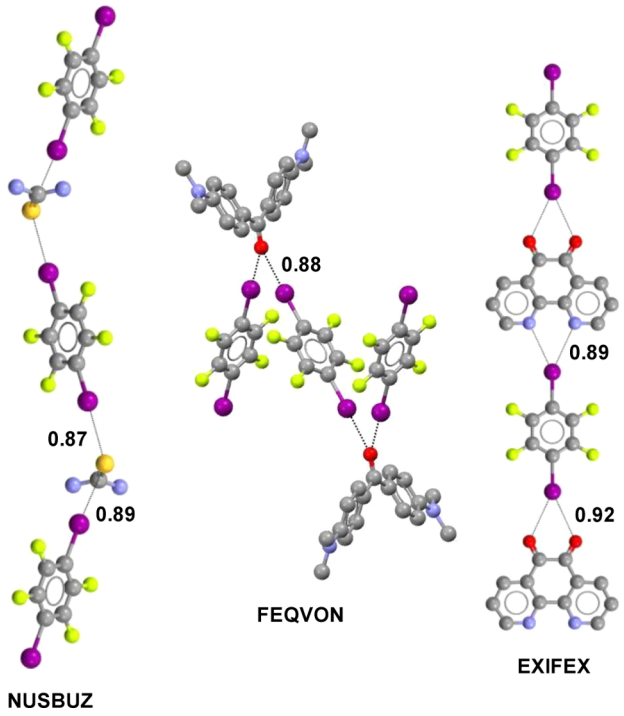

Figure 76. Representation of heteromeric 1D chains where 1,4-DITFB self-assembles with thiourea (NUSBUZ) and Michler's ketone (FEQVON), both functioning as monotopic XB acceptors where the heteroatom is a bifurcated site, and with 1,10-phenanthroline-5,6-dione (EXIFEX), forcing the iodine atoms of 1,4-DITFB to work as a bifurcated XB donor. Color code: carbon, gray; nitrogen, blue; oxygen, red; iodine, purple; bromine, light brown; sulfur, dark yellow; fluorine, yellow. XBs are dotted black lines. CSD Refcodes are reported.

3.1.3. Two and Three-Dimensional (2D and 3D) Systems. As discussed in the previous sections of this review, there is not a single strategy to assemble halogen-bonded discrete adducts or chains, and thus, there are several protocols to target 2D or 3D architectures. Increasing the number of XB donor and/or acceptor sites on the starting molecular modules is a strategy that has been largely and successfully applied during the years. The binding sites on the molecular scaffold should be oriented in such a way to elicit the desired binding profile of the interacting partners and afford the targeted network; for example, three, or four XB donor sites should be placed more or less orthogonal to each other if a 3D structure is pursued. In general, the higher the dimensionality of the targeted architecture, the more demanding the required design becomes and the more complex the synthesis of the starting building blocks may be.

When one or both of the interactive modules form three or more XBs, two-dimensional (2D) architectures are usually formed. Some examples involving neutral and anionic XB acceptors will be discussed in order, but before discussing examples afforded by structurally complex tectons, it is worth mentioning that dihalogens, the simplest molecules containing halogen atoms, assume in the solid state a 2D layered structure.[244,745] This well-defined assembly is related to the electron density distribution around the halogen atoms. I_2, Br_2, Cl_2, and F_2 molecules all possess two XB donor sites, the two σ-holes on the extensions of the covalent bonds, and two XB acceptor sites, the two belts rich in electron density and orthogonal to the covalent bonds. In solid Cl_2, for instance, the belt of one chlorine atom enters the hole of the chlorine of another molecule (Figure 50, YATKIP), and on repetition of this supramolecular synthon a flat 2D network is formed.

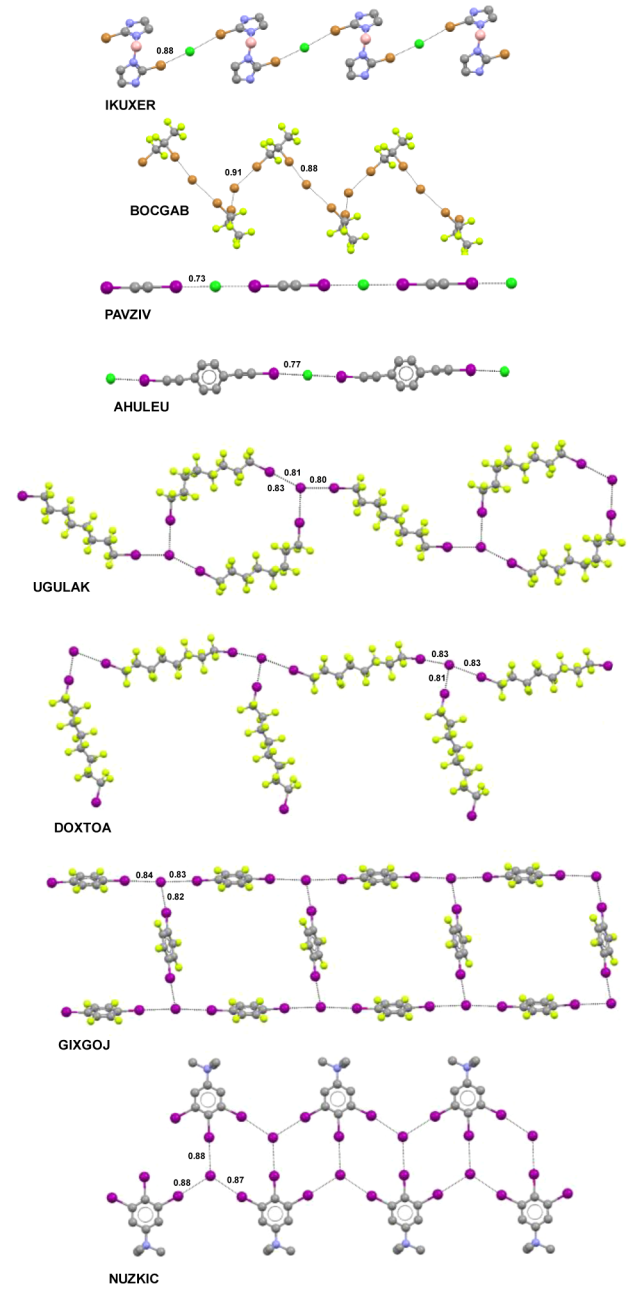

Figure 77. Infinite chains produced on C–Br···Cl^- XB formation in bis(2-bromoimidazole)boronium chloride (IKUXER),[742] C–Br···Br^- XB formation in (−)-sparteine hydrobromide/1,2-dibromohexafluoropropane (BOCGAB),[263] C–I···Cl^- XB formation in bis[bis(ethylenedithio)tetrathiafulvalene] chloride/diiodoacetylene (PAVZIV),[665] and C–I···Cl^- XB formation in tris[bis(ethylenedithio)-tetraselenafulvalene] chloride/1,4-bis(iodoethynyl)benzene (AHULEU).[743] Cations and hydrogen atoms are omitted for simplicity. "Rings and sticks" (UGULAK) and comblike (DOXTOA) architectures form when iodide anions (tridentate nodes) self-assemble with α,ω-diiodoperfluoroalkanes. Halogen-bonded ribbons form when iodide anions (tridentate nodes) self-assemble with 1,4-DITFB (GIXGOJ),[75] or with a triiodobenzene derivative (NUZKIC).[744] Color code: carbon, gray; nitrogen, blue; iodine, purple; chlorine, light green; boron, pink; fluorine, yellow. XBs are dotted black lines. CSD Refcodes are reported.

DOI: 10.1021/acs.chemrev.5b00484
Chem. Rev. 2016, 116, 2478−2601

A notable example of an infinite layer was reported by F. C. Pigge.[746] The trigonal molecule 1,3,5-tris[(4-iodophenoxy)-carbonyl]benzene (TIPB) functions as a self-complementary tecton when crystallized from chloroform and yields a 2D supramolecular network assembled thanks to I···O and I···π interactions. The bifurcated I···O and I···π XBs assist in the formation of triangular motifs which lead to the construction of 2D hexagonal patterns arranged in a parallel fashion. The honeycomb-like structure shows nanometer-sized channels filled by chloroform guest molecules (Figure 78A,B).

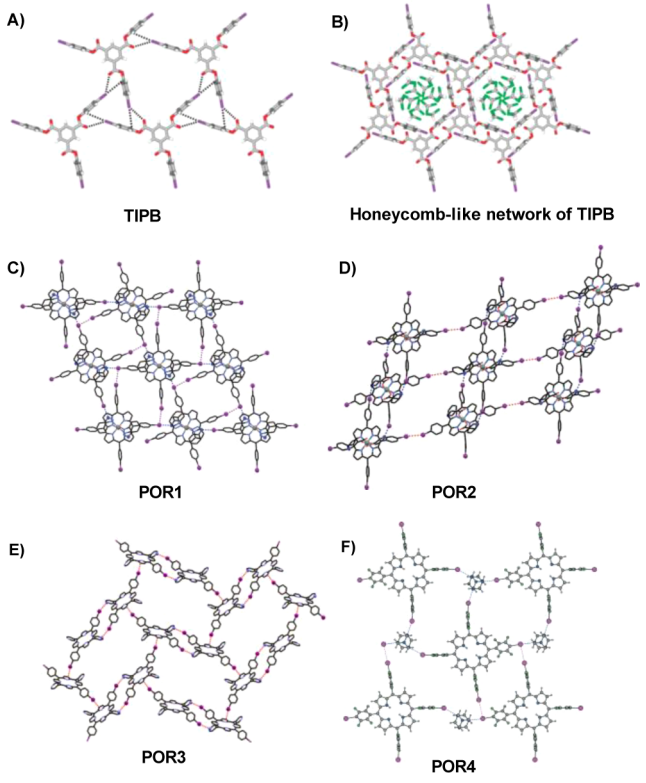

Figure 78. (A) Triangular motif sustained by bifurcated I···O and I···π XBs in the packing of TIPB. (B) Honeycomb-like network in TIPB. Hexagonal channels are filled by chloroform molecules (in green). (C) Two-dimensional array (sql) of tin tetrakis(iodophenyl)porphyrin with nicotinic acid (POR1) aligned parallel to the *ac* plane of the crystal. (D) Square-grid-type network in the crystal of tetrakis-(iodophenyl)porphyrin assembled with 1-hydroxybenzotriazole (POR2). Every porphyrin unit is involved in eight XB contacts. (E) View parallel to the crystal *ab* plane of bis(iodoaryl)dipyridylporphyrin free base (POR3). (F) Representative section of the halogen-bonded layer in POR4, viewed within the crystal *ac* plane. XBs are dotted lines. Panels A and B reprinted with permission from ref 746. Copyright 2008 Royal Society of Chemistry. Panels C and D reprinted with permission from ref 748. Copyright 2013 John Wiley and Sons. Panel E reprinted from ref 749. Copyright 2015 American Chemical Society. Panel F reprinted with permission from ref 750. Copyright 2014 Royal Society of Chemistry.

Porphyrin units functionalized with both XB donor and acceptor sites were used to construct 2D networks.[747] The tin tetrakis(iodophenyl)porphyrin with nicotinic acid (POR1) as an axial ligand formed in the solid state a layered grid-type arrangement wherein the porphyrin units were bridged by I···N XBs and I···I type I halogen−halogen contacts (Figure 78C). The topology of the two-dimensional porphyrin array was analyzed with TOPOS,[748] and the network was described as a square layer (sql). The substitution of 1-hydroxybenzotriazole for the axial ligand yielded a crystalline system (POR2) containing two-dimensional layers wherein the porphyrin units were connected to one another along the four equatorial directions by nearly linear C−I···N (N_c = 0.85) XBs. The corrugated nature of the layers allowed for their tight stacking in the normal direction, and disordered DMF molecules were accommodated in the interstitial channel voids of the structure (Figure 78D).

The free-base bis(iodoaryl)dipyridylporphyrin (POR3) adopts a crystal structure sustained by I···N and I···π XBs,[749] and the overall supramolecular arrangement is an open 2D herringbone pattern of the porphyrin molecules criss-crossed through XBs (Figure 78E).

A 2D porous framework is also obtained when a porphyrin with four iodotetrafluorobenzene residues in the meso positions is cocrystallized with hexamethylenetetramine (HMTA).[750] In the packing of the obtained system POR4 (Figure 78F), eight crystallographically different iodine atoms are present, and they are all involved in XBs. In the obtained layers, I···N XBs identify infinite ladder-type chains, which are connected to each other via short I···I interactions.

As already observed, anions have a moderate bias toward the formation of two or three XBs; it is thus not uncommon that 2D or 3D halogen-bonded supramolecular anions were obtained as a result of a design tailored to elicit a polydentate binding profile of halide anions. The number and geometry of the XB donor sites on the halocarbon tecton and the cation nature and size are also influential on the topology of the halogen-bonded anionic architecture, and a prediction of the structural aspects of the final network still remains a challenge.

The (6,3) network (honeycomb-like structure) is a frequently recurring pattern in 2D architectures formed on self-assembly of halide anions with a ditopic XB donor.[751] For instance, honeycomb-like structures were formed when Ph_4PBr and $(CH_3)_4NI$ were cocrystallized with 1,4-DITFB[75] and when potassium iodide and K.2.2.2 were cocrystallized with α,ω-diiodoperfluoroalkanes such as 1,2-diiodoperfluoroethane, 1,4-diiodoperfluorobutane, 1,6-diiodoperfluorohexane, and 1,8-diiodoperfluorooctane (Figure 79, TEHRAA).[68] In these structures, the halide units occupied the nodes of the (6,3) arrangement, while the dihalocarbon modules acted as bidentate XB donors that connected the nodes. The XB pattern around the halide anions adopted a pyramidal arrangement, and corrugated honeycomb-like layers were formed. Notably, in the tricomponent systems, strong segregation between the hydrocarbon moieties and perfluorocarbon units took place, and due to the presence of large cavities, some of the complexes showed an interpenetrated arrangement (see the next section for a detailed discussion of interpenetrated networks).

The deliberate construction of (6,3) networks was also achieved via XB-driven self-assembly of tetra-*n*-butylammonium perchlorate, periodate, and perrhenate with 1,4-DITFB (Figure 62, UZUQOW).[71] The mononegative oxyanions sit at network nodes and work as tridentate XB acceptors, the diiodobenzene derivatives space the nodes and function as bidentate XB donors, and the ammonium cations occupy the space encircled by the supramolecular (6,3) frames. Although perchlorate, periodate, and perrhenate anions have four XB acceptor sites, they function as tridentate nodes, and this behavior was explained in terms of decreasing overall electron density donor ability on the anion upon formation of the multiple XBs.

DOI: 10.1021/acs.chemrev.5b00484
Chem. Rev. 2016, 116, 2478−2601

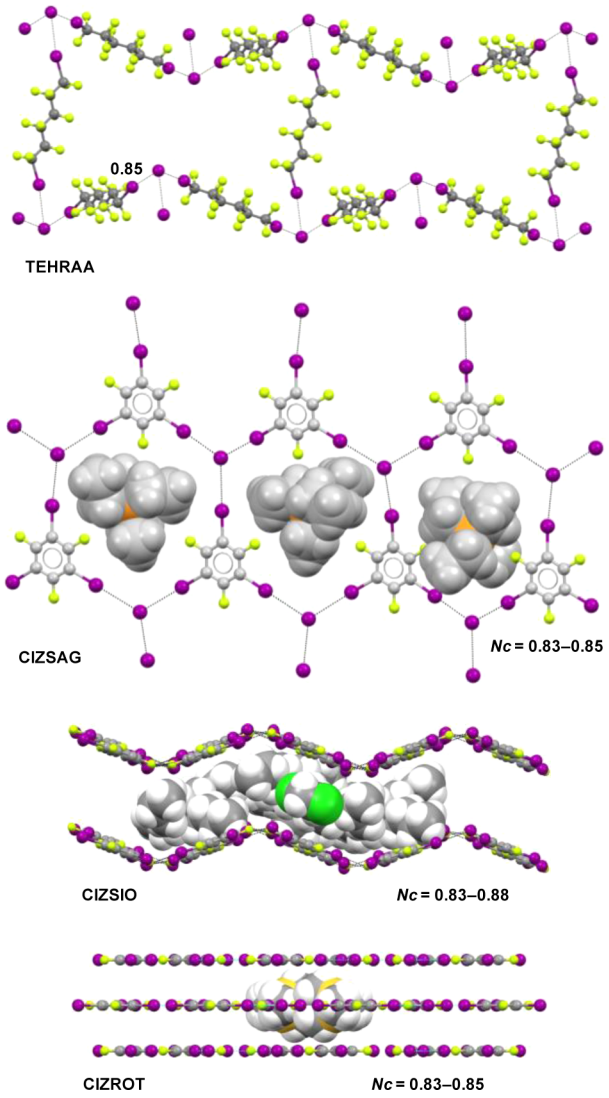

Figure 79. TEHRAA: side view of the (6,3) superanion network in the halogen-bonded adduct K.2.2.2/KI/DIPFH. Cations are omitted for clarity. CIZSAG: front view of the (6,3) network of tetraethylphosphonium iodide−1,3,5-triodo-2,4,6-trifluorobenzene. Cations are shown in space-filling style. CIZSIO: side view showing the undulated (6,3) anionic net of tetra-*n*-butylammonium iodide−1,3,5-triodo-2,4,6-trifluorobenzene dichloromethane solvate. Cations and dichloromethane are shown in space-filling style. CIZROT, side view showing the planarity of the (6,3) anionic network of trimethylsulfonium iodide−1,3,5-triodo-2,4,6-trifluorobenzene. Cations are shown in space-filling style. Color code: carbon, gray; nitrogen, blue; iodine, purple; phosphorus, orange; sulfur, dark yellow; fluorine, yellow. XBs are dotted black lines. CSD Refcodes are reported.

The formation of the (6,3) topology can be alternatively obtained by the self-assembly of tridentate XB donors with anions behaving as tridentate XB acceptors. In this case, the complementary tectons alternate at the nodes of the 2D architecture. Such halogen-bonded (6,3) networks are formed when CHI_3[480,752] self-assembles with onium halides and when 1,3,5-trifluoro-2,4,6-triiodobenzene (TITFB) is cocrystallized with onium iodides where the cation size matches the space encircled by the hexagonal framework.[539] For instance, (6,3) nets are obtained when Me_3SI, Me_4NI, Et_4PI, and *n*-Pr_4NI are employed (Figure 79, CIZROT and CIZSAG), but this is not the case for Ph_4PI as the cation is too large. It is interesting to observe that $Me_3S^+I^-$ affords a perfectly planar honeycomb-like anionic network (Figure 79, CIZROT), while on increasing the cation size (e.g., on moving from Me_4N^+ to Et_4P^+ and *n*-Pr_4N^+), the network becomes more and more corrugated (Figure 79, CIZSIO).

Another fairly common 2D topology afforded by XB tectons is the tiling where rhombs and octagons are present. Anions, usually halide anions, and bi- or tridentate XB donors all sit at the nodes of the rhombic and octagonal networks (Figure 80, HEDGOM and VAPXAM).[442,526]

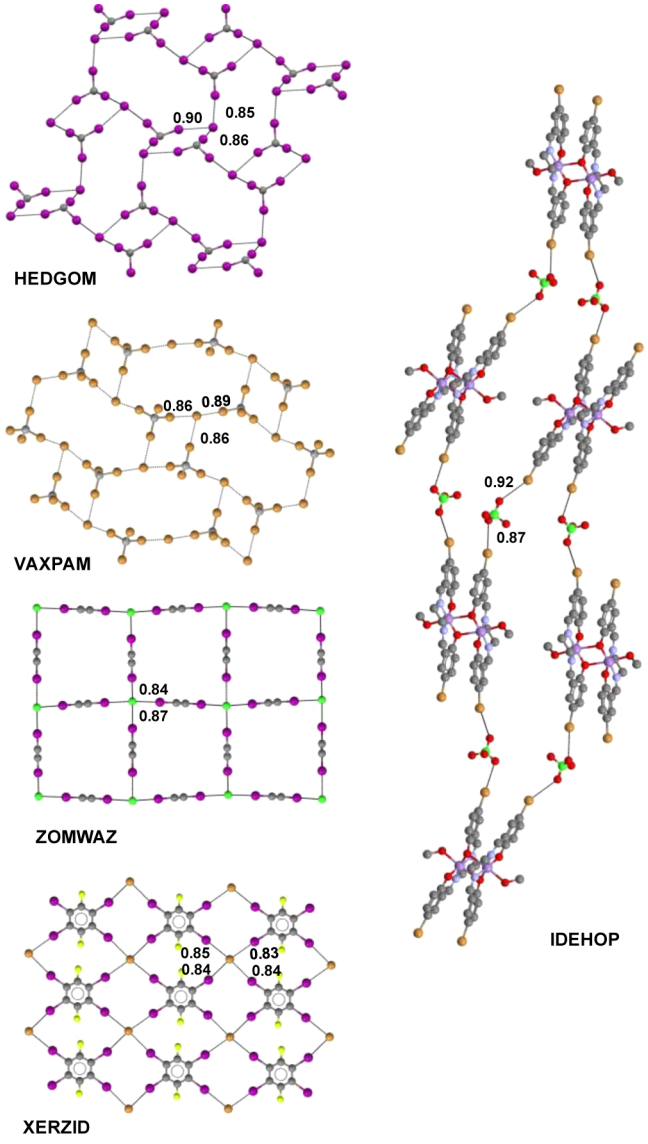

Figure 80. Tilings formed by octagons and rhombs and resulting on self-assembly of iodoform with benzyltrimethylammonium iodide (HEDGOM) and carbon tetrabromide with 1-aza-8-azoniabicyclo(5.4.0)undec-7-ene bromide (VAXPAM). (4,4) networks are obtained on self-assembly of diiodoacetylene with chloride anions (ZOMWAZ), 1,4-difluoro-2,3,5,6-tetraiodobenzene with bromide anions (XERZID), and [bis[[μ_2-*N*,*N*′-bis(5-bromosalicylaldehyde)-ethylenediamino]methanol]manganese(III)] perchlorate (IDEHOP). Hydrogen atoms and cations are omitted. Color code: carbon, gray; nitrogen, blue; oxygen, red; iodine, purple; bromine, light brown; chlorine, light green; fluorine, yellow. Mn atoms in IDEHOP are shown in gray-violet. XBs are dotted black lines. CSD Refcodes are reported.

DOI: 10.1021/acs.chemrev.5b00484
Chem. Rev. 2016, 116, 2478−2601

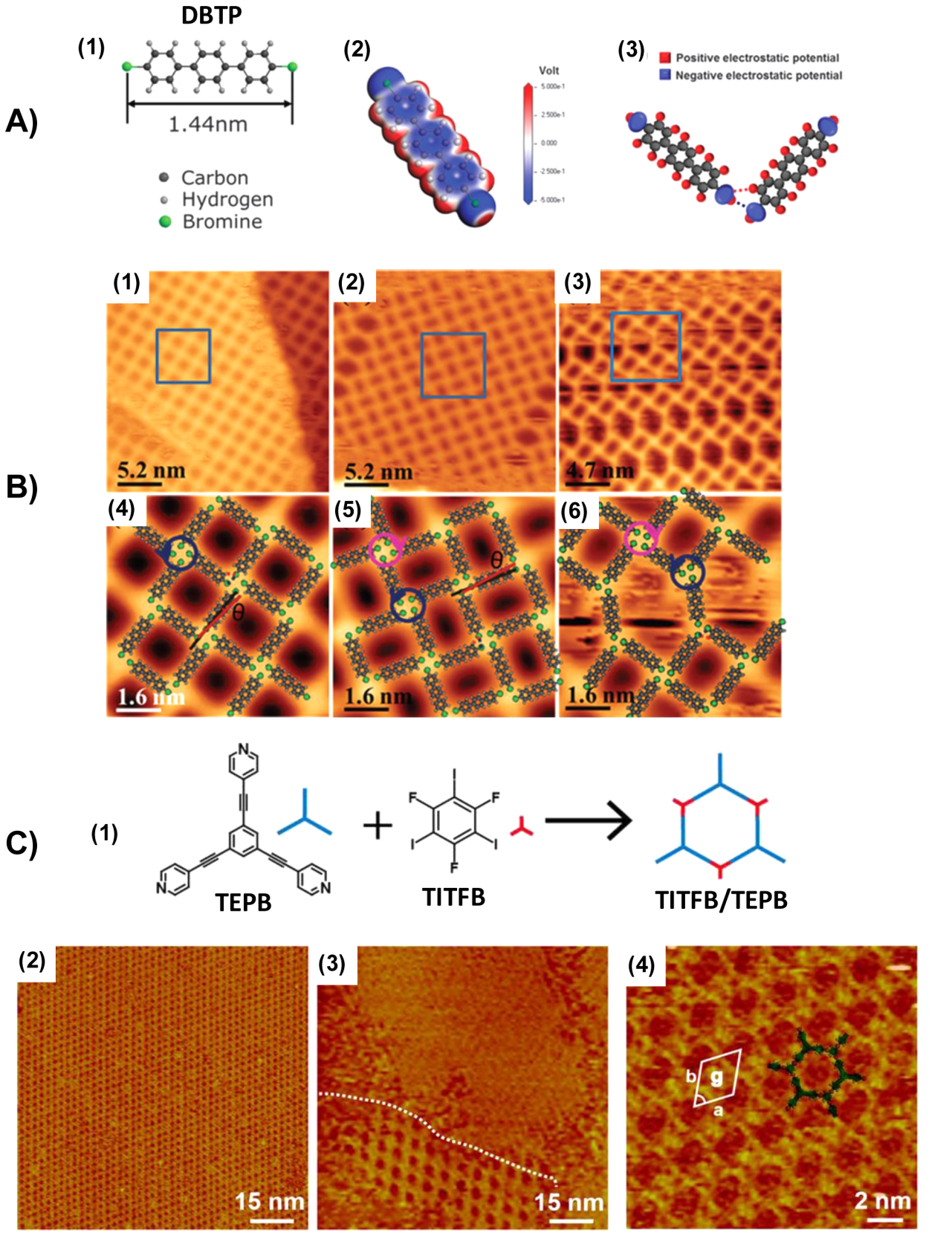

Figure 81. (A) (1) Chemical structure of DBTP. (2) Calculated molecular electrostatic potential distribution of DBTP at the isodensity surface shown in red (positive) and blue (negative). (3) Cartoon of two DBTP molecules with simplified electrostatic potential distributions around H and Br atoms (same color code as in (2)). Dotted blue lines indicate Br···Br XBs, and dotted red lines indicate Br···H HBs. (B) (1−3) STM topography images of three porous networks obtained after DBTP was deposited on Ag(111) at 80 K. (4−6) High-resolution STM images from the square-marked areas in (1), (2), and (3), respectively, with superimposed molecular models of DBTP. Adapted with permission from ref 756. Copyright 2011 Royal Society of Chemistry. (C) (1) Scheme of the self-assembly of tritopic XB acceptor TEPB and XB donor TITFB affording the TITFB/

DOI: 10.1021/acs.chemrev.5b00484
Chem. Rev. 2016, 116, 2478−2601

Figure 81. continued

TEPB honeycomb-like network where the two modules alternate at the nodes. (2) Large-scale STM image of the TITFB/TEPB honeycomb-like structure. (3) The STM image shows the coexistence of a TEPB close-packed structure and the TITFB/TEPB honeycomb-like network. (4) High-resolution STM image of the TITFB/TEPB honeycomb-like structure. Adapted from ref 755. Copyright 2015 American Chemical Society.

Also (4,4) networks have been obtained. In these networks, a tetradentate XB acceptor self-assembles with ditopic[664] or tetratopic[732] XB donors (Figure 80, ZOMWAZ and XERZID). The organization of the resulting (4,4) layers is dictated by the arrangement of the XBs around the halide anions. Oxyanions, by far the most numerous class of anions in organic chemistry, can also form 2D supramolecular networks with chloro-, bromo-, and iodocarbons (Figure 80, IDEHOP).[69,753]

When starting tectons organize on metal surfaces, the formation of halogen-bonded and self-assembled layers is governed by the same principles exemplified above in the formation of bulk crystalline adducts. We have already discussed how in crystalline dihalogens the negative belt on the halogen atom of one molecule enters the positive cap on the halogen of another molecule and layers are formed (Figure 50, YATKIP). Similarly, when 4,4″-dibromo-*p*-terphenyl (DBTP) is deposited on Ag(111), the negative belt of any bromine enters the positive cap of another bromine (Figure 81A) and a porous (4,4) network is formed where the sides of the squares are four terphenyl moieties and the vertexes are four arrays of halogen-bonded bromine atoms (Figure 81B).[754]

Any bromine atom behaves as an XB donor (via its positive cap) and attractively interacts with another bromine, which behaves as an XB acceptor (via its negative belt). Once again, the XB directionality translates the orthogonal arrangement of the binding sites on the starting module DBTP into the topology of the self-assembled porous layer, and the rodlike character of DBTP helps in this translation. H···Br HBs, involving the negative belt of the bromine, are also present in the layer and further pin DBTP modules in their position. However, we have also discussed how the anisotropic distribution of the electron density around covalently bound bromine atoms may account for their organization in the bulk into trigonal and self-complementary supramolecular synthons (Figure 26).

The same happens when DBTP is deposited on silver: Triangular motifs are assembled and hexagonal pores are generated where the sides are terphenyl moieties and the vertexes are three halogen-bonded bromine atoms. Scanning tunneling microscopy (STM) allows for the visualization of these arrays (Figure 81B). The formation of square porous networks on Au(111) by using 4,4″-dibromo-*p*-quaterphenyl (DBQP) was reported a few years after the results described above.[755] The network had chiral quadrupole nodes that were explained with four Br···Br XBs and four H···Br HBs.

XB was also applied to drive the self-assembly of a thienophenanthrene derivative (TPA) at the aliphatic acid/graphite interface using STM.[756] It was found that different nanosized structures could be formed by adjusting the TPA concentration. Even in this case the driving force was the formation of short Br···Br XBs.

Finally, Wan et al.[757] recently demonstrated the formation of XB-based open porous networks on a highly oriented pyrolytic graphite surface using 1,3,5-tris(ethynylpyridyl)benzene (TEPB) as an XB acceptor and TITFB, or analogous diiodinated tectons, as an XB donor. The formation of the 2D networks was driven by I···N XBs, and it was found that the electrical manipulation method of STM was a general method to engineer XB-based structures. In fact, by varying the XB acceptors across various pyridyl derivatives (ditopic, tetratopic), different XB-based binary supramolecular structures were obtained (Figure 81C).

Three-dimensional (3D) architectures can be formed when one or both of the interactive modules are tetradentate. The adamantanoid network is a common motif in 3D arrangements. These architectures have been obtained by using neutral self-complementary tetradentated building blocks containing two XB donor sites and two XB acceptors, by using neutral or anionic tetradentate XB acceptors sitting at the network nodes and being spaced by bidentated XB donors, or by using tetradentated XB donors and acceptors, which alternate at the nodes. Detailed discussion of these systems will be presented in the next section on interpenetrated networks. Here we describe a simple and noninterpenetrated adamantanoid network wherein tetrabromomethane and chloride anion function as the tetradentate XB donor and acceptor, respectively, and alternate at the nodes of the network (VAPVOY, Figure 82).[526] When chloride is replaced by iodide, which functions as an octadentate acceptor, a rhombododecahedron network is obtained instead (VAPWIZ, Figure 82).

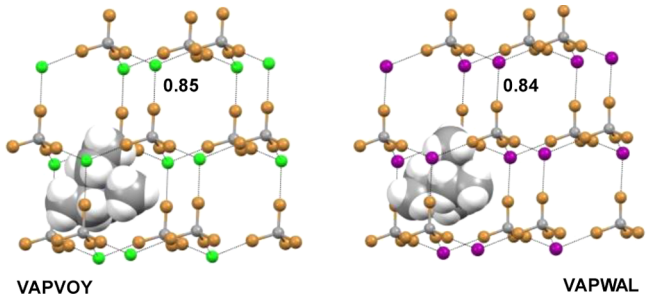

Figure 82. Isomorphous adamantanoid networks formed when tetrabromomethane (the tetradentate XB donor) alternates at the network nodes with chloride (VAPVOY) or iodide (VAPWAL) anions, which function as tetradentate XB acceptors. Cations at the center of the cage are shown in space-filling style. Only one $(C_2H_5)_4N^+$ is drawn for clarity. Color code: carbon, gray; iodine, purple; bromine, light brown; chlorine, light green; hydrogen, white. XBs are dotted black lines. CSD Refcodes are reported.

3.1.4. Interpenetrated Networks. The design and synthesis of entangled supramolecular networks with high structural complexity have always stimulated the scientific curiosity of chemists either due to the aesthetic beauty of these sophisticated architectures or due to the unique and useful functions they may possess, such as robustness or adaptive behavior. Interpenetrated networks are among the most intriguing three-dimensional (3D) systems, and the understanding of their topology is a particularly challenging task.[748,758]

An instrumental strategy for the construction of entangled networks by rational design is to translate the molecular geometry into the supramolecular geometry, namely, to

DOI: 10.1021/acs.chemrev.5b00484
Chem. Rev. 2016, 116, 2478−2601

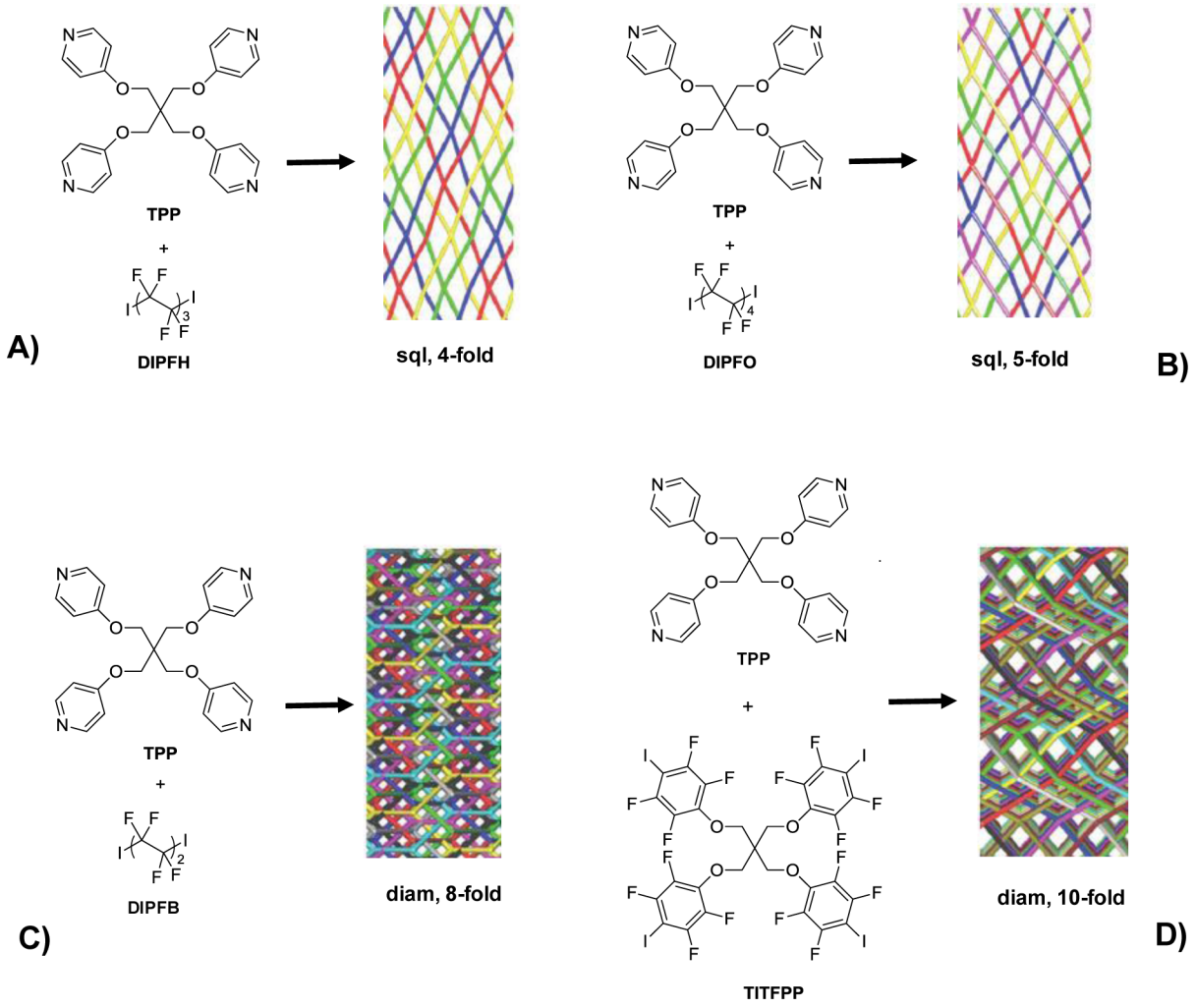

Figure 83. Structures of starting tectons and schematic views, obtained with TOPOS,[748] of the corresponding interpenetrated networks: (A) DIPFH/TPP (sql, 4-fold interpenetration); (B) DIPFO/TPP (sql, 5-fold interpenetration); (C) DIPFB/TPP (dia, 8-fold interpenetration); (D) TITFPP/TPP (dia, 10-fold interpenetration).

translate the topological information encoded in the starting building blocks into the supramolecular topology. This becomes feasible when a highly directional interaction is used to link donor and acceptor modules bearing the binding sites after a convenient geometry. Another possible strategy to influence the formation of interpenetrated systems is the assembly of rigid frameworks having large and uniform (potential) cavities. Entanglement involves several such frameworks, which mutually interlock to satisfy the close-packing requirements and to prevent the system from collapsing, as might be the case if the lack of interpenetration leaves voids in the packing.

As shown in previous sections, the XB is a strong and highly directional interaction, and thanks to these unique features, it could be successfully used to build up robust and rigid supramolecular nets for the assembly of interpenetrated networks.

Tectons with a tetrahedral core are often tailored to form 3D architectures, and if the arms on the core are sufficiently long and rigid to create large cavities, these motifs usually tend to interpenetrate. Following this principle, in 2001 G. R. Desiraju et al. used the 4,4′-diiodo-4″,4‴-dinitrotetraphenylmethane (DIDNTPM) as a self-complementary XB module to construct a supramolecular diamondoid network.[759] The structural characterization of the solid revealed the formation of an interpenetrated system composed by the combination of 5-fold diamondoid and 3-fold square grid networks both assembled by the I···O_2N synthon (N_c = 0.94−0.97).

A few years later, P. Metrangolo and G. Resnati[760] adopted a similar strategy and assembled highly interpenetrated architectures starting from XB donor and acceptor units having a tetrahedral core. The tetrakis(4-pyridyl)pentaerythritol (TPP) and the tetrakis(4-iodotetrafluorophenyl)pentaerythritol (TITFPP) were the XB acceptor and donor modules used in the study. These modules exhibited a greater flexibility than DIDNTPM due to the presence of the oxymethylene spacer bridging the tetrahedral core and the XB binding sites. The absence of a bias toward the diamondoid structure allowed for the obtainment of a small library of interpenetrated networks with quite different topologies and connectivities. In all of the cocrystals, TPP functioned as a robust tetradentate XB acceptor thanks to its four pyridyl rings, the N_c values for the I···N contacts spanned the 0.82−0.86 range, and all C−I···N angles were close to linear (160°−178°). When TPP was cocrystallized with 1,6-diiodoperfluorohexane (DIPFH) and 1,8-diiodoperfluorooctane (DIPFO), the corresponding adducts showed a 1:2 stoichiometry and two-dimensional (2D) square

DOI: 10.1021/acs.chemrev.5b00484
Chem. Rev. 2016, 116, 2478−2601

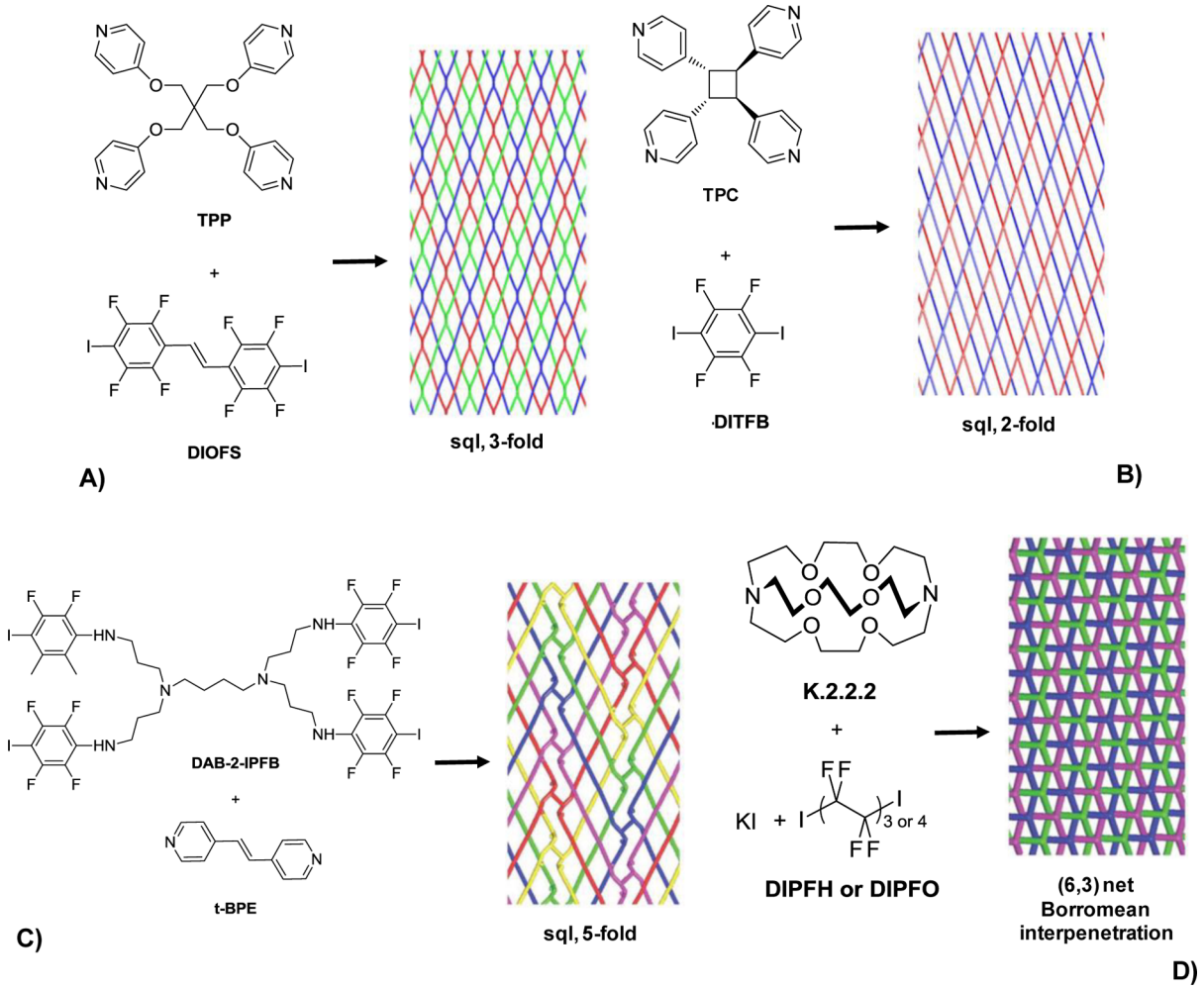

Figure 84. Structures of starting tectons and schematic views, obtained with TOPOS,[748] of the corresponding interpenetrated networks: (A) DIOFS/TPP adduct (sql, 3-fold interpenetration); (B) DITFB/TPC (sql, 2-fold interpenetration); (C) DAB-2-IPFB/*t*-BPE (sql, 5-fold interpenetration); (D) K.2.2.2/KI/DIPFH or DIPFO ((6,3) net, Borromean interpenetration).

4^4 layers (sql) with 4-fold and 5-fold interpenetrations, respectively (Figure 83).

When TPP was cocrystallized with 1,4-diiodoperfluorobutane (DIPFB) and TITFPP, adducts with 1:2 and 1:1 stoichiometries were obtained, respectively, and they both showed a diamondoid (dia) interpenetration with a rare 8-fold interpenetration of class Ia and a remarkable 5 × 2 = 10-fold interpenetration of class IIIa. The tendency of TPP to form interpenetrated nets was further confirmed when it was cocrystallized with 4,4′-diiodooctafluorostilbene (DIOFS), another rigid, linear, and ditopic XB acceptor. The X-ray characterization of the obtained cocrystal revealed that the self-assembled architecture was formed by alternating parallel layers having a square 4^4 topology, each layer resulting from the interpenetration of three different square networks (Figure 84).

When tetrakis(4-pyridyl)cyclobutane (TPC), a tetradentate tecton more rigid than TPP, was cocrystallized with 1,4-diiodotetrafluorobenzene (1,4-DITFB), an entangled network exhibited a 2D square 4^4 network with a 2-fold interpenetration of class IIa (Figure 84).[761]

A further example of halogen-bonded interpenetrated networks was achieved by the same authors[762] by using poly(propylenimine) dendrimer DAB-*dendr*-$(NHC_6F_4I)_2^2$ (DAB-2-IPFB) as the XB donor and *trans*-1,2-bis(4-pyridyl)-ethylene (*t*-BPE) as the XB acceptor. The construction of the supramolecular network was driven by the I···N synthon ($N_c \approx 0.8$), which thanks to its high directionality (C−I···N in the range of 173−178°) was able to effectively translate the tetragonal arrangement of the DAB-*dendr* tectons into the overall network. Topological analysis showed that the XB donor/acceptor modules were assembled in very large 2D square networks and the overall packing was composed of 5-fold interpenetrated and translationally related square 4^4 layers (Figure 84).

These examples of interpenetration, although limited in number, may suggest that the use of donor and acceptor modules with similar geometries and different sizes afford self-assembled networks with similar topologies and different sizes where the larger modules afford more extended networks and the resulting larger voids allow for a higher interpenetration.

Also anionic XB acceptors allowed for the obtainment of interpenetrated networks as was the case for some nets having iodide anions at the nodes of the nets and showing a Borromean entanglement. Borromean rings constitute one of the most fascinating patterns of topological entanglements, and their distinctive topological features lie in their mode of interpenetration: Three mutually disjoint simple closed curves form a link, yet no two rings are linked; thus, if one is cut, the

DOI: 10.1021/acs.chemrev.5b00484
Chem. Rev. 2016, 116, 2478−2601

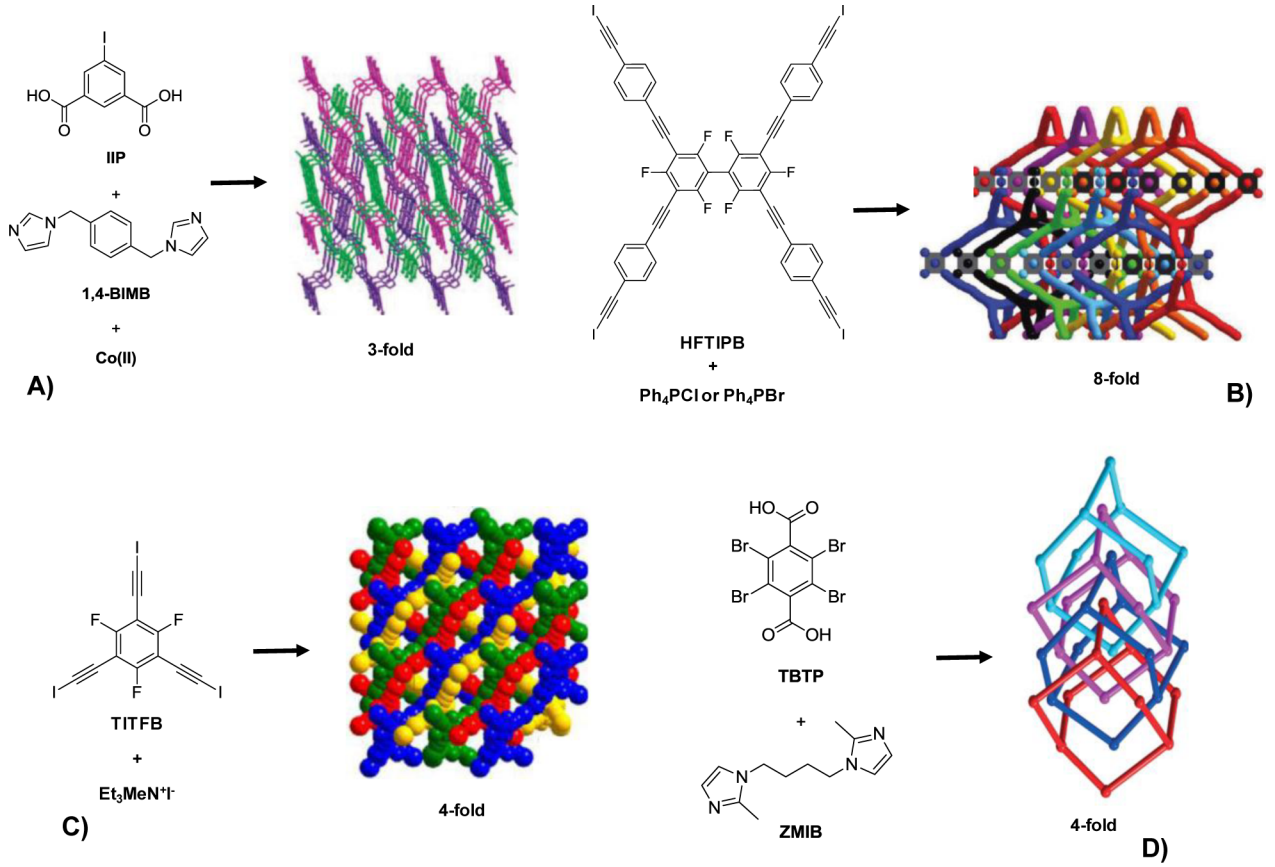

Figure 85. Structures of starting tectons and schematic views, obtained with TOPOS,[748] of the corresponding interpenetrated networks. (A) $[Co(1IP)(1,4\text{-BIMB})]_n$ (3-fold interpenetration). Adapted from ref 764. Copyright 2011 American Chemical Society. (B) HFTIPB/Ph_4PCl or Ph_4PBr (8-fold interpenetrated net of class Ia). Adapted from ref 765. Copyright 2011 American Chemical Society. (C) TITFB/$Et_3MeN^+I^-$ (4-fold interpenetration of class IIIa). Adapted from ref 766. Copyright 2013 American Chemical Society. (C) $[Zn_2(BMIB)(TBTP)_2{\cdot}2H_2O]_n$ (4-fold interpenetration dia of class IIIa). Adapted with permission from ref 767. Copyright 2014 Royal Society of Chemistry.

other two fall apart. In 2006, the first halogen-bonded Borromean networks were obtained on self-assembly of the kryptand 4,7,13,16,21,24-hexaoxa-1,10-diazabicyclo[8.8.8]-hexacosane (K.2.2.2), potassium iodide (KI), and DIPFH or DIPFO (Figure 84).[763] K.2.2.2 chelates K^+, and the formed naked iodide anion behaves as a tridentate XB acceptor, which sits at the nodes of the network and binds three different diiodoperfluoroalkanes, which, in turn, behave as bidentate XB donor spacers connecting the nodes. The final supramolecular architectures of K.2.2.2/KI/DIPFH and K.2.2.2/KI/DIPFO present infinite and highly undulated honeycomb-like sheets where each chair-shaped hexagon is defined by six noncoplanar iodide anions (vertexes) and six diiodoperfluoroalkanes (connectors). N_c values for $I\cdots I^-$ contacts are 0.83 and 0.85 for Borromean systems formed by DIPFH and DIPFO, respectively. Once again, the strength and directionality of XB, along with the stiffness of the perfluorinated modules, allowed the transfer, with great accuracy, of the arrangement of anions in the crystal packing to the XB donor tectons forming the undulated (6,3) honeycomb-like arrangement, which remained unmodified when the XB donor was changed. The fine balance between supramolecular synthon strength and module dimensions allowed for the formation of isostructural halogen-bonded hexagonal grids with large and uniform cavities, which have induced the fluorinated layers to mutually interlock in a Borromean fashion.

Several interpenetrated coordination polymers (CPs) have been obtained starting from manganese, zinc, or cobalt ions, different nitrogen ligands (such as *t*-BPE or 1,4-bis(imidazol-1-ylmethyl)benzene (1,4-BIMB) or its 1,3-analogue (1,3-BIMB)), and the rigid ligand 5-iodoisophthalic acid (IIP),[764] where the iodine atom was expected to support the supramolecular synthons I···O, I···N, I···π, and I···I. The CP $[Zn(IIP)(t\text{-}BPE)_{1.5}]_n$ featured interesting 3-fold parallel interpenetrated two-dimensional (2D) → 3D network motifs, which were stabilized by interlayer I···π, $\pi\cdots\pi$, and C−H···π interactions. In the structure $[Co(IIP)(1,4\text{-BIMB})]_n$, the ligand adopted a μ_2-bridge coordination mode through bis-monodentate carboxylate moieties linking two Co centers to form infinite chains along the *a*-axis, which were expanded into a 2D system through μ_2-bridged 1,4-BIMB ligands. The adjacent layers were connected by I···O contacts (N_c = 0.95−0.97) to form a 3D supramolecular structure, and three sets of them are interlocked with each other to display a 3-fold interpenetrating architecture (Figure 85A). The complex $[Co(IIP)(1,3\text{-BIMB})]_n$ also showed I···O XBs (N_c = 0.97), which promoted a rare 2-fold interpenetrating 3D supramolecular architecture.

Interpenetrated and halogen-bonded networks were serendipitously formed by R. Kato and M. Fourmigué[765] during the development of various nanowire crystals where the insulating networks were made of halide anions halogen-bonded to rigid neutral molecules. The authors synthesized an aromatic tecton with an extended skeleton, 2,2′,4,4′,6,6′-hexafluoro-3,3′,5,5′-

DOI: 10.1021/acs.chemrev.5b00484
Chem. Rev. 2016, 116, 2478−2601

tetrakis[[(4-(iodoethynyl)phenyl]ethynyl]biphenyl (HFTIPB) and possessing a pseudotetrahedral symmetry. Electrocrystallization experiments of this tecton with a bis(propylenedithio)-tetrathiafulvalene (BPTTF) derivative were performed in the presence of PPh_4Cl or PPh_4Br. The two corresponding cocrystals adopted a complex structure with mixed radical BPTTF cation/Br^- (or Cl^-) anion layers alternating with the neutral HFTIPB molecules. The halide anions behaved as tetradentate XB acceptors toward four iodine atoms of four different HFTIPB molecules, driving the formation of a square planar motif. The overall connectivity pattern around one halide anion led to the formation of a complex sublattice, which showed an 8-fold interpenetrated net of class Ia (Figure 85B).

The strategy to use halide anions and neutral XB tectons to develop supramolecular structures having conducting properties was further investigated by assembling 1,3,5-tris-(iodoethynyl)-2,4,6-trifluorobenzene (TITFB), a tritopic and neutral XB donor, with different haloorganic salts. It was expected that, similar to triiodotrifluorobenzene,[539] the tridentate XB donor TITFB could afford 2D (6,3) networks with large cavities, which could accommodate guest molecules or could form entangled networks. As anticipated, the cocrystallization of TITFB with several halide salts having different cations in a 1:1 ratio produced (6,3) honeycomb-like networks where the halide anions behaved as tridentate XB acceptors connecting three different TITFB units by I···X^- contacts (X = I, Br). Specifically, the adduct between TITFB and $Bu_3S^+I^-$ showed a highly corrugated and halogen-bonded (6,3) system where N_c for I···I^- was 0.82 and the (6,3) networks showed a 2-fold interpenetration. The self-asembly of TITFB and $Et_3MeN^+I^-$ afforded architectures with more sophisticated topologies. Iodide anions were tridentate, but while bridging three different TITFB molecules, the expected 2D (6,3) network was not formed, since one of the three TITFB units was rotated out of the network plane and a complex 3D anionic network was formed where the very large cavities enabled for a 4-fold interpenetration of class IIIa (Figure 85C).[766] A very rare example of an entangled halogen-bonded system was obtained when TITFB and $Et_3BuN^+Br^-$ were mixed in a 2:1 ratio. The assembly process driven by XB (N_c for I···Br^- is 0.83) produced a cubic structure where the bromide anion assumed an unprecedented hexadentate octahedral coordination, which, in combination with the trigonal nodes provided by the TITFB molecule, generated a hexagonal 3D network with a 2-fold interpenetration of class Ia.

Interpenetrated coordination polymers were also assembled by reacting, under solvothermal conditions, tetrabromoterephthalic acid (TBTP) with zinc ion and 1,4-bis(2-methyl-1*H*-imidazol-1-yl)butane (BMIB), a flexible ligand.[767] The single-crystal X-ray diffraction analysis of those crystals revealed that the $[Zn_2(BMIB)(TBTP)_2{\cdot}2H_2O]_n$ unit was assembled into single diamondoid networks with huge voids, which allowed other networks to entangle each other, leading to a 4-fold interpenetrated dia net of class IIIa (Figure 85D). The interpenetrated net was reinforced by several hydrogen bonds, type I halogen−halogen contacts, and Br···Br XBs occurring between close TBTP molecules belonging to different diamond networks (N_c for Br···Br is 0.96, and the C−Br···Br angle is 152°).

3.2. Applications

3.2.1. Porous Systems. The dynamic behavior of host−guest systems has received a lot of attention for its great relevance in applications such as encapsulation and separation, among others. The halogen bond has opened new avenues in this field thanks to its specificity for halocarbons, a class of industrially important compounds.

The first example in this field dates back to 1999, when P. Metrangolo and G. Resnati used the Lewis base (−)-sparteine hydrobromide to resolve the racemic 1,2-dibromohexafluoropropane. The resolution occurred as a result of a highly specific inclusion of only the (*S*)-enantiomer in a chiral crystal with a halogen-bonded helical arrangement formed by halogen bonds between the C-bound Br atoms of the perfluoropropane and the Br^- ions of the enantiopure base.[263]

Interestingly, in 2005 T. Takeuchi and co-workers[768] developed an imprinted polymer based on XB to be applied as a stationary phase in a separation technique. In general, molecularly imprinted polymers are host systems synthesized by copolymerization of functional monomer(s) and cross-linker(s) in the presence of a template guest molecule.[769] The resulting polymers have selective binding sites complementary to the template guest. In noncovalent imprinting, the functional monomers are selected to establish specific intermolecular interactions with the guest molecule. An approach based on supramolecular assembly has been largely promoted because (I) it facilitates the preorganization of complexes induced by the mutual recognition between the monomer(s) and the guest and (II) it favors the formation of the host cavities after the removal of the templates by washing.

The formation of an imprinted polymer host based on halogen bonding was achieved by the polymerization of the functional monomer 2,3,5,6-tetrafluoro-4-iodostyrene, the XB donor, with divinylbenzene and styrene as cross-linking agents, in the presence of 4-(dimethylamino)pyridine as the templating guest. It was expected that the XB acceptor template would recognize the XB donor sites on the host system, imprinting the molecular shape of the guest into the polymer and creating specific binding sites highly selective for the 4-(dimethylamino)pyridine guest and its structural analogues. The binding affinity and the imprinted properties of the resulting system were investigated by competitive experiments using different XB acceptors bearing either aliphatic or aromatic nitrogen groups. The 4-(dimethylamino)pyridine guest showed one of the highest affinities for the porous polymeric host among the different XB acceptors used. This behavior was rationalized by the fact that a synergistic effect deriving from the templating process occurred during the polymerization and the presence of two electron density donor sites on the guest. However, the XB-imprinted polymer showed an even higher affinity for the less bulky 4-aminopyridine, suggesting that steric hindrance sensibly influenced the recognition phenomena (Figure 86).

α,ω-Diiodoperfluoroalkanes ($I(CF_2)_mI$, $DIPFA_m$) are a class of key intermediates in the synthesis of various fluorochemicals and fluoropolymers,[770] and an elegant method for their effective separation was reported in 2009 and expanded the concept of dynamic recognition of host systems in the solid state. It was observed that when a mixture of α,ω-diiodoperfluoroalkanes and a given α,ω-bis-(trimethylammonium)alkane diiodide ($((CH_3)_3N(CH_2)_nN(CH_3)_3{\cdot}2I^-$, $BTMAA_n$) are crystallized from solution, the $BTMAA_n$ organic salt instantaneously forms a cocrystal, driven by the I···I^- XB, with $DIPFA_m$ when $m = n - 6$. The preferential molecular recognition of a given $DIPFA_m$ was due to the enhanced electrostatic binding strength in the ionic

DOI: 10.1021/acs.chemrev.5b00484
Chem. Rev. 2016, 116, 2478−2601

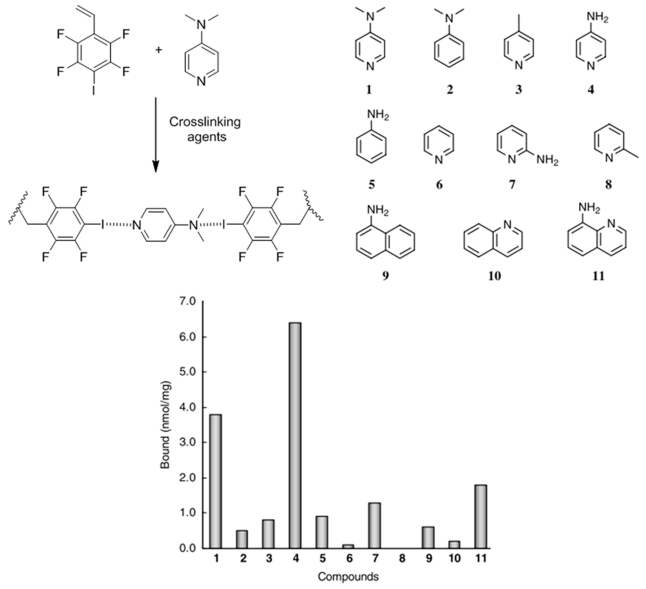

Figure 86. Top: possible structure of the molecularly imprinted polymer obtained using 2,3,5,6-tetrafluoro-4-iodostyrene as the monomer and 4-(dimethylamino)pyridine as the template. Bottom: binding affinities of different XB acceptors for the imprinted polymer. Adapted with permission from ref 768. Copyright 2005 Elsevier Ltd.

lattice wherein the size of the halogen-bonded superanion $I^-\cdots I(CF_2)_mI\cdots I^-$ matched that of the dicationic alkyl chain in the diammonium moiety. Several consistent examples proved that selective recognition occurred only when the "size-matching rule" was respected, namely, when the separation between the two iodide anions in the superanions matched the distance between the two positive N atoms in the cations by around 0.7−1 Å or less. This size complementarity is exemplified by the single-crystal structure of the complex $DIPFA_4\cdots BTMAA_{10}$ (Figure 87), where four alkyl dications define a rectangular parallelepiped cavity that encapsulates a $DIPFA_4$ molecule which is pinned in its position by strong XBs to the two I^- ions at either end. Here the difference between the intramolecular distance of the N atoms in the cation and the iodide ions' spacing is 0.85 Å.

It was found that even microcrystalline powders of the iodide organic salts could selectively and reversibly incorporate $DIPFA_m$ from the gas phase despite the absence of porosity in the starting crystal structures of $BTMAA_n$. The selective guest adsorption through a solid−gas reaction occurring under control by the size complementarity of the modules in the host−guest structure proved the dynamic behavior of these materials. Since the starting organic salts are not porous in nature, the formation of the size-matched halogen-bonded complexes occurred through a remarkable dynamic and reversible rearrangement of the $BTMAA_n$ crystal lattice, which created the space to accommodate the size-matched $DIPFA_m$ after an allosteric process, which was not observed in the mismatched complexes. Interestingly, a system where a $BTMAA_n$ is halogen bonded to a mismatched $DIPFA_m$ ($m \neq n - 6$) can also be obtained, and when powders of these materials are exposed to vapors of the size-matched $DIPFA_m$ ($m = n - 6$), the "right" $DIPFA_m$ substitutes for the "wrong" one in a gas−solid reaction. This confirms that bis(trimethylammonium)alkane diiodide salts are a very promising new class of dynamically porous materials.

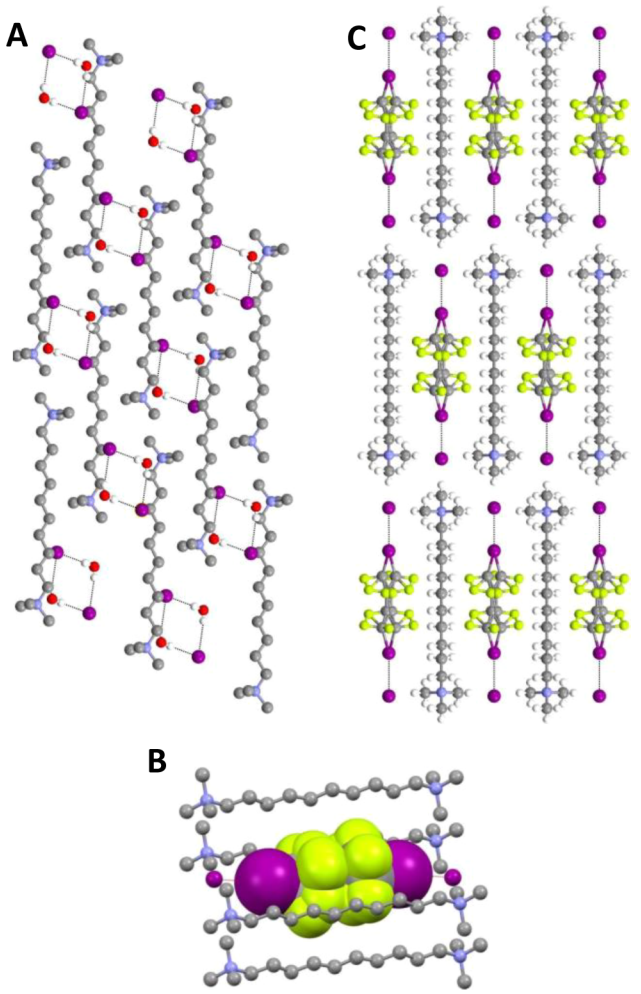

Figure 87. (A) Packing of bis(trimethylammonium)decane diiodide dihydrate (XOVBIU) viewed along the *a*-axis. (B) Complex bis(trimethylammonium)decane diiodide/diiodoperfluorobutane (XOVBAM) showing the molecular cavity defined by four alkyl dications, with encapsulated disordered guest molecules (space-filling style). This molecule is halogen-bonded to I^- ions at the top and the bottom. (C) Crystal packing of the same complex viewed along the *c*-axis. The α,ω-DIPFA molecules are disordered over two positions. In (A) only the water H atoms are reported. In (B) no hydrogen atoms are reported. Color code: carbon, gray; nitrogen, blue; oxygen, red; iodine, purple; fluorine, yellow; hydrogen, white. XBs and HBs are dotted black lines.

The dynamic behavior of bis(trimethylammonium)alkane diiodide salts was also exploited to trap the shortest and iodine-based XB donor, i.e., diiodine. The crystallization of the diiodide salt of 1,6-bis(trimethylammonium)hexane (HMET) with I_2 in a 1:1 ratio led to the quantitative formation of the discrete I_4^{2-} dianion (Figure 88A), a molecular entity that is a shallow minimum in the surface potential of systems compounded by I_2 and I^-.[771] Similarly, the triiodide of 2,2,9,9,16,16-hexamethyl-2,9,16-triazoniaheptadecane, a triammonium cation structurally related to HMET, trapped two I_2 molecules and formed the discrete I_7^{3-} trianion (Figure 88B).[772] In both cases, the formation of these unusual polyiodides as isolated species was driven by a combination of two factors: the ability of I^- to function as a very efficient XB acceptor toward I_2 and the size matching between the superanion units and the intraatomic N^+-N^+ separation in

DOI: 10.1021/acs.chemrev.5b00484
Chem. Rev. 2016, 116, 2478−2601

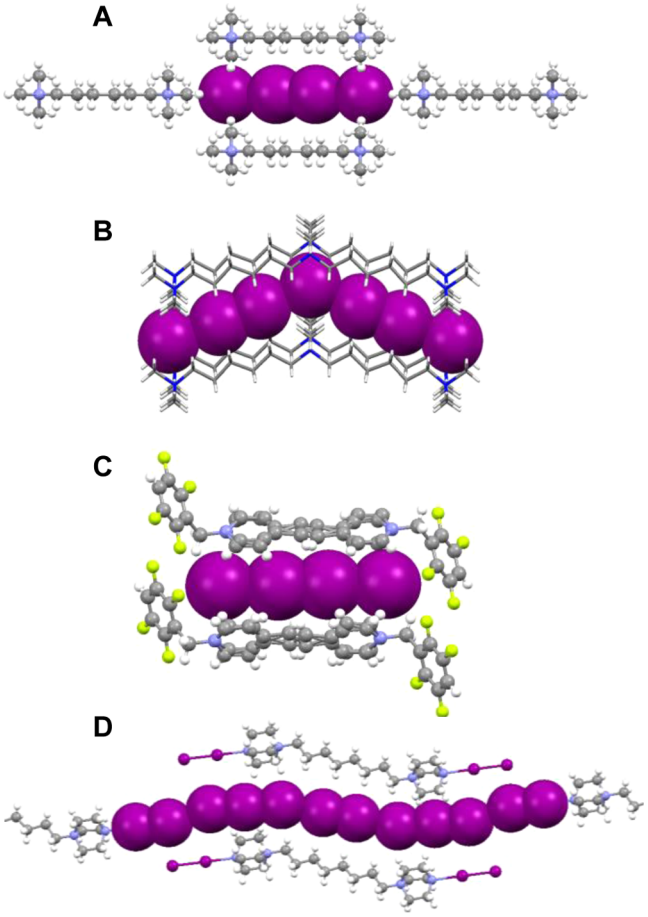

Figure 88. Partial view (ball-and-stick representation) of the crystal packing of (A) the discrete I_4^{2-} anion hosted in a size-matched cavity formed by four HMET units, (B) the discrete I_7^{3-} anion surrounded by four trication units, (C) the discrete I_4^{2-} anion caged between two *N*,*N*′-bis(tetrafluorobenzyl)-(*E*)-1,2-bis(4,4′-bipyridinium)ethylene units (the cations are disordered over two positions), and (D) the complex containing the discrete pseudolinear dodecaiodide species. Polyiodide anions are represented in space-filling style. Color code: carbon, gray; nitrogen, blue; iodine, purple; fluorine, yellow; hydrogen, white.

the cations. These discrete polyiodide systems were obtained from both solution and gas−solid reaction, and both the bi- and the triammonium cations were able to reversibly uptake and release I_2 by external stimuli, demonstrating further their dynamically porous character.

Some viologen derivatives with structurally different pendants on the nitrogen atoms of the pyridyl rings showed a similar uptake of XB donor guests under size-matching control. The pendants on the nitrogen atoms effectively hampered catenation of polyiodide species by capping the compartments of the crystal lattice identified by the dimensions of the viologen cations. Specifically, *N*,*N*′-bis-(tetrafluorobenzyl)-(*E*)-1,2-bis(4,4′-bipyridinium)ethylene was able to stabilize the I_4^{2-} superanion independently of the I_2 stoichiometry used during the crystallization process. The bipyridiniumethylene moieties adopted a nearly planar conformation, and four of them were the sides of a parallelepiped cage self-capped by the fluorophenyl rings of benzyl pendants (Figure 88C).[773]

The isolation of discrete halogen-bonded I_4^{2-} units was also achieved using perfluorobenzene-substituted bisphosphonium salts, where the superanion was positioned in a cavity and stabilized by anion···π interactions occurring with the perfluorinated rings.[163] Cation-templated synthesis was more recently adopted to obtain long and discrete polyiodide species, as is the case for dicationic N donors based on 1,4-diazabicyclo[2.2.2]octane, which was able to template discrete pseudolinear dodecaiodide species (Figure 88D).[774]

The dynamic response of bis(trimethylammonium)alkane dihalide salts toward the inclusion of XB donor guests was further exploited for the isolation of previously unknown mixed tetrahalides. It has been reported that, on reaction with 2 equiv of I_2, hexamethonium chloride and bromide afford the corresponding mixed trihalides XI_2^- (X = Cl, Br),[775] which undergo thermally induced crystal-to-crystal elimination of one I_2 molecule, yielding quantitatively the virtually unknown tetrahalides $[Cl_2I_2]^{2-}$ and $[Br_2I_2]^{2-}$ (Figure 89). In these tetrahalide dianions, the lighter Cl^- and Br^- halides double-pin a single I_2 molecule via short XBs, forming the tetrahalide units, which are selectively encapsulated by the HMET dications as a consequence of size matching of the self-assembled components. The starting units in the HMET·$2XI_2^-$ trihalides are preorganized to respond dynamically to heating and eliminate

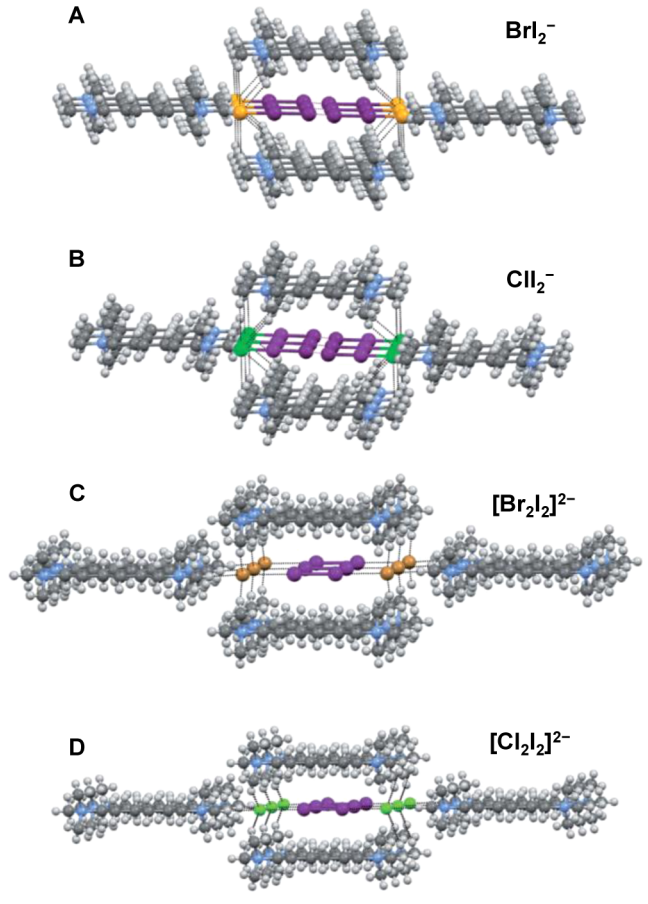

Figure 89. Partial view (ball-and-stick representation) of the crystal packing of (A, B) the mixed trihalide adducts HMET·$2XI_2^-$ (A, X = Br; B, X = Cl) and (C, D) the mixed tetrahalides $[Br_2I_2]^{2-}$ (C) and $[Cl_2I_2]^{2-}$ (D), obtained upon heating of the corresponding trihalides from (A) and (B). These mixed polyhalides are held together by XBs and are pinned by HBs in the cavities formed by four dication units. Color code: carbon, gray; nitrogen, blue; iodine, purple; bromine, light brown; chlorine, light green; fluorine, yellow; hydrogen, white. XBs and HBs are dotted black lines.

DOI: 10.1021/acs.chemrev.5b00484
Chem. Rev. 2016, 116, 2478−2601

one I_2 molecule and afford the tetrahalide. Interestingly, the second I_2 molecule was so tightly bound that it could be released only upon melting of the solid supramolecular system.[487]

The examples reported above showing the ability of bis(trimethylammonium)alkane dihalide salts to dynamically and reversibly encapsulate molecular guests demonstrate that the behavior is general and may have far-reaching applications for the encapsulation and separation of other guests of industrial relevance, for example the separation of dicarboxylic acids by engaging the halide ions of $BTMAA_n$ in interactions other than XB.

As for gas−solid reactions which produce halogen-bonded cocrystals, it has been reported that simple Cu(II) coordination complexes such as *trans*-$[CuCl_2(3\text{-Xpy})_2]$ (X = Cl, Br) react as crystalline solids with either hydrated or anhydrous HCl gas to give rise to the crystalline salts $(3\text{-Xpy})_2[CuCl_4]$. The absorption of the gaseous HCl induced a variation in the coordination sphere of the metal sites, which produced drastic solid-state rearrangements of the molecular structures. Crystallographic studies suggested that the reorganization of the HB and XB patterns present in the starting structures played a mayor role during the reorganization process.[776,777] In addition, the reactions were reversible, and the Cu(II) coordination complexes showed a good sensitivity to the HCl gas in the range of 200−20000 ppm.

The same authors extended the above-mentioned studies on HCl absorption by exposing the complex *trans*-$[CuBr_2(3\text{-Brpy})_2]$ to vapors of aqueous HBr. The resulting crystalline salt $(3\text{-BrpyH})_2[CuBr_4]$ showed the same chemical composition as above, but a different crystal structure compared to its $(3\text{-BrpyH})_2[CuCl_4]$ counterpart. Despite this structural difference on HX addition, the reverse reaction, i.e., removal of HX, returned each system to a common structural arrangement (Figure 90).[778]

The design of materials with channels or cavities for gas storage/separation or for reaction catalysis is a relatively recent and very important research topic. Metal−organic frameworks (MOFs) are the materials by far most commonly used for these purposes,[681,779] as the directionality and robustness of metal coordination allows for a careful design of the porosity of the systems. HB has recently received growing attention for the purpose,[780] while quite a few reports describe the preparation via XB of molecular frameworks possessing well-defined cavities in their lattice. In 2009 K. Rissanen et al. reported the successful use of XB for the rational design of porous materials obtained by the self-assembly of rigid macrocyclic building blocks.[184] Piperazine cyclophanes, thanks to the structural rigidity of their rings, could in principle accommodate small neutral guest molecules and were selected as starting building blocks. They were cocrystallized with 1,4-diiodotetrafluorobenzene (XB donor) in different molar ratios. The X-ray studies revealed that the cyclophane modules segregated into columns where the cyclophane cavities were piled up to form infinite tubular structures, with the different tubes cross-linked by I···N XBs. Chloroform molecules (crystallization solvent) occupied the intramolecular cavities of the cyclophanes (Figure 91). The calculated void revealed that the roughly cyclindrical voids represented 13% of the unit cell volume.

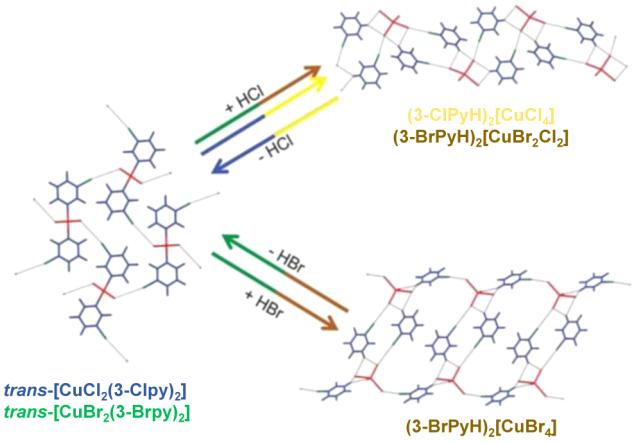

Figure 90. Different structural arrangements observed in the products of the reaction between crystalline *trans*-$[CuX_2(3\text{-Xpy})_2]$ and HCl or HBr gases. The colors of the arrows and of the chemical formulas are associated. Metal and halide ligands are shown in red, organic halogens in green, and all other atoms in blue (C, H, N). Black dotted lines represent HBs and XBs. Reprinted with permission from ref 778. Copyright 2011 Royal Society of Chemistry.

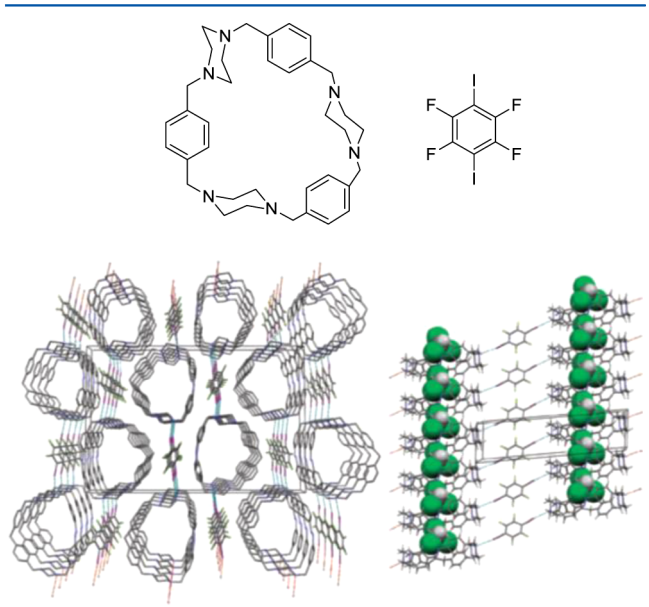

Figure 91. Top: molecular structures of the used XB donor and acceptor. Bottom: crystal packing of the halogen-bonded complex showing the ciclophane tubes. The XB is represented by dotted lines. The included chloroform molecules are omitted in the left plot and are shown in space-filling style in the right plot. Reprinted from ref 184. Copyright 2009 American Chemical Society.

The same group in 2012 reported the formation of molecular crystals with nanosized channels. These systems showed an unusual "breathing behavior", which allowed for the modulation of the volume and shape of the channels upon induced fit with the solvent guests. The basic supramolecular unit was composed by one hexamethylenetetramine (HMTA) unit and four *N*-iodosuccinimide (NIS) molecules, which were assembled by strong and highly directional I···N XBs ($N_c \approx 0.8$).[781] The $[NIS]_4$···[HMTA] complexes crystallized in three different polymorphic forms by varying the crystallization solvent. All the forms gave columnar assemblies as a primary motif, and the obtained supramolecular pillars, sustained by internal HB networks, were assembled parallel to each other to optimize the channel space for the selected guest molecules.

DOI: 10.1021/acs.chemrev.5b00484
Chem. Rev. 2016, 116, 2478−2601

Toluene, chloroform, nitromethane, and acetonitrile were hosted in the tubular channels. The inclusion of dichloromethane and carbon tetrachloride resulted, instead, in the formation of a very robust crystal lattice with well-defined square grid channels, which survived guest exchange by single-crystal to single-crystal transformation (Figure 92).

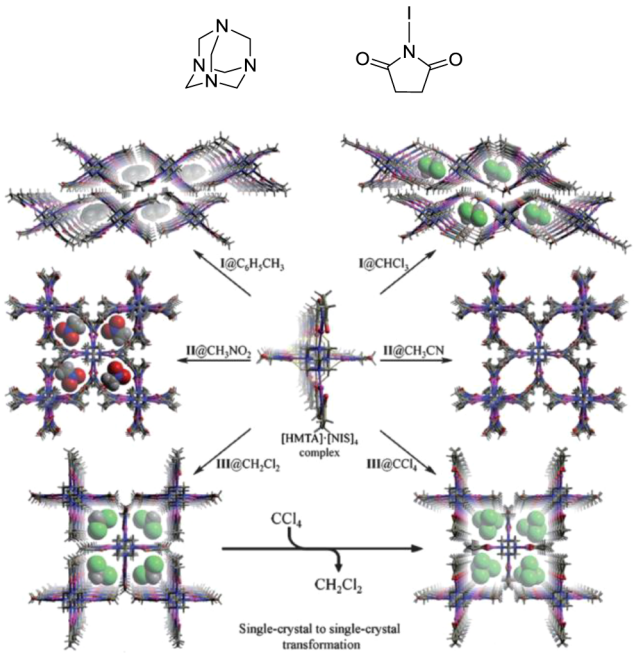

Figure 92. Top: molecular structures of the used XB acceptor and donor. Bottom: crystal structures of the $[NIS]_4$···[HMTA] complexes obtained upon crystallization from different solvents. Crystal structures of $[NIS]_4$···[HMTA]@$C_6H_5CH_3$ and $[NIS]_4$···[HMTA]@$CHCl_3$ as well as $[NIS]_4$···[HMTA]@CH_3CN and $[NIS]_4$···[HMTA]@CH_3NO_2 are isomorphs, whereas $[NIS]_4$···[HMTA]@CH_2Cl_2 and $[NIS]_4$···[HMTA]@CCl_4 are different, but can be interconverted via guest molecule exchange. Adapted with permission from ref 781. Copyright 2012 Royal Society of Chemistry.

In the same year, some of us reported the formation of a molecular open organic framework which showed 2D channels and was able to host various guest molecules and interchange them in single-crystal to single-crystal reactions.[782] The 4,4′-[1,2-bis(2,3,5,6-tetrafluoro-4-iodophenoxy)ethane-1,2-diyl]-dipyridine possessed two pairs of sites (the nitrogen and iodine atoms of pyridyl and iodotetrafluorophenyl rings, respectively) for potential chemically and geometrically orthogonal binding modes and was selected as a molecular building block for framework preparation. Consistent with the adopted design, the obtained framework was assembled via orthogonal and cooperative XB and HB. The inherent tendency of the molecular building block to self-assemble via I···N XBs was disrupted using hydrogen iodide, which functioned as a source of both H^+, a strong HB donor for the protonation of the pyridine moiety, and I^-, a strong XB acceptor for the binding of the iodotetrafluorophenyl ring. Both H^+ and I^- behaved as bidentate connectors and formed robust and linear I···I^-···I and N···H^+···N synthons. These synthons translated the cruciform shape of the starting module, having the four arms fully extended two-by-two to opposite sides, into the topology of the obtained network, comprising quasi-rectangular 2D grids. Two adjacent grid layers gave rise to a biporous network consisting of two channels with different shapes and chemical environments. The channels hosted various guest solvent molecules such as dioxane, nitrobenzene, or 1,3-dibromobenzene. The XB/HB network was robust enough to sustain a single-crystal to single-crystal and reversible exchange of the guest which occurred under gas−liquid conditions. Nitrobenzene and 1,3-dibromobenzene were, in fact, neatly substituted for dioxane without disrupting the framework topology (Figure 93).

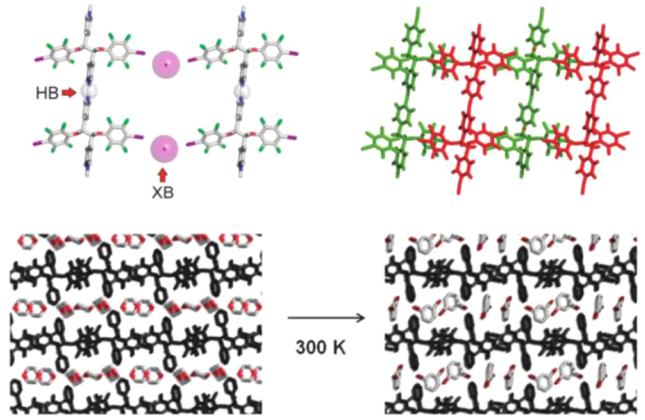

Figure 93. Top left: partial view (stick representation) of one layer of the ligand···HI adduct assembled by orthogonal HB and XB. I^- and H^+ ions are shown in space-filling representation. Top right: two adjacent layers (red and green) stack along the *a*-axis, resulting in the partitioning of the void in the rectangular grids. Dioxane molecules have been omitted for clarity. Bottom: partial views (stick representation) of the single-crystal X-ray structures of the ligand··· HI adducts containing dioxane (left) and 1,3-dibromobenzene (right). The latter system is obtained when a crystal of the former is divided into 1,3-dibromobenzene at room temperature. Reprinted with permission from ref 782. Copyright 2012 Royal Society of Chemistry.

Two further examples of frameworks constructed by XB are the anionic 3D network formed by [4-(benzoyloxy)-2,2,6,6-tetramethylpiperidinyl]-1-oxy, a free radical species, and molecular iodine[783] and the network based on an asymmetrically substituted and self-complementary arylporphyrin (Figure 94). Notably, in this case, all the halogen-bonded porphyrin layers were aligned in the same direction, imparting chirality upon the entire 3D assembly.[784]

The design and synthesis of molecular containers for guest encapsulation is a very topical area in supramolecular chemistry and after the pioneering work by Cram et al.[785] different approaches based on HB or metal−ligand coordination have been successful employed.

The first halogen-bonded capsule was a heteromeric system obtained in 2012 by C. B. Aakeröy, P. Metrangolo, and G. Resnati on self-assembly of a C-pentyltetrakis(4-pyridyl)-cavitand (XB acceptor) and a *p-tert*-butylcalix[4]arene tetrakis-[2-(4-iodotetrafluorophenoxy)ethyl ether] (XB donor).[786] The design assumed that the rigidity of the cavitand and the calix[4]arene scaffolds allows for the donor and acceptor sites to be preorganized for a multiple binding, and the conformational flexibility of the $-OCH_2CH_2O-$ bridges separating the calix[4]arene platform and the iodotetrafluorobenzene pendant enables an effective partner-induced fitting between the four XB donor and acceptor sites of the interacting partners. The cocrystallization of the two modules in CH_3CN afforded the halogen-bonded heteromeric capsule in the solid state thanks to the pairing of one cavitand unit and one tetrakis-

DOI: 10.1021/acs.chemrev.5b00484
Chem. Rev. 2016, 116, 2478−2601

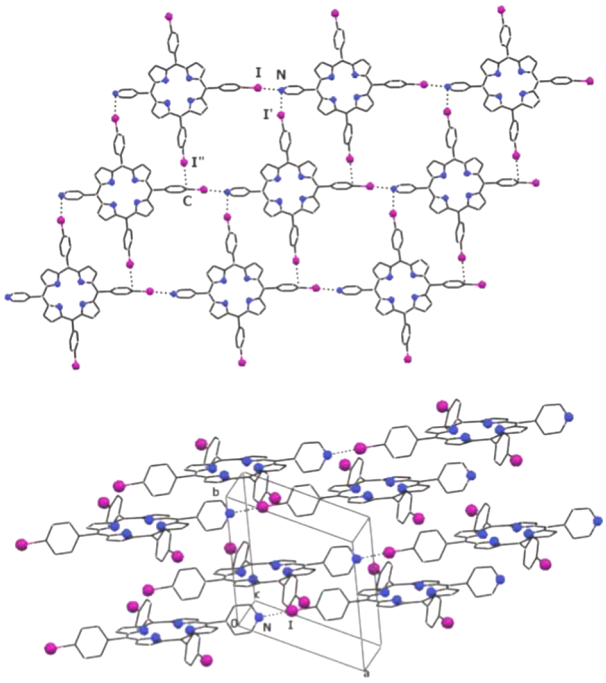

Figure 94. Top: partial view of a layer formed on assembly of the self-complementary porphyrin. XBs are in black dotted lines. Bottom: unidirectional arrangement of two successive layers. Adapted with permission from ref 784. Copyright 2008 Royal Society of Chemistry.

(iodotetrafluorophenyl)calix[4]arene via four I···N XBs (average N_c = 0.85 and C−I···N angle in the range of 169−177°). The pyridyl rings were all inwardly oriented and converged toward the same XB donor, and CH_3CN solvent molecules filled the cavities in the capsule (Figure 95).

More recently, N. K. Beyeh et al.[787] developed a dimeric capsule which was assembled by connecting molecular iodine with two macrocyclic molecules with a bowl-shaped structure, the *N*-cyclohexylammonium resorcinarene chloride. Differently from the previous capsule, the construction of this complex was driven by I···Cl^- XBs, which took place between the telechelic XB donor I_2 and the chloride anion of the resorcinarene units (N_c = 0.82−0.94). Thanks to the bowl-shaped XB acceptor modules, the capsule showed a single cavity (V = 511 Å^3) large enough to encapsulate three 1,4-dioxane guest molecules (Figure 96, left). Similar ammonium resorcinarene halide systems were used by the same group to develop halogen-bonded analogues of deep cavity cavitands.[788] The walls of the cavitands were formed by CCl_3Br molecules fixed in their position by Br···X^- contacts (X = Br or Cl).

Recently, F. Diederich and co-workers[789] reported the first case of a halogen-bonded molecular capsule formed in solution as verified by NMR studies. The capsule was assembled by using two resorcin[4]arene cavitands functionalized with pyridyl units, as XB acceptors, and with iodotetrafluorobenzene rings, as XB donors (Figure 96, middle).

J. Rebek and co-workers[790] used a supramolecular capsule formed via bifurcated hydrogen bonds involving modified cavitad modules to encapsulate a halogen-bonded complex. The cavity was large enough to accommodate the dimer between the XB donor and acceptor units (e.g., iodoperfluoropropane and the γ-picoline, Figure 96, right). It is known that weak intermolecular forces are difficult to observe in solution because the molecular encounters are short-lived and overwhelmed by

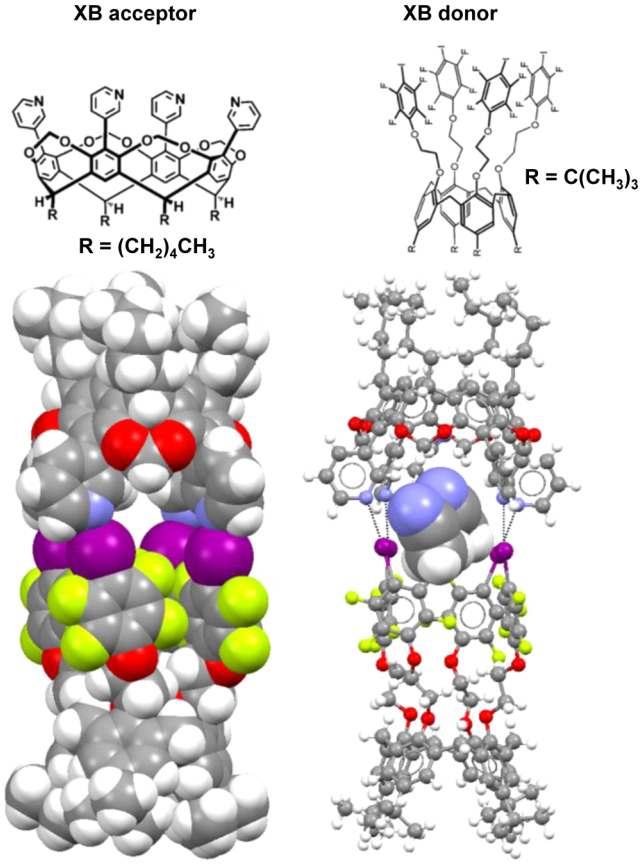

Figure 95. Top: molecular structures of the XB acceptor (left) and donor (right) used for the construction of the capsule. Bottom left: space-filling representation of the molecular capsule assembled via XB. The solvent molecule are omitted to show the cavity inside the capsule. Bottom right: ball-and-stick representation of the molecular capsule where the solvent molecules are shown in space-filling style and I···N XBs are shown as dotted black lines. Color code: carbon, gray; nitrogen, blue; oxygen, red; iodine, purple; fluorine, yellow; hydrogen, white.

the solvent. Differently, in the confined space within a capsule, the lifetime of noncovalent complexes is prolonged thanks to the isolation from the medium and the preorganization of the environment, which favors the self-assembly process. By monitoring with ^{19}F NMR solution systems containing the modified cavitad modules, the fluorinated XB donor, and the XB acceptor, Rebek observed a large shift in the ^{19}F spectrum of the XB donor consistent with the encapsulation of a halogen-bonded dimer.

The encapsulation of an XB donor was reported by W. M. Nau et al. in 2012 when the authors isolated the host−guest complexes between diiodine or dibromine and the barrel-shaped cucurbit[6]uril.[791] The crystal structures of the assembled systems showed that the encapsulated dihalogens adopted a tilted axial geometry and were held in place by two different types of XB interactions, one with a water molecule and the other with the ureido carbonyl groups of the molecular container itself (Figure 97).

A more sophisticated cage for molecular iodide encapsulation was constructed by Y.-C. Horng et al. in the same year.[792] The XB acceptor was a cylinder-shaped dimer formed by two tripodal trisulfide precursors connected by three dynamic disulfide bonds. The diiodine molecule was trapped in the cavity formed by the tripodal trisulfide capsule and was located

DOI: 10.1021/acs.chemrev.5b00484
Chem. Rev. 2016, 116, 2478−2601

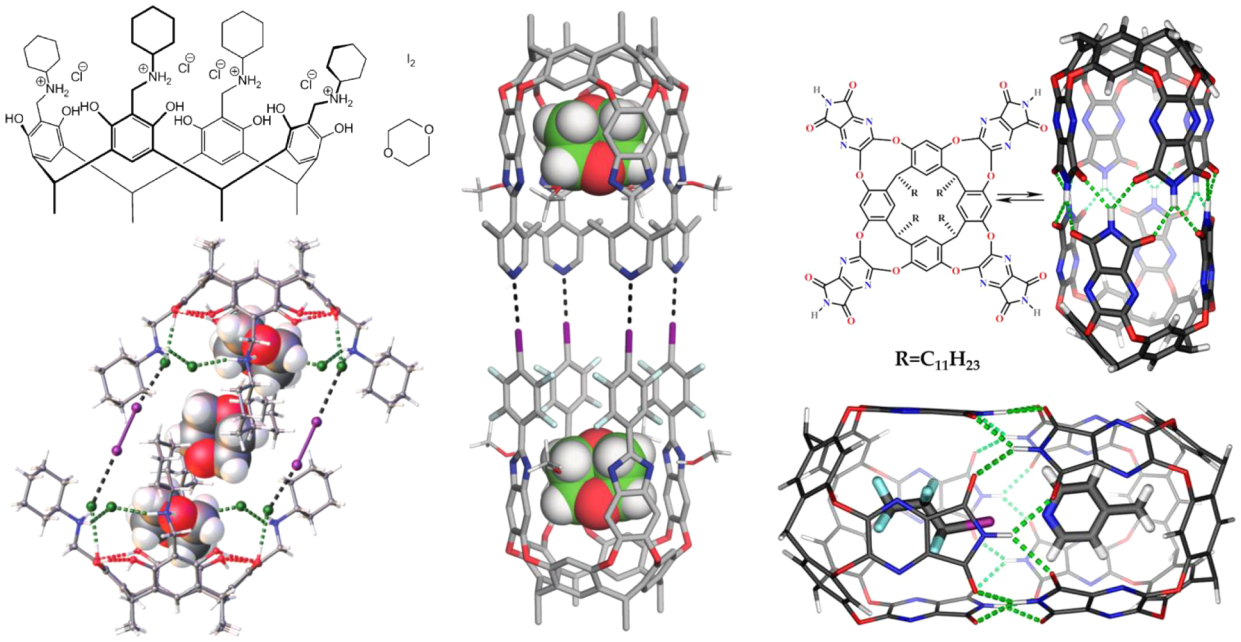

Figure 96. Left: molecular structures of the XB donor, XB acceptor, and guest molecule used for the assembly of N. K. Beyeh's capsule (top) and ball-and-stick representation of the halogen-bonded dimeric capsule with three 1,4-dioxane molecules in the cavity as space-filling CPK models (bottom). The XBs are shown in black and HBs as green and red dotted lines. Adapted with permission from ref 787. Copyright 2015 John Wiley and Sons. Middle: calculated model for the capsule developed by F. Diederich et al. with two 1,4-dioxane guests and four MeOH bridging units to stabilize intramolecular HB between imidazole walls (nearly optimized at the DFT:B3LYP/cc-pVDZ-LANL2DZ level of theory). Adapted with permission from ref 789. Copyright 2015 John Wiley and Sons. Right: chemical formula of the cavitand used by J. Rebek and co-workers and its computer-modeled dimeric capsule (top; HBs are shown as green dotted lines) and calculated model for the capsule with the encapsulated and halogen-bonded dimer (bottom). Full geometry optimization was carried out, including the capsule; the basis set for all atoms except iodine is 6-31G(d,p), and that for I is LANL2DZdp ECP. Adapted from ref 790. Copyright 2013 American Chemical Society.

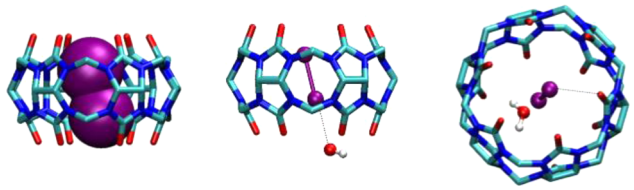

Figure 97. Stick-style views of the single-crystal X-ray structure of the cucurbit[6]uril–I_2 complex. Encapsulated diiodine, in space-filling style (left), is halogen-bonded with a water molecule (middle) and is bound to the carbonyl oxygen at the upper portal (right).

perpendicular to the benzene ring of the tripodal units. I_2 encapsulation was driven by a cooperative effect of XBs (between the σ-hole of I_2 and the aromatic π-systems) and HBs (between the negative belt of I_2 and NH groups of the tripodal units).

M. Fujita's coordination cages have shown the ability to accommodate different molecular guests, such as DNA duplexes[793] and fluorous aggregates.[794] Recently, it was shown that the XB between iodoperfluorocarbons (XB donors) and NO_3^- anions or H_2O molecules (XB acceptors) is enhanced if the XB donor is confined inside a self-assembled cage.[795] Fujita's cage was able to encapsulate various XB donors, and in all of cases the iodine atoms were located at the portals of the cage, thus allowing for the formation of XBs with either NO_3^- anions or H_2O molecules. Short I···O contacts were observed with both acceptors, and the XB formation was demonstrated by using single-crystal X-ray diffraction and NMR techniques (Figure 98A,B). Interestingly, the pairwise inclusion in the same cage of a halogen-bonded dimer formed by aniline and 1,3,5-triiodotrifluorobenzene was also reported.

A similar approach was exploited to encapsulate $CFCl_3$, a banned freon, in a tetragonal cage based on anion coordination.[796] The freon encapsulation was stabilized by weak Cl···π contacts as confirmed by the crystal structure (Figure 98 C). NMR studies and high-resolution ESI-MS experiments showed that the inclusion complex was formed even in solution.

3.2.2. Solid-State Synthesis. *3.2.2.1. Mechanochemistry.* The syntheses of halogen-bonded adducts via heterogeneous processes wherein a solid reagent interacts with a gas were discussed in the previous section. Here we describe heterogeneous processes resorting to mechanochemistry, namely, processes where a mechanical force is used to induce and/or sustain the chemical reaction between two solid reagents.[797] An intrinsic advantage of mechanochemistry is its easy scalability to large quantities in a solvent-free and environmentally compliant approach. In a recent review, T. Friščić highlighted the intimate connection between mechanochemistry and the principles of supramolecular chemistry.[798]

Mechanochemical methods have been applied, among others, to the synthesis of new polymorphs and cocrystals of active pharmaceutical ingredients (APIs) as well as to the large-scale production of porous metal–organic frameworks (MOFs). Mechanochemical methods have been largely exploited for the synthesis of hydrogen-bonded cocrystals,[797] while only a few examples of their use to produce halogen-bonded materials have been reported so far. The first example of mechanosynthesis of halogen-bonded systems appeared in 2008, carried out by D. Cincic et al.,[77] who systematically studied the assembly

DOI: 10.1021/acs.chemrev.5b00484
Chem. Rev. 2016, 116, 2478–2601

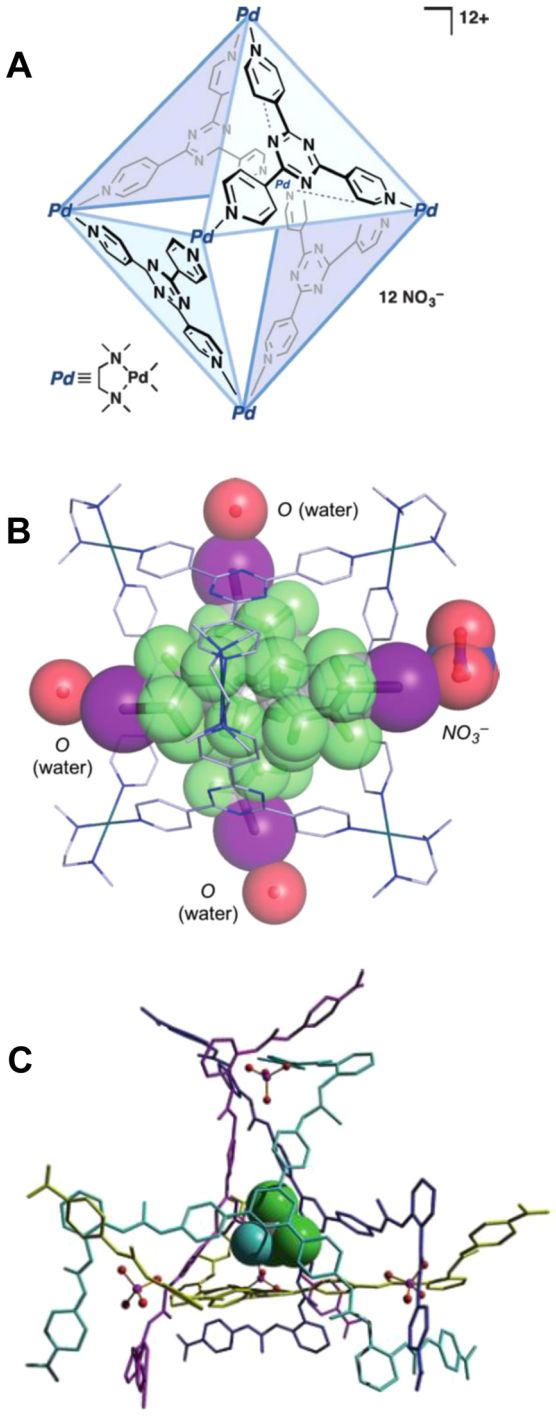

Figure 98. (A) Molecular structure of the self-assembled coordination cage by Fujita. (B) Single-crystal X-ray structure of the inclusion complex between Fujita's cage (stick representation) and 1,8-diiodoperfluorooctane (space-filling representation). Two molecules of the XB acceptor are hosted inside the cage. NO_3^- anions and H_2O molecules halogen-bonded to diiodoperfluorooctane molecules are shown as space-filling models. H atoms, NO_3^- anions, and H_2O molecuels that are not involved in XB have been omitted for clarity. Adapted with permission from ref 795. Copyright 2015 John Wiley and Sons. (C) Crystal structure of the inclusion complex between the anion-coordination-based tetragonal cage (stick representation) and $CFCl_3$. $CFCl_3$ is shown as a space-filling model. Adapted with permission from ref 796. Copyright 2015 John Wiley and Sons.

behavior of 1,4-diiodotetrafluorobenzene and 1,4-dibromotetrafluorobenzene with a series of structurally similar XB acceptors involving nitrogen, oxygen, or sulfur atoms. Powder and single-crystal X-ray diffraction analyses on the solid materials obtained upon neat grinding of the starting tectons revealed the formation of seven chemically different but isostructural cocrystals formed thanks to I···N, I···O, I···S, Br···N, and Br···O XBs. A few years later the same researchers used one of these cocrystals (i.e., the 1,4-diiodotetrafluorobenzene/thiomorpholine adduct) to perform kinetic studies with the aim of understanding the competition between different supramolecular interactions during the mechanochemical synthesis. By varying the grinding times, different stoichiometric ratios of donor to acceptor modules were obtained in the prepared halogen-bonded cocrystals. The 1:2 ratio appeared fast at short grinding times, while the 1:1 ratio was detected when using longer grinding times. Single-crystal X-ray analysis showed that the 1:1 adduct was assembled by the occurrence of simultaneous I···N and I···S XBs, while the 1:2 cocrystal showed only I···N XBs. This indicated a kinetic effect driven by the formation of the product based on the strongest XB possible, i.e., the I···N one (Figure 99).[609]

An important modification of the mechanochemical synthesis methodology is the addition of a few drops of a solvent to the solid-state materials just before grinding. Among others, this liquid-assisted grinding (LAG) methodology has been used in exploring the structure-directing (templating) properties of various guests during the formation of the succinic acid/caffeine cocrystal.[799] It was found that the templating effect of haloforms on the formation of the (succinic acid)·(caffeine)$_4$ framework was promoted by both C−H···O HBs and Br···N (or Cl···N) XBs (Figure 100).

In 2010 Friščić and co-workers[800] explored the possibility of using mechanochemical reactions to simulateneously form dynamic covalent bonds, metal coordination bonds, and XBs. The one-pot reaction between dibenzoylmethanate, morpholine or thiomorpholine, nickel(II) or cobalt(II) cations, and 1,4-diiodotetrafluorobenzene yielded the formation of an extended structure consisting of metal−organic complexes connected through XBs. A one-pot "all at once" milling approach was used, instead, in 2014 to assemble four components, Cu(OAc)$_2$·H$_2$O, 4-aminoacetophenone, 2-hydroxy-1-naphthaldehyde, and 1,4-diiodotetrafluorobenzene. The mechanochemical synthesis yielded the formation of a halogen-bonded metal−organic framework (MOF), where the metal−organic units were connected by strong I···O bonds (Figure 101).[801]

Many other examples of halogen-bonded systems obtained by mechanochemical methods are now reported in the literature, for example, for the synthesis of polyhalide[771] and interhalide[487] species, as well as of new polymorphs and cocrystals of halogenated APIs.[485] One remarkable example involving APIs is the $CaCl_2$ cocrystal of 3-iodo-2-propynyl *N*-butylcarbamate (IPBC), an iodinated antimicrobial product globally used as a preservative, fungicide, and algaecide.[477] When ball milling is used, IPBC affords a 4:1 cocrystal with $CaCl_2$, and the cocrystal can be easily obtained on a 10 g scale. Notably, this cocrystal shows improved technological properties compared to the pure IPBC, i.e., higher thermal stability and improved powder flow properties (Figure 102).[802]

3.2.2.2. Topochemical Reactions. The remarkable achievements obtained by crystal engineering and the continuous efforts in searching for new supramolecular strategies and tools to engineer molecular crystals are strictly linked to the need to

DOI: 10.1021/acs.chemrev.5b00484
Chem. Rev. 2016, 116, 2478−2601

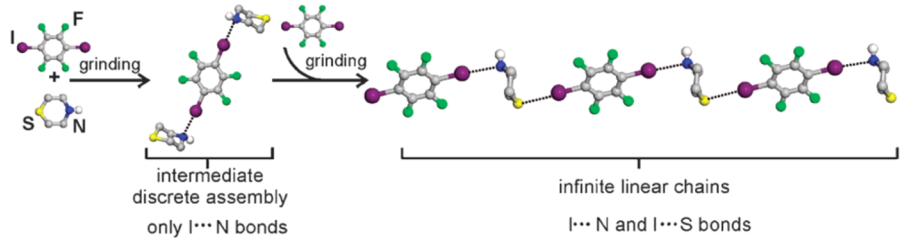

Figure 99. Schematic representation showing that on griding 1,4-diiodotetrafluorobenzene and thiomorpholine the 1:2 discrete adduct forms initially, which then evolves into 1:1 infinite chains on further grinding. Adapted with permission from ref 798. Copyright 2012 Royal Society of Chemistry.

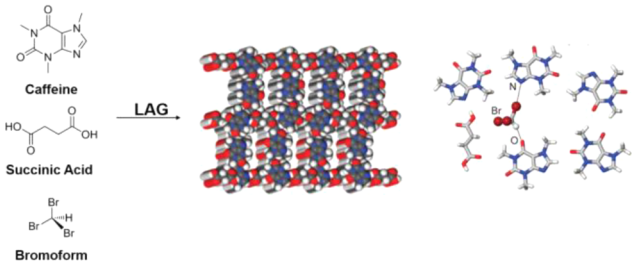

Figure 100. Left: structural formulas of tectons assembled via LAG methodology. Middle: (succinic acid)·(caffeine)$_4$ host framework with guests omitted. Right: view of the hydrogen C−H···O and halogen Br···N bonds involving the bromoform included in the (succinic acid)·(caffeine)$_4$ host framework. Adapted with permission from ref 798. Copyright 2012 Royal Society of Chemistry.

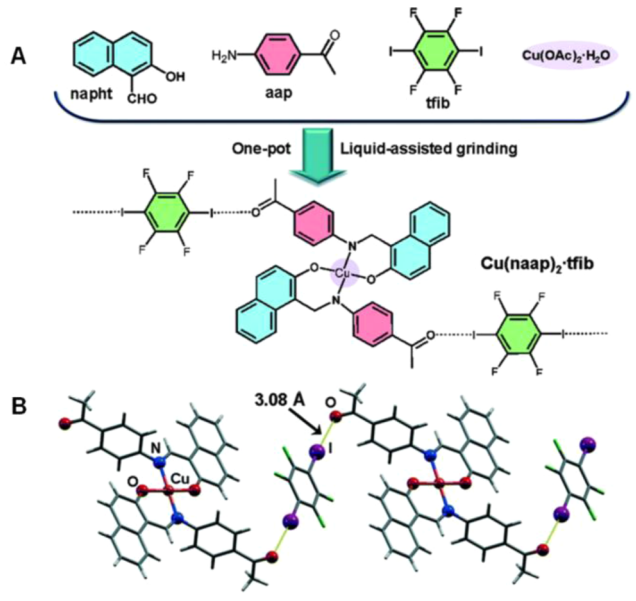

Figure 101. (A) Molecular structures of single compounds (top) employed in LAG synthesis of a halogen-bonded MOF (bottom). (B) Partial representation of the crystal structure resulting from a combination of covalent bond formation, coordination bonds, and XBs. I···O XBs are shown as yellow solid lines, and the I···O distance is reported (N_c = 0.88). Adapted with permission from ref 801. Copyright 2014 Royal Society of Chemistry.

master organization and reactivity in the solid state.[803] Compared to classical organic reactions performed in solution, solid-state reactions have several advantages that include high regio- and stereoselectivity, high scalability, and high reaction rates. Avoiding the use of solvents, solid-state reactions are cost-effective and have a lower impact on the environment than

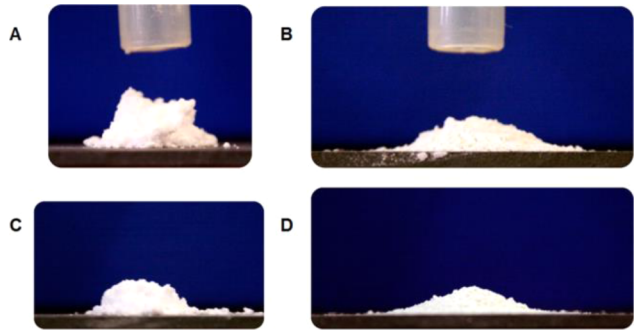

Figure 102. Pictures of cones of powders of pure IPBC (A, C) and its $CaCl_2$ cocrystal (B, D), taken after flowing the powders through a funnel from 25 mm (A, B) and 50 mm (C, D) heights. The cylindrical shape of the IPBC cones clearly indicates the high cohesion of the powders, while the flat cone shape of the $CaCl_2$ cocrystal indicates improved powder flow properties. Reprinted from ref 477. Copyright 2013 American Chemical Society.

reactions in solution. Topochemical reactions are defined as reactions "wherein the structure of the products is dictated by the geometry and proximity of the reactive sites of the precursors in the lattice".[804] During the years, various kinds of reactions, such as Diels−Alder or [4 + 4] reactions, have been explored in the solid state; however, the [2 + 2] photochemical reactions are by far the most studied in the solid state.[805] In 1918, Kohlschutter postulated the general topochemical principle that reactions in crystals proceed with a minimum amount of atomic and molecular movement.[806] The essential structural constraints for promoting photocycloaddition reactions in the solid state were first identified by Schmidt[807] thanks to a systematic study of photochemical reactivity on variously substituted cinnamic acids. The constraints are as follows: (I) The distance between centroids of two photoreactive double bonds must be within a distance of 3.5−4.5 Å. (II) The double bonds of the reacting molecules must be aligned in a parallel fashion.

Several supramolecular strategies based on HB, $\pi-\pi$ stacking, arene−fluoroarene interactions, or cation···π interactions have been exploited to conduct stereo- and regiocontrolled solid-state [2 + 2] reactions,[803] and also XB has recently proven its usefulness in this field.

The cocrystallization, by slow solvent diffusion, of *trans*-1,2-bis(4-pyridyl)ethylene and a pentaerythritol derivative bearing four iodotetrafluorobenzene units led to the formation of a cocrystal where the two modules were present in a 1:2 ratio and formed infinite, 1D, and halogen-bonded ribbons thanks to short and directional I···N XBs (the N_c values were 0.79 and 0.80, and the C−I···N angles were around 177°).[808] As expected, the pentaerythritol derivative behaved as a tetratopic

DOI: 10.1021/acs.chemrev.5b00484
Chem. Rev. 2016, 116, 2478−2601

XB donor, while the dipyridyl module acted as a ditopic XB acceptor (Figure 103). The conformation of the XB donor

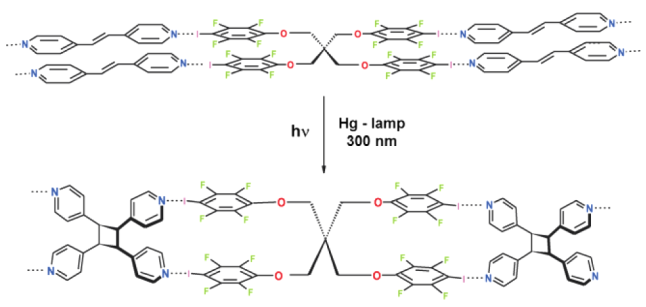

Figure 103. Schematic representation of the infinite, 1D, and halogen-bonded ribbons (top), which upon light irradiation in the solid state yield quantitatively the *rctt*-tetrakis(4-pyridyl)cyclobutane (bottom).

molecules was determined by intramolecular $\pi\cdots\pi$ stacking interactions between pairs of fluorophenyl rings which pointed outward at either side of the molecule in an almost parallel manner. The high directionality of the XB transferred this topochemical information to the olefins that were pinned in the ribbons in a parallel fashion with a distance of less than 4.5 Å between the olefins' centroids, nicely meeting Schmidt's requirements. A powdered crystalline sample of the above-described cocrystal was irradiated at 300 nm and readily underwent a photochemical cycloaddition reaction under topochemical control, yielding stereospecifically the corresponding *rctt*-tetrakis(4-pyridyl)cyclobutane in quantitative yields (Figure 103).

XB played a major role also in the convenient preorganization of a photoactive, heteroditopic, and self-complementary tecton (Figure 104). Specifically, the tecton possessed an

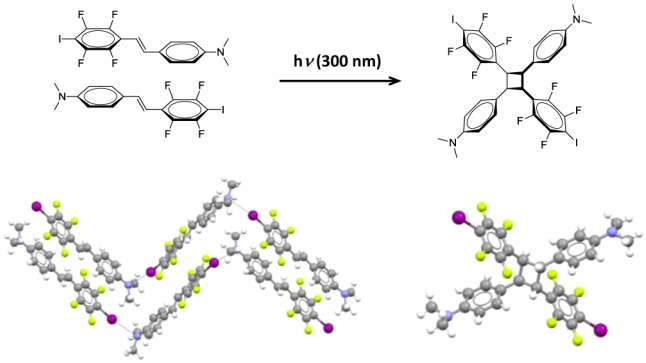

Figure 104. Top: schematic representation of the solid-state photoreaction of an XB-based self-complementary tecton to yield a tetratopic self-complementary cyclobutane derivative. Bottom: views of the crystal packing of two infinite and halogen-bonded chains formed in the solid state by the starting olefin (left, XBs as dotted black lines), and of the cyclobutane derivative obtained after UV irradiation (right). Color code: carbon, gray; nitrogen, blue; iodine, purple; fluorine, yellow; hydrogen, white. XBs are dotted black lines.

electron-poor aromatic terminal XB donor group connected by a double bond to an electron-rich aromatic terminal XB acceptor group.[722] Upon crystallization from chloroform, this self-complementary molecule organized into 1D infinite polar chains thanks to the expected I···N XB (N_c was 0.82, the C–I···N angle was 170°, and the I···N–C angle was 97.4°). As a result of the heterodipolar $\pi\cdots\pi$ stacking between adjacent chains, the double bonds of the different modules were organized to meet Schmidt's requirements for regiocontrolled photocyclization in the solid state, the centroids' separation being only 3.76 Å. Upon photoirradiation in the solid state, the double bonds underwent a [2 + 2] reaction, yielding the cycloadduct with complete regio- and stereospecificity. Thanks to the control exerted by the crystal packing, only the *rctt* isomer was obtained, with pairs of iodotetrafluorobenzene and dimethylaminobenzene pendants pointing in opposite directions with respect to the plane of the cyclobutane ring (Figure 104).

Another kind of reaction that may proceed under topochemical control is the thermal polymerization of diacetylenes.[804] These 1,4-addition reactions occur when specific structural requirements are met: (I) The maximum distance between the reactive C atoms of the monomeric diacetylene molecules is approximately 3.8 Å. (II) The diacetylene molecules are aligned linearly with an approximate repeat distance from 4.7 to 5.2 Å.[809] XBs was exploited for this kind of reaction by N. Goroff and co-workers, who targeted the 1,4-polymerization reaction of diiododiacetylenes in the solid state.[810] The cocrystallization of 1,4-diiodo-1,3-butadiyne (XB donor) with bis(3-picolyl)oxalamide (XB acceptor) led to the formation of a 2D supramolecular network thanks to a combination of XB and HB (Figure 105). Infinite 1D chains

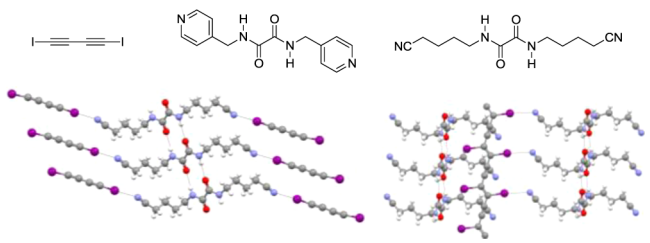

Figure 105. Top: schematic representation of XB donor and acceptors used for the photochemical polymerization of diacetylene modules. Bottom: partial views (ball-and-stick representation) of the 2D supramolecular architecture given by diiodobutadiyne and bis(4-cyanobutyl)oxalamide (left) and of the related photoreacted cocrystal between poly(diiododiacetylene) and bis(4-cyanobutyl)oxalamide (right). Color code: carbon, gray; nitrogen, blue; oxygen, red; iodine, purple; fluorine, yellow; hydrogen, white. XBs and HBs are dotted black lines.

are formed thanks to I···N bonds between the iodine atoms of the diyne molecules and the nitrogen atoms of the dipyridine molecules. These chains are then cross-linked into layers thanks to geometrically orthogonal HBs between the oxalamide residues of adjacent chains. These HBs also allow for the stacking of the dipyridyl units, and the information is transferred to the diyne molecules by the directional XBs, so that the requirements for polymerization are met. The 1,4-polymerization reaction was tried by applying high external pressure, and the formation of the polymer was evidenced with solid-state Raman scattering and magic angle spinning solid-state NMR. When the pyridyl-substituted XB acceptor was replaced by a structurally analogous oxalamide containing a nitrile group rather than a pyridyl group, the polymerization reaction took place spontaneously during the crystallization process, leading to the formation of the expected poly(diiododiacetylene).[811]

DOI: 10.1021/acs.chemrev.5b00484
Chem. Rev. 2016, 116, 2478–2601

4. SOFT MATERIALS

The use of XB in soft materials engineering is much less common than in crystalline solids engineering, and examples are especially scarce on polymeric and gel-phase materials. However, the same characteristics rendering the XB a first-class tool in crystal engineering (e.g., directionality and tunable interaction strength) motivate its use also in the context of supramolecular soft matter. Moreover, HB and XB present many similarities,[92] and many of the concepts in materials design elaborated with the former interaction can also be extended to the latter. A gradually increasing number of reports on halogen-bonded liquid crystals (LCs), polymers, and gels is appearing in the literature, and this section demonstrates the vast potential of XB in the design of these new types of soft matter. The three classes of soft materials mentioned above are rather interwoven. Many polymeric complexes exhibit liquid crystallinity,[812−814] and both polymeric gels[815,816] and liquid-crystal gels[817,818] have been widely studied. As a consequence, inclusion of a study in a given section may sometimes be a matter of presentation rather than topic.

Several issues remain to be studied also in the context of halogen-bonded LCs, the less unexplored area. Halogen-bonded discotic LCs have not been demonstrated, albeit hydrogen-bonded discotic LCs were among the first supramolecular LCs reported in 1989. Interesting opportunities might also be provided by ionic LCs,[819] in which fluorination has been reported to enhance lamellar phase segregation, thereby providing anisotropic conduction pathways and interesting charge-transport properties.[488,820] In supramolecular polymers and block copolymers, XB is foreseen to bring additional benefits in preparation of nanotechnology template materials due to its reversibility and the easy removal of the bond donor components from the system.[484] However, general guiding principles for XB-driven polymeric self-assembly should first be comprehensively understood. Therefore, several new openings and breakthroughs in regard to halogen-bonded soft matter are to be expected in the near future.

4.1. Liquid Crystals

Liquid crystals bear an immense technological potential because they combine the anisotropy of crystalline solids and the mobility of isotropic liquids in a unique manner. Liquid-crystal alignment can be modulated with external fields, which has a profound influence on how light propagates through the liquid crystal. Therefore, LCs are particularly promising for applications in display technology and photonics,[821−823] but they also constitute a unique template for designing complex self-assemblies[824] and have received increasing attention in applications related to biotechnology,[825,826] organic electronics,[827,828] and sensing.[829,830] The existence of thermotropic LC phases is inherently connected to noncovalent forces between anisotropic, typically rodlike or disklike, molecular constituents. HB is by far the most established noncovalent interaction in the creation of supramolecular liquid crystals, and the topic was comprehensively reviewed by C. M. Paleos and D. Tsiourvas in 2001.[831] Herein, we restrict ourselves to mention the seminal work of T. Kato and J. M. Frechet,[832−836] who were the first to demonstrate that new types of LC species can be created by coupling, via single HBs, components bearing pyridyl and carboxyl moieties. In this context, HB effectively elongates the rigid-rod segment, thus either generating liquid crystallinity into systems built from non-liquid-crystalline constituents, or modifying the LC behavior of the pair as compared to its building blocks.

It is stated by C. M. Paleos and D.Tsiourvas[831] that "For the formation of liquid-crystalline materials through HB interactions, complementarity of the interacting components coupled with the directionality of HBs are the main factors contributing to the exhibition of liquid crystallinity." Single HBs being able to form LC phases, it should be even more so in the case of the more directional XBs. This indeed turned out to be the case, as first shown in 2004.[837] Motivated by their earlier work on similar hydrogen-bonded LCs,[838−840] the authors of the paper used a series of alkoxystilbazoles and *para*-substituted tetrafluoroiodobenzenes as XB acceptors and donors, respectively (Figure 106A). These starting components are non-

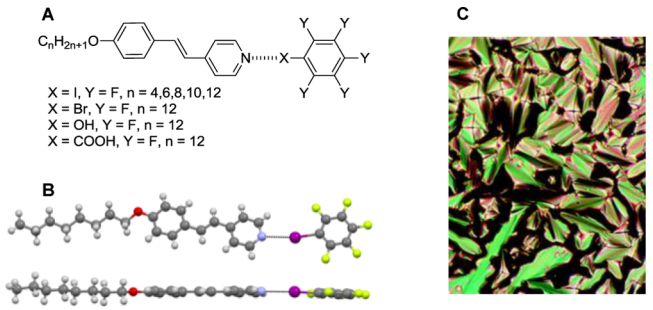

Figure 106. (A) Chemical structures of the halogen-bonded LCs reported in ref 837 and corresponding hydrogen-bonded analogues. (B) Crystal structure of the (octyloxy)stilbazole/iodopentafluorobenzene dimer evidencing the presence of I···N XB (shown as black dotted lines) and the coplanarity of the aromatic rings. Color code: gray, carbon; yellow, fluorine; purple, iodine; sky blue, nitrogen; white, hydrogen. (C) Polarized optical micrograph of the smectic A texture of the (hexyloxy)stilbazole/iodopentafluorobenzene dimer at 69° upon cooling. Reprinted from ref 837. Copyright 2004 American Chemical Society.

liquid-crystalline as pure species, and X-ray crystallographic studies (Figure 106B) proved that the XB connecting these components is responsible for the appearance of the liquid-crystalline phases, quadrupolar interactions, which play a central role in some other supramolecular LCs,[841−843] being absent. XB also gave rise to a color change of the material. While stilbazoles themselves are colorless, their absorption maximum red-shifted upon XB formation, and the formed adduct was yellow. The LC phase was dependent on the length of the alkoxy chain, progressing from nematic (short chains) to smectic A (long chains) (Figure 106C).[837] Attempts were also made to use bromopentafluorobenzene as the XB donor, but no evidence of compex formation was obtained. Probably the Br···N interaction is too weak to exist at the temperatures enabling liquid crystallinity (LC phases occurred at temperatures typically >70 °C). Importantly, the crystal-to-LC transition temperature was lower in halogen-bonded complexes than in hydrogen-bonded analogues. Since for many applications it is beneficial to have an operating temperature (i.e., the temperature at which the liquid crystallinity occurs) as low as possible, this may be a benefit of halogen-bonded as compared to hydrogen-bonded supramolecular liquid crystals.

J. Xu et al. reported on high molecular weight supramolecular LCs[845,846] obtained on self-assembly of bis-(iodotetrafluorophenoxy)alkanes (bidentate XB donors) with various mono- and bidentate XB bond acceptors (Figure

DOI: 10.1021/acs.chemrev.5b00484
Chem. Rev. 2016, 116, 2478−2601

107A). The occurrence of XB in many of the studied complexes was proven by detecting changes in the binding energies of the

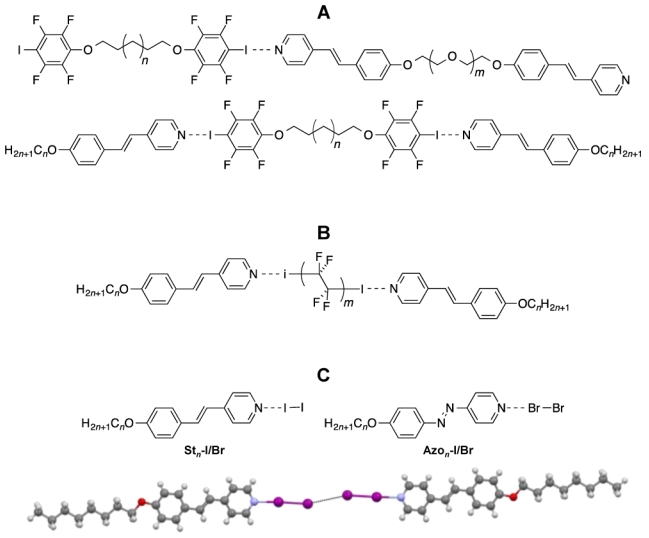

Figure 107. Chemical structures of high molecular weight polymeric (A, top) and trimeric (A, bottom) LCs,[845,846] trimeric LCs formed by diiodoperfluoroalkanes (B),[847] and dimeric systems formed by dihalogens (C, top).[850,851] (C) Representation of the crystal structure of two I_2···(octyloxy)stilbazole dimers interacting via type I I···I contacts. Color code: carbon, gray; nitrogen, blue; oxygen, red; iodine, purple; hydrogen, white.

1s orbitals at nitrogen and 3d orbitals at iodine via X-ray photoelectron spectra,[846] and since then, this technique has become a commonly used tool to verify XB formation. The LC temperature range of these halogen-bonded LCs is generally narrower than that of hydrogen-bonded LCs based on carboxyl−pyridine binding. The authors attributed the temperature range of hydrogen-bonded LCs to a weak secondary C═O···H—C HB (between the carbonyl oxygen and a hydrogen adjacent to the nitrogen atom in pyridine) which directs the complex to be planar and stabilizes the mesophase. Corresponding halogen-bonded complexes lack such a stabilizing secondary interaction due to the large size of iodine, and the mesophase range is narrower.

Low molecular weight supramolecular LCs were obtained by P. Metrangolo and G. Resnati et al. on XB-driven self-assembly of α,ω-diiodoperfluoroalkanes (bidentate XB donors) and alkoxystilbazoles (monodentate XB acceptors) (Figure 107B).[847] Long fluoroalkyl chains typically drive segregation of the fluorinated and nonfluorinated segments into lamellar smectic A phases (fluorophobic effect),[848,849] which most often precludes the appearance of nematic phases. Surprisingly, although such segregation was observed in the crystal structures of the complexes formed by α,ω-diiodoperfluoroalkanes, all the observed LC phases were monotropic nematic, even when the relatively long diiodoperfluorohexyl spacers separated the two XB donor sites. The same group also studied the halogen-bonded trimers formed by 1,4-DITFB with alkoxystilbazoles.[844] Monotropic nematic phases in a narrow temperature range were observed for the pure trimers, and upon mixing several alkoxystilbazoles bearing alkoxy pendants of different lengths, the material exhibited enantiotropic liquid crystallinity with an extended LC temperature range. Mixing differently sized components is a rather common method to suppress the melting points and to increase the mesophase range of LC materials, yet this was the first successful use of the approach in the context of halogen-bonded and supramolecular LCs.

Concerted use of XB and HB to induce liquid crystallinity was demonstrated by forming 2:1 complexes of alkoxystilbazoles and iodotetrafluorophenols.[852] In the same study and by using 1:1 complexes, it was shown that stilbazoles interact preferentially via HB. The synergistic use of XB and HB is particularly useful in LC polymers built from difunctional low molecular weight XB donors and acceptors. The quite narrow LC temperature ranges of halogen-bonded polymeric complexes[845] were attributed to the rigidity and high directionality of the XBs; by also introducing the less directional HBs into the polymeric supramolecular complex, the rigidity constraints are alleviated and the mesophase stability is significantly increased.[853] XB-driven chiral LC phases have also been reported. C. Präsang et al. observed spontaneous symmetry breaking and chiral nematic phases on self-assembly of nonchiral starting compounds, i.e., 1,3-diiodotetrafluorobenzenes and alkoxystilbazoles.[711] To account for their experimental observations, the authors argue that the nematic-to-isotropic transition is actually accompanied by XBs breaking. Upon cooling, a 1:1 complex is formed first (exhibiting a nematic phase), and shortly after that, the 2:1 complex re-forms (giving rise to the bent chiral nematic structure).

The studies described above report on several interesting findings, but they hardly afford conclusive design principles for halogen-bonded supramolecular mesogens. To address this issue, the Milano and York teams joined forces and carried out a systematic and comprehensive investigation using a series of XB donors and acceptors (some of them are shown in Figure 108A). By reporting 90 new dimeric halogen-bonded LC

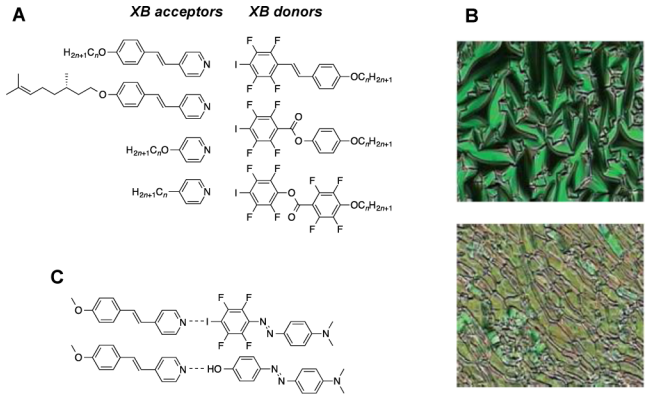

Figure 108. (A) A selection of XB donors and acceptors used in ref 854. (B) Birefringent textures of complexes formed by an (*S*)-citronellyl-substituted stilbazole with a butoxy-substituted iodotetrafluorostilbene, obtained upon cooling from the isotropic state. (C) Molecular structures of halogen-bonded (top) and hydrogen-bonded (bottom) stilbazole−azobenzene complexes. The halogen-bonded complex is liquid-crystalline; the hydrogen-bonded complex is not.[489]

species,[854] they were able to provide new insights into their structure−property relationships and to demonstrate that XB is a reliable tool for the systematic construction of supramolecular LCs.

Many of the reported complexes displayed enantiotropic LC phases with significantly broader LC temperature ranges (>20 °C) than those in previous reports. By using chiral citronellyl pendants on either the XB donor or the XB acceptor,

DOI: 10.1021/acs.chemrev.5b00484
Chem. Rev. 2016, 116, 2478−2601

enantiotropic chiral nematic mesophases were obtained with typical focal conic fan textures (Figure 108B, top), which changed after shear stress into planar textures with oily streaks (Figure 108B, bottom).

A particularly interesting observation was recently made using azobenzene-containing complexes,[489] which could be anticipated to exhibit no liquid crystallinity as they are devoid of flexible aliphatic chains. However, the halogen-bonded stilbazole−azobenzene complex (Figure 108C, top) shows a monotropic nematic phase with an isotropic-to-nematic transition at ca. 132 °C and a mesophase temperature range of ca. 18 °C. Most interestingly, the corresponding hydrogen-bonded complex (Figure 108C, bottom) was not liquid-crystalline. This difference highlights that XB not only parallels but can also override the performance of HB in LC materials.

All the aforementioned studies used iodotetrafluorobenzene moieties as XB donors (iodoperfluoroalkanes in ref 847). The first reports on the use of alternative XB motifs were published in 2013.[573,850] Complexes between alkoxystilbazoles and molecular iodine (Figure 107C, top left) exhibited unusually large mesophase stability and clearing points above 200 °C.[850] Interestingly, some of the complexes exhibited tilted SmC mesophases, and X-ray crystallographic studies showed that this phase was driven by the coupling of 1:1 dimers thanks to type I iodine···iodine contact. When replacing I_2 with Br_2, no liquid crystallinity was detected, and stilbazolium bromide in which one of the ethylenic hydrogens was replaced with bromine was formed. In another study,[851] the alkoxystilbazole was replaced with an azopyridine, to yield photoresponsive liquid crystals. In this case, both I_2 and Br_2 XB donors gave rise to liquid-crystalline complexes. This work demonstrated that not only can bromine-based XB donors be used in the successful design of supramolecular LCs, but, more surprisingly, dibromine significantly stabilized the mesophase compared to diiodine. For example, the complexes formed by I_2 and Br_2 with the azostilbazole bearing a dodecyloxy pendant both exhibited smectic A phases, and the respective temperature ranges were 119−135 and 70−158 °C. The reason for this unprecedented, bromine-induced stability remains unclear. Another interesting feature of the dihalogen-based LC complexes is that only smectic phases were observed, irrespective of the alkyl chain lengths on the XB acceptor units.

Iodoethynyl moieties are gaining in popularity as XB donors in general,[209,568,855] and a detailed study was recently reported on the use of 1,3- and 1,4-bis(iodoethynyl)benzenes (*p*-BIB and *m*-BIB, Figure 109A) to form trimeric LC complexes with benzonitrile and various pyridine acceptors.[573] The most important conclusion of this paper was that the use of XB donor mesogens bearing two iodoethynyl residues gives rise to mesophases with a higher degree of ordering compared to the use of the 1,4-DITFB donor. For instance, the 1:2 complex between *p*-BIB and *p*-(decyloxy)pyridine showed a crystal G mesophase, while the 1:2 complex between the same XB donor and a *p*-(benzoyloxy)pyridine showed a smectic B mesophase (parts B and C, respectively, of Figure 109). The former mesophase consists of tilted molecular layers with long-range three-dimensional order, while the latter has molecules exhibiting in-plane hexagonal ordering. On the other hand, *m*-BIB yielded liquid-crystalline complexes (Figure 109D) only when XB acceptors with three phenyl rings were used (specifically *p*-(benzoyloxy)stilbazoles). A polar SmAP phase, which is characteristic of bent-shaped molecules, was observed. None of these phases have been previously observed in

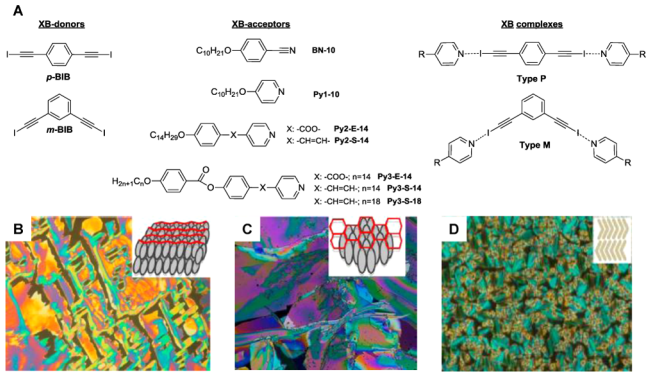

Figure 109. (A) Chemical structures of the XB donors and acceptors used in ref 573 and the general structures of the halogen-bonded complexes. Birefringence textures of the crystal G phase of the *p*-BIB/*p*-(decyloxy)pyridine complex (at 86 °C) (B), the smectic B phase of the *p*-BIB/*p*-[[*p*-(tetradecyloxy)benzoyl]oxy]stilbazole complex (at 108 °C) (C), and the smectic AP phase of the *m*-BIB/*p*-tetradecyloxy)stilbazole complex (at 131 °C) (D). Reprinted from ref 573. Copyright 2013 American Chemical Society.

halogen-bonded LCs, which clearly points out the promise of iodoethynyl units in the design of highly ordered supramolecular LCs and motivates further studies.

4.2. Polymers

Polymeric self-assemblies driven by XB have also been studied in parallel to LC dimers, trimers, and polymers built up from mono- and bidentate low molecular weight starting compounds. The preparation of fluorinated comb-shaped polymers driven by XB between poly(4-vinylpyridine) (P4VP) and α,ω-diiodoperfluoroalkanes (DIPFAs) was published as early as 2002.[473] The polymeric 2:1 P4VP/DIPFA complexes self-assembled into anisotropic comb-like structures, probably due to the high tendency of the polymer backbone and the fluorinated side chains to phase segregate. This study parallels the work of O. Ikkala and co-workers on phenol-based surfactants interacting by HB with comblike homopolymers and block copolymers containing a pyridine residue.[856,857] These early studies by the Milan group on the first example of halogen-bonded supramolecular assemblies involving polymers point to (i) finding optimal halogen-bonded side chains to drive the comblike self-assembly of these systems and (ii) controlling the morphology and self-assembly of block copolymers using halogen-bonded side chains. Studies on neither have been undertaken to date, but the complementarity between the perfluoroiodobenzene and pyridyl moieties has been used as a driving force for the formation of layer-by-layer polymeric films.[858] The resulting halogen-bonded multilayer polymer films were less stable than the corresponding hydrogen-bonded assemblies, yet the stability was improved by using hybrid films containing both halogen-bonded and hydrogen-bonded multilayers.

Recently, noncovalent interactions between a P4VP host matrix and azobenzene derivatives bearing XB donor sites have been used in the design of polymeric nonlinear optical and photoresponsive materials.[855,859,860] These materials are amorphous, their functionality is provided by XB, and they will be treated separately in the section of this review devoted to optical materials.

One of the most interesting recent studies on XB-driven self-assembly of polymers is the work of N. Houbenov et al. on spontaneous large-scale organization of halogen-bonded

DOI: 10.1021/acs.chemrev.5b00484
Chem. Rev. 2016, 116, 2478−2601

complexes between star-shaped polyethylene glycol (PEG) polymers and iodoperfluoroalkanes (Figure 110A).[484] Rapid

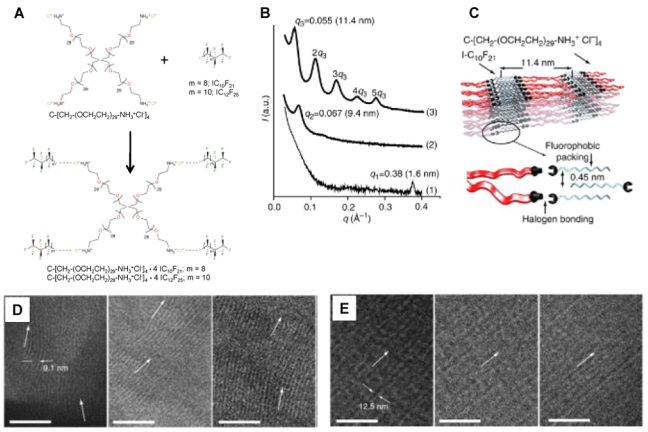

Figure 110. (A) Chemical structures of the PEG−iodoperfluoroalkane complexes used in ref 484. (B) Small-angle X-ray scattering patterns for iodoperfluorodecane (graph 1), PEG (graph 2), indicating poor self-assembly by segregation of the ionic end groups from the PEG core, and the supramolecular complex (graph 3), showing highly ordered self-assembly. (C) An illustration of the self-assembly mechanism of the halogen-bonded complex. (D) TEM micrographs at various locations of pure PEG showing a lack of macroscale alignment. (E) TEM micrographs of the halogen-bonded complex between PEG and 1-iodoperfluorododecane, showing exceptionally well-ordered lamellar nanostructures with overall macroscale order on the millimeter scale. The scale bars correspond to 100 nm. Reprinted with permission from ref 484. Copyright 2014 Nature Publishing Group.

and cost-effective protocols to achieve macroscopically aligned, nearly single-crystal, globally ordered, and self-assembled nanostructures remains a challenge. Importantly, the interplay between XB and the fluorophobic effect spontaneously leads to this goal in the model system of Figure 110A. The PEG polymers themselves give rise to nanoscale periodic structures (Figure 110B, graph 2) due to clustering of the charged end-group ammonium moieties, yet the material is macroscopically isotropic and exhibits poor overall alignment. Upon complexation with iodoperfluoroalkanes, highly ordered lamellar structures are obtained as demonstrated by the higher order peaks visible in the small-angle X-ray scattering pattern of the complexes (Figure 110B, graph 3). The increased ordering is driven by a combination of (i) XB between the chloride ions of the ammonium chloride end-capped PEG chains and the iodoperfluoroalkanes and (ii) the tight lateral packing of the fluorinated segments into phase-segregated layers. A model for the self-assembly mechanism is given in Figure 110C. The delicate balance between the different intermolecular interactions required to drive long-range self-assembly is evident from the fact that, like the starting polymer that exhibits no long-range alignment (Figure 110D), complexes with iodoperfluoroalkane chains with less than 10 carbon atoms are only locally ordered. Conversely, Figure 110E presents transmission electron microscopy (TEM) micrographs from several positions for a complex with iodoperfluorododecane, and the monodomain alignment spontaneously extends here into the millimeter length scale. As an additional benefit, the iodoperfluoroalkanes can be removed from the systems by combined vacuum/thermal treatment, which enables further use of the monodomain-oriented nanostructure as a nanotechnology template.

M. S. Taylor and A. Vanderkooy studied the solution self-assembly of complementary, multivalent XB donor and acceptor linear polymers, obtained from a methacrylate bearing iodoperfluoroarene residues and a 2-(dimethylamino)ethyl methacrylate, respectively.[861] They observed a variety of structures under relatively dilute conditions, ranging from spheres to wormlike nanotubes or more complex mixtures of the two (Figure 111). The structures appeared to be under

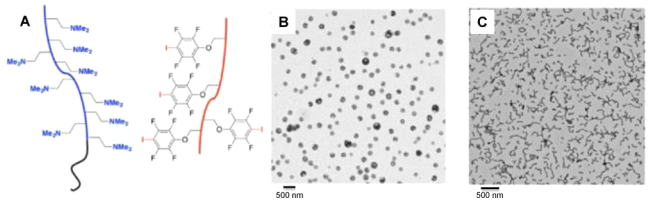

Figure 111. Cartoon representing complementary halogen-bonded polymers (A) and self-assembly in solution into vesicle (B) and wormlike (C) structures, as observed by TEM micrographs. Adapted from ref 861. Copyright 2015 American Chemical Society.

kinetic control and depended on a variety of factors such as the block length and polydispersity, the presence or absence of a solubilizing poly(ethylene oxide) segment in either polymer, and the assembly conditions, such as switching between different solvent systems.

4.3. Gels and Other Soft Systems

Supramolecular gel-phase materials are another important class of self-assembled soft matter, relevant for applications as diverse as regenerative medicine, drug delivery, and responsive optical/electronic materials.[862−864] The fibrous networks that provide supramolecular gels their solidlike rheological properties arise from complex hierarchical self-assemblies which are often initiated by HB-directed growth of one-dimensional fibrils. The dynamic self-association that nucleates the gel formation is very sensitive to competing noncovalent interactions; hence, such interactions can be used to control the gel strength, or in extreme cases to inhibit (or alternatively to "turn on") the gelation process altogether.[59−61] Recently, XB has also been added to the family of supramolecular interactions for controlling gelation.[83] Various bis(urea) compounds (Figure 112A) are nongelators in polar organic solvents or water−organic solvent mixtures. Conversely, an equimolar solution of 1,4-DITFB and 1,4-bis(3-pyridylureido)butane (BPUB) or 1,3-bis[(1-methyl-1-(3-pyridylureido)ethyl]benzene (DPUB) was found to gelate polar organic solvent−water mixtures. The single-crystal structure of the 1:1 complex between 1,4-DITFB and BPUB (Figure 112B) revealed that XB is present and probably turns on supramolecular gelation by preventing gel-inhibiting pyridyl−urea interactions. The generality of the role of XB in turning on supramolecular gelation was confirmed by the reversed system involving 4,4′-dipyridine (4,4′-DP) and 1,4-bis[(4-iodotetrafluorophenyl)ureido]butane (BIPUB), wherein the bis(urea) moiety was within the same molecule containing the XB donor sites (the iodine atom) and 4,4′-DP probably functioned as the XB acceptor and cross-linked the tapes formed by urea−urea interactions. Such a complex resulted in a network of fibers (Figure 112D) gelling various DMSO−water mixtures. Even a 1:1 mixture of BPUB and BIPUB provided a supramolecular gel consisting of an intricate

DOI: 10.1021/acs.chemrev.5b00484
Chem. Rev. 2016, 116, 2478−2601

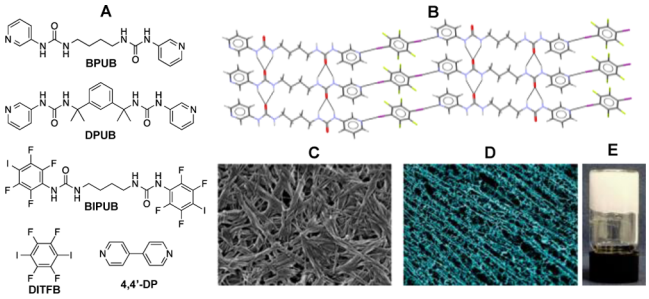

Figure 112. (A) Chemical structures of the compounds used in ref 83 to obtain supramolecular low molecular weight gels. (B) X-ray crystal structure of the 1:1 adduct between 1,4-DITFB and BPUB, which confirms the presence of gel-forming urea tapes cross-linked by XBs involving the pyridyl groups. (C, D) Scanning electron micrographs of dried 1:1 cogels formed by 4,4′-DP with BIPUB, and by BPUB with BIPUB, respectively. (E) Photograph of the 1,4-bis(3-pyridylureido)-butane/1,4-bis[(4-iodotetrafluorophenyl)ureido]butane cogel. Reprinted with permission from ref 83. Copyright 2013 Nature Publishing Group.

network of thin, homogeneous fibers showing some coalignment on the tens of micrometers scale, and linked by a more disordered secondary mesh of material (Figure 112D). These very thin fibers are consistent with the optical transparency of the gel. The results described above were the first demonstration that XB can play a role in driving the self-assembly of gel-phase materials even in polar media. Clearly, XB is sufficiently strong to interfere with competing gel-inhibitory HB interactions in a manner similar to that of metal coordination by bis(pyridylurea) gelators.[868] This provides new opportunities in the development of sophisticated gel-based functional materials and their supramolecular manipulation.

5. BIOMOLECULAR SYSTEMS

XB can now be considered a rather established interaction in supramolecular and material chemistry, while the presence and relevance of the interaction in biomolecular systems have begun to be studied only very recently. In general, halogen atoms are scarce in biomolecules, and this may account for the disparity mentioned above. The iodinated thyroid hormones T4 (thyroxine, 3,5,3′,5′-tetraiodothyronine) and T3 (3,5,3′-triiodothyronine) are probably the best known examples of naturally occurring halogenated compounds, and in the context of this review, it is important to observe that they work as XB donors in biomolecular systems.[27,249,869,870] However, halogen introduction is a traditional tool in drug optimization, for example, to increase the membrane permeability and half-life in vivo, and the recent years registered an ever growing interest in halogenated drugs.[871] Moreover, halogenated persistent organic pollutants are raising the attention on the biological relevance of halocarbons, and this is particularly the case for chlorinated and brominated diphenyls and diphenyl ethers, which are raising the highest concerns,[872−875] probably as their structural and chemical resemblance to thyroid hormones increases the impact of their presence in the biosphere. It can thus be anticipated that the interest in the role of XB in biological systems will increase in the future.

The first clear accounts on short Br···O contacts in biological systems were the 0.66 Å resolution structure of the inhibitor IDD594 with aldose reductase (AR)[876,877] and the structure of a four-stranded Holliday junction containing a bromouracyl unit.[878]

The former case was particularly informative as the high resolution of the structure allowed for the study of the geometry of the complex with a very low experimental error. It was thus possible to clearly observe how the Br of the inhibitor and the hydroxyl O of the Thr113 protein residue formed a short contact with a distance of 2.97 Å and a C−Br···O(γ) angle of 152.8°, thus substantially satisfying the requisites for an XB (Figure 113). This interaction was suggested to be the

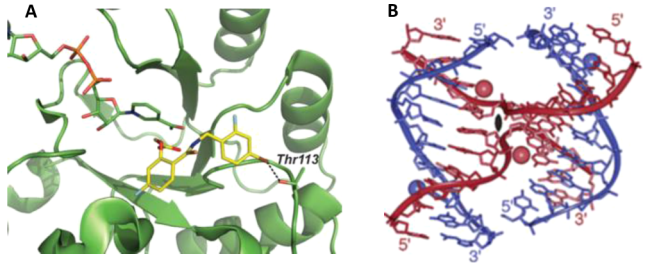

Figure 113. (A) XB (dotted black line) between the Br of IDD594 and the O(γ) of Thr113 in human aldose reductase. (B) Atomic structure of d(CCAGTACBr^{5}UGG), with bromine atoms rendered as spheres and the deoxyribose backbones as solid ribbons. Panel A reprinted with permission from ref 27. Copyright 2011 Royal Society of Chemistry. Panel B reprinted from ref 878. Copyright 2003 American Chemical Society.

reason underlying the specificity of IDD594 for AR over aldehyde reductase, in which Thr113 is replaced by a Tyr residue. Interestingly, when a single-atom mutation was performed by replacing Br with Cl, the IC_{50} value increased from 500 to 1300 nM, consistent with a decisive role of an XB in the recognition and binding event associated with enzyme inhibition. A similar situation was also found in the 2.1 Å resolution structure of aldose reductase with the inhibitor statil,[879] where a Br···O(γ) distance of 3.11 Å was recorded.

Holliday junctions are four-stranded intermediates associated with genetic recombination and recombination-dependent mechanisms such as DNA repair and integration. As part of a study on nucleotide sequences which stabilize Holliday junctions, P. S. Ho and co-workers reported the first evidence for a significant effect of the XB on a polynucleotide structure.[880] To help phase in X-ray diffraction data, they introduced the sequence CCAGTACBr^{5}UGG by substituting a thymine with a 5-bromouracil,[878] which led to a four-stranded Holliday junction. Conversely, both the native sequence with thymine and the analogous HB sequence with a non-halogenated uracil led to standard B-DNA duplexes. A short contact compatible with XB geometry was observed between the Br atom and a phosphodeoxyribose oxygen and replaced an analogous HB in the native junction.[881]

These studies prompted Ho and his group to perform a search in the Protein Data Bank (PDB)[249] with the goal of identifying short halogen−Lewis base (O, N, S) contacts which might have been previously overlooked, by defining two necessary prerequisites: a donor−acceptor distance lower than the sum of their respective van der Waals radii and a minimum angle of acceptor-to-donor approach of 120°. This first search yielded 113 hits, which were mostly complexes between proteins and halogenated ligands. Further surveys have been performed since then, and this number is now well above 700.[27,871,882−884]

DOI: 10.1021/acs.chemrev.5b00484
Chem. Rev. 2016, 116, 2478−2601

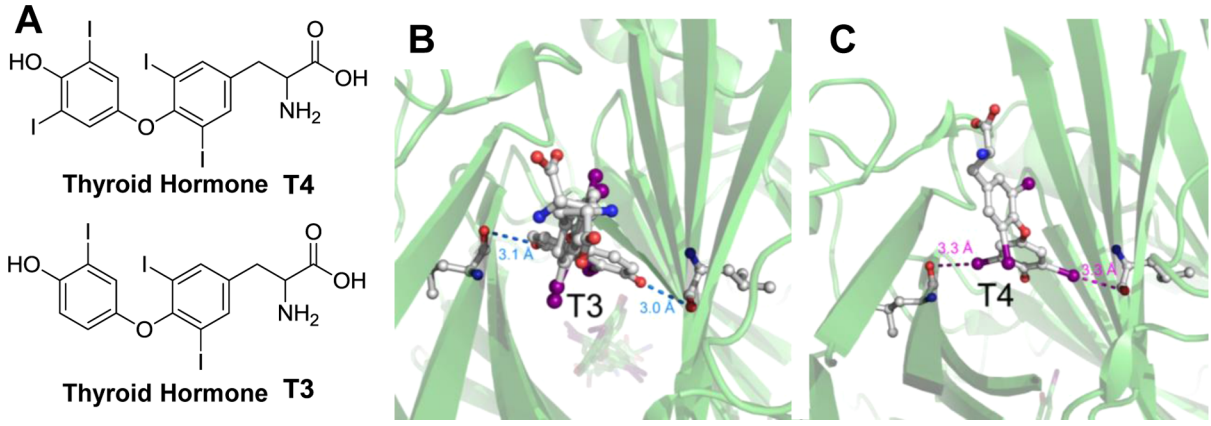

Figure 114. (A) Chemical formulas of the thyroid hormones T4 and T3. (B) HBs formed by T3 and (C) XBs formed by T4 with TTR. Reprinted with permission from ref 885. Copyright 2015 Springer.

5.1. Halogen Bond Donors

In most halogen-bonded biomolecular complexes, the donor is represented by a small halogenated molecule, while one or more specific sites of a biomacromolecule (typically a protein) act as acceptors.

The most important naturally occurring bioactive XB donors are the thyroid hormones T4 and T3, which contain four and three iodine atoms, respectively (Figure 114).

In humans and other backboned animals, proper development of the brain, skeleton, and organs is guaranteed by thyroid hormones, and is mediated by thyroid hormone receptors (THRs). Several I···O short contacts play a crucial role in the thyroid hormone recognition process,[886] and it was proposed that the higher T3 selectivity toward THRα in comparison to THRβ would be due to a shorter contact involving iodine.[887] In the blood, only a very small fraction (0.03−0.3%) of thyroid hormones is present in the biologically active free form, with the rest bound to transporter proteins such as transthyretin (TTR),[869,870] which has a higher selectivity for T4 over T3. It was shown that the iodines in the phenolic ring of T4 engage in two XBs with the TTR backbone, while this is not the case for the single iodine present on the phenol ring of T3.[888]

The activation of thyroid hormones, i.e., the conversion of T4 to T3 through cleavage of one C−I bond, is mediated by the selenoenzymes iodothyronine deiodinases; it was suggested that XB would be involved in their activity, through lengthening and activating the carbon−iodine covalent bonds.[889] By mimicking these systems, G. Mugesh and D. Manna have proposed a series of naphthalenes bearing thiol and selenol groups in the *peri*-position, which catalyze the deiodination of thyroid hormones through the combination of halogen and chalcogen bonds.[890]

As mentioned above, most of the known XB donors involved in biomolecular systems are non-naturally occurring small molecules, e.g., the volatile anesthetic halothane,[891,892] the antibacterial triclosan,[893−896] several nonsteroidal anti-inflammatory drugs (NSAIDs),[897−899] kinase inhibitors,[900−908] and several other drugs. Examples where the XB donor site is part of a biological macromolecule are understandably much more limited. Halogens are purposefully introduced into polynucleotides and proteins to facilitate structure determinations and can sometimes affect the obtained structure.[909−911] This was the case, for instance, for site-specific introduction of *p*-iodo-Phe to aid in protein structure determination.[911] For polynucleotides, examples include the introduction of halogenated uracils[878,882,912−914] and iodocytosine: A. Takénaka and co-workers observed that the introduction of an iodocytosine to obtain the sequence G^{I}CGAAAGCT changes the structure from a parallel intercalated duplex to a hexameric complex.[915,916]

In proteins, halogenation of amino acids (particularly Tyr) is known to occur naturally as a result of oxidative stress, catalyzed by enzymes such as myeloperoxidases[917] and eosinophil peroxidases.[918] Myeloperoxidase catalyzes the reaction of hydrogen peroxide and halide (Cl^-, Br^-, I^-) or pseudohalide (SCN^-) ions, generating hypohalous acids (HOX), which react rapidly with different targets in proteins including the sulfur atoms of cysteine or methionine, the nitrogen atoms of α-amino acids or histidine, lysine, and arginine side chains, and the aromatic rings of tyrosine and tryptophan.[919] Elevated levels of halogenated tyrosine residues have been detected in proteins isolated from patients with atherosclerosis, asthma, and cystic fibrosis.[920,921] While the occurrence of XBs involving such halogenated protein variants has not yet been proven, the fact that they can be recognized by polyclonal antibodies[922] suggests that XB may indeed be at work. Furthermore, recent studies on amyloidogenic short peptide fragments of human calcitonin showed an amplification of their fibribillation ability upon halogenation of Phe residues, with an effectiveness which follows the known XB strength scale Cl < Br < I.[923]

5.2. Halogen Bond Acceptors

In biologically relevant systems, the role of the XB acceptor is almost invariably played by biological macromolecules. In the recent survey by W. Zhu and co-workers,[871] it was shown that 778 short contacts involved halogens in high-quality structures of the PDB, and in 211 of them delocalized π electron systems were the interacting partner (halogen lone pair···π interactions were possibly included in these short contacts). Such delocalized π electron systems were, for instance, the guanidino groups in Arg residues[882,924] and other aromatic derivatives,[925] notable examples being Phe residues in protein kinases[900] and Tyr in the serine protease factor Xa (fXa).[926−930] Of the remaining 567 C−X···Y contacts, 430 are formed with protein residues. About 84% of these involve O atoms as XB acceptors, while N atoms are involved in only 10.4% of the cases (Figure 115); this distribution is remarkable when compared to the predominance of nitrogen compounds in halogen-bonded small molecular complexes. While being a relatively minor fraction,

DOI: 10.1021/acs.chemrev.5b00484
Chem. Rev. 2016, 116, 2478−2601

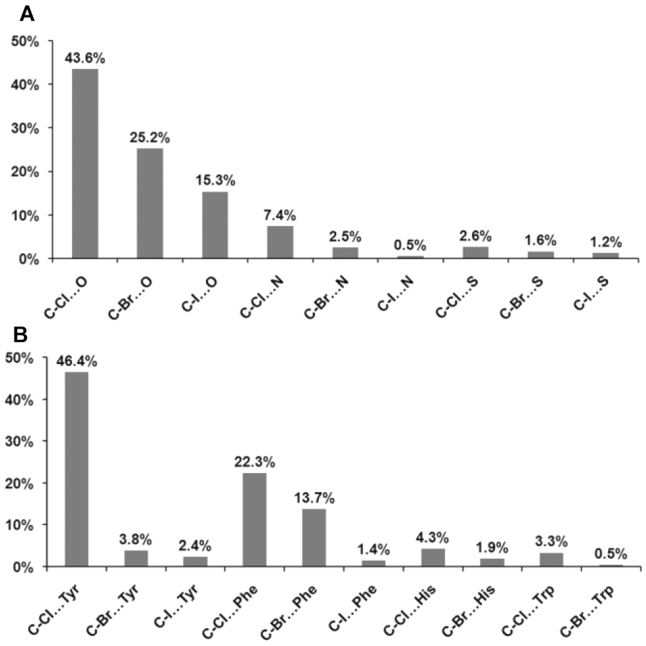

Figure 115. XBs in the PDB, divided as (A) C−X···Y and (B) C−X···π contacts (X = Cl, Br, I). Reprinted from ref 871. Copyright 2013 American Chemical Society.

XBs with S or Se atoms in the side chains of amino acids are also well documented.[890,892,899,931]

A more in-depth analysis reveals that 64.5% of C−X···Y contacts are formed with the protein backbone rather than amino acid side chains, possibly due to steric and solvent entropic costs in forming XBs with the latter.[885] The vast majority of these backbone XBs are established with the carbonyl oxygen rather than the amide nitrogen.[249,250,871,882,884,932] This was ascribed to two reasons, namely, (i) in C═O groups both oxygen lone pairs and the double bond can act as electron donors, whereas the nitrogen possesses only one electron lone pair, and (ii) accessing backbone nitrogens is a sterically more demanding phenomenon.[933] Interestingly, the peptide bond itself is also a potential XB acceptor.[249,934]

The only known cases of biomolecular XBs where the acceptor is not part of a biomacromolecule are when water molecules act as XB acceptors, most often with the ability for a single water molecule to be simultaneously involved both in XB and in HB.[935−937] Quantum chemical calculations suggested that XBs with water are thermodynamically more stable than other interactions involving water,[935] and it was shown in the most recent PDB survey that these interactions are around 16.6% of known biomolecular XBs.[871] The complexes of diclofenac with cytochrome P450[936] and lactoferrin[937] feature good examples of water molecules acting as bridges between halogen and hydrogen bonds. In the former case, XB with a water molecule featuring a Cl···O distance of 2.85 Å and a C−Cl···O angle of 158.1° was observed together with an HB involving the same water molecule and a carboxyl oxygen of the side chain of Glu297 (Figure 116). In the latter case a rather similar structure was observed, albeit with a slightly longer Cl···O distance, with a somewhat less linear angle, and involving Val591 in the HB.

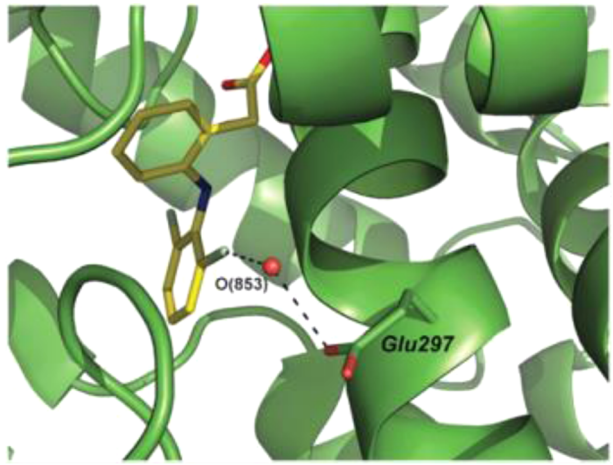

Figure 116. Diclofenac−cytochrome P450 complex showing that a water molecule forms at the same time an XB with one Cl atom of diclofenac (shown in pale green) and an HB with a carboxyl oxygen of the Glu297 side chain. Reprinted with permission from ref 27. Copyright 2011 Royal Society of Chemistry.

5.3. Geometrical Features

Similar to other fields, radial and angular geometric requirements are frequently employed to identify XBs in the biomolecular context. The radial requirement consists in the identification of a short contact between the halogen atom and the associated Lewis base atom, with an interatomic distance lower than the sum of their respective van der Waals radii.

Solely on the basis of the σ-hole model, the angular requirement would be for a linear C−X···B angle. However, a separate model has been proposed which takes into account the available surface area in halogen atoms for contact.[938] According to this model, the interaction probability is maximized for a C−X···B angle close to 170°, which corresponds nicely to the most common values found for small molecular complexes in the Cambridge Database[169,939] and to the distribution of short halogen contacts found in the PDB. This agreement is more strict for heavier halogens, such as Br and I, which form stronger XBs, while significant deviations are often observed when Cl atoms are involved[885] (Figure 117).

An interesting comparative study was performed for the binding of halogen-substituted benzenes into an internal nonpolar cavity of the Leu99 Ala bacteriophage T4 lysozyme mutant.[931] The I of iodopentafluorobenzene formed a 2.86 Å I···S contact with Met102 and a C−I···S angle of 166.3°, thus corresponding to a 0.5 Å shift and a 30° rotation with respect to the geometry found for benzene. A rather similar binding geometry was found for one of the two binding modes of the weaker XB donor iodobenzene, although with a significantly longer I···S contact (3.3 Å). Interestingly, the energy difference measured by isothermal titration calorimetry between these two complexes was 0.5−0.7 kcal/mol in favor of iodopentafluorobenzene; however, it should be noted that a difference in XB was likely only one of the differences responsible for this value. An XB was also found for one of the multiple binding modes displayed by bromopentafluorobenzene, which engaged a S atom of Met102 (Br···S distance 2.8 Å, C−Br···S angle 167°).

Another interesting example is the complex of the NSAID 3,5-diiodosalicylic acid with human serum albumin (HSA),[899] where one iodine was observed to form a contact with the

DOI: 10.1021/acs.chemrev.5b00484
Chem. Rev. 2016, 116, 2478−2601

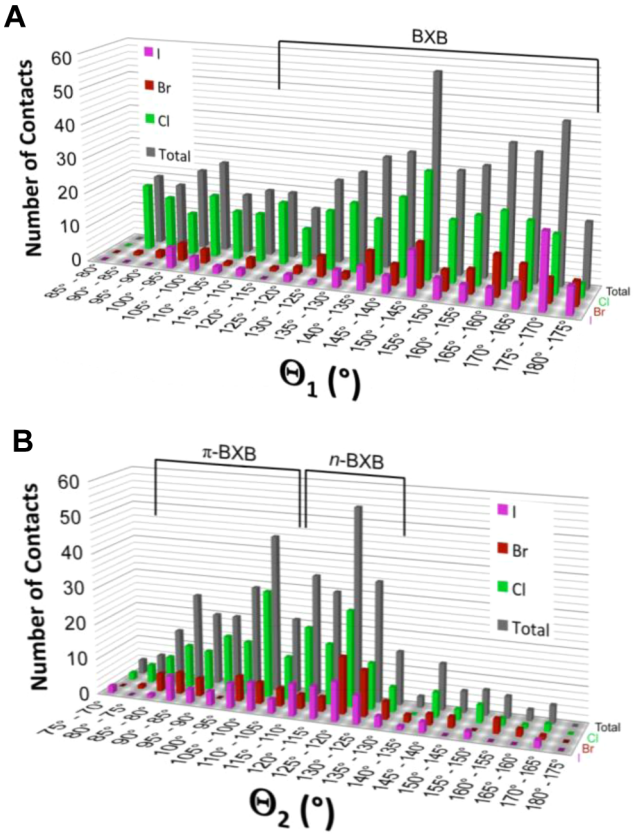

Figure 117. Number of short contacts involving halogens as a function of the angles: (A) C−X···B (θ_1) and (B) C−B···X (θ_2). π-BXB and n-BXB indicate biomolecular halogen bonds of the type C−X···π and C−X···Y, respectively. Reprinted with permission from ref 885. Copyright 2015 Springer.

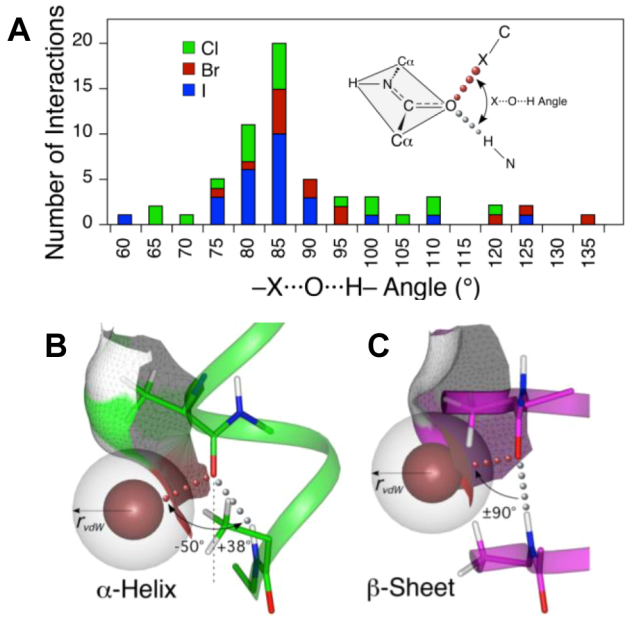

Figure 118. (A) Distribution of the relative angle of approach of HBs and XBs to a common Lewis base, subdivided by the halogen involved. Representations of the orthogonality of XBs and HBs in β-sheets (B) and α-helices (C); the white sphere represents the van der Waals radius of a Br atom. Reprinted with permission from ref 250. Copyright 2009 Nature Publishing Group.

carbonyl oxygen of Arg257, featuring an I···O distance of 3.46 Å and a C−I···O angle of 169.4°.

As mentioned above, far less ideal geometries are often observed for weaker XBs where chlorine atoms act as Lewis acids. In the complex of diclofenac, another NSAID, with the cyclooxygenase enzyme COX-2,[897] the main contributions to stabilization come from HB. However, in two out of the four independent complexes, short contacts were observed between a Cl atom and the hydroxyl oxygen of Ser530, with Cl···O distances of 3.23 and 3.18 Å, which are slightly shorter than the sum of the vdW radii of O and Cl, and C−Cl···O angles of 147.5° and 140.7°, respectively. These deviations from linearity are likely the result of geometrical constraints. Somewhat similarly, in the complex of COX-1 with (*S*)-indomethacin ethanolamide, a Cl···S contact is found with a distance of 3.29 Å and a C−Cl···S angle of 146.5°.[898]

The X···Y−C angle (X = XB donor; Y = XB acceptor) essentially depends on the distribution of electron-rich orbitals on the Lewis base Y atom. Among the XBs found in the PDB, an X···Y−C angle close to 120° is the most commonly found, which is consistent with an involvement of the nonbonding n orbitals of C═O groups. However, a local maximum occurs around 90°, particularly for the heavier halogen atoms,[249,885] which may be associated with interactions involving π orbitals of the Lewis base. This geometry is typically observed when XB and HB donors share a common acceptor, resulting in a strong X···O···H orthogonal arrangement, which is observed in both β-sheets and α-helices[250] (Figure 118). The orthogonality between the two interactions has also been shown on small molecular peptide models by both theoretical calculations[250] and experimental studies.[634] Orthogonality is not only geometrical, but also chemical, in the sense that the formation of XBs does not alter the HB-driven assemblies.

5.4. Energetical Considerations and Complex Stabilization Effects

Due to the difficulty of separating neatly the contributions of XBs from other contributions to adduct stabilization in systems as complex as those involving biomolecules, there are to date very few experimental measurements of XB binding energies in these systems. However, available data suggest contributions falling in the 1−5 kcal/mol range, which are rather consistent with what is observed in small molecular complexes.

The previously mentioned DNA Holliday junction system was used by P. S. Ho's group to study the competition between XBs and HBs. A junction was constructed containing two strands, each able to form either type of bond in competition with each other by using a 5-bromouracil or a cytosine, respectively. The relative stability of the two forms could be observed by means of a crystallographic titration assay[912,913,940] (Figure 119). On the basis of the observed isomer ratios, the halogen-bonded structure was found to be more stable by about 2 kcal/mol when the system was designed for competition of one XB versus two HBs, and by about 5 kcal/mol in a 2:2 competition.

The same assay was extended to include 5-halouracils containing different halogen substituents,[914] and the results confirmed that the bond stability increased on going from lighter to heavier halogens, at the same time also displaying more ideal geometries in terms of both radial and angular requirements of XB.

The DNA junctions were used to compare XB energies not only in crystals but also in solution. Differential scanning

DOI: 10.1021/acs.chemrev.5b00484
Chem. Rev. 2016, 116, 2478−2601

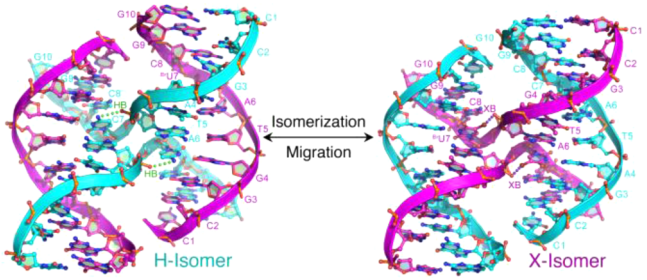

Figure 119. Competition between hydrogen-bonded (cyan strand) and halogen-bonded (magenta strand) structures in a four-stranded DNA junction. Reprinted with permission from ref 885. Copyright 2015 Springer.

calorimetry (DSC) was used to measure the heat required to melt DNA junctions involving Br and I as XB donors.[914,940] The results showed that while in these systems iodine allowed the most favorable enthalpic contribution (−5.9 versus −3.6 kcal/mol), it also brought forth a significant entropic cost, which made bromine favored in terms of overall free energy (−2.3 kcal/mol for I, −4.8 kcal/mol for Br).

C. D. Tatko and M. L. Waters conceived a study to measure the solution energy of biomolecular XBs involving aromatic groups as acceptors.[941] The thermal melting of β-hairpin peptides containing halogenated and nonhalogenated Phe residues was monitored by NMR, and the results showed that a single iodination of the aromatic Phe ring yielded a stabilization of −0.54 kcal/mol, while a double iodination could achieve a value of −1.01 kcal/mol.

Since a large number of the reported biomolecular XBs involve protein inhibitors, on a first degree of approximation, the stabilizing effect of XBs may be described in terms of dissociation constants and IC_{50} values, although a role is played by several other factors, such as dynamic structure differences, interactions with solvents, and accessibility of the active sites. The structures and IC_{50} values of cathepsin L complexes with a series of systematically selected halogenated, methylated, and hydrogenated inhibitors have been determined by F. Diederich and co-workers.[942] The replacement of a methyl group with different halogen atoms able to form short contacts with the carbonyl oxygen of Gly61 brought forth an IC_{50} reduction from 130 nM for the methyl to 22, 12, and 6.5 nM for Cl, Br, and I, respectively, which roughly corresponds to a stabilizing effect of 1−2 kcal/mol. The same study also demonstrated the possibility to finely tune the stabilization effect by using electron-withdrawing groups able to increase the XB donor ability of the halogens.

Several structures of tetrahalobenzimidazole inhibitors with the CK2 kinase are reported in the literature, where binding energies were calculated in the range of −8 to −11 kcal/mol.[901−905] As a rough comparison, the binding energy of the corresponding complex with 1*H*-indazole is reported to be −5.16 kcal/mol,[943] but the lack of a systematic study with closely related halogenated and nonhalogenated analogues makes it difficult to suggest a value for the specific stabilization induced by XB. A comparison of the binding energies found for 4,5,6,7-tetrahalobenzimidazoles[903,905] suggests a stronger stabilization by about 0.8 kcal/mol per established XB for the iodinated over the brominated analogue.

5.5. Relevance in the Pharmaceutical Field

About 40% of drugs in clinical trials or on the market are halogenated; at present about 25% of drugs in the launch phase and about 34% of those in the discovery phase are organohalogens. These numbers are a clear indication of the key role of halogen substituents in pharmaceuticals.[871] Furthermore, the presence of heavier organohalogens with respect to organofluorines shows a clear rising trend along the various phases of the drug discovery process, thus implying a strategic role of XB in the search for new lead compounds. In the National Cancer Institute's Diversity Set IV, which is a list of potential lead small-molecule compounds for high-throughput screening for cancer research, about 20% of the molecules contain I, Br, or Cl.[885,944] Standard docking algorithms cannot account for XB, potentially leading to a loss of viable lead compounds. On the other hand, halogens are incorporated into screening libraries used to search lead compounds as potential inhibitors against relevant therapeutic targets,[900,945−948] and the presence of an XB may affect protein−drug affinity to an extent significant enough to make the difference in a "go/no go" decision for a lead molecule.

Many of the reported small-molecule−protein complexes involve inhibitors with potential pharmaceutical and therapeutic interests. A noncomprehensive list of examples is reported below for illustration purposes; several entries have already been briefly described above in this section.

There is a particularly intense interest in protein kinases for their potential usefulness in the treatment of chronic inflammatory, cardiovascular, and neurodegenerative diseases, viral infections, and possibly even cancer; several complexes wherein XB is responsible for the binding of small molecules to these proteins have been reported.[900−908,947] Aldose reductase[876,877,882] and cathepsins[942,949] may have implications in a number of pathologies, including diabetic hyperglycemia and several cancers, and various halogen-bonded complexes involving them are available. XB has been a key factor in the design of potent and bioavailable inhibitors of the enzyme fXa, a serine protease factor, which has an important role in the blood coagulation cascade, and which was mentioned earlier as an example of biological XBs involving Cl/Br···π interactions.[926−930]

NSAIDs are used to reduce inflammation, pain, and fever. XB has been shown to occur, e.g., in the complexes of the NSAIDs diclofenac and (*S*)-indomethacin ethanolamide with cyclooxygenases,[897,898] as well as in that between 3,5-diiodosalicylic acid and HSA.[899] The latter is another example of the relevance of XBs in the biomolecular context, since nonspecific drug complexation with the overly abundant HSA is a well-known possible cause of reduced drug effectiveness.

Of course, this issue does not regard only NSAIDs. In the same study, a Cl···S XB was also found in the complex of HSA with diazepam. In the structure of cocrystals of the anesthetic halothane ($CF_3CHClBr$) with HSA, the Br atom was found to interact with several protein sites, the sulfur of a cysteine residue among others.[892] The physiological binding sites for halothane are presumed to be cavities within transmembrane 4-α-helix bundles of neurotransmitter receptors; while an exact structural determination of these sites remains elusive, similar motifs are found in ferritin, where hydrophobic cavities are formed between two protein monomers. In this system, the Br atom of halothane forms a 3.10 Å contact with the O of Leu24 at a C−Br···O angle of 144.9°, while the Cl forms a C−X···π XB with Tyr28, with the closest ring carbon at 3.3 Å.[891]

DOI: 10.1021/acs.chemrev.5b00484
Chem. Rev. 2016, 116, 2478−2601

One further particularly interesting example is offered by the HIV-1 reverse transcriptase (RT, a key enzyme used by HIV to form a new viral particle) and its complex with the inhibitor R221239.[950] In this complex, a 3.4 Å contact is formed between an iodine atom of the inhibitor and the backbone oxygen of Tyr 188, with a C−I···O angle of 161.6°. The special interest in this case comes from the fact that the inhibitor does not form relevant contacts with Tyr181, one of the amino acids involved in the most common mutations, which give rise to drug-resistant viruses.

A halogen-enriched library for molecules able to reactivate the functionality of the Y220C mutant of the p53 tumor suppressor has been designed and screened. These molecules could bind to the destabilizing surface crevice induced by the mutation, and thus shift the folding−unfolding equilibrium of the protein back toward the folded state.[946] The best binders displayed XBs between the iodine atom of the drug and the carbonyl oxygen of Leu145, with I···O distances of about 3.0 Å and C−I···O angles between 169° and 173° (Figure 120). A clear reduction in binding capability was observed by substituting bromine and chlorine for the iodine.

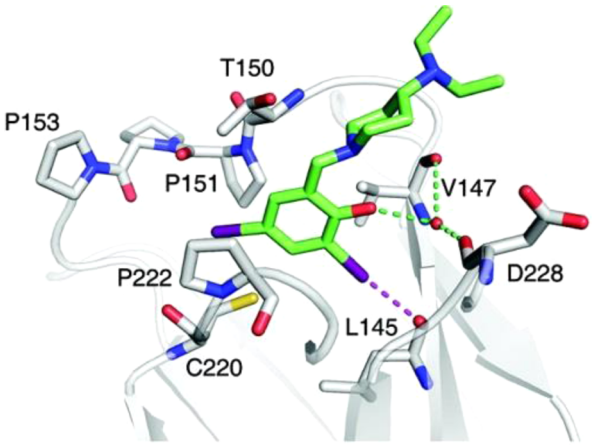

Figure 120. Crystal structure of the complex between the binder PhiKan5196 and the p53 mutant Y220C. The iodine atom is shown in magenta and forms an XB with the carbonyl oxygen of Leu145. Adapted from ref 946. Copyright 2012 American Chemical Society.

The interest in biomolecular XBs also extends beyond the therapeutic field. For example, triclosan is an antibacterial which acts as an inhibitor of bacterial fatty acid synthesis.[951] In the complex with the enoyl-acyl reductase (ENR) enzyme from *Plasmodium berghei*,[893] a 3.25 Å Cl···O contact is found with Gly204, bearing a C−Cl···O angle of 162.4°. A shorter and more linear XB can be observed with the Ala97 of ENR from *Bacillus anthracis*, where a Cl···O distance of 3.08 Å and a C−Cl···O angle of 166.2° are observed.[894]

Pseudilins are highly halogenated marine natural products and have been recently shown as promising herbicide compounds. XBs involving both Br and Cl atoms with protein backbone oxygens were found to contribute to the inhibition of IspD enzymes involved in the nonmevalonate pathway for isoprenoid biosynthesis, which is used by plants and many human pathogens, but not by animal organisms.[952]

5.6. Computational Models

From the findings and considerations reported above, the potential of XB in drug design is apparent; adequate modeling tools might nevertheless help in optimization.

One viable approach consists in hybrid quantum mechanical/molecular mechanics calculations (QM/MM),[947] as a reasonable compromise between the accuracy of QM and the speed of MM methods. This approach consists in using MM or molecular dynamics (MD) to model most of the biomacromolecule, while using QM for those parts which are of higher interest (e.g., a drug binding site) or which cannot be treated properly by MM or MD. This method could successfully model the geometry of XBs involving backbone carbonyl oxygens, although its accuracy in calculating interaction energies proved to be more on a qualitative level.

The positive extra point (PEP) approach[953,954] can be used to account for XBs in MM or MD methods used to evaluate the energies of biomacromolecules, such as OPLS-AA[955] or AMBER.[956] Since these methods assign by default an isotropic negative charge distribution to halogens, in the PEP the σ-hole is introduced by adding a positive pseudoatom at or near the halogen atom surface. This method, for example, allowed calculation of the binding energies of CK2 kinase complexes with several halogenated ligands, yielding values in good agreement with the experimental dissociation constants and IC_{50} values.[957] One drawback of this approach is that it tends to overestimate interatomic X···B distances; however, more accurate results could be achieved by careful positioning of the positive pseudoatom closer to the center of the XB.[958]

P. S. Ho and co-workers approached the issue by deriving a set of MM/MD force field equations based uniquely on the physical properties of covalently bound halogen atoms. They found functions for the Coulombic and Lennard-Jones potentials which describe the effective charge and shape of Br atoms as a function of the C−Br···Y angle.[938] This method was successfully used to model the structure−energy relationships relative to the DNA junction models studied by the same group.

To help identify XBs in biomolecular complexes, one knowledge-based approach has been devised by W. Zhu and co-workers to derive a set of scoring functions based on statistical distributions of XB geometries.[959] While such an approach is clearly influenced by the number and type of already available data (for example, there are currently very few structures including iodine atoms, mostly involving thyroid hormones), different binding modes may still show significant environmental similarities and thus be related.

6. FUNCTIONAL SYSTEMS

6.1. Organic Catalysis

In the field of noncovalent organocatalysis, HB plays an important role,[960,961] and several examples of HB donor catalysts have been reported.[210,962−968] Taking into account the similarities between HB and XB, in particular for their effective use in anion recognition,[69,70,741,967,968] many researchers started to investigate the possible use of XB donor molecules as catalysts in organic synthesis. However, it appeared immediately clear that the potential of the XB in this field may arise mainly from the peculiarities of halogen-bonded systems compared to related systems based on HB.[969] First, the higher directionality of XB[26] can be exploited in the design of multidentate XB donors with higher selectivity toward different substrates.[970] Second, halogen atoms being involved and particularly strong XB donors being associated with fluorinated backbones, XB can be considered as a hydrophobic alternative to HB. Accordingly, XB donors are more soluble in apolar

DOI: 10.1021/acs.chemrev.5b00484
Chem. Rev. 2016, 116, 2478−2601

solvents than their HB counterparts, which, on the other hand, often suffer from the competition of more polar HB donor/acceptor solvents.[971] Furthermore, since I, Br, Cl, and in some cases also F atoms can all be involved in XB, the interaction strength can be easily tuned by changing the halogen atom.[205] Finally, halogens are more polarizable and bigger in size than hydrogen, and XB donors can be classified as "softer" Lewis acids than those based on HB, with important consequences for the substrate preference of the final XB-based organocatalysts.

Halogen-bonded adducts have been invoked as transient species on the reaction pathways of different types of reactions.[972] For instance, the mechanistic scheme suggested for alkene bromination involves a noncovalent complex in which a Br_2 molecule approaches the carbon−carbon double bond at an angle of 180° (Figure 121).

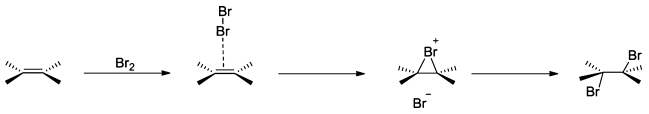

Figure 121. Representation of a schematic model of the mechanism of bromination of alkenes evidencing the formation of halogen-bonded adducts of the type X···π.

Similar halogen-bonded adducts also seem to be involved as intermediates in metathesis reactions between organic halides and organometallic compounds.[973] However, in these reactions the XB donor does not function as the catalyst since it is consumed during the reaction. In the remaining part of this section, we will examine only reactions where the XB donor functions as a catalyst and remains intact over the course of the reaction.

Elemental iodine is known to accelerate a wide variety of organic reactions, and its use in organic synthesis is well documented.[974−976] In several cases it has been claimed that the catalytic activity of I_2 is related to its Lewis acidity, as, for example, in reactions with carbonyl groups such as Strecker-type reactions,[977] acetal formation and cleavage,[978] imine formation, and Michael additions.[974,976] However, no detailed mechanistic studies have been reported in this respect, and modes of action of I_2 as a Lewis acid are not completely understood.

On the contrary, iodine trichloride (ICl_3) was reported in 2010 to catalyze the ring-opening polymerization of L-lactide in the presence of 11-bromo-1-undecanol (11-BU) as an initiator (Figure 122).[979] Through accurate FTIR and NMR studies, the authors were able to suggest a plausible polymerization mechanism occurring through a double activation of both the monomer L-lactide and the alcohol initiator (11-BU) by ICl_3.

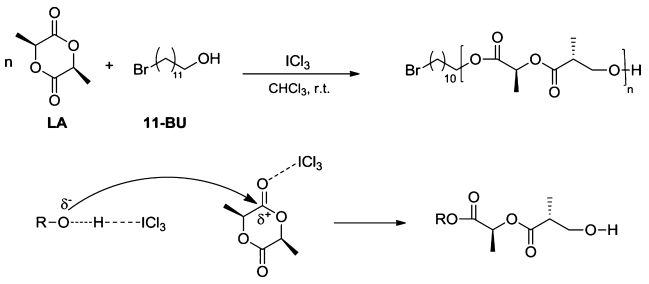

Figure 122. Top: polymerization of L-lactide to poly(L-lactide) with ICl_3. Bottom: proposed mechanism for the 2-fold activation.

The electrophilic activation of the carbonyl group of L-lactide by ICl_3 was shown by a blue shift of the C=O vibrational band and the downfield shift split of the ^{13}C NMR signals of L-lactide, both consistent with a transfer of electron density from the oxygen toward the iodine. On the other hand, a large downfield shift of the OH resonance of 11-BU suggested the formation of OH···Cl HBs. In the suggested polymerization pathway, XB and HB act in concert to accelerate the reaction (Figure 122). However, traces of HCl and HIO_3 deriving from the ICl_3 hydrolysis could be present in the reaction mixture, and it is difficult to ascertain if they play a role in the activation mechanism.

The first report about the purposeful use of organic XB donors as catalysts dates back to 2008, when C. Bölm et al. reported the reduction of 2-phenylquinoline by the Hantzsch ester catalyzed by haloperfluoroalkanes (Figure 123).[980] On the

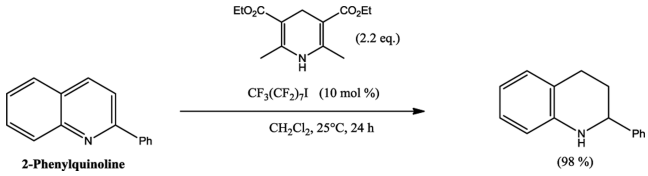

Figure 123. Reduction of 2-phenylquinoline in the presence of 1-iodoperfluorooctane.

basis of ^{19}F and ^{13}C NMR analyses, the authors demonstrated that the substrate activation for the reduction occurs through the formation of XB between I or Br atoms of the catalyst and the quinoline nitrogen atom of the substrate. Bromo- and iodoperfluoroalkanes of different lengths were tested in these experiments, with yields up to 98%. In particular, it has been evidenced that longer perfluoroalkanes produce higher yields, while for catalysts of comparable length, higher conversions are obtained with iodinated catalysts, consistent with the scale of the XB strength. To further corroborate the role of XB in these reactions, a competing XB acceptor, (2,2,6,6-tetramethyl-1-piperidinyl)oxy radical (TEMPO), was added to the reaction mixture, and as expected, a lower catalytic ability was obtained.

The same reduction can also be promoted with high efficiency by a bidentate, cationic XB donor based on a dihydroimidazoline core (Figure 124).[981] The reduction with

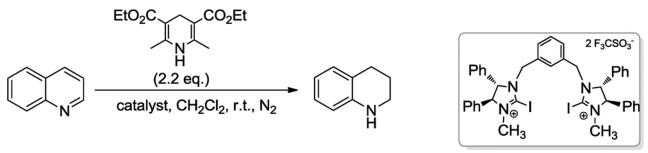

Figure 124. Hydrogenation of quinoline with the Hantzsch ester in the presence of a bidentate XB donor catalyst based on a dihydroimidazoline core (right).

the Hantzsch ester in dichloromethane proceeds with good yields (higher than 90%) both with quinolines and with imines, with a low catalyst loading of 2 mol %. NMR studies and isothermal calorimeric titrations confirmed the involvement of XB in the activation mechanism.

The fluoronium cation F^+, derived from *N*-fluorooropyridinium triflate, has beem used as a catalyst in aziridine synthesis starting from N-substituted imines and ethyl diazoacetate (Figure 125).[982] Due to its electrophilic character, the F^+ cation can be assumed to form strong XBs with the imine component,

DOI: 10.1021/acs.chemrev.5b00484
Chem. Rev. 2016, 116, 2478−2601

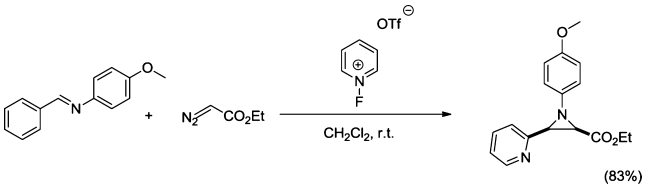

Figure 125. Aziridine synthesis in the presence of the fluoronium cation F^+.

activating it toward the following nucleophilic attack by ethyl diazoacetate.

Recently, Huber et al. reported the use of multidentate XB donors as activators or catalysts in organic synthesis.[970,983,984] In 2011 they reported the first use of bisimidazolium-based XB donors as catalysts in a Ritter-type reaction: the solvolysis of benzhydryl bromide in acetonitrile to obtain the *N*-benzhydrylacetamide (Figure 126).[983] Since the C−Br bond of the

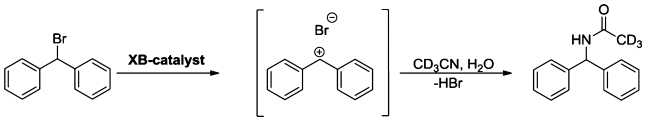

Figure 126. Solvolysis of benzhydryl bromide as a model reaction.

benzhydryl bromide is relatively weak and taking into account the ability of halide anions to act as XB acceptors, they reasoned that in the presence of a strong XB donor it should be relatively easy to activate the substrate toward a nucleophilic substitution reaction. The mechanism could be either S_N2 or S_N1 (Figure 127). In fact, either the XB donor could coordinate

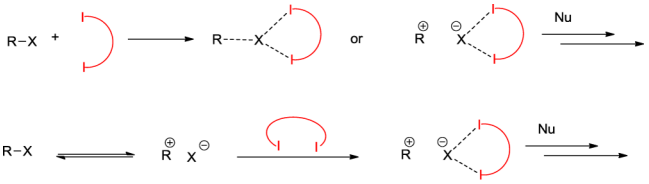

Figure 127. Possible modes of activation of a halogenated substrate by the bidentate XB donor catalyst (shown in red).

the bromine atom, polarizing the C−Br bond and thus facilitating the S_N2-type attack by the nucleophile, or alternatively the C−Br bond can break to form a carbocation intermediate, which undergoes an S_N1-type nucleophilic attack.

The solvolysis of benzhydryl bromide as reported in Figure 126 does not occur either without any catalyst or in the presence of the classical XB donors, e.g., 1,4-diiodotetrafluorobenzene and 1,3,5-triiodotrifluorobenzene. On the contrary, the use of the bisiodinated calalysts in Figure 128 as activating agents afforded yields of up to 80%. Upon addition of 1 equiv of the strong acid HOTf, the yields dropped down to 25%, allowing any possible role of acid impurities in the catalysis to be ruled out. According to the XB theory, by replacing iodine atoms with bromine, weaker XB donors are obtained; therefore, the corresponding bisbrominated activating agents afford lower conversions (54%). The replacement of the halogen atoms with hydrogens, instead, leads to a conversion of only 7%, demonstrating that in this reaction XB outperforms the HB.

Single-crystal X-ray analysis of one of the bisiodinated catalysts in Figure 128 revealed an O···I short contact between an oxygen atom of the triflate anion and an iodine atom of the

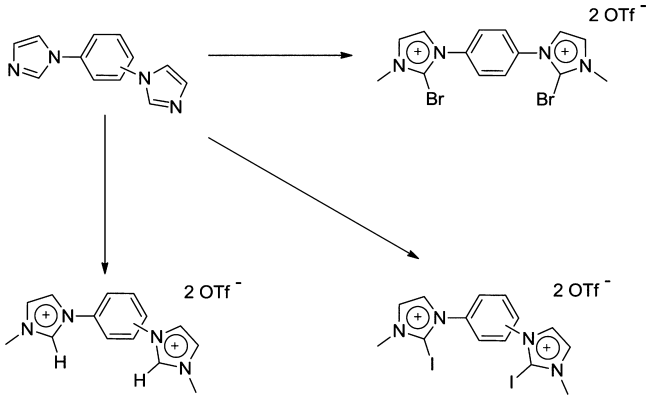

Figure 128. Halogenated and hydrogenated activating reagents.

bis(imidazolim) cation, suggesting a competition in the reaction mixture between the triflate and the reaction substrate for the activating agent. By replacing the triflate anion with the tetrafluoroborate, the yields increased to 97%, demonstrating the role of the counteranion in the activity of the XB donor catalyst.

Isothermal calorimetric titrations were also carried out to obtain further information on the ability of the synthesized catalysts to function as effective XB donors.[985] In these experiments, the catalysts were titrated with tetrabutylammonium chloride, bromide, and iodide in acetonitrile at room temperature, and the corresponding heats of binding were detected. This allowed the binding stoichiometries to be obtained and demonstrated that when the two iodoimidazolium synthons are in the *meta*-positions on the central phenyl ring, a bidentate halide coordination is obtained.

The effect of the alkyl chains bound to the imidazolium nitrogens was also investigated. By introducing longer alkyl chains (i.e., octyl instead of methyl), the solubility of the XB donor catalysts in apolar solvents increases. This is very important since, besides broadening the range of applicable solvents, stronger binding may be expected in these solvents.

More recently, Huber et al. demonstrated that dicationic XB donors with noncoordinating counteranions can also activate neutral carbonyl substrates toward Diels−Alder reactions (Figure 129).[986] Through DFT calculations they proved the

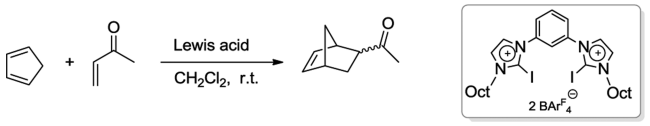

Figure 129. Left: Diels−Alder benchmark reaction. Right: dicationic XB donor activating agent $BAr^F = B[3,5\text{-}(CF_3)_2C_6H_3]_4^-$.

pivotal role of XB in the activation of the carbonyl group toward the Diels−Alder reaction, while by a series of experiments they were able to rule out the involvement of traces of acid, while demonstrating the role of the different structural features of the halogen bond donor.

As a closely related work, Takeda et al. reported in 2014 that 2-haloimidazolium salts efficiently catalyze the aza-Diels−Alder reaction of aldimines with the Danishefsky diene (Figure 130).

Comparative experiments demonstrated that no reaction occurs in the absence of catalysts, and also the classical XB donors, e.g., perfluoroalkyl iodides and iodoperfluorobenzenes, were inactive. On the contrary, in the presence of catalyst **A**

DOI: 10.1021/acs.chemrev.5b00484
Chem. Rev. 2016, 116, 2478−2601

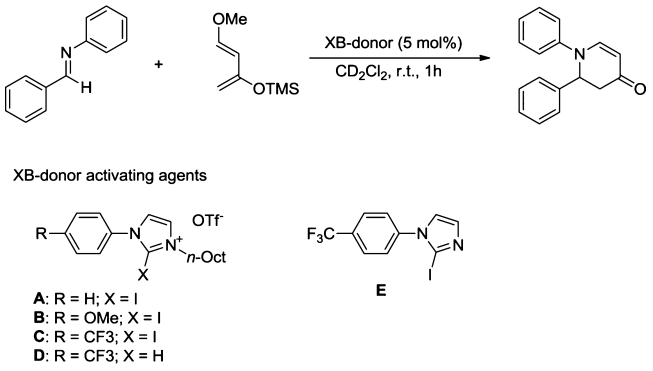

Figure 130. Top: Aza-Diels–Alder reaction of an aldimine with the Danishefsky diene. Bottom: structure of the used XB donor activating agents.

(Figure 130), a 57% conversion was obtained, and the introduction of CF_3 electron-withdrawing substituents on the molecular scaffold (catalyst **C**) increased the yields to 80%. No reaction occurred in the absence of iodine (catalyst **D**) or with the neutral XB donor **E**. All these experiments clearly demonstrated that the stronger the XB donor, the higher the yield of this kind of reaction and once again suggested the important role of XB in the activation mechanism.

To widen the library of multidentate XB donors to be used in organocatalysis, further compounds were developed and tested in Huber's group. First, the azobis(halopyridinium) compounds reported in Figure 131 were synthesized and tested in the solvolysis reaction of benzhydryl bromide.[984]

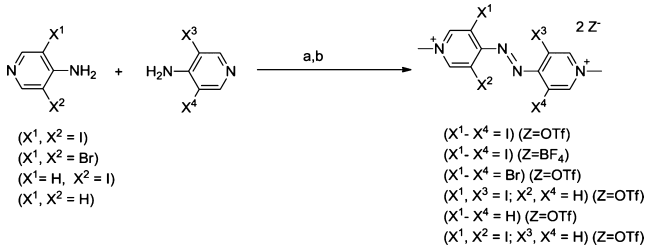

Figure 131. Synthesis of 4,4′-azobis(halopyridinium)-based XB donors and reference compounds.

Iodinated and brominated catalysts, in the presence of pyridine to quench traces of acid, were active in the solvolysis reaction, affording high yields, whereas the analogous non-halogenated compound, in the same conditions, gave only negligible yields. However, unexpectedly, in the absence of pyridine, the tetrahydrogenated catalyst was active in the solvolysis reaction, affording a 69% yield. Single-crystal X-ray analysis of this catalyst, obtained directly from the reaction mixture, helped in understanding this behavior. In fact, in the structure there were Br_4^{2-} anions interacting through XB with the cations. This suggested the formation of Br_2, during the reaction, by oxidation of HBr. Since Br_2 can act as an XB donor, it can activate the substrate toward the solvolysis reaction, explaining the unexpected yield obtained with the tetrahydrogenated catalyst in the absence of pyridine. Addition of cyclohexene quenches the activity of elemental bromine, allowing evaluation of the activation potential of the halopyridinium. Therefore, in the presence of pyridine and cyclohexene, the tetraiodinated and brominated catalysts gave yields of 93% and 76%, respectively, while only traces of the solvolysis product were obtained when using the tetrahydrogenated catalyst.

This behavior perfectly agrees with the XB theory and once again confirms the role of XB in the reaction activation process. Partly iodinated catalysts were also active in the solvolysis reaction, although they also afforded sizable amounts of benzhydrol and dibenzhydryl ether as byproducts.

Bi- and tridentate XB donors containing 5-iodo-1,2,3-triazolium moieties were also tested in Huber's group as activators in the solvolysis of benzhydryl bromide (Figure 132)[547] The iodinated bidentate compounds 1,3-I^{Bn}/OTf and

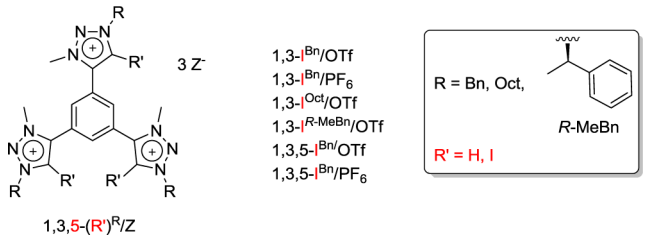

Figure 132. Bi- and tridentate polycationic XB donors based on the 5-iodo-1,2,3-triazolium synthon.

1,3-I^{Oct}/OTf gave, respectively, 78% and 62% conversions after 96 h of reaction, while the nonhalogenated compounds 1,3-H^{Bn}/OTf and 1,3-H^{Oct}/OTf afforded only 7% and 11% conversions, respectively, in the same reaction time, confirming the role of XB in the activation mechanism. The tridentate XB donor 1,3,5-I^{Bn}/OTf turned out to work far better with yields higher than 95% after only 48 h, suggesting a tridentate binding mechanism.

Besides these multidentate cationic XB donor catalysts, the same group also reported the use of polyfluorinated neutral activating agents.[987] Neutral XB donor catalysts can offer some advantages compared to the cationic ones. The latter, in fact, being soluble only in polar solvents, can be applied only to certain organic reactions. Moreover, complications may arise from the presence of anions that can compete with the substrate for the XB donor site.

In 2013 Huber et al. reported the first example of carbon–carbon bond formation catalyzed by the XB. In particular, they tested the XB donors **F**, **G**, and **H** (Figure 133) in the reaction of 1-chloroisochroman with silyl ketene acetals.

After 12 h at −78 °C, conversions of 37% and 91% were obtained in the presence of a 10 mol % concentration of the

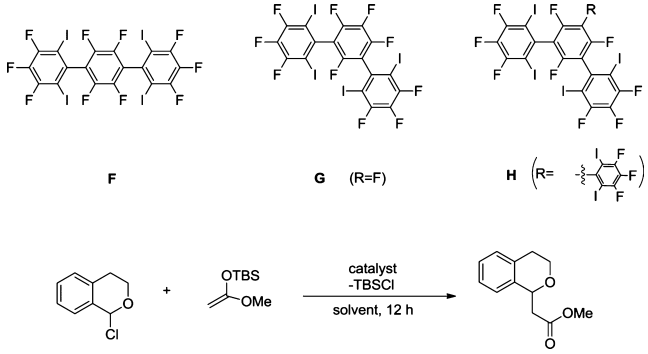

Figure 133. Top: structures of neutral polyfluorinated XB donors. Bottom: selected test reaction of 1-chloroisochromane (left) to the corresponding ester.

DOI: 10.1021/acs.chemrev.5b00484
Chem. Rev. 2016, 116, 2478–2601

iodinated XB donors **F** and **H**, respectively, while the analogous noniodinated species did not afford any reaction. The addition of strong XB acceptors (20 mol % tetrabutylammonium chloride) makes the XB donors **F** and **H** totally inactive, proving the role of XB in the activation process. Moreover, the *meta*-substituted compound **G** and the monodentate variant (1,3,5-triiodo-2,4,6-trifluorobenzene) were not active in this type of reaction, confirming the importance of the number and relative orientation of the iodine substituents.

Another important aspect in organocatalysis concerns catalyst recycling. Legros et al.[988] synthesized a *fluorous* organocatalyst by reacting diazabicyclooctane (DABCO) with 2 equiv of perfluorooctyl iodide, obtaining the trimeric halogen-bonded complex **I** in Figure 134. The perfluorinated chains

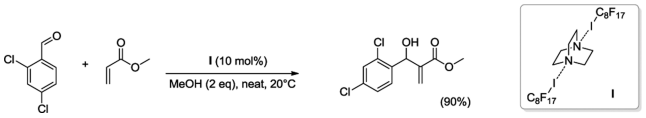

Figure 134.

deeply affect the solubility of the catalyst, which can be easily precipitated from the reaction mixture and recovered by filtration. This fluorous catalyst promoted the Morita–Baylis–Hillman reaction between aromatic aldehydes and Michael acceptors with yields as high as 92% (Figure 134). The recovered catalyst can be reused for up to five iterative cycles, albeit with a little decrease of the activity.

Finally, Charette et al.[989] reported on halogenated rhodium carboxylate catalysts that are active in the enantioselective cyclopropanation of alkenes with α-nitrodiazoacetophenones (Figure 135).

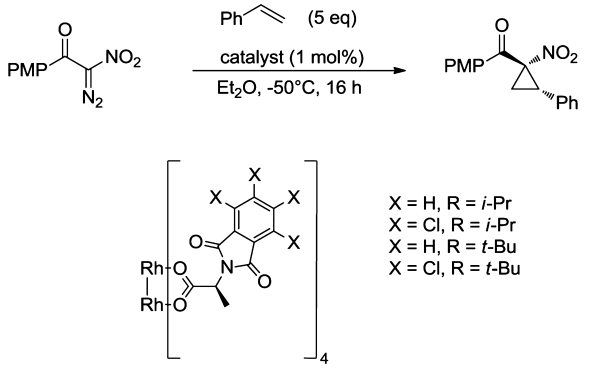

Figure 135. Cyclopropanation reaction with different Rh-based halogenated catalysts.

The tetrachlorinated catalysts showed enantioselectivities higher than those of the analogous hydrogenated compounds (80–93% ee vs 2–43% ee). Single-crystal X-ray analysis of the halogenated catalysts revealed an *all-up* conformation stabilized by Cl···O XBs between the chlorine atoms and oxygen atoms of the phthaloyl group. $^{1}H-^{13}C$ heteronuclear NOESY (nuclear Overhauser effect spectroscopy) experiments suggested that this *all-up* conformation is also kept in solution and is responsible for the high enentioselectivities observed.

6.2. Optical and Optoelectronic Systems

6.2.1. Light-Emitting Materials. Organic solid-state luminescent materials have in recent decades received a lot of attention due to their potential applications in organic electronics, photonics, and sensing.[990−992] The emissive properties of organic chromophores are greatly affected by their packing in the solid state.[993] On one hand, it is of interest to dynamically tune the packing, and consequently the optical properties, via external stimuli.[994,995] On the other hand, there is a need to predictively design solid-state materials with desired optical properties,[996] and XB-based crystal engineering has emerged as a promising tool for this. In this section we will discuss the role of halogenation in the emissive properties of organic chromophores and present the recent progress in halogen-bonded fluorescent and phosphorescent crystals as well as amorphous materials.

The bare size of halogen atoms plays an important role in the photoluminescence of halogenated chromophores. For instance, it has been reported that in halogenated monohydroxyl corroles the singlet-to-triplet intersystem crossing rate increases by a factor of 60 when using iodinated corroles as compared to their fluorinated counterparts.[997] This is explained through intramolecular spin–orbit perturbations, also known as the heavy-atom effect.[998,999] The heavy-atom effect renders halogenated chromophores of potential interest as photosensitizers in photodynamic therapy[1000] and as phosphorescence emitters, but for obtaining fluorescence emission with a high quantum yield, its role is typically detrimental. This is exemplified by comparing chromophores **10a** and **10b** shown in Figure 136A: The iodinated one, **10a**, showed a low

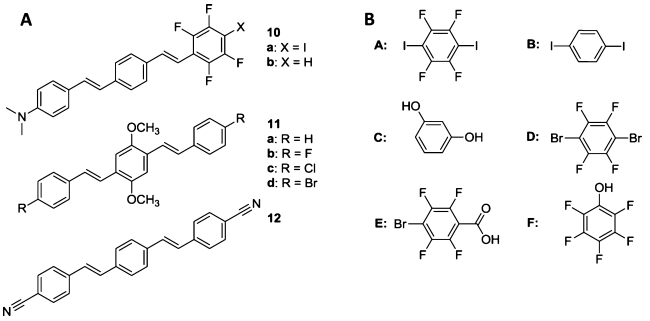

Figure 136. A selection of (A) fluorophores studied in refs 486, 1001, and 1002 and (B) halogen/hydrogen bond donors cocrystallized with **12** in ref 1002.

fluorescence quantum yield of 0.14 in toluene, while for the noniodinated **10b**, a quantum yield of 0.90 was reported.[486] Furthermore, for **10a** XB drives the self-assembly in the solid state into infinite chains that exhibit no fluorescence. **10b**, in turn, exhibits bright fluorescence due to J-type aggregation driven by aryl–fluoroaryl interactions.[486] As a counterexample, halogenation has a positive impact on the solid-state emission of compounds **11**.[1001] Microcrystals of **11c** exhibit an exceptionally high solid-state fluorescence quantum yield of 0.95, while crystals of **11d** outperform the other compounds in the efficiency of electrochemiluminescence. Clearly, more investigations are needed to comprehensively understand the effects of halogenation—and XB—on the photoluminescence of organic molecules and molecular crystals.

The first demonstration of the XB-based cocrystallization strategy to tune the fluorescence of solid-state materials was reported by Jones and co-workers in 2011.[1002] They employed the stilbene derivative **12** (Figure 136A), cocrystallized with several nonfluorescent halogen and hydrogen bond donors (Figure 136B) capable of interacting noncovalently with the

DOI: 10.1021/acs.chemrev.5b00484
Chem. Rev. 2016, 116, 2478–2601

cyano groups of **12**. Each of the cocrystals showed distinct crystal packing compared to the pure **12** (Figure 137, top).

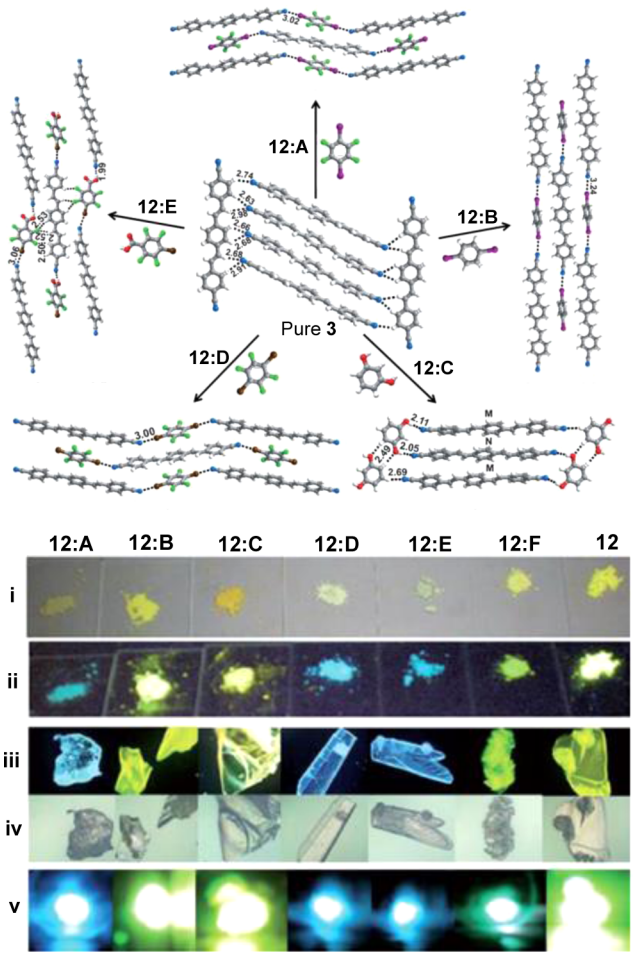

Figure 137. Top: crystal structures of pure **12** and related cocrystals **12**:**A**, **12**:**B**, **12**:**C**, **12**:**D**, and **12**:**E**, which each shows a distinct packing. Bottom: photographs of samples of pure **12** and of the related cocrystals. (i, ii) Powder samples under daylight and UV illumination, respectively. (iii, iv) Single-crystal samples under UV illumination and daylight as observed through a fluorescence microscope (50×). (v) Two-photon luminescence under 800 nm laser excitation. Reprinted with permission from ref 1002. Copyright 2011 Wiley-VCH.

This, in turn, strongly affected their optical properties as shown by the photographs of Figure 137, bottom, allowing the tuning of the emission color from blue to green to yellow as determined by the stacking arrangement of the chromophores.[1002] The cocrystals also served as efficient two-photon emitters when pumped with an 800 nm near-infrared light source. In a follow-up study, the same authors developed an ultrasound-assisted method to fabricate halogen-bonded nanococrystals.[1003] Their sonocrystallization procedure yielded monodisperse spherical 1:1 cocrystals of **12** and **A** with an average size of 60−70 nm (Figure 138A). Without the ultrasound treatment, no cocrystals were formed. The nanosized cocrystals may differ from their macroscopic counterparts in terms of their optical properties, as was also observed in this work. For example, the fluorescence lifetimes were prolonged by the nanoconfinement, and the emission spectrum exhibited distinct features as compared to that of the macrodimensional crystals. The emission from the nanococrystals could also be

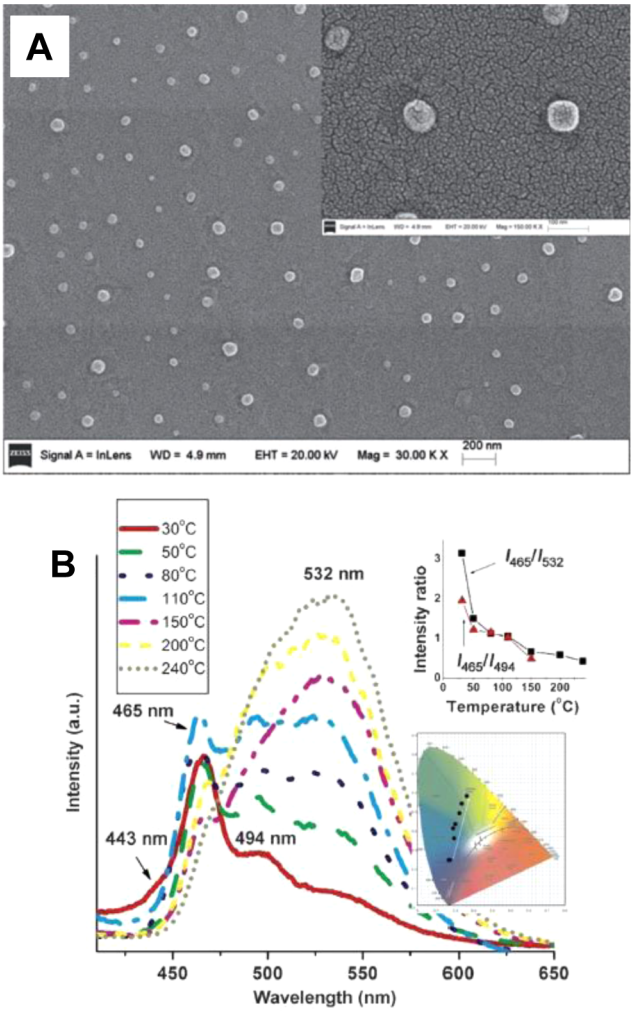

Figure 138. (A) Scanning electron micrograph of the **12**:**A** nanococrystals. (B) Fluorescence spectra of the nanococrystals at different temperatures. The inset shows the fluorescenece intensity ratios at I_{465nm}/I_{532nm} and the dependence of the color coordinates on the temperature. Reprinted with permission from ref 1003. Copyright 2013 Wiley-VCH.

reversibly tuned with the temperature (Figure 138B), whereas heating above 200 °C resulted in an irreversible structural change from **12**:**A** nanococrystals into nanocrystals of pure **12**. These two studies convincingly demonstrate that the XB-based cocrystallization strategy is a promising route toward tuning the emissive properties of organic crystalline materials.

Due to the heavy-atom effect, the large size of XB donor atoms renders XB-based solid-state materials particularly promising for the design of phosphorescent materials, as was first shown by the group of Jinsang Kim in 2011.[1004] Conventionally, materials exhibiting high-quantum-efficiency phosphorescence are based on organometallics;[1005,1006] purely organic, metal-free materials with efficient phosphorescence emission are rare.[1007,1008] XB, however, may change the picture, as was demonstrated using the materials shown in Figure 139A. The aromatic carbonyl group was used as a triplet generator. In solution, the compounds exhibited weak fluorescence, and the triplet emission was inactive. In the crystal form (Figure 139B), Br···O═C XB brings the aromatic carbonyls and the bromine atoms into close proximity, triggering the heavy-atom effect and giving rise to green phosphorescence with an emission

DOI: 10.1021/acs.chemrev.5b00484
Chem. Rev. 2016, 116, 2478−2601

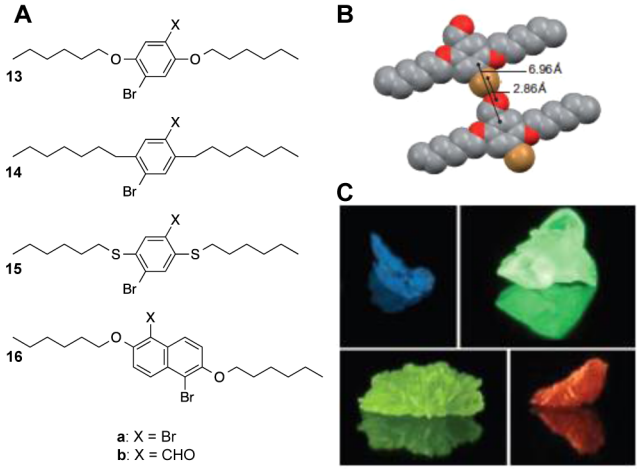

Figure 139. (A) Chemical structures of the hosts **a** and aldehydes **b** used in ref 1004. (B) Schematic depiction of the crystal packing of **13b**, highlighting the carbonyl oxygen−bromine XB. It is believed that this contact is responsible for the phosphorescence observed from crystals of **13b** (C). Reprinted with permission from ref 1004. Copyright 2011 Nature Publishing Group.

quantum yield of 2.9% (for the crystal of **13b**). By diluting the chromophore in a nonemissive but structurally similar host compound to prevent self-quenching (1 wt % **13b** in **13a**), an emission quantum yield as high as 55% was reported.[1004] Interestingly, when bromine was replaced with iodine, no phosphorescence was detected, which was attributed to inferior size matching between the iodine atom and the aldehyde group. By varying the electron density and conjugation length of the chromophore (Figure 139A), the emission color could be tuned from blue all the way to orange/red (Figure 139C). Compared to organometallics, the all-organic design may be beneficial in terms of material cost, tunability, and device stability, rendering the material concept of potential interest in display and lighting applications as well as in sensing. In a follow-up study,[1009] the authors showed that the quantum efficiency of phosphorescence is highly dependent on the composition of the mixed crystal, and that both too high and too low emitter concentrations severely diminish the emission efficiency. The optimum concentration range was found to be 1−10 wt %. The reduced quantum efficiency at the low-concentration regime was attributed to poor inclusion of the **13b** "impurities" in the crystal of **13a**. It was also shown that mismatch between the alkyl chain lengths between the emitter and the host reduced the phosphorescence quantum yield. This study further elucidated the findings of ref 1004, yet the quantum yield of 55% remained unbeatable.

The above studies revealed that bright, color-tunable room-temperature phosphorescence is achievable in organic crystals due to the XB-directed heavy-atom effect. However, in terms of practical applications, the crystal-engineering-based approach may not be the best, since the stringent requirement of high-quality crystals to activate the triplet emission complicates the sample preparation procedure. In this respect, amorphous film-forming materials would be more attractive, but they may suffer from pronounced vibrational dissipation and suppression of phosphorescence as compared to crystalline materials. Kim et al. also tackeled this issue, showing that efficient phosphorescence emission is indeed possible in glassy polymer matrixes.[1010] When embedded into atactic poly(methyl methacrylate) (PMMA), the organic phosphor **13b** exhibited green phosphorescence with a quantum yield of 0.7% at room temperature. Even if weak, the activation of phosphorescence was itself an indication of restricted vibrational decay due to the rigidity of the polymer matrix. Importantly, the phosphorescence quantum yield could be enhanced by an order of magnitude by using isotactic PMMA, due to reduced β-

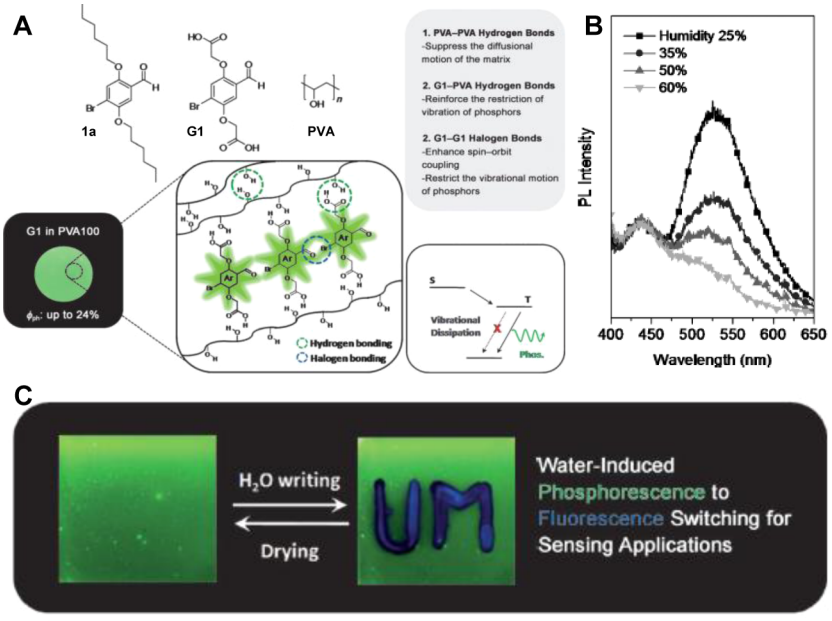

Figure 140. (A) Top: the new organic phosphor **G1** appears particularly promising in enhancing phosphorescence in an amorphous PVA matrix. Bottom: the green phosphorescence of **G1** embedded in PVA is explained by synergistic effects brought about by simultaneous use of halogen and hydrogen bonds. (B) The phosphorescence emission of 1 wt % **G1** in PVA depends linearly on the humidity, while the fluorescence emission is insensitive to the humidity, which allows (C) fluorescent watermarks to be reversibly written onto the amorphous polymer film. Reprinted with permission from ref 1011. Copyright 2014 Wiley-VCH.

DOI: 10.1021/acs.chemrev.5b00484
Chem. Rev. 2016, 116, 2478−2601

relaxations compared to those of atactic PMMA, which further suppressed the vibrational dissipation. The optimum emitter concentration was again around 1 wt %, suggesting that at very low concentrations the number density of the emitters is too low for the emission-enhancing chromophore−chromophore XB to occur. As a proof-of-principle application, the authors demonstrated the use of their amorphous phosphor as a temperature sensor in a microfluidic device.[1010] To further optimize the room-temperature emission in amorphous films, a design strategy combining halogen and hydrogen bonding was devised (Figure 140A).[1011] The role of the former was again to promote the intersystem crossing, while the latter served to supramolecularly cross-link the matrix polymer poly(vinyl alcohol) (PVA) and therefore further suppress the nonradiative decay processes from the triplet to the ground state. For this, a new organic phosphor (**G1**) (Figure 140A) was designed. In a material containing 1 wt % **G1** in PVA, a phosphorescence quantum yield of up to 24% was observed, which is a significant improvement compared to that of the previously reported **13b**−isotactic PMMA. The system is also strongly water-sensitive as the water molecules interfere with the HB between **G1** and the polymer matrix. As the bonds break, the phosphorescence emission is quenched, whereas the fluorescence emission remains intact (Figure 140B), which allows for humidity-triggered phosphorescence-to-fluorescence switching. This switching was used for reversible direct writing of fluorescent watermarks and moisture sensing (Figure 140C).

Parallel to the work of Kim et al., the XB-based design of organic phosphors has been intensively studied by the group of Prof. Wei Jun Jin, as has been recently reviewed in a book chapter.[1012] Their main target has been to harness halogen···π interactions, the type of XB that was quantified already in the 1940s and 1950s,[51,58,59] to engineer phosphorescent crystals. Two types of fluorophores were employed: (i) fluorene and its heterocyclic analogues[1013−1015] and (ii) polycyclic aromatic hydrocarbons,[649,1016−1018] typically cocrystallized with 1,4-diiodotetrafluorobenzene (DITFB). Cocrystals of DITFB and carbazole constitute a beautiful example of C−I···π XB-driven crystal engineering (Figure 141, left), where DITFB acts as both the cement to link the carbazole molecules via XB and also as a heavy-atom perturber to enhance the phosphorescence emission.[1013] The crystals assemble into a 2:1 DITFB/carbazole stoichiometry, forming infinite chains constructed by the C−I···π XBs and further stabilized by π−π stacking interactions between the DITFB molecules. The parallel chains are linked together by C−H···I HBs (Figure 141, left); hence, in these systems the iodine atom simultaneously acts as an XB donor and an HB acceptor. The resulting cocrystals exhibited strong phosphorescence in the solid state as well as in the form of microparticles suspended in water. The authors verified via powder X-ray diffraction experiments that the microparticles have the same structural characteristics as the cocrystals. The phosphorescence quantum yield of the microparticle suspension was determined to be 0.33.[1013] Also fluorene, dibenzofuran, and dibenzothiophene yielded C−I···π XB-driven phosphorescent cocrystals when complexed with DITFB,[1014] and especially the latter may turn out interesting in combining luminescence and electron transport in halogen-bonded crystals. In carbazole-containing crystals, the emission can be further tuned by *N*-methyl and *N*-ethyl substitutions.[1015] Compared to the unsubstituted carbazole,[1013] methyl substitution leads to red-shifted phosphorescence and a 1:1 stoichiometry between the donor and acceptor, while the emission from the ethyl-substituted carbazole is very weak and blue-shifted compared to its unsubstituted counterpart, and the donor-to-acceptor stoichiometry is 1:2. This highlights that substitution-induced changes in the crystal packing have a

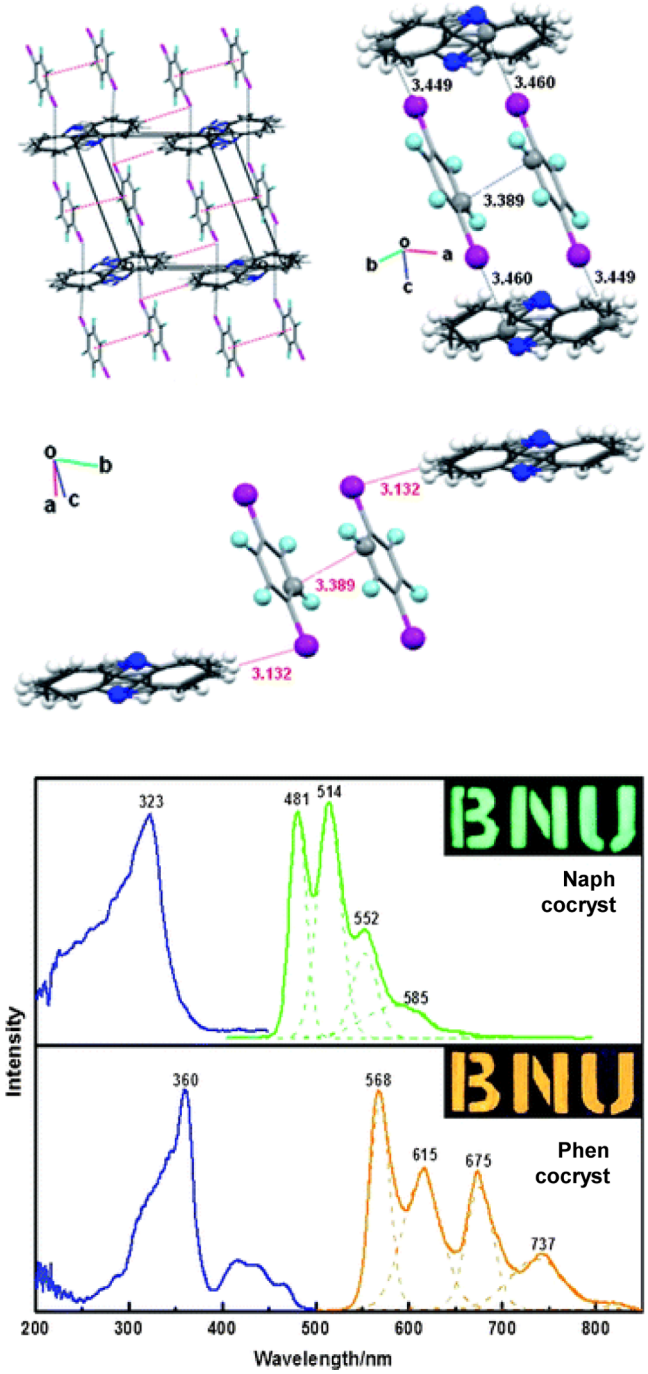

Figure 141. Top: infinite-chain structure of the carbazole/1,4-diiodotetrafluorobenzene cocrystals (left), driven by C−I···π XBs and further stabilized by π−π stacking (right). The adjacent chains are linked together by C−H···I HBs (bottom). Reprinted with permission from ref 1013. Copyright 2012 Royal Society of Chemistry. Bottom: phosphorescence excitation and emission from naphthalene/1,4-diiodotetrafluorobenzene (top) and phenanthrene/1,4-diiodotetrafluorobenzene (bottom) cocrystals. The insets display the phosphorescence color of the cocrystals under UV excitation through a mask. Reprinted with permission from ref 649. Copyright 2012 Royal Society of Chemistry.

DOI: 10.1021/acs.chemrev.5b00484
Chem. Rev. 2016, 116, 2478−2601

pronounced effect on the luminescence of materials (see also ref 1002). The luminescence and packing of cocrystals assembled between polycyclic aromatic hydrocarbons and diiodotetrafluorobenzenes depend delicately on the number of aromatic rings of the bond acceptor. In pyrene-containing cocrystals, the C−I···π XB did not take place,[1016] while it did occur in the smaller naphthalene- and phenanthrene-containing cocrystals, both exhibiting a 1:2 stoichiometry between the emitter and the diiodotetrafluorobenzene.[649] These two cocrystals emit strong green and orange phosphorescence (Figure 141, right), respectively, exhibiting monoexponential phosphorescence decays with lifetimes of 0.067 and 1.449 ms. In the phenanthrene cocrystal, phosphorescence was also obtained using 1,4-dibromotetrafluorobenzene as an XB donor,[1017] while this was unsuccessful in the case of carbazole-based organic phosphors.[1013]

Finally, Ventura et al. have studied the luminescence properties of several 1,8-napthalimide derivatives (Figure 142, top) in solution and in the crystal/cocrystal state,[1019] showing once again that XB makes a difference. This class of molecules is known for their rich optical properties, highly sensitive to the substituents particularly at the 4-position.[1020] In compounds **18**−**20**, the 4-substituted bromine plays the role of promoting intersystem crossing, whereas the methylpyridine substitution acts as an anchoring group able to form XBs with diiodotetrafluorobenzenes. The packing of the cocrystals was influenced by the position of the nitrogen atom in the pyridine ring due to steric hindrance, which in turn affected their emission properties. In another study, the authors showed that the luminescence properties of cocrystals of diiodotetrafluorobenzene and diphenylacetylene can be controlled with the stoichiometry of the crystal. Both 1:1 and 1:2 cocrystals were driven by halogen···π interactions, the former into a chevron-like arrangement and the latter into 2D C−I···π networks. Interestingly, the 1:1 stoichiometry leads to luminescence dominated by fluorescence, while the 1:2 cocrystal is a pure triplet emitter with a phosphorescence quantum yield of 6% at room temperature (Figure 142, bottom), pointing toward a new strategy for controlling the emissive properties of all-organic crystalline solids.[1021]

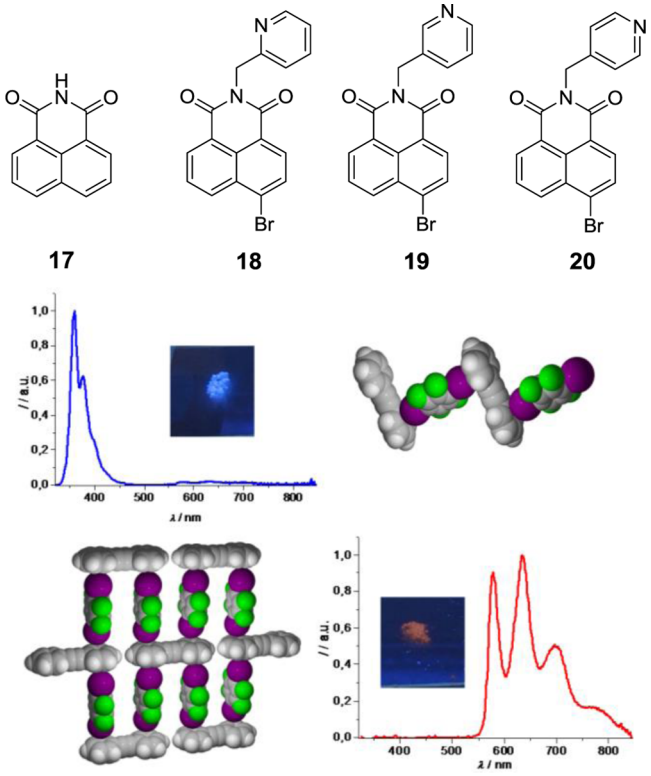

Figure 142. Top: chemical structures of the 1,8-napthalimide (**17**) derivatives with 4-bromine substitution and 2-, 3-, and 4-methylpyridine substitution at the imidic N-position (**18**, **19**, and **20**, respectively) used in ref 1019. Bottom: by controlling the stoichiometry of diphenylacetylene/1,4-diiodotetrafluorobenzene cocrystals from 1:1 (top) to 1:2 ratios (bottom), the photoluminescence can be "switched" between fluorescence and phosphorescence. Reprinted from ref 1021. Copyright 2015 American Chemical Society.

Overall, halogenated/halogen-bonded chromophores serve as a promising class of light-emitting solid-state materials diplaying unique properties brought about by XB (as convincingly illustrated by the examples of this section), in addition to being useful analytical tools. Some recent examples of the latter comprise the work of the Würthner group on the role of halogen−arene interactions in the self-assembly of squaraine dyes,[1022] the work of Beer et al. on porphyrin- and haloimidazolium-based receptors for anion recognition and sensing,[1023,1024] and the study of Xie et al. on the XB between molecular iodine and the photoinduced electron-transfer molecule ciprofloxacin under weakly alkaline conditions and its role in the charge-separation process.[1025]

6.2.2. Light-Responsive and Nonlinear Optical Materials. Since the first reports published in 2012,[489,859] XB has also appeared as a promising tool in the design of light-responsive, azobenzene-containing materials. Even if still in its infancy, this line of research is highly promising, comprising amorphous polymers,[855,859,860] liquid crystals,[489,851] and even crystals that deform under light irradiation.[1026,1027] The photoisomerization of azobenzene derivatives[1028] (Figure 143A) can give rise to a cascade of motions beyond the size scale of an individual molecule. In a polymeric or liquid-crystalline environment, the molecular alignment of the azobenzenes can be controlled with polarized light. This phenomenon is particularly useful in the context of liquid crystals, the alignment of which can be

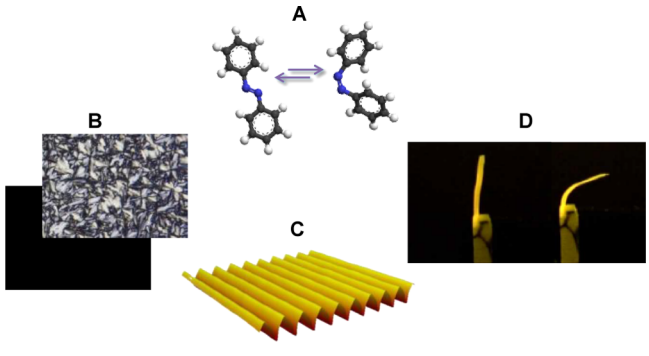

Figure 143. Photoisomerization of azobenzene (A) can give rise to a cascade of molecular motions into a material system it is incorporated into. The most relevant examples in the context of halogen-bonded functional materials are (B) photoinduced phase transitions in liquid-crystalline materials, (C) photoinduced surface patterning of initially flat polymer surfaces, and (D) photoinduced bending of azobenzene-containing cross-linked liquid-crystalline polymers or molecular (co)crystals. Reprinted with permission from ref 1040. Copyright 2005 Optical Society of America.

DOI: 10.1021/acs.chemrev.5b00484
Chem. Rev. 2016, 116, 2478−2601

controlled and modulated by thin layers of azobenzene "command surfaces", or by doping a small amount of azobenzene molecules into the liquid crystal.[1029,1030] In the latter case, the photoisomerization process can even give rise to isothermal phase transitions and turn an aligned liquid-crystal system into isotropic and vice versa (Figure 143B).[1031] Two other relevant processes triggered by azobenzene photoisomerization are photoinduced surface patterning and photoinduced bending. The former was first observed in 1995[1032,1033] when it was reported that, by irradiating an amorphous azopolymer film with a light interference pattern, the polymer starts to macroscopically move and forms a replica of the incident irradiation pattern onto the polymer surface in the form of a surface relief grating (SRG; Figure 143C). The SRGs are easily fabricated and intriguing both from the fundamental scientific perspective and in terms of their potential applications in photonics and nanostructuring.[1034,1035] The photoinduced bending (Figure 143D) takes place predominantly in cross-linked liquid-crystalline polymers and elastomers,[1036] and more recently also in azobenzene crystals,[1037,1038] triggered by alignment order changes in the solid state. XB-based supramolecular materials have something to offer on all these fronts as will be illustrated through the examples given in this subsection. The discussion follows a recent book chapter written by us,[1039] which we refer to for a more comprehensive treatment.

The first report on halogen-bonded azobenzene-containing materials was based on a polymeric XB acceptor (P4VP) complexed with azobenzenes **22**–**24** (Figure 144A).[859] The

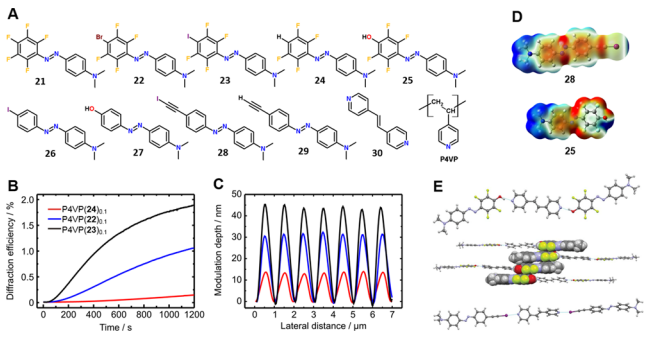

Figure 144. (A) Chemical structures of the azobenzene compounds studied in refs 859 and 855. Comparison of (B) the diffraction kinetics and (C) the AFM surface profile of thin films of complexes between **22**–**24** and P4VP (10 mol % azobenzenes in a P4VP matrix). The samples were spin-coated on silicon substrates, and their thickness was ca. 90 nm. Reprinted with permission from ref 859. Copyright 2012 Wily-VCH. (D) Electrostatic potential surfaces of compounds **28** (top) and **25** (bottom), ranging from −0.03 (red) to 0.03 (blue) au. (E) Ball-and-stick representation of the crystal packing of **30**·(**25**)$_2$ (top) and **30**·(**28**)$_2$ (bottom). Middle: view along the crystallographic *b*-axis of the cocrystal **30**·(**25**)$_2$, illustrating the tendency of **25** to interact via quadrupolar stacking. Reprinted with permission from ref 855. Copyright 2015 Royal Society of Chemistry.

choice of materials was based on previous work on phenol–pyridine hydrogen-bonded polymer–azobenzene complexes that had already proven their potential as efficient SRG-forming materials.[1041,1042] The rationale for replacing the relatively strong HBs with weaker XBs is that the electronic and photochemical properties (absorption spectrum, dipole moment, isomerization kinetics) of the molecules are mainly determined by the dimethylamino donor and the electron-withdrawing tetrafluorobenzene ring (Figure 144A), allowing the role of chromophore–polymer interaction to be decoupled from other effects that potentially influence the SRG formation. Therefore, this series allowed the study of the role of (i) the XB interaction strength (**22** vs **23**; 3.5 and 5.1 kcal/mol, respectively, based on DFT calculations) as well as the nature of the interaction (**22** vs **24**; XB vs HB, both of similar strength) in the surface patterning process. The surface deformation of spin-coated thin films of the polymer–azobenzene complexes was followed in situ by light-diffraction measurements (Figure 144B) and ex situ via atomic force microscopy (AFM) (Figure 144C). A strong dependence on the bond donor unit was observed as both the diffraction efficiency and the surface-modulation depth developed in the order **23** > **22** > **24**, i.e., I > Br > H. This result has two important implications. First, in the halogen-bonded complexes the surface patterning efficiency follows the strength of noncovalent bonding. Second, XB, presumably because of its higher directionality, seems to outperform hydrogen-bonded systems with a similar polymer–dye interaction strength in terms of SRG formation efficiency. Later on, a follow-up study was conducted, reporting on an extensive series of the nine polymer–azobenzene complexes shown in Figure 144A, to build up a "supramolecular hierarchy" among halogen and hydrogen bond donors in the surface patterning process.[855] This paper served to strengthen the conclusions made in ref 859. By comparing the complexes comprising **23** and **25** interacting through XB and structurally similar strong (11.8 kcal/mol) HB, respectively, it was shown that the final diffraction efficiencies of the **23**- and **25**-based complexes were approximately equal, but the buildup of the grating was much faster for the halogen-bonded complex. This is unambiguous proof of the high potential and special role of XB in mediating light-induced movements into photoresponsive polymer systems. Second, the paper introduced an iodoacetylene-functionalized azobenzene (**28**)that came out on top of the hierarchy. The use of a nonfluorinated dye to produce an XB-based complex with an efficient optical response may bring the advantage of reducing chromophore aggregation and phase separation (i.e., allowing higher chromophore concentrations to be used in the polymer matrix) as compared to the use fluorinated azobenzenes, which may be beneficial in applications that require high optical anisotropy or a nonlinear optical response. Due to the very different electrostatic potential surfaces of **25** and **28** (Figure 144D; the positive area is spread out in **24**, while it is narrowly focused on the extension of the C–I bond in **28** and **23**), model cocrystals also constructed with **30** exhibited very different packing features, the latter being highly linear and the former adapting a zigzag arrangement with an extremely short O···N distance. The higher directionality of XB gives rise to a more rigid polymer–azobenzene junction, which in turn enhances the light-induced mass transport.[855]

As already brought up previously, XB offers interesting prospects in designing new types of supramolecular liquid crystals from non-liquid-crystalline building blocks, which in turn opens up a new route toward light-functional liquid crystals. This was first shown using the complex presented in Figure 145A,[489] which exhibited a monotropic nematic LC phase upon cooling from the isotropic phase. Note that neither of the constituents contains any flexible chains that are conventionally used in designing small-molecule liquid-crystalline complexes, which in combination with the presence

DOI: 10.1021/acs.chemrev.5b00484
Chem. Rev. 2016, 116, 2478–2601

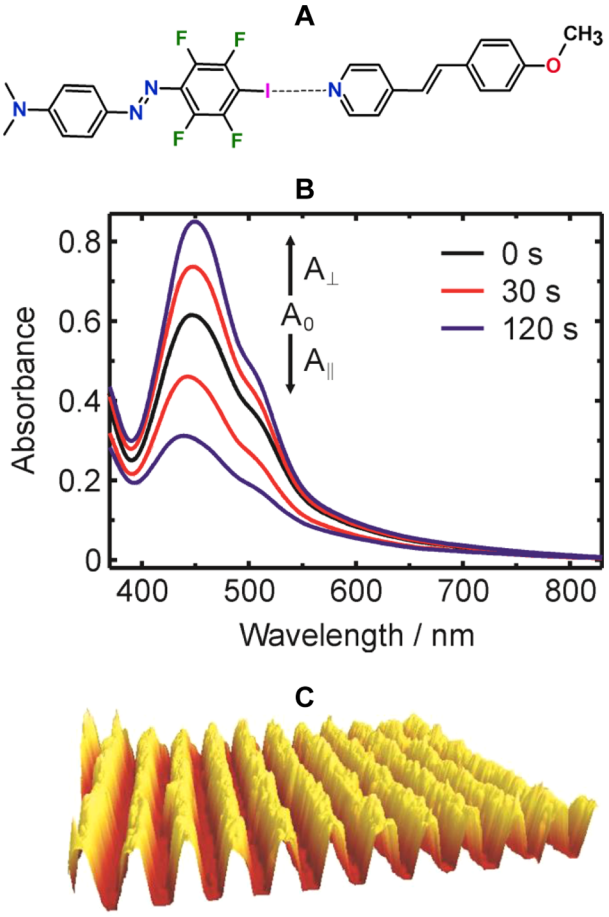

Figure 145. (A) Chemical structure of the halogen-bonded liquid-crystalline complex employed in ref 489. (B) Polarized absorption spectra of a thin film (250 nm) of the complex shown in (A). Black curve: initial spectrum (same for both polarizations). The red and blue curves correspond to the polarized absorption spectra in the directions parallel ($A_{\parallel} < A_0$) and perpendicular ($A_{\perp} > A_0$) to the polarization plane, taken after 30 and 120 s of irradiation (488 nm, 100 mW/cm^2), respectively. The absorption anisotropy is an unambiguous sign of photoinduced reorientation of the azobenzene chromophores. (C) Atomic force microscopy view of the spin-coated thin film of the complex shown in (A) after SRG inscription (5 min, 488 nm, 300 mW/cm^2). The surface-modulation depth after the SRG inscription was 600 nm, 2.4 times the initial film thickness. Reprinted with permission from ref 489. Copyright 2012 Wiley-VCH.

of the dimethylamino group should promote the surface patterning efficiency.[1043,1044] The high-temperature LC phase, in turn, should promote photoalignment.[1045,1046] The photoresponsive properties of the complex were indeed unique. Because of the presence of the azobenzene moiety, initially isotropic, polycrystalline spin-coated thin films of the complex could be uniaxially aligned by irradiation with polarized light, achieving a high order parameter of molecular alignment of 0.55 (Figure 145B). Interestingly, the films underwent irreversible crystalline-to-amorphous transformation upon irradiation with visible light (488 nm, 100 mW/cm^2, 30 s). Furthermore, as illustrated in Figure 145C, within an inscription time of only a few minutes, a grating with modulation depth of 600 nm could be inscribed on a film with a starting thickness of only 250 nm. This result stands out as among the most efficient SRG-forming materials reported.[489]

The second example of halogen-bonded photoresponsive LCs, published in 2014, demonstrated a photoinduced LC-to-isotropic phase transition in complexes between azopyridines and molecular iodine (see Figure 107C for the chemical structures). The phase transition was detected by irradiating the I_2 complex (n = 12) with UV light under a polarized optical microscope, at a temperature at which it exhibited a liquid-crystalline (smectic A) phase. As shown in Figure 146, the

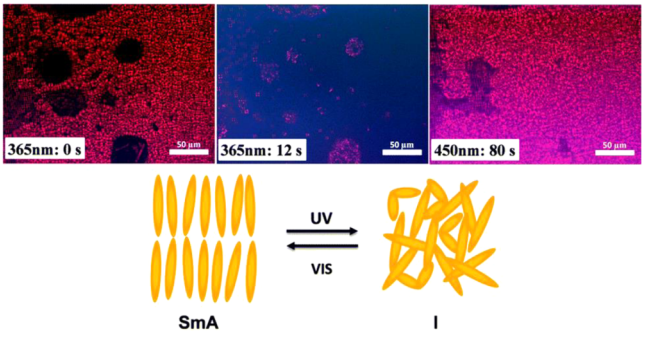

Figure 146. Polarized optical micrographs of an azopyridine–I_2 complex (see Figure 107C) at its liquid-crystalline phase before (left) and after (right) UV irradiation. The decreased contrast indicates photoinduced phase transition due to *trans–cis* photoisomerization. Upon irradiation with visible light, the colored pattern can be retained due to reverse *cis–trans* isomerization. Reprinted with permission from ref 851. Copyright 2014 Royal Society of Chemistry.

liquid crystallinity quickly disappeared upon irradiation, as evidenced by reduced contrast in the polarized optical microscopy (POM) image that turned from colored to dark. The color was recovered after the isotropic sample was irradiated with visible light. This is a clear sign that the phase transition is initiated by reversible *trans–cis* photoisomerization. Interestingly, the corresponding bromine-containing complexes that provided more stable mesophases[851] were not photoresponsive. Even if further studies are needed to fully understand the photoresponse of these complexes, this result points toward the use of XB in building, e.g., supramolecular photoactuators[1047] and functional halogen-bonded liquid crystals and networks.[1048]

Despite the fact that the photoisomerization may be hindered in constrained environments, the photomechanical effects have in recent years also been studied in the crystalline state.[1037,1038,1049] XB and fluorination have several things to offer in this context. Bléger et al. have shown that *ortho*-fluorination of azobenzenes significantly increases the thermal half-life of the *cis*-isomers, up to months or even years.[1050,1051] Barrett, Friščić, and co-workers[1026] used the long half-lives to grow single crystals of the *cis*-forms of symmetrically substituted 4,4′-haloperfluoroazobenzenes (Figure 147, top) that were subjected to X-ray crystallographic and photomechanical characterization. Compared to *trans*-crystals, the *cis*-crystals are of lower density, allowing for the *cis–trans* isomerization to occur in single crystals, whereas the reverse isomerization was inactive (Figure 147, bottom right). Upon irradiating the *cis*-single crystal with 457 nm laser light, the crystal bent away from the direction of the incoming light (Figure 147, bottom left). The deformation was irreversible, and was accompanied by a crystal-to-crystal transition from a *cis*-single crystal to a polycrystalline aggregate of *trans*-crystals,

DOI: 10.1021/acs.chemrev.5b00484
Chem. Rev. 2016, 116, 2478–2601

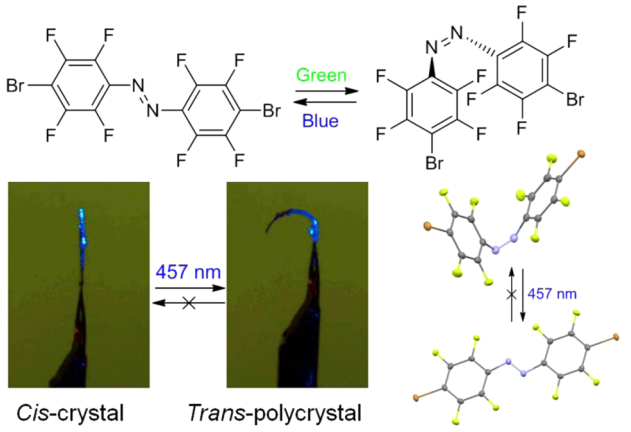

Figure 147. Top: *trans*- and *cis*-forms of 4,4′-dibromoperfluoroazobenzene. Bottom right: in the crystal state, the photoisomerization proceeds only from the *cis*- to the *trans*-state, not vice versa. Upon *cis*-to-*trans* isomerization, thin crystals bend irreversibly away from the irradiation source. Reprinted from ref 1026. Copyright 2013 American Chemical Society.

being the first demonstration of permanent photomechanical modification of crystal shape in azobenzene crystals.[1026]

The difunctional 4,4′-haloperfluoroazobenzenes have also been used as building blocks for halogen-bonded cocrystals,[1052,1053] which may bring additional flexibility to the material design of the photomechanical crystals. Indeed, Barrett and Friščić et al. recently demonstrated the ability of such cocrystals to undergo photoinduced deformation,[1027] employing the materials shown in Figure 148A. As Figure 148B exemplifies, the geometry of the tectons is beautifully translated into the geometry of the cocrystal, thanks to the directionality of the XB: The *all-trans*-cocrystal (*trans*-**31**)·(*trans*-**bpe**) forms infinite linear halogen-bonded chains, whereas the *all-cis*-cocrystal (*cis*-**32**)·(*cis*-**bpe**) takes a V-shaped zigzag geometry. Due to the lower packing density, only the crystals containing the *cis*-form of **31** or **32** underwent (irreversible) photomechanical deformation. Surprisingly, the crystals remained of high enough quality even after photoirradiation, which for the first time enabled in situ monitoring of the photoisomerization process via X-ray diffraction analysis. Such studies revealed that the crystal-to-crystal isomerization proceeded via an amorphization phase followed by recrystallization, as illustrated in Figure 148C.[1027]

The field of nonlinear optics[1054] (NLO) may also benefit from XB, especially when dealing with second-order NLO phenomena occurring only in noncentrosymmetric media. Typical chromophores for second-order NLO comprise a π-conjugated system that is asymmetrically end-capped with electron-donating and -accepting moieties. Due to the electronegative fluorine atoms, a tetrafluoroiodobenzene unit may simultaneously act as an XB donor and an intramolecular electron acceptor, therefore being an ideal building block for supramolecular NLO materials. However, before building up solid-state NLO materials or devices, it is imperative to characterize and understand the NLO response at the molecular level. This can be achieved either using electric-field-induced second-harmonic generation (EFISH) or hyper-Rayleigh scattering (HRS). The first, and thus far the only, study on XB-based tuning of molecular-level NLO response was performed by Cariati et al., who compared the molecular hyperpolarizabilities of **33** and **34** (Figure 149A) in chloroform and in dimethylformamide (DMF) using EFISH.[1055] The

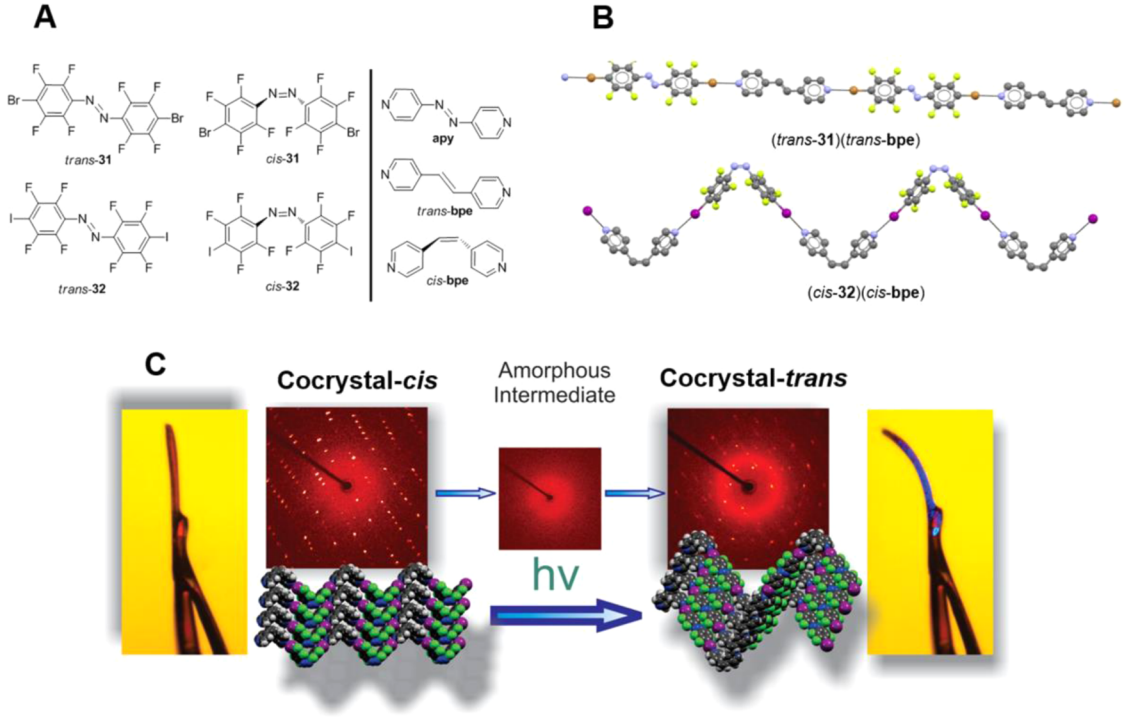

Figure 148. (A) Compounds used in ref 1027. (B) Linear structure of supramolecular chains of (*trans*-**31**)·(*trans*-**bpe**) and the zigzag structure of (*cis*-**32**)·(*cis*-**bpe**) as determined by single-crystal X-ray diffraction analysis. (C) Photoinduced bending of halogen-bonded cocrystals, followed by in situ X-ray diffraction, reveals that the transition from the unbent *cis*-single crystal to the bent polycrystalline *trans*-state proceeds through an amorphous intermediate phase. Reprinted with permission from ref 1027. Copyright 2014 Royal Society of Chemistry.

DOI: 10.1021/acs.chemrev.5b00484
Chem. Rev. 2016, 116, 2478−2601

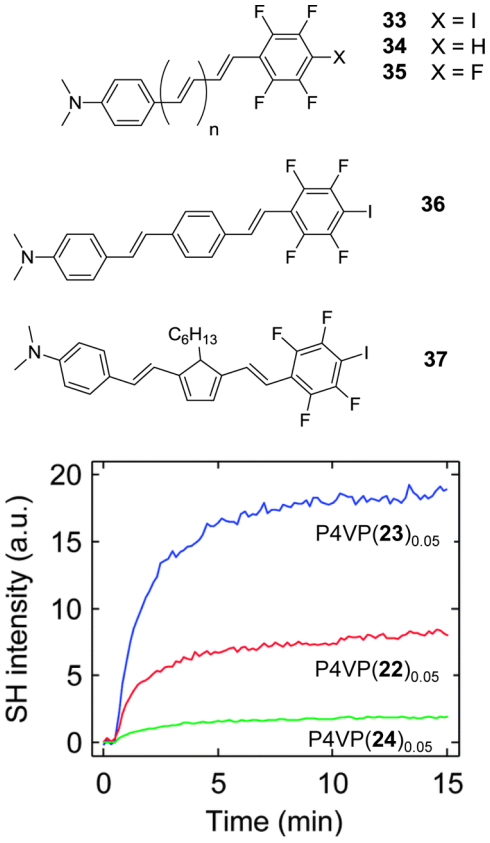

Figure 149. (A, top) A selection of NLO-phores containing XB donor groups. (B, bottom) Upon optical poling of azobenzene chromophores **22**, **23**, and **24** of Figure 144A in a P4VP matrix (the molar ratio between the azobenzenes and the polymer repeat units is 1:20), XB clearly boosts the second-order nonlinear optical response of the material system. Reprinted with permission from ref 860. Copyright 2015 Royal Society of Chemistry.

former is essentially uncapable of participating in noncovalent interactions, while DMF is a rather strong XB acceptor. In chloroform the EFISH signal, which actually consists of the product of molecular dipole moment μ and the hyperpolarizability component along the dipolar axis β, was positive in sign and of similar magnitude for both compounds, matching the value reported for the pentafluorinated derivative **35**.[1056] This shows that the *para*-substituent of the fluorinated ring, while extremely pertinent for the ability of the molecule to form noncovalent interactions, does not play a major role in the molecular-level NLO properties. The situation becomes markedly different in DMF. For the non-halogen-bonded reference compound **34**, $\mu\beta$ decreased somewhat but remained positive, while for **33** $\mu\beta$ was reversed in sign and increased by a factor of almost 2.5. The authors attributed the sign inversion to a change in direction of μ due to the presence of two competing electron donor sites, the $-NMe_2$ and the solvent molecule halogen-bonded to the tetrafluoroiodobenzene moiety. This work shows that XB can be harnessed to tune the optical nonlinearities of organic compounds at the molecular level.

For building actual NLO devices, the goal with second-order NLO materials always lies in the solid state. In other words, it is not sufficient to have noncentrosymmetric molecular constituents, but these constituents must adopt an overall noncentrosymmetric arrangement. This requirement is met in noncentrosymmetric crystals, and an attempt toward this direction was taken by Cariati and co-workers using the self-complementary molecules **36** and **37** (Figure 149A).[723] The molecules showed high molecular-level nonlinearities, and crystallized into head-to-tail halogen-bonded polar chains. Unfortunately, the chains stacked into a centrosymmetric arrangement, giving rise to no bulk second-harmonic signal. On the basis of the knowledge gained on hydrogen-bonded supramolecular structures,[1057,1058] the most promising methods to order, e.g., **36** and **37**, into a noncentrosymmetric alignment are based on vapor-phase deposition. Due to the self-complementarity of these molecules, this approach may lead to spontaneous noncentrosymmetric self-organization of the bulk structure without applying external fields. This route to construct halogen-bonded solid-state NLO materials, however, remains yet to be demonstrated.

Also azobenzene molecules are highly promising as NLO chromophores,[1059] and they possess the additional benefit of allowing the NLO response at both the molecular[1060] and macroscopic[1061] levels to be switched through photoisomerization. The photoisomerization process also allows an initially isotropic azobenzene-containing material system to be optically poled,[1062] and in fact, the only example that XB makes a difference in solid-state second-order NLO properties employs this method.[860] The materials used in this work are shown in Figure 144A (compounds **22**, **23**, and **24**), incorporated into a P4VP matrix in a 1:20 (azobenzene/polymer repeat unit) molar fraction. The results demonstrated that stronger chromophore−polymer XB resulted in an increased second-harmonic signal when the bond strength was the only variable (**22** vs **23**), and compared to hydrogen-bonded systems, XB seemed to prevail (**22**/**23** vs **24**). When the polymer matrix was replaced with polystyrene, which lacks the electron-donating nitrogen atom, the NLO response developed in the same order (**23** > **22** > **24**), but the overall magnitude of the response was significantly lower than in P4VP. This was attributed to weak, yet non-negligible, halogen···π interactons between the building blocks. These observations are interesting, but further studies at both the molecular (hyper-Rayleigh scattering) and macroscopic (electric-field poling) levels are needed to profoundly understand them, and to unambiguously judge the applicability of XB in the design of solid-state polymeric NLO materials. Further studies along these lines are presently in progress.

6.3. Conductive and Magnetic Materials

XB-based crystal engineering has resulted in several examples of conducting and magnetic materials, based on controlled organization of radical species in the crystalline state. As brought up by Fourmigué,[1063] XB can play a dual role in crystals comprising radical species. On one hand, it provides structural control over their solid-state organization, bringing predictability in the crystal design and control in the conductivity and magnetic-interaction pathways. On the other hand, XB may play an electronic role and contribute to the band dispersion of organic stacks, which may further affect the conductive and magnetic properties of the crystals. Several aspects to be covered here have been reviewed by Fourmigué,[576,602,1063] while Mercuri et al. have recently highlighted the advancements in tailoring magnetic properties of molecular materials through noncovalent interactions.[1064] We direct an interested reader toward these works for further details.

The design of halogen-bonded conductive materials is largely based upon the use of halogenated tetrathiafulvalene (TTF)

DOI: 10.1021/acs.chemrev.5b00484
Chem. Rev. 2016, 116, 2478−2601

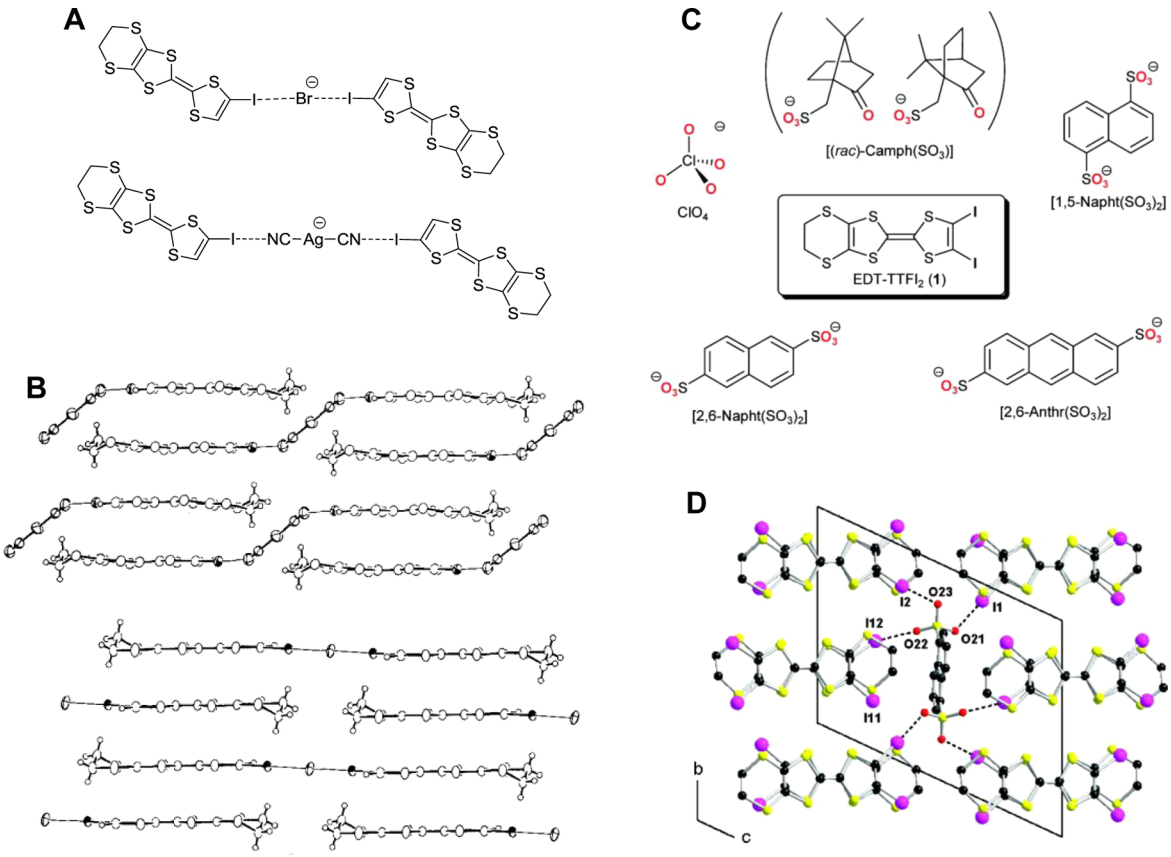

Figure 150. (A) Halogen-bonded radical cation salts formed between partially oxidized halogenated TTF molecules and halide (top) or cyanometalate (bottom) anions were the first examples of halogen-bond-based molecular conductors.[600] (B) Crystal structures of the $Ag(CN)_2$ (top) and Br^- (bottom) salts. Reprinted with permission from ref 600. Copyright Elsevier 1995. (C) Chemical structures of the TTF cation and various anions used in ref 1074. (D) Projection view, along the stacking axis, of the unit cell of the salt $(\mathbf{38})_4[1,5\text{-Napht}(SO_3)_2]$, showing the XBs as dotted lines. Reprinted from ref 1074. Copyright 2011 American Chemical Society.

derivatives as XB donors. TTF has been at the very heart of organic electronics research as a π electron donor[1065] since the discovery of the formation of highly conducting charge-transfer complexes with the electron acceptor tetracyano-*p*-quinodimethane (TCNQ).[1066] It can be reversibly oxidized into cationic TTF^+ and TTF^{2+} states,[1067] and it is the mixed valence state that is required for obtaining high conductivities.[602] Partial oxidation may also enhance the ability of the TTF derivatives to act as both HB and XB donors.[576,1065] Imakubo and Kato were the first to report on halogen-bonded radical cocrystals, obtained by electrocrystallization of iodinated TTF derivatives in the presence of bromide and cyanometalate counterions acting as XB acceptors (Figure 150A).[600] The crystal packing of the resultant structures was driven by I···Br^- and I···N XBs, respectively, yet being rather different for the two as dictated by the shape of the anion (Figure 150B). This pioneering study has prompted several follow-up studies using different couterions as bond acceptors, to yield a family of highly conducting, halogen-bonded salts.[574,665,670,672,1068−1073] The strength of XB in TTF-based salts is evident from the contraction of van der Waals radii[215] upon complexation. For example, Fourmigué et al. investigated a series of cation radical salts of the donor molecule 3,4-diiodo-3′,3′-(ethylenedithio)-tetrathiafulvalene (EDT-$TTFI_2$, **38**) with ClO_4^- and various organic sulfonates (Figure 150C), identifying I···O distances as short as 77% of the sums of the van der Waals radii of iodine and oxygen.[1074,1075] In their studies, organic sulfonates appeared as powerful XB acceptors, giving rise to high conductivities of up to 8 S/cm^{-1} in crystals of $(\mathbf{38})_4\cdot[1,5\text{-Napht}(SO_3)_2]$ ($1,5\text{-Napht}(SO_3)_2$ = 1,5-naphthalenebis-(sulfonate), Figure 150D).

Chiral iodinated TTF salts have also been actively studied, with the aim of devising multifunctional materials in which the chirality may modulate structural features, gives rise to magnetochiral anisotropy, and ultimately leads to supramolecular systems combining conductivity and magnetism.[1076,1077] In the case of halogen-bonded TTF salts, chirality can be induced either by using chiral counteranions such as enantiopure camphorsulfonate[1078] or by using TTF derivatives that are both halogenated and chiral.[1079] These studies indicate that using chiral counterions favors the presence of multiple crystallographically independent molecules with different degrees of charge transfer, whereas in the only example employing a chiral halogenated TTF derivative,[1079] the conductivity was limited by steric constraints imposed by the bulky chiral substituents.

Another approach to utilize XB in the context of conductive materials, also demonstrated by Kato and co-workers, uses halogen-bonded supramolecular networks between anions and iodinated "innocent" molecules for the creation of multicomponent molecular conductors.[575,1080,1081] A particularly elegant example is given in ref 1080 in which a halogen-bonded supramolecular network is used as an insulating network sheathing conducting TTF-based 1D nanowires. An example of

DOI: 10.1021/acs.chemrev.5b00484
Chem. Rev. 2016, 116, 2478−2601

a structure consisting of TSF stacks isolated by a network of HFTIEB and Cl^- (see Figure 151A for the chemical structures)

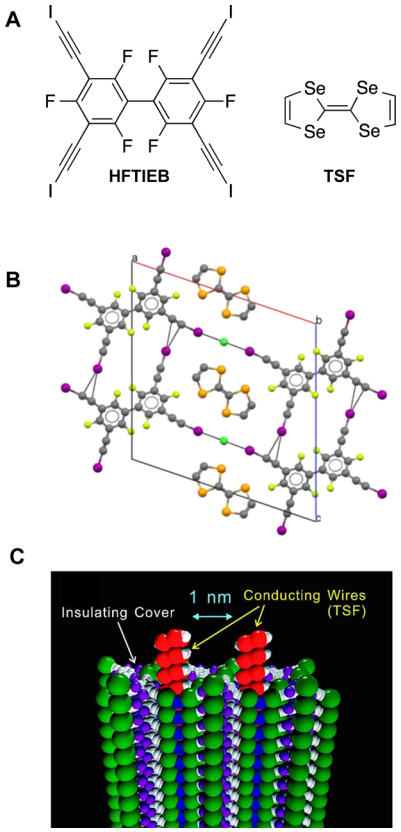

Figure 151. (A) Chemical structures of a cation radical (TSF) and the XB donor (HFTIEB) used to construct sheathed molecular nanowires. (B) and (C) display the crystal structure and the CPK model of TSF stacks isolated by a network of HFTIEB and Cl^- ions. Reprinted from ref 1080. Copyright 2008 American Chemical Society.

is given in Figure 151B,C. Astonishingly, an insulating layer with a thickness of only 1 nm produces an anisotropy in resistivity of 8 orders of magnidude along and perpendicular to the wire axis. This is the highest anisotropy value reported for a single chemical substance at room temperature.

In the search for halogen-bonded magnetic materials, neutral nitroxide free radicals have appeared as promising ever since the first demonstration of a neutral nitroxide ferromagnet.[1082] In the solution state, Lucarini et al. have performed electron paramagnetic resonance (EPR) spectroscopy of the radical XB acceptor (2,2,6,6-tetramethylpiperidin-1-yl)oxyl (TEMPO) in perfluorocarbon solution. They showed that, upon addition of iodoperfluorocarbon, nitrogen hyperfine splitting of the nitroxide group increased significantly, which the authors attributed to redistribution of the spin density when nitroxide free radicals are involved in XB formation.[668] Cavallotti et al. combined ^{19}F NMR measurements and theoretical calculations to study the TEMPO−iodoperfluorocarbon complexes, and their observations also indicated spin transfer between the TEMPO and the iodoperfluorocarbon molecules.[669] Cimino et al. have in turn carried out theoretical studies on the magnetic properties of TEMPO-based supramolecular complexes.[1083]

In the solid state, Schöllhorn and co-workers cocrystallized TEMPO radicals with diiodotetrafluorobenzenes, providing the first examples of halogen-bonded nitroxide complexes in the solid state.[610] The self-assembly of (2-phenyl)-4,4,5,5-tetramethylimidazolin-1-oxyl-3-oxide and 1,4-diiodotetrafluorobenzene (PTIO and DITFB, respectively, in Figure 152A) yielded

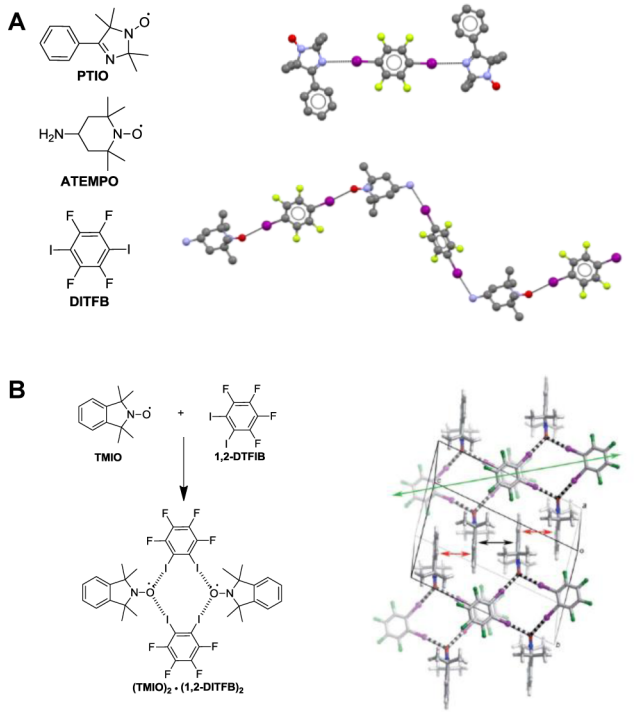

Figure 152. (A) Self-assembly of DITFB with (2-phenyl)-4,4,5,5-tetramethylimidazolin-1-oxyl-3-oxide (PTIO) gives rise to trimeric complexes (top right), while complexes between DITFB and ATEMPO assemble into linear chains (bottom right). Reprinted with permission from ref 610. Copyright 2006 Elsevier. (B) The assembly between TMIO and 1,2-DITFB results in a cyclic tetrameric complex. Reprinted with permission from ref 1084. Copyright 2011 Royal Society of Chemistry.

trimers interacting through I···N XB, whereas the difunctional molecule (4-amino-2,2,6,6-tetramethylpiperidin-1-yl)oxy (ATEMPO) (Figure 152A) afforded 1D chains driven by both I···O and I···N interactions. Halogen-bonded trimers and tetramers bearing mononitroxyl radicals as simple or bifurcated XB acceptors have been reported by Micallef and co-workers (see Figure 152B as an example).[1084,1085]

Minguez Espallargas et al.,[1086] in turn, have applied XB to organize nitronyl nitroxide radicals[603] as one-dimensional magnetic chains. By changing the XB donor, they controlled both the separation of the radical chains, aiming at enhanced magnetic isolation between the chains by increasing the length of the XB donors, and the intrachain packing of the radicals. Indeed, crystals employing 4,4′-diiodooctafluorobiphenyl donors exhibited much stronger antiferromagnetic interactions than crystals employing the shorter 1,4-diiodotetrafluorobenzene units (Figure 153A). In this work, XB played a structural role: The lack of magnetic exchange through XBs was confirmed via EPR spectroscopy.[1086] As a final example, the group of Wei Jun Jin recently reported on XB-induced modulation of the magnetic properties of [4-(benzoyloxy)-2,2,6,6-tetramethylpiperidin-1-yl]oxy (BTEMPO) free radicals by cocrystallization with 1,4- and 1,2-diiodotetrafluorobenzene (DITFB).[1087] Cocrystals with 1,4-DITFB tend to form infinite 1D chains (Figure 153B, top right), whereas 1,2-DITFB favors

DOI: 10.1021/acs.chemrev.5b00484
Chem. Rev. 2016, 116, 2478−2601

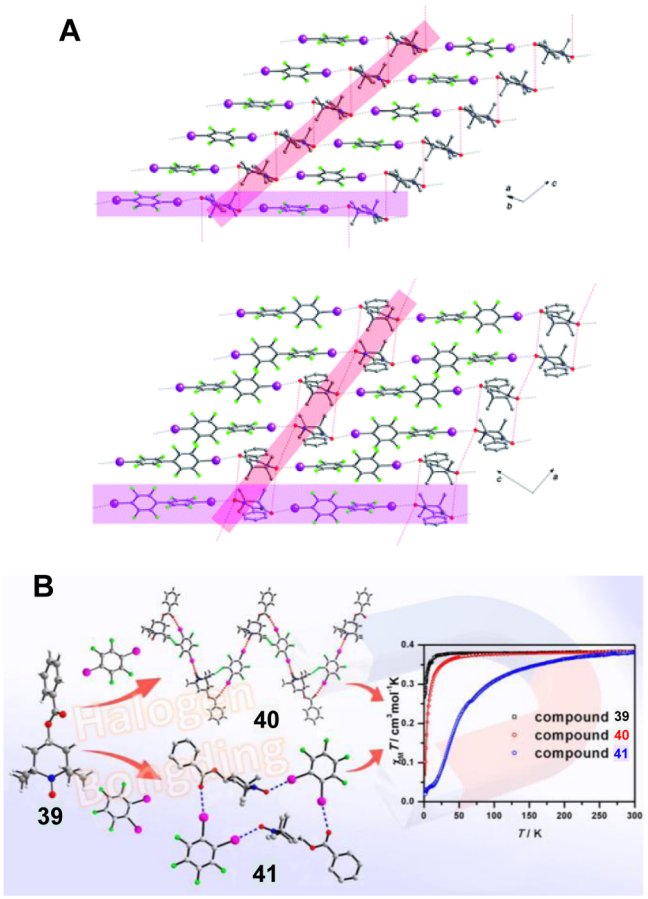

Figure 153. (A) One-dimensional halogen-bonded supramolecular chains in complexes between (3-phenyl-2,2,5,5-tetramethylimidazolin-1-yl)oxy and 1,4-diiodotetrafluorobenzene (top) and 4,4′-diiodooctafluorobiphenyl (bottom). In both cases the radicals form magnetic chains isolated by the XB donors, and within the chains, the radicals pack into dimeric units. Reprinted with permission from ref 1086. Copyright Royal Society of Chemistry 2012. (B) Halogen-bonded cocrystals **40** and **41** containing the BTEMPO radical **39** exhibit enhanced antiferromagnetic coupling as compared to the pure single crystal of **39**. Reprinted from ref 1087. Copyright 2013 American Chemical Society.

the formation of cyclic tetramers (Figure 153B, bottom right). All crystals were antiferromagnetic, but compared to single crystals of pure BTEMPO, both halogen-bonded cocrystals exhibited higher antiferromagnetic coupling, the strongest being the tetrameric complex of 1,2-DITFB. According to the authors, in these cocrystals the role of XB is not limited to structural control, but it also allows transmission of spin polarization from the donor to the acceptor connected by the XB.[1087]

Nitroxide free radicals are not the only building blocks used to construct halogen-bonded molecular magnets. Brammer and co-workers have extensively studied the ability of halometalates to act as XB acceptors,[455,554,1088] and they have also prepared halogen-bonded ferromagnetic chains based on Co(II) coordination polymers, with the aim of investigating the role of XB on interchain magnetic interactions.[1089] Molecular spin-crossover complexes[1090] involving XB have also recently been reported.[1091,1092] Finally, Mercuri et al. have performed a comprehensive characterization of a family of chiral, halogen-bonded tris(haloanilato)metalate(III)-based complexes, also pinpointing the dual role of XB, directing the molecular packing, varying the electron density of the anilato ring, and affecting the magnetic behavior of the complexes.[1093]

6.4. Miscellanea

In this review we have aimed at bringing out the many faces of XB by comprehensively treating the different fields of research where it is playing a role, yet some important developments in organic electronics,[488,820,1094] nanoparticle assemblies,[1095−1098] polymer−carbon nanotube composites,[1099,1100] and on-surface crystallization[1101,1102] do not fall into the categories defined earlier and warrant a separate discussion.

In section 4 (Soft Materials), we already mentioned that fluorinated ionic liquids and liquid crystals provide a promising route to improve the performance of fully organic electronic devices. It has been shown that, compared to a conventional ionic liquid electrolyte (1-butyl-3-methylimidazolium iodide) used in dye-sensitized solar cells, the use of a fluorinated ionic liquid may improve the efficiency of the device by improving charge transport within the electrolyte material, and the charge-transfer dynamics at the organic−inorganic sensitizer/electrolyte−TiO_2 interface.[820] This behavior was tentatively attributed to the low affinity of perfluorocarbons for organic and aqueous phases, which may drive the long alkyl chains of the sensitizer (Z907 was used) into densely packed layers to minimize interactions with the fluorinated electrolyte, and also lead to higher I_3^- diffusion coefficient in the bulk of the electrolyte. Depending on the length of the alkyl substituents, the imidazolium iodide-based ionic liquids may even exhibit liquid-crystalline properties, showing smectic A phases over wide temperature ranges[819] and promoting anisotropic charge transport in I^-/I_3^- redox couple electrolytes.[1103] Abate et al.[488] have shown that, for a fluorinated ionic liquid crystal, the phase segregation may be further assisted by the fluorophobic effect, and as a result, after the addition of I_2 to generate the I^-/I_3^- redox couple,[771] the mesophase is not destabilized, but the crystal-to-LC phase transition temperature is reduced by 20 K. Their material also had the tendency to supercool, allowing retention of the long-range smectic order in the solid film at room temperature, which may be of importance in, e.g., solar cells, supercapacitors, and lithium batteries.[488] Neither of these works utilizes XB per se, but they do demonstrate the power of fluorinated salts in organic electronic applications. Noteworthy is also the fact that halide anions are very efficient XB acceptors, and therefore, halogen-bonded ionic liquids and liquid crystals, and their use in organic electronics, will be reported in the foreseeable future.

On top of the two examples described in the previous paragraph, XB has also been shown to give a contribution in solar cell technology, as reported in 2014 by the Snaith group.[1094] Presently, perovskite-based materials are among the most studied in solar-cell research, combining high energy conversion efficiency and low cost in a unique manner.[1104,1105] The state-of-the-art perovskite-based materials employ lead halide compounds, having a chemical formula of $CH_3NH_3PbX_3$ (X = I^-, Br^-, Cl^-). The surface of the perovskite crystals contains an excess of halide anions (which are efficient XB-accepting moieties), which can be passivated with XB donors (Figure 154, top). As shown in Figure 154, bottom, this passivation has significant concequences on the performance of the solar cell. Whereas the untreated device delivers a power conversion efficiency of 13% and a fill factor of 0.57, the surface passivation via XBs leads to a significant improvement of these values to 15.7% and 0.67, respectively. The authors explain the

DOI: 10.1021/acs.chemrev.5b00484
Chem. Rev. 2016, 116, 2478−2601

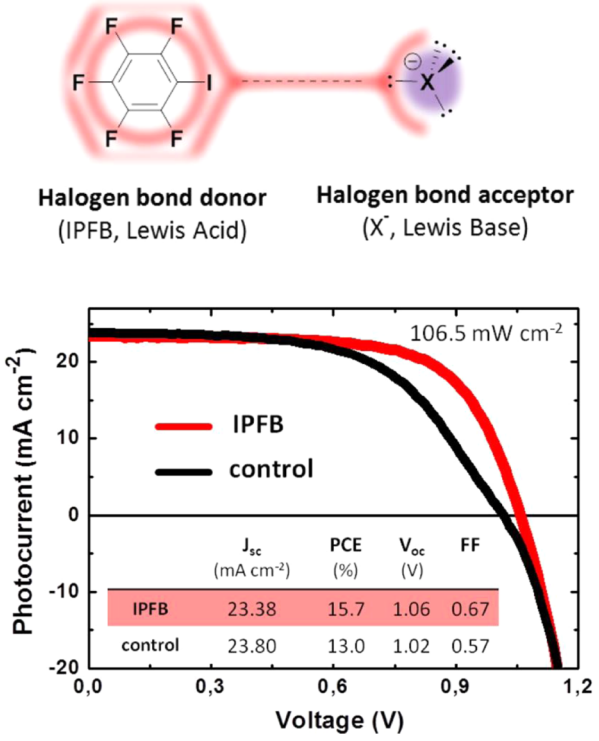

Figure 154. Top: schematic representation of the XB between the passivating iodopentafluorobenzene (IPFB) unit and a generic halide anion at the perovskite surface. Bottom: performance of the perovskite solar cells with (red) and without (black) surface passivation, using spiro-OMeTAD as the hole transporter. Reprinted from ref 1094. Copyright 2014 American Chemical Society.

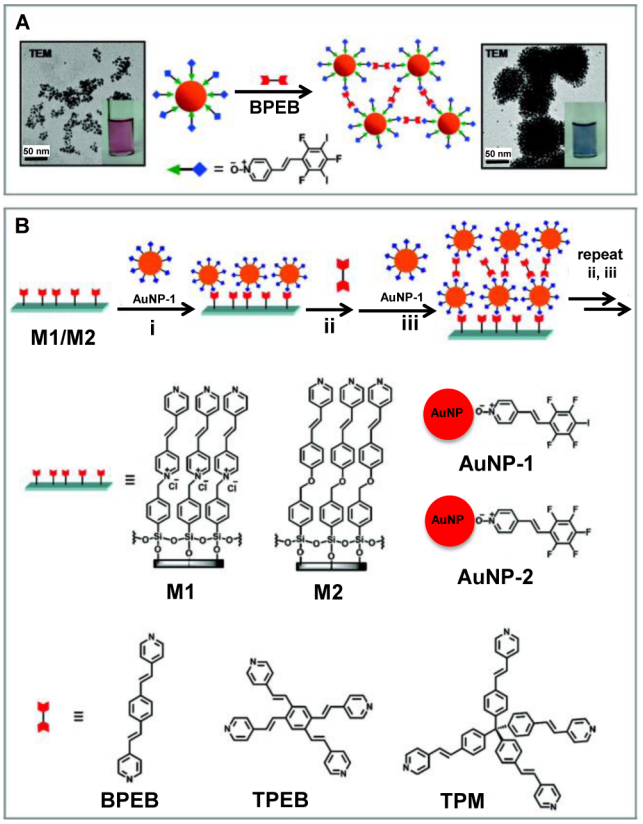

Figure 155. (A) Schematics of the formation of assemblies of functionalized gold nanoparticles (AuNPs) in the presence of bipyridyl cross-linkers (BPEB, TPEB, TPM) via XB. (B) Stepwise generation of assemblies consisting of functionalized gold nanoparticles and different XB-accepting cross-linkers on organic monolayers (M1 and M2). Reprinted from ref 1096. Copyright 2011 American Chemical Society.

improvement as follows: Without passivation, the halide anions act as hole traps, leading to accumulation of charges at the perovskite−hole-transport-layer heterojunction. XB-induced passivation prevents this undesired charge accumulation, and therefore improves the device performance.

In a completely different context, Milko van der Boom and co-workers have utilized XB as a supramolecular tool to assemble nanoparticles. They functionalized gold nanoparticles with XB-donating stilbene derivatives (Figure 155A), which upon mixing with bifunctional XB acceptors formed either chainlike structures or large, dense assemblies, depending on the concentration of the bipyridyl cross-linker (BPEB, TPEB, TPM; Figure 155B, bottom).[1095] The XB-driven aggregation of the gold nanoparticles led to a red shift of the plasmon resonance from ca. 520 to ca. 600 nm, accompanied by a color change from red to blue, as observed by the naked eye. To unambiguously associate the observed behavior with XB,[1098] a control experiment was performed where the XB donors on the gold surface were replaced with their perfluorinated counterparts (lacking the XB-donating site). In this case, no aggregation or color change occurred even within several weeks, whereas the XB-driven aggregates formed already within a few hours. As a continuation, they prepared surface-confined structures, attaching the nanoparticles onto silicon and glass substrates functionalized with pyridine groups (Figure 155B). Multilayer structures, with controlled morphology obtained by varying the structure of the cross-linker and by the number of deposition steps, were prepared by successive depositions of nanoparticles and pyridine-containing cross-linkers. The nanoparticle-functionalized surfaces were also shown to exhibit surface-enhanced Raman scattering.[1096]

It has also been recently shown that iodoperfluorobenzene compounds can directly bind to gold nanoparticle surfaces. Blakey et al. used a combination of UV−vis difference spectroscopy, surface-enhanced Raman scattering, and synchrotron X-ray photoelectron spectroscopy to show that the binding occurs through iodine atoms, for a range of both fluorinated and nonfluorinated iodo compounds.[1097] An interesting utilization of the gold−iodine interaction has been performed by Kiguchi et al., who formed single-molecule junctions of gold electrodes bound with 1,4-diiodobenzene and studied their conductance by the scanning tunneling microscopy break junction technique (Figure 156).[1098] They showed that the iodine site can be utilized as an anchoring group to build single-molecule junctions, whereas the junctions were not formed using dibrominated or dichlorinated benzenes, which was attributed to gold−iodine XB. The authors used the distances needed to break the single-molecule junctions as an indication of the binding strength between the electrodes and the bringing molecules, and concluded that the Au···I bond is stronger than the Au···NH_2 bond, but significantly weaker than the Au···SH bond. An interesting follow-up for this study could be to use 1,4-diiodotetrafluorobenzene or 1,4-bis(iodoethynyl)benzene to increase the strength of XB, therefore modifying the properties of the single-molecule junctions.

In the context of carbon-based nanomaterials, XB has been reported to enhance the thermal and mechanical properties of

DOI: 10.1021/acs.chemrev.5b00484
Chem. Rev. 2016, 116, 2478−2601

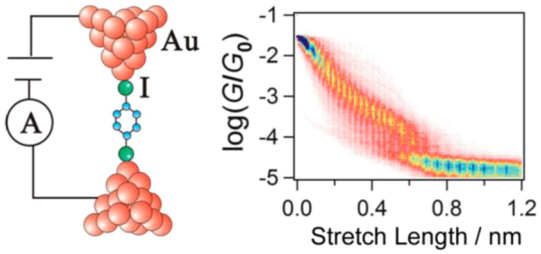

Figure 156. Left: schematics of a diiodobenzene-bridged single-molecule junction. Right: the authors used 2D conductance histograms to determine the conductance of the molecular junction and to conclude that sufficiently strong XB is required for the junction to form. Reprinted from ref 1098. Copyright 2013 American Chemical Society.

polymer−carbon nanotube (CNT) composites.[1099,1100] Salavagione et al. have studied dispersions of multiwalled, alkyl-modified CNTs in a poly(vinyl chloride) (PVC) matrix. The PVC matrix acts as an efficient "solubilizing agent" for the nanotubes, leading to composites with excellent mechanical and thermal properties, which depend on the tacticity of the polymer host. The high performance was in part attributed to C—Cl···O═C XB, which improved the dispersion of CNTs in the matrix.

As the final example, we bring up the work of Facchetti and van der Boom et al. on on-surface crystallization of halogen-bonded materials via physical vapor deposition (PVD), controlled by surface functionalization and the compound to be deposited.[1101,1102] In 2008, the authors proposed stilbazole derivatives to be ideal candidates for PVD experiments, due to their high thermal stability and high volatility. Using molecules containing both XB donor and acceptor functionalities, they constructed highly crystalline unimolecular halogen-bonded networks on the surface with a structure identical to that of solution-grown crystals.[1101] More recently, they reported on the on-surface, solvent-free crystal-to-cocrystal conversion process, driven by XB. They exposed a surface-confined polycrystalline film of a molecule containing XB-accepting groups, prepared by physical vapor deposition, into vapors of a complementary molecule bearing XB donor moieties. The subsequent transformation into a halogen-bonded cocrystal was accompanied by significant changes in the surface morphology, crystallinity, and optical properties of the deposited materials. Such a stepwise vapor-deposition-based approach using XBs might develop as a facile and intriguing approach toward the formation of multicomponent organic thin films for functional organic devices.[1102]

7. CONCLUSIONS

It has been more than 200 years since the first halogen-bonded complex, I_2···NH_3, was prepared in a chemical laboratory,[12] and it has been nearly 150 years since it was assigned the correct composition.[13] A fairly extensive review giving a brief history of the interaction and a snapshot of where we are now, and, perhaps, where we are going, seemed therefore particularly timely.

During the years, experimental observations and theoretical modeling have consistently contributed to the development of the present understanding of the nature of the XB and the potential of its current exploitations. The most important of these contributions have been described in previous sections of this review, and it is now possible to pinpoint briefly two pieces of information at the crossover between the historical perspective and the theoretical understanding developed in the past 15 years.

As acknowledged by the IUPAC definition,[9] the core feature of the XB is the electrophilic behavior of halogen atoms. Hydrogen is the electrophilic atom most frequently involved in attractive interactions with donors of electron density, and HB is by far the most studied and used noncovalent interaction. Similarities between XB and HB are numerous and have been the subjects of specific studies.[859] Analogies in the behavior of hydrogen and halogens have been recognized from the very early times to the point that some old versions of the periodic table put hydrogen in the same group as halogens, and not on top of the alkali metals. This was the case for J. Newlands' table published in 1863 when he described his law of octaves,[1106,1107] or for J. W. Retgers' table (Figure 157).[1108] Interestingly, the

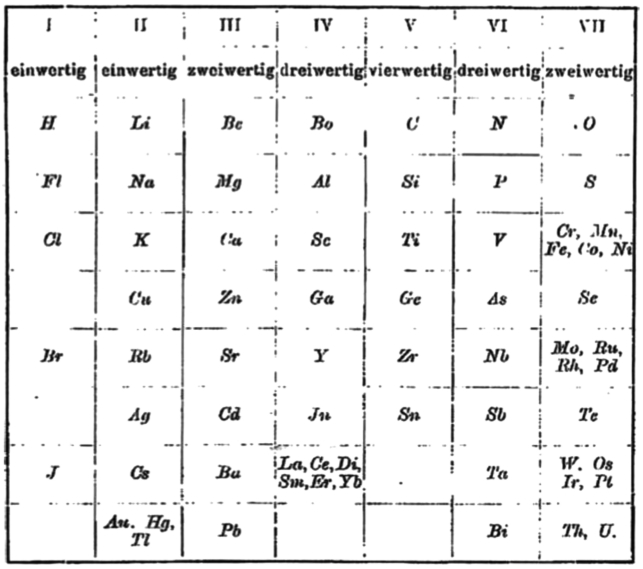

I	II	III	IV	V	VI	VII
einwertig	einwertig	zweiwertig	dreiwertig	vierwertig	dreiwertig	zweiwertig
H	Li	Be	Bo	C	N	O
Fl	Na	Mg	Al	Si	P	S
Cl	K	Ca	Sc	Ti	V	Cr, Mn, Fe, Co, Ni
	Cu	Zn	Ga	Ge	As	Se
Br	Rb	Sr	Y	Zr	Nb	Mo, Ru, Rh, Pd
	Ag	Cd	In	Sn	Sb	Te
J	Cs	Ba	La, Ce, Di, Sm, Er, Yb		Ta	W, Os Ir, Pt
	Au, Hg, Tl	Pb			Bi	Th, U.

Figure 157. Periodic table published by J. W. Retgers in 1895 in his paper in *Z. Phys. Chem.*,[1108] a journal established in 1887 by W. Ostwald, J. H. van 't Hoff, and S. A. Arrhenius as the first journal tailored to scientific papers on physical chemistry.

analogy between the two interactions was somehow implied and envisaged also by F. Guthrie in 1863, when he assigned the formula $NH_3 \cdot I_2$ to the halogen-bonded adduct between ammonia and iodine and commented on the analogy between this adduct and the one formed by ammonia with hydrogen iodide.[13]

While the analogies between XB and HB were valuable in the recent past to understand the features of the XB, the differences between the two interactions may help in the future to identify the most beneficial applications of the former interaction, namely, those where the specific properties of the XB represent an added value. For instance, directionality, tunability, hydrophobicity, and variable size of the donor atom are four unique features of the XB, which offer new opportunities if compared to the well-established use of the HB.[1109] This was, for example, the case for directionality when allowing some XBs to outperform stronger HBs in writing surface-relief gratings on thin films of supramolecular polymers,[489,855,859] or for donor atom size when altering by the heavy-atom effect the light-emitting properties of halogenated dyes by promoting singlet-to-triplet intersystem crossing.[997] Many other examples of

DOI: 10.1021/acs.chemrev.5b00484
Chem. Rev. 2016, 116, 2478−2601

specific advantages brought up by the use of XB have been demonstrated in quite different fields spanning from material sciences (e.g., liquid crystals[844,854,1110] and gels[83]) to separation and sensing (e.g., anion recognition[550,657,719] and transport[213,214]).

Applications in the field of small-molecule−protein interaction and, more in general, in biology and pharmacology are becoming more and more numerous, but it can be expected they will increase exponentially. In fact, in a biological scenario, directionality can offer the possibility to boost specificity and selectivity in binding and recognition processes, tunability can allow for optimizing the interaction strength by single-atom mutation, and hydrophobicity already belongs to the well-established advantages of introducing halogen atoms.

One of the advantages that the XB has in the fields of biology and nanomedicine over classical electrostatic, steric, and HB interactions is that halogen atoms in biological molecules are uncommon, and therefore, site-specific incorporation of halogenated amino acids or nucleotides into proteins or DNA can confer a very high degree of control and specificity. A marvelous example of this is the thyroid hormones, i.e., thyroxine (T_4), which is the relatively inactive prohormone, and the active hormone, triiodothyronine (T_3) (Figure 158).

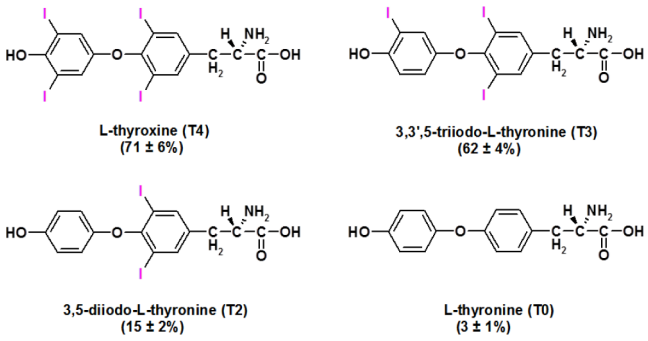

Figure 158. Molecular structures of thyroid hormones and the binding activities of the RNA aptamer complexes described in ref 1111.

Thyroid hormones basically regulate the development, growth, and metabolism of every single cell in our body. Structural studies have demonstrated that XB plays an important role in the binding[1112] of thyroid hormones to the body's hormone receptor and affects their activity.[1111] The fact that Nature has used iodinated hormones and XBs might find a possible explanation in the fine-tuning needed by the complex regulatory system of the thyroid gland. In fact, by single-atom mutations, i.e., removal of one iodine atom from the hormone structure, our body discriminates what is inactive and needs to be transported in the target organs, T_4, from what is the active hormone, T_3, and what needs to be recycled, T_2, to recover the iodine needed to again convert T_3 into T_4.

The properties of a nanostructured system partly result from the chemical and physical characteristics of the single constituent molecules and partly depend on the structural organization of the molecules in the given structure. Intermolecular interactions play a major role in determining the structure of any aggregate, and different structures may result in different properties, like in the case of polymorphs. When a new interaction becomes available, new structures, namely, new functions, become available. This was the case for the XB that only recently has become a routine tool for controlling aggregation and assembly phenomena. Applications are at a very initial stage, and will probably grow in the near future. With new applications of XB being pursued and identified, the quest for a deeper and more subtle understanding of the interaction will increase and will prompt further studies on the fundamental aspects. The scope of this review is to be a tool for those interested in either fundamental or applicative studies on XB.

AUTHOR INFORMATION

Corresponding Authors

*E-mail: pierangelo.metrangolo@polimi.it.
*E-mail: giuseppe.resnati@polimi.it.

Notes

The authors declare no competing financial interest.

Biographies

Gabriella Cavallo obtained her Ph.D. in chemistry in 2006 at the University of Salerno (Italy). After two years of activity in Pirelli Laboratories, a research unit of Pirelli Tyres, she joined the NFMLab at the Politecnico di Milano in 2008 as a postdoctoral researcher. Then she became an ssistant professor in 2012 at the same university. In 2011 she was a visiting researcher at the VTT-Technical Research Centre of Finland. Her research interests are in the synthesis of halofluorinated compounds for recognition processes and molecular materials. In 2011 she was a cofounder of FLUORIT, a Politecnico di Milano spin-off company for fluorine technologies.

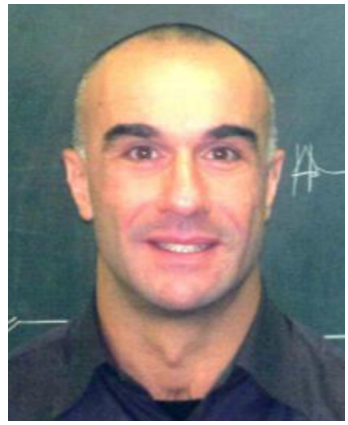

Pierangelo Metrangolo is a full professor at the Politecnico di Milano (since 2011) and a part-time research professor of molecular recognition at the VTT-Technical Research Centre of Finland (since 2010). In 2015 he was appointed as a visiting professor at the Centre of Excellence in Molecular Engineering of Biosynthetic Hybrid Materials of Aalto University, Finland. He was a European Union Fellow at the University of Toulouse (France, 2001) and a visiting

DOI: 10.1021/acs.chemrev.5b00484
Chem. Rev. 2016, 116, 2478−2601

professor at the University of York (U.K., 2005) and the University of Jyväskylä (Finland, 2006). His awards include the 2005 "G. Ciamician" medal of the Division of Organic Chemistry of the Italian Chemical Society and the 2005 Journals Grant Award of the Royal Society of Chemistry (RSC). He was a cofounder of the NFMLab at the Politecnico of Milano in 2003 and of the spin-off company FLUORIT in 2011. He is on the editorial boards of *CrystEngComm* (RSC) and *Crystal Growth and Design* (American Chemical Society), and is a coeditor of *Acta Crystallographica Section B* (International Union of Crystallography). In 2013 he was awarded a European Research Council Consolidator grant (ERC-StG2012) entitled "FOLDHALO—Folding with Halogen Bonding". In 2015 he was elected a titular member of the Physical and Biophysical Chemistry Division of IUPAC. The focus of his research is on supramolecular chemistry and nanomedicine with a particular interest in the design of functional and biomimetic materials.

Roberto Milani obtained a joint Ph.D. degree in materials science and engineering at the University of Padova and in structure and dynamics of reactive systems at the University of Lille I (France) in 2008. He was an invited postdoc at the University of Lille I in 2009. He was a senior postdoc at the Center for Nanoscience and Technology of the Italian Institute of Technology (2010–2011), and was appointed as a research scientist at the VTT-Technical Research Centre of Finland in 2012. In 2014 he received an Academy of Finland Research Fellowship. His research interests include supramolecular chemistry, biomimetic and hybrid materials, and surface functionalization.

Tullio Pilati retired as a senior researcher of the National Research Council in 2011. Since then, he has been a research associate at the NFMLab of the Politecnico di Milano. His research interests are in the field of crystallography of perfluorocarbon–hydrocarbon hybrid materials, bioactive compounds, and minerals. He is also developing software packages for analysis of lattice dynamics and crystal geometry.

Arri Priimagi earned his PhD degree in 2009 from the Department of Applied Physics, Helsinki University of Technology (nowadays known as Aalto University), Finland. After a two-year postdoc at Chemical Resources Laboratory, Tokyo Institute of Technology, and a 10-month International Fellowship at Politecnico di Milano, he was in 2014 appointed to the position of a tenure-track assistant professor at the Department of Chemistry and Bioengineering at Tampere University of Technology, Finland. In 2014 he received an Academy of Finland research Fellowship, and in 2015 was awarded an European Research Council Starting Grant entitled "Tunable Photonic Structures via Photomechanical Actuation". His research interests lie in functional soft matter, with a particular emphasis in photonic and light-responsive materials.

Giancarlo Terraneo became an assistant professor at the Politecnico di Milano in 2008. He was a VLAG Fellow at the University of Wageningen (The Netherlands, 2003) and a visiting scientist at the University of Zurich (Switzerland, 2004) and the University of York (U.K., 2008). He received a silver medal at "Premio Primo Levi 2007—Società Chimica Italiana" and has served since 2013 on the Doctoral Program Board of the Ph.D. in industrial chemistry and chemical engineering at the Politecnico di Milano. In 2011 he was a cofounder of FLUORIT, a Politecnico di Milano spin-off company for fluorine technologies. In 2015 he was promoted to associate professor at the same university. His research interests are on self-assembly and crystal engineering with a focus on structural studies via X-ray crystallography.

DOI: 10.1021/acs.chemrev.5b00484
Chem. Rev. 2016, 116, 2478–2601

Giuseppe Resnati became a full professor at the Politecnico di Milano in 2001. He was a NATO fellow at the University of Clemson (United States, 1990) and a visiting professor at the Université Paris Sud XI (France, 1993), Nagoya University (Japan, 2001), and Université de Strasbourg (France, 2012). He was awarded the 2008 Research Prize of the Division of Organic Chemistry of the Italian Chemical Society and the European Lectureship in Chemical Science by the Royal Society of Chemistry in 2010. He is on the editorial boards of the *Journal of Fluorine Chemistry* (Elsevier) and *Crystal Growth and Design* (American Chemical Society). He is a member of Academia Europaea. He was a cofounder of the NFMLab at the Politecnico of Milano in 2003 and of FLUORIT in 2011. His interests are in fluorine chemistry, spanning the synthesis of fluoroorganic compounds and their use in material chemistry, and in self-assembly processes, where he focuses on halogen-driven recognition phenomena (halogen bonding).

ACKNOWLEDGMENTS

We are grateful to all colleagues, graduate and Ph.D. students, and postdoctoral associates who worked with us on the XB. Some of them are mentioned in the references. Their dedication and enthusiasm have been fundamental. P.M. gratefully acknowledges the financial contribution from the European Research Council under the project FOLDHALO, Starting Grant ERC-2012-StG_20111012 (Grant Agreement Number 307108). R.M. gratefully acknowledges the financial contribution from the Academy of Finland, project SelfSmart (Decision Number 276537).

GLOSSARY

AR	aldose reductase
m-BIB	1,3-bis(iodoethynyl)benzene
p-BIB	1,4-bis(iodoethynyl)benzene
1,3-BIMB	1,3-bis(imidazol-1-ylmethyl)benzene
1,4-BIMB	1,4-bis(imidazol-1-ylmethyl)benzene
t-BPE	*trans*-1,2-bis(4-pyridyl)ethylene
BPTTF	bis(propylenedithio)tetrathiafulvalene
BIPUB	1,4-bis[(4-iodotetrafluorophenyl)ureido]butane
BPUB	1,4-bis(3-pyridylureido)butane
$BTMAA_n$	α,ω-bis(trimethylammonium)alkane diiodide
CP	coordination polymer
DAB-2-IPFB	poly(propylenimine) dendrimer DAB-*dendr*-$(NHC_6F_4I)_2^2$
DIDNTPM	4,4′-diiodo-4″,4‴-dinitrotetraphenylmethane
$DIPFA_m$	α,ω-diiodoperfluoroalkane
DPUB	1,3-bis[(1-methyl-1-(3-pyridylureido)ethyl]-benzene
DIPFB	1,4-diiodoperfluorobutane
DIPFH	1,6-diiodoperfluorohexane
DIOFS	4,4′-diiodooctafluorostilbene
DIPFO	1,8-diiodoperfluorooctane
1,4-DITFB	1,4-diiodotetrafluorobenzene
ETS	extended transition state
HB	hydrogen bond
HMTA	hexamethylenetetramine
HMET	1,6-bis(trimethylammonium)hexane diiodide
HOMO	highest occupied molecular orbital
HTIPEB	2,2′,4,4′,6,6′-hexafluoro-3,3′,5,5′-tetrakis[[4-(iodoethynyl)phenyl]ethynyl]biphenyl
IIF	5-iodoisophthalic acid
K.2.2.2	4,7,13,16,21,24-hexaoxa-1,10-diazabicyclo[8.8.8]-hexacosane
LAG	liquid-assisted grinding
LC	liquid crystal
LUMO	lowest unoccupied molecular orbital
MO	molecular orbital
MOF	metal−organic framework
NSAIDs	nonsteroidal anti-inflammatory drugs
NIS	*N*-iodosuccinimide
NOCV	natural orbitals for chemical valence
P4VP	poly(4-vinylpyridine)
PEG	polyethylene glycol
RT	reverse transcriptase
T3	3,5,3′-triiodothyronine
T4	thyroxine, 3,5,3′,5′-tetraiodothyronine
TBTP	tetrabromoterephthalic acid
TEMPO	(2,2,6,6-tetramethyl-1-piperidinyl)oxy radical
THR	thyroid hormone receptor
TITFPP	tetrakis(4-iodotetrafluorophenyl)pentaerythritol
TPC	tetrakis(4-pyridyl)cyclobutane
TPP	tetrakis(4-pyridyl)pentaerythritol
TTF	tetrathiafulvalene
TTR	transthyretin
XB	halogen bond

REFERENCES

(1) Hantzsch, A. Die Chromoisomerie Der P-Dioxy-Terepthalsaure Derivate Als Phenol-Enol-Isomerie. *Ber. Dtsch. Chem. Ges.* **1915**, *48*, 797−816.

(2) Nakamoto, K.; Margoshes, M.; Rundle, R. E. Stretching Frequencies as a Function of Distances in Hydrogen Bonds. *J. Am. Chem. Soc.* **1955**, *77*, 6480−6486.

(3) Schleyer, P. V. R.; West, R. Comparison of Covalently Bonded Electronegative Atoms as Proton Acceptor Groups in Hydrogen Bonding. *J. Am. Chem. Soc.* **1959**, *81*, 3164−3165.

(4) Metrangolo, P.; Resnati, G. Metal-Bound Halogen Atoms in Crystal Engineering. *Chem. Commun.* **2013**, *49*, 1783−1785.

(5) *Halogen Bonding. Fundamentals and Applications*; Metrangolo, P., Resnati, G., Eds.; Springer-Verlag: Berlin, Heidelberg, 2008.

(6) Murray, J. S.; Lane, P.; Politzer, P. Expansion of the σ-Hole Concept. *J. Mol. Model.* **2009**, *15*, 723−729.

(7) Politzer, P.; Murray, J. S.; Clark, T. Halogen Bonding and Other σ-Hole Interactions: A Perspective. *Phys. Chem. Chem. Phys.* **2013**, *15*, 11178−11189.

(8) Project No. 2009-032-1-100. Categorizing Halogen Bonding and Other Noncovalent Interactions Involving Halogen Atoms. *Chem. Int.* **2010**, *32*, 20−21. http://www.iupac.org/publications/ci/2010/3202/pp1_2009-032-1-100.html.

(9) Desiraju, G. R.; Ho, P. S.; Kloo, L.; Legon, A. C.; Marquardt, R.; Metrangolo, P.; Politzer, P.; Resnati, G.; Rissanen, K. Definition of the Halogen Bond (IUPAC Recommendations 2013). *Pure Appl. Chem.* **2013**, *85*, 1711−1713.

(10) Metrangolo, P.; Resnati, G. Halogen Bonding: A Paradigm in Supramolecular Chemistry. *Chem. - Eur. J.* **2001**, *7*, 2511−2519.

DOI: 10.1021/acs.chemrev.5b00484
Chem. Rev. 2016, 116, 2478−2601

(11) Colin, M. M.; Gaultier de Claubry, H. Sur Le Combinaisons de L'iode Avec Les Substances Végétales et Animales. *Ann. Chim.* **1814**, *90*, 87−100.
(12) Colin, M. Note Sur Quelques Combinaisons de L'iode. *Ann. Chim.* **1814**, *91*, 252−272.
(13) Guthrie, F. On the Iodide of Iodammonium. *J. Chem. Soc.* **1863**, *16*, 239−244.
(14) Mulliken, R. S. Structures of Complexes Formed by Halogen Molecules with Aromatic and with Oxygenated Solvents. *J. Am. Chem. Soc.* **1950**, *72*, 600−608.
(15) Hassel, O. Structural Aspects of Interatomic Charge-Transfer Bonding. http://www.nobelprize.org/nobel_prizes/chemistry/laureates/1969/hassel-lecture.pdf.
(16) Pelletier, P.; Caventou, J. Sur Un Nouvel Alcali Végétal (la Strychine) Trouvé Dans La Fève de Saint-Ignace, La Noix Vomique Etc. *Ann. Chim. Phys.* **1819**, *10*, 142−177.
(17) Svensson, P. H.; Kloo, L. Synthesis, Structure, and Bonding in Polyiodide and Metal Iodide-Iodine Systems. *Chem. Rev.* **2003**, *103*, 1649−1684.
(18) Jörgensen, S. M. Ueber Einige Anorganische Superjodide. *J. Prakt. Chem.* **1870**, *2*, 347−360.
(19) Rhoussopoulos, O. Einwirkung von Chinolin Auf Chloroform Und Jodoform. *Ber. Dtsch. Chem. Ges.* **1883**, *16*, 202−203.
(20) Remsen, I.; Norris, J. F. Action of the Halogens on the Methylamines. *Am. Chem. J.* **1896**, *18*, 90−95.
(21) Ault, B. S.; Andrews, L. Infrared and Raman Spectra of the M +F3- Ion Pairs and Their Mixed Chlorine-Fluorine Counterparts in Solid Argon. *Inorg. Chem.* **1977**, *16*, 2024−2028.
(22) Ault, B. S.; Andrews, L. Matrix Reactions of Alkali Metal Fluoride Molecules with Fluorine. Infrared and Raman Spectra of the Trifluoride Ion in the M+F3- Species. *J. Am. Chem. Soc.* **1976**, *98*, 1591−1593.
(23) Riedel, S.; Köchner, T.; Wang, X.; Andrews, L. Polyfluoride Anions, a Matrix-Isolation and Quantum-Chemical Investigation. *Inorg. Chem.* **2010**, *49*, 7156−7164.
(24) Legon, A. C. Prereactive Complexes of Dihalogens XY with Lewis Bases B in the Gas Phase: A Systematic Case for the Halogen Analogue B···XY of the Hydrogen Bond B···HX. *Angew. Chem., Int. Ed.* **1999**, *38*, 2686−2714.
(25) Metrangolo, P.; Meyer, F.; Pilati, T.; Resnati, G.; Terraneo, G. Halogen Bonding in Supramolecular Chemistry. *Angew. Chem., Int. Ed.* **2008**, *47*, 6114−6127.
(26) Politzer, P.; Murray, J. S.; Clark, T. Halogen Bonding: An Electrostatically-Driven Highly Directional Noncovalent Interaction. *Phys. Chem. Chem. Phys.* **2010**, *12*, 7748−7757.
(27) Parisini, E.; Metrangolo, P.; Pilati, T.; Resnati, G.; Terraneo, G. Halogen Bonding in Halocarbon-Protein Complexes: A Structural Survey. *Chem. Soc. Rev.* **2011**, *40*, 2267−2278.
(28) Cardillo, P.; Corradi, E.; Lunghi, A.; Meille, S. V.; Messina, M. T.; Metrangolo, P.; Resnati, G. The N···I Intermolecular Interaction as a General Protocol for the Formation of Perfluorocarbon-Hydrocarbon Supramolecular Architectures. *Tetrahedron* **2000**, *56*, 5535−5550.
(29) Metrangolo, P.; Murray, J. S.; Pilati, T.; Politzer, P.; Resnati, G.; Terraneo, G. Fluorine-Centered Halogen Bonding: A Factor in Recognition Phenomena and Reactivity. *Cryst. Growth Des.* **2011**, *11*, 4238−4246.
(30) Cametti, M.; Crousse, B.; Metrangolo, P.; Milani, R.; Resnati, G. The Fluorous Effect in Biomolecular Applications. *Chem. Soc. Rev.* **2012**, *41*, 31−42.
(31) Pavan, M. S.; Durga Prasad, K.; Row, T. N. G. Halogen Bonding in Fluorine: Experimental Charge Density Study on Intermolecular F···F and F···S Donor-Acceptor Contacts. *Chem. Commun.* **2013**, *49*, 7558−7560.
(32) Schwerdtfeger, P. Atomic Static Dipole Polarizabilities. In *Atoms, Molecules and Clusters in Electric Fields*; Maroulis, G., Ed.; Imperial College Press: London, 2006; pp 1−32.
(33) Dojahn, J. G.; Chen, E. C. M.; Wentworth, W. E. Characterization of Homonuclear Diatomic Ions by Semi-Empirical Morse Potential Energy Curves. 1. The Halogen Anions. *J. Phys. Chem.* **1996**, *100*, 9649−9657.
(34) Alkorta, I.; Blanco, F.; Solimannejad, M.; Elguero, J. Competition of Hydrogen Bonds and Halogen Bonds in Complexes of Hypohalous Acids with Nitrogenated Bases. *J. Phys. Chem. A* **2008**, *112*, 10856−10863.
(35) Hermann, A.; Hoffmann, R.; Ashcroft, N. W. Condensed Astatine: Monatomic and Metallic. *Phys. Rev. Lett.* **2013**, *111*, 116404.
(36) Mulliken, R. S.; Person, W. B. *Molecular Complexes: A Lecture and Reprint Volume*; Wiley-Interscience: New York, 1969.
(37) Mulliken, R. S. Spectroscopy, Molecular Orbitals, and Chemical Bonding. http://www.nobelprize.org/nobel_prizes/chemistry/laureates/1966/mulliken-lecture.pdf.
(38) Kleinberg, J. The Positive Character of the Halogens. *J. Chem. Educ.* **1946**, *23*, 559−562.
(39) Andrews, L.; Keefer, R. *Molecular Complexes in Organic Chemistry*; Holden-day Inc: San Francisco, London, Amsterdam, 1964.
(40) Foster, R. *Organic Charge-Transfer Complexes*; Academic Press: New York, 1969.
(41) Chaudhuri, J. N.; Basu, S. Charge-Transfer Interaction between Iodine and Aza-Aromatics. *Trans. Faraday Soc.* **1959**, *55*, 898.
(42) Yada, H.; Tanaka, J.; Nagakura, S. Infrared Absorption Spectrum of Charge-Transfer Complex between Trimethylamine and Iodine. *J. Mol. Spectrosc.* **1962**, *9*, 461−468.
(43) Hayward, G. C.; Hendra, P. J. The Far Infra-Red and Raman Spectra of the Trihalide Ions IBr−2 and I−3. *Spectrochim. Acta, Part A* **1967**, *23*, 2309−2314.
(44) Maki, A. G.; Forneris, R. Infrared and Spectra of Some Trihalide Ions: ICl−2,IBr−2, I−3, I2Br−, and BrICl−. *Spectrochim. Acta, Part A* **1967**, *23*, 867−880.
(45) Gayles, J. N. Amine−Halogen Charge-Transfer Interactions: Vibrational Spectra and Intramolecular Potentials. *J. Chem. Phys.* **1968**, *49*, 1840−1847.
(46) Kiefer, W.; Bernstein, H. J. The UV-Laser Excited Resonance Raman Spectrum of the I−3 Ion. *Chem. Phys. Lett.* **1972**, *16*, 5−9.
(47) Gabes, W.; Gerding, H. Vibrational Spectra and Structures of the Trihalide Ions. *J. Mol. Struct.* **1972**, *14*, 267−279.
(48) Yarwood, J.; Brownson, G. W. Infrared Intensity and Band Shape Measurements on Molecular Complexes of the Halogens. *Adv. Mol. Relax. Processes* **1973**, *5*, 1−9.
(49) Kleinberg, J.; Davidson, A. W. The Nature of Iodine Solutions. *Chem. Rev.* **1948**, *42*, 601−609.
(50) Benesi, H. A.; Hildebrand, J. H. Ultraviolet Absorption Bands of Iodine in Aromatic Hydrocarbons. *J. Am. Chem. Soc.* **1948**, *70*, 2832−2833.
(51) Benesi, H. A.; Hildebrand, J. H. A Spectrophotometric Investigation of the Interaction of Iodine with Aromatic Hydrocarbons. *J. Am. Chem. Soc.* **1949**, *71*, 2703−2707.
(52) Mulliken, R. S. Molecular Compounds and Their Spectra. II. *J. Am. Chem. Soc.* **1952**, *74*, 811−824.
(53) Mulliken, R. S. Molecular Compounds and Their Spectra. III. The Interaction of Electron Donors and Acceptors. *J. Phys. Chem.* **1952**, *56*, 801−822.
(54) Rosokha, S.; Kochi, J. X-Ray Structures and Electronic Spectra of the π-Halogen Complexes between Halogen Donors and Acceptors with π-Receptors. In *Halogen Bonding. Fundamentals and Applications*; Metrangolo, P., Resnati, G., Eds.; Springer-Verlag: Berlin, Heidelberg, 2008; Vol. *126*, pp 137−160.
(55) Burdeniuc, J.; Sanford, M.; Crabtree, R. H. Amine Charge Transfer Complexes of Perfluoroalkanes and an Application to Poly(tetrafluoroethylene) Surface Functionalization. *J. Fluorine Chem.* **1998**, *91*, 49−54.
(56) Hassel, O.; Hvoslef, J. The Structure of Bromine 1,4-Dioxanate. *Acta Chem. Scand.* **1954**, *8*, 873.
(57) Hassel, O.; Romming, C. Direct Structural Evidence for Weak Charge-Transfer Bonds in Solids Containing Chemically Saturated Molecules. *Q. Rev., Chem. Soc.* **1962**, *16*, 1−18.

DOI: 10.1021/acs.chemrev.5b00484
Chem. Rev. 2016, 116, 2478−2601

(58) Hassel, O.; Stromme, K. O. Structure of the Crystalline Compound Benzene-Bromine (1:1). *Acta Chem. Scand.* **1958**, *12*, 1146.
(59) Hassel, O.; Stromme, K. O. Crystal Structure of the Addition Compound Benzene-Chlorine (1:1). *Acta Chem. Scand.* **1959**, *13*, 1781−1786.
(60) Vasilyev, A. V.; Lindeman, S. V.; Kochi, J. K. Noncovalent Binding of the Halogens to Aromatic Donors. Discrete Structures of Labile Br2 Complexes with Benzene and Toluene. *Chem. Commun.* **2001**, 909−910.
(61) Brown, R. S. Investigation of the Early Steps in Electrophilic Bromination through the Study of the Reaction with Sterically Encumbered Olefins. *Acc. Chem. Res.* **1997**, *30*, 131−137.
(62) Lenoir, D.; Chiappe, C. What Is the Nature of the First-Formed Intermediates in the Electrophilic Halogenation of Alkenes, Alkynes, and Allenes? *Chem. - Eur. J.* **2003**, *9*, 1036−1044.
(63) Cavallo, G.; Metrangolo, P.; Pilati, T.; Resnati, G.; Terraneo, G. Halogen Bond: A Long Overlooked Interaction. In *Halogen Bonding I: Impact on Materials Chemistry and Life Science*; Metrangolo, P., Resnati, G., Eds.; Springer International Publishing: Cham, Switzerland, 2015; pp 1−18.
(64) Bent, H. Structural Chemistry of Donor-Acceptor Interactions. *Chem. Rev.* **1968**, *68*, 587−648.
(65) Ramasubbu, N.; Parthasarathy, R.; Murray-Rust, P. Angular Preferences of Intermolecular Forces around Halogen Centers: Preferred Directions of Approach of Electrophiles and Nucleophiles around Carbon-Halogen Bond. *J. Am. Chem. Soc.* **1986**, *108*, 4308−4314.
(66) Dumas, J.-M.; Gomel, M.; Guerin, M. Molecular Interactions Involving Organic Halides. In *Halides, Pseudo-Halides and Azides: Volume 2*; John Wiley & Sons, Ltd.: Chichester, U.K., 1983; pp 985−1020.
(67) Legon, A. C. Pi-Electron "Donor-Acceptor" Complexes B···ClF and the Existence of the "Chlorine Bond. *Chem. - Eur. J.* **1998**, *4*, 1890−1897.
(68) Liantonio, R.; Metrangolo, P.; Pilati, T.; Resnati, G. Fluorous Interpenetrated Layers in a Three-Component Crystal Matrix. *Cryst. Growth Des.* **2003**, *3*, 355−361.
(69) Cavallo, G.; Metrangolo, P.; Pilati, T.; Resnati, G.; Sansotera, M.; Terraneo, G. Halogen Bonding: A General Route in Anion Recognition and Coordination. *Chem. Soc. Rev.* **2010**, *39*, 3772−3783.
(70) Metrangolo, P.; Pilati, T.; Terraneo, G.; Biella, S.; Resnati, G. Anion Coordination and Anion-Templated Assembly under Halogen Bonding Control. *CrystEngComm* **2009**, *11*, 1187−1196.
(71) Abate, A.; Martí-Rujas, J.; Metrangolo, P.; Pilati, T.; Resnati, G.; Terraneo, G. Tetrahedral Oxyanions in Halogen-Bonded Coordination Networks. *Cryst. Growth Des.* **2011**, *11*, 4220−4226.
(72) Abate, A.; Biella, S.; Cavallo, G.; Meyer, F.; Neukirch, H.; Metrangolo, P.; Pilati, T.; Resnati, G.; Terraneo, G. Halide Anions Driven Self-Assembly of Haloperfluoroarenes: Formation of One-Dimensional Non-Covalent Copolymers. *J. Fluorine Chem.* **2009**, *130*, 1171−1177.
(73) Cauliez, P.; Polo, V.; Roisnel, T.; Llusar, R.; Fourmigué, M. The Thiocyanate Anion as a Polydentate Halogen Bond Acceptor. *CrystEngComm* **2010**, *12*, 558.
(74) Viger-Gravel, J.; Leclerc, S.; Korobkov, I.; Bryce, D. L. Correlation between C-13 Chemical Shifts and the Halogen Bonding Environment in a Series of Solid Para-Diiodotetrafluorobenzene Complexes. *CrystEngComm* **2013**, *15*, 3168−3177.
(75) Grebe, J.; Geiseler, G.; Harms, K.; Dehnicke, K. Donor-Akzeptor-Komplexe von Halogenidionen Mit 1.4-Diiodtetrafluorbenzol/Donor-Acceptor Complexes of Halide Ions with 1,4-Diiodotetrafluorobenzene. *Z. Naturforsch., B: J. Chem. Sci.* **1999**, *54*, 77−86.
(76) Walsh, R. B.; Padgett, C. W.; Metrangolo, P.; Resnati, G.; Hanks, T. W.; Pennington, W. T. Crystal Engineering through Halogen Bonding: Complexes of Nitrogen Heterocycles with Organic Iodides. *Cryst. Growth Des.* **2001**, *1*, 165−175.
(77) Cinčić, D.; Friščić, T.; Jones, W. Isostructural Materials Achieved by Using Structurally Equivalent Donors and Acceptors in Halogen-Bonded Cocrystals. *Chem. - Eur. J.* **2008**, *14*, 747−753.
(78) Arman, H. D.; Gieseking, R. L.; Hanks, T. W.; Pennington, W. T. Complementary Halogen and Hydrogen Bonding: Sulfur···iodine Interactions and Thioamide Ribbons. *Chem. Commun.* **2010**, *46*, 1854−1856.
(79) Arman, H. D.; Rafferty, E. R.; Bayse, C. a.; Pennington, W. T. Complementary Selenium···iodine Halogen Bonding and Phenyl Embraces: Cocrystals of Triphenylphosphine Selenide with Organoiodides. *Cryst. Growth Des.* **2012**, *12*, 4315−4323.
(80) Corradi, E.; Meille, S. V.; Messina, M. T.; Metrangolo, P.; Resnati, G. Halogen Bonding versus Hydrogen Bonding in Driving Self-Assembly Processes. *Angew. Chem., Int. Ed.* **2000**, *39*, 1782−1786.
(81) Sgarbossa, P.; Bertani, R.; Di Noto, V.; Piga, M.; Giffin, G. A.; Terraneo, G.; Pilati, T.; Metrangolo, P.; Resnati, G. Interplay between Structural and Dielectric Features of New Low K Hybrid Organic-Organometallic Supramolecular Ribbons. *Cryst. Growth Des.* **2012**, *12*, 297−305.
(82) Aakeroy, C. B.; Desper, J.; Helfrich, B. A.; Metrangolo, P.; Pilati, T.; Resnati, G.; Stevenazzi, A. Combining Halogen Bonds and Hydrogen Bonds in the Modular Assembly of Heteromeric Infinite 1-D Chains. *Chem. Commun.* **2007**, 4236−4238.
(83) Meazza, L.; Foster, J. A.; Fucke, K.; Metrangolo, P.; Resnati, G.; Steed, J. W. Halogen-Bonding-Triggered Supramolecular Gel Formation. *Nat. Chem.* **2013**, *5*, 42−47.
(84) Messina, M. T.; Metrangolo, P.; Panzeri, W.; Pilati, T.; Resnati, G. Intermolecular Recognition between Hydrocarbon Oxygen-Donors and Perfluorocarbon Iodine-Acceptors: The Shortest O···I Non-Covalent Bond. *Tetrahedron* **2001**, *57*, 8543−8550.
(85) Liantonio, R.; Luzzati, S.; Metrangolo, P.; Pilati, T.; Resnati, G. Perfluorocarbon-Hydrocarbon Self-Assembly. Part 16: Anilines as New Electron Donor Modules for Halogen Bonded Infinite Chain Formation. *Tetrahedron* **2002**, *58*, 4023−4029.
(86) Liu, P.; Ruan, C.; Li, T.; Ji, B. Cyclohexa-2,5-Diene-1,4-Dione-1,2,4,5-Tetrafluoro-3,6-Diiodobenzene (1/1). *Acta Crystallogr., Sect. E: Struct. Rep. Online* **2012**, *E68*, o1431 .
(87) Britton, D.; Gleason, W. B. Dicyanodurene-P-Tetrafluorodiiodobenzene (1/1). *Acta Crystallogr., Sect. E: Struct. Rep. Online* **2002**, *E58*, o1375−o1377.
(88) Lunghi, A.; Cardillo, P.; Messina, T.; Metrangolo, P.; Panzeri, W.; Resnati, G. Perfluorocarbon-Hydrocarbon Self Assembling. Thermal and Vibrational Analyses of One-Dimensional Networks Formed by A,w-Diiodoperfluoroalkanes with K.2.2. and K.2.2.2. *J. Fluorine Chem.* **1998**, *91*, 191−194.
(89) Brinck, T.; Murray, J. S.; Politzer, P. Surface Electrostatic Potentials of Halogenated Methanes as Indicators of Directional Intermolecular Interactions. *Int. J. Quantum Chem.* **1992**, *44*, 57−64.
(90) Brinck, T.; Murray, J. S.; Politzer, P. Molecular Surface Electrostatic Potentials and Local Ionization Energies of Group V−VII Hydrides and Their Anions: Relationships for Aqueous and Gas-Phase Acidities. *Int. J. Quantum Chem.* **1993**, *48*, 73−88.
(91) Murray, J. S.; Paulsen, K.; Politzer, P. Molecular Surface Electrostatic Potentials in the Analysis of Non-Hydrogen-Bonding Noncovalent Interactions. *Proc.—Indian Acad. Sci., Chem. Sci.* **1994**, *106*, 267−275.
(92) Metrangolo, P.; Neukirch, H.; Pilati, T.; Resnati, G. Halogen Bonding Based Recognition Processes: A World Parallel to Hydrogen Bonding. *Acc. Chem. Res.* **2005**, *38*, 386−395.
(93) Erdelyi, M. Scientific Conferences: A Big Hello to Halogen Bonding. *Nat. Chem.* **2014**, *6*, 762−764.
(94) Novick, S. E.; Janda, K. C.; Klemperer, W. HFClF: Structure and Bonding. *J. Chem. Phys.* **1976**, *65*, 5115.
(95) Desiraju, G. R.; Steiner, T. *The Weak Hydrogen Bond in Structural Chemistry and Biology*; Oxford University Press: Oxford, U.K., 1999.
(96) Alkorta, I.; Elguero, J. Non-Conventional Hydrogen Bonds. *Chem. Soc. Rev.* **1998**, *27*, 163−170.

DOI: 10.1021/acs.chemrev.5b00484
Chem. Rev. 2016, 116, 2478−2601

(97) Zingaro, R. A.; Hedges, M. Phosphine Oxide-Halogen Complexes: Effect on P-O and P-S Stretching Frequencies. *J. Phys. Chem.* **1961**, *65*, 1132−1138.
(98) Martire, D. E.; Sheridan, J. P.; King, J. W.; O'Donnell, S. E. Thermodynamics of Molecular Association. 9. An NMR Study of Hydrogen Bonding of CHCl3 and CHBr3 to Di-N-Octyl Ether, Di-N-Octyl Thioether and Di-N-Octylmethylamine. *J. Am. Chem. Soc.* **1976**, *98*, 3101−3106.
(99) Glaser, R.; Murphy, R. F. What's in a Name? Noncovalent Ar-Cl·(H-Ar′)n Interactions and Terminology Based on Structure and Nature of the Bonding. *CrystEngComm* **2006**, *8*, 948−951.
(100) Chopra, D.; Row, T. N. G. Role of Organic Fluorine in Crystal Engineering. *CrystEngComm* **2011**, *13*, 2175−2186.
(101) Laurence, C.; Graton, J.; Gal, J. F. An Overview of Lewis Basicity and Affinity Scales. *J. Chem. Educ.* **2011**, *88*, 1651−1657.
(102) Lu, Y.-X.; Zou, J.-W.; Yu, Q.-S.; Jiang, Y.-J.; Zhao, W.-N. Ab Initio Investigation of Halogen Bonding Interactions Involving Fluorine as an Electron Acceptor. *Chem. Phys. Lett.* **2007**, *449*, 6−10.
(103) Karan, N. K.; Arunan, E. Chlorine Bond Distances in ClF and Cl2 Complexes. *J. Mol. Struct.* **2004**, *688*, 203−205.
(104) Raghavendra, B.; Arunan, E. Unpaired and Sigma Bond Electrons as H, Cl, and Li Bond Acceptors: An Anomalous One-Electron Blue-Shifting Chlorine Bond. *J. Phys. Chem. A* **2007**, *111*, 9699−9706.
(105) Rosokha, S. V.; Neretin, I. S.; Rosokha, T. Y.; Hecht, J.; Kochi, J. K. Charge-Transfer Character of Halogen Bonding: Molecular Structures and Electronic Spectroscopy of Carbon Tetrabromide and Bromoform Complexes with Organic σ- and π-Donors. *Heteroat. Chem.* **2006**, *17*, 449−459.
(106) Imakubo, T.; Tajima, N.; Shirahata, T.; Miyake, A.; Sawa, H.; Nakamura, T.; Ohnuki, H.; Tamura, M.; Kato, R.; Izumi, M.; et al. Crystal Design of Organic Conductors Using the Iodine Bond. *Synth. Met.* **2003**, *135−136*, 601−602.
(107) Laurence, C.; Graton, J.; Berthelot, M.; El Ghomari, M. J. The Diiodine Basicity Scale: Toward a General Halogen-Bond Basicity Scale. *Chem. - Eur. J.* **2011**, *17*, 10431−10444.
(108) Zefirov, N. S.; Koz'min, A. S.; Kasumov, T.; Potekhin, K. A.; Sorokin, V. D.; Brel, V. K.; Abramkin, E. V.; Struchkov, Yu. T.; Zhdankin, V. V.; Stang, P. J. Interaction of an Allene with Polyvalent Iodine Derivatives. Preparation, X-Ray Molecular Structure, and Some Reactions of phenyl(2,2-Dimethyl-4-(diethylphosphono)-2,5-Dihydro-3-Furyl)iodonium Salts. *J. Org. Chem.* **1992**, *57*, 2433−2437.
(109) Matveeva, E. D.; Podrugina, T. A.; Grishin, Y. K.; Tkachev, V. V.; Zhdankin, V. V.; Aldoshin, S. M.; Zefirov, N. S. Synthesis and Structure of Mixed Phosphonium-Iodonium Ylide. *Russ. J. Org. Chem.* **2003**, *39*, 536−541.
(110) Frohn, H. J.; Giesen, M.; Welting, D.; Henkel, G. Contributions to the Chemistry of Brominetrifluoride 0.2. Bis-(pentafluorophenyl)bromonium Cations with Weak Nucleophilic Fluoroelementate Anions. *Eur. J. Solid State Inorg. Chem.* **1996**, *33*, 841.
(111) Murray, J. S.; Lane, P.; Clark, T.; Politzer, P. Sigma-Hole Bonding: Molecules Containing Group VI Atoms. *J. Mol. Model.* **2007**, *13*, 1033−1038.
(112) Clark, T.; Murray, J. S.; Lane, P.; Politzer, P. Why Are Dimethyl Sulfoxide and Dimethyl Sulfone Such Good Solvents? *J. Mol. Model.* **2008**, *14*, 689−697.
(113) Murray, J. S.; Concha, M. C.; Lane, P.; Hobza, P.; Politzer, P. Blue Shifts vs Red Shifts in Sigma-Hole Bonding. *J. Mol. Model.* **2008**, *14*, 699−704.
(114) Murray, J. S.; Lane, P.; Politzer, P. Simultaneous Sigma-Hole and Hydrogen Bonding by Sulfur- and Selenium- Containing Heterocycles. *Int. J. Quantum Chem.* **2008**, *108*, 2770−2781.
(115) Wang, W.; Ji, B.; Zhang, Y. Chalcogen Bond: A Sister Noncovalent Bond to Halogen Bond. *J. Phys. Chem. A* **2009**, *113*, 8132−8135.
(116) Shishkin, O. V.; Omelchenko, I. V.; Kalyuzhny, A. L.; Paponov, B. V. Intramolecular S···O Chalcogen Bond in Thioindirubin. *Struct. Chem.* **2010**, *21*, 1005−1011.
(117) Metrangolo, P.; Resnati, G. Enzyme Mimics: Halogen and Chalcogen Team Up. *Nat. Chem.* **2012**, *4*, 437−438.
(118) Li, Q. Z.; Li, R.; Guo, P.; Li, H.; Li, W. Z.; Cheng, J. B. Competition of Chalcogen Bond, Halogen Bond, and Hydrogen Bond in SCS-HOX and SeCSe-HOX (X = Cl and Br) Complexes. *Comput. Theor. Chem.* **2012**, *980*, 56−61.
(119) Politzer, P.; Riley, K. E.; Bulat, F. A.; Murray, J. S. Perspectives on Halogen Bonding and Other Sigma-Hole Interactions: Lex Parsimoniae (Occam's Razor). *Comput. Theor. Chem.* **2012**, *998*, 2−8.
(120) Kapecki, J. A.; Baldwin, J. E. Extended Huckel Calculations on Two Heterocyclic Systems Containing 2.41- and 2.64-Å Sulfur-Oxygen Distances. *J. Am. Chem. Soc.* **1969**, *91*, 1120−1123.
(121) Rosenfield, R. E.; Parthasarathy, R.; Dunitz, J. D. Directional Preferences of Nonbonded Atomic Contacts with Divalent Sulfur. 1. Electrophiles and Nucleophiles. *J. Am. Chem. Soc.* **1977**, *99*, 4860−4862.
(122) Row, T. N. G.; Parthasarathy, R. Directional Preferences of Nonbonded Atomic Contacts with Divalent Sulfur in Terms of Its Orbital Orientations. 2. S···S Interactions and Nonspherical Shape of Sulfur in Crystals. *J. Am. Chem. Soc.* **1981**, *103*, 477−479.
(123) Iwaoka, M.; Takemoto, S.; Tomoda, S. Statistical and Theoretical Investigations on the Directionality of Nonbonded S···O Interactions. Implications for Molecular Design and Protein Engineering. *J. Am. Chem. Soc.* **2002**, *124*, 10613−10620.
(124) Junming, L.; Yunxiang, L.; Subin, Y.; Weiliang, Z. Theoretical and Crystallographic Data Investigations of Noncovalent S···O Interactions. *Struct. Chem.* **2011**, *22*, 757−763.
(125) Burling, F. T.; Goldstein, B. M. Computational Studies of Nonbonded Sulfur-Oxygen and Selenium-Oxygen Interactions in the Thiazole and Selenazole Nucleosides. *J. Am. Chem. Soc.* **1992**, *114*, 2313−2320.
(126) Drago, R. S.; Wong, N.; Ferris, D. C. The E, C, T Interpretation of Bond Dissociation Energies and Anion-Neutral Molecule Interactions. *J. Am. Chem. Soc.* **1991**, *113*, 1970−1977.
(127) Widhalm, M.; Kratky, C. Synthesis and X-Ray Structure of Binaphthyl-Based Macrocyclic Diphosphanes and Their Ni(II) and Pd(II) Complexes. *Chem. Ber.* **1992**, *125*, 679−689.
(128) Carré, F.; Chuit, C.; Corriu, R. J. P.; Monforte, P.; Nayyar, N. K.; Reyé, C. Intramolecular Coordination at Phosphorus: Donor-Acceptor Interaction in Three- and Four-Coordinated Phosphorus Compounds. *J. Organomet. Chem.* **1995**, *499*, 147−154.
(129) Mitzel, N. W.; Blake, A. J.; Rankin, D. W. H. Beta-Donor Bonds in SiON Units: An Inherent Structure-Determining Property Leading to (4 + 4)-Coordination in Tetrakis-(N,N-Dimethylhydroxylamido)silane. *J. Am. Chem. Soc.* **1997**, *119*, 4143−4148.
(130) Losehand, U.; Mitzel, N. W.; Rankin, D. W. H. Synthesis and Molecular Structures of N,N-Dimethylhydroxylamino-Trichlorosilane and -Germane. *J. Chem. Soc., Dalton Trans.* **1999**, 4291−4297.
(131) Liu, F.; Du, L.; Gao, J.; Wang, L.; Song, B.; Liu, C. Application of Polarizable Ellipsoidal Force Field Model to Pnicogen Bonds. *J. Comput. Chem.* **2015**, *36*, 441−448.
(132) Mohajeri, A.; Pakiari, A. H.; Bagheri, N. Theoretical Studies on the Nature of Bonding in Sigma-Hole Complexes. *Chem. Phys. Lett.* **2009**, *467*, 393−397.
(133) Murray, J. S.; Lane, P.; Politzer, P. A Predicted New Type of Directional Noncovalent Interaction. *Int. J. Quantum Chem.* **2007**, *107*, 2286−2292.
(134) Politzer, P.; Murray, J.; Janjić, G.; Zarić, S. σ-Hole Interactions of Covalently-Bonded Nitrogen, Phosphorus and Arsenic: A Survey of Crystal Structures. *Crystals* **2014**, *4*, 12−31.
(135) Politzer, P.; Murray, J. S.; Lane, P.; Concha, M. C. Electrostatically Driven Complexes of SiF4 With Amines. *Int. J. Quantum Chem.* **2009**, *109*, 3773−3780.
(136) Bundhun, A.; Ramasami, P.; Murray, J. S.; Politzer, P. Trends in σ-Hole Strengths and Interactions of F3MX Molecules (M = C, Si, Ge and X = F, Cl, Br, I). *J. Mol. Model.* **2013**, *19*, 2739−2746.
(137) Watanabe, A.; Tasaki, S.; Wada, Y.; Nakamachi, H. Polymorphism of Thiamine Hydrochloride. II. Crystal Structure of

DOI: 10.1021/acs.chemrev.5b00484
Chem. Rev. 2016, 116, 2478−2601

Thiamine Hydrochloride Hemihydrate and Its Stability. *Chem. Pharm. Bull.* **1979**, *27*, 2751−2759.
(138) Hu, N.-H.; Liu, W.; Aoki, K. Thiamine as a Cationic Host in Anion Coordination Chemistry. Crystal Structures of Five Anion Salts of Thiamine Monophosphate. *Bull. Chem. Soc. Jpn.* **2000**, *73*, 1043−1052.
(139) Price, J.; Lui, M.; Jones, N. D.; Ragogna, P. J. Group 15 Pnictenium Cations Supported by a Conjugated Bithiophene Backbone. *Inorg. Chem.* **2011**, *50*, 12810.
(140) Cameron, J. U.; Killean, R. C. G. Arsenic Trichloride Dipyridil, $AsCl_3(NC_5H_5)_2$. *Cryst. Struct. Commun.* **1972**, *1*, 31.
(141) Murray, J. S.; Lane, P.; Clark, T.; Riley, K. E.; Politzer, P. Sigma-Holes, Pi-Holes and Electrostatically-Driven Interactions. *J. Mol. Model.* **2012**, *18*, 541−548.
(142) Murray, J. S.; Macaveiu, L.; Politzer, P. Factors Affecting the Strengths of σ-Hole Electrostatic Potentials. *J. Comput. Sci.* **2014**, *5*, 590−596.
(143) Politzer, P.; Murray, J. S.; Concha, M. C. Sigma-Hole Bonding between like Atoms; a Fallacy of Atomic Charges. *J. Mol. Model.* **2008**, *14*, 659−665.
(144) Politzer, P.; Murray, J. S.; Clark, T. σ-Hole Bonding: A Physical Interpretation. In *Halogen Bonding I: Impact on Materials Chemistry and Life Science*; Metrangolo, P., Resnati, G., Eds.; Springer International Publishing: Cham, Switzerland, 2015; pp 19−42.
(145) Clark, T.; Hennemann, M.; Murray, J. S.; Politzer, P. Halogen Bonding: The Sigma-Hole. *J. Mol. Model.* **2007**, *13*, 291−296.
(146) Ramasami, P.; Ford, T. A. Chalcogen-Bonded Complexes. Selenium-Bound Adducts of NH_3, H_2O, PH_3, and H_2S with OCSe, SCSe, and CSe_2. *J. Mol. Model.* **2015**, *21*, 10.1007/s00894-014-2562-4.
(147) Zahn, S.; Frank, R.; Hey-Hawkins, E.; Kirchner, B. Pnicogen Bonds: A New Molecular Linker? *Chem. - Eur. J.* **2011**, *17*, 6034−6038.
(148) Alkorta, I.; Elguero, J.; Grabowski, S. J. Pnicogen and Hydrogen Bonds: Complexes between PH3X+ and PH2X Systems. *Phys. Chem. Chem. Phys.* **2015**, *17*, 3261−3272.
(149) Setiawan, D.; Kraka, E.; Cremer, D. *J. Phys. Chem. A* **2015**, *119*, 1642−1656.
(150) Mani, D.; Arunan, E. The X-C···Y (X = O/F, Y = O/S/F/Cl/Br/N/P) "Carbon Bond" and Hydrophobic Interactions. *Phys. Chem. Chem. Phys.* **2013**, *15*, 14377−14383.
(151) Thomas, S. P.; Pavan, M. S.; Guru Row, T. N. Experimental Evidence for "Carbon Bonding" in the Solid State from Charge Density Analysis. *Chem. Commun.* **2014**, *50*, 49−51.
(152) Bauzá, A.; Mooibroek, T. J.; Frontera, A. Tetrel-Bonding Interaction: Rediscovered Supramolecular Force? *Angew. Chem., Int. Ed.* **2013**, *52*, 12317−12321.
(153) Esrafili, M. D.; Mohammadian-Sabet, F. Exploring σ-Hole Bonding in XH3Si···HMY (X = H, F, CN; M = Be, Mg; Y = H, F, CH3) Complexes: A "tetrel-Hydride" Interaction. *J. Mol. Model.* **2015**, *21*, 60.
(154) Cavallo, G.; Metrangolo, P.; Pilati, T.; Resnati, G.; Terraneo, G. Naming Interactions from the Electrophilic Site. *Cryst. Growth Des.* **2014**, *14*, 2697−2702.
(155) Collin, L. R. The Crystal Structure of Solid Chlorine. *Acta Crystallogr.* **1952**, *5*, 431.
(156) Tsirelson, V. G.; Zhou, P. F.; Tang, T.-H.; Bader, R. F. W. Topological Definition of Crystal Structure: Determination of the Bonded Interactions in Solid Molecular Chlorine. *Acta Crystallogr., Sect. A: Found. Crystallogr.* **1995**, *51*, 143−153.
(157) Sakurai, T.; Sundaralingam, M.; Jeffrey, G. A. A Nuclear Quadrupole Resonance and X-Ray Study of Crystal Structure of 2,5-Dichloroaniline. *Acta Crystallogr.* **1963**, *16*, 354.
(158) Desiraju, G. R.; Parthasarathy, R. The Nature of Halogen··· halogen Interactions: Are Short Halogen Contacts due to Specific Attractive Forces or due to Close Packing of Nonspherical Atoms? *J. Am. Chem. Soc.* **1989**, *111*, 8725−8726.
(159) Chopra, D. Is Organic Fluorine Really "Not" Polarizable? *Cryst. Growth Des.* **2012**, *12*, 541−546.
(160) Mukherjee, A.; Tothadi, S.; Desiraju, G. R. Halogen Bonds in Crystal Engineering: Like Hydrogen Bonds yet Different. *Acc. Chem. Res.* **2014**, *47*, 2514−2524.
(161) Allen, F. H. The Cambridge Structural Database: A Quarter of a Million Crystal Structures and Rising. *Acta Crystallogr., Sect. B: Struct. Sci.* **2002**, *58*, 380−388.
(162) Xu, K.; Ho, D. M.; Pascal, R. A. Azaaromatic Chlorides: A Prescription for Crystal Structures with Extensive Nitrogen-Chlorine Donor-Acceptor Interactions. *J. Am. Chem. Soc.* **1994**, *116*, 105−110.
(163) Müller, M.; Albrecht, M.; Gossen, V.; Peters, T.; Hoffmann, A.; Raabe, G.; Valkonen, A.; Rissanen, K. Anion-π Interactions in Salts with Polyhalide Anions: Trapping of I4 2-. *Chem. - Eur. J.* **2010**, *16*, 12446−12453.
(164) Wendler, K.; Thar, J.; Zahn, S.; Kirchner, B. Estimating the Hydrogen Bond Energy. *J. Phys. Chem. A* **2010**, *114*, 9529−9536.
(165) Aakeröy, C. B.; Chopade, P. D.; Desper, J. Avoiding "Synthon Crossover" in Crystal Engineering with Halogen Bonds and Hydrogen Bonds. *Cryst. Growth Des.* **2011**, *11*, 5333−5336.
(166) Aakeröy, C. B.; Fasulo, M.; Schultheiss, N.; Desper, J.; Moore, C. Structural Competition between Hydrogen Bonds and Halogen Bonds. *J. Am. Chem. Soc.* **2007**, *129*, 13772−13773.
(167) Saccone, M.; Cavallo, G.; Metrangolo, P.; Pace, A.; Pibiri, I.; Pilati, T.; Resnati, G.; Terraneo, G. Halogen Bond Directionality Translates Tecton Geometry into Self-Assembled Architecture Geometry. *CrystEngComm* **2013**, *15*, 3102−3105.
(168) Bianchi, R.; Forni, A.; Pilati, T. Experimental Electron Density Study of the Supramolecular Aggregation between 4,4′-Dipyridyl-N,N′-Dioxide and 1,4-Diiodotetrafluorobenzene at 90 K. *Acta Crystallogr., Sect. B: Struct. Sci.* **2004**, *60*, 559−568.
(169) Lommerse, J. P. M.; Stone, A. J.; Taylor, R.; Allen, F. H. The Nature and Geometry of Intermolecular Interactions between Halogens and Oxygen or Nitrogen. *J. Am. Chem. Soc.* **1996**, *118*, 3108−3116.
(170) Forni, A.; Metrangolo, P.; Pilati, T.; Resnati, G. Halogen Bond Distance as a Function of Temperature. *Cryst. Growth Des.* **2004**, *4*, 291−295.
(171) Padgett, C. W.; Walsh, R. D.; Drake, G. W.; Hanks, T. W.; Pennington, W. T. New Conformations and Binding Modes in Halogen-Bonded and Ionic Complexes of 2,3,5,6-tetra(2′-Pyridyl)-pyrazine. *Cryst. Growth Des.* **2005**, *5*, 745−753.
(172) Khavasi, H. R.; Tehrani, A. A. Influence of Halogen Bonding Interaction on Supramolecular Assembly of Coordination Compounds; Head-to-Tail N···X Synthon Repetitivity. *Inorg. Chem.* **2013**, *52*, 2891−2905.
(173) Crihfield, A.; Hartwell, J.; Phelps, D.; Walsh, R. B.; Harris, J. L.; Payne, J. F.; Pennington, W. T.; Hanks, T. W. Crystal Engineering through Halogen Bonding. 2. Complexes of Diacetylene-Linked Heterocycles with Organic Iodides. *Cryst. Growth Des.* **2003**, *3*, 313−320.
(174) Bjorvatten, T.; Hassel, O. Crystal Structure of the 1:3 Addition Compound Iodoform-Quinoline. *Acta Chem. Scand.* **1962**, *16*, 249−255.
(175) Pigge, F. C.; Vangala, V. R.; Swenson, D. C. Relative Importance of X···O═C vs. X···X Halogen Bonding as Structural Determinants in 4-Halotriaroylbenzenes. *Chem. Commun.* **2006**, 2123−2125.
(176) Syssa-Magalé, J.-L.; Boubekeur, K.; Schöllhorn, B. First Molecular Self-Assembly of 1,4-Diiodo-Tetrafluoro-Benzene and a Ketone via (O···I) Non-Covalent Halogen Bonds. *J. Mol. Struct.* **2005**, *737*, 103−107.
(177) Naso, F.; Cardellicchio, C.; Capozzi, M. A. M.; Capitelli, F.; Bertolasi, V. Self-Assemblies of Chiral P-Haloaryl Sulfoxides through C−H···O Short Contacts and Halogen Involving Interactions. *New J. Chem.* **2006**, *30*, 1782.
(178) Nayak, S. K.; Terraneo, G.; Forni, A.; Metrangolo, P.; Resnati, G. C-BrO Supramolecular Synthon: In Situ Cryocrystallography of Low Melting Halogen-Bonded Complexes. *CrystEngComm* **2012**, *14*, 4259−4261.

DOI: 10.1021/acs.chemrev.5b00484
Chem. Rev. 2016, 116, 2478−2601

(179) Bertolotti, F.; Cavallo, G.; Metrangolo, P.; Nayak, S. K.; Resnati, G.; Terraneo, G. C-halogen···O Supramolecular Synthons: In Situ Cryocrystallization of 1,2-dihalotetrafluoroethane/HMPA Adducts. *Supramol. Chem.* **2013**, *25*, 718−727.
(180) Syssa-Magalé, J. L.; Boubekeur, K.; Palvadeau, P.; Meerschaut, A.; Schöllhorn, B. Self-Assembly via (N···I) Non-Covalent Bonds between 1,4-Diiodo-Tetrafluoro-Benzene and a Tetra-Imino Ferrocenophane. *J. Mol. Struct.* **2004**, *691*, 79−84.
(181) Evangelisti, L.; Feng, G.; Gou, Q.; Grabow, J. U.; Caminati, W. Halogen Bond and Free Internal Rotation: The Microwave Spectrum of CF3Cl-Dimethyl Ether. *J. Phys. Chem. A* **2014**, *118*, 579−582.
(182) Holmesland, O.; Romming, C. Crystal Structure of the (1:1) Addition Compounds of Diiodoacetylene with 1,4-Dithiane and 1,4-Dieselenane Respectively. *Acta Chem. Scand.* **1966**, *20*, 2601−2610.
(183) Cinčić, D.; Friščić, T.; Jones, W. Experimental and Database Studies of Three-Centered Halogen Bonds with Bifurcated Acceptors Present in Molecular Crystals, Cocrystals and Salts. *CrystEngComm* **2011**, *13*, 3224.
(184) Raatikainen, K.; Huuskonen, J.; Lahtinen, M.; Metrangolo, P.; Rissanen, K. Halogen Bonding Drives the Self-Assembly of Piperazine Cyclophanes into Tubular Structures. *Chem. Commun.* **2009**, 2160−2162.
(185) Amico, V.; Meille, S. V.; Corradi, E.; Messina, M. T.; Resnati, G. Infinite Chain Formation Driven by Nitrogen···Iodine Interactions. *J. Am. Chem. Soc.* **1998**, *120*, 8261−8262.
(186) Chu, Q.; Wang, Z.; Huang, Q.; Yan, C.; Zhu, S. Fluorine-Containing Donor-Acceptor Complexes: Crystallographic Study of the Interactions between Electronegative Atoms (N, O, S) and Halogen Atoms (I, Br). *New J. Chem.* **2003**, *27*, 1522−1527.
(187) Cooke, S. A.; Cotti, G.; Evans, C. M.; Holloway, J. H.; Kisiel, Z.; Legon, A. C.; Thumwood, J. M. Pre-Reactive Complexes in Mixtures of Water Vapour with Halogens: Characterisation of H2O···ClF and H2O···F2 by a Combination of Rotational Spectroscopy and Ab Initio Calculations. *Chem. - Eur. J.* **2001**, *7*, 2295−2305.
(188) Hill, J. G.; Legon, A. C.; Tew, D. P.; Walker, N. R. Halogen Bonding in the Gas-Phase: A Comparison of the Iodine Bond in B···ICl and B···ICF_3 for Simple Lewis Bases B. In *Halogen Bonding I: Impact on Materials Chemistry and Life Science*; Metrangolo, P., Resnati, G., Eds.; Springer International Publishing: Cham, Switzerland, 2015; pp 43−77.
(189) Stephens, S. L.; Mizukami, W.; Tew, D. P.; Walker, N. R.; Legon, A. C. The Halogen Bond between Ethene and a Simple Perfluoroiodoalkane: C2H4···ICF3 Identified by Broadband Rotational Spectroscopy. *J. Mol. Spectrosc.* **2012**, *280*, 47−53.
(190) Messina, M. T.; Metrangolo, P.; Panzeri, W.; Ragg, E.; Resnati, G. Perfluorocarbon-Hydrocarbon Self-Assembly. Part 3. Liquid Phase Interactions between Perfluoroalkylhalides and Heteroatom Containing Hydrocarbons. *Tetrahedron Lett.* **1998**, *39*, 9069−9072.
(191) Metrangolo, P.; Panzeri, W.; Recupero, F.; Resnati, G. Perfluorocarbon-Hydrocarbon Self-Assembly Part 16. 19F NMR Study of the Halogen Bonding between Halo-Perfluorocarbons and Heteroatom Containing Hydrocarbons. *J. Fluorine Chem.* **2002**, *114*, 27−33.
(192) Bjorvatten, T. Crystal Structures of Chloro and Bromo Cyanoacetylene. *Acta Chem. Scand.* **1968**, *22*, 410.
(193) Borgen, B.; Hassel, O.; Römming, C. Mutual Arrangement of Iodo-Cyano-Acetylene Molecules in the Solid. *Acta Chem. Scand.* **1962**, *16*, 2469−2470.
(194) Desiraju, G. R.; Harlow, R. L. Cyano-Halogen Interactions and Their Role in the Crystal Structures of the 4-Halobenzonitriles. *J. Am. Chem. Soc.* **1989**, *111*, 6757−6764.
(195) Metrangolo, P.; Murray, J. S.; Pilati, T.; Politzer, P.; Resnati, G.; Terraneo, G. The Fluorine Atom as a Halogen Bond Donor, Viz. a Positive Site. *CrystEngComm* **2011**, *13*, 6593−6896.
(196) Rege, P. D.; Malkina, O. L.; Goroff, N. S. The Effect of Lewis Bases on the 13C NMR of Iodoalkynes. *J. Am. Chem. Soc.* **2002**, *124*, 370−371.
(197) Perkins, C.; Libri, S.; Adams, H.; Brammer, L. Diiodoacetylene: Compact, Strong Ditopic Halogen Bond Donor. *CrystEngComm* **2012**, *14*, 3033−3038.
(198) Bock, H.; Holl, S. Crystallization and Structure Determination of Sigma-Donor-Acceptor Complexes between 1,4-Dioxane and the Polyiodine Molecules I2, I2C═CI2, (IC)4S and (IC)4NR. *Z. Naturforsch., B: J. Chem. Sci.* **2001**, *56*, 111−121.
(199) Gagnaux, P.; Susz, B. P. Etudes de Composés D'addition Des Acides de LEWIS. XII. Structure, Spectre Infrarouge et Polarisation Moléculaire Du Composé D'addition Dioxanne-1, 4−diiodacétylène. *Helv. Chim. Acta* **1960**, *43*, 948−956.
(200) Bjorvatten, T. Crystal Structure of the 2:1 Addition Compound Iodoform-1,4-Diselenane, (CHI3)2.C4H8Se2. *Acta Chem. Scand.* **1963**, *17*, 2292−2300.
(201) Glaser, R.; Chen, N.; Wu, H.; Knotts, N.; Kaupp, M. 13C NMR Study of Halogen Bonding of Haloarenes: Measurements of Solvent Effects and Theoretical Analysis. *J. Am. Chem. Soc.* **2004**, *126*, 4412−4419.
(202) Präsang, C.; Whitwood, A. C.; Bruce, D. W. Halogen-Bonded Cocrystals of 4-(N,N-Dimethylamino)pyridine with Fluorinated Iodobenzenes. *Cryst. Growth Des.* **2009**, *9*, 5319−5326.
(203) De Santis, A.; Forni, A.; Liantonio, R.; Metrangolo, P.; Pilati, T.; Resnati, G. N ··· Br Halogen Bonding: One-Dimensional Infinite Chains through the Self-Assembly of Dibromotetrafluorobenzenes with Dipyridyl Derivatives. *Chem. - Eur. J.* **2003**, *9*, 3974−3983.
(204) Valerio, G.; Raos, G.; Meille, S. V.; Metrangolo, P.; Resnati, G. Halogen Bonding in Fluoroalkylhalides: A Quantum Chemical Study of Increasing Fluorine Substitution. *J. Phys. Chem. A* **2000**, *104*, 1617−1620.
(205) Riley, K. E.; Murray, J. S.; Fanfrlík, J.; Řezáč, J.; Solá, R. J.; Concha, M. C.; Ramos, F. M.; Politzer, P. Halogen Bond Tunability I: The Effects of Aromatic Fluorine Substitution on the Strengths of Halogen-Bonding Interactions Involving Chlorine, Bromine, and Iodine. *J. Mol. Model.* **2011**, *17*, 3309−3318.
(206) Raatikainen, K.; Cametti, M.; Rissanen, K. The Subtle Balance of Weak Supramolecular Interactions: The Hierarchy of Halogen and Hydrogen Bonds in Haloanilinium and Halopyridinium Salts. *Beilstein J. Org. Chem.* **2010**, *6*, 4.
(207) Logothetis, T. A.; Meyer, F.; Metrangolo, P.; Pilati, T.; Resnati, G. Crystal Engineering of Brominated Tectons: N-Methyl-3,5-Dibromo-Pyridinium Iodide Gives Particularly Short C-Br···I Halogen Bonding. *New J. Chem.* **2004**, *28*, 760−763.
(208) Liantonio, R.; Metrangolo, P.; Pilati, T.; Resnati, G.; Stevenazzi, A. Perfluorocarbon-Hydrocarbon Self-Assembly: First Crystalline Halogen-Bonded Complex Involving Bromoperfluoroalkanes. *Cryst. Growth Des.* **2003**, *3*, 799−803.
(209) Aakeröy, C. B.; Baldrighi, M.; Desper, J.; Metrangolo, P.; Resnati, G. Supramolecular Hierarchy among Halogen-Bond Donors. *Chem. - Eur. J.* **2013**, *19*, 16240−16247.
(210) Etter, M. C. Encoding and Decoding Hydrogen-Bond Patterns of Organic Compounds. *Acc. Chem. Res.* **1990**, *23*, 120−126.
(211) Russo, L.; Biella, S.; Lahtinen, M.; Liantonio, R.; Metrangolo, P.; Resnati, G.; Rissanen, K. Solution Stoichiometry Determines Crystal Stoichiometry in Halogen-Bonded Supramolecular Complexes. *CrystEngComm* **2007**, *9*, 341−344.
(212) Vargas Jentzsch, A.; Emery, D.; Mareda, J.; Metrangolo, P.; Resnati, G.; Matile, S. Ditopic Ion Transport Systems: Anion-π Interactions and Halogen Bonds at Work. *Angew. Chem., Int. Ed.* **2011**, *50*, 11675−11678.
(213) Vargas Jentzsch, A.; Matile, S. Transmembrane Halogen-Bonding Cascades. *J. Am. Chem. Soc.* **2013**, *135*, 5302−5303.
(214) Jentzsch, A. V.; Emery, D.; Mareda, J.; Nayak, S. K.; Metrangolo, P.; Resnati, G.; Sakai, N.; Matile, S. Transmembrane Anion Transport Mediated by Halogen-Bond Donors. *Nat. Commun.* **2012**, *3*, 905.
(215) Bondi, A. Van Der Waals Volumes and Radii. *J. Phys. Chem.* **1964**, *68*, 441−451.
(216) Syssa-Magalé, J.-L.; Boubekeur, K.; Palvadeau, P.; Meerschaut, A.; Schollhorn, B. The Tailoring of Crystal Structures via the Self-

DOI: 10.1021/acs.chemrev.5b00484
Chem. Rev. 2016, 116, 2478−2601

Assembly of Organic Coordination Compounds by NI Non-Covalent Halogen Bonds: Co-Crystals of Sterically Hindered N-Heterocycles and 1,4-Diiodo-Tetrafluorobenzene. *CrystEngComm* **2005**, *7*, 302−308.
(217) Huber, S. M.; Jimenez-Izal, E.; Ugalde, J. M.; Infante, I. Unexpected Trends in Halogen-Bond Based Noncovalent Adducts. *Chem. Commun.* **2012**, *48*, 7708−7710.
(218) Rosokha, S. V.; Vinakos, M. K. Hybrid Network Formation via Halogen Bonding of the Neutral Bromo-Substituted Organic Molecules with Anionic Metal-Bromide Complexes. *Cryst. Growth Des.* **2012**, *12*, 4149−4156.
(219) Wolters, L. P.; Schyman, P.; Pavan, M. J.; Jorgensen, W. L.; Bickelhaupt, F. M.; Kozuch, S. The Many Faces of Halogen Bonding: A Review of Theoretical Models and Methods. *Wiley Interdiscip. Rev. Comput. Mol. Sci.* **2014**, *4*, 523−54010.1002/wcms.1189.
(220) Kozuch, S.; Martin, J. M. L. Halogen Bonds: Benchmarks and Theoretical Analysis. *J. Chem. Theory Comput.* **2013**, *9*, 1918−1931.
(221) Chudzinski, M. G.; Taylor, M. S. Correlations between Computation and Experimental Thermodynamics of Halogen Bonding. *J. Org. Chem.* **2012**, *77*, 3483−3491.
(222) Řezáč, J.; Riley, K. E.; Hobza, P. Benchmark Calculations of Noncovalent Interactions of Halogenated Molecules. *J. Chem. Theory Comput.* **2012**, *8*, 4285−4292.
(223) Politzer, P.; Murray, J. S. Halogen Bonding: An Interim Discussion. *ChemPhysChem* **2013**, *14*, 278−294.
(224) Palusiak, M. On the Nature of Halogen Bond - The Kohn-Sham Molecular Orbital Approach. *J. Mol. Struct.: THEOCHEM* **2010**, *945*, 89−92.
(225) Riley, K. E.; Hobza, P. Investigations into the Nature of Halogen Bonding Including Symmetry Adapted Perturbation Theory Analyses. *J. Chem. Theory Comput.* **2008**, *4*, 232−242.
(226) Wang, C.; Danovich, D.; Mo, Y.; Shaik, S. On The Nature of the Halogen Bond. *J. Chem. Theory Comput.* **2014**, *10*, 3726−3737.
(227) Syzgantseva, O. a.; Tognetti, V.; Joubert, L. On the Physical Nature of Halogen Bonds: A QTAIM Study. *J. Phys. Chem. A* **2013**, *117*, 8969−8980.
(228) Wolters, L. P.; Bickelhaupt, F. M. Halogen Bonding versus Hydrogen Bonding: A Molecular Orbital Perspective. *ChemistryOpen* **2012**, *1*, 96−105.
(229) Pinter, B.; Nagels, N.; Herrebout, W. A.; De Proft, F. Halogen Bonding from a Hard and Soft Acids and Bases Perspective: Investigation by Using Density Functional Theory Reactivity Indices. *Chem. - Eur. J.* **2013**, *19*, 519−530.
(230) Clark, T. σ-Holes. *Wiley Interdiscip. Rev. Comput. Mol. Sci.* **2013**, *3*, 13−20.
(231) Clark, T.; Politzer, P.; Murray, J. S. Correct Electrostatic Treatment of Noncovalent Interactions: The Importance of Polarization. *Wiley Interdiscip. Rev. Comput. Mol. Sci.* **2015**, *5*, 169−177.
(232) Hobza, P.; Zahradník, R. An Essay on the Theory and Calculations of Intermolecular Interactions. *Int. J. Quantum Chem.* **1992**, *42*, 581−590.
(233) Kolář, M. H.; Deepa, P.; Ajani, H.; Pecina, A.; Hobza, P. Characteristics of a σ-Hole and the Nature of a Halogen Bond. In *Halogen Bonding II: Impact on Material Chemistry and Life Science*; Metrangolo, P., Resnati, G., Eds.; Springer International Publishing: Cham, Switzerland, 2015; pp 1−25.
(234) Kolar, M. H.; Carloni, P.; Hobza, P. Statistical Analysis of σ-Holes: A Novel Complementary View on Halogen Bonding. *Phys. Chem. Chem. Phys.* **2014**, *16*, 19111−19114.
(235) Murray-Rust, P.; Motherwell, W. D. S. Computer Retrieval and Analysis of Molecular Geometry. 4. Intermolecular Interactions. *J. Am. Chem. Soc.* **1979**, *101*, 4374−4376.
(236) Murray-Rust, P.; Stallings, W. C.; Monti, C. T.; Preston, R. K.; Glusker, J. P. Intermolecular Interactions of the C-F Bond. The Crystallographic Environment of Fluorinated Carboxylic Acids and Related Structures. *J. Am. Chem. Soc.* **1983**, *105*, 3206−3214.
(237) Delgado-Barrio, G.; Prat, R. F. Deformed Hartree-Fock Solutions for Atoms. III. Convergent Iterative Process and Results for O−. *Phys. Rev. A: At., Mol., Opt. Phys.* **1975**, *12*, 2288−2297.
(238) Weinstein, H.; Politzer, P.; Srebrenik, S. A Misconception Concerning the Electronic Density Distribution of an Atom. *Theor. Chim. Acta* **1975**, *38*, 159−163.
(239) Politzer, P.; Murray, J. S. The Fundamental Nature and Role of the Electrostatic Potential in Atoms and Molecules. *Theor. Chem. Acc.* **2002**, *108*, 134−142.
(240) Stewart, R. F. On the Mapping of Electrostatic Properties from Bragg Diffraction Data. *Chem. Phys. Lett.* **1979**, *65*, 335−342.
(241) Politzer, P.; Truhlar, D. G. *Chemical Applications of Atomic and Molecular Electrostatic Potentials*; Politzer, P., Truhlar, D. G., Eds.; Springer: New York, 1981; Vol. *X*.
(242) Bader, R. F. W.; Carroll, M. T.; Cheeseman, J. R.; Chang, C. Properties of Atoms in Molecules: Atomic Volumes. *J. Am. Chem. Soc.* **1987**, *109*, 7968−7979.
(243) Murray, J. S.; Politzer, P. Molecular Surfaces, van Der Waals Radii and Electrostatic Potentials in Relation to Noncovalent Interactions. *Croat. Chem. Acta* **2009**, *82*, 267−275.
(244) Stevens, E. D. Experimental Electron Density Distribution of Molecular Chlorine. *Mol. Phys.* **1979**, *37*, 27−45.
(245) Nyburg, S. C.; Faerman, C. H. A Revision of van Der Waals Atomic Radii for Molecular Crystals: N, O, F, S, Cl, Se, Br and I Bonded to Carbon. *Acta Crystallogr., Sect. B: Struct. Sci.* **1985**, *B41*, 274−279.
(246) Awwadi, F. F.; Willett, R. D.; Peterson, K. a.; Twamley, B. The Nature of Halogen···halogen Synthons: Crystallographic and Theoretical Studies. *Chem. - Eur. J.* **2006**, *12*, 8952−8960.
(247) Bilewicz, E.; Rybarczyk-Pirek, A. J.; Dubis, A. T.; Grabowski, S. J. Halogen Bonding in Crystal Structure of 1-Methylpyrrol-2-Yl Trichloromethyl Ketone. *J. Mol. Struct.* **2007**, *829*, 208−211.
(248) Hathwar, V. R.; Chopra, D.; Panini, P.; Row, T. N. G. Revealing the Polarizability of Organic Fluorine in the Trifluoromethyl Group: Implications in Supramolecular Chemistry. *Cryst. Growth Des.* **2014**, *14*, 5366−5369.
(249) Auffinger, P.; Hays, F. A.; Westhof, E.; Ho, P. S. Halogen Bonds in Biological Molecules. *Proc. Natl. Acad. Sci. U. S. A.* **2004**, *101*, 16789−16794.
(250) Voth, A. R.; Khuu, P.; Oishi, K.; Ho, P. S. Halogen Bonds as Orthogonal Molecular Interactions to Hydrogen Bonds. *Nat. Chem.* **2009**, *1*, 74−79.
(251) Politzer, P.; Murray, J. S.; Concha, M. C. Halogen Bonding and the Design of New Materials: Organic Bromides, Chlorides and Perhaps Even Fluorides as Donors. *J. Mol. Model.* **2007**, *13*, 643−650.
(252) Politzer, P.; Lane, P.; Concha, M. C.; Ma, Y.; Murray, J. S. An Overview of Halogen Bonding. *J. Mol. Model.* **2007**, *13*, 305−311.
(253) Riley, K. E.; Murray, J. S.; Fanfrlík, J.; Řezáč, J.; Solá, R. J.; Concha, M. C.; Ramos, F. M.; Politzer, P. Halogen Bond Tunability II: The Varying Roles of Electrostatic and Dispersion Contributions to Attraction in Halogen Bonds. *J. Mol. Model.* **2013**, *19*, 4651−4659.
(254) Shields, Z. P.; Murray, J. S.; Politzer, P. Directional Tendencies of Halogen and Hydrogen Bonds. *Int. J. Quantum Chem.* **2010**, *110*, 2823−2832.
(255) Lu, Y.; Zou, J.; Wang, H.; Yu, Q.; Zhang, H.; Jiang, Y. Triangular Halogen Trimers. A DFT Study of the Structure, Cooperativity, and Vibrational Properties. *J. Phys. Chem. A* **2005**, *109*, 11956−11961.
(256) Wang, F. F.; Hou, J. H.; Li, Z. R.; Wu, D.; Li, Y.; Lu, Z. Y.; Cao, W. L. Unusual Halogen-Bonded Complex F Br δ + ··· Br δ + F and Hydrogen-Bonded Complex F Br δ + ··· H δ + F Formed by Interactions between Two Positively Charged Atoms of Different Polar Molecules. *J. Chem. Phys.* **2007**, *126*, 144301.
(257) Riley, K. E.; Murray, J. S.; Politzer, P.; Concha, M. C.; Hobza, P. Br···O Complexes as Probes of Factors Affecting Halogen Bonding: Interactions of Bromobenzenes and Bromopyrimidines with Acetone. *J. Chem. Theory Comput.* **2009**, *5*, 155−163.
(258) Kolář, M.; Hostaš, J.; Hobza, P. The Strength and Directionality of a Halogen Bond Are Co-Determined by the Magnitude and Size of the σ-Hole. *Phys. Chem. Chem. Phys.* **2014**, *16*, 9987−9996.

DOI: 10.1021/acs.chemrev.5b00484
Chem. Rev. 2016, 116, 2478−2601

(259) Grant Hill, J. The Halogen Bond in thiirane···ClF: An Example of a Mulliken Inner Complex. *Phys. Chem. Chem. Phys.* **2014**, *16*, 19137−19140.
(260) Poleshchuk, O. K.; Branchadell, V.; Brycki, B.; Fateev, A. V.; Legon, A. C. HFI and DFT Study of the Bonding in Complexes of Halogen and Interhalogen Diatomics with Lewis Base. *J. Mol. Struct.: THEOCHEM* **2006**, *760*, 175−182.
(261) Alkorta, I.; Rozas, I.; Elguero, J. Charge-Transfer Complexes between Dihalogen Compounds and Electron Donors. *J. Phys. Chem. A* **1998**, *102*, 9278−9285.
(262) Legon, A. C. C. The Interaction of Dihalogens and Hydrogen Halides with Lewis Bases in the Gas Phase: An Experimental Comparison of the Halogen Bond and the Hydrogen Bond. In *Halogen Bonding. Fundamentals and Applications*; Metrangolo, P., Resnati, G., Eds.; Structure and Bonding, Vol. *126*; Springer-Verlag: Berlin, Heidelberg, 2008; pp 17−64.
(263) Farina, A.; Meille, S. V.; Messina, M. T.; Metrangolo, P.; Resnati, G.; Vecchio, G. Resolution of Racemic 1,2-Dibromohexafluoropropane through Halogen-Binded Supramolecular Helices. *Angew. Chem., Int. Ed.* **1999**, *38*, 2433−2436.
(264) Rosokha, S. V.; Stern, C. L.; Ritzert, J. T. Experimental and Computational Probes of the Nature of Halogen Bonding: Complexes of Bromine-Containing Molecules with Bromide Anions. *Chem. - Eur. J.* **2013**, *19*, 8774−8788.
(265) Rosokha, S. V.; Stern, C. L.; Swartz, A.; Stewart, R. Halogen Bonding of Electrophilic Bromocarbons with Pseudohalide Anions. *Phys. Chem. Chem. Phys.* **2014**, *16*, 12968−12979.
(266) Rosokha, S. V.; Vinakos, M. K. Halogen Bond-Assisted Electron Transfer Reactions of Aliphatic Bromosubstituted Electrophiles. *Phys. Chem. Chem. Phys.* **2014**, *16*, 1809−1813.
(267) Rosokha, S. V.; Kochi, J. K. Fresh Look at Electron-Transfer Mechanisms via the Donor/acceptor Bindings in the Critical Encounter Complex. *Acc. Chem. Res.* **2008**, *41*, 641−653.
(268) Lenoir, D. The Electrophilic Substitution of Arenes: Is the π Complex a Key Intermediate and What Is Its Nature? *Angew. Chem., Int. Ed.* **2003**, *42*, 854−857.
(269) Wang, Z.; Zheng, B.; Yu, X.; Li, X.; Yi, P. Structure, Properties, and Nature of the Pyridine-XY (X, Y = F, Cl, Br) Complexes: An Ab Initio Study. *J. Chem. Phys.* **2010**, *132*, 164104.
(270) Mitoraj, M. P.; Michalak, A. Theoretical Description of Halogen Bonding - An Insight Based on the Natural Orbitals for Chemical Valence Combined with the Extended-Transition- State Method (ETS-NOCV). *J. Mol. Model.* **2013**, *19*, 4681−4688.
(271) Plyler, E. K.; Mulliken, R. S. Molecular Complexes and Their Spectra. IX. Infrared Absorption by Iodine in Its Pyridine Complexes and in Benzene. *J. Am. Chem. Soc.* **1959**, *81*, 823−826.
(272) Mulliken, R. S. Note on the Charge-Transfer Band of the Pyridine-Iodine Complex. *J. Am. Chem. Soc.* **1969**, *91*, 1237.
(273) Legon, A. C. The Halogen Bond: An Interim Perspective. *Phys. Chem. Chem. Phys.* **2010**, *12*, 7736−7747.
(274) Metrangolo, P.; Resnati, G. Halogen versus Hydrogen. *Science* **2008**, *321*, 918−919.
(275) Deepa, P.; Pandiyan, B. V.; Kolandaivel, P.; Hobza, P. Halogen Bonds in Crystal TTF Derivatives: An Ab Initio Quantum Mechanical Study. *Phys. Chem. Chem. Phys.* **2014**, *16*, 2038−2047.
(276) Ding, X.; Tuikka, M.; Haukka, M. Halogen Bonding in Crystal Engineering. In *Recent Advances in Crystallography*; Benedict, J. B., Ed.; InTech: Rijeka, Croatia, 2012; pp 143−168.
(277) Politzer, P.; Murray, J. S.; Clark, T. Mathematical Modeling and Physical Reality in Noncovalent Interactions. *J. Mol. Model.* **2015**, *21*, 52.
(278) Riley, K. E.; Hobza, P. The Relative Roles of Electrostatics and Dispersion in the Stabilization of Halogen Bonds. *Phys. Chem. Chem. Phys.* **2013**, *15*, 17742−17751.
(279) Stone, A. J. Are Halogen Bonded Structures Electrostatically Driven? *J. Am. Chem. Soc.* **2013**, *135*, 7005−7009.
(280) Eskandari, K.; Zariny, H. Halogen Bonding: A Lump-Hole Interaction. *Chem. Phys. Lett.* **2010**, *492*, 9−13.
(281) Duarte, D. J. R.; Sosa, G. L.; Peruchena, N. M. Nature of Halogen Bonding. A Study Based on the Topological Analysis of the Laplacian of the Electron Charge Density and an Energy Decomposition Analysis. *J. Mol. Model.* **2013**, *19*, 2035−2041.
(282) Springer, S. D.; Rivera-Rivera, L. A.; McElmurry, B. A.; Wang, Z.; Leonov, I. I.; Lucchese, R. R.; Legon, A. C.; Bevan, J. W. CMM-RS Potential for Characterization of the Properties of the Halogen-Bonded OC-Cl2 Complex, and a Comparison with Hydrogen-Bonded OC-HCl. *J. Phys. Chem. A* **2012**, *116*, 1213−1223.
(283) Townes, C. H.; Schawlow, A. L. *Microwave Spectroscopy*; McGraw-Hill: New York, Toronto, London, 1955.
(284) Balle, T. J. Fabry−Perot Cavity Pulsed Fourier Transform Microwave Spectrometer with a Pulsed Nozzle Particle Source. *Rev. Sci. Instrum.* **1981**, *52*, 33−45.
(285) Legon, A. C. Fourier Transform Microwave Spectroscopy. In *Atomic and Molecular Beam Methods*; Scoles, G., Ed.; Oxford University Press: New York, 1992; Vol. *2*, pp 289−308.
(286) Brown, G. G.; Dian, B. C.; Douglass, K. O.; Geyer, S. M.; Shipman, S. T.; Pate, B. H. A Broadband Fourier Transform Microwave Spectrometer Based on Chirped Pulse Excitation. *Rev. Sci. Instrum.* **2008**, *79*, 053103.
(287) Stephens, S. L.; Walker, N. R. Determination of Nuclear Spin−rotation Coupling Constants in CF3I by Chirped-Pulse Fourier-Transform Microwave Spectroscopy. *J. Mol. Spectrosc.* **2010**, *263*, 27−33.
(288) Cooke, S. A.; Cotti, G.; Evans, C. M.; Holloway, J. H.; Legon, A. C. Rotational Spectrum and Properties of a Gas-Phase Complex of Molecular Fluorine and Hydrogen Cyanide. *Chem. Phys. Lett.* **1996**, *262*, 308−314.
(289) Cotti, G.; Evans, C. M.; Holloway, J. H.; Legon, A. C. Rotational Spectroscopy of a Pre-Reactive Mixture of H2S and F2: Detection and Characterisation of the Weakly Bound Complex H2S···F2. *Chem. Phys. Lett.* **1997**, *264*, 513−521.
(290) Bloemink, H. I.; Hinds, K.; Holloway, J. H.; Legon, A. C. Characterisation of a Pre-Reactive Intermediate in Gas-Phase Mixtures of Fluorine and Ammonia: The Rotational Spectrum of the H3N···F2 Complex. *Chem. Phys. Lett.* **1995**, *245*, 598−604.
(291) Evans, C. M.; Holloway, J. H.; Legon, A. C. Rotational Spectrum and Angular Geometry of a Pre-Reactive Complex of Oxirane and F2. *Chem. Phys. Lett.* **1997**, *267*, 281−287.
(292) Bloemink, H. I.; Cooke, S. A.; Legon, A. C.; Holloway, J. H. Rotational Spectroscopy of Mixtures of Trimethylamine and Fluorine: Identification of the Ion Pair [(CH3)3NF]+··· F− in the Gas Phase. *Angew. Chem., Int. Ed. Engl.* **1997**, *36*, 1340−1342.
(293) Bloemink, H. I.; Hinds, K.; Legon, A. C.; Thorn, J. C. Characterisation of the Intermediate C2H4···Cl2, in a Gaseous Mixture of Ethene and Chlorine by Rotational Spectroscopy: A Weak Pi-Type Complex. *Chem. - Eur. J.* **1995**, *1*, 17−25.
(294) Legon, A. C. Mulliken n.aσ and bπ.aσ Complexes B···Cl2 in the Gas Phase: Rules for Predicting Angular Geometries and Nature of the Interaction. *Chem. Phys. Lett.* **1995**, *237*, 291−298.
(295) Baiocchi, F. A. The Structure and Hyperfine Constants of HF−Cl2. *J. Chem. Phys.* **1982**, *77*, 1632−1638.
(296) Bloemink, H. I.; Hinds, K.; Legon, A. C.; Thorn, J. C. Properties of the Intermediate ethyne···Cl2 from Its Rotational Spectrum and Some Generalisations for a Series B···Cl2. *Chem. Phys. Lett.* **1994**, *223*, 162−166.
(297) Jager, W.; Xu, Y.; Gerry, M. C. L. Microwave Spectroscopic Investigation of the Weakly Bound Dimer Carbon Monoxide-Chlorine (OCCl2). *J. Phys. Chem.* **1993**, *97*, 3685−3689.
(298) Legon, A. C.; Warner, H. E. Isolation of Stable Intermediates in Reactive Gas Mixtures: Rotational Spectrum of H3P···Cl2 in a Pulsed Jet. *J. Chem. Phys.* **1993**, *98*, 3827−3832.
(299) Bloemink, H. I.; Dolling, S. J.; Hinds, K.; Legon, A. C. H2S-Cl2 Characterised in a Pre-Reactive Gas Mixture of Hydrogen Sulfide and Chlorine through Rotational Spectroscopy: The Nature of the Interaction. *J. Chem. Soc., Faraday Trans.* **1995**, *91*, 2059−2066.
(300) Bloemink, H. I.; Cooke, S. A.; Hinds, K.; Legon, A. C.; Thorn, J. C. The bπ.aσ Complex C2H2···Cl2 Characterised by Rotational

DOI: 10.1021/acs.chemrev.5b00484
Chem. Rev. 2016, 116, 2478−2601

Spectroscopy as an Intermediate in a Reactive Mixture of Ethyne and Chlorine. *J. Chem. Soc., Faraday Trans.* **1995**, *91*, 1891−1900.
(301) Legon, A. C.; Thorn, J. C. Identification and Characterisation of the Gas-Phase Complex HCN···Cl2 by Rotational Spectroscopy. *J. Chem. Soc., Faraday Trans.* **1993**, *89*, 4157−4162.
(302) Legon, A. C.; Lister, D. G.; Thorn, J. C. Non-Reactive Interaction of Ammonia and Molecular Chlorine: Rotational Spectrum of the "Charge-Transfer" Complex H3N···Cl2. *J. Chem. Soc., Faraday Trans.* **1994**, *90*, 3205−3212.
(303) Bloemink, H. I.; Legon, A. C. The Complex H3N···Br2 Characterized in the Gas Phase by Rotational Spectroscopy. *J. Chem. Phys.* **1995**, *103*, 876−882.
(304) Waclawik, E. R.; Thumwood, J. M. A.; Lister, D. G.; Fowler, P. W.; Legon, A. C. Geometry, Strength of Binding and Br2 Charge Redistribution in the Complex OC···Br2 Determined by Rotational Spectroscopy. *Mol. Phys.* **1999**, *97*, 159−166.
(305) Cooke, S. A.; Cotti, G.; Evans, C. M.; Holloway, J. H.; Legon, A. C. The Pre-Reactive Complex H2O···ClF Identified in Mixtures of Water Vapour and Chlorine Monofluoride by Rotational Spectroscopy. *Chem. Commun.* **1996**, 2327−2328.
(306) Cooke, S. A.; Cotti, G.; Hinds, K.; Holloway, J. H.; Legon, A. C.; Lister, D. G. Rotational Spectrum and Molecular Properties of the Dinitrogen-Chlorine Monofluoride Complex. *J. Chem. Soc., Faraday Trans.* **1996**, *92*, 2671−2676.
(307) Hinds, K.; Holloway, J. H.; Legon, A. C. The Complex OC··· ClF Identified as a Pre-Chemical Intermediate by Rotational Spectroscopy of Carbon Monoxide-Chlorine Monofluoride Mixtures. *Chem. Phys. Lett.* **1995**, *242*, 407−414.
(308) Hinds, K.; Holloway, J. H.; Legon, A. C. Evidence for a Pre-Reactive Intermediate in a Gaseous Mixture of Ethyne and Chlorine Monofluoride. Rotational Spectrum of the Mulliken bπ·aσ Complex C2H2···ClF. *J. Chem. Soc., Faraday Trans.* **1996**, *92*, 1291.
(309) Bloemink, H. I.; Holloway, J. H.; Legon, A. C. Geometry and Nature of the Binding of the Pre-Reactive Complex C2H4···ClF from Its Rotational Spectrum. *Chem. Phys. Lett.* **1996**, *250*, 567−575.
(310) Hinds, K.; Legon, A. C.; Holloway, J. H. Rotational Spectrum and Properties of a Complex of Hydrogen Cyanide and Chlorine Monofluoride. *Mol. Phys.* **1996**, *88*, 673−682.
(311) Bloemink, H. I.; Hinds, K.; Holloway, J. H.; Legon, A. C. Isolation of H2S···ClF in a Pre-Reactive Mixture of H2S and ClF Expanded in a Coaxial Jet and Characterisation by Rotational Spectroscopy. *Chem. Phys. Lett.* **1995**, *242*, 113−120.
(312) Bloemink, H. I.; Evans, C. M.; Holloway, J. H.; Legon, A. C. Is the Gas-Phase Complex of Ammonia and Chlorine Monofluoride H3N···ClF or [H3NCl]+···F−? Evidence from Rotational Spectroscopy. *Chem. Phys. Lett.* **1996**, *248*, 260−268.
(313) Cooke, S. A.; Corlett, G. K.; Evans, C. M.; Holloway, J. H.; Legon, A. C. Configuration at Oxygen and Deviation of the O···Cl-F System from Linearity in 2,5-dihydrofuran···ClF from Rotational Spectroscopy. *Chem. Phys. Lett.* **1997**, *275*, 269−277.
(314) Cooke, S. A.; Corlett, G. K.; Evans, C. M.; Legon, A. C.; Holloway, J. H. Angular Geometries of Complexes Containing the O··· Cl−F Linkage: Rotational Spectrum of Formaldehyde···Chlorine Monofluoride. *J. Chem. Phys.* **1998**, *108*, 39.
(315) Bloemink, H. I.; Evans, C. M.; Holloway, J. H.; Legon, A. C. Are B···Cl-F Bonds Linear? The Angular Geometry of a Pre-Reactive Complex of Oxirane and Chlorine Monofluoride from Rotational Spectroscopy. *Chem. Phys. Lett.* **1996**, *251*, 275−286.
(316) Evans, C. M.; Holloway, J. H.; Legon, A. C. Nature and Angular Geometry of the Pre-Reactive Complex Thiirane-Chlorine Monofluoride from Its Rotational Spectrum. *Chem. Phys. Lett.* **1996**, *255*, 119−128.
(317) Cotti, G.; Holloway, J. H.; Legon, A. C. Molecular Geometry of SO2···ClF from Its Rotational Spectrum: A Cis, Planar Complex with a Linear O···Cl-F Bond. *Chem. Phys. Lett.* **1996**, *255*, 401−409.
(318) Hinds, N.; Holloway, J. H.; Legon, A. C. A Pseudo-π Analogue of a Mulliken bπ.aσ Type Complex: The Rotational Spectrum of Cyclopropane−chlorine Monofluoride. *J. Chem. Soc., Faraday Trans.* **1997**, *93*, 373−378.
(319) Cooke, S. A.; Holloway, J. H.; Legon, A. C. Identification and Geometry of the Pre-Reactive Complex Buta-1,3-diene···ClF by Rotational Spectroscopy. *J. Chem. Soc., Faraday Trans.* **1997**, *93*, 2361−2365.
(320) Cooke, S. A.; Holloway, J. H.; Legon, A. C. The Rotational Spectrum and Angular Geometry of a Pre-Reactive Complex of Allene and Chlorine Monofluoride. *Chem. Phys. Lett.* **1997**, *266*, 61−69.
(321) Cooke, S. A.; Holloway, J. H.; Legon, A. C. Identification and Characterization of a Gas-Phase Complex of Methylenecyclopropane and Chlorine Monofluoride by Rotational Spectroscopy. *J. Chem. Soc., Faraday Trans.* **1997**, *93*, 4253−4258.
(322) Cooke, S. A.; Evans, C. M.; Holloway, J. H.; Legon, A. C. Interaction of Benzene and Halogens in the Gas-Phase: Rotational Spectrum of C6H6···ClF. *J. Chem. Soc., Faraday Trans.* **1998**, *94*, 2295−2302.
(323) Cooke, S. A.; Corlett, G. K.; Holloway, J. H.; Legon, A. C. Evidence Concerning the Relative Nucleophilicities of Non-Bonding and π-Bonding Electrons in Furan from the Rotational Spectrum of furan···ClF. *J. Chem. Soc., Faraday Trans.* **1998**, *94*, 2675−2680.
(324) Cooke, S. A.; Holloway, J. H.; Legon, A. C. Rotational Spectrum of Thiophene···ClF and the Role of Thiophene as a π- or n-Electron Pair Donor in Weakly Bound Complexes. *Chem. Phys. Lett.* **1998**, *298*, 151−160.
(325) Bloemink, H. I.; Holloway, J. H.; Legon, A. C. Mulliken Inner Complexes [(CH3)3 NCl]+···F− in Pre-Reactive Mixtures of Trimethylamine and Chlorine Monofluoride: Identification and Characterisation by Rotational Spectroscopy. *Chem. Phys. Lett.* **1996**, *254*, 59−68.
(326) Legon, A. C. Donor-Acceptor Complexes of Lewis Bases with Bromine Monochloride in the Gas Phase. Some Generalisations from Rotational Spectroscopy. *J. Chem. Soc., Faraday Trans.* **1995**, *91*, 1881−1883.
(327) Blanco, S.; Legon, A. C.; Thorn, J. C. Rotational Spectrum of the Gas-Phase Dimer OC···BrCl. *J. Chem. Soc., Faraday Trans.* **1994**, *90*, 1365−1371.
(328) Bloemink, H. I.; Hinds, K.; Legon, A. C.; Thorn, J. C. Nonreactive Interactions between Ethene and Halogens: Detection of a π-Donor Complex C2H4-BrCl by Rotational Spectroscopy. *Angew. Chem., Int. Ed. Engl.* **1994**, *33*, 1512−1513.
(329) Bloemink, H. I.; Hinds, K.; Legon, A. C.; Thorn, J. C. Intermediates in the Gas-Phase Reactions of Acetylene and Halogens: The Identification of the Acetylene-BrCl Complex by Rotational Spectroscopy. *J. Chem. Soc., Chem. Commun.* **1994**, 1229−1230.
(330) Bloemink, H. I.; Legon, A. C. The Pre-Reactive Complex of H2S and BrCl; Observation and Characterisation by Rotational Spectroscopy. *Chem. - Eur. J.* **1996**, *2*, 265−270.
(331) Hinds, K.; Legon, A. C. The Geometry and Intermolecular Binding of HCN···BrCl Probed by Rotational Spectroscopy. *Chem. Phys. Lett.* **1995**, *240*, 467−473.
(332) Bloemink, H. I.; Legon, A. C.; Thorn, J. C. "Charge-Transfer" Complexes of Ammonia with Halogens. Nature of the Binding in H3N···BrCl from Its Rotational Spectrum. *J. Chem. Soc., Faraday Trans.* **1995**, *91*, 781−787.
(333) Davey, J. B.; Legon, A. C.; Waclawik, E. R. Measurement of Inter- and Intramolecular Charge Transfer in the Complex N2···ICl from Analysis of Halogen Nuclear Quadrupole Hyperfine Structure in the Rotational Spectrum. *J. Mol. Struct.: THEOCHEM* **2000**, *500*, 403−411.
(334) Davey, J. B.; Legon, A C.; Waclawik, E. R. Inter- and Intramolecular Electron Transfer in the Complex OC···ICl Determined from Iodine and Chlorine Nuclear Quadrupole Hyperfine Structure in Its Rotational Spectrum. *Phys. Chem. Chem. Phys.* **1999**, *1*, 3097−3101.
(335) Davey, J. B.; Legon, A. C. Rotational Spectroscopy of Mixtures of Ethyne and Iodine Monochloride: Isolation and Characterisation of the π-Type Complex C2H2···ICl. *Phys. Chem. Chem. Phys.* **1999**, *1*, 3721−3726.
(336) Thumwood, J. M. A.; Legon, A. C. A π-Electron Donor−acceptor Complex of Ethene and Iodine Monochloride: Geometry,

DOI: 10.1021/acs.chemrev.5b00484
Chem. Rev. 2016, 116, 2478−2601

Binding Strength and Charge Redistribution Determined by Rotational Spectroscopy. *Chem. Phys. Lett.* **1999**, *310*, 88−96.
(337) Davey, J. B.; Legon, A. C.; Waclawik, E. R. An Investigation of the Gas-Phase Complex of Water and Iodine Monochloride by Microwave Spectroscopy: Geometry, Binding Strength and Electron Redistribution. *Phys. Chem. Chem. Phys.* **2000**, *2*, 1659−1665.
(338) Legon, A. C.; Waclawik, E. R. Angular Geometry, Binding Strength and Charge Transfer for the Complex H2S···ICl Determined by Rotational Spectroscopy. *Chem. Phys. Lett.* **1999**, *312*, 385−393.
(339) Waclawik, E. R.; Legon, A. C. Halogen Nuclear Quadrupole Coupling in the Rotational Spectrum of H3N···ICl as a Probe of Inter- and Intramolecular Charge Transfer. *Phys. Chem. Chem. Phys.* **1999**, *1*, 4695−4700.
(340) Davey, J. B.; Legon, A. C.; Waclawik, E. R. Inter- and Intramolecular Electronic Transfer on Formation of H3P···ICl as Determined by Rotational Spectroscopy. *Phys. Chem. Chem. Phys.* **2000**, *2*, 2265−2269.
(341) Herrebout, W. A.; Legon, A. C.; Waclawik, E. R. Is There a Significant Intermolecular Charge Transfer in the Ground State of the HCN···ICl Complex? An Answer from Rotational Spectroscopy. *Phys. Chem. Chem. Phys.* **1999**, *1*, 4961−4966.
(342) Anable, J. P.; Hird, D. E.; Stephens, S. L.; Zaleski, D. P.; Walker, N. R.; Legon, A. C. Characterisation of the Weak Halogen Bond in N2···ICF3 by Pure Rotational Spectroscopy. *Chem. Phys. Lett.* **2015**, *625*, 179−185.
(343) Stephens, S. L.; Walker, N. R.; Legon, A. C. Rotational Spectra and Properties of Complexes B···ICF3 (B = Kr or CO) and a Comparison of the Efficacy of ICl and ICF3 as Iodine Donors in Halogen Bond Formation. *J. Chem. Phys.* **2011**, *135*, 224309.
(344) Stephens, S. L.; Walker, N. R.; Legon, A. C. Molecular Geometries of H2S···ICF3 and H2O···ICF3 Characterised by Broadband Rotational Spectroscopy. *Phys. Chem. Chem. Phys.* **2011**, *13*, 21093−21101.
(345) Stephens, S. L.; Walker, N. R.; Legon, A. C. Internal Rotation and Halogen Bonds in CF3I···NH3 and CF3I···N(CH3)3 Probed by Broadband Rotational Spectroscopy. *Phys. Chem. Chem. Phys.* **2011**, *13*, 20736−20744.
(346) Legon, A. C. Nature of Complexes B···ClF in the Gas Phase: Conclusions from Systematic Variation of the Lewis Base B and a Comparison of the B···ClF/B···HCl Series. *Chem. Phys. Lett.* **1997**, *279*, 55−64.
(347) Legon, A. C. Quantitative Gas-Phase Electrophilicities of the Dihalogen Molecules XY = F2, Cl2, Br2, BrCl and ClF. *Chem. Commun.* **1998**, 2585−2586.
(348) Legon, A. C. Angular and Radial Geometries, Charge Transfer and Binding Strength in Isolated Complexes B···ICl: Some Generalisations. *Chem. Phys. Lett.* **1999**, *314*, 472−480.
(349) Legon, A. C. The Nature of the Interaction of Molecular Fluorine and Lewis Bases B from a Comparison of the Properties of B···F2 and B···HF. *Chem. Commun.* **1998**, 2737−2738.
(350) Legon, A. C.; Millen, D. J. Determination of Properties of Hydrogen-Bonded Dimers by Rotational Spectroscopy and a Classification of Dimer Geometries. *Faraday Discuss. Chem. Soc.* **1982**, *73*, 71−87.
(351) Legon, A. C.; Millen, D. J. Directional Character, Strength, and Nature of the Hydrogen Bond in Gas-Phase Dimers. *Acc. Chem. Res.* **1987**, *20*, 39−46.
(352) Legon, A. C.; Millen, D. J. Angular Geometries and Other Properties of Hydrogen-Bonded Dimers: A Simple Electrostatic Interpretation of the Success of the Electron-Pair Model. *Chem. Soc. Rev.* **1987**, *16*, 467−498.
(353) Kisiel, Z.; Pietrewicz, B. A.; Fowler, P. W.; Legon, A. C.; Steiner, E. Rotational Spectra of the Less Common Isotopomers, Electric Dipole Moment and the Double Minimum Inversion Potential of H2O···HCl. *J. Phys. Chem. A* **2000**, *104*, 6970−6978.
(354) Davey, J. B.; Legon, A. C.; Thumwood, J. M. A. Interaction of Water and Dichlorine in the Gas Phase: An Investigation of H2O···Cl2 by Rotational Spectroscopy and Ab Initio Calculations. *J. Chem. Phys.* **2001**, *114*, 6190−6202.
(355) Peebles, S. A.; Fowler, E. W.; Legon, A. C. Anisotropic Repulsion in Complexes B···Cl2 and B···HCl: The Shape of the Chlorine Atom-in-a-Molecule. *Chem. Phys. Lett.* **1995**, *240*, 130−134.
(356) Legon, A. C.; Millen, D. J. Hydrogen Bonding as a Probe of Electron Densities: Limiting Gas-Phase Nucleophilicities and Electrophilicities of B and HX. *J. Am. Chem. Soc.* **1987**, *109*, 356−358.
(357) Legon, A. C. A Reduced Radial Potential Energy Function for the Halogen Bond and the Hydrogen Bond in Complexes B···XY and B···HX, Where X and Y Are Halogen Atoms. *Phys. Chem. Chem. Phys.* **2014**, *16*, 12415−12421.
(358) Hauchecorne, D.; Nagels, N.; van der Veken, B. J.; Herrebout, W. A. C−X···π Halogen and C−H···π Hydrogen Bonding: Interactions of CF3X (X = Cl, Br, I or H) with Ethene and Propene. *Phys. Chem. Chem. Phys.* **2012**, *14*, 681−690.
(359) Hill, J. G.; Hu, X. Theoretical Insights into the Nature of Halogen Bonding in Prereactive Complexes. *Chem. - Eur. J.* **2013**, *19*, 3620−3628.
(360) Cheetham, N. F.; McNaught, I. J.; Pullin, A. D. E. Donor-Acceptor Complexes Formed by Perfluoro-Organobromides and Iodides with Nitrogenous and Other Bases. III Qualitative Examination of Condensed Phase Spectra of CF3I and CF3Br and of Their Complexes with Trimethylamine and Other Bases. *Aust. J. Chem.* **1974**, *27*, 973−985.
(361) Haque, I.; Wood, J. L. The Infra-Red Spectra of Pyridine-Halogen Complexes. *Spectrochim. Acta, Part A* **1967**, *23*, 959−967.
(362) Yarwood, J.; Person, W. B. Far-Infrared Intensity Studies of Iodine Complexes. *J. Am. Chem. Soc.* **1968**, *90*, 594−600.
(363) Augdahl, E.; Klaboe, P. Spectrocopic Studies of Charge Transfer complexes—VI. *Spectrochim. Acta* **1963**, *19*, 1665−1673.
(364) Klaboe, P. The Raman Spectra of Some Iodine, Bromine, and Iodine Monochloride Charge-Transfer Complexes in Solution. *J. Am. Chem. Soc.* **1967**, *89*, 3667−3676.
(365) Maes, G. The Infrared and Raman Intensity of the Halogen Stretching Vibrations in Complexes of Iodine and Bromine with Pyridines. *J. Mol. Struct.* **1980**, *61*, 95−100.
(366) Besnard, M.; Del Campo, N.; Yarwood, J. Molecular Relaxation Processes in Liquid Mixtures Containing Iodine Complexes. *J. Mol. Liq.* **1991**, *48*, 165−182.
(367) Yokobayashi, K.; Watari, F.; Aida, K. Infra-Red Absorption Spectra of Charge-Transfer Complexes of Trimethylamine: (CH3)3N·I2, (CH3)3N·IBr and (CH3)3N·ICl. *Spectrochim. Acta, Part A* **1968**, *24*, 1651−1655.
(368) Maes, G.; Zeegers-Huyskens, T. Raman Intensity Study of the νBr-Br Vibration in Charge Transfer Complexes of Bromine with Pyridines. *J. Phys. Chem.* **1978**, *82*, 2391−2395.
(369) Popov, A. I.; Marshall, J. C.; Stute, F. B.; Person, W. B. Studies on the Chemistry of Halogens and of Polyhalides. XXI. Halogen Complexes of 4,4′-Bipyridine and the Infrared Spectra of Pyridine Complexes. *J. Am. Chem. Soc.* **1961**, *83*, 3586−3590.
(370) Yagi, Y.; Popov, A. I.; Person, W. B. Chemistry of Halogens and of Polyhalides. XXVI. Infrared Absorption Spectra of Iodine Bromide and Its Complexes. *J. Phys. Chem.* **1967**, *71*, 2439−2444.
(371) Ginn, S. G. W.; Wood, J. L. Intermolecular Vibrations of Charge Transfer Complexes. *Trans. Faraday Soc.* **1966**, *62*, 777−787.
(372) Bowmaker, G.; Hacobian, S. Nuclear Quadrupole Resonance of Charge Transfer Complexes. I. The Trihalide Ions. *Aust. J. Chem.* **1968**, *21*, 551−564.
(373) Yahagi, E.; Matsumura, S.; Imai, Y.; Aida, K. Far-i.r. Spectra of Charge-Transfer Complexes between IX (X = Cl, Br) and Some Pyridine and Quinoline Bases. *Spectrochim. Acta, Part A* **1987**, *43*, 711−713.
(374) Person, W. B.; Humphrey, R. E.; Popov, A. I. Infrared Spectra of Charge Transfer Complexes. II. Iodine Cyanide Complexes. *J. Am. Chem. Soc.* **1959**, *81*, 273−277.
(375) Messina, M. T.; Metrangolo, P.; Navarrini, W.; Radice, S.; Resnati, G.; Zerbi, G. Infrared and Raman Analyses of the Halogen-Bonded Non-Covalent Adducts Formed by α,ω-Diiodoperfluoroalkanes with DABCO and Other Electron Donors. *J. Mol. Struct.* **2000**, *524*, 87−94.

DOI: 10.1021/acs.chemrev.5b00484
Chem. Rev. 2016, 116, 2478−2601

(376) Haque, I.; Wood, J. L. The Infra-Red Spectra of γ-Picoline—halogen Complexes. *Spectrochim. Acta, Part A* **1967**, *23*, 2523−2533.
(377) Tassaing, T.; Besnard, M.; Yarwood, J. Vibrational Spectroscopic Studies of the Chemical Dynamics in Charge Transfer Complexes of the Type Iodine-Pyridine 1. Experimental Results. *Mol. Phys.* **1997**, *92*, 271−280.
(378) Tassaing, T.; Besnard, M. Ionization Reaction in Iodine/Pyridine Solutions: What Can We Learn from Conductivity Measurements, Far-Infrared Spectroscopy, and Raman Scattering? *J. Phys. Chem. A* **1997**, *101*, 2803−2808.
(379) Haque, I.; Wood, J. L. The Vibrational Spectra and Structure of the bis(pyridine)iodine(I), bis(pyridine)bromine(I), Bis(γ-Picoline)-iodine-(I) and Bis(γ-picoline)bromine(I) Cations. *J. Mol. Struct.* **1968**, *2*, 217−238.
(380) Baruah, S. K. Infrared Studies of Some Sensitive Vibrational Modes of Pyridines on Complex Formation with Halogens and Interhalogens. *Asian J. Chem.* **2004**, *16*, 706−710.
(381) Person, W. B.; Anderson, G. R.; Fordemwalt, J. N.; Stammreich, H.; Forneris, R. Infrared and Raman Spectra, Force Constants, and the Structures of Some Polyhalide Ions: ICl2−, ICl4−, BrCl2−, and Br3−. *J. Chem. Phys.* **1961**, *35*, 908−914.
(382) Sasaki, K.; Aida, K. IR Spectra of Charge-Transfer Complexes between IX(X = Cl, Br) and Aminopyridines. *J. Inorg. Nucl. Chem.* **1980**, *42*, 13−15.
(383) Kaya, K.; Mikami, N.; Udagawa, Y.; Ito, M. Resonance Raman Effect of I−3 Ion by Ultraviolet Laser Excitation. *Chem. Phys. Lett.* **1972**, *16*, 151−153.
(384) Johnson, A. E.; Myers, A. B. Emission Cross Sections and Line Shapes for Photodissociating Triiodide in Ethanol: Experimental and Computational Studies. *J. Chem. Phys.* **1995**, *102*, 3519−3533.
(385) Johnson, A. E.; Myers, A. B. A Comparison of Time- and Frequency-Domain Resonance Raman Spectroscopy in Triiodide. *J. Chem. Phys.* **1996**, *104*, 2497−2507.
(386) Johnson, A. E.; Myers, A. B. Solvent Effects in the Raman Spectra of the Triiodide Ion: Observation of Dynamic Symmetry Breaking and Solvent Degrees of Freedom. *J. Phys. Chem.* **1996**, *100*, 7778−7788.
(387) Al-Hashimi, N. A. Spectroscopic Studies of the Reaction of Iodine with 2,3-Diaminopyridine. *Spectrochim. Acta, Part A* **2004**, *60*, 2181−2184.
(388) Sato, H.; Hirata, F.; Myers, A. B. Theoretical Study of the Solvent Effect on Triiodide Ion in Solutions. *J. Phys. Chem. A* **1998**, *102*, 2065−2071.
(389) Margulis, C. J.; Coker, D. F.; Lynden-Bell, R. M. Symmetry Breaking of the Triiodide Ion in Acetonitrile Solution. *Chem. Phys. Lett.* **2001**, *341*, 557−560.
(390) Zhang, F.; Lynden-Bell, R. Solvent-Induced Symmetry Breaking. *Phys. Rev. Lett.* **2003**, *90*, 185505.
(391) Zhang, F. S.; Lynden-Bell, R. M. Temperature and Solvent Dependence of Vibrational Relaxation of Tri-Iodide: A Simulation Study. *J. Chem. Phys.* **2003**, *119*, 6119−6131.
(392) Zhang, F.; Lynden-Bell, R. Solvent-Induced Symmetry Breaking: Varying Solvent Strength. *Phys. Rev. E* **2005**, *71*, 021502.
(393) Zhang, F. S.; Lynden-Bell, R. M. Interactions of Triiodide Cluster Ion with Solvents. *Eur. Phys. J. D* **2005**, *34*, 129−132.
(394) Schmulbach, C. D.; Drago, R. S. Molecular Addition Compounds of Iodine. III. An Infrared Investigation of the Interaction Between Dimethylacetamide and Iodine. *J. Am. Chem. Soc.* **1960**, *82*, 4484−4487.
(395) Klaboe, P.; Kloster-Jensen, E. Raman Spectra and Revised Vibrational Assignments of Some Halogeno Cyanoacetylenes. *Spectrochim. Acta, Part A* **1967**, *23*, 1981−1990.
(396) Christensen, D. H.; Johnsen, I.; Klaboe, P.; Kloster-Jensen, E. Far Infrared Spectra and Thermodynamic Functions of Some Halogeno Cyanoacetylenes and Monohalogeno Diacetylenes. *Spectrochim. Acta, Part A* **1969**, *25*, 1569−1576.
(397) Sellier, G.; Wojtkowiak, B. Étude par Spectroscopie d'Absorption Infrarouge de Quelques Complexes de Transfert de Charge Donnés par l'Iodo-1-pentyne-1. *C. R. Hebd. Seances Acad. Sci., Ser. B* **1966**, *263*, 974−976.
(398) Webb, J. A.; Klijn, J. E.; Hill, P. A.; Bennett, J. L.; Goroff, N. S. Experimental Studies of the 13C NMR of Iodoalkynes in Lewis-Basic Solvents. *J. Org. Chem.* **2004**, *69*, 660−664.
(399) Gao, K.; Goroff, N. S. Two New Iodine-Capped Carbon Rods. *J. Am. Chem. Soc.* **2000**, *122*, 9320−9321.
(400) Laurence, C.; Queignec-Cabanetos, M.; Dziembowska, T.; Queignec, R.; Wojtkowiak, B. 1-Iodoacetylenes. 1. Spectroscopic Evidence of Their Complexes with Lewis Bases. A Spectroscopic Scale of Soft Basicity. *J. Am. Chem. Soc.* **1981**, *103*, 2567−2573.
(401) Laurence, C.; Queignec-Cabanetos, M.; Wojtkowiak, B. 1-Iodoacetylenes. Part 2. Formation Constants of Their Complexes with Lewis Bases. *J. Chem. Soc., Perkin Trans. 2* **1982**, 1605−1610.
(402) Cheetham, N. F.; Pullin, A. D. E. Donor-Acceptor Complexes Formed by Perfluoro-Organobromides and Iodides with Nitrogenous and Other Bases. II. *Aust. J. Chem.* **1971**, *24*, 479−487.
(403) Cheetham, N. F.; Pullin, A. D. E. A Gas-Phase Donor-Acceptor Complex. *Chem. Commun.* **1967**, 233−234.
(404) Cheetham, N.; McNaught, I.; Pullin, A. Donor-Acceptor Complexes Formed by Perfluoro-Organo Bromides and Iodides with Nitrogenous and Other Bases. IV. Analysis of the Infrared Spectra of CF3I·N(CH3)3 and CF3 Br·N(CH3)3 and Related Complexes. *Aust. J. Chem.* **1974**, *27*, 987−1007.
(405) McNaught, I. J.; Pullin, A. D. E. Donor-Acceptor Complexes Formed by Perfluoro-Organo Bromides and Iodides with Nitrogenous and Other Bases. V. Comparison of Liquid Phase Complexes of CFI3, C2F5I or C3F7I with NMe3, NEt3 or NPr3; IR, FAR-IR and NMR Spectra. *Aust. J. Chem.* **1974**, *27*, 1009−1015.
(406) Corradi, E.; Meille, S. V.; Messina, M. T.; Metrangolo, P.; Resnati, G. Perfluorocarbon-Hydrocarbon Self-Assembly. Part 6: α,ω-Diiodoperfluoroalkanes as Pseudohalogens in Supramolecular Synthesis. *Tetrahedron Lett.* **1999**, *40*, 7519−7523.
(407) Messina, M. T.; Metrangolo, P.; Resnati, G.; Quici, S.; Manfredi, A.; Pilati, T. Herringbone Infinite Networks Formed by Terpyridine and Haloperfluoroarene Modules. *Supramol. Chem.* **2001**, *12*, 405−410.
(408) Hawthorne, B.; Fan-Hagenstein, H.; Wood, E.; Smith, J.; Hanks, T. Study of the Halogen Bonding between Pyridine and Perfluoroalkyl Iodide in Solution Phase Using the Combination of FTIR and 19F NMR. *Int. J. Spectrosc.* **2013**, *2013*, 1−10.
(409) Hauchecorne, D.; Van Der Veken, B. J.; Moiana, A.; Herrebout, W. A. The C-Cl···N Halogen Bond, the Weaker Relative of the C-I and C-Br···N Halogen Bonds, Finally Characterized in Solution. *Chem. Phys.* **2010**, *374*, 30−36.
(410) Hauchecorne, D.; Szostak, R.; Herrebout, W. A.; Van Der Veken, B. J. C-X···O Halogen Bonding: Interactions of Trifluoromethyl Halides with Dimethyl Ether. *ChemPhysChem* **2009**, *10*, 2105−2115.
(411) Hauchecorne, D.; Moiana, A.; van der Veken, B. J.; Herrebout, W. A. Halogen Bonding to a Divalent Sulfur Atom: An Experimental Study of the Interactions of CF3X (X = Cl, Br, I) with Dimethyl Sulfide. *Phys. Chem. Chem. Phys.* **2011**, *13*, 10204−10213.
(412) Hauchecorne, D.; Herrebout, W. A. Experimental Characterization of C-X···Y-C (X = Br, I; Y = F, Cl) Halogen-Halogen Bonds. *J. Phys. Chem. A* **2013**, *117*, 11548−11557.
(413) Nagels, N.; Hauchecorne, D.; Herrebout, W. A. Exploring the C-X···pi Halogen Bonding Motif: An Infrared and Raman Study of the Complexes of CF3X (X = Cl, Br and I) with the Aromatic Model Compounds Benzene and Toluene. *Molecules* **2013**, *18*, 6829−6851.
(414) Nagels, N.; Herrebout, W. A. A Cryospectroscopic Infrared and Raman Study of the C−X···π Halogen Bonding Motif: Complexes of the CF3Cl, CF3Br, and CF3I with Ethyne, Propyne and 2-Butyne. *Spectrochim. Acta, Part A* **2015**, *136*, 16−26.
(415) Vanspeybrouck, W.; Herrebout, W. A.; van der Veken, B. J.; Lundell, J.; Perutz, R. N. Direct Measurement of the Stability of the Supramolecular Synthon C6H6·C6F6. *J. Phys. Chem. B* **2003**, *107*, 13855−13861.

DOI: 10.1021/acs.chemrev.5b00484
Chem. Rev. 2016, 116, 2478−2601

(416) Delanoye, S. N.; Herrebout, W. A.; van der Veken, B. J. Stabilities of the C-H···O Bonded Complexes of the Haloforms HCClnF3-n (n = 0−3) with Dimethyl Ether, Oxirane, and Acetone: An Experimental and Theoretical Study. *J. Phys. Chem. A* **2005**, *109*, 9836−9843.
(417) Herrebout, W. Infrared and Raman Measurements of Halogen Bonding in Cryogenic Solutions. In *Halogen Bonding I: Impact on Materials Chemistry and Life Science*; Metrangolo, P., Resnati, G., Eds.; Springer International Publishing: Cham, Switzerland, 2015; pp 79−154.
(418) Wang, W.; Hobza, P. Origin of the X - Hal (Hal = Cl, Br) Bond-Length Change in the Halogen-Bonded Complexes. *J. Phys. Chem. A* **2008**, *112*, 4114−4119.
(419) Wang, W.; Wang, D.; Zhang, Y.; Ji, B.; Tian, A. Hydrogen Bond and Halogen Bond inside the Carbon Nanotube. *J. Chem. Phys.* **2011**, *134*, 054317.
(420) Wang, W.; Zhang, Y.; Ji, B. On the Difference of the Properties between the Blue-Shifting Halogen Bond and the Blue-Shifting Hydrogen Bond. *J. Phys. Chem. A* **2010**, *114*, 7257−7260.
(421) Michielsen, B.; Verlackt, C.; van der Veken, B. J.; Herrebout, W. A. C−H···X (X = S, P) Hydrogen Bonding: The Complexes of Halothane with Dimethyl Sulfide and Trimethylphosphine. *J. Mol. Struct.* **2012**, *1023*, 90−95.
(422) Michielsen, B.; Dom, J. J. J.; van der Veken, B. J.; Hesse, S.; Suhm, M. A.; Herrebout, W. A. Solute−solvent Interactions in Cryosolutions: A Study of Halothane−ammonia Complexes. *Phys. Chem. Chem. Phys.* **2012**, *14*, 6469−6478.
(423) Michielsen, B.; Dom, J. J. J.; van der Veken, B. J.; Hesse, S.; Xue, Z.; Suhm, M. A.; Herrebout, W. A. The Complexes of Halothane with Benzene: The Temperature Dependent Direction of the Complexation Shift of the Aliphatic C-H Stretching. *Phys. Chem. Chem. Phys.* **2010**, *12*, 14034−14044.
(424) Michielsen, B.; Herrebout, W. A.; van der Veken, B. J. Intermolecular Interactions between Halothane and Dimethyl Ether: A Cryosolution Infrared and Ab Initio Study. *ChemPhysChem* **2007**, *8*, 1188−1198.
(425) Michielsen, B.; Herrebout, W. A.; van der Veken, B. J. C-H Bonds with a Positive Dipole Gradient Can Form Blue-Shifting Hydrogen Bonds: The Complex of Halothane with Methyl Fluoride. *ChemPhysChem* **2008**, *9*, 1693−1701.
(426) Nagels, N.; Geboes, Y.; Pinter, B.; De Proft, F.; Herrebout, W. A. Tuning the Halogen/Hydrogen Bond Competition: A Spectroscopic and Conceptual DFT Study of Some Model Complexes Involving CHF2I. *Chem. - Eur. J.* **2014**, *20*, 8433−8443.
(427) Geboes, Y.; Nagels, N.; Pinter, B.; De Proft, F.; Herrebout, W. A. Competition of C(sp2)-X···O Halogen Bonding and Lone Pair···π Interactions: Cryospectroscopic Study of the Complexes of C2F3X (X = F, Cl, Br, and I) and Dimethyl Ether. *J. Phys. Chem. A* **2015**, *119*, 2502−2516.
(428) Drago, R. S.; Bafus, D. The N.M.R. Spectra of Dimethylpropionamide−iodine Solutions. *J. Phys. Chem.* **1961**, *65*, 1066−1067.
(429) Larsen, D. W.; Allred, A. L. Halogen Complexes. I. An Investigation by Nuclear Magnetic Resonance of Complexes Formed by Iodine and Some Para-Substituted Phenyl Methyl Sulfides. *J. Am. Chem. Soc.* **1965**, *87*, 1216−1219.
(430) Larsen, D. W.; Allred, A. L. Halogen Complexes. II. The Types and Mean Lifetimes of Complexes Formed by Iodine and 2,4,6-Trimethylpyridine. *J. Am. Chem. Soc.* **1965**, *87*, 1219−1226.
(431) Larsen, D. W.; Allred, A. L. Halogen Complexes. III. The Association of 2,4,6-Trimethylpyridine and Trifluoroiodomethane. *J. Phys. Chem.* **1965**, *69*, 2400−2401.
(432) Schuster, I. I.; Roberts, J. D. Halogen Complexes of Pyridines. A Proton and Carbon-13 Nuclear Magnetic Resonance Study. *J. Org. Chem.* **1979**, *44*, 2658−2662.
(433) Baruah, S. K.; Baruah, P. K. Studies of Nuclear Magnetic Resonance Spectra of Positive Halogen Salts of Pyridine and Substituted Pyridines. *Asian J. Chem.* **2004**, *16*, 688−694.
(434) Carlsson, A. C. C.; Gräfenstein, J.; Budnjo, A.; Laurila, J. L.; Bergquist, J.; Karim, A.; Kleinmaier, R.; Brath, U.; Erdélyi, M. Symmetric Halogen Bonding Is Preferred in Solution. *J. Am. Chem. Soc.* **2012**, *134*, 5706−5715.
(435) Carlsson, A.-C. C.; Uhrbom, M.; Karim, A.; Brath, U.; Gräfenstein, J.; Erdélyi, M. Solvent Effects on Halogen Bond Symmetry. *CrystEngComm* **2013**, *15*, 3087−3092.
(436) Carlsson, A.-C. C.; Gräfenstein, J.; Laurila, J. L.; Bergquist, J.; Erdelyi, M. Symmetry of [N-X-N]+ Halogen Bonds in Solution. *Chem. Commun.* **2012**, *48*, 1458−1460.
(437) Saunders, M.; Jaffe, M. H.; Vogel, P. New Method for Measuring Equilibrium Deuterium Isotope Effects. Isomerization of 3-Deuterio-2,3-dimethylbutyl-2-ium Ion. *J. Am. Chem. Soc.* **1971**, *93*, 2558−2559.
(438) Siehl, H.-U. *Advances in Physical Organic Chemistry*; Academic Press: London, 1987; Vol. 23.
(439) Wynter, C. I. Mössbauer Effect of 129I in Pyridine Complexes of Iodine Monohalides. *J. Chem. Phys.* **1969**, *50*, 3872.
(440) Robertson, C. C.; Perutz, R. N.; Brammer, L.; Hunter, C. A. A Solvent-Resistant Halogen Bond. *Chem. Sci.* **2014**, *5*, 4179−4183.
(441) Green, R. D.; Martin, J. S. Anion-Molecule Complexes in Solution. I. Nuclear Magnetic Resonance and Infrared Studies of Halide Ion-Trihalomethane Association. *J. Am. Chem. Soc.* **1968**, *90*, 3659−3668.
(442) Loehr, H. G.; Engel, A.; Josel, H.-P. H. P.; Voegtle, F.; Schuh, W.; Puff, H. Three-Dimensional Linkage by Electron Donor-Acceptor Interactions: Complexes of Organic Ammonium Halides with Triiodomethane. *J. Org. Chem.* **1984**, *49*, 1621−1627.
(443) Bertrán, J. F.; Rodríguez, M. Detection of Halogen Bond Formation by Correlation of Proton Solvent Shifts. 1. Haloforms in n-Electron Donor Solvents. *Org. Magn. Reson.* **1979**, *12*, 92−94.
(444) Bertrán, J. F.; Rodríguez, M. Detection of Halogen Bond Formation by Correlation of Proton Solvent Shifts. II−methylene Halides in n-Electron Donor Solvents. *Org. Magn. Reson.* **1980**, *14*, 244−246.
(445) Laurence, C.; Queignec-Cabanetos, M.; Wojtkowiak, B. 1-Iodoacetylenes. IV. Relations Structure-Reactivite Pour La Complexation Des 1-Iodoacetylenes Substitues Avec Des Bases de Lewis. *Can. J. Chem.* **1983**, *61*, 135−138.
(446) Zhao, X. R.; Shen, Q. J.; Jin, W. J. Acceptor Number of Halogenated Solvents and Its Potential as a Criterion for the Ability of Halogen Bonding as a Specific Solvent Effect Using the 31P NMR Chemical Shift of Triethylphosphine Oxide as a Probe. *Chem. Phys. Lett.* **2013**, *566*, 60−66.
(447) Esrafili, M. D. Investigation of H-Bonding and Halogen-Bonding Effects in Dichloroacetic Acid: DFT Calculations of NQR Parameters and QTAIM Analysis. *J. Mol. Model.* **2012**, *18*, 5005−5016.
(448) Esrafili, M. D. A DFT Investigation on Hydrogen- and Halogen-Bonding Interactions in Dichloroacetic Acid: Application of NMR-GIAO and Bader Theories. *Struct. Chem.* **2013**, *24*, 39−47.
(449) Ciancaleoni, G.; Bertani, R.; Rocchigiani, L.; Sgarbossa, P.; Zuccaccia, C.; Macchioni, A. Discriminating Halogen-Bonding from Other Noncovalent Interactions by a Combined NOE NMR/DFT Approach. *Chem. - Eur. J.* **2015**, *21*, 440−447.
(450) Navarrini, W.; Metrangolo, P.; Pilati, T.; Resnati, G. Crown Ethers as Pre-Organised Exo-Receptors in the Divergent Recognition of α,ω-Diiodoperfluoroalkanes. *New J. Chem.* **2000**, *24*, 777−780.
(451) Van Dyke Tiers, G. Detection of Oriented Association via NMR Dilution Shifts in Tetramethylsilane Solvent. 3. Perfluoroalkyl Halides; Association with Acetone, Esters, Nitriles, and Tertiary Amines, and Lack of Evidence for Self-Association. *J. Fluorine Chem.* **1999**, *98*, 89−95.
(452) Van Dyke Tiers, G. Detection of Oriented Association via NMR Dilution Shifts in Tetramethylsilane Solvent. 4. Temperature Coefficients for Perfluoroalkyl Halide Systems. *J. Fluorine Chem.* **2000**, *102*, 175−184.
(453) Cabot, R.; Hunter, C. A. Non-Covalent Interactions between Iodo-Perfluorocarbons and Hydrogen Bond Acceptors. *Chem. Commun.* **2009**, 2005−2007.

DOI: 10.1021/acs.chemrev.5b00484
Chem. Rev. 2016, 116, 2478−2601

(454) Sarwar, M. G.; Dragisic, B.; Salsberg, L. J.; Gouliaras, C.; Taylor, M. S. Thermodynamics of Halogen Bonding in Solution: Substituent, Structural, and Solvent Effects. *J. Am. Chem. Soc.* **2010**, *132*, 1646−1653.
(455) Libri, S.; Jasim, N. A.; Perutz, R. N.; Brammer, L. Metal Fluorides Form Strong Hydrogen Bonds and Halogen Bonds: Measuring Interaction Enthalpies and Entropies in Solution. *J. Am. Chem. Soc.* **2008**, *130*, 7842−7844.
(456) Ma, N.; Zhang, Y.; Ji, B.; Tian, A.; Wang, W. Structural Competition between Halogen Bonds and Lone-Pair···π Interactions in Solution. *ChemPhysChem* **2012**, *13*, 1411−1414.
(457) Thorson, R. A.; Woller, G. R.; Driscoll, Z. L.; Geiger, B. E.; Moss, C. A.; Schlapper, A. L.; Speetzen, E. D.; Bosch, E.; Erdélyi, M.; Bowling, N. P. Intramolecular Halogen Bonding in Solution: 15N, 13C, and 19F NMR Studies of Temperature and Solvent Effects. *Eur. J. Org. Chem.* **2015**, *2015*, 1685−1695.
(458) Sarwar, M. G.; Dragisic, B.; Sagoo, S.; Taylor, M. S. A Tridentate Halogen-Bonding Receptor for Tight Binding of Halide Anions. *Angew. Chem., Int. Ed.* **2010**, *49*, 1674−1677.
(459) Tepper, R.; Schulze, B.; Jäger, M.; Friebe, C.; Scharf, D. H.; Görls, H.; Schubert, U. S. Anion Receptors Based on Halogen Bonding with Halo-1,2,3-Triazoliums. *J. Org. Chem.* **2015**, *80*, 3139−3150.
(460) Kilah, N. L.; Wise, M. D.; Serpell, C. J.; Thompson, A. L.; White, N. G.; Christensen, K. E.; Beer, P. D. Enhancement of Anion Recognition Exhibited by a Halogen-Bonding Rotaxane Host System. *J. Am. Chem. Soc.* **2010**, *132*, 11893−11895.
(461) Bryce, D. L.; Viger-Gravel, J. Solid-State NMR Study of Halogen-Bonded Adducts. In *Halogen Bonding I: Impact on Materials Chemistry and Life Science*; Metrangolo, P., Resnati, G., Eds.; Springer International Publishing: Cham, Switzerland, 2015; pp 183−203.
(462) Perras, F. A.; Bryce, D. L. Direct Investigation of Covalently Bound Chlorine in Organic Compounds by Solid-State 35Cl NMR Spectroscopy and Exact Spectral Line-Shape Simulations. *Angew. Chem., Int. Ed.* **2012**, *51*, 4227−4230.
(463) Semin, G. K.; Babushkina, T. A.; Khrlakyan, S. P.; Pervova, E. Y.; Shokina, V. V.; Knunyants, I. L. I127 NQR Spectra of Fluorinated Alpha,omega-Diiodoalkanes and Complexes with Amines. *Theor. Exp. Chem.* **1971**, *4*, 179−181.
(464) Bowmaker, G.; Hacobian, S. Nuclear Quadrupole Resonance of Charge-Transfer Complexes. II. The Aminehalogen Complexes. *Aust. J. Chem.* **1969**, *22*, 2047−2059.
(465) Bowmaker, G. A. Nuclear Quadrupole Resonance of Charge Transfer Complexes. Part 3.−A 14N and 35Cl n.q.r. Study of the 1:1 Complex of 3,5-Dichloropyridine with Iodine Monochloride. *J. Chem. Soc., Faraday Trans. 2* **1976**, *72*, 1964−1969.
(466) Bowmaker, G. A.; Boyd, P. D. W. An SCF-MS-Xα Study of the Bonding and Nuclear Quadrupole Coupling in 1:1 Complexes of Amines with Diatomic Halogens and Interhalogens. *J. Chem. Soc., Faraday Trans. 2* **1987**, *83*, 2211−2223.
(467) Viger-Gravel, J.; Korobkov, I.; Bryce, D. L. Multinuclear Solid-State Magnetic Resonance and X-Ray Diffraction Study of Some Thiocyanate and Selenocyanate Complexes Exhibiting Halogen Bonding. *Cryst. Growth Des.* **2011**, *11*, 4984−4995.
(468) Viger-Gravel, J.; Meyer, J. E.; Korobkov, I.; Bryce, D. L. Probing Halogen Bonds with Solid-State NMR Spectroscopy: Observation and Interpretation of J(77Se, 31 P) Coupling in Halogen-Bonded P═Se···I Motifs. *CrystEngComm* **2014**, *16*, 7285−7297.
(469) Attrell, R. J.; Widdifield, C. M.; Korobkov, I.; Bryce, D. L. Weak Halogen Bonding in Solid Haloanilinium Halides Probed Directly via Chlorine-35, Bromine-81, and Iodine-127 NMR Spectroscopy. *Cryst. Growth Des.* **2012**, *12*, 1641−1653.
(470) Widdifield, C. M.; Cavallo, G.; Facey, G. A.; Pilati, T.; Lin, J.; Metrangolo, P.; Resnati, G.; Bryce, D. L. Multinuclear Solid-State Magnetic Resonance as a Sensitive Probe of Structural Changes upon the Occurrence of Halogen Bonding in Co-Crystals. *Chem. - Eur. J.* **2013**, *19*, 11949−11962.
(471) Bouchmella, K.; Dutremez, S. G.; Alonso, B.; Mauri, F.; Gervais, C. 1H, 13C, and 15N Solid-State NMR Studies of Imidazole- and Morpholine-Based Model Compounds Possessing Halogen and Hydrogen Bonding Capabilities. *Cryst. Growth Des.* **2008**, *8*, 3941−3950.
(472) Blackstock, S. C.; Lorand, J. P.; Kochi, J. K. Charge-Transfer Interactions of Amines with Tetrahalomethanes. X-Ray Crystal Structures of the Donor-Acceptor Complexes of Quinuclidine and Diazabicyclo [2.2.2]octane with Carbon Tetrabromide. *J. Org. Chem.* **1987**, *52*, 1451−1460.
(473) Bertani, R.; Metrangolo, P.; Moiana, A.; Perez, E.; Pilati, T.; Resnati, G.; Rico-Lattes, I.; Sassi, A. Supramolecular Route to Fluorinated Coatings: Self-Assembly between poly(4-Vinylpyridines) and Haloperfluorocarbons. *Adv. Mater.* **2002**, *14*, 1197−1201.
(474) Weingarth, M.; Raouafi, N.; Jouvelet, B.; Duma, L.; Bodenhausen, G.; Boujlel, K.; Schöllhorn, B.; Tekely, P. Revealing Molecular Self-Assembly and Geometry of Non-Covalent Halogen Bonding by Solid-State NMR Spectroscopy. *Chem. Commun.* **2008**, 5981−5983.
(475) García, M. Á.; Cabildo, P.; Claramunt, R. M.; Pinilla, E.; Rosario Torres, M.; Alkorta, I.; Elguero, J. The Interplay of Hydrogen Bonds and Halogen Bonds in the Structure of NH-Pyrazoles Bearing C-Aryl and C-Halogen Substituents. *Inorg. Chim. Acta* **2010**, *363*, 1332−1342.
(476) Nonappa; Lahtinen, M.; Kolehmainen, E.; Haarala, J.; Shevchenko, A. Evidence of Weak Halogen Bonding: New Insights on Itraconazole and Its Succinic Acid Cocrystal. *Cryst. Growth Des.* **2013**, *13*, 346−351.
(477) Baldrighi, M.; Cavallo, G.; Chierotti, M. R.; Gobetto, R.; Metrangolo, P.; Pilati, T.; Resnati, G.; Terraneo, G. Halogen Bonding and Pharmaceutical Cocrystals: The Case of a Widely Used Preservative. *Mol. Pharmaceutics* **2013**, *10*, 1760−1772.
(478) Bricklebank, N.; Godfrey, S. M.; Mackie, A. G.; McAuliffe, C. A.; Pritchard, R. G.; Kobryn, P. J. Diiodophosphoranes. Synthesis and Structure in the Solid State and in Solution. *J. Chem. Soc., Dalton Trans.* **1993**, 101−103.
(479) Dillon, K. B.; Waddington, T. C. Structures of Some Dihalotriphenylphosphorus(V) Compounds. *Nature, Phys. Sci.* **1971**, *230*, 158−159.
(480) Dahl, T.; Hassel, O. Solid Adducts of Hexamethylenetetramine and Trihalogenomethanes. Crystal Structure of the 1:1 Iodoform Compound. *Acta Chem. Scand.* **1970**, *24*, 377−383.
(481) Metrangolo, P.; Meyer, F.; Resnati, G.; Ursini, M. Haloperfluorocarbons: Versatile Tectons in Halogen Bonding Based Crystal Engineering. *ACS Symp. Ser.* **2005**, *911*, 514−542.
(482) Bertani, R.; Sgarbossa, P.; Venzo, A.; Lelj, F.; Amati, M.; Resnati, G.; Pilati, T.; Metrangolo, P.; Terraneo, G. Halogen Bonding in Metal-Organic-Supramolecular Networks. *Coord. Chem. Rev.* **2010**, *254*, 677−695.
(483) Dey, A.; Metrangolo, P.; Pilati, T.; Resnati, G.; Terraneo, G.; Wlassics, I. The Disorder of Perfluoroalkyl Chains in Crystals: Two Case Histories of Interpretation and Refinement. *J. Fluorine Chem.* **2009**, *130*, 816−823.
(484) Houbenov, N.; Milani, R.; Poutanen, M.; Haataja, J.; Dichiarante, V.; Sainio, J.; Ruokolainen, J.; Resnati, G.; Metrangolo, P.; Ikkala, O. Halogen-Bonded Mesogens Direct Polymer Self-Assemblies up to Millimetre Length Scale. *Nat. Commun.* **2014**, *5*, 4043.
(485) Baldrighi, M.; Bartesaghi, D.; Cavallo, G.; Chierotti, M. R.; Gobetto, R.; Metrangolo, P.; Pilati, T.; Resnati, G.; Terraneo, G. Polymorphs and Co-Crystals of Haloprogin: An Antifungal Agent. *CrystEngComm* **2014**, *16*, 5897−5904.
(486) Botta, C.; Cariati, E.; Cavallo, G.; Dichiarante, V.; Forni, A.; Metrangolo, P.; Pilati, T.; Resnati, G.; Righetto, S.; Terraneo, G.; et al. Fluorine-Induced J-Aggregation Enhances Emissive Properties of a New NLO Push-Pull Chromophore. *J. Mater. Chem. C* **2014**, *2*, 5275−5279.
(487) Martí-Rujas, J.; Meazza, L.; Lim, G. K.; Terraneo, G.; Pilati, T.; Harris, K. D. M.; Metrangolo, P.; Resnati, G. An Adaptable and Dynamically Porous Organic Salt Traps Unique Tetrahalide Dianions. *Angew. Chem., Int. Ed.* **2013**, *52*, 13444−13448.

DOI: 10.1021/acs.chemrev.5b00484
Chem. Rev. 2016, 116, 2478−2601

(488) Abate, A.; Petrozza, A.; Cavallo, G.; Lanzani, G.; Matteucci, F.; Bruce, D. W.; Houbenov, N.; Metrangolo, P.; Resnati, G. Anisotropic Ionic Conductivity in Fluorinated Ionic Liquid Crystals Suitable for Optoelectronic Applications. *J. Mater. Chem. A* **2013**, *1*, 6572−6578.
(489) Priimagi, A.; Saccone, M.; Cavallo, G.; Shishido, A.; Pilati, T.; Metrangolo, P.; Resnati, G. Photoalignment and Surface-Relief-Grating Formation Are Efficiently Combined in Low-Molecular-Weight Halogen-Bonded Complexes. *Adv. Mater.* **2012**, *24*, OP345−OP352.
(490) Metrangolo, P.; Resnati, G.; Pilati, T.; Liantonio, R.; Meyer, F. Engineering Functional Materials by Halogen Bonding. *J. Polym. Sci., Part A: Polym. Chem.* **2007**, *45*, 1−15.
(491) Metrangolo, P.; Resnati, G.; Pilati, T.; Biella, S. Halogen Bonding in Crystal Engineering. *Struct. Bonding (Berlin, Ger.)* **2008**, *126*, 105−136.
(492) Amati, M.; Lelj, F.; Liantonio, R.; Metrangolo, P.; Luzzati, S.; Pilati, T.; Resnati, G. Hybrid Iodoperfluoroalkane-Ferrocene Supramolecular Arrays: The Shortest Contacts Iodine Forms with Nitrogen Atoms and Unsaturated Moieties. *J. Fluorine Chem.* **2004**, *125*, 629−640.
(493) Troff, R. W.; Mäkelä, T.; Topić, F.; Valkonen, A.; Raatikainen, K.; Rissanen, K. Alternative Motifs for Halogen Bonding. *Eur. J. Org. Chem.* **2013**, *2013*, 1617−1637.
(494) Bailey, R. D.; Buchanan, M. L.; Pennington, W. T. Molecular Complexes of 1,4-Diazines with Iodine. *Acta Crystallogr., Sect. C: Cryst. Struct. Commun.* **1992**, *48*, 2259−2262.
(495) Aragoni, M. C.; Arca, M.; Devillanova, F. A.; Hursthouse, M. B.; Huth, S. L.; Isaia, F.; Lippolis, V.; Mancini, A.; Ogilvie, H. R.; Verani, G. Reactions of Pyridyl Donors with Halogens and Interhalogens: An X-Ray Diffraction and FT-Raman Investigation. *J. Organomet. Chem.* **2005**, *690*, 1923−1934.
(496) Batsanov, A. S.; Howard, J. A. K.; Lightfoot, A. P.; Twiddle, S. J. R.; Whiting, A. Stereoselective Chloro-Deboronation Reactions Induced by Substituted Pyridine−Iodine Chloride Complexes. *Eur. J. Org. Chem.* **2005**, *2005*, 1876−1883.
(497) Mascal, M.; Richardson, J. L.; Blake, A. J.; Li, W. Molecular Structure of the S-Triazine-Br2 Complex. *Tetrahedron Lett.* **1996**, *37*, 3505−3506.
(498) Boese, R.; Boese, A. D.; Bláser, D.; Antipin, M. Y.; Ellern, A.; Seppelt, K. The Surprising Crystal Packing of Chlorinefluoride. *Angew. Chem., Int. Ed. Engl.* **1997**, *36*, 1489−1492.
(499) Hassel, O.; Stromme, K. O. Crystal Structure of the Addition Compound 1,4-Dioxan-Chlorine. *Acta Chem. Scand.* **1959**, *13*, 1775−1780.
(500) Ketelaar, J. A. A.; Zwartsenberg, J. W. The Crystal Structure of the Cyanogen Halides. *Recl. Trav. Chim. Pays-Bas* **1939**, *58*, 448−452.
(501) Kempe, R.; Kessenich, E.; Schulz, A. *Inorg. Chem.* **2001**, *40*, 5182−5187.
(502) Bailey, R. D.; Drake, G. W.; Grabarczyk, M.; Hanks, T. W.; Hook, L. L.; Pennington, W. T. Synthesis, Structure and Thermal Decomposition of Nitrogen − Iodine Charge-Transfer Complexes. *J. Chem. Soc., Perkin Trans. 2* **1997**, 2773−2779.
(503) Cecconi, F.; Ghilardi, C. A.; Midollini, S.; Orlandini, A.; Vacca, A. Synthesis, Characterization and X-Ray Structure of the Organomercurial Complex [Hg(C6F5) (np3)](CF3SO3). *Polyhedron* **2001**, *20*, 2885−2888.
(504) Sessler, J. L.; An, D.; Cho, W. S.; Lynch, V. Calix[n]bipyrroles: Synthesis, Characterization, and Anion-Binding Studies. *Angew. Chem., Int. Ed.* **2003**, *42*, 2278−2281.
(505) Pettinari, C.; Pettinari, R.; Marchetti, F.; Macchioni, A.; Zuccaccia, D.; Skelton, B. W.; White, A. H. Synthesis, Reactivity, Spectroscopic Characterization, X-Ray Structures, PGSE, and NOE NMR Studies of (eta5-C5Me5)-Rhodium and -Iridium Derivatives Containing Bis(pyrazolyl)alkane Ligands. *Inorg. Chem.* **2007**, *46*, 896−906.
(506) Tulloch, A. A. D.; Danopoulos, A. A.; Tizzard, G. J.; Coles, S. J.; Hursthouse, M. B.; Hay-Motherwell, R. S.; Motherwell, W. B. Chiral 2,6-Lutidinyl-Biscarbene Complexes of Palladium. *Chem. Commun.* **2001**, 1270−1271.
(507) Oberhauser, W.; Bachmann, C.; Bruggeller, P. PdII and PtII Complexes Containing 1,1,4,7,10,10-Hexaphenyl-1,4,7,10-Tetraphosphadecane: 1st X-Ray Structure of a Pd-Tetraphos Complex. *Polyhedron* **1995**, *14*, 787−792.
(508) Chen, A.-J.; Su, C.-C.; Tsai, F.-Y.; Lee, J.-J.; Huang, T.-M.; Yang, C.-S.; Lee, G.-H.; Wang, Y.; Chen, J.-T. A New Stable Intermediary Mode between η3−2-Aminoallyl Complexes and Metallacyclobutanimines. Synthesis and Structural Characteristic of η3-Azatrimethylenemethane and N-Protonated, N-Alkylated, N-Arylated η3-Azatrimethylenemethane Complexes of Pt and Pd. *J. Organomet. Chem.* **1998**, *569*, 39−54.
(509) Adkine, P.; Cantat, T.; Deschamps, E.; Ricard, L.; Mézailles, N.; Le Floch, P.; Geoffroy, M. EPR and DFT Studies of the One-Electron Reduction Product of Phospholium Cations. *Phys. Chem. Chem. Phys.* **2006**, *8*, 862−868.
(510) Ruiz, J.; Arauz, R.; Riera, V.; Vivanco, M.; Garcia-Granda, S.; Pérez-Carreno, E. Carbene Complexes from Coordinated Bis(diphenylphosphino)methane. Synthesis and X-Ray Structure Determination of the Remarkable Heterotrimetallic Derivative [{Fe(CNPh)4((PPh2)2C)}2Hg]I2. *J. Chem. Soc., Chem. Commun.* **1993**, *94*, 740−742.
(511) Serli, B.; Zangrando, E.; Iengo, E.; Alessio, E. Novel Mono- and Dinuclear Ruthenium Nitrosyls with Coordinated Pyrazine. *Inorg. Chim. Acta* **2002**, *339*, 265−272.
(512) Hill, A. F.; White, A. J. P.; Williams, D. J.; Wilton-ely, J. D. E. T. Synthesis and Reactivity of [TpRh(PPh)] (Tp = Hydridotris(pyrazol-1-Yl)borate). *Organometallics* **1998**, *17*, 3152−3154.
(513) van den Beuken, E. K.; Meetsma, A.; Kooijman, H.; Spek, A. L.; Feringa, B. L. New Palladium, Platinum and Nickel Complexes Based on Rigid Phosphorus and Nitrogen Containing Ligands. *Inorg. Chim. Acta* **1997**, *264*, 171−183.
(514) Stace, J. J.; Lambert, K. D.; Krause, J. A.; Connick, W. B. Rhodium Dimers with 2,2-Dimethyl-1,3-Diisocyano and Bis(diphenylphosphino)methane Bridging Ligands. *Inorg. Chem.* **2006**, *45*, 9123−9131.
(515) Tay, E. P. L.; Kuan, S. L.; Leong, W. K.; Goh, L. Y. Synthetic and X-Ray Structural and Reactivity Studies of Cp*Ru IV Complexes Containing Bidentate Dithiocarbonate, Xanthate, Carbonate, and Phosphinate Ligands (Cp* = eta5-C5Me5). *Inorg. Chem.* **2007**, *46*, 1440−1450.
(516) Hensen, K.; Mayr-Stein, R.; Stumpf, T.; Pickel, P.; Bolte, M.; Fleischer, H. Halogen Exchange and Expulsion: Ligand Stabilized Dihalogen Silicon Dications. *J. Chem. Soc. Dalt. Trans.* **2000**, 473−477.
(517) Iwaoka, M.; Komatsu, H.; Tomoda, S. Structural Characteristics of Areneselenenyl Bromide and Areneselenenyl Chloride Stabilized by Hypervalent Coordination with a Halide Anion in the Solid State. *J. Organomet. Chem.* **2000**, *611*, 164−171.
(518) Hensen, K.; Kettner, M.; Pickel, P.; Bolte, M. New Dicationic Silicon Complexes with N-Methylimidazole. *Z. Naturforsch., B: J. Chem. Sci.* **1999**, *54*, 200−208.
(519) Burchell, T. J.; Eisler, D. J.; Jennings, M. C.; Puddephatt, R. J. Ring-Opening Polymerization of Gold Macrocycles and Self-Assembly of a Coordination Polymer through Hydrogen-Bonding. *Chem. Commun.* **2003**, 2228−2229.
(520) Etter, M. C.; Kress, R. B.; Bernstein, J.; Cash, D. J. Solid-State Chemistry and Structures of a New Class of Mixed Dyes. Cyanine-Oxonol. *J. Am. Chem. Soc.* **1984**, *106*, 6921−6927.
(521) Cowley, A. R.; Dilworth, J. R.; Salichou, M. Syntheses and Structures of Pyrazolylmethane Complexes of rhenium(III), (IV) and (V). *Dalton Trans.* **2007**, 1621−1629.
(522) Song, L. C.; Jin, G. X.; Wang, H. T.; Zhang, W. X.; Hu, Q. M. Self-Assembly of Cationic Pd(II)/Pt(II) Metallomacrocycles Containing Tetrahedral C2Co2 Clusters from Rigid Cluster-Bridged Bipyridine (4-C5H4N)2C2Co 2(CO)6 and Diphosphine- Or Diarsine-Chelated Pd(II)/Pt(II) Complexes [M(dppb)(H2O)2]-[OTf]2 (M = Pd, Pt). *Organometallics* **2005**, *24*, 6464−6471.
(523) Song, R.-F.; Xie, Y.-B.; Li, J.-R.; Bu, X.-H. Formation of Novel Discrete silver(I) Coordination Architectures with Quinoline-Based Monothioethers: Adjusting the Intramolecular Ag?Ag Distances and

DOI: 10.1021/acs.chemrev.5b00484
Chem. Rev. 2016, 116, 2478−2601

Complex Structures by Ligands Modifications and Variations of Counter Anions. *Dalton Trans.* **2003**, *6*, 4742.
(524) Britton, D. 3,5-Dichloro-4-Cyanobenzoic Acid Co-Crystals with Carbon Tetrachloride, Naphthalene, and Anthracene. *J. Chem. Crystallogr.* **2012**, *42*, 851−855.
(525) Mohlen, M.; Neumuller, B.; Dashti-Mommertz, A.; Muller, C.; Massa, W.; Dehnicke, K. On the Tri(phosphorano)borazinium Monocation [H3B3(NPEt3)3Cl2]+. Crystal Structures of Me3-SiNPR3 · BH3 (R = Et, Ph), [H3B3(NPEt3)3Cl1.85Br0.15]Br · CCl4, and of the Product of Hydrolysis NH4[B5O6(OH)4] · 2 H2O. *Z. Anorg. Allg. Chem.* **1999**, *625*, 1631−1637.
(526) Lindeman, S. V.; Hecht, J.; Kochi, J. K. The Charge-Transfer Motif in Crystal Engineering. Self-Assembly of Acentric (diamondoid) Networks from Halide Salts and Carbon Tetrabromide as Electron-Donor/acceptor Synthons. *J. Am. Chem. Soc.* **2003**, *125*, 11597−11606.
(527) Rosokha, S. V.; Lu, J.; Rosokha, T. Y.; Kochi, J. K. Halogen-Bonded Assembly of Hybrid Inorganic/organic 3D-Networks from Dibromocuprate Salts and Tetrabromomethane. *Chem. Commun.* **2007**, *4*, 3383−3385.
(528) Bertolotti, F.; Gervasio, G. Crystal Structure of Iodoform at 106 K and of the Adduct CHI3·3(C9H7N). Iodoform as a Building Block of Co-Crystals. *J. Mol. Struct.* **2013**, *1036*, 305−310.
(529) Pohl, S. Carbon Tetraiodide. *Z. Kristallogr., Kristallgeom., Kristallphys., Kristallchem.* **1982**, *159*, 211.
(530) Asaftei, S.; Reichelt, M.; Reuter, H.; Rosemeyer, H. Synthesis and Crystal Structures of Two 9-(2-Bromoethyl)-Substituted 7-Deazapurines. *Helv. Chim. Acta* **2009**, *92*, 1944−1951.
(531) Abraham, F.; Mernari, B.; Lagrenée, M.; Sueur, S. Structure Cristalline de La Chloro-4 Bis(chlorométhyl)-3,6 Pyridazine. *Acta Crystallogr., Sect. C: Cryst. Struct. Commun.* **1989**, *45*, 1327−1329.
(532) Kieltsch, I.; Eisenberger, P.; Togni, A. Mild Electrophilic Trifluoromethylation of Carbon- and Sulfur-Centered Nucleophiles by a Hypervalent iodine(III)-CF3 Reagent. *Angew. Chem., Int. Ed.* **2007**, *46*, 754−757.
(533) Eisenberger, P.; Gischig, S.; Togni, A. Novel 10-I-3 Hypervalent Iodine-Based Compounds for Electrophilic Trifluoromethylation. *Chem. - Eur. J.* **2006**, *12*, 2579−2586.
(534) Niedermann, K.; Welch, J. M.; Koller, R.; Cvengros, J.; Santschi, N.; Battaglia, P.; Togni, A. New Hypervalent Iodine Reagents for Electrophilic Trifluoromethylation and Their Precursors: Synthesis, Structure, and Reactivity. *Tetrahedron* **2010**, *66*, 5753−5761.
(535) Wang, W. Halogen Bond Involving Hypervalent Halogen: CSD Search and Theoretical Study. *J. Phys. Chem. A* **2011**, *115*, 9294−9299.
(536) Fontana, F.; Forni, A.; Metrangolo, P.; Panzeri, W.; Pilati, T.; Resnati, G. Perfluorocarbon-Hydrocarbon Discrete Intermolecular Aggregates: An Exceptionally Short N···I Contact. *Supramol. Chem.* **2002**, *14*, 47−55.
(537) Cavallo, G.; Metrangolo, P.; Pilati, T.; Resnati, G.; Terraneo, G. Tetraphenylphosphonium Iodide-1,3,5-Trifluoro-2,4,6-Triiodobenzene-Methanol (3/4/1). *Acta Crystallogr., Sect. E: Struct. Rep. Online* **2013**, *69*, o865−o866.
(538) Wasilewska, A.; Gdaniec, M.; Połoński, T. Co-Crystals of Iodopentafluorobenzene with Nitrogen Donors: 2-D Molecular Assemblies through Halogen Bonding and Aryl-Perfluoroaryl Interactions. *CrystEngComm* **2007**, *9*, 203−206.
(539) Metrangolo, P.; Meyer, F.; Pilati, T.; Resnati, G.; Terraneo, G. Mutual Induced Coordination in Halogen-Bonded Anionic Assemblies with (6,3) Cation-Templated Topologies. *Chem. Commun.* **2008**, 1635−1637.
(540) Molski, M. J.; Mollenhauer, D.; Gohr, S.; Paulus, B.; Khanfar, M. A.; Shorafa, H.; Strauss, S. H.; Seppelt, K. Halogenated Benzene Cation Radicals. *Chem. - Eur. J.* **2012**, *18*, 6644−6654.
(541) Huse, G.; Powell, H. M. 266. The Crystal Structure of Picryl Iodide. *J. Chem. Soc.* **1940**, 1398−1402.
(542) Weiss, R.; Schwab, O.; Hampel, F. Ion-Pair Strain as the Driving Force for Hypervalent Adduct Formation between Iodide Ions and Substituted Iodobenzenes: Structural Alternatives to Meisenheimer Complexes. *Chem. - Eur. J.* **1999**, *5*, 968−974.
(543) Ghosh, S.; Reddy, C. M.; Desiraju, G. R. Hexaiodo-Benzene: A Redetermination at 100K. *Acta Crystallogr., Sect. E: Struct. Rep. Online* **2007**, *63*, o910−o911.
(544) Guardigli, C.; Liantonio, R.; Mele, M. L.; Metrangolo, P.; Resnati, G.; Pilati, T. Design and Synthesis of New Tectons for Halogen Bonding-Driven Crystal Engineering. *Supramol. Chem.* **2003**, *15*, 177−188.
(545) White, N. G.; Caballero, A.; Beer, P. D. Observation of Strong Halogen Bonds in the Solid State Structures of Bis-Haloimidazolium Macrocycles. *CrystEngComm* **2014**, *16*, 3722−3729.
(546) Subramanian, T.; Parkin, S.; Spielmann, H. P. Synthesis of Farnesol Analogues Containing Triazoles in Place of Isoprenes through "Click Chemistry. *Synlett* **2012**, *23*, 2539−2543.
(547) Kniep, F.; Rout, L.; Walter, S. M.; Bensch, H. K. V.; Jungbauer, S. H.; Herdtweck, E.; Huber, S. M. 5-Iodo-1,2,3-Triazolium-Based Multidentate Halogen-Bond Donors as Activating Reagents. *Chem. Commun.* **2012**, *48*, 9299−9301.
(548) Brotherton, W. S.; Clark, R. J.; Zhu, L. Synthesis of 5-Iodo-1,4-Disubstituted-1,2,3-Triazoles Mediated by in Situ Generated copper(I) Catalyst and Electrophilic Triiodide Ion. *J. Org. Chem.* **2012**, *77*, 6443−6455.
(549) Dubrovina, N. V.; Domke, L.; Shuklov, I. a.; Spannenberg, A.; Franke, R.; Villinger, A.; Börner, A. New Mono- and Bidentate P-Ligands Using One-Pot Click-Chemistry: Synthesis and Application in Rh-Catalyzed Hydroformylation. *Tetrahedron* **2013**, *69*, 8809−8817.
(550) Mullaney, B. R.; Thompson, A. L.; Beer, P. D. An All-Halogen Bonding Rotaxane for Selective Sensing of Halides in Aqueous Media. *Angew. Chem., Int. Ed.* **2014**, *53*, 11458−11462.
(551) Freytag, M.; Jones, P. G.; Ahrens, B.; Fischer, A. K. Hydrogen Bonding and Halogen-Halogen Interactions in 4-Halopyridinium Halides. *New J. Chem.* **1999**, *23*, 1137−1139.
(552) Haddad, S. F.; Al-Far, R. H. Crystal Structure of Three Isomorphous Compounds of 2,5-Dibromopyridine with tetrahalometalate(II) Ions. *J. Chem. Crystallogr.* **2008**, *38*, 663−669.
(553) Brammer, L.; Espallargas, G. M.; Adams, H. Involving Metals in Halogen-Halogen Interactions: Second-Sphere Lewis Acid Ligands for Perhalometallate Ions (M-X···X′-C). *CrystEngComm* **2003**, *5*, 343−345.
(554) Mínguez Espallargas, G.; Brammer, L.; Sherwood, P. Designing Intermolecular Interactions between Halogenated Peripheries of Inorganic and Organic Molecules: Electrostatically Directed M-X···X′- C Halogen Bonds. *Angew. Chem., Int. Ed.* **2006**, *45*, 435−440.
(555) Awwadi, F. F.; Willett, R. D.; Peterson, K. A.; Twamley, B. The Nature of Halogen···halide Synthons: Theoretical and Crystallographic Studies. *J. Phys. Chem. A* **2007**, *111*, 2319−2328.
(556) Awwadi, F. F.; Taher, D.; Haddad, S. F.; Turnbull, M. M. Competition between Hydrogen and Halogen Bonding Interactions: Theoretical and Crystallographic Studies. *Cryst. Growth Des.* **2014**, *14*, 1961−1971.
(557) Espallargas, G. M.; Zordan, F.; Marín, L. A.; Adams, H.; Shankland, K.; van de Streek, J.; Brammer, L. Rational Modification of the Hierarchy of Intermolecular Interactions in Molecular Crystal Structures by Using Tunable Halogen Bonds. *Chem. - Eur. J.* **2009**, *15*, 7554−7568.
(558) Willett, R. D.; Awwadi, F.; Butcher, R.; Haddad, S.; Twamley, B. The Aryl Bromine - Halide Ion Synthon and Its Role in the Control of the Crystal Structures of Tetrahalocuprate (II) Ions. *Cryst. Growth Des.* **2003**, *3*, 301−311.
(559) Andrews, M. B.; Cahill, C. L. Utilizing Hydrogen Bonds and Halogen−halogen Interactions in the Design of Uranyl Hybrid Materials. *Dalton Trans.* **2012**, *41*, 3911−3914.
(560) Andrews, M. B.; Cahill, C. L. Metal−organic Hybrids Involving the [UO2Cl3(NO3)]2− Tecton and the Role of Halogen Polarizability. *CrystEngComm* **2013**, *15*, 3082−3086.
(561) Surbella, R. G., III; Cahill, C. L. The Exploration of Supramolecular Interactions Stemming from the [UO2(NCS)4-

DOI: 10.1021/acs.chemrev.5b00484
Chem. Rev. 2016, 116, 2478−2601

(H2O)]2− Tecton and Substituted Pyridinium Cations. *CrystEngComm* **2014**, *16*, 2352−2364.
(562) Sayapin, Y. A.; Duong, B. N.; Komissarov, V. N.; Dorogan, I. V.; Makarova, N. I.; Bondareva, I. O.; Tkachev, V. V.; Shilov, G. V.; Aldoshin, S. M.; Minkin, V. I. Synthesis, Structure, and Photoisomerization of Derivatives of 2-(2-Quinolyl)-1,3-Tropolones Prepared by the Condensation of 2-Methylquinolines with 3,4,5,6-Tetrachloro-1,2-Benzoquinone. *Tetrahedron* **2010**, *66*, 8763−8771.
(563) Cametti, M.; Raatikainen, K.; Metrangolo, P.; Pilati, T.; Terraneo, G.; Resnati, G. 2-Iodo-Imidazolium Receptor Binds Oxoanions via Charge-Assisted Halogen Bonding. *Org. Biomol. Chem.* **2012**, *10*, 1329−1333.
(564) Cole, M. L.; Jones, C.; Junk, P. C. Studies of the Reactivity of N-Heterocyclic Carbenes with Halogen and Halide Sources. *New J. Chem.* **2002**, *26*, 1296−1303.
(565) Scheele, U. J.; Dechert, S.; Meyer, F. A Versatile Access to Pyridazines with Tethered Imidazolium Groups-New Precursors for Mono- and Binucleating NHC/pyridazine Hybrid Ligands. *Tetrahedron Lett.* **2007**, *48*, 8366−8370.
(566) Liu, Q.-X.; Song, H.-B.; Xu, F.-B.; Li, Q.-S.; Zeng, X.-S.; Leng, X.-B.; Zhang, Z.-Z. Synthesis, Crystal Structure and Photophysical Properties of N-Heterocyclic Carbene Pd(II), Pt(II) Complexes and Iodine Adduct. *Polyhedron* **2003**, *22*, 1515−1521.
(567) Lauher, J. W.; Fowler, F. W.; Goroff, N. S. Single-Crystal-to-Single-Crystal Topochemical Polymerizations by Design. *Acc. Chem. Res.* **2008**, *41*, 1215−1229.
(568) Dumele, O.; Wu, D.; Trapp, N.; Goroff, N. S.; Diederich, F. Halogen Bonding of (Iodoethynyl)benzene Derivatives in Solution. *Org. Lett.* **2014**, *16*, 4722−4725.
(569) Jin, H.; Plonka, A. M.; Parise, J. B.; Goroff, N. S. Pressure Induced Topochemical Polymerization of Diiodobutadiyne: A Single-Crystal-to-Single-Crystal Transformation. *CrystEngComm* **2013**, *15*, 3106−3110.
(570) Miao, Z.; Xu, M.; Hoffmann, B.; Bernet, B.; Vasella, A. Functionalised Bicyclic Exo-Glycals by Alkynol Cycloisomerisation of Hydroxy 1,3-Diynes and Hydroxy Haloalkynes. *Helv. Chim. Acta* **2005**, *88*, 1885−1912.
(571) Braje, W. M.; Frackenpohl, J.; Schrake, O.; Wartchow, R.; Beil, W.; Hoffmann, H. M. R. Synthesis of 10,11-Didehydro Cinchona Alkaloids and Key Derivatives. *Helv. Chim. Acta* **2000**, *83*, 777−792.
(572) Kawai, H.; Utamura, T.; Motoi, E.; Takahashi, T.; Sugino, H.; Tamura, M.; Ohkita, M.; Fujiwara, K.; Saito, T.; Tsuji, T.; et al. Hydrindacene-Based Acetylenic Macrocycles with Horizontally and Vertically Ordered Functionality Arrays. *Chem. - Eur. J.* **2013**, *19*, 4513−4524.
(573) González, L.; Gimeno, N.; Tejedor, R. M.; Polo, V.; Ros, M. B.; Uriel, S.; Serrano, J. L. Halogen-Bonding Complexes Based on Bis(iodoethynyl)benzene Units: A New Versatile Route to Supramolecular Materials. *Chem. Mater.* **2013**, *25*, 4503−4510.
(574) Barrès, A.-L.; El-Ghayoury, A.; Zorina, L. V.; Canadell, E.; Auban-Senzier, P.; Batail, P. The 8:1: 1 Ternary Hybrid Framework in the System [EDT-TTF +][1,4-bis(iodoethynyl)benzene][Re6Se8(CN)6]4-: Dual Noncovalent Expression of the Octahedral Halogen-Bond Hexa-Acceptor Nanonode. *Chem. Commun.* **2008**, *8*, 2194−2196.
(575) Yamamoto, H. M.; Yamaura, J. I.; Kato, R. Multicomponent Molecular Conductors with Supramolecular Assembly: Iodine-Containing Neutral Molecules as Building Blocks. *J. Am. Chem. Soc.* **1998**, *120*, 5905−5913.
(576) Fourmigué, M.; Batail, P. Activation of Hydrogen- and Halogen-Bonding Interactions in Tetrathiafulvalene-Based Crystalline Molecular Conductors. *Chem. Rev.* **2004**, *104*, 5379−5418.
(577) Koskinen, L.; Hirva, P.; Kalenius, E.; Jääskeläinen, S.; Rissanen, K.; Haukka, M. Halogen Bonds with Coordinative Nature: Halogen Bonding in a S−I+−S Iodonium Complex. *CrystEngComm* **2015**, *17*, 1231−1236.
(578) Neverov, A. A.; Brown, R. S. Mechanistic Evaluation of the Transfer of Br+ from Bis(sym-Collidine)bromonium Triflate to Acceptor Alkenes. *J. Org. Chem.* **1998**, *63*, 5977−5982.
(579) Nosco, D. L.; Heeg, M. J.; Glick, M. D.; Elder, R. C.; Deutsch, E. Coordination Stabilization of Organic Intermediates. Crystal Structure of {[(en)2Co(SCH2CH2NH2)]2I}(NO3)5.4H2O, a Stable Complex of iodine(I). *J. Am. Chem. Soc.* **1980**, *102*, 7784−7786.
(580) Manjare, S. T.; Singh, H. B.; Butcher, R. J. Oxidation of Carbene-Derived Selenium Diiodide with Silver Tetrafluoroborate − Isolation of Iodonium Ion Complexes with Selones. *Eur. J. Inorg. Chem.* **2013**, *2013*, 2161−2166.
(581) Kotali, E.; Varvoglis, A.; Bozopoulos, A.; Rentzeperis, P. A Stable Dibenzoiodolyl Pyrrolidinedithiocarbamate. *J. Chem. Soc., Chem. Commun.* **1985**, 1819−1820.
(582) Antos, A.; Elemes, Y.; Michaelides, A.; Nyxas, J. a.; Skoulika, S.; Hadjiarapoglou, L. P. The Question of Electrophilic vs Nucleophilic Addition of Cyclic β-Dicarbonyl Phenyliodonium Ylides: Electrophilic Cycloaddition of Diphenylketene. *J. Org. Chem.* **2012**, *77*, 10949−10954.
(583) Batchelor, R. J.; Birchall, T.; Sawyer, J. F. Crystal Structure and Iodine-127 Moessbauer Spectrum of Diphenyliodonium-2-Carboxylate Hydrate, C13H9IO2·H2O: Secondary vs. Hydrogen Bonding. *Inorg. Chem.* **1986**, *25*, 1415−1420.
(584) Justik, M. W.; Protasiewicz, J. D.; Updegraff, J. B. Preparation and X-Ray Structures of 2-[(aryl)iodonio]benzenesulfonates: Novel Diaryliodonium Betaines. *Tetrahedron Lett.* **2009**, *50*, 6072−6075.
(585) Ochiai, M.; Miyamoto, K.; Suefuji, T.; Shiro, M.; Sakamoto, S.; Yamaguchi, K. Synthesis and Structure of Supramolecular Complexes between 1-Alkynyl(phenyl) (tetrafluoroborato)-λ3-Iodanes and 18-Crown-6. *Tetrahedron* **2003**, *59*, 10153−10158.
(586) Ochiai, M.; Suefuji, T.; Miyamoto, K.; Shiro, M. Solid State Structures of Pentacoordinated lambda3-Iodanes with a Trigonal Bipyramidal Geometry: Synthesis of Diphenyl- and Alkynyl(phenyl)-lambda3-Iodane Complexes with 1,10-Phenanthroline. *Chem. Commun.* **2003**, *120*, 1438−1439.
(587) Ochiai, M.; Nakano, A.; Yoshimura, A.; Miyamoto, K.; Hayashi, S.; Nakanishi, W. Imido Transfer of Sulfonylimino-lambda3-Bromane Makes Possible the Synthesis of Sulfonylimino-lambda3-Iodanes. *Chem. Commun.* **2009**, 959−961.
(588) Ochiai, M.; Miyamoto, K.; Yokota, Y.; Suefuji, T.; Shiro, M. Synthesis, Characterization, and Reaction of Crown Ether Complexes of Aqua(hydroxy) (aryl)iodonium Ions. *Angew. Chem., Int. Ed.* **2004**, *44*, 75−78.
(589) Ochiai, M.; Suefuji, T.; Miyamoto, K.; Tada, N.; Goto, S.; Shiro, M.; Sakamoto, S.; Yamaguchi, K. Secondary Hypervalent I(III)···O Interactions: Synthesis and Structure of Hypervalent Complexes of Diphenyl-lambda(3)-Iodanes with 18-Crown-6. *J. Am. Chem. Soc.* **2003**, *125*, 769−773.
(590) Dixon, L. I.; Carroll, M. a.; Gregson, T. J.; Ellames, G. J.; Harrington, R. W.; Clegg, W. Synthesis and Reactivity of Aryl-(alkynyl)iodonium Salts. *Eur. J. Org. Chem.* **2013**, *2013*, 2334−2345.
(591) Murray, S. J.; Müller-Bunz, H.; Ibrahim, H. Congested C2-Symmetric Aryliodanes Based on an Anti-Dimethanoanthracene Backbone. *Chem. Commun.* **2012**, *48*, 6268.
(592) Frohn, H.-J.; Wenda, A.; Flörke, U. [(C6F5)2IF2][BF4], the First Salt with the Electrophilic Cation [(C6F5)2IF2]+: Synthesis, Reactivity, and Structure. *Z. Anorg. Allg. Chem.* **2008**, *634*, 764−770.
(593) Hoyer, S.; Seppelt, K. Phenyliodine(V) Fluorides. *J. Fluorine Chem.* **2004**, *125*, 989−996.
(594) Hirschberg, M. E.; Barthen, P.; Frohn, H.-J.; Bläser, D.; Tobey, B.; Jansen, G. Interaction of the Electrophilic Bis(pentafluorophenyl)-iodonium Cation [(C6F5)2I]+ with the Ambident Pseudohalogenide Anions [SCN]− and [CN]−. *J. Fluorine Chem.* **2014**, *163*, 28−33.
(595) Raatikainen, K.; Rissanen, K. Interaction between Amines and N-Haloimides: A New Motif for Unprecedentedly Short Br···N and I···N Halogen Bonds. *CrystEngComm* **2011**, *13*, 6972−6977.
(596) Padmanabhan, K.; Paul, I. C.; Curtin, D. Y. Structure of N-Lodosuccinimide. *Acta Crystallogr., Sect. C: Cryst. Struct. Commun.* **1990**, *C46*, 88−92.
(597) Svensson, C.; Albertsson, J.; Eberson, L. Structure of Tetraethylammonium Mono(N-Bromo-succinimide)bromate(1-). *Acta Chem. Scand.* **1988**, *42b*, 596−600.

DOI: 10.1021/acs.chemrev.5b00484
Chem. Rev. 2016, 116, 2478−2601

(598) Elding, M.; Albertsson, J.; Svensson, G.; Eberson, L. Organic 'Hypervalent' Bromine Compounds: the Structure of a Linear N-Bromotetramethylsuccinimide-Tetramethylsuccinimidate Complex in the Solid State. *Acta Chem. Scand.* **1990**, *44*, 135−138.
(599) Crowston, E. H.; Lobo, A. M.; Parbhakar, S.; Rzepa, H. S.; Williams, D. J. X-Ray and SCF-MO Model Study of the Complex Formed between N-Bromosuccinimide and 1,4-Diazabicyclo[2.2.2]-octane. *J. Chem. Soc., Chem. Commun.* **1984**, 276−278.
(600) Imakubo, T.; Sawa, H.; Kato, R. Novel Radical Cation Salts of Organic Pi-Donors Containing Iodine Atom(s): The First Application of Strong Intermolecular-I···X-(X = CN, Halogen Atom) Interaction to Molecular Conductors. *Synth. Met.* **1995**, *73*, 117−122.
(601) Devic, T.; Domercq, B.; Auban-senzier, P.; Molinié, P.; Fourmigué, T.M. Cyano-Halogen Interactions in [EDT-TTF-I]2[Ni-(mnt)2] and [EDT-TTF-I2]2[Ni(mnt)2] and Geometrical Evolutions within Mixed-Valence or Fully Oxidized TTF Dyads. *Eur. J. Inorg. Chem.* **2002**, *2002*, 2844−2849.
(602) Fourmigué, M. Halogen Bonding in Conducting or Magnetic Molecular Materials. In *Halogen Bonding. Fundamentals and Applications*; Metrangolo, P., Resnati, G., Eds.; Springer: Berlin, Heidelberg, 2008; Vol. *126*, pp 181−207.
(603) Hosokoshi, Y.; Tamura, M.; Nozawa, K.; Suzuki, S.; Kinoshita, M.; Sawa, H.; Kato, R. Magnetic Properties and Crystal Structures of 2-Hydro and 2-Halo Nitronyl Nitroxide Radical Crystals. *Synth. Met.* **1995**, *71*, 1795−1796.
(604) Zhu, S.; Xing, C.; Xu, W.; Li, Z. Hydrogen Bonding and Halogen Bonding Co-Existing in the Reaction of Heptafluorobenzyl Iodide with N,N,N′,N′-Tetramethylethylene Diamine. *Tetrahedron Lett.* **2004**, *45*, 777−780.
(605) Peuronen, A.; Valkonen, A.; Kortelainen, M.; Rissanen, K.; Lahtinen, M. Halogen Bonding-Based Catch and Release: Reversible Solid-State Entrapment of Elemental Iodine with Monoalkylated DABCO Salts. *Cryst. Growth Des.* **2012**, *12*, 4157−4169.
(606) Raatikainen, K.; Rissanen, K. Hierarchical Halogen Bonding Induces Polymorphism. *CrystEngComm* **2009**, *11*, 750−752.
(607) Huang, Q.; Wang, Z.; Chu, Q.; Zhu, S. Crystal Structure of a Supramolecular Complex Formed between 1-Bromo-2-Iodo-Tetrafluoroethane and N,N,N′,N′-Tetramethyl- Ethylenediamine. *J. Inclusion Phenom. Mol. Recognit. Chem.* **2006**, *54*, 177−180.
(608) Cinčić, D.; Friščić, T.; Jones, W. Structural Equivalence of Br and I Halogen Bonds: A Route to Isostructural Materials with Controllable Properties. *Chem. Mater.* **2008**, *20*, 6623−6626.
(609) Cinčić, D.; Friščić, T.; Jones, W. A Stepwise Mechanism for the Mechanochemical Synthesis of Halogen-Bonded Cocrystal Architectures. *J. Am. Chem. Soc.* **2008**, *130*, 7524−7525.
(610) Boubekeur, K.; Syssa-Magalé, J. L.; Palvadeau, P.; Schöllhorn, B. Self-Assembly of Nitroxide Radicals via Halogen Bonding-Directional NO· ···I Interactions. *Tetrahedron Lett.* **2006**, *47*, 1249−1252.
(611) Raatikainen, K.; Rissanen, K. Modulation of N···I and + N-H··· Cl-···I Halogen Bonding: Folding, Inclusion, and Self-Assembly of Tri- and Tetraamino Piperazine Cyclophanes. *Cryst. Growth Des.* **2010**, *10*, 3638−3646.
(612) Bhattacharya, S.; Saha, B. K. Isostructurality in the Guest Free Forms and in the Clathrates of 1,3,5-Triethyl-2,4,6-tris(4-Halophenoxy)methylbenzenes. *Cryst. Growth Des.* **2012**, *12*, 169−178.
(613) Bertani, R.; Chaux, F.; Gleria, M.; Metrangolo, P.; Milani, R.; Pilati, T.; Resnati, G.; Sansotera, M.; Venzo, A. Supramolecular Rods via Halogen Bonding-Based Self-Assembly of Fluorinated Phosphazene Nanopillars. *Inorg. Chim. Acta* **2007**, *360*, 1191−1199.
(614) Ji, B.; Wang, W.; Deng, D.; Zhang, Y. Symmetrical Bifurcated Halogen Bond: Design and Synthesis. *Cryst. Growth Des.* **2011**, *11*, 3622−3628.
(615) de Lima Ferreira, M.; de Souza, M. V. N.; Wardell, S. M. S. V; Wardell, J. L.; Tiekink, E. R. T. N-(4-Bromophenyl)pyrazine-2-Carboxamide. *Acta Crystallogr., Sect. E: Struct. Rep. Online* **2010**, *66*, o2722−o2723.
(616) Vodak, D. T.; Kim, K.; Iordanidis, L.; Rasmussen, P. G.; Matzger, A. J.; Yaghi, O. M. Computation of Aromatic C3N4 Networks and Synthesis of the Molecular Precursor N(C3N3)3Cl 6. *Chem. - Eur. J.* **2003**, *9*, 4197−4201.
(617) Tragl, S.; Gibson, K.; Meyer, H. J. HN(C3N3Cl2)2 Und N(C 3N3Cl2)3 - Mögliche Molekulare Zwischenstufen Bei Der Synthese von kohlenstoff(IV)-Nitriden. *Z. Anorg. Allg. Chem.* **2004**, *630*, 2373−2376.
(618) Aakeröy, C. B.; Wijethunga, T. K.; Haj, M. A.; Desper, J.; Moore, C. The Structural Landscape of Heteroaryl-2-Imidazoles: Competing Halogen- and Hydrogen-Bond Interactions. *CrystEngComm* **2014**, *16*, 7218−7225.
(619) Wang, D. Y.; You, L. Y.; Wang, J. L.; Wang, H.; Zhang, D. W.; Li, Z. T. Complexation of Two Macrocycles for Amide, Saccharide, and Halide Derivatives: The Capacity of 1,2,3-Triazole as Hydrogen and Halogen Bonding Acceptors. *Tetrahedron Lett.* **2013**, *54*, 6967−6970.
(620) Gainsford, G. J.; Mason, J. M.; Gulab, S. A. 7-Benzyloxymethyl-9-bromo-6-chloro-9-deazapurine. *Acta Crystallogr., Sect. E: Struct. Rep. Online* **2010**, *66*, o13810.1107/S1600536809050879
(621) Schlemper, E. O.; Britton, D. The Crystal Structure of P-Iodobenzonitrile. *Acta Crystallogr.* **1965**, *18*, 419−424.
(622) Metrangolo, P.; Pilati, T.; Resnati, G.; Stevenazzi, A. Metric Engineering of Perfluorocarbon-Hydrocarbon Layered Solids Driven by the Halogen Bonding. *Chem. Commun.* **2004**, 1492−1493.
(623) Bond, A. D.; Griffiths, J.; Rawson, J. M.; Hulliger, J. Inducing Structural Polarity Using Fluorinated Organics: X-Ray Crystal Structures of P-XC6F4CN (X = Cl, Br, I). *Chem. Commun.* **2001**, 2488−2489.
(624) Hatlevik, Ø.; Arif, A. M.; Miller, J. S. Synthesis and Characterization of hexakis(acetonitrile)chromium(III) Tetrafluoroborate, [CrIII(NCMe)6][BF4] 3. A Nonaqueous CrIII Source. *J. Phys. Chem. Solids* **2004**, *65*, 61−63.
(625) Niedzicki, L.; Karpierz, E.; Zawadzki, M.; Dranka, M.; Kasprzyk, M.; Zalewska, A.; Marcinek, M.; Zachara, J.; Domańska, U.; Wieczorek, W. Lithium Cation Conducting TDI Anion-Based Ionic Liquids. *Phys. Chem. Chem. Phys.* **2014**, *16*, 11417−11425.
(626) Liu, M.-G.; Ni, C.-L. Bis[(4-Bromo-2-Fluorobenzyl)-triphenylphosphonium] bis(1,2-Dicyanoethene-1,2-dithiolato)-nickelate(II). *Acta Crystallogr., Sect. E: Struct. Rep. Online* **2006**, *62*, m2851−m2852.
(627) Purushothaman, M.; Thanigaimani, K.; Arshad, S.; Silambarasan, S.; Razak, I. A.; Ali, K. M. S. 2,6-Diamino-4-(4-Chlorophenyl)-1-Methyl-1,4-Dihydropyridine-3,5-Dicarbonitrile. *Acta Crystallogr., Sect. E: Struct. Rep. Online* **2014**, *70*, o812−o813.
(628) Delgado-Rebollo, M.; Canseco-Gonzalez, D.; Hollering, M.; Mueller-Bunz, H.; Albrecht, M. Synthesis and Catalytic Alcohol Oxidation and Ketone Transfer Hydrogenation Activity of Donor-Functionalized Mesoionic Triazolylidene ruthenium(II) Complexes. *Dalton Trans.* **2014**, *43*, 4462−4473.
(629) Barnes, N. A.; Flower, K. R.; Fyyaz, S. A.; Godfrey, S. M.; Mcgown, A. T.; Miles, P. J.; Pritchard, R. G.; Warren, J. E. Can the Solid State Structures of the Dihalogen Adducts R3EX2 (E = P, As; R = Alkyl, Aryl; X = Br, I) with the Molecular Spoke Geometry Be Considered Good Mimics of the gold(I) Systems [(R3E)AuX] (E = As, P; R = Alkyl, Aryl; X = Cl, Br, I)? *CrystEngComm* **2010**, *12*, 784−794.
(630) Barnes, N. A.; Flower, K. R.; Godfrey, S. M.; Hurst, P. A.; Khan, R. Z.; Pritchard, R. G. Structural Relationships between O-, M- and P-Tolyl Substituted R3EI2 (E = As, P) and [(R3E)AuX] (E = As, P; X = Cl, Br, I). *CrystEngComm* **2010**, *12*, 4240.
(631) Aakeröy, C. B.; Schultheiss, N. C.; Rajbanshi, A.; Desper, J.; Moore, C. Supramolecular Synthesis Based on a Combination of Hydrogen and Halogen Bonds. *Cryst. Growth Des.* **2009**, *9*, 432−441.
(632) Aakeröy, C. B.; Panikkattu, S.; Chopade, P. D.; Desper, J. Competing Hydrogen-Bond and Halogen-Bond Donors in Crystal Engineering. *CrystEngComm* **2013**, *15*, 3125−3136.
(633) Moss, D. K.; Spence, J. D.; Nantz, M. H. Effects of Propargylic Substitution and Annelation on the Cycloaromatization of a Bicyclo[7.3.1] Enediyne. *J. Org. Chem.* **1999**, *64*, 4339−4343.

DOI: 10.1021/acs.chemrev.5b00484
Chem. Rev. 2016, 116, 2478−2601

(634) Vasylyeva, V.; Nayak, S. K.; Terraneo, G.; Cavallo, G.; Metrangolo, P.; Resnati, G. Orthogonal Halogen and Hydrogen Bonds Involving a Peptide Bond Model. *CrystEngComm* **2014**, *16*, 8102−8105.
(635) Choi, H. D.; Seo, P. J.; Lee, U. 2-(4-Fluorophenyl)-5-Iodo-3-Isopropylsulfonyl-1-Benzofuran. *Acta Crystallogr., Sect. E: Struct. Rep. Online* **2012**, *68*, o3192.
(636) Britton, D. 2,3,5,6-Tetrafluoro-1,4-Diiodobenzene−dimethyl Sulfoxide (1/1). *Acta Crystallogr., Sect. E: Struct. Rep. Online* **2003**, *59*, o1332−o1333.
(637) Eccles, K. S.; Morrison, R. E.; Stokes, S. P.; O'Mahony, G. E.; Hayes, J. A.; Kelly, D. M.; O'Boyle, N. M.; Fabian, L.; Moynihan, H. A.; Maguire, A. R.; Lawrence, S. E. Utilizing Sulfoxide···Iodine Halogen Bonding for Cocrystallization. *Cryst. Growth Des.* **2012**, *12*, 2969−2977.
(638) Takemura, A.; McAllister, L. J.; Karadakov, P. B.; Pridmore, N. E.; Whitwood, A. C.; Bruce, D. W. Competition and Cooperation: Hydrogen and Halogen Bonding in Co-Crystals Involving 4-Iodotetrafluorobenzoic Acid, 4-Iodotetrafluorophenol and 4-Bromotetrafluorophenol. *CrystEngComm* **2014**, *16*, 4254−4264.
(639) Tuikka, M.; Hirva, P.; Rissanen, K.; Korppi-Tommola, J.; Haukka, M. Halogen Bonding-a Key Step in Charge Recombination of the Dye-Sensitized Solar Cell. *Chem. Commun.* **2011**, *47*, 4499−4501.
(640) Tamilselvi, A.; Mugesh, G. Interaction of Heterocyclic Thiols/thiones Eliminated from Cephalosporins with Iodine and Its Biological Implications. *Bioorg. Med. Chem. Lett.* **2010**, *20*, 3692−3697.
(641) Mueller, B.; Takaluoma, T. T.; Laitinen, R. S.; Seppelt, K. Syntheses and Structures of Two Dimethyl Diselenide−Diiodine Adducts and the First Well Characterized Diorgano Disulfide−Nitrosonium Adduct. *Eur. J. Inorg. Chem.* **2011**, *2011*, 4970−4977.
(642) Faoro, E.; de Oliveira, G. M.; Lang, E. S. Attainment of New TeII and TeIV Iodides by Unexpected Removal of the Mesityl Group of [mesTeI2]−: Synthesis and Structural Features of [TeI4][Co(en)3] · I, [TeI6][Co(en)3] · I, [{TeI6}{Te2I10}][Co(NH3)6]2 · 2I · 6H2O and [(mesTeI2)2(μ-I2)][Co(bpy)3] · I3. *Polyhedron* **2009**, *28*, 63−68.
(643) Aullón, G.; Bellamy, D.; Brammer, L.; Bruton, E. A.; Guy Orpen, A. Metal-Bound Chlorine Often Accepts Hydrogen Bonds. *Chem. Commun.* **1998**, 653−654.
(644) Zordan, F.; Brammer, L.; Sherwood, P. Supramolecular Chemistry of Halogens: Complementary Features of Inorganic (M-X) and Organic (C-X′) Halogens Applied to M-X···X′-C Halogen Bond Formation. *J. Am. Chem. Soc.* **2005**, *127*, 5979−5989.
(645) Johnson, M. T.; Džolić, Z.; Cetina, M.; Wendt, O. F.; Öhrström, L.; Rissanen, K. Neutral Organometallic Halogen Bond Acceptors: Halogen Bonding in Complexes of PCPPdX (X = Cl, Br, I) with Iodine (I2), 1,2-Diiodotetrafluorobenzene (F4DIBz), and 1,4-Diiodooctafluorobutane (F8DIBu). *Cryst. Growth Des.* **2012**, *12*, 362−368.
(646) Bakhmutov, V. I. *Dihydrogen Bond: Principles, Experiments, and Applications*; Wiley-Interscience: Hoboken, NJ, 2008.
(647) Smith, D. A.; Brammer, L.; Hunter, C. A.; Perutz, R. N. Metal Hydrides Form Halogen Bonds: Measurement of Energetics of Binding. *J. Am. Chem. Soc.* **2014**, *136*, 1288−1291.
(648) Jenny, N. M.; Wang, H.; Neuburger, M.; Fuchs, H.; Chi, L.; Mayor, M. Synthesis and Solid-State Investigations of Oligo-Phenylene−Ethynylene Structures with Halide End-Groups. *Eur. J. Org. Chem.* **2012**, *2012*, 2738−2747.
(649) Shen, Q. J.; Pang, X.; Zhao, X. R.; Gao, H. Y.; Sun, H.-L.; Jin, W. J. Phosphorescent Cocrystals Constructed by 1,4-Diiodotetrafluorobenzene and Polyaromatic Hydrocarbons Based on C−I···π Halogen Bonding and Other Assisting Weak Interactions. *CrystEngComm* **2012**, *14*, 5027−5034.
(650) Chiappe, C.; Lenoir, D.; Silvio Pomelli, C.; Bianchini, R. Influence of Alkene Structure on the Stability of alkene−Br2 Complexes: Effect of Chlorine Substitution. *Phys. Chem. Chem. Phys.* **2004**, *6*, 3235−3240.
(651) Vasilyev, A. V.; Lindeman, S. V.; Kochi, J. K. Molecular Structures of the Metastable Charge-Transfer Complexes of Benzene (and Toluene) with Bromine as the Pre-Reactive Intermediates in Electrophilic Aromatic Bromination. *New J. Chem.* **2002**, *26*, 582−592.
(652) Resnati, G.; Metrangolo, P.; Pilati, T.; Biella, S.; Terraneo, G. Anion Coordination under Halogen Bonding Control. *Abstract of Papers*, 238th ACS National Meeting, Washington, DC, Aug 16−20, 2009; American Chemical Society: Washington, DC, 2009; ORGN-143.
(653) Farnham, W. B.; Dixon, D. a; Calabrese, J. C. Novel Fluorine-Bridged Polyfluorinated Iodine Structures. Presence of Fluorine as the Central Atom in a Five-Center, Six-Electron Bond. *J. Am. Chem. Soc.* **1988**, *110*, 8453−8461.
(654) Mercurio, J. M.; Knighton, R. C.; Cookson, J.; Beer, P. D. Halotriazolium Axle Functionalised [2]Rotaxanes for Anion Recognition: Investigating the Effects of Halogen-Bond Donor and Preorganisation. *Chem. - Eur. J.* **2014**, *20*, 11740−11749.
(655) Mullen, K. M.; Mercurio, J.; Serpell, C. J.; Beer, P. D. Exploiting the 1,2,3-Triazolium Motif in Anion-Templated Formation of a Bromide-Selective Rotaxane Host Assembly. *Angew. Chem., Int. Ed.* **2009**, *48*, 4781−4784.
(656) Caballero, A.; Swan, L.; Zapata, F.; Beer, P. D. Iodide-Induced Shuttling of a Halogen- and Hydrogen-Bonding Two-Station Rotaxane. *Angew. Chem., Int. Ed.* **2014**, *53*, 11854−11858.
(657) Langton, M. J.; Robinson, S. W.; Marques, I.; Félix, V.; Beer, P. D. Halogen Bonding in Water Results in Enhanced Anion Recognition in Acyclic and Rotaxane Hosts. *Nat. Chem.* **2014**, *6*, 1039−1043.
(658) Caballero, A.; Zapata, F.; White, N. G.; Costa, P. J.; Félix, V.; Beer, P. D. A Halogen-Bonding Catenane for Anion Recognition and Sensing. *Angew. Chem., Int. Ed.* **2012**, *51*, 1876−1880.
(659) Freytag, M.; Jones, P. G. Hydrogen Bonds C − H···Cl as a Structure-Determining Factor in the gold(I) Complex Bis (3-bromopyridine)gold(I) dichloroaurate(I). *Chem. Commun.* **2000**, 277−278.
(660) Valle, G.; Ettorre, R. Bis(3-Bromoimidazolium) tetrachloropalladate(II). *Acta Crystallogr., Sect. C: Cryst. Struct. Commun.* **1994**, *50*, 1221−1222.
(661) Boyall, A. J.; Dillon, K. B.; Howard, J. a K.; Monks, P. K.; Thompson, A. L. Novel (n + 1 + 1) Cycloaddition Reactions; the Formation of Cyclic Tetraphosphonium Dications with Four Linked Phosphorus Atoms and an Organic Backbone. *Dalton Trans.* **2007**, 1374−1376.
(662) Imakubo, T.; Tajima, N.; Tamura, M.; Kato, R.; Nishio, Y.; Kajita, K. A Supramolecular Superconductor θ-(DIETS)2[Au(CN)4]. *J. Mater. Chem.* **2002**, *12*, 159−161.
(663) Ghassemzadeh, M.; Harms, K.; Dehnicke, K. Complexes of Halide Ions with 1-Halogen-2-Phenylacetylenes. *Chem. Ber.* **1996**, *129*, 115−120.
(664) Ghassemzadeh, M.; Harms, K.; Dehnicke, K. Komplexe von Halogenid-Ionen Mit Diiodacetylen. Die Kristallstrukturen von PPh4[X(I-C≡C-I)2] Mit X = Cl, Br, I. *Chem. Ber.* **1996**, *129*, 259−262.
(665) Yamamoto, H. M.; Yamaura, J.; Kato, R. Structural and Electrical Properties of (BEDT-TTF)2X(diiodoacetylene) (X = Cl, Br): The Novel Self-Assembly of Neutral Lewis-Acidic Molecules and Halide Anions in a Molecular Metal. *J. Mater. Chem.* **1998**, *8*, 15−16.
(666) Imakubo, T.; Sawa, H.; Kato, R. Novel Molecular Conductors, (DIETS)4M(CN)4 (M Donor-Anion Contacts by -I-NC- Interaction. *J. Chem. Soc., Chem. Commun.* **1995**, *4*, 1667−1668.
(667) Bock, H.; Holl, S. Interaction in Molecular Crystals. 179. Sigma-Donor-Acceptor Complexes of Tetraiodoethene in Tetra(n-butyl)ammonium Halide Salts. *Z. Naturforsch., B: J. Chem. Sci.* **2002**, *57*, 713−725.
(668) Mugnaini, V.; Punta, C.; Liantonio, R.; Metrangolo, P.; Recupero, F.; Resnati, G.; Pedulli, G. F.; Lucarini, M. Noncovalent Paramagnetic Complexes: Detection of Halogen Bonding in Solution by ESR Spectroscopy. *Tetrahedron Lett.* **2006**, *47*, 3265−3269.
(669) Cavallotti, C.; Metrangolo, P.; Meyer, F.; Recupero, F.; Resnati, G. Binding Energies and 19F Nuclear Magnetic Deshielding in Paramagnetic Halogen-Bonded Complexes of TEMPO with Haloperfluorocarbons. *J. Phys. Chem. A* **2008**, *112*, 9911−9918.

DOI: 10.1021/acs.chemrev.5b00484
Chem. Rev. 2016, 116, 2478−2601

(670) Hervé, K.; Cador, O.; Golhen, S.; Costuas, K.; Halet, J.-F.; Shirahata, T.; Muto, T.; Imakubo, T.; Miyazaki, A.; Ouahab, L. Iodine Substituted Tetrathiafulvalene Radical Cation Salts with [M(isoq)2-(NCS)4]- Anions Where M = CrIII, GaIII: Role of I···S and S···S Contacts on Structural and Magnetic Properties. *Chem. Mater.* **2006**, *18*, 790−797.
(671) Shirahata, T.; Kibune, M.; Maesato, M.; Kawashima, T.; Saito, G.; Imakubo, T. New Organic Conductors Based on Dibromo- and Diiodo-TSeFs with Magnetic and Non-Magnetic MX4 Counter Anions (M = Fe, Ga; X = Cl, Br). *J. Mater. Chem.* **2006**, *16*, 3381−3390.
(672) Nishijo, J.; Ogura, E.; Yamaura, J.; Miyazaki, A.; Enoki, T.; Takano, T.; Kuwatani, Y.; Iyoda, M. Molecular Metals with Ferromagnetic Interaction between Localized Magnetic Moments. *Solid State Commun.* **2000**, *116*, 661−664.
(673) Imakubo, T.; Sawa, H.; Kato, R. Synthesis and Crystal Structure of the Molecular Metal Based on Iodine-Bonded Pi-Donor, (IEDT)[Pd(dmit)2]. *J. Chem. Soc., Chem. Commun.* **1995**, 1097−1098.
(674) Le Questel, J.-Y.; Laurence, C.; Graton, J. Halogen-Bond Interactions: A Crystallographic Basicity Scale towards Iodoorganic Compounds. *CrystEngComm* **2013**, *15*, 3212−3221.
(675) Lehn, J. M. Supramolecular Chemistry. *Science* **1993**, *260*, 1762−1763.
(676) Bosman, A. W.; Sijbesma, R. P.; Meijer, E. W. Supramolecular Polymers at Work. *Mater. Today* **2004**, *7*, 34−39.
(677) Bohne, C. Supramolecular Dynamics. *Chem. Soc. Rev.* **2014**, *43*, 4037−4050.
(678) Stupp, S. I.; Palmer, L. C. Supramolecular Chemistry and Self-Assembly in Organic Materials Design. *Chem. Mater.* **2014**, *26*, 507−518.
(679) Oshovsky, G. V.; Reinhoudt, D. N.; Verboom, W. Supramolecular Chemistry in Water. *Angew. Chem., Int. Ed.* **2007**, *46*, 2366−2393.
(680) Cook, T. R.; Zheng, Y. R.; Stang, P. J. Metal-Organic Frameworks and Self-Assembled Supramolecular Coordination Complexes: Comparing and Contrasting the Design, Synthesis, and Functionality of Metal-Organic Materials. *Chem. Rev.* **2013**, *113*, 734−777.
(681) Li, H.; Eddaoudi, M.; O'Keeffe, M.; Yaghi, O. M. Design and Synthesis of an Exceptionally Stable and Highly Porous Metal-Organic Framework. *Nature* **1999**, *402*, 276−279.
(682) Kovbasyuk, L.; Krämer, R. Allosteric Supramolecular Receptors and Catalysts. *Chem. Rev.* **2004**, *104*, 3161−3187.
(683) Yan, X.; Wang, F.; Zheng, B.; Huang, F. Stimuli-Responsive Supramolecular Polymeric Materials. *Chem. Soc. Rev.* **2012**, *41*, 6042−6065.
(684) Sangeetha, N. M.; Maitra, U. Supramolecular Gels: Functions and Uses. *Chem. Soc. Rev.* **2005**, *34*, 821−836.
(685) Buerkle, L. E.; Rowan, S. J. Supramolecular Gels Formed from Multi-Component Low Molecular Weight Species. *Chem. Soc. Rev.* **2012**, *41*, 6089.
(686) Aida, T.; Meijer, E. W.; Stupp, S. I. Functional Supramolecular Polymers. *Science* **2012**, *335*, 813−817.
(687) Hartgerink, J. D.; Beniash, E.; Stupp, S. I. Self-Assembly and Mineralization of Peptide-Amphiphile Nanofibers. *Science* **2001**, *294*, 1684−1688.
(688) Alexeev, Y. E.; Kharisov, B. I.; García, T. C. H.; Garnovskii, A. D. Coordination Motifs in Modern Supramolecular Chemistry. *Coord. Chem. Rev.* **2010**, *254*, 794−831.
(689) Schalley, C. A. Supramolecular Chemistry Goes Gas Phase: The Mass Spectrometric Examination of Noncovalent Interactions in Host-Guest Chemistry and Molecular Recognition. *Int. J. Mass Spectrom.* **2000**, *194*, 11−39.
(690) Thalladi, V. R.; Goud, B. S.; Hoy, V. J.; Allen, F. H.; Howard, J. A. K.; Desiraju, G. R. Supramolecular Synthons in Crystal Engineering. Structure Simplification, Synthon Robustness and Supramolecular Retrosynthesis. *Chem. Commun.* **1996**, 401−402.
(691) Aakeröy, C. B.; Champness, N. R.; Janiak, C. Recent Advances in Crystal Engineering. *CrystEngComm* **2010**, *12*, 22−43.
(692) Desiraju, G. R. Supramolecular Synthons in Crystal Engineering−A New Organic Synthesis. *Angew. Chem., Int. Ed. Engl.* **1995**, *34*, 2311−2327.
(693) Aakeroy, C. B.; Seddon, K. R. The Hydrogen Bond and Crystal Engineering. *Chem. Soc. Rev.* **1993**, *22*, 397−407.
(694) Jabay, O.; Pritzkow, H.; Jander, J. Untersuchungen an Stickstoff-Brom-Verbindungen, IV/Studies on Nitrogen-Bromine Compounds, IV. *Z. Naturforsch., B: J. Chem. Sci.* **1977**, *32*, 1416−1420.
(695) Ghassemzadeh, M.; Harms, K.; Dehnicke, K.; Magull, J. μ2-Chlorokomplexe von Succinimid Und N-Chlorsuccinimid. Die Kristallstrukturen von PPh4[Cl(Succinimid)2], PPh4[[CI(N-Cl-Succinimid)2] Und N-Chlorphthalimid. *Z. Naturforsch., B: J. Chem. Sci.* **1994**, *49*, 506−512.
(696) Bosch, E. Serendipity and the Search for Short N - I Halogen Bonds. *Cryst. Growth Des.* **2014**, *14*, 126−130.
(697) Batsanov, A. S.; Howard, J. A. K. Morpholine-Beta-Iodophenylacetylene (1/1) Revisited: An Exceptionally Short I···N Contact. *Acta Crystallogr., Sect. C: Cryst. Struct. Commun.* **2000**, *56*, 252−253.
(698) Cinčić, D.; Friščić, T.; Jones, W. A Cocrystallisation-Based Strategy to Construct Isostructural Solids. *New J. Chem.* **2008**, *32*, 1776−1781.
(699) Stromme, K. O. An X-Ray Analysis of the 1:1 Compound Trimethylamine-Iodine. *Acta Chem. Scand.* **1959**, *13*, 268−274.
(700) McAuliffe, C. A.; Beagley, B.; Gott, C. A.; Mackie, A. G.; MacRory, P. P.; Pritchard, R. G. Structure of Triphenylarsane Diiodide, [Ph3As · I2], a Compound Formed in the Thermal Decomposition of [Mn(OAsPh3)3I2 (SO2)2]. *Angew. Chem., Int. Ed. Engl.* **1987**, *26*, 264−265.
(701) Arca, M.; Devillanova, F. A.; Garau, A.; Isaia, F.; Lippolis, V.; Verani, G.; Demartin, F. 31P CP-MAS NMR, Vibrational, and X-Ray Characterization of the Adducts of Triphenylphosphine Sulfide with ICl and IBr. *Z. Anorg. Allg. Chem.* **1998**, *624*, 745−749.
(702) Cross, W. I.; Dahalan, M. Z.; Godfrey, S. M.; Jaiboon, N.; McAuliffe, C. A.; Pritchard, R. G.; Thompson, G. M. (Triphenylarsine)iodinemonobromine: A Charge-Transfer Adduct in Which Arsenic Selectively Bonds to Iodine. *Acta Crystallogr., Sect. C: Cryst. Struct. Commun.* **2000**, *56*, 140−141.
(703) Bannister, C.; Burns, K.; Prout, K.; Watkin, D. J.; Cooper, D. G.; Durant, G. J.; Ganellin, C. R.; Ife, R. J.; Sach, G. S. Structures of Histamine H1-Receptor Antagonists Derived from the Cimetidine Group of Histamine H2-Receptor Antagonists. *Acta Crystallogr., Sect. B: Struct. Sci.* **1994**, *50*, 221−243.
(704) Polson, M.; Turnbull, M. M.; Wikaira, J. L. 2-Amino-5-Iodopyridinium Bromide Hemihydrate and 2-Amino-5-Iodopyridinium Chloride Monohydrate. *Acta Crystallogr., Sect. C: Cryst. Struct. Commun.* **2013**, *69*, 1152−1156.
(705) Frey, M.; Jones, P. G. Secondary Bonding Interactions in Some Halopyridinium and Dihalopyridinium Halides. *Z. Naturforsch., B: J. Chem. Sci.* **2001**, *56*, 889−896.
(706) Fletcher Claville, M. O.; Payne, R. J.; Parker, B. C.; Fronczek, F. R. (Bromomethyl)trimethylammonium Bromide. *Acta Crystallogr., Sect. E: Struct. Rep. Online* **2007**, *63*, o2601−u1137.
(707) Anders, E.; Opitz, A.; Wermann, K.; Wiedel, B.; Walther, M.; Imhof, W.; Görls, H. Preparation and Conversion of N-Halomethylpyridinium Halides. Comparison with Related Compounds. *J. Org. Chem.* **1999**, *64*, 3113−3121.
(708) Kolomeitsev, A.; Schoth, R.-M.; Lork, E.; Roschenthaler, G.-V. Facile New Method for Synthezising N-Polyfluoroalkylated Heterocycles - Molecular Structure of N-(bromodifluoromethyl)-4-Dimethylaminopyridinium Bromide. *Chem. Commun.* **1996**, 335−336.
(709) Mori, T.; Kobayashi, A.; Sasaki, Y.; Kobayashi, H.; Saito, G.; Inokuchi, H. Band Structures Of Two Types Of (BEDT-TTF)2I3. *Chem. Lett.* **1984**, 957−960.
(710) Oh, S. Y.; Nickels, C. W.; Garcia, F.; Jones, W.; Friscic, T. Switching between Halogen- and Hydrogen-Bonding in Stoichiometric Variations of a Cocrystal of a Phosphine Oxide. *CrystEngComm* **2012**, *14*, 6110−6114.

DOI: 10.1021/acs.chemrev.5b00484
Chem. Rev. 2016, 116, 2478−2601

(711) Präsang, C.; Whitwood, A. C.; Bruce, D. W. Spontaneous Symmetry-Breaking in Halogen-Bonded, Bent-Core Liquid Crystals: Observation of a Chemically Driven Iso-N-N* Phase Sequence. *Chem. Commun.* **2008**, 2137−2139.
(712) Takemura, A.; McAllister, L. J.; Hart, S.; Pridmore, N. E.; Karadakov, P. B.; Whitwood, A. C.; Bruce, D. W. Halogen- and Hydrogen-Bonded Salts and Co-Crystals Formed from 4-Halo-2,3,5,6-Tetrafluorophenol and Cyclic Secondary and Tertiary Amines: Orthogonal and Non-Orthogonal Halogen and Hydrogen Bonding, and Synthetic Analogues of Halogen-Bonded Biological Syst. *Chem. - Eur. J.* **2014**, *20*, 6721−6732.
(713) Wang, H.; Hu, R. X.; Pang, X.; Gao, H. Y.; Jin, W. J. The Phosphorescent Co-Crystals of 1,4-Diiodotetrafluorobenzene and Bent 3-Ring-N-Heterocyclic Hydrocarbons by C-I···N and C-I···π Halogen Bonds. *CrystEngComm* **2014**, *16*, 7942−7948.
(714) Aakeröy, C. B.; Chopade, P. D.; Desper, J. Establishing a Hierarchy of Halogen Bonding by Engineering Crystals without Disorder. *Cryst. Growth Des.* **2013**, *13*, 4145−4150.
(715) Tucker, D. A.; White, P. S.; Trojan, K. L.; Kirk, M. L.; Hatfield, W. E. Identification of a Novel Tetragonally Compressed Six-Coordinate Copper (II) Complex: Preparation and Characterization of a 3-Chloroanilinium Copper Chloride Complex, (3-chloroanilinium)8[CuCl6]Cl4. *Inorg. Chem.* **1991**, *30*, 823−826.
(716) Desper, J. M.; Vyvyan, J. R.; Mayer, M. J.; Ochrymowycz, L. A.; Gellman, S. H. Nickel(II) Chelation by Three Bicyclic Tetrathioethers: Solution and Solid-State Data. *Inorg. Chem.* **1993**, *32*, 381−382.
(717) Mele, A.; Metrangolo, P.; Neukirch, H.; Pilati, T.; Resnati, G. A Halogen-Bonding-Based Heteroditopic Receptor for Alkali Metal Halides. *J. Am. Chem. Soc.* **2005**, *127*, 14972−14973.
(718) Chudzinski, M. G.; McClary, C. A.; Taylor, M. S. Anion Receptors Composed of Hydrogen- and Halogen-Bond Donor Groups: Modulating Selectivity with Combinations of Distinct Noncovalent Interactions. *J. Am. Chem. Soc.* **2011**, *133*, 10559−10567.
(719) Gilday, L. C.; Beer, P. D. Halogen- and Hydrogen-Bonding Catenanes for Halide-Anion Recognition. *Chem. - Eur. J.* **2014**, *20*, 8379−8385.
(720) You, L. Y.; Chen, S. G.; Zhao, X.; Liu, Y.; Lan, W. X.; Zhang, Y.; Lu, H. J.; Cao, C. Y.; Li, Z. T. C-H···O Hydrogen Bonding Induced Triazole Foldamers: Efficient Halogen Bonding Receptors for Organohalogens. *Angew. Chem., Int. Ed.* **2012**, *51*, 1657−1661.
(721) Zapata, F.; Caballero, A.; Molina, P.; Alkorta, I.; Elguero, J. Open Bis(triazolium) Structural Motifs as a Benchmark To Study Combined Hydrogen- and Halogen-Bonding Interactions in Oxoanion Recognition Processes. *J. Org. Chem.* **2014**, *79*, 6959−6969.
(722) Marras, G.; Metrangolo, P.; Meyer, F.; Pilati, T.; Resnati, G.; Vij, A. Solid State Synthesis under Supramolecular Control of a 2D Heterotetratopic Self-Complementary Tecton Tailored to Halogen Bonding. *New J. Chem.* **2006**, *30*, 1397−1402.
(723) Cariati, E.; Cavallo, G.; Forni, A.; Leem, G.; Metrangolo, P.; Meyer, F.; Pilati, T.; Resnati, G.; Righetto, S.; Terraneo, G.; et al. Self-Complementary Nonlinear Optical-Phores Targeted to Halogen Bond-Driven Self-Assembly of Electro-Optic Materials. *Cryst. Growth Des.* **2011**, *11*, 5642−5648.
(724) Leroy, J.; Schöllhorn, B.; Syssa-Magalé, J. L.; Boubekeur, K.; Palvadeau, P. A Convenient Preparation of 2,3,5,6-Tetrafluoro-4-Iodo-Benzaldehyde and Its Application in Porphyrin Synthesis. *J. Fluorine Chem.* **2004**, *125*, 1379−1382.
(725) Collings, J. C.; Burke, J. M.; Smith, P. S.; Batsanov, A. S.; Howard, J. A. K.; Marder, T. B. The Synthesis and Crystal Structures of Halogenated Tolans P-X-C6H4-C[triple bond]C-C6F5 and P-X-C6F4-C[triple bond]C-C6H5(X = F, Cl, Br, I). *Org. Biomol. Chem.* **2004**, *2*, 3172−3178.
(726) Ferrer, M.; Gutiérrez, A.; Mounir, M.; Rodríguez, L.; Rossell, O.; Font-Bardia, M.; Gómez-Sal, P.; Martín, A.; Solans, X. Design and Synthesis of Polytopic Metalloligands Based on Fluoroaryl Gold(I) Organometallic Compounds. *Organometallics* **2011**, *30*, 3419−3429.
(727) Stein, M.; Berger, R.; Seichter, W.; Hulliger, J.; Weber, E. Specific Interaction Modes in the Crystal Structures of Oligofluorinated Tolanes Featuring Additional Electron Donor and Acceptor Groups. *J. Fluorine Chem.* **2012**, *135*, 231−239.
(728) Balasubramanian, T.; Muthiah, P. T. Hydrogen-Bonding Patterns in Substituted Oxines. Redetermination of 8-Hydroxy-7-Iodoquinoline-5-Sulfonic Acid. *Acta Crystallogr., Sect. C: Cryst. Struct. Commun.* **1996**, *52*, 2072−2073.
(729) Hašek, J.; Obrda, J.; Huml, K.; Nešpurek, S.; Šorm, M. Study of Photochromic Sydnones. II. Structure of 4-Bromo-3-(3-Pyridyl)-sydnone. *Acta Crystallogr., Sect. B: Struct. Crystallogr. Cryst. Chem.* **1979**, *35*, 437−440.
(730) Hope, H.; Thiessen, W. E. The Structures of 4,4′-Dichloro-3,3′-Ethylenebis-Sydnone and 3,3′-Ethylenebis-Sydnone. *Acta Crystallogr., Sect. B: Struct. Crystallogr. Cryst. Chem.* **1969**, *25*, 1237−1247.
(731) Hulliger, J.; Langley, P. J. On Intrinsic and Extrinsic Defect-Forming Mechanisms Determining the Disordered Structure of 4-Iodo-4′-Nitrobiphenyl Crystals. *Chem. Commun.* **1998**, 2557−2558.
(732) Bailey, R. D.; Hook, L. L.; Watson, R. P.; Hanks, T. W.; Pennington, W. T. Tetraiodoethylene: A Supramolecular Host for Lewis Base Donors. *Cryst. Eng.* **2000**, *3*, 155−171.
(733) Lucassen, A. C. B.; Vartanian, M.; Leitus, G.; Van Der Boom, M. E. 4′-Bromo-2′,3′,5′,6′-Tetrafluorostilbazole: Donor and Acceptor Site for Halogen Bonding and π-Stacking in One Rigid-Rod-Type Molecule. *Cryst. Growth Des.* **2005**, *5*, 1671−1673.
(734) Burton, D. D.; Fontana, F.; Metrangolo, P.; Pilati, T.; Resnati, G. Halogen Bonding Driven Self-Assembly of (E)-1,2-Diiodo-1,2-Difluoroethene with Nitrogen Substituted Hydrocarbons. *Tetrahedron Lett.* **2003**, *44*, 645−648.
(735) Metrangolo, P.; Meyer, F.; Pilati, T.; Resnati, G.; Terraneo, G. 4,4′-Bipyridine−2,4,5,6-Tetrafluoro-1,3-Diiodobenzene (1/1). *Acta Crystallogr., Sect. E: Struct. Rep. Online* **2007**, *63*, o4243.
(736) Liantonio, R.; Metrangolo, P.; Pilati, T.; Resnati, G. 4,4′-Bipyridine 1,2-Diiodo-3,4,5,6-Tetrafluorobenzene. *Acta Crystallogr., Sect. E: Struct. Rep. Online* **2002**, *58*, o575−o577.
(737) Chu, Q.; Wang, Z.; Huang, Q.; Yan, C.; Zhu, S. Fluorine-Containing Donor-Acceptor Complex: Infinite Chain Formed by Oxygen···Iodine Interaction. *J. Am. Chem. Soc.* **2001**, *123*, 11069−11070.
(738) Neukirch, H.; Guido, E.; Liantonio, R.; Metrangolo, P.; Pilati, T.; Resnati, G. Spontaneous Resolution in a Halogen Bonded Supramolecular Architecture. *Chem. Commun.* **2005**, 1534−1536.
(739) Huang, K. S.; Haddadin, M. J.; Olmstead, M. M.; Kurth, M. J. Synthesis and Reactions of Some Heterocyclic Azacyanines. *J. Org. Chem.* **2001**, *66*, 1310−1315.
(740) Gattuso, G.; Notti, A.; Pappalardo, S.; Parisi, M. F.; Pilati, T.; Resnati, G.; Terraneo, G. Ion-Pair Separation via Selective Inclusion/segregation Processes. *CrystEngComm* **2009**, *11*, 1204−1206.
(741) Biella, S.; Gattuso, G.; Notti, A.; Metrangolo, P.; Pappalardo, S.; Parisi, M. F.; Pilati, T.; Resnati, G.; Terraneo, G. Halogen Bonding-Based Anion Coordination in Calixarene/inorganic Halide/diiodoperfluorocarbon Assemblies. *Supramol. Chem.* **2009**, *21*, 149−156.
(742) Weiss, A.; Barba, V.; Pritzkow, H.; Siebert, W. Synthesis, Structures and Reactivity of Macrocyclic Imidazolylboranes. *J. Organomet. Chem.* **2003**, *680*, 294−300.
(743) Yamamoto, H. M.; Maeda, R.; Yamaura, J.-I.; Kato, R. Structural and Physical Properties of Conducting Cation Radical Salts Containing Supramolecular Assemblies Based on p-Bis(iodoethynyl)-benzene Derivatives. *Annu. Rev. Synth. Met.* **2001**, *11*, 101−102.
(744) Dick, S. Crystal Structure of N,N,N-Trimethyl-N-(3,4,5-Triiodphenyl)ammonium Iodide Dimethylsulfoxide Solvate, [C6H2I3N(CH3)3)]I × (CH3)2SO. *Z. Kristallogr. - New Cryst. Struct.* **1998**, *213*, 357−358.
(745) Bertolotti, F.; Shishkina, A. V.; Forni, A.; Gervasio, G.; Stash, A. I.; Tsirelson, V. G. Intermolecular Bonding Features in Solid Iodine. *Cryst. Growth Des.* **2014**, *14*, 3587−3595.
(746) Pigge, F. C.; Vangala, V. R.; Kapadia, P. P.; Swenson, D. C.; Rath, N. P. Hexagonal Crystalline Inclusion Complexes of 4-Iodophenoxy Trimesoate. *Chem. Commun.* **2008**, 4726−4728.
(747) Titi, H. M.; Patra, R.; Goldberg, I. Exploring Supramolecular Self-Assembly of Tetraarylporphyrins by Halogen Bonding: Crystal

DOI: 10.1021/acs.chemrev.5b00484
Chem. Rev. 2016, 116, 2478−2601

Engineering with Diversely Functionalized Six-Coordinate tin(L)2-Porphyrin Tectons. *Chem. - Eur. J.* **2013**, *19*, 14941−14949.
(748) Blatov, V. A.; Shevchenko, A. P.; Proserpio, D. M. Applied Topological Analysis of Crystal Structures with the Program Package ToposPro. *Cryst. Growth Des.* **2014**, *14*, 3576−3586.
(749) Titi, H. M.; Nandi, G.; Tripuramallu, B. K.; Goldberg, I. Exploring Supramolecular Self-Assembly of Tetraarylporphyrins by Halogen Interactions. 3. Tin(L)2 (A2B2-Porphyrin) Arrays Supported by Concerted Halogen and Hydrogen Bonding. *Cryst. Growth Des.* **2015**, *15*, 3063−3075.
(750) Syssa-Magalé, J.-L.; Boubekeur, K.; Leroy, J.; Chamoreau, L.-M.; Fave, C.; Schöllhorn, B. Directed Synthesis of a Halogen-Bonded Open Porphyrin Network. *CrystEngComm* **2014**, *16*, 10380−10384.
(751) Cavallo, G.; Biella, S.; Lü, J.; Metrangolo, P.; Pilati, T.; Resnati, G.; Terraneo, G. Halide Anion-Templated Assembly of Di- and Triiodoperfluorobenzenes into 2D and 3D Supramolecular Networks. *J. Fluorine Chem.* **2010**, *131*, 1165−1172.
(752) du Mont, W.-W.; Stenzel, V.; Jeske, J.; Jones, P. C.; Sebald, A.; Pohl, S.; Saak, W.; Batcher, M. Destructive or Cooperative Attack of Iodide Anions on Alkyltriiodophosphonium Cations: Elimination of Iodine in Solution and Layer Structures in the Solid State. *Inorg. Chem.* **1994**, *33*, 1502−1505.
(753) Lü, Z.; Yuan, M.; Pan, F.; Gao, S.; Zhang, D.; Zhu, D. Syntheses, Crystal Structures, and Magnetic Characterization of Five New Dimeric Manganese(III) Tetradentate Schiff Base Complexes Exhibiting Single-Molecule-Magnet Behavior. *Inorg. Chem.* **2006**, *45*, 3538−3548.
(754) Chung, K.-H.; Park, J.; Kim, K. Y.; Yoon, J. K.; Kim, H.; Han, S.; Kahng, S.-J. Polymorphic Porous Supramolecular Networks Mediated by Halogen Bonds on Ag(111). *Chem. Commun.* **2011**, *47*, 11492−11494.
(755) Jang, W. J.; Chung, K.-H.; Lee, M. W.; Kim, H.; Lee, S.; Kahng, S.-J. Tetragonal Porous Networks Made by Rod-like Molecules on Au(111) with Halogen Bonds. *Appl. Surf. Sci.* **2014**, *309*, 74−78.
(756) Zha, B.; Miao, X.; Liu, P.; Wu, Y.; Deng, W. Concentration Dependent Halogen-Bond Density in the 2D Self-Assembly of a Thienophenanthrene Derivative at the Aliphatic Acid/graphite Interface. *Chem. Commun.* **2014**, *50*, 9003−9006.
(757) Zheng, Q.-N.; Liu, X.-H.; Chen, T.; Yan, H.-J.; Cook, T.; Wang, D.; Stang, P. J.; Wan, L.-J. Formation of Halogen Bond-Based 2D Supramolecular Assemblies by Electric Manipulation. *J. Am. Chem. Soc.* **2015**, *137*, 6128−6131.
(758) Baburin, I. A.; Blatov, V. A.; Carlucci, L.; Ciani, G.; Proserpio, D. M. Interpenetrating Metal-Organic and Inorganic 3D Networks: A Computer-Aided Systematic Investigation. Part II [1]. Analysis of the Inorganic Crystal Structure Database (ICSD). *J. Solid State Chem.* **2005**, *178*, 2452−2474.
(759) Thaimattam, R.; Sharma, C. V. K.; Clearfield, A.; Desiraju, G. R. Diamondoid and Square Grid Networks in the Same Structure. Crystal Engineering with the Iodo···Nitro Supramolecular Synthon. *Cryst. Growth Des.* **2001**, *1*, 103−106.
(760) Metrangolo, P.; Meyer, F.; Pilati, T.; Proserpio, D. M.; Resnati, G. Highly Interpenetrated Supramolecular Networks Supported by N···I Halogen Bonding. *Chem. - Eur. J.* **2007**, *13*, 5765−5772.
(761) Baldrighi, M.; Metrangolo, P.; Meyer, F.; Pilati, T.; Proserpio, D.; Resnati, G.; Terraneo, G. Halogen-Bonded and Interpenetrated Networks through the Self-Assembly of Diiodoperfluoroarene and Tetrapyridyl Tectons. *J. Fluorine Chem.* **2010**, *131*, 1218−1224.
(762) Metrangolo, P.; Meyer, F.; Pilati, T.; Proserpio, D. M.; Resnati, G. Dendrimeric Tectons in Halogen Bonding-Based Crystal Engineering. *Cryst. Growth Des.* **2008**, *8*, 654−659.
(763) Liantonio, R.; Metrangolo, P.; Meyer, F.; Pilati, T.; Navarrini, W.; Resnati, G. Metric Engineering of Supramolecular Borromean Rings. *Chem. Commun.* **2006**, 1819−1821.
(764) Zang, S.-Q.; Fan, Y.-J.; Li, J.-B.; Hou, H.-W.; Mak, T. C. W. Halogen Bonding in the Assembly of Coordination Polymers Based on 5-Iodo-Isophthalic Acid. *Cryst. Growth Des.* **2011**, *11*, 3395−3405.
(765) Lieffrig, J.; Yamamoto, H. M.; Kusamoto, T.; Cui, H.; Jeannin, O.; Fourmigué, M.; Kato, R. Halogen-Bonded, Eight-Fold PtS-Type Interpenetrated Supramolecular Network. A Study toward Redundant and Cross-Bar Supramolecular Nanowire Crystal. *Cryst. Growth Des.* **2011**, *11*, 4267−4271.
(766) Lieffrig, J.; Jeannin, O.; Fourmigué, M. Expanded Halogen-Bonded Anion Organic Networks with Star-Shaped Iodoethynyl-Substituted Molecules: From Corrugated 2D Hexagonal Lattices to Pyrite-Type 2-Fold Interpenetrated Cubic Lattices. *J. Am. Chem. Soc.* **2013**, *135*, 6200−6210.
(767) Yan, Z.-H.; Han, L.-L.; Zhao, Y.-Q.; Li, X.-Y.; Wang, X.-P.; Wang, L.; Sun, D. Three Mixed-Ligand Coordination Networks Modulated by Flexible N-Donor Ligands: Syntheses, Topological Structures, and Temperature-Sensitive Luminescence Properties. *CrystEngComm* **2014**, *16*, 8747.
(768) Takeuchi, T.; Minato, Y.; Takase, M.; Shinmori, H. Molecularly Imprinted Polymers with Halogen Bonding-Based Molecular Recognition Sites. *Tetrahedron Lett.* **2005**, *46*, 9025−9027.
(769) Cheong, W. J.; Yang, S. H.; Ali, F. Molecular Imprinted Polymers for Separation Science: A Review of Reviews. *J. Sep. Sci.* **2013**, *36*, 609−628.
(770) Metrangolo, P.; Carcenac, Y.; Lahtinen, M.; Pilati, T.; Rissanen, K.; Vij, A.; Resnati, G. Nonporous Organic Solids Capable of Dynamically Resolving Mixtures of Diiodoperfluoroalkanes. *Science* **2009**, *323*, 1461−1464.
(771) Abate, A.; Brischetto, M.; Cavallo, G.; Lahtinen, M.; Metrangolo, P.; Pilati, T.; Radice, S.; Resnati, G.; Rissanen, K.; Terraneo, G. Dimensional Encapsulation of I(−)···I(2)···I(−) in an Organic Salt Crystal Matrix. *Chem. Commun.* **2010**, *46*, 2724−2726.
(772) Lin, J.; Martí-Rujas, J.; Metrangolo, P.; Pilati, T.; Radice, S.; Resnati, G.; Terraneo, G. Solution and Solid State Synthesis of the Discrete Polyiodide I 7 3- under Modular Cation Templation. *Cryst. Growth Des.* **2012**, *12*, 5757−5762.
(773) García, M. D.; Martí-Rujas, J.; Metrangolo, P.; Peinador, C.; Pilati, T.; Resnati, G.; Terraneo, G.; Ursini, M. Dimensional Caging of Polyiodides: Cation-Templated Synthesis Using Bipyridinium Salts. *CrystEngComm* **2011**, *13*, 4411−4416.
(774) Peuronen, A.; Rinta, H.; Lahtinen, M. N···I Halogen Bonding Supported Stabilization of a Discrete Pseudo-Linear [I12]2− Polyiodide. *CrystEngComm* **2015**, *17*, 1736−1740.
(775) Meazza, L.; Martí-Rujas, J.; Terraneo, G.; Castiglioni, C.; Milani, A.; Pilati, T.; Metrangolo, P.; Resnati, G. Solid-State Synthesis of Mixed Trihalides via Reversible Absorption of Dihalogens by Non Porous Onium Salts. *CrystEngComm* **2011**, *13*, 4427−4435.
(776) Mínguez Espallargas, G.; Van De Streek, J.; Fernandes, P.; Florence, A. J.; Brunelli, M.; Shankland, K.; Brammer, L. Mechanistic Insights into a Gas-Solid Reaction in Molecular Crystals: The Role of Hydrogen Bonding. *Angew. Chem., Int. Ed.* **2010**, *49*, 8892−8896.
(777) Vitorica-Yrezabal, I. J.; Sullivan, R. a.; Purver, S. L.; Curfs, C.; Tang, C. C.; Brammer, L. Synthesis and Polymorphism of (4-ClpyH)2[CuCl4]: Solid−gas and Solid−solid Reactions. *CrystEngComm* **2011**, *13*, 3189−3196.
(778) Mínguez Espallargas, G.; Florence, A. J.; van de Streek, J.; Brammer, L. Different Structural Destinations: Comparing Reactions of [CuBr2(3-Brpy)2] Crystals with HBr and HCl Gas. *CrystEngComm* **2011**, *13*, 4400−4404.
(779) Yoshizawa, M.; Tamura, M.; Fujita, M. Diels-Alder in Aqueous Molecular Hosts: Unusual Regioselectivity and Efficient Catalysis. *Science* **2006**, *312*, 251−254.
(780) Brunet, P.; Simard, M.; Wuest, J. D. Molecular Tectonics. Porous Hydrogen-Bonded Networks with Unprecedented Structural Integrity. *J. Am. Chem. Soc.* **1997**, *119*, 2737−2738.
(781) Raatikainen, K.; Rissanen, K. Breathing Molecular Crystals: Halogen- and Hydrogen-Bonded Porous Molecular Crystals with Solvent Induced Adaptation of the Nanosized Channels. *Chem. Sci.* **2012**, *3*, 1235−1239.
(782) Martí-Rujas, J.; Colombo, L.; Lü, J.; Dey, A.; Terraneo, G.; Metrangolo, P.; Pilati, T.; Resnati, G. Hydrogen and Halogen Bonding Drive the Orthogonal Self-Assembly of an Organic Framework Possessing 2D Channels. *Chem. Commun.* **2012**, *48*, 8207−8209.

DOI: 10.1021/acs.chemrev.5b00484
Chem. Rev. 2016, 116, 2478−2601

(783) Pang, X.; Wang, H.; Zhao, X. R.; Jin, W. J. Anionic 3D Cage Networks Self-Assembled by Iodine and V-Shaped Pentaiodides Using Dimeric Oxoammonium Cations Produced in Situ as Templates. *Dalton Trans.* **2013**, *42*, 8788−8795.
(784) Muniappan, S.; Lipstman, S.; Goldberg, I. Rational Design of Supramolecular Chirality in Porphyrin Assemblies: The Halogen Bond Case. *Chem. Commun.* **2008**, 1777−1779.
(785) Cram, D. J.; Karbach, S.; Kim, Y. H.; Baczynskyj, L.; Kallemeyn, G. W. Shell Closure of Two Cavitands Forms Carcerand Complexes with Components of the Medium as Permanent Guests. *J. Am. Chem. Soc.* **1985**, *107*, 2575−2576.
(786) Aakeröy, C. B.; Rajbanshi, A.; Metrangolo, P.; Resnati, G.; Parisi, M. F.; Desper, J.; Pilati, T. The Quest for a Molecular Capsule Assembled via Halogen Bonds. *CrystEngComm* **2012**, *14*, 6366−6368.
(787) Beyeh, N. K.; Pan, F.; Rissanen, K. A Halogen-Bonded Dimeric Resorcinarene Capsule. *Angew. Chem.* **2015**, *127*, 7411−7415.
(788) Beyeh, N. K.; Cetina, M.; Rissanen, K. Halogen Bonded Analogues of Deep Cavity Cavitands. *Chem. Commun.* **2014**, *50*, 1959−1961.
(789) Dumele, O.; Trapp, N.; Diederich, F. Halogen Bonding Molecular Capsules. *Angew. Chem., Int. Ed.* **2015**, *54*, 12339−12344.
(790) Sarwar, M. G.; Ajami, D.; Theodorakopoulos, G.; Petsalakis, I. D.; Rebek, J. Amplified Halogen Bonding in a Small Space. *J. Am. Chem. Soc.* **2013**, *135*, 13672−13675.
(791) El-Sheshtawy, H. S.; Bassil, B. S.; Assaf, K. I.; Kortz, U.; Nau, W. M. Halogen Bonding inside a Molecular Container. *J. Am. Chem. Soc.* **2012**, *134*, 19935−19941.
(792) Huang, P.-S.; Kuo, C.-H.; Hsieh, C.-C.; Horng, Y.-C. Selective Capture of Volatile Iodine Using Amorphous Molecular Organic Solids. *Chem. Commun.* **2012**, *48*, 3227−3229.
(793) Sawada, T.; Fujita, M. A Single Watson−Crick G·C Base Pair in Water: Aqueous Hydrogen Bonds in Hydrophobic Cavities. *J. Am. Chem. Soc.* **2010**, *132*, 7194−7201.
(794) Takezawa, H.; Murase, T.; Resnati, G.; Metrangolo, P.; Fujita, M. Recognition of Polyfluorinated Compounds Through Self-Aggregation in a Cavity. *J. Am. Chem. Soc.* **2014**, *136*, 1786−1788.
(795) Takezawa, H.; Murase, T.; Resnati, G.; Metrangolo, P.; Fujita, M. Halogen-Bond-Assisted Guest Inclusion in a Synthetic Cavity. *Angew. Chem., Int. Ed.* **2015**, *54*, 8411−8414.
(796) Yang, D.; Zhao, J.; Zhao, Y.; Lei, Y.; Cao, L.; Yang, X.-J.; Davi, M.; de Sousa Amadeu, N.; Janiak, C.; Zhang, Z.; et al. Encapsulation of Halocarbons in a Tetrahedral Anion Cage. *Angew. Chem., Int. Ed.* **2015**, *54*, 8658−8661.
(797) James, S. L.; Adams, C. J.; Bolm, C.; Braga, D.; Collier, P.; Friscic, T.; Grepioni, F.; Harris, K. D. M.; Hyett, G.; Jones, W.; et al. Mechanochemistry: Opportunities for New and Cleaner Synthesis. *Chem. Soc. Rev.* **2012**, *41*, 413−447.
(798) Friščić, T. Supramolecular Concepts and New Techniques in Mechanochemistry: Cocrystals, Cages, Rotaxanes, Open Metal−organic Frameworks. *Chem. Soc. Rev.* **2012**, *41*, 3493−3510.
(799) Friščić, T.; Trask, A. V.; Motherwell, W. D. S.; Jones, W. Guest-Directed Assembly of Caffeine and Succinic Acid into Topologically Different Heteromolecular Host Networks upon Grinding. *Cryst. Growth Des.* **2008**, *8*, 1605−1609.
(800) Lapadula, G.; Judaš, N.; Friščić, T.; Jones, W. A Three-Component Modular Strategy to Extend and Link Coordination Complexes by Using Halogen Bonds to O, S and π Acceptors. *Chem. - Eur. J.* **2010**, *16*, 7400−7403.
(801) Cinčić, D.; Friščić, T. Synthesis of an Extended Halogen-Bonded Metal−organic Structure in a One-Pot Mechanochemical Reaction That Combines Covalent Bonding, Coordination Chemistry and Supramolecular Synthesis. *CrystEngComm* **2014**, *16*, 10169−10172.
(802) Baldrighi, M.; Metrangolo, P.; Resnati, G.; Terraneo, G. Co-Crystals of 3-Iodopropynyl Butylcarbamate. IT1411006B1, 2013; accession number 2014:1954502, CAN 161:711319, CAPLUS.
(803) Biradha, K.; Santra, R. Crystal Engineering of Topochemical Solid State Reactions. *Chem. Soc. Rev.* **2013**, *42*, 950−967.
(804) Wegner, G. Solid-State Polymerization Mechanisms. *Pure Appl. Chem.* **1977**, *49*, 443−454.
(805) Macgillivray, L.; Papaefstathiou, G.; Friscić, T.; Hamilton, T. D.; Bucar, D.; Chu, Q.; Varshney, D.; Georgiev, I. Supramolecular Control of Reactivity in the Solid State: From Templates to Ladderanes to Metal - Organic Frameworks. *Acc. Chem. Res.* **2008**, *41*, 280−291.
(806) Hertel, E.; Schneider, K. Transformations in Crystal Lattices. *Z. Elektrochem.* **1931**, *37*, 536−538.
(807) Schmidt, G. M. J. Photodimerization in the Solid State. *Pure Appl. Chem.* **1971**, *27*, 647−678.
(808) Caronna, T.; Liantonio, R.; Logothetis, T. a.; Metrangolo, P.; Pilati, T.; Resnati, G. Halogen Bonding and π···π Stacking Control Reactivity in the Solid State. *J. Am. Chem. Soc.* **2004**, *126*, 4500−4501.
(809) Baughman, R. H. Solid-State Synthesis of Large Polymer Single Crystals. *J. Polym. Sci., Polym. Phys. Ed.* **1974**, *12*, 1511−1535.
(810) Wilhelm, C.; Boyd, S. A.; Chawda, S.; Fowler, F. W.; Goroff, N. S.; Halada, G. P.; Grey, C. P.; Lauher, J. W.; Luo, L.; Martin, C. D.; et al. Pressure-Induced Polymerization of Diiodobutadiyne in Assembled Cocrystals. *J. Am. Chem. Soc.* **2008**, *130*, 4415−4420.
(811) Sun, A.; Lauher, J. W.; Goroff, N. S. Preparation of Poly(diiododiacetylene), an Ordered Conjugated Polymer of Carbon and Iodine. *Science* **2006**, *312*, 1030−1034.
(812) Pollino, J. M.; Weck, M. Non-Covalent Side-Chain Polymers: Design Principles, Functionalization Strategies, and Perspectives. *Chem. Soc. Rev.* **2005**, *34*, 193−207.
(813) Kato, T.; Mizoshita, N.; Kishimoto, K. Functional Liquid-Crystalline Assemblies: Self-Organized Soft Materials. *Angew. Chem., Int. Ed.* **2005**, *45*, 38−68.
(814) Hammond, M. R.; Mezzenga, R. Supramolecular Routes towards Liquid Crystalline Side-Chain Polymers. *Soft Matter* **2008**, *4*, 952−961.
(815) Ahn, S.; Kasi, R. M.; Kim, S.-C.; Sharma, N.; Zhou, Y. Stimuli-Responsive Polymer Gels. *Soft Matter* **2008**, *4*, 1151−1157.
(816) Noro, A.; Hayashi, M.; Matsushita, Y. Design and Properties of Supramolecular Polymer Gels. *Soft Matter* **2012**, *8*, 6416−6429.
(817) Kato, T.; Hirai, Y.; Nakaso, S.; Moriyama, M. Liquid-Crystalline Physical Gels. *Chem. Soc. Rev.* **2007**, *36*, 1857−1867.
(818) Castles, F.; Morris, S. M.; Hung, J. M. C.; Qasim, M. M.; Wright, A. D.; Nosheen, S.; Choi, S. S.; Outram, B. I.; Elston, S. J.; Burgess, C.; et al. Stretchable Liquid-Crystal Blue-Phase Gels. *Nat. Mater.* **2014**, *13*, 817−821.
(819) Axenov, K. V.; Laschat, S. Thermotropic Ionic Liquid Crystals. *Materials* **2011**, *4*, 206−259.
(820) Abate, A.; Petrozza, A.; Roiati, V.; Guarnera, S.; Snaith, H.; Matteucci, F.; Lanzani, G.; Metrangolo, P.; Resnati, G. A Polyfluoroalkyl Imidazolium Ionic Liquid as Iodide Ion Source in Dye Sensitized Solar Cells. *Org. Electron.* **2012**, *13*, 2474−2478.
(821) Beeckman, J.; Neyts, K.; Vanbrabant, P. J. M. Liquid-Crystal Photonic Applications. *Opt. Eng.* **2011**, *50*, 081202.
(822) Chigrinov, V. G. *Liquid Crystal Photonics*; Nova Science Publishers: New York, 2014.
(823) Coles, H.; Morris, S. Liquid-Crystal Lasers. *Nat. Photonics* **2010**, *4*, 676−685.
(824) Tschierske, C. Development of Structural Complexity by Liquid-Crystal Self-Assembly. *Angew. Chem., Int. Ed.* **2013**, *52*, 8828−8878.
(825) Woltman, S. J.; Jay, G. D.; Crawford, G. P. Liquid-Crystal Materials Find a New Order in Biomedical Applications. *Nat. Mater.* **2007**, *6*, 929−938.
(826) Lin, Y.-H. Liquid Crystals for Bio-Medical Applications. *Top. Appl. Phys.* **2015**, *129*, 337−354.
(827) Pisula, W.; Zorn, M.; Chang, J. Y.; Müllen, K.; Zentel, R. Liquid Crystalline Ordering and Charge Transport In Semiconducting Materials. *Macromol. Rapid Commun.* **2009**, *30*, 1179−1202.
(828) O'Neill, M.; Kelly, S. M. Ordered Materials for Organic Electronics and Photonics. *Adv. Mater.* **2011**, *23*, 566−584.
(829) De Haan, L. T.; Verjans, J. M. N.; Broer, D. J.; Bastiaansen, C. W. M.; Schenning, A. P. H. J. Humidity-Responsive Liquid Crystalline

DOI: 10.1021/acs.chemrev.5b00484
Chem. Rev. 2016, 116, 2478−2601

Polymer Actuators with an Asymmetry in the Molecular Trigger That Bend, Fold, and Curl. *J. Am. Chem. Soc.* **2014**, *136*, 10585−10588.
(830) Carlton, R. J.; Hunter, J. T.; Miller, D. S.; Abbasi, R.; Mushenheim, P. C.; Tan, L. N.; Abbott, N. L. Chemical and Biological Sensing Using Liquid Crystals. *Liq. Cryst. Rev.* **2013**, *1*, 29−51.
(831) Paleos, C. M.; Tsiourvas, D. Supramolecular Hydrogen-Bonded Liquid Crystals. *Liq. Cryst.* **2001**, *28*, 1127−1161.
(832) Kato, T.; Frechet, J. M. J. A New Approach to Mesophase Stabilization through Hydrogen Bonding Molecular Interactions in Binary Mixtures. *J. Am. Chem. Soc.* **1989**, *111*, 8533−8534.
(833) Kato, T.; Frechet, J. M. J. Stabilization of a Liquid-Crystalline Phase through Noncovalent Interaction with a Polymer Side Chain. *Macromolecules* **1989**, *22*, 3818−3819.
(834) Kato, T.; Frechet, J. M. J.; Wilson, P. G.; Saito, T.; Uryu, T.; Fujishima, A.; Jin, C.; Kaneuchi, F. Hydrogen-Bonded Liquid Crystals. Novel Mesogens Incorporating Nonmesogenic Bipyridyl Compounds through Complexation between Hydrogen-Bond Donor and Acceptor Moieties. *Chem. Mater.* **1993**, *5*, 1094−1100.
(835) Kato, T.; Kihara, H.; Kumar, U.; Uryu, T.; Fréchet, J. M. J. A Liquid-Crystalline Polymer Network Built by Molecular Self-Assembly through Intermolecular Hydrogen Bonding. *Angew. Chem., Int. Ed. Engl.* **1994**, *33*, 1644−1645.
(836) Kato, T.; Fukumasa, M.; Frechet, J. M. J. Supramolecular Liquid-Crystalline Complexes Exhibiting Room-Temperature Mesophases and Electrooptic Effects. Hydrogen-Bonded Mesogens Derived from Alkylpyridines and Benzoic Acids. *Chem. Mater.* **1995**, *7*, 368−372.
(837) Nguyen, H. L.; Horton, P. N.; Hursthouse, M. B.; Legon, A. C.; Bruce, D. W. Halogen Bonding: A New Interaction for Liquid Crystal Formation. *J. Am. Chem. Soc.* **2004**, *126*, 16−17.
(838) Bruce, D. W.; Dunmur, D. A.; Lalinde, E.; Maitlis, P. M.; Styring, P. 4-Alkyloxy-4′-Stilbazoles New Heterocyclic Mesogens. *Liq. Cryst.* **1988**, *3*, 385−395.
(839) Willis, K.; Price, D. J.; Adams, H.; Ungar, G.; Bruce, D. W. Hydrogen-Bonded Liquid Crystals from Alkoxystilbazoles and 3-Cyanophenols: Structural Control of Mesomorphism. Molecular Structure of the Complex between 4-Cyanophenol and 4-Octyloxystilbazole. *J. Mater. Chem.* **1995**, *5*, 2195−2199.
(840) Price, D. J.; Willis, K.; Richardson, T.; Ungar, G.; Bruce, D. W. Hydrogen Bonded Liquid Crystals from Nitrophenols and Alkoxystilbazoles. *J. Mater. Chem.* **1997**, *7*, 883−891.
(841) Dai, C.; Nguyen, P.; Marder, T. B.; Marder, T. B.; Scott, A. J.; Clegg, W.; Viney, C.; Viney, C. Control of Single Crystal Structure and Liquid Crystal Phase Behaviour via Arene−perfluoroarene Interactions. *Chem. Commun.* **1999**, 2493−2494.
(842) Kishikawa, K.; Aikyo, S.; Akiyama, S.; Inoue, T.; Takahashi, M.; Yagai, S.; Aonuma, H.; Kohmoto, S. Realization of a Lateral Directional Order in Nematic and Smectic A Phases of Rodlike Molecules by Using Perfluoroarene-Arene Interactions. *Soft Matter* **2011**, *7*, 5176−5187.
(843) Kishikawa, K. Utilization of the Perfluoroarene-Arene Interaction for Stabilization of Liquid Crystal Phases. *Isr. J. Chem.* **2012**, *52*, 800−808.
(844) Bruce, D. W.; Metrangolo, P.; Meyer, F.; Prasang, C.; Resnati, G.; Terraneo, G.; Whitwood, A. C.; et al. Mesogenic, Trimeric, Halogen-Bonded Complexes from Alkoxystilbazoles and 1,4-Diiodotetrafluorobenzene. *New J. Chem.* **2008**, *32*, 477−482.
(845) Xu, J.; Liu, X.; Lin, T.; Huang, J.; He, C. Synthesis and Self-Assembly of Difunctional Halogen-Bonding Molecules: A New Family of Supramolecular Liquid-Crystalline Polymers. *Macromolecules* **2005**, *38*, 3554−3557.
(846) Xu, J.; Liu, X.; Ng, J. K.-P.; Lin, T.; He, C. Trimeric Supramolecular Liquid Crystals Induced by Halogen Bonds. *J. Mater. Chem.* **2006**, *16*, 3540−3545.
(847) Metrangolo, P.; Präsang, C.; Resnati, G.; Liantonio, R.; Whitwood, A. C.; Bruce, D. W. Fluorinated Liquid Crystals Formed by Halogen Bonding. *Chem. Commun.* **2006**, 3290−3292.
(848) Tschierske, C. Non-Conventional Liquid Crystals-the Importance of Micro-Segregation for Self-Organisation. *J. Mater. Chem.* **1998**, *8*, 1485−1508.
(849) Yano, M.; Taketsugu, T.; Hori, K.; Okamoto, H.; Takenaka, S. The Effect of Fluorination: A Crystallographic and Computational Study of Mesogenic Alkyl 4-[2-(Perfluorooctyl)ethoxy]benzoates. *Chem. - Eur. J.* **2004**, *10*, 3991−3999.
(850) McAllister, L. J.; Präsang, C.; Wong, J. P.-W.; Thatcher, R. J.; Whitwood, A. C.; Donnio, B.; O'Brien, P.; Karadakov, P. B.; Bruce, D. W. Halogen-Bonded Liquid Crystals of 4-Alkoxystilbazoles with Molecular Iodine: A Very Short Halogen Bond and Unusual Mesophase Stability. *Chem. Commun.* **2013**, *49*, 3946−3948.
(851) Chen, Y.; Yu, H.; Zhang, L.; Yang, H.; Lu, Y. Photoresponsive Liquid Crystals Based on Halogen Bonding of Azopyridines. *Chem. Commun.* **2014**, *50*, 9647−9649.
(852) Präsang, C.; Nguyen, H. L.; Horton, P. N.; Whitwood, A. C.; Bruce, D. W. Trimeric Liquid Crystals Assembled Using Both Hydrogen and Halogen Bonding. *Chem. Commun.* **2008**, 6164−6166.
(853) Cho, C. M.; Wang, X.; Li, J. J.; He, C.; Xu, J. Synthesis and Self-Assembly of Halogen-Bond Donor−spacer−hydrogen-Bond Donor Molecules: Polymeric Liquid Crystals Induced by Combination of Intermolecular Halogen- and Hydrogen-Bonding Interactions. *Liq. Cryst.* **2013**, *40*, 185−196.
(854) Bruce, D. W.; Metrangolo, P.; Meyer, F.; Pilati, T.; Praesang, C.; Resnati, G.; Terraneo, G.; Wainwright, S. G.; Whitwood, A. C. Structure-Function Relationships in Liquid-Crystalline Halogen-Bonded Complexes. *Chem. - Eur. J.* **2010**, *16*, 9511−9524.
(855) Saccone, M.; Dichiarante, V.; Forni, A.; Goulet-Hanssens, A.; Cavallo, G.; Vapaavuori, J.; Terraneo, G.; Barrett, C. J.; Resnati, G.; Metrangolo, P.; et al. Supramolecular Hierarchy among Halogen and Hydrogen Bond Donors in Light-Induced Surface Patterning. *J. Mater. Chem. C* **2015**, *3*, 759−768.
(856) Ruokolainen, J.; ten Brinke, G.; Ikkala, O.; Torkkeli, M.; Serimaa, R. Mesomorphic Structures in Flexible Polymer−Surfactant Systems Due to Hydrogen Bonding: Poly(4-vinylpyridine)−Pentadecylphenol. *Macromolecules* **1996**, *29*, 3409−3415.
(857) Ten Brinke, G.; Ikkala, O. Smart Materials Based on Self-Assembled Hydrogen-Bonded Comb-Shaped Supramolecules. *Chem. Rec.* **2004**, *4*, 219−230.
(858) Wang, F.; Ma, N.; Chen, Q.; Wang, W.; Wang, L. Halogen Bonding as a New Driving Force for Layer-by-Layer Assembly. *Langmuir* **2007**, *23*, 9540−9542.
(859) Priimagi, A.; Cavallo, G.; Forni, A.; Gorynsztejn-Leben, M.; Kaivola, M.; Metrangolo, P.; Milani, R.; Shishido, A.; Pilati, T.; Resnati, G.; et al. Halogen Bonding versus Hydrogen Bonding in Driving Self-Assembly and Performance of Light-Responsive Supramolecular Polymers. *Adv. Funct. Mater.* **2012**, *22*, 2572−2579.
(860) Virkki, M.; Tuominen, O.; Forni, A.; Saccone, M.; Metrangolo, P.; Resnati, G.; Kauranen, M.; Priimagi, A. Halogen Bonding Enhances Nonlinear Optical Response in Poled Supramolecular Polymers. *J. Mater. Chem. C* **2015**, *3*, 3003−3006.
(861) Vanderkooy, A.; Taylor, M. S. Solution-Phase Self-Assembly of Complementary Halogen Bonding Polymers. *J. Am. Chem. Soc.* **2015**, *137*, 5080−5086.
(862) Hirst, A. R.; Escuder, B.; Miravet, J. F.; Smith, D. K. High-Tech Applications of Self-Assembling Supramolecular Nanostructured Gel-Phase Materials: From Regenerative Medicine to Electronic Devices. *Angew. Chem., Int. Ed.* **2008**, *47*, 8002−8018.
(863) Piepenbrock, M. O. M.; Lloyd, G. O.; Clarke, N.; Steed, J. W. Metal- and Anion-Binding Supramolecular Gels. *Chem. Rev.* **2010**, *110*, 1960−2004.
(864) Babu, S. S.; Praveen, V. K.; Ajayaghosh, A. Functional π-Gelators and Their Applications. *Chem. Rev.* **2014**, *114*, 1973−2129.
(865) Lloyd, G. O.; Steed, J. W. Anion-Tuning of Supramolecular Gel Properties. *Nat. Chem.* **2009**, *1*, 437−442.
(866) Foster, J. A.; Piepenbrock, M.-O. M.; Lloyd, G. O.; Clarke, N.; Howard, J. A. K.; Steed, J. W. Anion-Switchable Supramolecular Gels for Controlling Pharmaceutical Crystal Growth. *Nat. Chem.* **2010**, *2*, 1037−1043.

DOI: 10.1021/acs.chemrev.5b00484
Chem. Rev. 2016, 116, 2478−2601

(867) Steed, J. W. Anion-Tuned Supramolecular Gels: A Natural Evolution from Urea Supramolecular Chemistry. *Chem. Soc. Rev.* **2010**, *39*, 3686−3699.
(868) Byrne, P.; Lloyd, G. O.; Applegarth, L.; Anderson, K. M.; Clarke, N.; Steed, J. W. Metal-Induced Gelation in Dipyridyl Ureas. *New J. Chem.* **2010**, *34*, 2261−2274.
(869) Griffin, J. E. The Thyroid. In *Textbook of Endocrine Physiology*, 2nd ed.; Griffin, J. E., Ojeda, S. R., Eds.; Oxford University Press: New York, 1992; pp 224−246.
(870) Bartelena, L.; Robbins, J. Thyroid Hormone Transport Proteins. *Clin. Lab. Med.* **1993**, *13*, 583−598.
(871) Xu, Z.; Yang, Z.; Liu, Y.; Lu, Y.; Chen, K.; Zhu, W. Halogen Bond: Its Role beyond Drug-Target Binding Affinity for Drug Discovery and Development. *J. Chem. Inf. Model.* **2014**, *54*, 69−78.
(872) Janssen, C.; Roose, P. *Monitoring Chemical Pollution in Europe's Seas. Programmes, Practices and Priorities for Research*; Position Paper 16; Marine Board, European Science Foundation: Oostende, Belgium, 2011.
(873) Bergman, Å.; Heindel, J. J.; Jobling, S.; Kidd, K. A.; Zoeller, R. T. *State of the Science of Endocrine Disrupting Chemicals—2012*, an assessment of the state of the science of endocrine disruptors prepared by a group of experts for the United Nations Environment Programme (UNEP) and WHO; UNEP: Nairobi, Kenya; World Health Organization: Geneva, Switzerland, 2012.
(874) *Commission Regulation (EU) No 756/2010 of 24 August 2010 Amending Regulation (EC) No 850/2004 of the European Parliament and of the Council on Persistent Organic Pollutants as Regards Annexes IV and V*; European Union: Brussels, Belgium, 2010.
(875) *Proposal for a Directive Amending the Water Framework Directive (WFD) and the Directive on Environmental Quality Standards (EQFD)*; Council of the European Union: Brussels, Belgium, 2011.
(876) Howard, E. I.; Sanishvili, R.; Cachau, R. E.; Mitschler, A.; Chevrier, B.; Barth, P.; Lamour, V.; Van Zandt, M.; Sibley, E.; Bon, C.; et al. Ultrahigh Resolution Drug Design I: Details of Interactions in Human Aldose Reductase-Inhibitor Complex at 0.66 Å. *Proteins: Struct., Funct., Genet.* **2004**, *55*, 792−804.
(877) Muzet, N.; Guillot, B.; Jelsch, C.; Howard, E.; Lecomte, C. Electrostatic Complementarity in an Aldose Reductase Complex from Ultra-High-Resolution Crystallography and First-Principles Calculations. *Proc. Natl. Acad. Sci. U. S. A.* **2003**, *100*, 8742−8747.
(878) Hays, F. A.; Vargason, J. M.; Ho, P. S. Effect of Sequence on the Conformation of DNA Holliday Junctions. *Biochemistry* **2003**, *42*, 9586−9597.
(879) El-Kabbani, O.; Ramsland, P.; Darmanin, C.; Chung, R. P. T.; Podjarny, A. Structure of Human Aldose Reductase Holoenzyme in Complex with Statil: An Approach to Structure-Based Inhibitor Design of the Enzyme. *Proteins: Struct., Funct., Genet.* **2003**, *50*, 230−238.
(880) Hays, F. A.; Teegarden, A.; Jones, Z. J. R.; Harms, M.; Raup, D.; Watson, J.; Cavaliere, E.; Ho, P. S. How Sequence Defines Structure: A Crystallographic Map of DNA Structure and Conformation. *Proc. Natl. Acad. Sci. U. S. A.* **2005**, *102*, 7157−7162.
(881) Eichman, B. F.; Vargason, J. M.; Mooers, B. H. M.; Ho, P. S. The Holliday Junction in an Inverted Repeat DNA Sequence: Sequence Effects on the Structure of Four-Way Junctions. *Proc. Natl. Acad. Sci. U. S. A.* **2000**, *97*, 3971−3976.
(882) Scholfield, M. R.; Vander Zanden, C. M.; Carter, M.; Ho, P. S. Halogen Bonding (X-Bonding): A Biological Perspective. *Protein Sci.* **2013**, *22*, 139−152.
(883) Panigrahi, S. K.; Desiraju, G. R. Strong and Weak Hydrogen Bonds in the Protein-Ligand Interface. *Proteins: Struct., Funct., Genet.* **2007**, *67*, 128−141.
(884) Zhou, P.; Tian, F.; Zou, J.; Shang, Z. Rediscovery of Halogen Bonds in Protein-Ligand Complexes. *Mini-Rev. Med. Chem.* **2010**, *10*, 309−314.
(885) Ho, P. S. Biomolecular Halogen Bonds. In *Halogen Bonding I: Impact on Materials Chemistry and Life Science*; Metrangolo, P., Resnati, G., Eds.; Springer International Publishing: Cham, Switzerland, 2015; pp 241−276.
(886) Wojtczak, A.; Cody, V.; Luft, J. R.; Pangborn, W. Structure of Rat Transthyretin (rTTR) Complex with Thyroxine at 2.5 Å Resolution: First Non-Biased Insight into Thyroxine Binding Reveals Different Hormone Orientation in Two Binding Sites. *Acta Crystallogr., Sect. D: Biol. Crystallogr.* **2001**, *57*, 1061−1070.
(887) Valadares, N. F.; Salum, L. B.; Polikarpov, I.; Andricopulo, A. D.; Garratt, R. C. Role of Halogen Bonds in Thyroid Hormone Receptor Selectivity: Pharmacophore-Based 3d-QSSR Studies. *J. Chem. Inf. Model.* **2009**, *49*, 2606−2616.
(888) Eneqvist, T.; Lundberg, E.; Karlsson, A.; Huang, S.; Santos, C. R. A.; Power, D. M.; Sauer-Eriksson, A. E. High Resolution Crystal Structures of Piscine Transthyretin Reveal Different Binding Modes for Triiodothyronine and Thyroxine. *J. Biol. Chem.* **2004**, *279*, 26411−26416.
(889) Bayse, C. A.; Rafferty, E. R. Is Halogen Bonding the Basis for Iodothyronine Deiodinase Activity? *Inorg. Chem.* **2010**, *49*, 5365−5367.
(890) Manna, D.; Mugesh, G. Regioselective Deiodination of Thyroxine by Iodothyronine Deiodinase Mimics: An Unusual Mechanistic Pathway Involving Cooperative Chalcogen and Halogen Bonding. *J. Am. Chem. Soc.* **2012**, *134*, 4269−4279.
(891) Liu, R.; Loll, P. J.; Eckenhoff, R. G. Structural Basis for High-Affinity Volatile Anesthetic Binding in a Natural 4-Helix Bundle Protein. *FASEB J.* **2005**, *19*, 567−576.
(892) Bhattacharya, A. A.; Curry, S.; Franks, N. P. Binding of the General Anesthetics Propofol and Halothane to Human Serum Albumin: High Resolution Crystal Structures. *J. Biol. Chem.* **2000**, *275*, 38731−38738.
(893) Yu, M.; Kumar, T. R. S.; Nkrumah, L. J.; Coppi, A.; Retzlaff, S.; Li, C. D.; Kelly, B. J.; Moura, P. A.; Lakshmanan, V.; Freundlich, J. S.; et al. The Fatty Acid Biosynthesis Enzyme FabI Plays a Key Role in the Development of Liver-Stage Malarial Parasites. *Cell Host Microbe* **2008**, *4*, 567−578.
(894) Tipparaju, S. K.; Mulhearn, D. C.; Klein, G. M.; Chen, Y.; Tapadar, S.; Bishop, M. H.; Yang, S.; Chen, J.; Ghassemi, M.; Santarsiero, B. D.; et al. Design and Synthesis of Aryl Ether Inhibitors of the Bacillus Anthracis Enoyl-ACP Reductase. *ChemMedChem* **2008**, *3*, 1250−1268.
(895) Priyadarshi, A.; Kim, E. E.; Hwang, K. Y. Structural Insights into Staphylococcus Aureus Enoyl-ACP Reductase (FabI), in Complex with NADP and Triclosan. *Proteins: Struct., Funct., Genet.* **2010**, *78*, 480−486.
(896) Freundlich, J. S.; Wang, F.; Vilchèze, C.; Gulten, G.; Langley, R.; Schiehser, G. A.; Jacobus, D. P.; Jacobs, W. R.; Sacchettini, J. C. Triclosan Derivatives: Towards Potent Inhibitors of Drug-Sensitive and Drug-Resistant Mycobacterium Tuberculosis. *ChemMedChem* **2009**, *4*, 241−248.
(897) Rowlinson, S. W.; Kiefer, J. R.; Prusakiewicz, J. J.; Pawlitz, J. L.; Kozak, K. R.; Kalgutkar, A. S.; Stallings, W. C.; Kurumbail, R. G.; Marnett, L. J. A Novel Mechanism of Cyclooxygenase-2 Inhibition Involving Interactions with Ser-530 and Tyr-385. *J. Biol. Chem.* **2003**, *278*, 45763−45769.
(898) Harman, C. A.; Turman, M. V.; Kozak, K. R.; Marnett, L. J.; Smith, W. L.; Garavito, R. M. Structural Basis of Enantioselective Inhibition of Cyclooxygenase-1 by S-Alpha-Substituted Indomethacin Ethanolamides. *J. Biol. Chem.* **2007**, *282*, 28096−28105.
(899) Ghuman, J.; Zunszain, P. A.; Petitpas, I.; Bhattacharya, A. A.; Otagiri, M.; Curry, S. Structural Basis of the Drug-Binding Specificity of Human Serum Albumin. *J. Mol. Biol.* **2005**, *353*, 38−52.
(900) Voth, A. R.; Ho, P. S. The Role of Halogen Bonding in Inhibitor Recognition and Binding by Protein Kinases. *Curr. Top. Med. Chem.* **2007**, *7*, 1336−1348.
(901) Battistutta, R.; De Moliner, E.; Sarno, S.; Zanotti, G.; Pinna, L. A. Structural Features Underlying Selective Inhibition of Protein Kinase CK2 by ATP Site-Directed Tetrabromo-2-Benzotriazole. *Protein Sci.* **2001**, *10*, 2200−2206.
(902) Battistutta, R.; Mazzorana, M.; Sarno, S.; Kazimierczuk, Z.; Zanotti, G.; Pinna, L. A. Inspecting the Structure-Activity Relationship

DOI: 10.1021/acs.chemrev.5b00484
Chem. Rev. 2016, 116, 2478−2601

of Protein Kinase CK2 Inhibitors Derived from Tetrabromo-Benzimidazole. *Chem. Biol.* **2005**, *12*, 1211−1219.
(903) Battistutta, R.; Mazzorana, M.; Cendron, L.; Bortolato, A.; Sarno, S.; Kazimierczuk, Z.; Zanotti, G.; Moro, S.; Pinna, L. A. The ATP-Binding Site of Protein Kinase CK2 Holds a Positive Electrostatic Area and Conserved Water Molecules. *ChemBioChem* **2007**, *8*, 1804−1809.
(904) Dobeš, P.; Řezáč, J.; Fanfrlík, J.; Otyepka, M.; Hobza, P. Semiempirical Quantum Mechanical Method PM6-DH2X Describes the Geometry and Energetics of CK2-Inhibitor Complexes Involving Halogen Bonds Well, While the Empirical Potential Fails. *J. Phys. Chem. B* **2011**, *115*, 8581−8589.
(905) Sarno, S.; Papinutto, E.; Franchin, C.; Bain, J.; Elliott, M.; Meggio, F.; Kazimierczuk, Z.; Orzeszko, A.; Zanotti, G.; Battistutta, R.; et al. ATP Site-Directed Inhibitors of Protein Kinase CK2: An Update. *Curr. Top. Med. Chem.* **2011**, *11*, 1340−1351.
(906) Fedorov, O.; Huber, K.; Eisenreich, A.; Filippakopoulos, P.; King, O.; Bullock, A. N.; Szklarczyk, D.; Jensen, L. J.; Fabbro, D.; Trappe, J.; et al. Specific CLK Inhibitors from a Novel Chemotype for Regulation of Alternative Splicing. *Chem. Biol.* **2011**, *18*, 67−76.
(907) De Moliner, E.; Moro, S.; Sarno, S.; Zagotto, G.; Zanotti, G.; Pinna, L. A.; Battistutta, R. Inhibition of Protein Kinase CK2 by Anthraquinone-Related Compounds: A Structural Insight. *J. Biol. Chem.* **2003**, *278*, 1831−1836.
(908) Wãsik, R.; Łebska, M.; Felczak, K.; Poznański, J.; Shugar, D. Relative Role of Halogen Bonds and Hydrophobic Interactions in Inhibition of Human Protein Kinase CK2α by Tetrabromobenzotriazole and Some C(5)-Substituted Analogues. *J. Phys. Chem. B* **2010**, *114*, 10601−10611.
(909) Beck, T.; Gruene, T.; Sheldrick, G. M. The Magic Triangle Goes MAD: Experimental Phasing with a Bromine Derivative. *Acta Crystallogr., Sect. D: Biol. Crystallogr.* **2010**, *66*, 374−380.
(910) Vallejos, M.; Auffinger, P.; Ho, P. Halogen Interactions in Biomolecular Crystal Structures. In *International Tables for Crystallography Vol. F: Crystallography of Biological Macromolecules*; Arnold, E., Himmel, D. M., Rossmann, G., Eds.; Wiley: Chichester, U.K., 2012; pp 821−826.
(911) Xie, J.; Wang, L.; Wu, N.; Brock, A.; Spraggon, G.; Schultz, P. G. The Site-Specific Incorporation of P-Iodo-L-Phenylalanine into Proteins for Structure Determination. *Nat. Biotechnol.* **2004**, *22*, 1297−1301.
(912) Voth, A. R.; Hays, F. A.; Ho, P. S. Directing Macromolecular Conformation through Halogen Bonds. *Proc. Natl. Acad. Sci. U. S. A.* **2007**, *104*, 6188−6193.
(913) Carter, M.; Ho, P. S. Assaying the Energies of Biological Halogen Bonds. *Cryst. Growth Des.* **2011**, *11*, 5087−5095.
(914) Carter, M.; Voth, A. R.; Scholfield, M. R.; Rummel, B.; Sowers, L. C.; Ho, P. S. Enthalpy-Entropy Compensation in Biomolecular Halogen Bonds Measured in DNA Junctions. *Biochemistry* **2013**, *52*, 4891−4903.
(915) Sunami, T.; Kondo, J.; Hirao, I.; Watanabe, K.; Miura, K.; Takénaka, A. Structures of d(GCGAAGC) and d(GCGAAAGC) (tetragonal Form): A Switching of Partners of the Sheared G.A Pairs to Form a Functional G.AxA.G Crossing. *Acta Crystallogr., Sect. D: Biol. Crystallogr.* **2004**, *60*, 422−431.
(916) Sunami, T.; Kondo, J.; Hirao, I.; Watanabe, K.; Miura, K. I.; Takénaka, A. Structure of d(GCGAAAGC) (hexagonal Form): A Base-Intercalated Duplex as a Stable Structure. *Acta Crystallogr., Sect. D: Biol. Crystallogr.* **2004**, *60*, 90−96.
(917) Domigan, N. M.; Charlton, T. S.; Duncan, M. W.; Winterbourn, C. C.; Kettle, A. J. Chlorination of Tyrosyl Residues in Peptides by Myeloperoxidase and Human Neutrophils. *J. Biol. Chem.* **1995**, *270*, 16542−16548.
(918) Wu, W.; Chen, Y.; d'Avignon, A.; Hazen, S. L. 3-Bromotyrosine and 3,5-Dibromotyrosine Are Major Products of Protein Oxidation by Eosinophil Peroxidase: Potential Markers for Eosinophil-Dependent Tissue Injury in Vivo. *Biochemistry* **1999**, *38*, 3538−3548.
(919) Davies, M. J. Myeloperoxidase-Derived Oxidation: Mechanisms of Biological Damage and Its Prevention. *J. Clin. Biochem. Nutr.* **2011**, *48*, 8−19.
(920) Wu, W.; Samoszuk, M. K.; Comhair, S. A.; Thomassen, M. J.; Farver, C. F.; Dweik, R. A.; Kavuru, M. S.; Erzurum, S. C.; Hazen, S. L. Eosinophils Generate Brominating Oxidants in Allergen-Induced Asthma. *J. Clin. Invest.* **2000**, *105*, 1455−1463.
(921) Pattison, D. I.; Davies, M. J. Kinetic Analysis of the Reactions of Hypobromous Acid with Protein Components: Implications for Cellular Damage and Use of 3-Bromotyrosine as a Marker of Oxidative Stress. *Biochemistry* **2004**, *43*, 4799−4809.
(922) Kambayashi, Y.; Ogino, K.; Takemoto, K.; Imagama, T.; Takigawa, T.; Kimura, S.; Hibino, Y.; Hitomi, Y.; Nakamura, H. Preparation and Characterization of a Polyclonal Antibody against Brominated Protein. *J. Clin. Biochem. Nutr.* **2009**, *44*, 95−103.
(923) Bertolani, A.; Pirrie, L.; Houbenov, N.; Haataja, J.; Stefan, L.; Catalano, L.; Terraneo, G.; Giancane, G.; Valli, L.; Milani, R.; et al. Supramolecular Amplification of Amyloid Self-Assembly by Iodination. *Nat. Commun.* **2015**, *6*, 7574.
(924) Kortagere, S.; Ekins, S.; Welsh, W. J. Halogenated Ligands and Their Interactions with Amino Acids: Implications for Structure-Activity and Structure-Toxicity Relationships. *J. Mol. Graphics Modell.* **2008**, *27*, 170−177.
(925) Saraogi, I.; Vijay, V. G.; Das, S.; Sekar, K.; Guru Row, T. N. C-Halogen···π Interactions in Proteins: A Database Study. *Cryst. Eng.* **2003**, *6*, 69−77.
(926) Matter, H.; Nazaré, M.; Güssregen, S.; Will, D. W.; Schreuder, H.; Bauer, A.; Urmann, M.; Ritter, K.; Wagner, M.; Wehner, V. Evidence for C-Cl/C-Br···π Interactions as an Important Contribution to Protein-Ligand Binding Affinity. *Angew. Chem., Int. Ed.* **2009**, *48*, 2911−2916.
(927) Nazaré, M.; Will, D. W.; Matter, H.; Schreuder, H.; Ritter, K.; Urmann, M.; Essrich, M.; Bauer, A.; Wagner, M.; Czech, J.; et al. Probing the Subpockets of Factor Xa Reveals Two Binding Modes for Inhibitors Based on a 2-Carboxyindole Scaffold: A Study Combining Structure-Activity Relationship and X-Ray Crystallography. *J. Med. Chem.* **2005**, *48*, 4511−4525.
(928) Matter, H.; Will, D. W.; Nazaré, M.; Schreuder, H.; Laux, V.; Wehner, V. Structural Requirements for Factor Xa Inhibition by 3-Oxybenzamides with Neutral P1 Substituents: Combining X-Ray Crystallography, 3D-QSAR, and Tailored Scoring Functions. *J. Med. Chem.* **2005**, *48*, 3290−3312.
(929) Shi, Y.; Sitkoff, D.; Zhang, J.; Klei, H. E.; Kish, K.; Liu, E. C.-K.; Hartl, K. S.; Seiler, S. M.; Chang, M.; Huang, C.; et al. Design, Structure-Activity Relationships, X-Ray Crystal Structure, and Energetic Contributions of a Critical P1 Pharmacophore: 3-Chloroindole-7-Yl-Based Factor Xa Inhibitors. *J. Med. Chem.* **2008**, *51*, 7541−7551.
(930) Adler, M.; Kochanny, M. J.; Ye, B.; Rumennik, G.; Light, D. R.; Biancalana, S.; Whitlow, M. Crystal Structures of Two Potent Nonamidine Inhibitors Bound to Factor Xa. *Biochemistry* **2002**, *41*, 15514−15523.
(931) Liu, L.; Baase, W. A.; Matthews, B. W. Halogenated Benzenes Bound within a Non-Polar Cavity in T4 Lysozyme Provide Examples of I···S and I···Se Halogen-Bonding. *J. Mol. Biol.* **2009**, *385*, 595−605.
(932) Wilcken, R.; Zimmermann, M. O.; Lange, A.; Zahn, S.; Boeckler, F. M. Using Halogen Bonds to Address the Protein Backbone: A Systematic Evaluation. *J. Comput.-Aided Mol. Des.* **2012**, *26*, 935−945.
(933) Lu, Y.; Wang, Y.; Zhu, W. Nonbonding Interactions of Organic Halogens in Biological Systems: Implications for Drug Discovery and Biomolecular Design. *Phys. Chem. Chem. Phys.* **2010**, *12*, 4543−4551.
(934) Paulini, R.; Müller, K.; Diederich, F. Orthogonal Multipolar Interactions in Structural Chemistry and Biology. *Angew. Chem., Int. Ed.* **2005**, *44*, 1788−1805.
(935) Zhou, P.; Lv, J.; Zou, J.; Tian, F.; Shang, Z. Halogen-Water-Hydrogen Bridges in Biomolecules. *J. Struct. Biol.* **2010**, *169*, 172−182.
(936) Wester, M. R.; Johnson, E. F.; Marques-Soares, C.; Dijols, S.; Dansette, P. M.; Mansuy, D.; Stout, C. D. Structure of Mammalian

DOI: 10.1021/acs.chemrev.5b00484
Chem. Rev. 2016, 116, 2478−2601

Cytochrome P450 2C5 Complexed with Diclofenac at 2.1 Å Resolution: Evidence for an Induced Fit Model of Substrate Binding. *Biochemistry* **2003**, *42*, 9335−9345.
(937) Mir, R.; Singh, N.; Vikram, G.; Kumar, R. P.; Sinha, M.; Bhushan, A.; Kaur, P.; Srinivasan, A.; Sharma, S.; Singh, T. P. The Structural Basis for the Prevention of Nonsteroidal Antiinflammatory Drug-Induced Gastrointestinal Tract Damage by the C-Lobe of Bovine Colostrum Lactoferrin. *Biophys. J.* **2009**, *97*, 3178−3186.
(938) Carter, M.; Rappé, A. K.; Ho, P. S. Scalable Anisotropic Shape and Electrostatic Models for Biological Bromine Halogen Bonds. *J. Chem. Theory Comput.* **2012**, *8*, 2461−2473.
(939) Ouvrard, C.; Le Questel, J. Y.; Berthelot, M.; Laurence, C. Halogen-Bond Geometry: A Crystallographic Database Investigation of Dihalogen Complexes. *Acta Crystallogr., Sect. B: Struct. Sci.* **2003**, *59*, 512−526.
(940) Vander Zanden, C. M.; Carter, M.; Ho, P. S. Determining Thermodynamic Properties of Molecular Interactions from Single Crystal Studies. *Methods* **2013**, *64*, 12−18.
(941) Tatko, C. D.; Waters, M. L. Effect of Halogenation on Edge − Face Aromatic Interactions in a Beta-Hairpin Peptide: Enhanced Affinity with Iodo-Substituents. *Org. Lett.* **2004**, *6*, 3969−3972.
(942) Hardegger, L. A.; Kuhn, B.; Spinnler, B.; Anselm, L.; Ecabert, R.; Stihle, M.; Gsell, B.; Thoma, R.; Diez, J.; Benz, J.; et al. Systematic Investigation of Halogen Bonding in Protein-Ligand Interactions. *Angew. Chem., Int. Ed.* **2011**, *50*, 314−318.
(943) Wyatt, P. G.; Woodhead, A. J.; Berdini, V.; Boulstridge, J. A.; Carr, M. G.; Cross, D. M.; Davis, D. J.; Devine, L. A.; Early, T. R.; Feltell, R. E.; et al. Identification of N-(4-Piperidinyl)-4-(2,6-Dichlorobenzoylamino)-1H-Pyrazole-3-Carboxamide (AT7519), a Novel Cyclin Dependent Kinase Inhibitor Using Fragment-Based X-Ray Crystallography and Structure Based Drug Design. *J. Med. Chem.* **2008**, *51*, 4986−4999.
(944) National Cancer Institute/National Institutes of Health (NCI/NIH). Developmental Therapeutics Program, 2014. http://dtp.nci.nih.gov/index.html.
(945) Lu, Y.; Liu, Y.; Xu, Z.; Li, H.; Liu, H.; Zhu, W. Halogen Bonding for Rational Drug Design and New Drug Discovery. *Expert Opin. Drug Discovery* **2012**, *7*, 375−383.
(946) Wilcken, R.; Liu, X.; Zimmermann, M. O.; Rutherford, T. J.; Fersht, A. R.; Joerger, A. C.; Boeckler, F. M. Halogen-Enriched Fragment Libraries as Leads for Drug Rescue of Mutant p53. *J. Am. Chem. Soc.* **2012**, *134*, 6810−6818.
(947) Lu, Y.; Shi, T.; Wang, Y.; Yang, H.; Yan, X.; Luo, X.; Jiang, H.; Zhu, W. Halogen Bonding - A Novel Interaction for Rational Drug Design? *J. Med. Chem.* **2009**, *52*, 2854−2862.
(948) Hernandes, M. Z.; Cavalcanti, S. M.; Moreira, D. R.; de Azevedo, W. F., Jr.; Leite, A. C. Halogen Atoms in the Modern Medicinal Chemistry: Hints for the Drug Design. *Curr. Drug Targets* **2010**, *11*, 303−314.
(949) Hardegger, L. A.; Kuhn, B.; Spinnler, B.; Anselm, L.; Ecabert, R.; Stihle, M.; Gsell, B.; Thoma, R.; Diez, J.; Benz, J.; et al. Halogen Bonding at the Active Sites of Human Cathepsin L and MEK1 Kinase: Efficient Interactions in Different Environments. *ChemMedChem* **2011**, *6*, 2048−2054.
(950) Himmel, D. M.; Das, K.; Clark, A. D.; Hughes, S. H.; Benjahad, A.; Oumouch, S.; Guillemont, J.; Coupa, S.; Poncelet, A.; Csoka, I.; et al. Crystal Structures for HIV-1 Reverse Transcriptase in Complexes with Three Pyridinone Derivatives: A New Class of Non-Nucleoside Inhibitors Effective against a Broad Range of Drug-Resistant Strains. *J. Med. Chem.* **2005**, *48*, 7582−7591.
(951) Heath, R. J.; Su, N.; Murphy, C. K.; Rock, C. O. The Enoyl-[acyl-Carrier-Protein] Reductases FabI and FabL fromBacillus Subtilis. *J. Biol. Chem.* **2000**, *275*, 40128−40133.
(952) Kunfermann, A.; Witschel, M.; Illarionov, B.; Martin, R.; Rottmann, M.; Höffken, H. W.; Seet, M.; Eisenreich, W.; Knölker, H.-J.; Fischer, M.; et al. Pseudilins: Halogenated, Allosteric Inhibitors of the Non-Mevalonate Pathway Enzyme IspD. *Angew. Chem., Int. Ed.* **2014**, *53*, 2235−2239.
(953) Ibrahim, M. A. A. Molecular Mechanical Study of Halogen Bonding in Drug Discovery. *J. Comput. Chem.* **2011**, *32*, 2564−2574.
(954) Rendine, S.; Pieraccini, S.; Forni, A.; Sironi, M. Halogen Bonding in Ligand−receptor Systems in the Framework of Classical Force Fields. *Phys. Chem. Chem. Phys.* **2011**, *13*, 19508−19516.
(955) Jorgensen, W. L.; Schyman, P. Treatment of Halogen Bonding in the OPLS-AA Force Field: Application to Potent Anti-HIV Agents. *J. Chem. Theory Comput.* **2012**, *8*, 3895−3901.
(956) Case, D. A.; Cheatham, T. E.; Darden, T.; Gohlke, H.; Luo, R.; Merz, K. M.; Onufriev, A.; Simmerling, C.; Wang, B.; Woods, R. J. The Amber Biomolecular Simulation Programs. *J. Comput. Chem.* **2005**, *26*, 1668−1688.
(957) Ibrahim, M. A. A. AMBER Empirical Potential Describes the Geometry and Energy of Noncovalent Halogen Interactions Better than Advanced Semiempirical Quantum Mechanical Method PM6-DH2X. *J. Phys. Chem. B* **2012**, *116*, 3659−3669.
(958) Kolář, M.; Hobza, P. On Extension of the Current Biomolecular Empirical Force Field for the Description of Halogen Bonds. *J. Chem. Theory Comput.* **2012**, *8*, 1325−1333.
(959) Liu, Y.; Xu, Z.; Yang, Z.; Chen, K.; Zhu, W. A Knowledge-Based Halogen Bonding Scoring Function for Predicting Protein-Ligand Interactions. *J. Mol. Model.* **2013**, *19*, 5015−5030.
(960) Jeffrey, G. A. *An Introduction to Hydrogen Bonding*; Oxford University Press: Oxford, U.K., 1997.
(961) Steed, J. W.; Atwood, J. L. *Supramolecular Chemistry*, 2nd ed.; Wiley: Weinheim, Germany, 2009.
(962) Gholami, M. R.; Talebi, B. A. Gas-Phase Diels-Alder Cycloaddition Reaction in the Presence of Methanol and Water Vapor. *J. Phys. Org. Chem.* **2003**, *16*, 79−83.
(963) Curran, D. P.; Kuo, L. H. Altering the Stereochemistry of Allylation Reactions of Cyclic α-Sulfinyl Radicals with Diarylureas. *J. Org. Chem.* **1994**, *59*, 3259−3261.
(964) Curran, D. P. Acceleration of a Dipolar Claisen Rearrangement by Hydrogen Bonding to a Soluble Diaryl Urea. *Tetrahedron Lett.* **1995**, *36*, 6647−6650.
(965) Etter, M. C.; Panunto, T. W. 1,3-Bis(m-Nitrophenyl)urea: An Exceptionally Good Complexing Agent for Proton Acceptors. *J. Am. Chem. Soc.* **1988**, *110*, 5896−5897.
(966) Hine, J.; Linden, S.-M.; Kanagasabapathy, V. M. 1,8-Biphenylenediol Is a Double-Hydrogen-Bonding Catalyst for Reaction of an Epoxide With a Nucleophile. *J. Am. Chem. Soc.* **1985**, *107*, 1082−1083.
(967) Schreiner, P. R. Metal-Free Organocatalysis through Explicit Hydrogen Bonding Interactions. *Chem. Soc. Rev.* **2003**, *32*, 289−296.
(968) Zhang, Z.; Schreiner, P. R. (Thio)urea Organocatalysis−what Can Be Learnt from Anion Recognition? *Chem. Soc. Rev.* **2009**, *38*, 1187−1198.
(969) Schindler, S.; Huber, S. M. Halogen Bonds in Organic Synthesis and Organocatalysis. In *Halogen Bonding II: Impact on Material Chemistry and Life Science*; Metrangolo, P., Resnati, G., Eds.; Springer International Publishing: Cham, Switzerland, 2015; pp 167−203.
(970) Kniep, F.; Jungbauer, S. H.; Zhang, Q.; Walter, S. M.; Schindler, S.; Schnapperelle, I.; Herdtweck, E.; Huber, S. M. Organocatalysis by Neutral Multidentate Halogen-Bond Donors. *Angew. Chem., Int. Ed.* **2013**, *52*, 7028−7032.
(971) Lu, Y.; Li, H.; Zhu, X.; Zhu, W.; Liu, H. How Does Halogen Bonding Behave in Solution? A Theoretical Study Using Implicit Solvation Model. *J. Phys. Chem. A* **2011**, *115*, 4467−4475.
(972) Zefirov, N. S.; Makhon'kov, D. I. X-Philic Reactions. *Chem. Rev.* **1982**, *82*, 615−624.
(973) Bailey, W. F.; Patricia, J. J. The Mechanism of the Lithium - Halogen Interchange Reaction: A Review of the Literature. *J. Organomet. Chem.* **1988**, *352*, 1−46.
(974) Banerjee, A. K.; Vera, W.; Mora, H.; Laya, M. S.; Bedoya, L.; Cabrera, E. V. Iodine in Organic Synthesis. *J. Sci. Ind. Res.* **2006**, *65*, 299−308.
(975) Togo, H.; Iida, S. Synthetic Use of Molecular Iodine for Organic Synthesis. *Synlett* **2006**, *2006*, 2159−2175.

DOI: 10.1021/acs.chemrev.5b00484
Chem. Rev. 2016, 116, 2478−2601

(976) Jereb, M.; Vražič, D.; Zupan, M. Iodine-Catalyzed Transformation of Molecules Containing Oxygen Functional Groups. *Tetrahedron* **2011**, *67*, 1355−1387.
(977) Alcaide, B.; Almendros, P.; Cabrero, G.; Ruiz, M. P. Direct Synthesis of Protected Enantiopure 5-Cyano-3,4-Dihydroxypyrrolidin-2-Ones from β-Lactam Aldehydes Catalyzed by Iodine. *Synthesis* **2008**, *2008*, 2835−2839.
(978) Das, S.; Borah, R.; Devi, R. R.; Thakur, A. J. Molecular Iodine in Protection and Deprotection Chemistry. *Synlett* **2008**, *2008*, 2741−2762.
(979) Coulembier, O.; Meyer, F.; Dubois, P. Controlled Room Temperature ROP of L-Lactide by ICl3: A Simple Halogen-Bonding Catalyst. *Polym. Chem.* **2010**, *1*, 434−437.
(980) Bruckmann, A.; Pena, M. A.; Bolm, C. Organocatalysis through Halogen-Bond Activation. *Synlett* **2008**, *2008*, 900−902.
(981) He, W.; Ge, Y. C.; Tan, C. H. Halogen-Bonding-Induced Hydrogen Transfer to C═N Bond with Hantzsch Ester. *Org. Lett.* **2014**, *16*, 3244−3247.
(982) Bew, S. P.; Fairhurst, S. A.; Hughes, D. L.; Legentil, L.; Liddle, J.; Pesce, P.; Nigudkar, S.; Wilson, M. A. Organocatalytic Aziridine Synthesis Using F+ Salts. *Org. Lett.* **2009**, *11*, 4552−4555.
(983) Walter, S. M.; Kniep, F.; Herdtweck, E.; Huber, S. M. Halogen-Bond-Induced Activation of a Carbon-Heteroatom Bond. *Angew. Chem., Int. Ed.* **2011**, *50*, 7187−7191.
(984) Kniep, F.; Walter, S. M.; Herdtweck, E.; Huber, S. M. 4,4′-Azobis(halopyridinium) Derivatives: Strong Multidentate Halogen-Bond Donors with a Redox-Active Core. *Chem. - Eur. J.* **2012**, *18*, 1306−1310.
(985) Walter, S. M.; Kniep, F.; Rout, L.; Schmidtchen, F. P.; Herdtweck, E.; Huber, S. M. Isothermal Calorimetric Titrations on Charge-Assisted Halogen Bonds: Role of Entropy, Counterions, Solvent, and Temperature. *J. Am. Chem. Soc.* **2012**, *134*, 8507−8512.
(986) Jungbauer, S. H.; Walter, S. M.; Schindler, S.; Rout, L.; Kniep, F.; Huber, S. M. Activation of a Carbonyl Compound by Halogen Bonding. *Chem. Commun.* **2014**, *50*, 6281−6284.
(987) Walter, S. M.; Jungbauer, S. H.; Kniep, F.; Schindler, S.; Herdtweck, E.; Huber, S. M. Polyfluorinated versus Cationic Multidentate Halogen-Bond Donors: A Direct Comparison. *J. Fluorine Chem.* **2013**, *150*, 14−20.
(988) Dordonne, S.; Crousse, B.; Bonnet-Delpon, D.; Legros, J. Fluorous Tagging of DABCO through Halogen Bonding: Recyclable Catalyst for the Morita-Baylis-Hillman Reaction. *Chem. Commun.* **2011**, *47*, 5855−5857.
(989) Lindsay, V. N. G.; Lin, W.; Charette, A. B. Experimental Evidence for the All-up Reactive Conformation of Chiral rhodium(II) Carboxylate Catalysts: Enantioselective Synthesis of Cis-Cyclopropane α-Amino Acids. *J. Am. Chem. Soc.* **2009**, *131*, 16383−16385.
(990) D'Andrade, B. W.; Forrest, S. R. White Organic Light-Emitting Devices for Solid-State Lighting. *Adv. Mater.* **2004**, *16*, 1585−1595.
(991) Xiao, L.; Chen, Z.; Qu, B.; Luo, J.; Kong, S.; Gong, Q.; Kido, J. Recent Progresses on Materials for Electrophosphorescent Organic Light-Emitting Devices. *Adv. Mater.* **2011**, *23*, 926−952.
(992) Zhao, Q.; Li, F.; Huang, C. Phosphorescent Chemosensors Based on Heavy-Metal Complexes. *Chem. Soc. Rev.* **2010**, *39*, 3007−3030.
(993) Varghese, S.; Das, S. Role of Molecular Packing in Determining Solid-State Optical Properties of π-Conjugated Materials. *J. Phys. Chem. Lett.* **2011**, *2*, 863−873.
(994) Sagara, Y.; Kato, T. Mechanically Induced Luminescence Changes in Molecular Assemblies. *Nat. Chem.* **2009**, *1*, 605−610.
(995) Chung, J. W.; Yoon, S.-J.; An, B.-K.; Park, S. Y. High-Contrast On/Off Fluorescence Switching via Reversible E−Z Isomerization of Diphenylstilbene Containing the α-Cyanostilbenic Moiety. *J. Phys. Chem. C* **2013**, *117*, 11285−11291.
(996) Gierschner, J.; Park, S. Y. Luminescent Distyrylbenzenes: Tailoring Molecular Structure and Crystalline Morphology. *J. Mater. Chem. C* **2013**, *1*, 5818−5832.
(997) Shi, L.; Liu, H.-Y.; Shen, H.; Hu, J.; Zhang, G.-L.; Wang, H.; Ji, L.-N.; Chang, C.-K.; Jiang, H.-F. Fluorescence Properties of Halogenated Mono-Hydroxyl Corroles: The Heavy-Atom Effects. *J. Porphyrins Phthalocyanines* **2009**, *13*, 1221−1226.
(998) Koziar, J. C.; Cowan, D. O. Photochemical Heavy-Atom Effects. *Acc. Chem. Res.* **1978**, *11*, 334−341.
(999) Solov'ev, K. N.; Borisevich, E. A. Intramolecular Heavy-Atom Effect in the Photophysics of Organic Molecules. *Usp. Fiz. Nauk* **2005**, *175*, 247.
(1000) Gorman, A.; Killoran, J.; O'Shea, C.; Kenna, T.; Gallagher, W. M.; O'Shea, D. F. In Vitro Demonstration of the Heavy-Atom Effect for Photodynamic Therapy. *J. Am. Chem. Soc.* **2004**, *126*, 10619−10631.
(1001) Sun, C. L.; Li, J.; Geng, H. W.; Li, H.; Ai, Y.; Wang, Q.; Pan, S. L.; Zhang, H. L. Understanding the Unconventional Effects of Halogenation on the Luminescent Properties of Oligo(phenylene Vinylene) Molecules. *Chem. - Asian J.* **2013**, *8*, 3091−3100.
(1002) Yan, D.; Delori, A.; Lloyd, G. O.; Friščić, T.; Day, G. M.; Jones, W.; Lu, J.; Wei, M.; Evans, D. G.; Duan, X. A Cocrystal Strategy to Tune the Luminescent Properties of Stilbene-Type Organic Solid-State Materials. *Angew. Chem., Int. Ed.* **2011**, *50*, 12483−12486.
(1003) Yan, D.; Bučar, D. K.; Delori, A.; Patel, B.; Lloyd, G. O.; Jones, W.; Duan, X. Ultrasound-Assisted Construction of Halogen-Bonded Nanosized Cocrystals That Exhibit Thermosensitive Luminescence. *Chem. - Eur. J.* **2013**, *19*, 8213−8219.
(1004) Bolton, O.; Lee, K.; Kim, H.-J.; Lin, K. Y.; Kim, J. Activating Efficient Phosphorescence from Purely Organic Materials by Crystal Design. *Nat. Chem.* **2011**, *3*, 205−210.
(1005) You, Y.; Park, S. Y. Phosphorescent iridium(III) Complexes: Toward High Phosphorescence Quantum Efficiency through Ligand Control. *Dalton Trans.* **2009**, 1267−1282.
(1006) Zhao, Q.; Huang, C.; Li, F. Phosphorescent Heavy-Metal Complexes for Bioimaging. *Chem. Soc. Rev.* **2011**, *40*, 2508−2524.
(1007) Yuan, W. Z.; Shen, X. Y.; Zhao, H.; Lam, J. W. Y.; Tang, L.; Lu, P.; Wang, C.; Liu, Y.; Wang, Z.; Zheng, Q.; et al. Crystallization-Induced Phosphorescence of Pure Organic Luminogens at Room Temperature. *J. Phys. Chem. C* **2010**, *114*, 6090−6099.
(1008) Hirata, S.; Adachi, C.; Watanabe, T.; Totani, K. Efficient Persistent Room Temperature Phosphorescence in Organic Materials. *Kobunshi Ronbunshu* **2013**, *70*, 623−636.
(1009) Bolton, O.; Lee, D.; Jung, J.; Kim, J. Tuning the Photophysical Properties of Metal-Free Room Temperature Organic Phosphors via Compositional Variations in Bromobenzaldehyde/Dibromobenzene Mixed Crystals. *Chem. Mater.* **2014**, *26*, 6644−6649.
(1010) Lee, D.; Bolton, O.; Kim, B. C.; Youk, J. H.; Takayama, S.; Kim, J. Room Temperature Phosphorescence of Metal-Free Organic Materials in Amorphous Polymer Matrices. *J. Am. Chem. Soc.* **2013**, *135*, 6325−6329.
(1011) Kwon, M. S.; Lee, D.; Seo, S.; Jung, J.; Kim, J. Tailoring Intermolecular Interactions for Efficient Room-Temperature Phosphorescence from Purely Organic Materials in Amorphous Polymer Matrices. *Angew. Chem., Int. Ed.* **2014**, *53*, 11177−11181.
(1012) Pang, X.; Jin, W. J. Halogen Bonding in the Design of Organic Phosphors. In *Halogen Bonding II: Impact on Material Chemistry and Life Science*; Metrangolo, P., Resnati, G., Eds.; Springer International Publishing: Cham, Switzerland, 2015; pp 115−146.
(1013) Gao, H. Y.; Shen, Q. J.; Zhao, X. R.; Yan, X. Q.; Pang, X.; Jin, W. J. Phosphorescent Co-Crystal Assembled by 1,4-Diiodotetrafluorobenzene with Carbazole Based on C−I···π Halogen Bonding. *J. Mater. Chem.* **2012**, *22*, 5336−5343.
(1014) Gao, H. Y.; Zhao, X. R.; Wang, H.; Pang, X.; Jin, W. J. Phosphorescent Cocrystals Assembled by 1,4- Diiodotetrafluorobenzene and Fluorene and Its Heterocyclic Analogues Based on C−I···π Halogen Bonding. *Cryst. Growth Des.* **2012**, *12*, 4377−4387.
(1015) Zhu, Q.; Gao, Y. J.; Gao, H. Y.; Jin, W. J. Effect of N-Methyl and Ethyl on Phosphorescence of Carbazole in Cocrystals Assembled by C-I···π Halogen Bond, π-Hole···π Bond and Other Interactions Using 1,4-Diiodotetrafluorobenzene as Donor. *J. Photochem. Photobiol., A* **2014**, *289*, 31−38.
(1016) Shen, Q. J.; Wei, H. Q.; Zou, W. S.; Sun, H. L.; Jin, W. J. Cocrystals Assembled by Pyrene and 1,2- or 1,4-Diiodotetrafluor-

DOI: 10.1021/acs.chemrev.5b00484
Chem. Rev. 2016, 116, 2478−2601

obenzenes and Their Phosphorescent Behaviors Modulated by Local Molecular Environment. *CrystEngComm* **2012**, *14*, 1010−1015.
(1017) Pang, X.; Wang, H.; Zhao, X. R.; Jin, W. J. Co-Crystallization Turned on the Phosphorescence of Phenanthrene by C−Br···π Halogen Bonding, π−hole···π Bonding and Other Assisting Interactions. *CrystEngComm* **2013**, *15*, 2722−2730.
(1018) Zhu, Q.; Wang, H.; Zhao, X. R.; Jin, W. J. The Phosphorescent Behaviors of 9-Bromo- and 9-Iodophenanthrene in Crystals Modulated by π-π Interactions, C-H···π Hydrogen Bond and C-I···π Halogen Bond. *J. Photochem. Photobiol., A* **2014**, *274*, 98−107.
(1019) Ventura, B.; Bertocco, A.; Braga, D.; Catalano, L.; D'Agostino, S.; Grepioni, F.; Taddei, P. Luminescence Properties of 1,8-Naphthalimide Derivatives in Solution, in Their Crystals, and in Co-Crystals: Toward Room-Temperature Phosphorescence from Organic Materials. *J. Phys. Chem. C* **2014**, *118*, 18646−18658.
(1020) Kucheryavy, P.; Li, G.; Vyas, S.; Hadad, C.; Glusac, K. D. Electronic Properties of 4-Substituted Naphthalimides. *J. Phys. Chem. A* **2009**, *113*, 6453−6461.
(1021) D'Agostino, S.; Grepioni, F.; Braga, D.; Ventura, B. Tipping the Balance with the Aid of Stoichiometry: Room Temperature Phosphorescence versus Fluorescence in Organic Cocrystals. *Cryst. Growth Des.* **2015**, *15*, 2039−2045.
(1022) Mayerhöffer, U.; Würthner, F. Halogen-Arene Interactions Assist in Self-Assembly of Dyes. *Angew. Chem., Int. Ed.* **2012**, *51*, 5615−5619.
(1023) Zapata, F.; Caballero, A.; White, N. G.; Claridge, T. D. W.; Costa, P. J.; Félix, V.; Beer, P. D. Fluorescent Charge-Assisted Halogen-Bonding Macrocyclic Halo-Imidazolium Receptors for Anion Recognition and Sensing in Aqueous Media. *J. Am. Chem. Soc.* **2012**, *134*, 11533−11541.
(1024) Gilday, L. C.; White, N. G.; Beer, P. D. Halogen- and Hydrogen-Bonding Triazole-Functionalised Porphyrin-Based Receptors for Anion Recognition. *Dalton Trans.* **2013**, *42*, 15766−15773.
(1025) Zou, W.-S.; Lin, S.; Li, J.-Y.; Wei, H.-Q.; Zhang, X.-Q.; Shen, D.-X.; Qiao, J.-Q.; Lian, H.-Z.; Xie, D.-Q.; Ge, X. Mechanism and Application of Halogen Bond Induced Fluorescence Enhancement and Iodine Molecule Cleavage in Solution. *New J. Chem.* **2015**, *39*, 262−272.
(1026) Bushuyev, O. S.; Tomberg, A.; Friščić, T.; Barrett, C. J. Shaping Crystals with Light: Crystal-to-Crystal Isomerization and Photomechanical Effect in Fluorinated Azobenzenes. *J. Am. Chem. Soc.* **2013**, *135*, 12556−12559.
(1027) Bushuyev, O. S.; Corkery, T. C.; Barrett, C. J.; Friščić, T. Photo-Mechanical Azobenzene Cocrystals and in Situ X-Ray Diffraction Monitoring of Their Optically-Induced Crystal-to-Crystal Isomerisation. *Chem. Sci.* **2014**, *5*, 3158−3164.
(1028) Bandara, H. M. D.; Burdette, S. C. Photoisomerization in Different Classes of Azobenzene. *Chem. Soc. Rev.* **2012**, *41*, 1809−1825.
(1029) Seki, T. New Strategies and Implications for the Photoalignment of Liquid Crystalline Polymers. *Polym. J.* **2014**, *46*, 751−768.
(1030) Yaroshchuk, O.; Reznikov, Y. Photoalignment of Liquid Crystals: Basics and Current Trends. *J. Mater. Chem.* **2012**, *22*, 286−300.
(1031) Ikeda, T. Photomodulation of Liquid Crystal Orientations for Photonic Applications. *J. Mater. Chem.* **2003**, *13*, 2037−2057.
(1032) Rochon, P.; Batalla, E.; Natansohn, A. Optically Induced Surface Gratings on Azoaromatic Polymer Films. *Appl. Phys. Lett.* **1995**, *66*, 136−138.
(1033) Kim, D. Y.; Tripathy, S. K.; Li, L.; Kumar, J. Laser-Induced Holographic Surface Relief Gratings on Nonlinear Optical Polymer Films. *Appl. Phys. Lett.* **1995**, *66*, 1166−1168.
(1034) Lee, S.; Kang, H. S.; Park, J. K. Directional Photofluidization Lithography: Micro/nanostructural Evolution by Photofluidic Motions of Azobenzene Materials. *Adv. Mater.* **2012**, *24*, 2069−2103.
(1035) Priimagi, A.; Shevchenko, A. Azopolymer-Based Micro- and Nanopatterning for Photonic Applications. *J. Polym. Sci., Part B: Polym. Phys.* **2014**, *52*, 163−182.
(1036) Ube, T.; Ikeda, T. Photomobile Polymer Materials with Crosslinked Liquid-Crystalline Structures: Molecular Design, Fabrication, and Functions. *Angew. Chem., Int. Ed.* **2014**, *53*, 10290−10299.
(1037) Koshima, H.; Ojima, N.; Uchimoto, H. Mechanical Motion of Azobenzene Crystals upon Photoirradiation. *J. Am. Chem. Soc.* **2009**, *131*, 6890−6891.
(1038) Kim, T.; Zhu, L.; Al-Kaysi, R. O.; Bardeen, C. J. Organic Photomechanical Materials. *ChemPhysChem* **2014**, *15*, 400−414.
(1039) Saccone, M.; Cavallo, G.; Metrangolo, P.; Resnati, G.; Priimagi, A. Halogen-Bonded Photoresponsive Materials. In Halogen Bonding II: Impact on Material Chemistry and Life Science; *Top. Curr. Chem.*; 2015, *359*, pp 147−166. Metrangolo, P.; Resnati, G. Eds.; Springer International Publishing: Cham, Switzerland.
(1040) Tabiryan, N.; Serak, S.; Dai, X.-M.; Bunning, T. Polymer Film with Optically Controlled Form and Actuation. *Opt. Express* **2005**, *13*, 7442−7448.
(1041) Priimagi, A.; Lindfors, K.; Kaivola, M.; Rochon, P. Efficient Surface-Relief Gratings in Hydrogen-Bonded Polymer−Azobenzene Complexes. *ACS Appl. Mater. Interfaces* **2009**, *1*, 1183−1189.
(1042) Vapaavuori, J.; Priimagi, A.; Kaivola, M. Photoinduced Surface-Relief Gratings in Films of Supramolecular Polymer-Bisazobenzene Complexes. *J. Mater. Chem.* **2010**, *20*, 5260−5264.
(1043) Zhang, Q.; Wang, X.; Barrett, C. J.; Bazuin, C. G. Spacer-Free Ionic Dye−Polyelectrolyte Complexes: Influence of Molecular Structure on Liquid Crystal Order and Photoinduced Motion. *Chem. Mater.* **2009**, *21*, 3216−3227.
(1044) Han, G.; Zhang, H.; Chen, J.; Sun, Q.; Zhang, Y.; Zhang, H. Easily Crosslinkable Side-Chain Azobenzene Polymers for Fast and Persistent Fixation of Surface Relief Gratings. *New J. Chem.* **2015**, *39*, 1410−1420.
(1045) Zakrevskyy, Y.; Stumpe, J.; Faul, C. F. J. A Supramolecular Approach to Optically Anisotropic Materials: Photosensitive Ionic Self-Assembly Complexes. *Adv. Mater.* **2006**, *18*, 2133−2136.
(1046) Kreger, K.; Wolfer, P.; Audorff, H.; Kador, L.; Stingelin-Stutzmann, N.; Smith, P.; Schmidt, H.-W. Stable Holographic Gratings with Small-Molecular Trisazobenzene Derivatives. *J. Am. Chem. Soc.* **2010**, *132*, 509−516.
(1047) Mamiya, J.; Yoshitake, A.; Kondo, M.; Yu, Y.; Ikeda, T. Is Chemical Crosslinking Necessary for the Photoinduced Bending of Polymer Films? *J. Mater. Chem.* **2008**, *18*, 63−65.
(1048) Broer, D. J.; Bastiaansen, C. M. W.; Debije, M. G.; Schenning, A. P. H. J. Functional Organic Materials Based on Polymerized Liquid-Crystal Monomers: Supramolecular Hydrogen-Bonded Systems. *Angew. Chem., Int. Ed.* **2012**, *51*, 7102−7109.
(1049) Kobatake, S.; Takami, S.; Muto, H.; Ishikawa, T.; Irie, M. Rapid and Reversible Shape Changes of Molecular Crystals on Photoirradiation. *Nature* **2007**, *446*, 778−781.
(1050) Bléger, D.; Schwarz, J.; Brouwer, A. M.; Hecht, S. O-Fluoroazobenzenes as Readily Synthesized Photoswitches Offering Nearly Quantitative Two-Way Isomerization with Visible Light. *J. Am. Chem. Soc.* **2012**, *134*, 20597−20600.
(1051) Knie, C.; Utecht, M.; Zhao, F.; Kulla, H.; Kovalenko, S.; Brouwer, A. M.; Saalfrank, P.; Hecht, S.; Bléger, D. Ortho-Fluoroazobenzenes: Visible Light Switches with Very Long-Lived Z Isomers. *Chem. - Eur. J.* **2014**, *20*, 16492−16501.
(1052) Saccone, M.; Terraneo, G.; Pilati, T.; Cavallo, G.; Priimagi, A.; Metrangolo, P.; Resnati, G. Azobenzene-Based Difunctional Halogen-Bond Donor: Towards the Engineering of Photoresponsive Co-Crystals. *Acta Crystallogr., Sect. B: Struct. Sci., Cryst. Eng. Mater.* **2014**, *70*, 149−156.
(1053) Bushuyev, O. S.; Tan, D.; Barrett, C. J.; Friscic, T. Fluorinated Azobenzenes with Highly Strained Geometries for Halogen Bond-Driven Self-Assembly in the Solid State. *CrystEngComm* **2015**, *17*, 73−80.
(1054) Boyd, R. In *Nonlinear Optics*; Boyd, R., Ed.; Academic Press: Burlington, MA, 2008.
(1055) Cariati, E.; Forni, A.; Biella, S.; Metrangolo, P.; Meyer, F.; Resnati, G.; Righetto, S.; Tordin, E.; Ugo, R. Tuning Second-Order

DOI: 10.1021/acs.chemrev.5b00484
Chem. Rev. 2016, 116, 2478−2601

NLO Responses through Halogen Bonding. *Chem. Commun.* **2007**, 2590−2592.
(1056) Papagni, A.; Maiorana, S.; Buttero, P. D.; Perdicchia, D.; Cariati, F.; Cariati, E.; Marcolli, W. Synthesis and Spectroscopic and NLO Properties of "Push-Pull" Structures Incorporating the Inductive Electron-Withdrawing Pentafluorophenyl Group. *Eur. J. Org. Chem.* **2002**, *2002*, 1380−1384.
(1057) Facchetti, A.; Annoni, E.; Beverina, L.; Morone, M.; Zhu, P.; Marks, T. J.; Pagani, G. A. Very Large Electro-Optic Responses in H-Bonded Heteroaromatic Films Grown by Physical Vapour Deposition. *Nat. Mater.* **2004**, *3*, 910−917.
(1058) Rashid, A. N.; Erny, C.; Gunter, P. Hydrogen-Bond-Directed Orientation in Nonlinear Optical Thin Films. *Adv. Mater.* **2003**, *15*, 2024−2027.
(1059) Yesodha, S. K.; Sadashiva Pillai, C. K.; Tsutsumi, N. Stable Polymeric Materials for Nonlinear Optics: A Review Based on Azobenzene Systems. *Prog. Polym. Sci.* **2004**, *29*, 45−74.
(1060) Delaire, J. A.; Nakatani, K. Linear and Nonlinear Optical Properties of Photochromic Molecules and Materials. *Chem. Rev.* **2000**, *100*, 1817−1846.
(1061) Priimagi, A.; Ogawa, K.; Virkki, M.; Mamiya, J.; Kauranen, M.; Shishido, A. High-Contrast Photoswitching of Nonlinear Optical Response in Crosslinked Ferroelectric Liquid-Crystalline Polymers. *Adv. Mater.* **2012**, *24*, 6410−6415.
(1062) Fiorini, C.; Charra, F.; Nunzi, J.-M.; Raimond, P. Quasi-Permanent All-Optical Encoding of Noncentrosymmetry in Azo-Dye Polymers. *J. Opt. Soc. Am. B* **1997**, *14*, 1984−2003.
(1063) Fourmigué, M.; Lieffrig, J. Organizing Radical Species in the Solid State with Halogen Bonding. In *Halogen Bonding II: Impact on Material Chemistry and Life Science*; Metrangolo, P., Resnati, G., Eds.; Springer International Publishing: Cham, Switzerland, 2015; pp 91−113.
(1064) Atzori, M.; Serpe, A.; Deplano, P.; Schlueter, J. A.; Laura Mercuri, M. Tailoring Magnetic Properties of Molecular Materials through Non-Covalent Interactions. *Inorg. Chem. Front.* **2015**, *2*, 108−115.
(1065) Bryce, B. M. R. Tetrathiafulvalenes as π-Electron Donors for Intramolecular Charge-Transfer Materials. *Adv. Mater.* **1999**, *11*, 11−23.
(1066) Ferraris, J.; Cowan, D. O.; Walatka, V.; Perlstein, J. H. Electron Transfer in a New Highly Conducting Donor-Acceptor Complex. *J. Am. Chem. Soc.* **1973**, *95*, 948−949.
(1067) Canevet, D.; Sallé, M.; Zhang, G.; Zhang, D.; Zhu, D. Tetrathiafulvalene (TTF) Derivatives: Key Building-Blocks for Switchable Processes. *Chem. Commun.* **2009**, 2245−2269.
(1068) Gompper, R.; Hock, J.; Polborn, K.; Dormann, E.; Winter, H. The Radical Cation Iodide of the New Electron Donor Tetraiodotetrathiafulvalene: Magnetic Properties and Crystal Structure. *Adv. Mater.* **1995**, *7*, 41−43.
(1069) Imakubo, T.; Shirahata, T.; Hervé, K.; Ouahab, L. Supramolecular Organic Conductors Based on Diiodo-TTFs and Spherical Halide Ion X−(X = Cl, Br). *J. Mater. Chem.* **2006**, *16*, 162−173.
(1070) Domercq, B.; Devic, T.; Fourmigué, M.; AubanSenzier, P.; Canadell, E. Hal···Hal Interactions in a Series of Three Isostructural Salts of Halogenated Tetrathiafulvalenes. Contribution of the Halogen Atoms to the HOMO−HOMO Overlap Interactions. *J. Mater. Chem.* **2001**, *11*, 1570−1575.
(1071) Ranganathan, A.; El-Ghayoury, A.; Mézière, C.; Hartê, E.; Clérac, R.; Batail, P. Balancing Framework Densification with Charged, Halogen-Bonded-π-Conjugated Linkages: [PPh4]2{[E-TTF-I2]-[Re6Se8(CN)6]} versus [PPh4]2[EDT-TTF-I]2{[EDT-TTF-I]-[Re6Se8(CN)6]}. *Chem. Commun.* **2006**, 2878−2880.
(1072) Alberola, A.; Fourmigué, M.; Gómez-García, C. J.; Llusar, R.; Triguero, S. Halogen Bonding Interactions with the [Mo3S7Cl6]2− Cluster Anion in the Mixed Valence Salt [EDT-TTFI2]4[Mo3S7Cl6]·CH3CN. *New J. Chem.* **2008**, *32*, 1103−1109.
(1073) Fourmigué, M.; Auban-Senzier, P. Anionic Layered Networks Reconstructed from [Cd(SCN)3]∞- Chains in Pseudo One-Dimensional Conducting Salts of Halogenated Tetrathiafulvalenes. *Inorg. Chem.* **2008**, *47*, 9979−9986.
(1074) Shin, K.; Brezgunova, M.; Jeannin, O.; Roisnel, T.; Camerel, F.; Auban-senzier, P.; Fourmigué, M. Strong Iodine···Oxygen Interactions in Molecular Conductors Incorporating Sulfonate Anions. *Cryst. Growth Des.* **2011**, *11*, 5337−5345.
(1075) Shin, K.-S.; Jeannin, O.; Brezgunova, M.; Dahaoui, S.; Aubert, E.; Espinosa, E.; Auban-Senzier, P.; Świetlik, R.; Frąckowiak, A.; Fourmigué, M. Inter-Layer Charge Disproportionation in the Dual-Layer Organic Metal (tTTF-I)2ClO4 with Unsymmetrical I···O Halogen Bond Interactions. *Dalton Trans.* **2014**, *43*, 5280−5291.
(1076) Avarvari, N.; Wallis, J. D. Strategies towards Chiral Molecular Conductors. *J. Mater. Chem.* **2009**, *19*, 4061−4076.
(1077) Pop, F.; Auban-Senzier, P.; Canadell, E.; Rikken, G. L. J. A.; Avarvari, N. Electrical Magnetochiral Anisotropy in a Bulk Chiral Molecular Conductor. *Nat. Commun.* **2014**, *5*, 3757.
(1078) Brezgunova, M.; Shin, K.-S.; Auban-Senzier, P.; Jeannin, O.; Fourmigué, M. Combining Halogen Bonding and Chirality in a Two-Dimensional Organic Metal (EDT-TTF-I2)2(D-camphorsulfonate)·H2O. *Chem. Commun.* **2010**, *46*, 3926−3928.
(1079) Lieffrig, J.; Le Pennec, R.; Jeannin, O.; Auban-Senzier, P.; Fourmigué, M. Toward Chiral Conductors: Combining Halogen Bonding Ability and Chirality within a Single Tetrathiafulvalene Molecule. *CrystEngComm* **2013**, *15*, 4408−4412.
(1080) Yamamoto, H. M.; Kosaka, Y.; Maeda, R.; Yamaura, J. I.; Nakao, A.; Nakamura, T.; Kato, R. Supramolecular Insulating Networks Sheathing Conducting Nanowires Based on Organic Radical Cations. *ACS Nano* **2008**, *2*, 143−155.
(1081) Yamamoto, H. M.; Yamaura, J.-I.; Kato, R. Preparation of Multicomponent Molecular Conductors with Supramolecular Assembly. *Synth. Met.* **1999**, *102*, 1448−1451.
(1082) Tamura, M.; Nakazawa, Y.; Shiomi, D.; Nozawa, K.; Hosokoshi, Y.; Ishikawa, M.; Takahashi, M.; Kinoshita, M. Bulk Ferromagnetism in the β-Phase Crystal of the P-Nitrophenyl Nitronyl Nitroxide Radical. *Chem. Phys. Lett.* **1991**, *186*, 401−404.
(1083) Cimino, P.; Pavone, M.; Barone, V. Halogen Bonds between 2,2,6,6-Tetramethylpiperidine-N-Oxyl Radical and CxHyFzi Species: DFT Calculations of Physicochemical Properties and Comparison with Hydrogen Bonded Adducts. *J. Phys. Chem. A* **2007**, *111*, 8482−8490.
(1084) Davy, K. J. P.; McMurtrie, J.; Rintoul, L.; Bernhardt, P. V.; Micallef, A. S. Vapour Phase Assembly of a Halogen Bonded Complex of an Isoindoline Nitroxide and 1,2-Diiodotetrafluorobenzene. *CrystEngComm* **2011**, *13*, 5062−5070.
(1085) Hanson, G. R.; Jensen, P.; McMurtrie, J.; Rintoul, L.; Micallef, A. S. Halogen Bonding between an Isoindoline Nitroxide and 1,4-Diiodotetrafluorobenzene: New Tools and Tectons for Self-Assembling Organic Spin Systems. *Chem. - Eur. J.* **2009**, *15*, 4156−4164.
(1086) Espallargas, G. M.; Recuenco, A.; Romero, F. M.; Brammer, L.; Libri, S. One-Dimensional Organization of Free Radicals via Halogen Bonding. *CrystEngComm* **2012**, *14*, 6381−6383.
(1087) Pang, X.; Zhao, X. R.; Wang, H.; Sun, H. L.; Jin, W. J. Modulating Crystal Packing and Magnetic Properties of Nitroxide Free Radicals by Halogen Bonding. *Cryst. Growth Des.* **2013**, *13*, 3739−3745.
(1088) Beweries, T.; Brammer, L.; Jasim, N. a.; McGrady, J. E.; Perutz, R. N.; Whitwood, A. C. Energetics of Halogen Bonding of Group 10 Metal Fluoride Complexes. *J. Am. Chem. Soc.* **2011**, *133*, 14338−14348.
(1089) Clemente-Juan, J. M.; Coronado, E.; Minguez Espallargas, G.; Adams, H.; Brammer, L. Effects of Halogen Bonding in Ferromagnetic Chains Based on Co(II) Coordination Plymers. *CrystEngComm* **2010**, *12*, 2339−2342.
(1090) Halcrow, M. A. Structure:function Relationships in Molecular Spin-Crossover Complexes. *Chem. Soc. Rev.* **2011**, *40*, 4119−4142.
(1091) Fukuroi, K.; Takahashi, K.; Mochida, T.; Sakurai, T.; Ohta, H.; Yamamoto, T.; Einaga, Y.; Mori, H. Synergistic Spin Transition between Spin Crossover and Spin-Peierls-like Singlet Formation in the

DOI: 10.1021/acs.chemrev.5b00484
Chem. Rev. 2016, 116, 2478−2601

Halogen-Bonded Molecular Hybrid System: [Fe(Iqsal) 2][Ni(dmit)2] × CH3CN × H2O. *Angew. Chem., Int. Ed.* **2014**, *53*, 1983−1986.
(1092) Nassirinia, N.; Amani, S.; Teat, S. J.; Roubeau, O.; Gamez, P. Enhancement of Spin-Crossover Cooperativity Mediated by Lone Pair-π Interactions and Halogen Bonding. *Chem. Commun.* **2014**, *50*, 1003−1005.
(1093) Atzori, M.; Artizzu, F.; Sessini, E.; Marchio, L.; Loche, D.; Serpe, A.; Deplano, P.; Concas, G.; Pop, F.; Avarvari, N.; et al. Halogen-Bonding in a New Family of Tris(haloanilato)metallate(iii) Magnetic Molecular Building Blocks. *Dalton Trans.* **2014**, *43*, 7006−7019.
(1094) Abate, A.; Saliba, M.; Hollman, D. J.; Stranks, S. D.; Wojciechowski, K.; Avolio, R.; Grancini, G.; Petrozza, A.; Snaith, H. J. Supramolecular Halogen Bond Passivation of Organic−Inorganic Halide Perovskite Solar Cells. *Nano Lett.* **2014**, *14*, 3247−3254.
(1095) Shirman, T.; Arad, T.; Van Der Boom, M. E. Halogen Bonding: A Supramolecular Entry for Assembling Nanoparticles. *Angew. Chem., Int. Ed.* **2010**, *49*, 926−929.
(1096) Shirman, T.; Kaminker, R.; Freeman, D.; Van Der Boom, M. E. Halogen-Bonding Mediated Stepwise Assembly of Gold Nanoparticles onto Planar Surfaces. *ACS Nano* **2011**, *5*, 6553−6563.
(1097) Blakey, I.; Merican, Z.; Rintoul, L.; Chuang, Y.-M.; Jack, K. S.; Micallef, A. S. Interactions of Iodoperfluorobenzene Compounds with Gold Nanoparticles. *Phys. Chem. Chem. Phys.* **2012**, *14*, 3604−3611.
(1098) Komoto, Y.; Fujii, S.; Hara, K.; Kiguchi, M. Single Molecular Bridging of Au Nanogap Using Aryl Halide Molecules. *J. Phys. Chem. C* **2013**, *117*, 24277−24282.
(1099) Salavagione, H. J.; Martínez, G.; Marco, C. A Polymer/solvent Synergetic Effect to Improve the Solubility of Modified Multi-Walled Carbon Nanotubes. *J. Mater. Chem.* **2012**, *22*, 7020.
(1100) Salavagione, H. J.; Ellis, G.; Martínez, G. Poly(vinyl chloride)/Multiwalled Carbon Nanotube Nanocomposites: Effect of the Tacticity Distribution on the Polymer/Nanofiller Interface. *J. Phys. Chem. C* **2012**, *116*, 18256−18262.
(1101) Shirman, T.; Freeman, D.; Posner, Y. D.; Feldman, I.; Facchetti, A.; Van Der Boom, M. E. Assembly of Crystalline Halogen-Bonded Materials by Physical Vapor Deposition. *J. Am. Chem. Soc.* **2008**, *130*, 8162−8163.
(1102) Boterashvili, M.; Lahav, M.; Shankar, S.; Facchetti, A.; van der Boom, M. E. On-Surface Solvent-Free Crystal-to-Co-Crystal Conversion by Non-Covalent Interactions. *J. Am. Chem. Soc.* **2014**, *136*, 11926−11929.
(1103) Yamanaka, N.; Kawano, R.; Kubo, W.; Kitamura, T.; Wada, Y.; Watanabe, M.; Yanagida, S. Ionic Liquid Crystal as a Hole Transport Layer of Dye-Sensitized Solar Cells. *Chem. Commun.* **2005**, 740−742.
(1104) Green, M. A.; Ho-Baillie, A.; Snaith, H. J. The Emergence of Perovskite Solar Cells. *Nat. Photonics* **2014**, *8*, 506−514.
(1105) Kazim, S.; Nazeeruddin, M. K.; Grätzel, M.; Ahmad, S. Perovskite as Light Harvester: A Game Changer in Photovoltaics. *Angew. Chem., Int. Ed.* **2014**, *53*, 2812−2824.
(1106) Newlands, J. A. R. On Relations among the Equivalents. *Chem. News* **1864**, *10*, 94−95.
(1107) Newlands, J. A. R. On the Law of Octaves. *Chem. News* **1865**, *12*, 83.
(1108) Retgers, J. W. Über Einige Änderungen Im Periodischen System Der Elemente. *Z. Phys. Chem.* **1895**, *16*, 644.
(1109) Priimagi, A.; Cavallo, G.; Metrangolo, P.; Resnati, G. The Halogen Bond in the Design of Functional Supramolecular Materials: Recent Advances. *Acc. Chem. Res.* **2013**, *46*, 2686−2695.
(1110) Bruce, D. W. Halogen-Bonded Liquid Crystals. In *Halogen Bonding. Fundamentals and Applications*; Metrangolo, P., Resnati, G., Eds.; Structure and Bonding, Vol. *126*; Springer-Verlag: Berlin, Heidelberg, 2008; pp 161−180.
(1111) Lévesque, D.; Beaudoin, J.-D.; Roy, S.; Perreault, J.-P. In Vitro Selection and Characterization of RNA Aptamers Binding Thyroxine Hormone. *Biochem. J.* **2007**, *403*, 129−138.
(1112) Sandler, B.; Webb, P.; Apriletti, J. W.; Huber, B. R.; Togashi, M.; Lima, S. T. C.; Juric, S.; Nilsson, S.; Wagner, R.; Fletterick, R. J.; et al. Thyroxine-Thyroid Hormone Receptor Interactions. *J. Biol. Chem.* **2004**, *279*, 55801−55808.

DOI: 10.1021/acs.chemrev.5b00484
Chem. Rev. 2016, 116, 2478−2601